Base-Modified Peptide Nucleic Acid Analogues as Hybridization Probes in Nucleic Acid Diagnostics

A thesis

Submitted in partial fulfillment of the requirements

For the degree of

Doctor of Philosophy

By

Pramod Madhavrao Sabale

Reg. No. 20113138

INDIAN INSTITUTE OF SCIENCE EDUCATION
AND RESEARCH PUNE
2017

This thesis is dedicated
to my family

INDIAN INSTITUTE OF SCIENCE EDUCATION AND RESEARCH (IISER), PUNE
(An Autonomous Institution, Ministry of Human Resource Development, Govt. of India)
Dr. Homi Bhabha Road, Pashan, Pune–411 008

Dr. Seergazhi G. Srivatsan
Associate Professor, Chemistry

Dr. Seergazhi G. Srivatsan
Associate Professor
Department of Chemistry
IISER, Pune

CERTIFICATE

Certified that the work incorporated in the thesis entitled *"**Base-Modified Peptide Nucleic Acid Analogues as Hybridization Probes in Nucleic Acid Diagnostics**"* submitted by Mr. Pramod M. Sabale was carried out by the candidate under my supervision. The work presented here or any part of it has not been included in any other thesis submitted previously for the award of any degree or diploma from any other University or Institution.

S.G. Srivatsan

Date: May 8, 2017
Place: Pune

Dr. Seergazhi G. Srivatsan

Tel.: +91-20-25908086 Fax: +91-20-25908186 E-mail: srivatsan@iiserpune.ac.in

DECLARATION

I declare that this written submission represents my ideas in my own words and where others ideas have included; I have adequately cited and referenced the original sources. I also declare that I have adhered to all principles of academic honesty and integrity and have not misrepresented or fabricated or falsified any idea/data/fact/source in my submission. I understand that violation of the above will be cause for disciplinary action by the institute and can also evoke penal action from the sources which have thus not been properly cited or from whom proper permission has not been taken when needed.

The work reported in this thesis is the original work done by me under the guidance of Dr. S. G. Srivatsan.

Date: May 8, 2017 Mr. Pramod Madhavrao Sabale

Place: Pune Reg. No. 20113138

Acknowledgements

I would like to express special appreciation to my enthusiastic mentor Dr. S. G. Srivatsan for his constant support and guidance during the courses of study. I admire his creativity in designing and executing experiments with great thinking. His guidance has helped me during the time of research and writing of this thesis. I thank Dr. Srivatsan, not only for his valuable inputs and consistent encouragement during my PhD, but also for his generous support in my personal life. I am very fortunate to have an opportunity to work under his supervision.

I sincerely thank to Prof. K. N. Ganesh (Director, IISER Pune) for providing the excellent infrastructure and facilities to pursue my doctoral research. I would like to express my sincere gratitude to Prof. K. N. Ganesh for being one of the research advisory committee (RAC) members and providing critical suggestion during RAC meeting. I also would like to acknowledge Dr. G. J. Sanjayan (NCL Pune) for his valuable comments during RAC meetings. I would like to thank Dr. Kundan Sengupta, particularly his student Ajay Labade for their help in initial cell culture experiments. I am sincerely grateful to Prof. M. Jayakannan (Chair, Department of Chemistry) for his help during PhD. I would also like to acknowledge Dr. S. K. Asha from NCL, Pune for allowing me to perform fluorescence experiments in her lab.

I am very fortunate to have wonderful colleagues working with me like Dr. Maroti, Dr. Arun, Dr. Anupam, Dr. Vyankat, Dr. Cornelia, Ashok, Sudeshna, Jerrin, Manisha, Pankaj, Saddam, Uddhav, Anurag, Neel, Sangamesh and Progya. I thank them for their support and keeping cheerful atmosphere in the lab during my doctoral research. I am thankful to all students of Prof. K. N. Ganesh, for their help in understanding PNA chemistry in initial days. In particular, Dr. Deepak, Dr. Vijay, Dr. Nitin and Dr. Satish for teaching me PNA synthesis. I thank Sushil and Balu for their help and support. I am thankful to all IISER Pune colleagues, with whom I discussed my ups and downs of research, and for giving the relaxation needed in tough times of research. I would like to extend my gratitude to all faculty members for their constant support and encouragement. It is my prime duty to acknowledge Council of Scientific and Industrial Research (CSIR) India for my graduate research fellowship. I would like to thank those who helped me directly and indirectly during my research.

I shall always remain indebted to my parents and my entire family, for their unconditional love, blessings, sacrifices, patience and support during my study. The values

and virtues they have instilled in me have made me to achieve whatever I have achieved so far. I would like to thank a very special person, my lovely wife, Shweta for her unconditional support and trust. Finally, I would like to thank my cute son Advik, whose smile has always made me to forget all the tension and frustration during the courses of research.

Pramod Madhavrao Sabale

Chapter 2 is reprint of: 1) **P. M. Sabale**, A. Nuthanakanti and S. G. Srivatsan, Synthesis and fluorescence properties of a full set of extended RNA base analogues. *Ind. J. Chem.*, 2013, **52A**, 1004–1013.
2) **P. M. Sabale** and S. G. Srivatsan, Responsive fluorescent PNA analogue as a tool for detecting G-quadruplex motifs of oncogenes and activity of toxic ribosome-inactivating proteins. *ChemBioChem*, 2016, **17**, 1665–1673.
The dissertation author is the main author and researcher for this work.

Chapter 3A is reprint of: **P. M. Sabale**, J. T. George and S. G. Srivatsan, A base-modified PNA-graphene oxide platform as a turn-on fluorescence sensor for the detection of human telomeric repeats. *Nanoscale*, 2014, **6**, 10460–10469.
The dissertation author is the main author and researcher for this work.

Chapter 3B is a reprint of: **P. M. Sabale** and S. G. Srivatsan, Responsive fluorescent PNA analogue as a tool for detecting G-quadruplex motifs of oncogenes and activity of toxic ribosome-inactivating proteins. *ChemBioChem*, 2016, **17**, 1665–1673.
The dissertation author is one of the main authors and researcher for this work.

Table of content

Abbreviations

2-AP	2-Aminopurine	DBCO	Dibenzocyclooctyne
A	Adenine	EDC	1-Ethyl-3-(3-dimethylaminopropyl)carbodiimide
Abs	Absorption	EDTA	Ethylenediaminetetraacetic acid
Ac	Acetyl	*em*	Emission
ACN	Acetonitrile	ESI	Electrospray ionization
aeg	Aminoethylglycine	Et	Ethyl
AMP	Adenosine monophosphate	EBA	Ethylbromo acetate
BSA	Bovine serum albumin	EtOAc	Ethyl acetate
NBS	*N*-Bromosuccinimide	EPR	Electron paramagnetic resonance
FBS	Fetal bovine serum	FRET	Förster resonance energy transfer
(Boc)2O	Boc anhydride	Fmoc	9-Fluorenylmethoxycarbonyl
Bn	Benzyl	FI	Fluorescence intensity
C	Cytosine	FISH	Fluorescence *in situ* hybridization
CD	Circular dichroism	GO	Graphene oxide
CMP	Cytidine monophosphate	G	Guanine
Cu	Copper	GFP	Green fluorescent protein
CuAAC	Copper(I)-catalyzed alkyne-azide cycloaddition	GMP	Guanosine monophosphate
$CuSO_4$	Copper sulphate	GQ	G-quadruplex
CHCA	α-Cyano-4-hydroxycinnamic acid	Gly	Glycine
Cbz	Benzyloxycarbonyl	h-Telo	Human telomeric
Calcd	Calculated	HPLC	High performance liquid chromatography
CPP	Cell penetrating peptide	h	Hours
DMADHP	2-Dimethylamino-4,6-dihydroxypyrimidine	HBTU	2-(1H-Benzotriazole-1-yl)-1,1,3,3 tetramethyluronum-hexafluoro-phosphate
DAPI	4',6-Diamidino-2-phenylindole	HOBt	*N*-Hydroxybenzotriazole
DFHBI	3,5-Difluoro-4-hydroxybenzylidene imidazolinone	IEDDA	Inverse-electron demand Diels-Alder
DHB	2,5-Dihydroxybenzoic acid	IR	Infrared
DNA	Deoxyribonucleic acid	*in vitro*	Outside living organism
DMAP	4-Dimethylaminopyridine	*in vivo*	Inside living organism
DMSO	Dimethyl sulfoxide	ISH	*In situ* hybridization
DMF	*N*, *N*-Dimethylformamide	K_{ap}	Apparent rate constant
ds	Double stranded	K_{sv}	Stern-Volmer quenching constant
DMEM	Dulbecco's Modified Eagle Medium	LSM	Laser scanning microscope
DCM	Dichloromethane	LED	Light emitting diode
DIPEA	*N,N*-Diisopropylethylamine	Lys	Lysine
DMG	Dimethylguanidine	L	Levo-
DA	Diels-Alder	ε	Molar extinction coefficient

max	Maximum
MeOH	Methanol
mRNA	Messenger RNA
mM	Milimolar
MALDI-TOF	Matrix assisted laser desorption ionisation-time of flight
mg	Milligram
MHz	Megahertz
MBHA	4-Methyl benzhydryl amine
MS	Mass spectrometry
min	Minute
µM	Micro molar
µg	Microgram
µL	Microliter
mmol	Millimoles
MW	Molecular weight
MRI	Magnetic resonance imaging
nM	Nanomolar
ng	Nanogram
nmol	Nanomoles
nm	Nanometer
NMP	*N*-Methyl-2-pyrrolidone
NMR	Nuclear magnetic resonance
N	Normal
NMP	Nucleoside monophosphate
NHS	*N*-hydroxysuccinimide
Obsvd	Observed
ON	Oligonucleotide
PAGE	Polyacrylamide gel electrophoresis
Pd	Palladium
PDS	Pyridostatin
PBS	Phosphate buffered saline
ppm	Parts per million
PNA	Peptide nucleic acid
PS-oligo	Phosphorothioate-oligo
PCR	Polymerase chain reaction
RPMI	Roswell park memorial institute
rel	Relative
Rf	Retention factor
RNA	Ribonucleic acid
rRNA	Ribosomal RNA
RP	Reverse Phase
RT	Room temperature
RIPs	Ribosome inactivating proteins
siRNA	Small interfering RNA
SPPS	Solid-phase peptide synthesis
ss	Single strand/single stranded
SPAAC	strain-promoted alkyne-azide cycloadditions
SNP	Single nucleotide polymorphism
SSC	Saline-sodium citrate
TCSPC	Time correlated single photon counting
TERRA	Telomeric repeat-containing RNA
THF	Tetrahydrofuron
THPTA	*tris*-(3-Hydroxypropyl triazolylmethyl)amine
tRNA	Transfer RNA
TLC	Thin layer chromatography
Tm	Thermal melting
Tris	Tris (hydroxymethyl) amino methane
TEMED	Tetramethylethylenediamine
TFA	Trifluoroacetic acid
TFMSA	Trifluoromethane sulfonic acid
T	Thymine
TEG	Triethylene glycol
VRC	Vanadyl ribonucleoside complex
U	Uridine
UV-Vis	Ultraviolet-Visible
UMP	Uridine monophosphate
UV	Ultraviolet
WC	Watson-Crick

Synopsis

Base-Modified Peptide Nucleic Acid Analogues as Hybridization Probes in Nucleic Acid Diagnostics

Background

Nucleic acids adopt several complex secondary and tertiary structures to perform functions like storage and transfer of genetic information, catalysis and regulation of gene expression.[1] Several biophysical tools have been developed to detect nucleic acid sequences and also understand the structure and function of nucleic acids.[2] In particular, fluorescence-based techniques, which are highly sensitive and offer detection of analytes in real time, have been widely utilized for the detection of nucleic acid sequences in cell-free and cellular systems.[3] As natural nucleobases are practically nonemissive, often in these studies, a complementary oligonucleotide (ON) labeled with an appropriate fluorescent reporter or reporters (e.g., FRET pair) is used as a probe to target the nucleic acid sequence of interest.[4] Upon hybridization to the target nucleic acid, the reporter signals the binding event via changes in its fluorescence properties, which is used in detecting as well as imaging specific nucleic acid motifs *in vitro* and in live cells. Alternatively, environment-sensitive fluorescent nucleoside analogue probes incorporated into ONs have been extensively used in studying nucleic acid lesions (e.g., abasic site, mismatch base pair) and the conformational changes that occur at the nucleotide level during a binding event or in a reaction involving nucleic acids.[5] Although the utility of such ON reporters are arguably undeniable, low fluorescence efficiency upon incorporation into ON sequences, background fluorescence, poor hybridization efficiency and nucleases mediated degradation limit the practical utility of many such labeled ON probes, particularly in cellular environment.[6] Therefore, it is highly desirable to develop robust fluorescence hybridization tools with properties suitable for cell-free and in-cell analysis of nucleic acids. In this context, a synthetic nucleic acid analogue, peptide nucleic acid (PNA), containing an uncharged and achiral pseudo-peptide backbone would be appropriate as it is resistant to nucleases and proteases, and base-pairs strongly with complementary DNA and RNA ONs.[7] Inspired by many of the useful properties of PNA and base-modified nucleobase analogues, we hypothesized that constructing PNA oligomer probes containing microenvironment- and conformation-sensitive fluorescent nucleobase

analogues would provide ample opportunities to develop new and robust diagnostic tools for studying the structure and functions of nucleic acids in both cell-free and cellular systems.[8]

This thesis illustrates the design, synthesis and photophysical characterization of fluorescent PNA analogues obtained by attaching heterobicyclic rings (benzofuran and benzothiophene) at the 5-position of the uracil base. The fluorescence properties of PNA base analogues are highly sensitive to changes in their microenvironment. Importantly, the sensitivity of the fluorescent PNA analogues to neighbouring base environment in PNA-DNA and PNA-RNA duplexes enabled the development of fluorescence hybridization assays to detect telomeric DNA repeats, G-quadruplex (GQ) forming proto-oncogenes and abasic sites in RNA. For example, benzofuran-modified PNA oligomer has been used to develop a simple turn-on fluorescence hybridization assay for the detection of telomeric DNA repeats using graphene oxide (GO) platform. Benzothiophene-modified PNA oligomers enabled the detection of GQ-forming sequences in proto-oncogenes and depurination activity of a toxic ribosome inactivating proteins (RIPs) toxin. Furthermore, PNA analogue based on the Lucifer chromophore, with the ability to positively signal the presence of adenosine repeat, has been utilized in imaging of poly(A) tails of mRNA in cells.

Although development of robust fluorescence-based PNA probes is challenging, development of efficient methods to incorporate such reporters into PNA oligomers is equally important. The last part of the thesis describes the development of a post-synthetic PNA labeling technology by using chemoselective reactions. PNA oligomers containing chemoselective reactive handles have been prepared and post-synthetically functionalized with variety of biophysical tags by using copper(I)-catalyzed azide-alkyne cycloaddition (CuAAC), strain-promoted azide-alkyne cycloaddition (SPAAC), azide-phosphine Staudinger ligation and palladium-catalyzed reactions. Taken together, novel environment-sensitive fluorescent PNA probes and chemical labeling techniques reported in this thesis will expand the scope of PNA in devising new platforms to detect, image and target biologically relevant nucleic acid motifs.

The thesis is organized as follows:

Chapter 1: Introduction to nucleic acids and PNA

This chapter briefly describes different tools that have been developed to advance our understanding of the structure and function of nucleic acids. The detection of nucleic acids

by using synthetic ON probes in cell-free as well as cellular conditions is elaborated. Structure, properties and various modifications carried out on PNA for detecting and targeting nucleic acids are also discussed. In particular, fluorescent base-modified PNA probes for studying structure and conformation of nucleic acids are elaborated. Further, we provide a detailed discussion on the applications of PNA in nucleic acid therapeutics, molecular biology, PCR clamping, microarrays and biosensors, and nucleic acid diagnostics. Finally, the limitations of presently available fluorescent PNA analogues and PNA labeling methodologies followed by motivation for the present research work are provided.

Chapter 2: Synthesis, incorporation and photophysical analysis of 5-heterobicycle-modified uracil PNA analogues

In order to modify appropriate nucleobase (A/T/G/C) in the context to PNA, we have taken the advantage of fluorescent uridine analogues (5-benzothiophene-uridine and 5-benzofuran-uridine) reported by our group.[9] We first synthesized full set of benzofuran-conjugated ribonucleoside analogues and compared their photophysical properties in solvents of different polarity and viscosity.[10] From these results, we observed that benzofuran uridine analogue exhibits probe like property because, it shows a) emission maximum in the visible region, b) reasonable quantum yield, and c) good solvatochromism. Based on these observations, PNA base analogues made of 5-benzothiophene (^{BT}U)- and 5-benzofuran (^{BF}U)-conjugated uracil core were synthesized (Figure 1A). Preliminary photophysical analysis of emissive PNA analogues revealed that the ^{BT}U- and ^{BF}U-modified PNA analogues are highly sensitive to their microenvironment (Figure 1B and 1C).

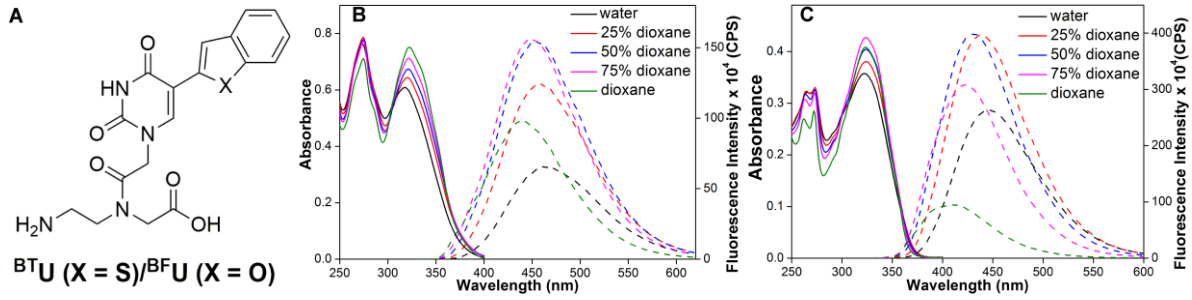

Figure 1. (**A**) Chemical structure of nucleobase-modified PNA analogues (^{BT}U and ^{BF}U). Absorption (solid line) and emission (dashed line) spectra of monomers in water, dioxane and its mixtures. Absorption and emission spectra for ^{BT}U (**B**) and ^{BF}U (**C**). With change in solvent polarity, absorption spectrum is marginally affected, while emission spectrum is significantly affected.

^{BT}U and ^{BF}U were incorporated into model PNA oligomers, wherein the emissive base was placed in-between different flanking bases. Subsequent hybridization with various DNA

ONs and photophysical analysis revealed that the fluorescence properties of emissive PNA analogues are sensitive to neighbouring base environment (Figure 2).[11] Importantly, UV-thermal melting and circular dichroism (CD) studies of unmodified and modified PNA-DNA heteroduplexes pointed out that benzothiophene- and benzofuran-modifications had only marginal impact on the structure and stability of duplexes. Interestingly, the PNA oligomer containing ^{BT}U PNA base flanked in-between C residues, selectively signaled the presence of perfect complementary base dA in a DNA ON (in GAG base set) with the appreciable enhancement in fluorescence intensity as compared to corresponding single-stranded PNA and mismatched PNA-DNA duplexes (Figure 2B).[11] The ability of ^{BF}U PNA to report complementary DNA ONs and ^{BT}U PNA to selectively signal the presence of a GAG base set in DNA ON with significant enhancement in fluorescence efficiency has been utilized in devising assays to detect the human telomeric DNA repeat and GQ forming proto-oncogenes, and monitor the depurination activity of plant toxins. These applications are discussed in the following chapters.

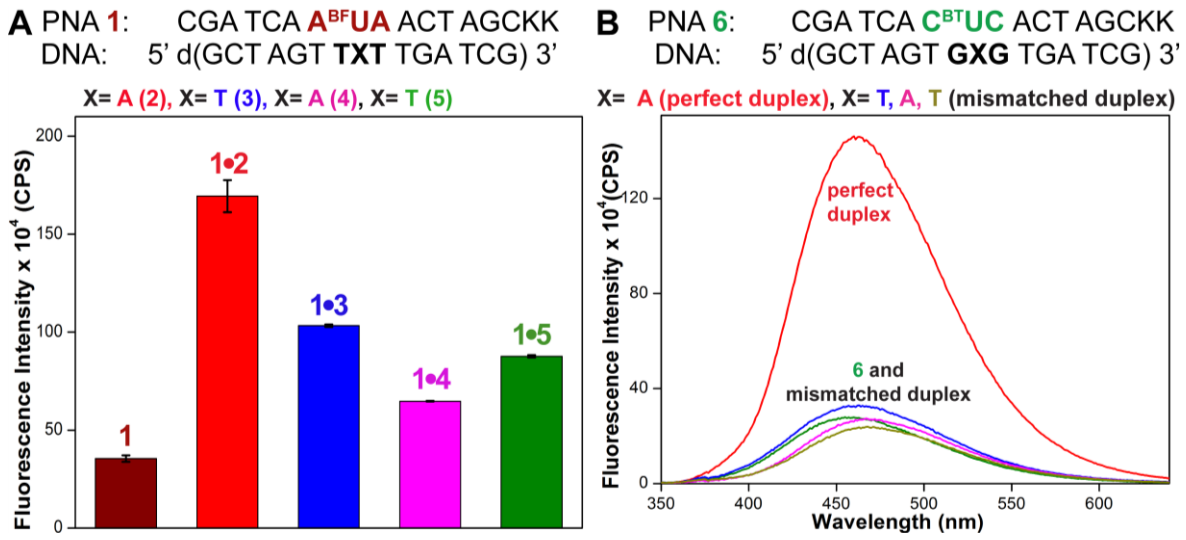

Figure 2. (**A**) Fluorescence intensity of ^{BF}U-modified PNA **1** (^{BF}U flanked in-between A residues) and their PNA-DNA heteroduplexes. ^{BF}U reports complementary ONs with enhancement in fluorescence intensity. (**B**) Fluorescence spectra of ^{BT}U-modified PNA **6** (^{BT}U flanked in-between C residues) and its PNA-DNA heteroduplexes. ^{BT}U selectively signals the presence of perfect complementary base dA in DNA ON (GAG base set) with significant enhancement in fluorescence intensity as compared to single-stranded and mismatched duplexes.

Chapter 3: Fluorescence detection of noncanonical nucleic acid motifs and depurination activity of plant toxins using fluorescent PNA probes

Chapter 3A: Fluorescent PNA-graphene oxide platform as a turn-on sensor for the detection of human telomeric DNA repeats

This chapter describes the development of a fluorescence turn-on platform to detect the human telomeric DNA repeat $(TTAGGG)_n$ by using benzofuran-modified uracil PNA analogue (^{BF}U) and graphene oxide (GO) (Figure 3A).[12] This sensor assembly is made of a PNA oligomer labeled with ^{BF}U, which retains its fluorescence efficiency upon hybridization to the target ON (e.g., human telomeric DNA repeat) and GO, an excellent fluorescence quencher, which shows significantly higher binding affinity for single stranded (ss) ONs over the double stranded (ds) and folded ONs. A ^{BF}U-labeled PNA probe complementary to the human telomeric DNA ON (telo-DNA) was synthesized (Figure 3B). Upon addition of ss fluorescent PNA probe to an aqueous dispersion of GO, reasonable quenching in fluorescence intensity was observed as a result of binding of PNA probe to GO. Further, addition of telo-DNA ON resulted in a significant enhancement in fluorescence intensity, which was due to desorption of PNA probe from GO surface and subsequent duplex formation with complementary telo-DNA ON (Figure 3C). Fluorescence anisotropy experiments also corroborated with the observed results. This assay also enabled the fluorescence detection of biologically relevant higher order GQ structures of human telomeric DNA repeat.[12] Further, the suitability of this detection method in setting up a rudimentary assay in identifying small molecule G-quadruplex binders was explored. Taken together, the results demonstrate that this method, which does not involve rigorous assay setup, could provide new opportunities to detect telomeric DNA repeats and discover efficient G-quadruplex binders.

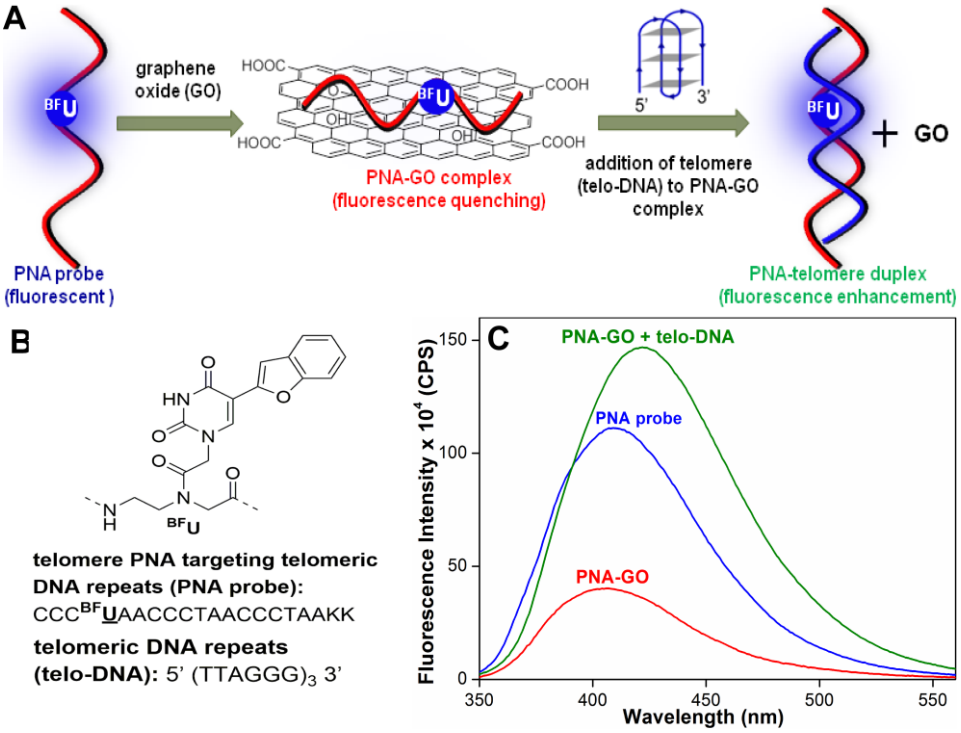

Figure 3. (**A**) A schematic illustration of the fluorescence turn-on assay to detect the human telomeric DNA repeats by using ^{BF}U-modified fluorescent PNA-GO platform. (**B**) ^{BF}U-modified fluorescent PNA probe targeting telomeric DNA ON (telo-DNA) are shown. (**C**) Fluorescence detection of telomere DNA using PNA-GO platform. Upon addition of ^{BF}U-PNA probe GO, it shows reduction in fluorescence intensity due to formation of PNA-GO complex. Subsequent addition of telomere target (telo-DNA) results in appreciable enhancement in fluorescence due to desorption of PNA probe from GO and formation of PNA-telomere duplex.

Chapter 3B: Benzothiophene-conjugated uracil PNA analogue as a fluorescence tool for detecting oncogenic G-quadruplex motifs and activity of toxic ribosome inactivating proteins

The PNA oligomer containing ^{BT}U, flanked in between C-residue (C^{BT}UC), selectively signaled the presence of GAG base in a complementary DNA ON with significant enhancement in fluorescence intensity (discussed in chapter 2).[11] The GAG triplet base sets are constituents of many functionally important nucleic acid motifs such as G-quadruplex (GQ) forming sequences in the promoter (c-myc, c-myb, c-kit etc.) and untranslated regions (UTRs) of mRNA (NRAS, BCL-2 etc.) of a number of oncogenes.[13] In addition, GAG base set is also present in the highly conserved sarcin-ricin loop of eukaryotic 28S rRNA, which is a critical site for the binding of elongation factors to ribosome during protein synthesis process.[14] The adenosine residue (A_{4324}) of the GAG base set present in the sarcin-ricin loop is specifically depurinated by ribosome inactivating protein (RIP) toxins to produce an RNA abasic site.[14] In this chapter, we describe the utility of the responsiveness of the ^{BT}U PNA

analogue to develop a simple turn-on fluorescence hybridization assay to detect GQ motifs of proto-oncogenes (c-myc and c-kit), and to monitor as well as estimate the depurination activity of ribosome inactivating protein (RIP) toxins (Figure 4A and Figure 5A).

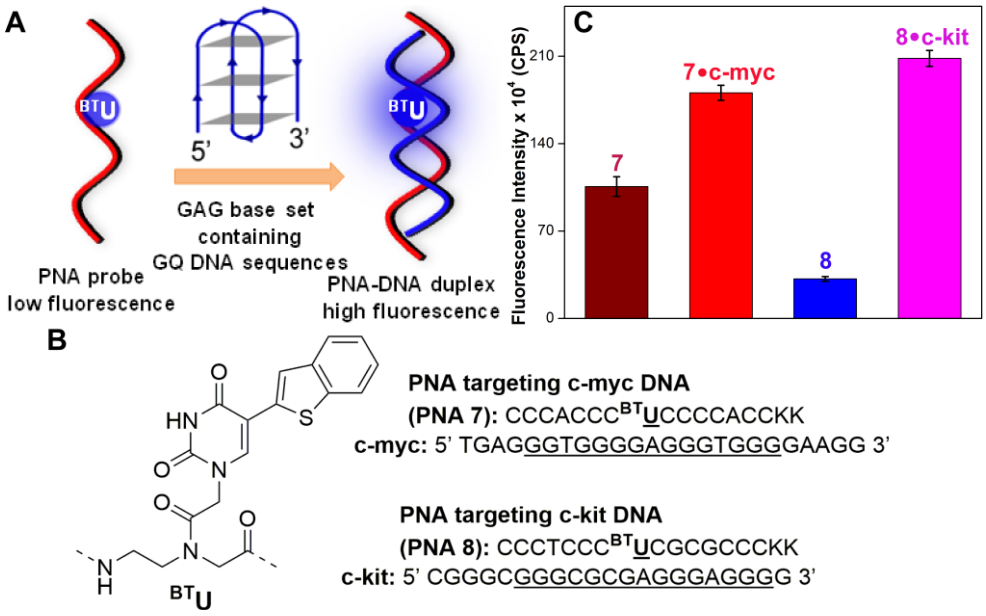

Figure 4. (**A**) A schematic illustration of the fluorescence turn-on assay to detect the GAG base set containing GQ forming DNA sequences using emissive PNA probes (**B**) ^{BT}U-modified fluorescent PNA probes **7** and **8** targeting c-myc and c-kit DNA ONs, respectively are shown. (**C**) ^{BT}U-PNA probes (**7** and **8**) detect c-myc and c-kit DNA ONs by the formation of PNA-DNA heteroduplex (**7**•c-myc and **8**•c-kit2) with enhancement in fluorescence intensity.

To setup a hybridization assay, ^{BT}U-modified PNA oligomers **7**, **8** and **9** (^{BT}U flanked in-between C residues) complementary to c-myc, c-kit and RNA containing the conserved region of the sarcin-ricin stem-loop domain of rRNA ONs were synthesized by using SPPS (Figure 4B and Figure 5B). PNA probes were initially hybridized to respective ON target and subjected to fluorescence analysis. The heteroduplex of PNA probe **7** and **8** with c-myc and c-kit displayed significant enhancement in fluorescence intensity as compared to corresponding ss PNA oligomer (Figure 4C). Moreover, strand invasion ability of PNA probe **7** and **8** were evaluated by incubating them with preformed GQ structures of c-myc and c-kit ON, respectively, at physiological conditions. This experiment showed that PNA probe **8** was able to invade GQ formed by c-kit ON, while PNA probe **7** was not very effective in invading the GQ structure of c-myc. Taken together, our results validate that ^{BT}U-modified PNA oligomers could be potentially utilized as fluorescence turn-on probes to detect certain GQ forming motifs.[11]

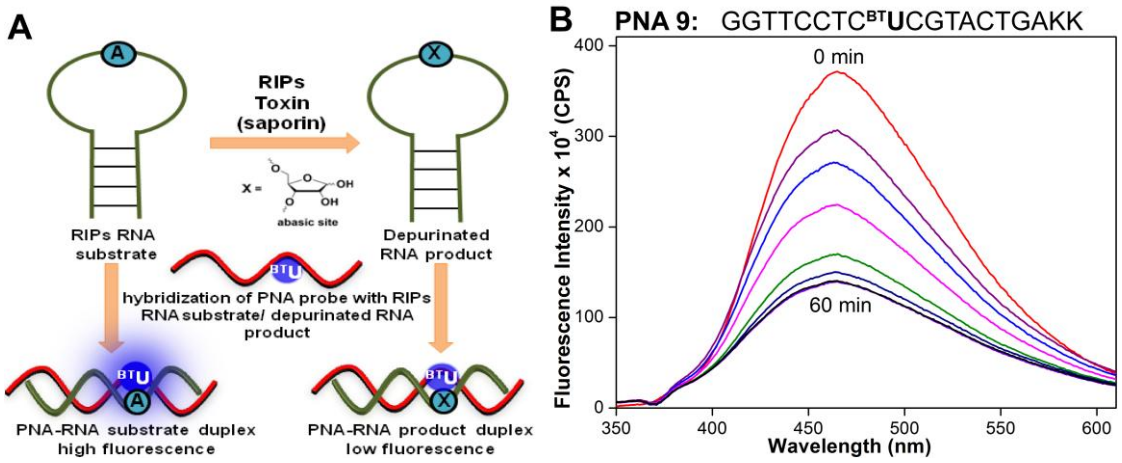

Figure 5. (**A**) Study of depurination activity of ribosome inactivating protein (RIP) toxin using fluorescent PNA oligomer probe. (**B**) Saporin mediated depurination of RIPs RNA substrate monitored by fluorescent ^{BT}U-PNA probe **9**. Fluorescence intensity is gradually decreased as a function of time due to the formation of PNA-RNA product duplex with ^{BT}U-opposite to developing abasic site.

The ability of the ^{BT}U-modified PNA **9** to differentiate between a complementary base in a GAG base set and an abasic site in a PNA-RNA heteroduplex by change in the fluorescence intensity was utilized in monitoring the depurination activity of RIP toxins (e.g. saporin, Figure 5A). Thermally folded RIPs RNA substrate was incubated with various concentration of saporin and then aliquots of reaction mixtures was immediately hybridized with PNA probe **9**. In the PNA-RNA substrate duplex the emissive base would be paired with the complementary base A and in the PNA-RNA product duplex the probe would be located opposite to an abasic site. Fluorescence spectra of aliquots revealed a time-dependent quenching in emission intensity as a result of generation of an abasic site by saporin, which enabled the detection as well as kinetic evaluation of the activity of saporin (Figure 5B). These results demonstrate that ^{BT}U, when placed opposite to a developing abasic site in RNA, could be used to detect and estimate the depurination activity of RIP toxins, irrespective of the protein's identity.[11]

Chapter 4: Lucifer chromophore-based fluorescent PNA probe for imaging poly(A) tail of mRNA

^{BT}U and ^{BF}U PNA analogues reported in the previous chapters, though very useful, have excitation maximum in the UV region, which would limit their application in cell-based analysis. In this chapter, design and synthesis of a set of emissive PNA analogues based on Lucifer[15] (^{Nap}U and ^{Amnap}U) and pyrene[16] (^{Py}U) chromophores, which have excitation and

emission maximum suitable for confocal microscopy, are described (Figure 6A). The fluorescence property of ^{Nap}U PNA analogue is highly sensitive to its microenvironment as compared to ^{Amnap}U and ^{Py}U PNA analogues (Figure 6B). Further, ^{Nap}U PNA analogue was incorporated into model PNA oligomers, where ^{Nap}U-modification was placed in-between different flanking bases (A, T, G and C residues) and subjected to fluorescence analysis. Among all model PNA designed, one of the emissive PNA oligomer (^{Nap}U-flanked in between T residues) was able to preferentially detect A-repeat in DNA ON with significant enhancement in fluorescence intensity (Figure 6C). Moreover, the excitation and emission profiles of ^{Nap}U analogue incorporated into PNA oligomer are compatible for cell imaging using fluorescence microscopy.

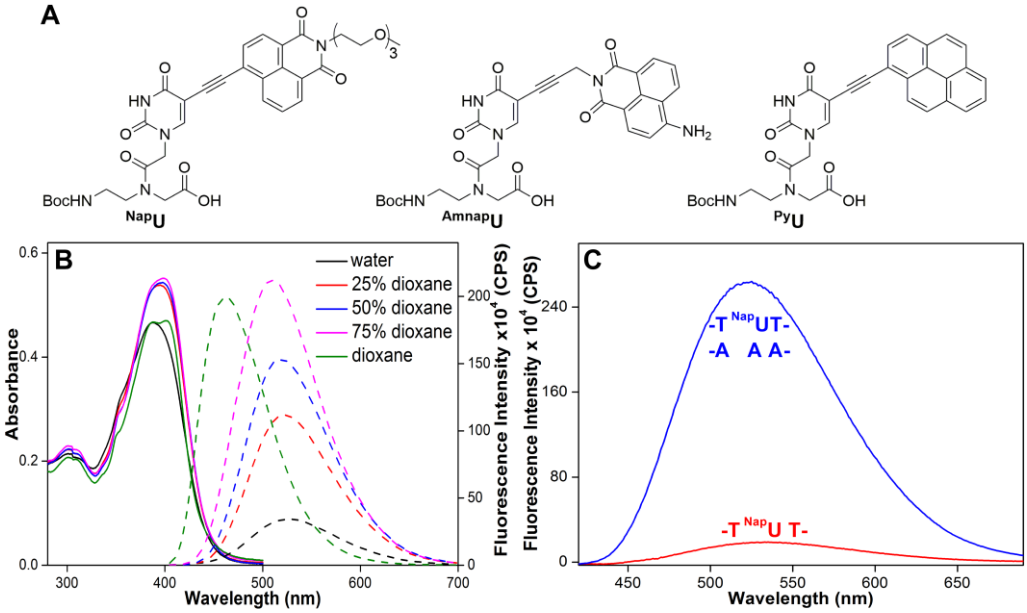

Figure 6. (**A**) Chemical structure of nucleobase-modified PNA analogues based on Lucifer (^{Nap}U and ^{Amnap}U) and pyrene (^{Py}U) fluorophores are shown. Absorption (solid line) and emission (dashed line) spectra of monomers in water, dioxane and its mixtures. (**B**) Absorption and emission spectra for ^{Nap}U. With change in solvent polarity, absorption spectrum is marginally affected, while emission spectrum is significantly affected. (**C**) Utility of ^{Nap}U to preferentially detect adenosine dA repeats (-AAA-) in DNA ON with significant enhancement in fluorescence is demonstrated.

Typically, A-repeats [poly(A) tail] are present at the 3′-UTR region of eukaryotic mRNA.[17] The poly(A) tail performs various functions such as it provides stability to mRNA in cytoplasm and assists in the translation process.[17] The ability of ^{Nap}U PNA analogue to report the presence of a triplet A encouraged us to design a hybridization assay for the detection of poly(A) mRNA in cell-free as well as cellular conditions. In this regard, fluorescent poly(T) PNA probe (TTTTT^{Nap}UTTTTTTKK) was synthesized, which was found

to photophysically distinguish between poly(A) DNA and poly(A) RNA. This property of the poly(T) PNA probe was utilized in imaging endogenous mRNA in fixed cells by confocal microscopy (Figure 7).

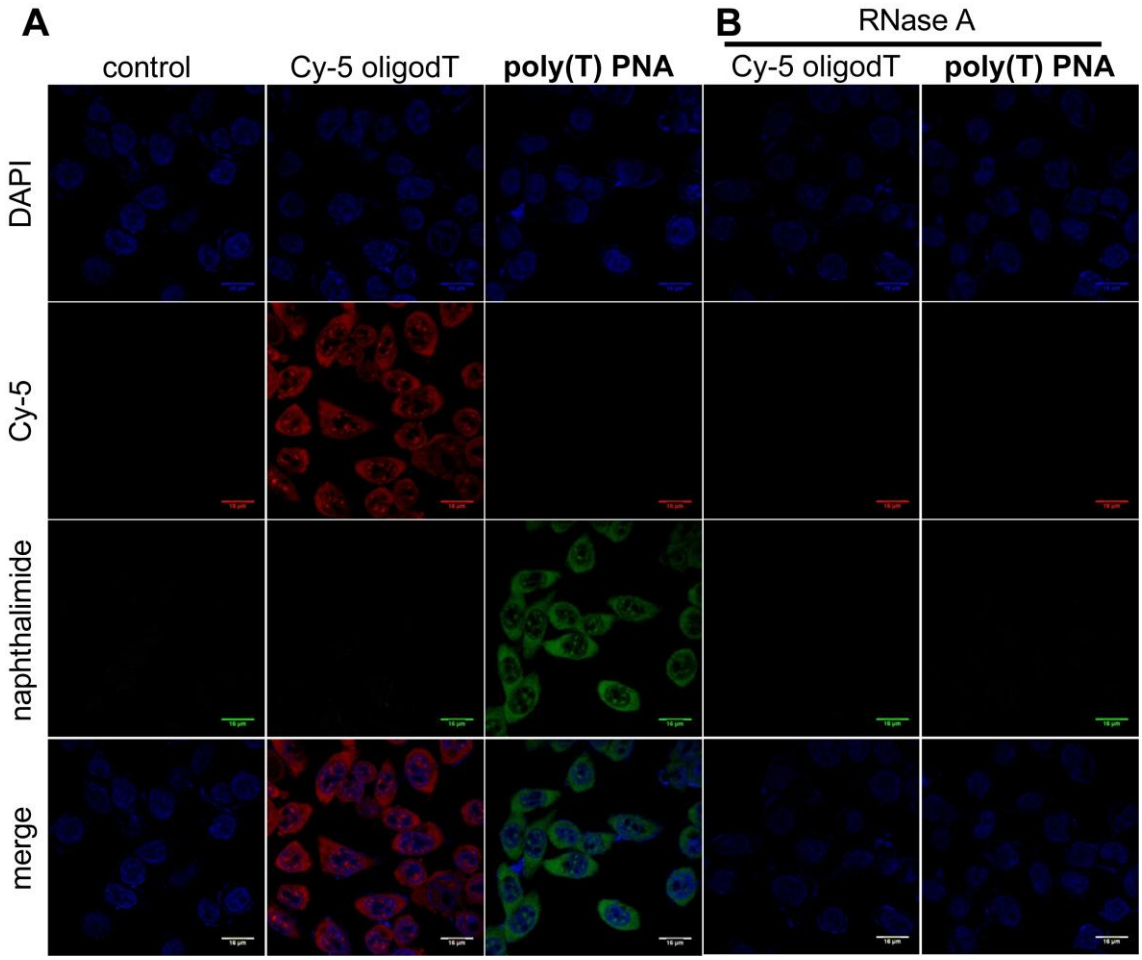

Figure 7. (**A**) Imaging cellular poly(A) mRNA using Cy-5 oligo-dT and poly(T) PNA probe. Cultured DLD1 cells were fixed, permeabilized and hybridized with Cy-5 oligo-dT (0.5 µM) and poly(T) PNA probe (1.0 µM) for 2.5 h at 37 °C. (**B**) Cells were treated with RNase A (single-stranded RNA cleaving enzyme) and hybridized with Cy-5 oligo-dT (1.0 µM) and poly(T) PNA probe (1.0 µM) under similar conditions.

As a control, poly(A) mRNA was imaged by incubating cells with a commercially available poly(A) mRNA probe, Cy-5 oligo-dT_{30}. Oligo-dT probe exhibited characteristic poly(A) mRNA distribution pattern (red colour in Cy-5 channel) in cytoplasm with punctated nuclear staining, which was consistent with literature reports (Figure 7A).[18] Similar staining pattern was observed with our fluorescent poly(T) PNA probe (green colour in naphthalimide channel, Figure 7A). The disappearance of poly(A) staining pattern after RNase A treatment (Figure 7B) and other control experiments using unmodified poly(T) PNA probe and random PNA oligomers confirmed the specific staining of the poly(A) mRNA in fixed cells by ^{Nap}U-

modified PNA probe. Interestingly, competition experiments with different ratios of Cy-5 oligo-dT_{30} and fluorescent poly(T) PNA probe indicated that PNA probe preferentially and strongly binds to poly(A) mRNA as compared to commercially available oligo-dT probe. Collectively, the ability of PNA to displace/invade nucleic acid structures and the results presented in this chapter underscore the potential of Lucifer-based PNA oligomers as efficient probes for detecting and imaging specific nucleic acid sequences in cells.

Chapter 5: Postsynthetic chemical labeling of PNA oligomers by using bioorthogonal chemical reactions

Given the importance of functionalized PNA probes in nucleic acid diagnosis and therapeutics, development of new methods to introduce complex functionalities that are not straightforwardly possible by solid-phase are highly desired. In this regard, the chemoselective reactions such as CuAAC, SPAAC, Staudinger ligation and palladium-catalyzed reactions have been useful in labeling nucleic acids.[19] We sought to explore the potential of these reactions in the context of ssPNA and PNA hybridized to biologically relevant nucleic acid motifs with the view of implementing these reactions in imaging and pulling down of specific nucleic acid sequences in cells.

In this chapter, we report the synthesis of alkyne (^{OD}U)-, azide (^{TGAz}U)- and iodo (^{I}U)-modified uracil PNA analogues (Figure 8A). These PNA analogues containing a small chemoselective reactive handle were incorporated into PNA oligomers by solid-phase method and subsequent chemical functionalization was achieved by performing CuAAC, SPAAC, Staudinger ligation and palladium-catalyzed reactions with respective reactive counterpart possessing a reporter or an affinity tag (e.g., fluorescent reporters, sugar, biotin tag, Figure 8B and 8C). The azide-alkyne and azide-phosphine click reactions worked very well in solution and the respective products could be isolated in respectable yields that would be sufficient enough for downstream biophysical analysis. Further, palladium-catalyzed Suzuki-Miyaura and Cu-free Sonogashira reactions of an ^{I}U-modified PNA oligomer with boronic acid (e.g., benzothiophene and CF_3 benzene boronic acids) and alkyne (naphthalimide and glucose alkyne) substrates gave the coupled products in low to moderate yields. Reaction with benzothiophene boronic acid and naphthalimide alkyne produced environment-sensitive fluorescent PNA probes and a reaction with CF_3 benzene boronic acid generated a 19F isotope-labeled PNA probe suitable for 19F NMR analysis. CuAAC, SPAAC and Staudinger ligation reactions have been further extended to label specific PNA-DNA heteroduplexes

(post-hybridization labeling) with fluorophores and an affinity tag. The reactions proceeded very well indicating that such post-hybridization chemical labeling techniques could be used for imaging specific nucleic acid sequences in the cells.

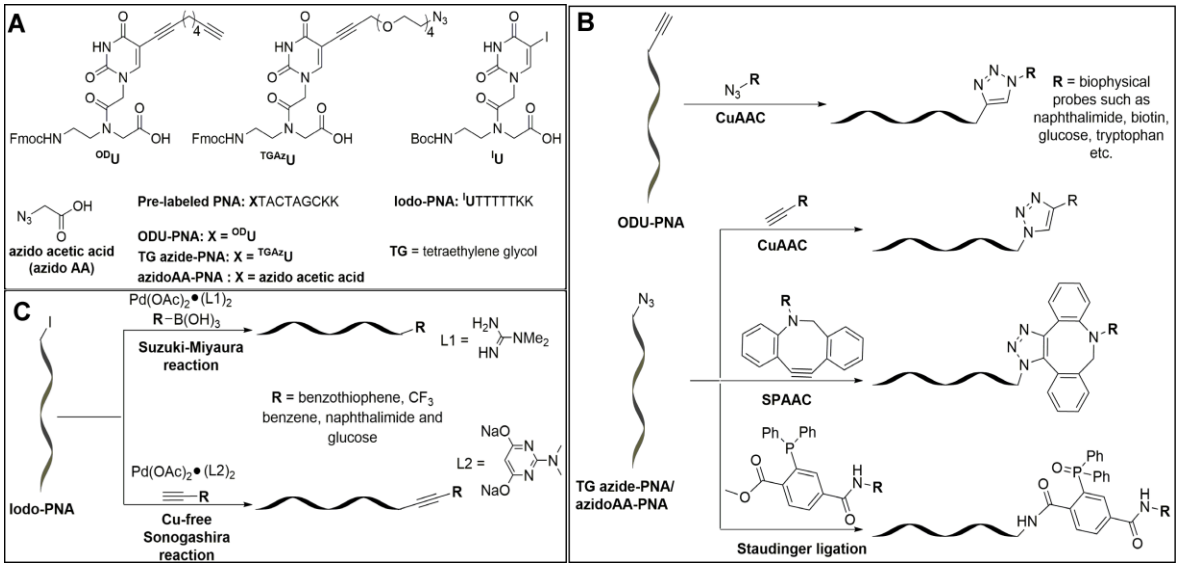

Figure 8. (**A**) Chemical structure of ^{OD}U, ^{TGAz}U and ^{I}U PNA analogues, and azido acetic acid are shown. Sequences of ODU-PNA, TG azide-PNA, azidoAA-PNA and iodo-PNA are also given. (**B**) Postsynthetic chemical functionalization of ODU- and TG azide- and azidoAA-PNA by CuAAC reaction. TG azide- and azidoAA-PNA by SPAAC and Staudinger ligation reactions. (**C**) Postsynthetic chemical functionalization of iodo-PNA by palladium-catalyzed reactions.

References:

1. a) I. Tinoco Jr and C. J. Bustamante, *Mol. Biol.*, 1999, **293**, 271–281; b) T. Hermann and D. J. Patel, *Structure*, 2000, **8**, 47–54; c) P. Murat and S. Balasubramanian, *Curr. Opin. Genet. Dev.*, 2014, **25**, 22–29.
2. F. Wachowius, C. Höbartner, *ChemBioChem*, 2010, **11**, 469–480.
3. U. Asseline, *Curr. Org. Chem.*, 2006, **10**, 491–518;
4. a) G. Bao, W. J. Rhee and A. Tsourkas, *Annu. Rev. Biomed. Eng.*, 2009, **11**, 25–47; b) J. Guo, J. Ju and N. J. Turro, *Anal. Bioanal. Chem.*, 2012, **402**, 3115–3125.
5. a) R. W. Sinkeldam, N. J. Greco and Y. Tor, *Chem. Rev.*, 2010, **110**, 2579–2619; b) S. G. Srivatsan and A. A. Sawant, *Pure Appl. Chem.*, 2011, **83**, 213–232.
6. a) R. W. Dirks and H. J. Tanke, *BioTechniques*, 2006, **40**, 489–496; b) S. Sixou, F. C. Szoka, Jr., G. A. Green, B. Giusti, G. Zon and D. J. Chin, *Nucleic Acids Res.*, 1994, **22**, 662–668.
7. P. E. Nielsen, M. Egholm, R. H. Berg and O. Buchardt, *Science*, 1991, **254**, 1497–1500.
8. a) B. P. Gangamani, V. A. Kumar and K. N. Ganesh, *Chem. Commun.*, 1997, 1913–1914; b) F. Wojciechowski and R. H. E. Hudson, *J. Am. Chem. Soc.*, 2008, **130**, 12574–12575; c) C. Boonlua, C. Vilaivan, H.-A. Wagenknecht and T. Vilaivan, *Chem.-Asian J.*, 2011, **6**, 3251–3259; d) S. Müllar, J. Strohmeier and U. Diederichsen, *Org. Lett.*, 2011, **14**, 1382–1385; e) A. H. St. Amant and R. H. E. Hudson, *Org. Biomol. Chem.*, 2012, **10**, 876–881.

9. a) M. G. Pawar and S. G. Srivatsan, *Org. Lett.*, 2011, **13**, 1114–1117; b) A. A. Tanpure and S. G. Srivatsan, *Chem. Eur. J.*, 2011, **17**, 12820–12827.
10. P. M. Sabale, A. Nuthanakanti and S. G. Srivatsan, *Ind. J. Chem. A*, 2013, **52**, 1004–1013.
11. P. M. Sabale and S. G. Srivatsan, *ChemBioChem*, 2016, **17**, 1665–1673.
12. P. M. Sabale, J. T. George and S. G. Srivatsan, *Nanoscale*, 2014, **6**, 10460–10469.
13. G. W. Collie and G. N. Parkinson, *Chem. Soc. Rev.*, 2011, **40**, 5867–5892.
14. a) Y. Endo, A. Glück and I. G. Wool, *J. Mol. Biol.*, 1991, **221**, 193–207; b) L. Barbieri, M. G. Battelli and F. Stirpe, *Biochim. Biophys. Acta.*, 1993, **1154**, 237–282.
15. a) W. W. Stewart, *Nature*, 1981, **292**, 17–21; b) R. M. Duke, E. B. Veale, F. M. Pfeffer, P. E. Kruger and T. Gunnlaugsson, *Chem. Soc. Rev.*, 2010, **39**, 3936–3953; c) A. A. Tanpure and S. G. Srivatsan, *ChemBioChem*, 2014, **15**, 1309–1316.
16. a) C. Wu, C. Wang, L. Yan and C. J. Yang, *J. Biomed. Nanotechnol.*, 2009, **5**, 495–504; b) M. E. Østergaard and P. J. Hrdlicka, *Chem. Soc., Rev.*, 2011, **40**, 5771–5788; c) J. N. Wilson, J. Gao and E. T. Kool, *Tetrahedron***,** 2007**, 63,** 3427–3433.
17. a) D. F. Colgan and J. L. Manley, *Genes & Dev.*, 1997, **11**, 2755–2766; b) A. O. Subtelny, S. W. Eichhorn, G. R. Chen, H. Sive and D. P. Bartel, *Nature*, 2014, **508**, 66–71; c) T. H. Beilharz, T. Preiss, *Methods*, 2009, **48**, 294–300.
18. a) D. O. Wang, H. Matsuno, S. Ikeda, A. Nakamura, H. Yanagisawa, Y. Hayashi and A. Okamoto, *RNA*, 2012, **18**, 166–175; b) R. S. McIsaac, S. J. Silverman, L. Parsons, P. Xu, R. Briehof, M. N. McClean, D. Botstein, *J. Vis. Exp.*, 2013, **76**, e50382; c) A. Gebhardt, M. Habjan, C. Benda, A. Meiler, D. A. Haas, M. Y. Hein, A. Mann, M. Mann, B. Habermann and A. Pichlmair, *Nat. Commun.*, 2015, **6**, 8192.
19. C. D. Spicer and B. G. Davis, *Nat. Commun.*, 2014, **5**, 4740.

List of Publications

1. **P. M. Sabale**, A. Nuthanakanti and S. G. Srivatsan, Synthesis and fluorescence properties of a full set of extended RNA base analogues. *Ind. J. Chem.*, 2013, **52A**, 1004–1013.
2. **P. M. Sabale**, J. T. George and S. G. Srivatsan, A base-modified PNA-graphene oxide platform as a turn-on fluorescence sensor for the detection of human telomeric repeats. *Nanoscale*, 2014, **6**, 10460–10469.
3. **P. M. Sabale** and S. G. Srivatsan, Responsive fluorescent PNA analogue as a tool for detecting G-quadruplex motifs of oncogenes and activity of toxic ribosome-inactivating proteins. *ChemBioChem*, 2016, **17**, 1665–1673.
4. **P. M. Sabale,** U. Ambi and S. G. Srivatsan, Lucifer chromophore-based fluorescent PNA probe for imaging poly(A) tail of mRNA (Manuscript under preparation).
5. **P. M. Sabale** and S. G. Srivatsan, Synthesis of telomere targeting PNA oligomer probes by using bio-orthogonal chemical reactions (Manuscript under preparation).

Chapter 1

Peptide nucleic acid as hybridization probes for targeting and detecting nucleic acids

1.1 Introduction

The fundamental functions such as storage and transfer of genetic information in living systems are performed by nucleic acids (DNA/RNA).[1] Apart from this, they participate in catalysing reactions (e.g., ribozymes)[2], regulating gene expression (e.g., RNA interference by miRNA and siRNA),[3] regulating the biosynthesis of certain metabolities (e.g., riboswitches)[4] and gene editing (e.g., CRISPR).[5] Nucleic acids perform the aforementioned functions by interacting with other biomolecules, and in doing so, they adopt complex secondary canonical and non-canonical structures (Figure 1).[6] The major driving forces like hydrogen bonding, π-stacking and metal ion interactions are responsible for the formation of different structural motifs. Therefore, to study the structure-function relationship, several biophysical and biochemical tools have been developed. Techniques namely fluorescence, nuclear magnetic resonance (NMR), electron paramagnetic resonance (EPR), X-ray crystallography and microscopy have been widely utilized.[7] Notably, nucleic acids have to be labeled with appropriate reporter molecule due to the lack of intrinsic reporter like functionality of natural nucleic acids. Among these, fluorescence is a widely used technique because it offers high sensitivity, rapid and real-time analysis.[8]

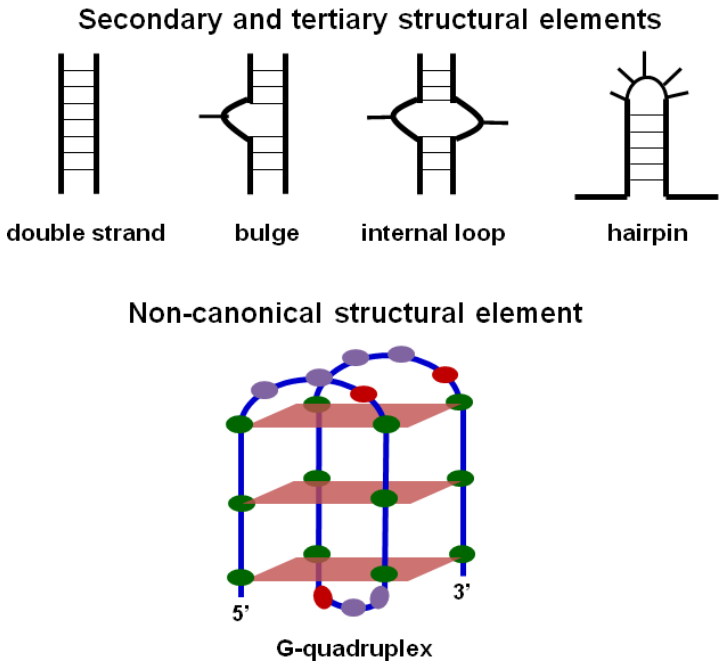

Figure 1. Various structural elements adopted by nucleic acids.

There are various methods available for understanding the structure and dynamics of nucleic acids in cell-free and cellular conditions.[9] Typically, cellular DNA and RNA oligonucleotides (ONs) have been visualized by covalent labeling such as incorporating modified nucleosides or by non-covalent labeling with small fluorescent dyes that are known

to bind to either DNA or RNA specifically (e.g., DAPI, Hoechst, SYTO etc.).[10] These methods provide overall imaging of cellular DNA and RNA inside cells. However, these methods cannot be used to detect specific sequences in the cell. In this regard, strategies based on the hybridization of complementary ON probes with nucleic acid targets have been widely employed for detection of specific nucleic acid sequences.[11] Currently, DNA microarrays, and *in situ* hybridization based on the molecular recognition of ON labeled with different biophysical tags have been applied in molecular diagnostics, and therapeutics.[7a] In particular, ON probes conjugated to fluorescent tags (e.g., fluorescein, rhodamine, Alexa and cyanine dyes) have been routinely used for developing hybridization assays.[7a]

Fluorescence *in situ* hybridization (FISH) using linear ON probes has provided valuable information about spatial and temporal distribution including the expression, localization, degradation, and storage of nucleic acid sequences in cellular milieu (Figure 2A).[12] Fluorescein-labeled DNA ONs were first explored for detection and tracking of endogenous poly(A) mRNA inside cells.[13] However, this linear ON FISH probe was unable to distinguish between unbound probe and probe hybridized to nucleic acid targets.[14] Moreover, these ON probes exhibit poor signal-to-noise ratio (background fluorescence problem), which precludes their utility for live cell imaging. These shortcomings were further overcome by using "turn on" probes such as molecular beacons[15] and FIT (forced intercalation) PNA probes, which upon hybridization to target nucleic acid display significant enhancement in fluorescence. Utility of FIT PNA probes are discussed in section 1.2.5.3. On the other hand, the molecular beacon consists of ON sequences with fluorophore-quencher pair at the end, which forms hairpin loop structure in the absence of target nucleic acids (Figure 2B). Molecular beacon exhibits reduced fluorescence in the absence of complementary target due to the proximity of quencher and fluorophore in hairpin loop structure. Upon hybridization with target nucleic acid the hairpin loop structure would open and separate the fluorophore and quencher, which results in the intense fluorescence signal.

In parallel, small molecules that emit very high fluorescence upon binding to specific RNA sequences have been recently used for aptamer based fluorescence detection of nucleic acids in living cells (Figure 2C).[16] In this approach, small molecule e.g., 3,5-difluoro-4-hydroxybenzylidene imidazolinone (DFHBI) upon binding to RNA aptamer (Spinach, Spinach2, Broccoli) result in enhanced green coloured fluorescence. In another strategy, fluorescent protein [green fluorescent protein (GFP)] fused to bacterial phage MS2 coat protein, which specifically binds to hairpin loop motif of target mRNA has been utilized for cell imaging (Figure 2D).[17] Although, all above methods have been regularly used for global

detection of specific nucleic acids inside cells, these methods lack the detection of conformational changes occurring at nucleotide level in a specific nucleic acid sequence.

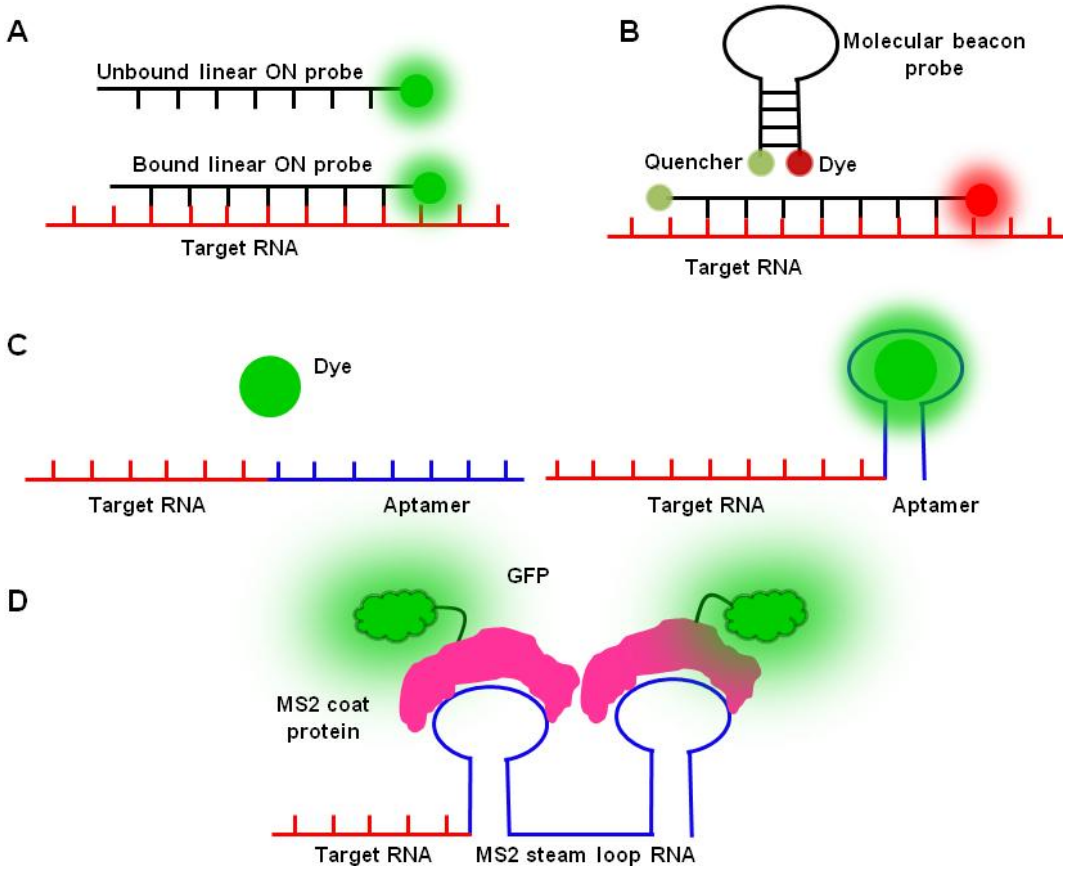

Figure 2. Different methods to visualize nucleic acid (particularly RNA) in fixed and live cells. (**A** and **B**) FISH using linear ON and molecular beacon probes. (**C** and **D**) Aptamer and vector based imaging of specific RNA molecules upon binding to fluorescent reporters.

ONs probes have also been shown to modulate gene expression of disease-causing protein upon sequences-specific binding to target nucleic acids.[18] Typically, there are two main strategies involved, i) targeting dsDNA using complementary ON probes, which is known to form triplex with dsDNA (*antigene therapy*), ii) targeting mRNA using complementary ON probes (*antisense therapy*) (Figure 3).[19] Small interfering RNA (siRNA) and micro RNA (miRNA) inhibits the gene expression of specific proteins by binding to complementary mRNA.[20] DNA ONs have also been shown to regulate gene expression upon hybridizing to complementary mRNA sequences, which were further used for therapeutic applications.[21] Despite these elegant strategies in regulating gene expression, natural ON probes have limitations such as poor hybridization efficiency and half-life in cellular conditions.[22]

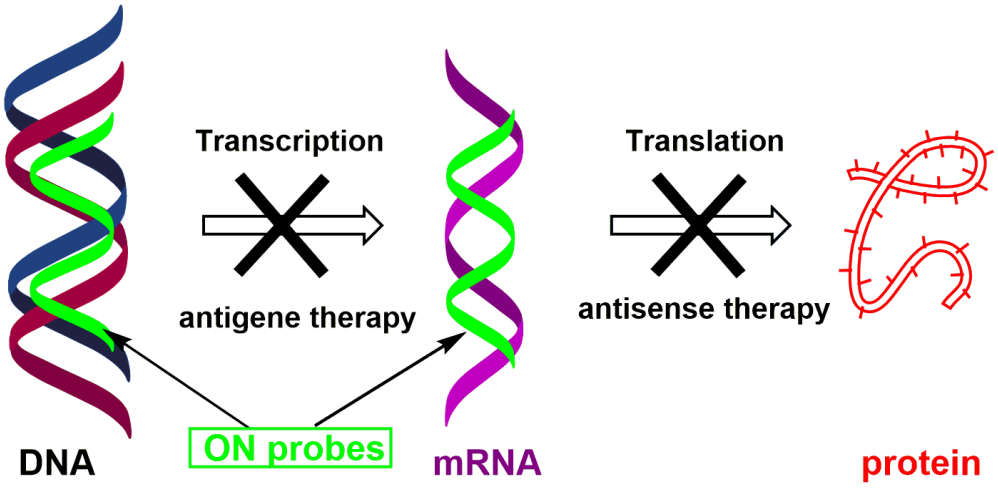

Figure 3. The design principle of antigene and antisense therapy using ON probes.

Owing to the practical limitations of natural DNA/RNA ON hybridization probes in detecting as well as targeting therapeutically relevant nucleic acid sequences, several synthetic nucleic acid mimics have been developed. In this chapter, an overview of the different synthetic nucleic acid mimics, particularly peptide nucleic acid (PNA) as hybridization probes in nucleic acid diagnostics has been discussed. Moreover, different synthetic strategies to synthesize labeled PNA oligomers and shortcomings in available fluorescent base-modified PNA analogues are described. Finally, the motivation behind the present research work of developing microenvironment-sensitive fluorescent PNA probes and labeling methodologies for nucleic acid detection is discussed.

1.2 Peptide nucleic acid (PNA) as hybridization probe

1.2.1 Background

To overcome the drawbacks of natural ONs, several synthetic nucleic acid analogues have been developed over the years by replacing the sugar-phosphate backbone or the phosphodiester linkage with charged or neutral backbone. synthetic analogues such as phosphorothioate (PS)[23] ON, locked nucleic acid (LNA)[24], morpholino[25] ON and peptide nucleic acid (PNA)[26] have been introduced by various research groups (Figure 4A). Most of the above analogues displayed superior properties such as strong binding affinity and/or higher stability in cell-free and cellular conditions as compared to natural ONs. Among all the modified ON designed, PNA is highly useful hybridization probe, because of its very strong binding to complementary ONs and is highly resistant to hydrolytic cleavage (nuclease or protease.[27] Unlike most of the above ON probes, PNA in PNA-DNA duplex consist of neutral peptide backbone, which eliminates the inter-strand electrostatic repulsion prevalent

in natural ON duplexes (Figure 4B). These useful features of PNA have been widely implemented in developing robust hybridization probes in nucleic acid diagnosis and biosensors applications.[27a,28]

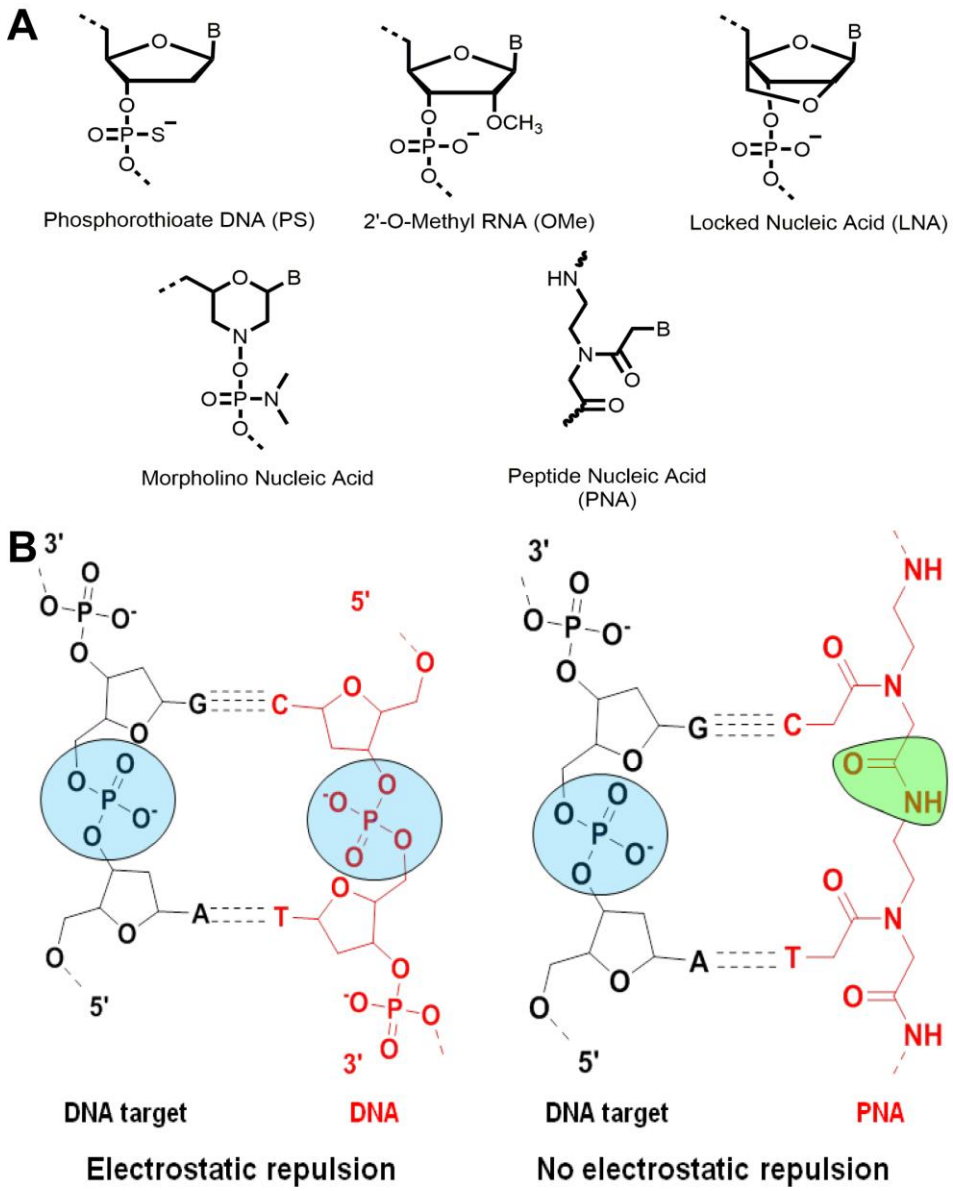

Figure 4. (**A**) The structures of few synthetic nucleic acid mimics. (**B**) Schematic illustration of strong binding hybridization probes for nucleic acid diagnostics as compared to ON probes.

1.2.2 Peptide nucleic acid (PNA) structure and properties

Nielsen and co-worker first introduced peptide nucleic acid (PNA) in 1991.[26] Since then, an enormous amount of studies explaining their synthesis, characterization, and applications have been published in several hundreds of research articles. In PNA, the sugar-phosphodiester backbone of nucleic acid is replaced by repeating units of an achiral pseudo-peptide backbone, *N*-(2-aminoethyl)glycine (*aeg*) with nitrogenous bases attached to the

backbone via methylene carbonyl spacer (Figure 5).[29] By convention, the PNA sequences are always written from the N- to the C-terminus. Neutral PNA backbone exhibits no electrostatic repulsion when PNAs hybridized to complementary ONs. Hence, it shows a very high binding affinity for complementary DNA and RNA ONs as compared to natural DNA or RNA ONs.[30] Greater stability results in improved thermal melting temperature (T_m) for PNA-ON duplexes as compared to corresponding DNA-DNA or DNA-RNA duplexes. Additionally, the binding affinity of PNA oligomers is independent of ionic strength due to its neutral *aeg*-backbone, which shows that T_m values of PNA-DNA duplex are less affected by low ionic strength.[31] This property can be further explored for targeting secondary structural motifs adopted by DNA or RNA ONs, which are destabilized by low ionic strength. PNA is neither a nucleic acid nor a peptide and which essentially provides resistance to hydrolysis by nucleases and protease.[32] Moreover, PNA oligomers are not recognized by polymerases, and hence cannot be used as primers for polymerase reactions. Besides, the neutral backbone of PNAs is responsible for its poor solubility and self-aggregation in an aqueous medium. [32,33]

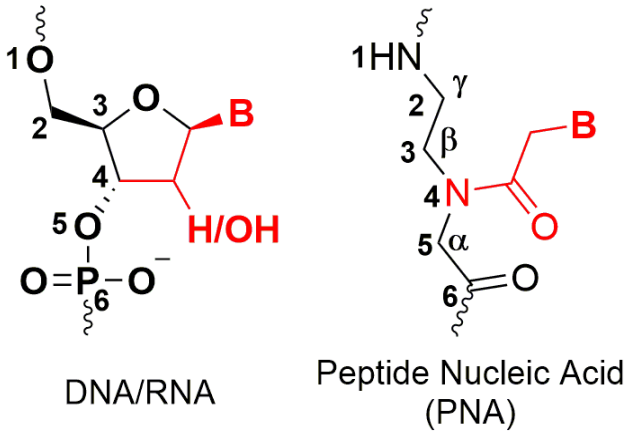

Figure 5. Chemical structure of DNA/RNA and PNA.

Although, PNA structurally deviates from DNA/RNA ONs due to the absence of the sugar phosphate backbone, it possesses useful properties as compared to DNA/RNA ONs.[34] In DNA/RNA duplexes two strands are always oriented in the antiparallel direction (with the 5'-end of one strand opposite to the 3'-end of the other), while in PNA-DNA or PNA-RNA duplexes two strands can be oriented in parallel or antiparallel orientation (Figure 6). However, the antiparallel orientation is strongly preferred in PNA-DNA and PNA-RNA duplexes.[35] PNA double helix is formed by hydrogen bonding as well as π-stacking between nucleobases with a smaller twist and larger π-overlap between the neighboring bases. PNAs

are known to form B- and A-type structures when associated with DNA and RNA, respectively.[35] Techniques such as NMR, and X-ray crystallography have been implemented to solve the three-dimensional structure of PNA-DNA[36], PNA-RNA[37] duplexes and $(PNA)_2$-DNA[38] triplex. From these techniques, it was concluded that PNA-RNA and PNA-DNA duplexes form distinct helical structures termed as 'P-form' helix.[34]

A mismatch in PNA-DNA or PNA-RNA duplex is significantly destabilized than a mismatch in corresponding DNA-DNA or DNA-RNA or RNA-RNA duplex.[39] This single base discrimination ability of PNA probes could offer high specificity and thus allows the further development of several PNA-based strategies for molecular diagnostics. Although PNA was initially designed as potential drug candidates for antisense and antigene therapy, today there are various applications of these molecules in molecular biology and biotechnology, drug discovery, diagnostics and biosensors, and material chemistry.

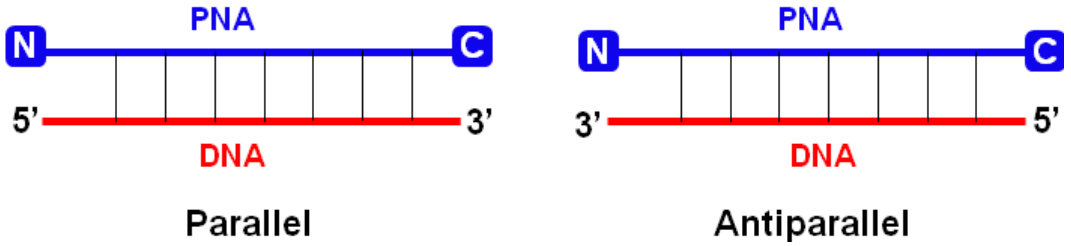

Figure 6. Parallel and antiparallel modes of PNA-DNA duplex.

1.2.3 Triplex formation and strand-invasion by PNA

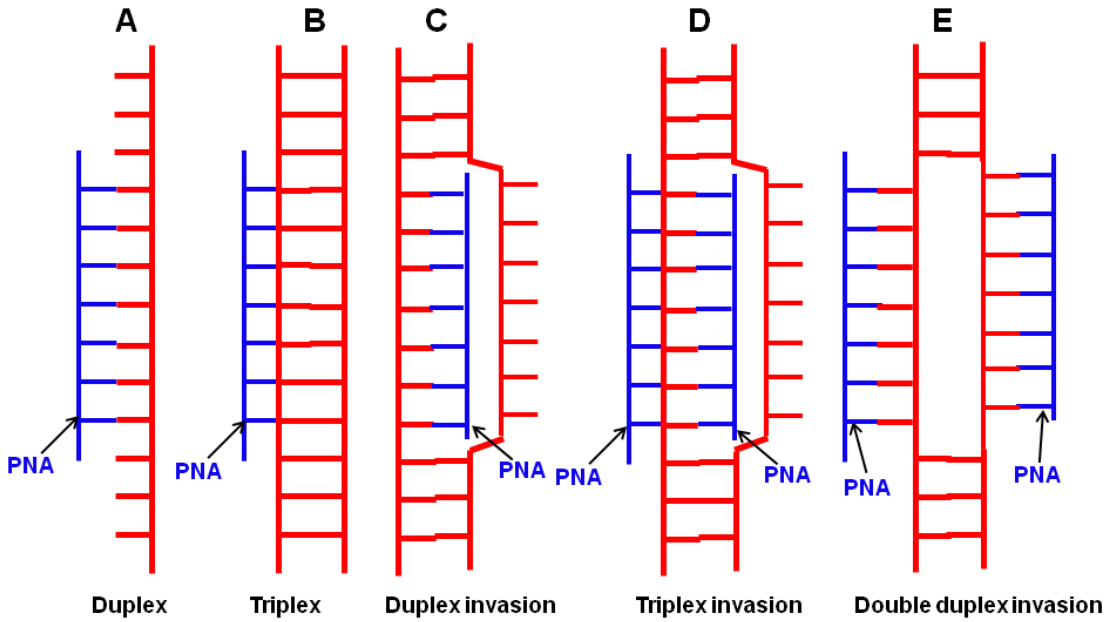

Figure 7. Schematic illustration of the modes by which PNA binds to single-strand and double-strand DNA targets. PNA oligomers and DNA are shown in green and red, respectively.

Apart from PNA-DNA heteroduplex (Figure 7A), PNA is also known to form stable triplexes upon binding to double-stranded DNA, for example, cytosine-rich PNAs and guanine/cytosine-rich DNA duplexes produce PNA-$(DNA)_2$ triplexes by Hoogsteen base-pairing (Figure 7B).[40a,40b] Formation of extremely stable PNA-DNA duplex using duplex invasion by purine-rich PNA oligomers is also reported (Figure 7C).[40d] Further, homopyrimidine-rich PNAs and homopurine DNA strand from DNA-DNA duplex forms $(PNA)_2$-DNA triplexes through triplex invasion by Watson-Crick and Hoogsteen base-pairing (Figure 7D).[40c] Finally, double duplex invasion complex is reported using pseudo complementary PNA with diaminopurine-thiouracil base pair, that destabilizes PNA-PNA duplex by steric interaction (Figure 7E).[40e]

1.2.4 Drawbacks of original *aeg*-PNA

Original *aeg*-PNA oligomer exhibits certain limitations such as low aqueous solubility, poor cellular permeability, ambiguity in DNA binding orientation (antiparallel or parallel) and self-aggregations.[29,34] Several design strategies have been adopted to improve the binding affinity, aqueous solubility and specificity of PNA by modifying the backbone or the nucleobase.

1.2.5 Chemical modifications of PNA

Various backbone- and nucleobase-modified PNA analogues have been introduced to overcome above mentioned shortcomings of PNA by different research groups. Few of the modified-PNA analogues are discussed below.

1.2.5.1 Backbone modifications

PNA backbone can be modified in the ethylene diamine side or glycine part or methylene carbonyl linker or a combination of above.[29] The design principle behind the backbone modifications are i) attachment of cationic groups in the backbone or at the N- or C-terminus to improve solubility and cellular permeability, ii) replacement of acyclic backbone with conformationally constrained cyclic backbone to improve the selective binding affinity for either DNA or RNA ONs, iii) introduction of chirality in achiral PNA to improve binding orientation to complementary DNA/RNA (Figure 8).[29]

The initial modification was carried out in *aeg*-PNA analogue **1**[26] by extending methylene group to either at ethylene diamine or glycine side or methylene carbonyl linker between nucleobase and backbone (Figure 8). PNA analogues, *N*-(2-aminoethyl)-β-alanine

2[41] and *N*-(3-aminopropyl)glycine **3**[42] backbone and ethylene carbonyl linked nucleobase **4**[42] obtained by above design resulted in large destabilization of PNA-DNA duplexes as compared to *aeg*-PNA-DNA duplex. To improve the binding affinity and solubility, the amide linkage of *aeg*-PNA was substituted with tertiary amine, which is positively charged at neutral pH. The cationic PNA analogue **5**[43] with flexible linkage synthesized by above strategy was highly soluble in aqueous medium but with reduced thermal stability (T_m) towards complementary DNA ONs. This observation underscores the importance of amide bond in constrained flexibility of PNA backbone. The tertiary amide bond in *aeg*-PNA is responsible for *cis* and *trans* rotamers, which interferes in the orientation during hybridization process. To overcome this difficulty, olefinic polyamide nucleic acid analogues **6**[44] and **7**[44] were introduced by replacing the amide linkage with olefinic C=C double bond E and Z, respectively.

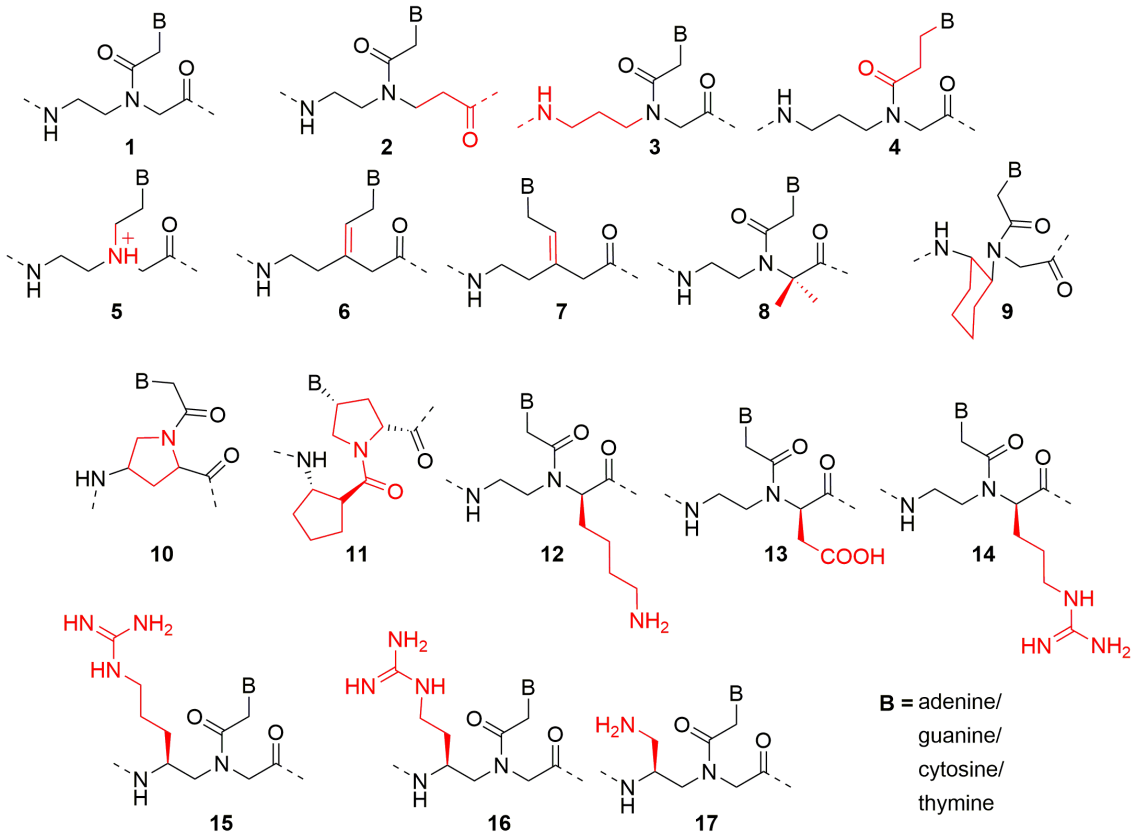

Figure 8. Structures of representative backbone-modified PNA analogues.

Further, the appropriate constrained flexibility in PNA backbone to improve its binding affinity towards complementary DNA ON has been evaluated. For this purposes, PNA backbone was modified by either substituting alkyl groups (in the ethylene diamine or glycine side) or by cyclization of backbone (in aminoethyl or glycine side). Series of PNA

analogues were reported by substituting alkyl groups at α-or γ-position in PNA backbone. For example, Ganesh *et al*. have recently reported the synthesis of sterically constrained PNA analogue **8**[45] with *gem*-dimethyl substituent at α-position in glycine side (Figure 8). This analogue exhibited superior binding affinity for DNA as compared to RNA ON. Further, the cyclization of PNA backbone in aminoethyl or glycine side has been systematically carried out to generate PNAs with better selectivity and binding orientation for the DNA or RNA ONs. They have also introduced a chiral cyclohexyl-derived backbone, which resulted in a conformationally constrained *cis*-cyclohexyl PNA analogue **9**[46]. This analogue showed an unprecedented binding affinity for RNA as compared to DNA ON. Further, conformational flexibility was achieved by proline-based PNA, where the tertiary amide linker was replaced with a pyrrolidine ring. Several proline-based PNA analogues have been reported so far.[47] Among them, 4-aminoprolyl PNA analogue **10**[48] exhibited a higher binding to complementary DNA ON, while most of the remaining analogues resulted in reduction in the hybridization efficiency for complementary ONs as compared to original *aeg*-PNA. Vilavian *et al*. have reported a pyrrolidinyl PNA **11**[49] consisting of D-prolyl-2-aminocyclopentanecarboxylic acid (ACPC) backbone with considerably better specificity towards DNA ONs than original *aeg*-PNA.

Further, to introduce the chirality, various amino acid residues with desired stereochemistry have been attached at α-or γ-position in PNA backbone by Nielsen *et al*.[50] PNA analogue **12**[50] derived by positively charged D-lysine at α-position in glycine side was able to stabilize PNA-DNA duplexes as compared to unmodified PNA-DNA duplex due to the electrostatic attraction with negatively charged phosphate backbone of DNA (Figure 8). Besides, lysine-modified PNA monomer showed significantly better solubility in aqueous conditions.[50] However, analogues derived from negatively charged amino acids (e.g., **13**[50]) significantly destabilized the PNA-DNA duplex due to electrostatic repulsion. Recently, Heemstra and co-workers have evaluated the detailed effect of ionic strength on duplex stability of PNA oligomers containing negatively or positively charged side chains.[51] These studies showed that the electrostatic interactions do play a role in PNA binding; at medium to high salt concentrations negatively charged PNA binds more strongly to DNA and RNA than positively charged PNA oligomers. PNA analogues with hydrophobic amino acid also showed a reduced binding affinity towards complementary DNA ON. When thermal stability of PNA analogues derived from L and D amino acids were compared, PNA monomers containing D-amino acids exhibited a stronger binding affinity for complementary antiparallel

DNA strands than L-monomers. In general, backbone modification has often resulted in the destabilization of PNA-RNA duplexes as compared to PNA-DNA duplexes.

To overcome the problem of poor cell permeability and aqueous solubility of original *aeg*-PNA, Ly *et al*. have replaced the glycine part with D-arginine to obtain chiral PNA analogue **14**[52]. Despite the positively charged guanidinium group, the thermal melting analysis suggested that a single modification in decamer PNA sequence destabilized the PNA-DNA duplex by 2–4 °C. However, multiple modifications incorporated at the alternate position in PNA sequence, stabilized the PNA-DNA duplex.[53] Next, cell permeability studies were performed in human HCT116 (colon), Sao2 (Osteosarcoma) and HeLa cell lines, and it was found that these cationic PNAs permeabilized through the cell membrane and accumulated specifically in the nucleus.[52] Further, they synthesized second generation guanidino PNA **15**[54] by incorporating guanidinium group at the γ-position in the backbone. The thermal melting and cell permeability studies confirmed that PNA sequences containing analogue **15** were bound tightly to complementary DNA ON and was taken up easily into HeLa cells compared to the original *aeg*-PNA. Ganesh *et al*. have also reported cationic γ-PNA analogues **16**[55] and **17**[56] by incorporating guanidinium and amino group at γ-position in the backbone, respectively. Moreover, better binding affinity and cell permeability of PNA sequences containing above analogues were further confirmed by thermal melting and cell penetration studies in HeLa cell lines. In general, except for a few backbone modifications, most of the attempts have resulted in PNA oligomers with lower affinity for complementary ONs as compared to the original *aeg*-PNA.

1.2.5.2 Nucleobase modifications

Unnatural and modified bases have been substituted in place of canonical nucleobases to enhance the binding of PNA oligomers to complementary nucleic acids (Figure 9).[29] The nucleobase-modified PNAs reported so far are limited in number as compared to backbone-modified PNAs discussed earlier. 2,6-Diaminopurine analogue **18**[57] binds to thymine in complementary ONs with significantly stronger affinity (Figure 9). Further, 2,6-diaminopurine **18**–thiouracil **19** pair[58] has been effectively utilized as a sterically compromised base pair in designing PNA oligomers for double duplex-invasion of DNA or RNA (Figure 9). Cytosine has also been replaced with pseudoisocytosine **20**[59] to obtain highly stable triplex-forming PNA analogue at physiological pH (Figure 9). 2-Aminopurine PNA analogue **21**[60] was introduced for reverse Watson-Crick base-pairing with uracil and thymine, which was inherently fluorescent and was utilized for studying the hybridization of

PNA to complementary ONs by fluorescence spectroscopy (Figure 9). 6-Thioguanine **22**[61] incorporated into PNA displayed a characteristic shift in absorption maximum upon hybridization to complementary ON, however it reduced the thermal stability of PNA-DNA heteroduplex. A number of bi- and tricyclic cytosine and thymine analogues (e.g., **23**[62]) have also been introduced into PNA oligomers. These modifications have resulted in better stabilization of the PNA-DNA duplexes by enhanced base paring and stacking interactions (Figure 9). An attempt has also been made to synthesize PNA analogue **24**[63] by completely replacing nucleobase with potential anti-tumor agent-naphthalimide for intercalation studies, but it resulted in destabilization of PNA-DNA heteroduplex.

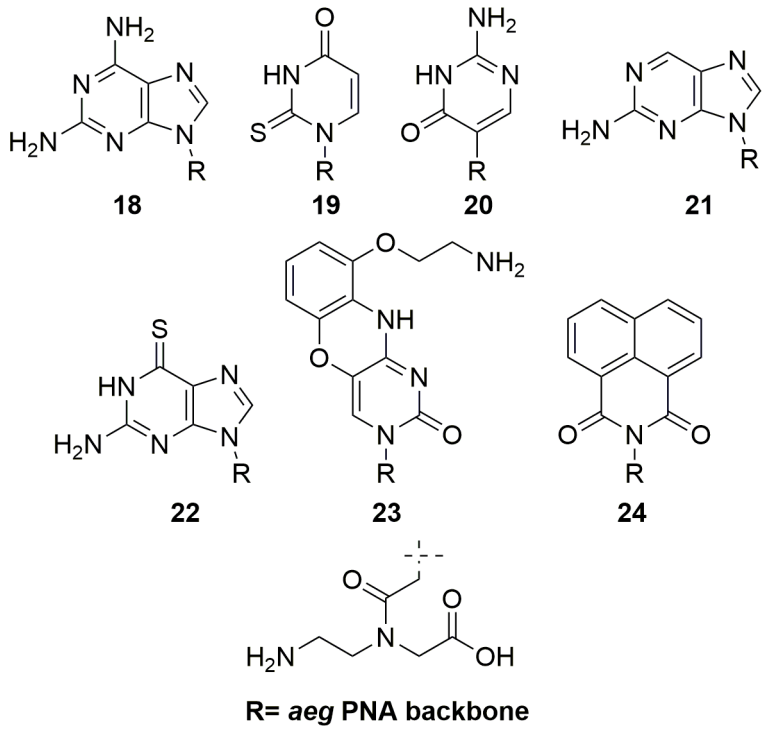

Figure 9. Structures of base-modified PNA analogues.

1.2.5.3 Fluorescent nucleobase-modified PNA analogues

Nucleobases in *aeg*-PNA have been further modified with a known fluorophores or heterocyclic rings to impart the useful fluorescence properties, which are essential for the diagnosis and imaging applications, as natural nucleobases are practically non-emissive. Fluorescent nucleobase-modified PNA analogues can be utilized to detect the conformational changes occurring at the nucleotide level. In this regards, very few microenvironment sensitive emissive PNA analogues are reported so far, and those are discussed below.

2-Aminopurine PNA analogue **22**[59] has been incorporated into a PNA oligomer and was hybridized to a complementary DNA ON by Ganesh *et al*. (Figure 9). Binding affinity

and kinetics of hybridization process of fluorescent PNA-DNA hetroduplex were studied by thermal melting analysis and fluorescence decay kinetics, respectively. Further, emissive 8-vinylguanine PNA analogue **25**[64] was synthesized and incorporated into PNA oligomers by Diederichsen *et al.* (Figure 10). The emissive PNA oligomers containing **25** have been developed for distinguishing the quadruplex formation in RNA ON from single-strand PNA by the change in fluorescence intensity. Both of the analogues, 2-aminopurine **22** and 8-vinylguanine **25** were found to be minimally perturbing when hybridized to complementary ONs. However, they exhibited excitation and emission maxima in the UV-region, which limits their practical utility in a cell-based analysis.

Phenylpyrrolocytosine PNA analogue **26**[65] reported by Hudson *et al.* displayed emission maximum in the visible region with the quantum yield of 0.32 in buffer solution (Figure 10). The analogue exhibited good microenvironment sensitivity and was able to report the hybridization process to complementary DNA ON with higher binding affinity for guanine base. However, the hybridization with complementary DNA displayed a quenching in fluorescence intensity as compared to single-strand phenylpyrrolocytosine PNA oligomer. Further, phenylpyrrolocytosine PNA containing nine D-lysine residues has been shown to internalized into cytoplasm, when incubated into GM04281 (fibroblast) cell lines for one or nine days by Corey *et al.*[66] In another example, pyrene-labeled uracil pyrrolidinyl PNA analogue **27**[67] has been incorporated into PNA oligomers and was used as a base-discriminating fluorescent base by Vilaivan and co-workers (Figure 10).

Seitz *et al*. have reported fluorogenic PNA-based FIT (forced intercalation) probes (**28, 29** and **30**)[68] by completely replacing nucleobase with hybridization responsive cyanine fluorophores, e.g., thiozole orange (TO), oxazole yellow (OY) and pyridinium-linked dye (BO) etc. (Figure 10). The fluorescence of single-stranded FIT-PNA probes was completely quenched, while it was significantly increased upon hybridization to complementary DNA/RNA ONs. This was possible due to the restricted intramolecular rotation caused by intercalation of cyanine fluorophores (TO or OY) in PNA-DNA/RNA heteroduplex. These FIT-PNA probes have been efficiently utilized for the detection and imaging of cellular nucleic acid targets such as viral mRNA, K-ras mRNA and miRNA-122 within living cells.[68–70] Further, PNA FIT-probes have been explored for single-nucleotide-specific genotyping by quantitative PCR (qPCR).[71] Recently, Nishizawa *et al*. investigated the utility of triplex forming PNA oligomer containing TO-base surrogate for fluorescence sensing of dsRNA sequences.[72] The PNA probe exhibited remarkable light-up response of the TO unit upon PNA-dsRNA triplex formation through Hoogsteen base pairing at acidic pH. Although

these PNA FIT-probes lack a hydrogen bonding face, they have been elegantly explored for the detection of mismatched base as well as single nucleotide polymorphism (SNP) in nucleic acid sequences.[68]

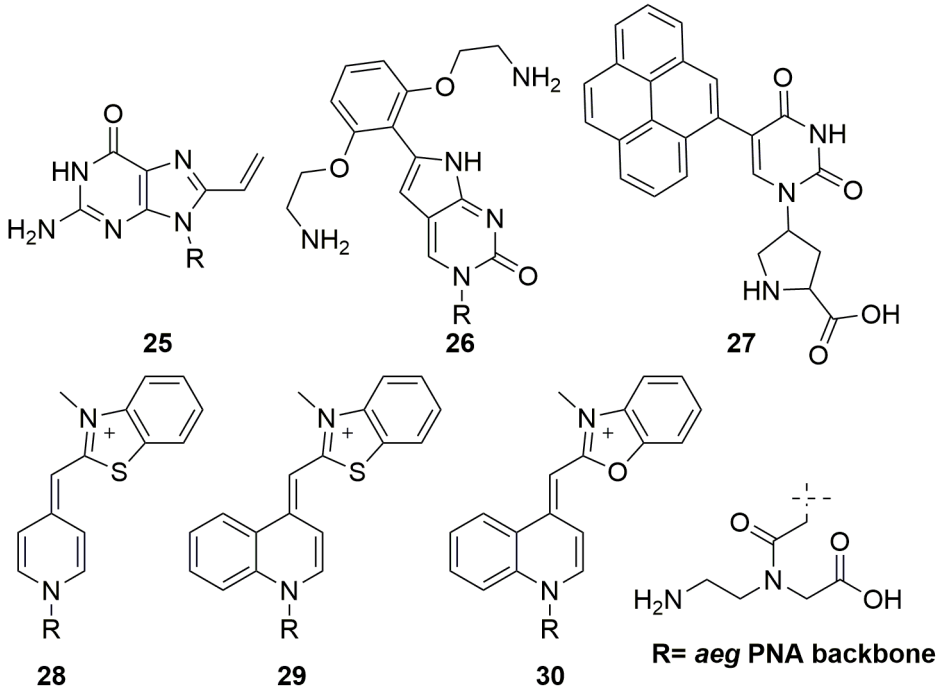

Figure 10. Structures of fluorescent base-modified PNA analogues.

1.2.6 Application of PNA oligomers

This section describes various applications of unmodified and modified *aeg*-PNA oligomers in gene therapy and as molecular biology probe, PCR clamping tool, and nucleic acid diagnostic tool.

1.2.6.1 PNA as antisense and antigene agents

The PNA was initially developed for sequence specific binding to the complementary dsDNA or ssmRNA and thereby regulating gene expression of disease-causing proteins.[26] Moreover, the inability of RNaseH to recognize PNA-RNA duplex has been aptly exploited in regulating protein expression levels by targeting mRNAs.[73] However, the failure of RNaseH in recognizing PNA-RNA duplex requires the PNA in stoichiometric amount for antisense application, which could be one of the limitation of PNA as antisense drug. In this regards, PNA possesses useful properties such as strong binding, strand invasion ability, and higher biological stability required for gene therapy. Although, extensively utilized in cell-free systems, low strand invasion kinetics, and poor solubility and cell permeability due to the neutral and hydrophobic nature of PNAs have hampered its effective use in cell-based

studies. Several transfection protocols for PNA have been established till now, which include microinjection, electroporation, co-transfection with DNA, and conjugation to lipophilic moieties, cell-penetrating peptides, nanoparticales, etc.[74] Enormous amount of studies have been devoted on targeting particular genes using complementary PNA oligomers *in vitro* as well as *in vivo*.

Gait *et al*. have used electroporation of a PNA oligomer as well as PNA containing four additional lysine residues (positively charged amino acid residues) at the terminus to explicitly block miR-122 activity in human and rat liver cells.[75] Further, the splicing correction of mRNA using PNA oligomers conjugated with peptides has been demonstrated in a mouse model of Duchenne muscular dystrophy by Wood and co-workers.[76] Corey *et al*. reported the inhibition of human telomerase activity by PNA targeting to RNA component of human telomerase (hTR).[77] These results suggested that PNA inhibits the activity of human telomerase by 10- to 50-fold more efficiently than phosphorothioate (PS) ONs with IC_{50} values within picomolar to nanomolar range. Fabbri and co-workers have reported that PNA conjugated to octaarginine is easily taken up by the human leukemic K562 cells, thereby inhibiting the activity of target microRNA-210.[78] The detailed study on the principles of using different cell penetrating peptide-PNA conjugates for cellular delivery of antisense oligomers have been reported by Nielsen and Shiraishi.[79] In another example, limited cellular uptake and low bioavailability has been overcome by conjugating PNA oligomers with cholesterol and cholic acid derivatives.[80] These PNA oligomers exhibited antisense activity in cultured HeLa pLuc705 cells. Pandey, Patino and co-workers demonstrated that cyclic PNAs conjugated to cell penetrating vector (triphenylphosphonium cation) via a disulfide linkage inhibited the activity of HIV replication by targeting the HIV-1 TAR RNA loop.[81]

1.2.6.2 PNA as PCR clamp

The strong binding affinity and specificity of PNA towards complementary ON and inability of DNA polymerases to process PNA-DNA duplex has been utilized in PCR clamping.[82] PNA-mediated PCR clamping has been introduced by Stanley and Nielsen *et al*. for selective amplification of ribosomal DNAs (rDNAs), which are not abundant in clone libraries generated by standard PCR.[83] This technique enabled the differentiatation of two sequences, which differed by only one base pair. PNA-clamp method has also been introduced for detection of mutations caused in epidermal growth factor receptor (EGFR) gene, which are associated with resistant to Gefitinib therapy in lung cancer.[84] This method has been

subsequently used for single nucleotide polymorphism (SNP) specific genotyping of the gene of interest (mutant screening). For example, globin reduction PNA targeting to human blood gamma globin RNA was able to suppress the amplification of the globin RNA during cDNA synthesis.[84] In another example, PNA complementary to chloroplast and mitochondrial 16S sequences has been explored as a PCR blocker for studying genetic material recovered directly from environmental samples (metagenomics).[85]

1.2.6.3 PNA as biosensor and microarrays

PNA can be used on microarrays and other biosensors, where its specific hybridization to complementary DNA or RNA was detected by various biophysical tools such as surface plasmon resonance (SPR), time-of-flight secondary ion mass spectrometry (TOF-SIMS), electrochemical detection, or direct electronic detection and fluorescence-based techniques.[86]

Appella *et al*. have demonstrated the colorimetric sandwich-hybridization assay for detection of anthrax DNA using PNA oligomers.[87] In this strategy, one of the PNA (capture probe) was immobilized on the surface, and then complementary DNA was incubated followed by another PNA (detection probe). This assay has been conveniently carried out in 96-well plate format. The biotin labeled PNA with commercially available avidin-horseradish peroxidase conjugate (HRP-avidin) and tetramethylbenzidine (TMB) has been used to generate a signal in the presence of target DNA. Further, PNA in combination with gold and silver nanoparticles (AuNPs and AgNPs) has been explored in colorimetric detection of nucleic acids by Su and Kanjanawarut.[88] This method utilizes the interesting property of nanoparticles by controlling the particle aggregation and dispersion in the presence of PNA and PNA-DNA complexes. This assay has enabled the detection of a specific DNA sequence with single-base-mismatch resolution by color change. Park *et al*. have reported an electrochemical method to identify mutations in human gene by using PNA-modified electrode and a single-stranded DNA specific endonuclease.[89] Recently, Kelley and co-workers have reported immobilization of PNA on nanostructured microelectrodes (Au electrodeposited with a fine layer of Pd) for electrochemical assay.[90] This assay helped in the detection of circulating tumor DNA collected from lung cancer and melanoma patients with great sensitivity and specificity.

In another example, Fernandez *et al.* has introduced the proline-based oligo-T PNA probe attached to magnetic beads for sequence-specific purification of mRNA.[91] Poly(A) tail in mRNA was recognized by oligo-T PNA upon incubation with a pool of nucleic acids and was specifically separated from genomic DNA and rRNA by applying a magnetic field.

Schultz, Harris and co-workers have demonstrated a simple methodology to identify and monitor the activity of enzymes using PNA-encoded small molecule microarrays.[92] In this method, small molecules and fluorescent tag (fluorescein) were conjugated to PNA and then incubated with cell lysates. Subsequently, PNAs that did not interact with proteins were removed by size exclusion filtration, and remaining mixture was subjected to a microarray with complementary ON. Fluorescence signal obtained from various positions on chip gave the amount of protein present in cell lysates. Recently, label-free detection of DNA targets by a combination of cationic-conjugated polymers (CCP) and PNA probe containing FRET pair has been demonstrated by Liu and Bazan.[93] In this method, fluorescent PNA probe was allowed to hybridize with target nucleic acids followed by incubation with fluorescent CCP. CCP in association with negatively charged DNA target by electrostatic attraction and which is also in proximity to the hybridized PNA probe to DNA target. Then selective excitation of the CCP resulted in very efficient FRET to fluorescent PNA probe. Recently, Kumar and co-workers have combined the properties of graphene oxide (GO) and PNA to develop fluorescence hybridization assay for the detection of specific DNA sequences.[94]

1.2.6.4 PNA as hybridization probes

Notably, over the last few years much of the interest has been focused on the use of PNA oligomers as hybridization probes in nucleic acid diagnostics. The tighter binding affinity, and strand invasion ability of PNA oligomers even at low ionic strength suggested that PNA can be more useful for hybridization applications, such as sequence-specific capture of single-stranded and double-strand nucleic acids, as compared to that of natural or synthetic ON probes.[27a] Several biophysical techniques have been utilized for studying nucleic acids by using PNA as hybridization probes for various applications like detection, imaging, pull down assay etc.

Traditionally, nucleic acids are analyzed by standard hybridization techniques, such as Southern and Northern blotting.[27a] In this regards, PNA pre-gel hybridization process have been developed as an alternative to Southern/Northern analysis, where labeled PNA oligomers were subjected to hybridization with denatured dsDNA/RNA sample at low ionic strength prior to loading on the gel and resolved. The PNA-DNA hybrids were then blotted onto a nylon membrane and detected using standard chemiluminescent techniques up to single mismatch in DNA sample by Egholm and co-workers.[95] Alternatively, affinity electrophoresis (gel-based method) has been introduced for detection of nucleic acids, where the mobility of DNA bound to PNA probes slowed down as compared to unbound DNA in

the gel matrix. Nordén *et al.* have studied the kinetics of PNA-DNA and PNA-RNA hybridization in real time by using biomolecular interaction analysis (BIAcore) technique.[39b]

PNA is especially good for *in situ* hybridization (ISH) because it can bind to DNA or RNA quickly even under low salt or other unfavorable conditions for ON probes.[96] Additionally, PNA exhibits low background signals, mild washing protocol and high stability of PNA probe in biological fluid. Also, PNA oligomers are compatible with variety of reporter molecules such as digoxigenin (DIG), biotin, and fluorescent tags like fluorescein, rhodamine, cyanine, Alexa etc. In this direction, variety of labeled PNA probes has been commercialized and being used for detection and imaging of target nucleic acids in cellular conditions.

Biotin-labeled PNA probes have been used for the detection of human parvovirus B19 nucleic acids in clinical specimen by Gallinel and co-workers.[97] This PNA-based *in situ* hybridization assay has been more practical and faster to perform as compared to standardized DNA-based ISH assay. These results suggested that the PNA-ISH was highly specific and sensitive as compared to a PCR assay. In another example, Burton *et al.* have developed a DIG-labeled PNA probe for the detection of *lactobacilli* PCR amplicons samples using denaturing gradient gel electrophoresis (DGGE) blots.[98] The *lactobacillus*-specific PNA probe was able to distinguish DNA fragments from *lactobacilli* from other bacterial species, including those that migrated to a similar position. DIG-labeled PNA probes in combination with digoxigenin antibodies could be further explored for the detection of nucleic acid sequences by *in situ* hybridization assay similar to DIG-labeled DNA probes, but with better selectivity and sensitivity.[97]

Fluorescence *in situ* hybridization (FISH) assay is one of most widely used techniques in molecular biology. The PNA-FISH assay has been first introduced by Lansdorp *et al.* for the quantitative detection of human telomeric DNA repeats using fluorescein labeled PNA probe and was able to estimate the telomere length as compared to other DNA/RNA probes.[99] Further, multicolor FISH with fluorescent PNA probes have been carried for detecting and enumerating specific chromosomes in interphase and metaphase cells.[100] Cy-5 labeled PNA probe has been explored for studying the dynamic behavior of telomeric DNA in living human osteosarcoma U2OS cells by Dirks and co-workers.[101] Telomeric PNA probes have also been utilized in several FISH assay of cancer and ageing related diseases. In another example, fluorescently-labeled PNA probes targeting species-specific rRNA sequences have been utilized for identification of gram-negative and gram-positive bacteria using FISH assay by Perry-O'Keefe *et al.*[102] The specificity and sensitivity of fluorescently-labeled PNA

probes were evaluated using 28 representative species and were in good agreement with available rDNA sequence information.

Recently, FISH assay has been performed for sensing miRNA, which regulates diverse gene expression at the post-transcriptional level using fluorescent PNA probe and nano graphene oxide (NGO) complex by Min and co-workers.[103] Fluorescence of PNA probe in PNA-NGO complex was initially quenched by π-stacking with GO surface. Upon incubation of PNA-NGO complex into cancer cells with specific miRNA over-expressed were able to detect in live cells with much lower background signals.

1.3 Methods to synthesize modified PNA probes

1.3.1 Solid-phase peptide synthesis (SPPS)

Unmodified and modified PNA oligomers are synthesized by a well-established solid-phase peptide synthesis (SPPS) protocol using *t*-butoxycarbonyl (Boc) or fluorenylmethyloxycarbonyl (Fmoc) chemistry (Figure 11).[34] For SPPS, amino group of *aeg*-backbone is commonly protected by either Boc or Fmoc group depending upon the chemistry, while carboxyl group is free for coupling with amino counterpart. The exocyclic amino groups present in purines (A and G) and pyrimidines (C) for Boc-and Fmoc- PNA monomers are protected with Cbz-and Bhoc-group, respectively.

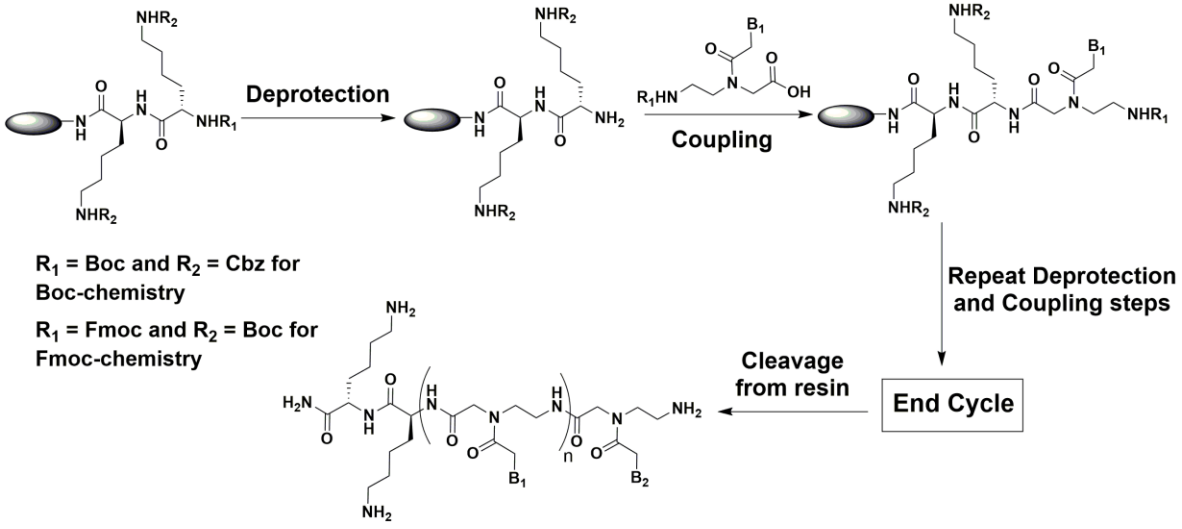

Figure 11. A schematic diagram for the synthesis of PNA oligomers by solid-phase peptide synthesis (SPPS) using Boc-and Fmoc-chemistry.[34]

First, the PNA oligomer T_{10} was synthesized using Boc-chemistry by Nielsen and co-workers.[26] This strategy involves strong acidic condition (50% TFA in dichloromethane) for deprotection of Boc-group during SPPS cycle followed by coupling with appropriate Boc-

PNA monomer in presence of coupling reagents HOBt, HBTU and DIPEA in dry DMF (Figure 11). Further, PNA oligomer is cleaved from the solid support using strongly acidic conditions such as TFMSA in TFA or HF in anisole. The MBHA resin is used as solid support for Boc-chemistry. While, currently Fmoc-chemistry is being majorly used for synthesis of PNA oligomers due to its milder reaction protocols. Fmoc-group is deprotected during SPPS cycle using 20% piperidine in DMF, followed by coupling with Fmoc-PNA monomers in presence of coupling reagents HOBt, HBTU and DIPEA in dry DMF. Then desired length of PNA oligomer is isolated after cleavage using TFA. Finally, crude PNA oligomers isolated after cleavage and further purified by RP-HPLC and characterized by mass spectrometry. Therefore, labeled PNA probes for various applications can be synthesized by SPPS or SPPS followed by chemical ligation such as acid-amine coupling or thiol-maleimide reaction.

1.3.2 Postsynthetic chemical modifications

Despite the success of SPPS in generating labeled PNA oligomers, several modified PNA analogues exhibits poor stability under the stringent solid-phase synthesis condition or show poor coupling efficiency. Therefore, there is a significant demand for the development of chemical functionalization methods that would allow easy access to a variety of labeled PNA oligomers. In this regards, bulky reporter molecules can be conjugated to PNA oligomers after SPPS by chemical ligation such as acid-amine coupling or thiol-maleimide reaction.[104] Unfortunately, poor stability of the activated esters and less chemoselectivity due to intrinsic amine and alcohol groups in biomolecules has restricted their utility. Moreover, these chemoselective reactions exhibit certain drawbacks such as pH sensitivity of acid-amine coupling and oxidation of thiols.[105]

Alternatively, postsynthetic functionalizations of biomolecules including proteins, glycans and nucleic acids have been achevied using chemoselective reactions, such as copper (I)-catalyzed azide-alkyne cycloaddition (CuAAC), strain-promoted azide-alkyne cycloaddition (SPAAC), azide-phosphine Staudinger ligation, inverse electron demand Diels-Alder reactions (IEDDA), and palladium-catalyzed reactions with various biophysical tags.[106,107] Therefore, this chemoseletive reactions could be further extended for labeling of PNA with a variety of reporters. In this approach, PNA monomer containing a small reactive group has to be incorporated into oligomers using SPPS followed by a chemoselective reaction with a suitable reactive counterpart containing a desired biophysical probe (Figure 12). In context to PNA, postsynthetic chemical modification such as CuAAC has been

carried out on solid support as well as in solutions to label PNA oligomers with fluorescent tags, peptide, ligand molecules.[108–111]

Kumar *et al.* have introduced a CuAAC reaction for synthesis of PNA-peptide conjugates in *tert*-butyl alcohol-water mixture for better cell permeability in antisense therapy.[108] In another example, CuAAC reaction has been carried out on PNA oligomer with solid support (resin) for synthesis of fluorescent and ligand labeled PNA probes by Hudson and co-workers.[109] Recently, Manicardi *et al.* have reported the synthesis of furan-PNA oligomer using CuAAC reaction in solution for covalent targeting of single stranded DNA through a crosslinking strategy.[110] In one of the example, SPAAC reaction has also been utilized for the synthesis of Cy-5 labled γ-PNA oligomers in acidic buffer (pH 4), which was subsequently used for designing 3D DNA nanocage strcutures by Fromme and co-workers.[111] However, postsynthetic chemical methodologies with milder reaction conditions are not very well explored for labeling of PNA oligomers with diverse biophysical reporters including fluorophores, affinity tags etc.

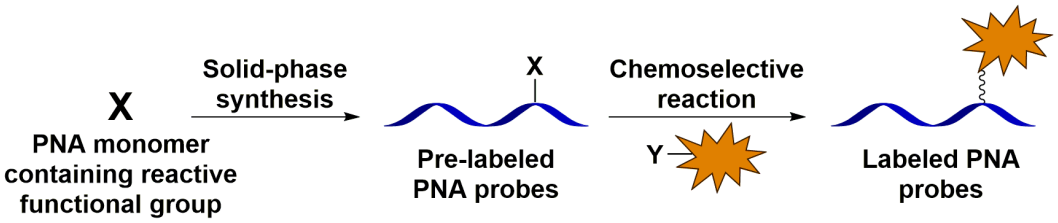

Figure 12. Design of postsynthetic chemical functionalization on PNA oligomers with different biophysical probes.

1.4 Statement of research problem

In recent years, PNA has been mainly used as a hybridization probe in nucleic acid diagnosis and biosensor applications. In general, hybridization assays use PNA probes conjugated to bulky fluorophores through linker, which can be used for detection of nucleic acids globally.[11,12b] However, various conformational changes occurring at the nucleotide level are difficult to analyze by the above PNA probes. In this regards, very few minimally perturbing microenvironment-sensitive nucleobase-modified PNA analogues have been incorporated into PNA and used in studying nucleic acids by a hybridization process. However, the minimally perturbing analogues have excitation and emission maximum in the UV region and or exhibit decrease in fluorescence intensity upon hybridization to complementary ONs. In this regard, development of minimally perturbing PNA base analogues, which (i) display emission in the visible region, (ii) retain reasonable fluorescence efficiency upon incorporation into PNA oligomers, and importantly (iii) are responsive to changes in

surrounding environment are highly desired. Such a PNA base analogue incorporated into a PNA oligomer and hybridized to a complementary target nucleic acid sequence would not only enable the detection but also could be used to modulate the function of the target nucleic acid.

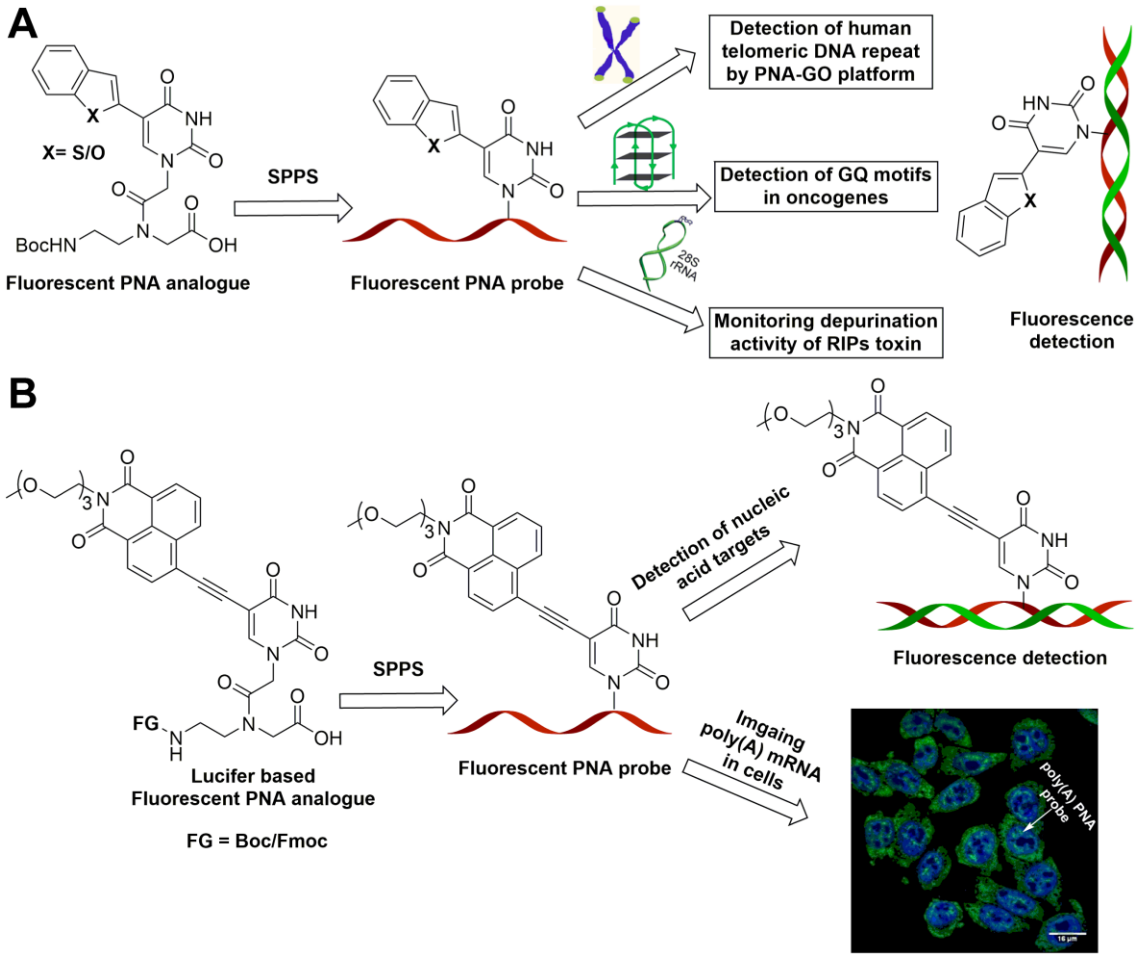

Figure 13. (**A**) Design of fluorescent 5-heterobicycle-conjugated uracil PNA oligomers as hybridization probes for fluorescence detection of nucleic acids. (**B**) Design of highly emissive nucleobase-modified PNA analogues based on Lucifer chromophore chromospheres for the detection and imaging of poly(A) mRNA in cell-free and cellular conditions.

This thesis describes the design, synthesis and applications of a novel series of emissive PNA analogues derived by conjugating heterobicycles (benzofuran and benzothiophene) at the 5-position of uracil base (Figure 13A). The PNA base analogues show emission in the visible region and exhibit excellent solvatochromism. The analogues incorporated into model PNA oligomers are structurally minimally invasive and interestingly, their fluorescence properties are highly sensitive to changes in neighbouring base environment. Depending on the photophysical behaviour, the benzofuran- and benzothiophene-modified PNA oligomers were used in the establishing assay to detect non-canonical G-quadruplex structures of telomeric DNA repeat and oncogenic DNA promoters,

and in the monitoring the depurination activity of ribosome inactivating protein (RIP) toxins. Further, the development of PNA uracil base analogues based on the Lucifer chromophore as tools for imaging ploy(A) mRNA sequences in cells have been described (Figure 13B).

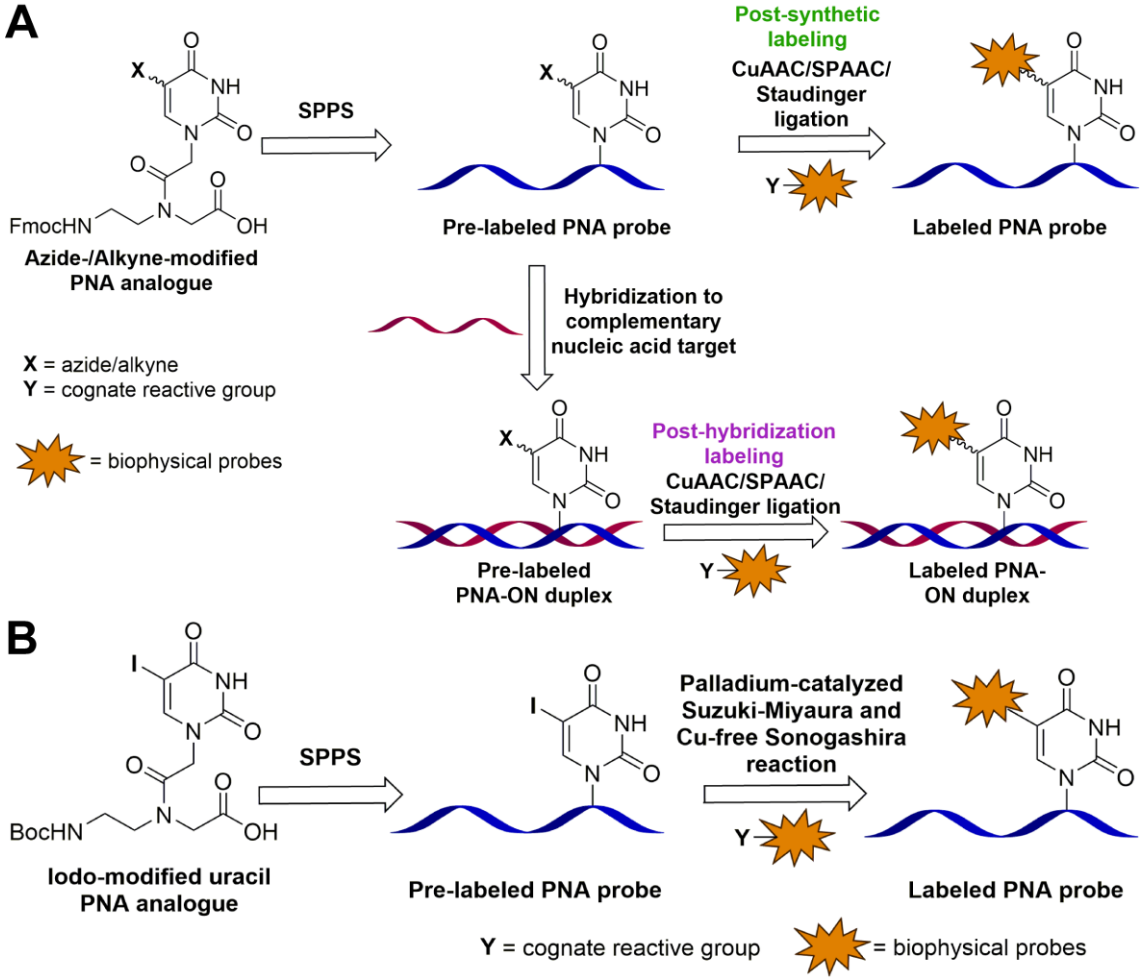

Figure 14. Design and incorporation of azide-, alkyne-, and iodo-modified uracil PNA analogues into PNA oligomers by SPPS followed by labeling with biophysical probes. (**A**) Postsynthetic labeling of single-stranded alkyne- and azide-modified PNA oligomers, and post-hybridization labeling of alkyne- and azide-modified PNA-ON duplex with CuAAC, SPAAC and Staudinger ligation reactions. (**B**) Postsynthetic labeling of single-stranded iodo-modified PNA oligomers by using palladium-catalyzed reactions.

Although development of robust fluorescence-based PNA probes is challenging, development of efficient methods to incorporate such reporters into PNA oligomers is equally important. In this context, development of postsynthetic chemical methodologies for labeling PNA oligomers with variety of biophysical reporters by using CuAAC, SPAAC, Staudinger ligation and palladium-catalyzed reactions is described in the final chapter (Figure 14). CuAAC, SPAAC and Staudinger ligation have been further extended to label specific PNA-DNA heteroduplexes (post-hybridization labeling) with fluorophores and a biotin affinity tag (Figure 14A). Such post-hybridization labeling techniques could be used for multiplexed

imaging of specific nucleic acid sequences in the cells. Taken together, the development and applications of the biophysical tools as well as the labeling methodologies described in this thesis will definitely expand the scope of PNA as a useful tool in diagnostic and therapeutic applications.

1.5 References

1. P. Ahlquist, *Science*, 2002, **296**, 1270–1273.
2. S. Altman, M. Baer, C. Guerrier-Takada and A. Vioque, *Trends Biochem. Sci*., 1986, **11**, 515–518.
3. L. Timmons, H. Tabara, C. C. Mello and A. Z. Fire, *Mol. Biol. Cell*, 2003, **14**, 2972–2983.
4. A. Nahvi, N. Sudarsan, M. S. Ebert, X. Zou, K. L. Brown and R. R. Breaker, *Chem. Biol.*, 2002, **9**, 1043–1049.
5. R. Mout, M. Ray, Y.-W. Lee, F. Scaletti and V. M. Rotello, *Bioconjugate Chem.*, 2017, **28**, 880−884.
6. a) I. Tinoco Jr and C. J. Bustamante, *Mol. Biol.*, 1999, **293**, 271–281; b) T. Hermann and D. J. Patel, *Structure*, 2000, **8**, 47–54; c) P. Murat and S. Balasubramanian, *Curr. Opin. Genet. Dev.*, 2014, **25**, 22–29.
7. a) U. Asseline, *Curr. Org. Chem.*, 2006, **10**, 491–518; b) N. Piton, Y. Mu, G. Stock, T. F. Prisner, O. Schiemann and J. W. Engels, *Nucl. Acids Res.*, 2007, **35**, 3128–3143; c) P. Z. Qin, K. Hideg, J. Feigon and W. L. Hubbell, *Biochemistry*, 2003, **42**, 6772–6783; d) V. Olieric, U. Rieder, K. Lang, A. Serganov, C. Schulze-Briese, R. Micura, P. Dumas and E. Ennifar, *RNA*, 2009, **15**, 707–715.
8. a) N. G. Walter, *Curr. Protoc. Nucl. Acid Chem.*, 2003, Unit 11.10; b) R. Zhao and D. Rueda, *Methods*, 2009, **49**, 112–117; c) L. Zhao and T. Xia, *Methods*, 2009, **49**, 128–135.
9. a) A. S. Boutorine, D. S. Novopashina, O. A. Krasheninina, K. Nozeret and A. G. Venyaminova, *Molecules*, 2013, **18**, 15357–15397; b) J. M. Holstein and A. Rentmeister, *Methods*, 2016, **98**, 18–25; c) J. T. George and S. G. Srivatsan, *Methods*, 2017, **doi.**org/10.1016/j.ymeth.2017.02.004.
10. a) Q. Li, Y. Kim, J. Namm, A. Kulkarni, G. R. Rosania, Y.-H. Ahn and Y.-T. Chang, *Chem. Biol.*, 2006, **13**, 615–623; b) R. M. Martin, H. Leonhardt and M. C. Cardoso, *Cytometry Part A*, 2005, **67A**, 45–52; c) J. Kapuscinski, *Biotech. Histochem.*, 1995, **70**, 220–233.
11. J. Guo, J. Ju and N. J. Turro, *Anal. Bioanal. Chem.*, 2012, **402**, 3115–3125.
12. a) S. Paillasson, M. Van De Corput, R. W. Dirks, H. J. Tanke, M. Robert-Nicoud, X. Ronot, *Exp. Cell Res.*, 1997, **231**, 226–233; b) R. W. Dirks and H. J. Tanke, *BioTechniques*, 2006, **40**, 489–496.
13. J. C. Politz, K. L. Taneja and R. H. Singer, *Nucleic Acids Res.*, 1995, **23**, 4946–4953.
14. G. Bao, W. J. Rhee and A. Tsourkas, *Annu. Rev. Biomed. Eng.*, 2009, **11**, 25–47.
15. D. P. Bratu, B. J. Cha, M. M. Mhlanga, F. R. Kramer and S. Tyagi, *Proc. Natl. Acad. Sci. U. S. A.*, 2003, **100**, 13308–13313.
16. a) J. S. Paige, K. Y. Wu and S. R. Jaffrey, *Science*, 2011, **333**, 642–646; b) R. L. Strack, M. D. Disney and S. R. Jaffrey, *Nat. Methods*, 2013, **10**, 1219–1224; c) G. S. Filonov, J. D. Moon, N. Svensen and S. R. Jaffrey, *J. Am. Chem. Soc.*, 2014, **136**, 16299–16308.
17. a) E. Bertrand, P. Chartrand, M. Schaefer, S. M. Shenoy, R. H. Singer and R. M. Long, *Mol. Cell*, 1998, **2**, 437–445; b) M. Valencia-Burton, R. M. McCullough, C. R. Cantor and N. E. Broude, *Nat. Methods*, 2007, **4**, 421–427; c) H. Y. Park, H. Lim, Y. J. Yoon,

A. Follenzi, C. Nwokafor, M. Lopez-Jones, X. Meng and R. H. Singer, *Science*, 2014, **343**, 422–424.
18. C. Frank Bennett and E. E. Swayze, *Annu. Rev. Pharmacol. Toxicol.*, 2010, **50**, 259–293.
19. a) J.-J.Toule, Antisense oligonucleotides and antisense RNA: *Novel Pharmacological and Therapeutic Agents.* (Weiss, B., ed), CRC press, 1997, 1–16; b) R. W. Wagner, *Nat. Med.*, 1995, **1**, 1116–1118; c) V. N. Soyfer and V. N. Potamann, *Triple Helical Nucleic Acids*, 1996, Springer-Verlag, NY; d) P. P. Chan and P. M. Glazer, *J. Mol. Med.*, 1997, **75** , 267–282.
20. B. J. Dolnick, *Pharmacol. Ther.*, 1997, **75**, 179–184.
21. a) M. L. Stephenson and P. C. Zamecnik, *Proc. Natl. Acad. Sci. U. S. A.*, 1978, **75**, 285–288; b) J. G. Izant and H. Weintraub, *Cell*, 1984, **36**, 1007–1015.
22. S. Sixou, F. C. Szoka, Jr., G. A. Green, B. Giusti, G. Zon and D. J. Chin, *Nucleic Acids Res.*, 1994, **22**, 662–668.
23. C. A. Stein and J. S. Cohen, Phoshorothioate oligodeoxynucleotide analogues. In Cohen J. S. (ed.): Oligodeoxynucleotides-Antisense Inhibitors of Gene Expression. London: Macmillan Press, 1989, p. 97.
24. H. Orum and J. Wengel, *Curr. Opinion Mol. Ther.*, 2001, **3**, 239–243.
25. J. Summerton, *Biochim. Biophys. Acta.*, 1999, **1489**, 141–158.
26. P. E. Nielsen, M. Egholm, R. H. Berg and O. Buchardt, *Science*, 1991, **254**, 1497–1500.
27. a) F. Pellestor and P. Paulasova, *Eur. J. Hum. Genet.*, 2004, **12**, 694–700; b) Luca Mologni & Carlo Gambacorti-Passerini, *Letters in Peptide Science*, 2004, **10**, 297–308.
28. a) M. Pooga, T. Land, T. Bartfai and Ü. Langel, *Biomolecular Engineering*, 2001, **17**, 183–192; b) J. Wang, *Current Issues Molec. Biol.*, 1999, **1**, 117–122.
29. K. N. Ganesh and P. E. Nielsen, *Curr. Org. Chem.*, 2000, **4**, 931–943.
30. M. Egholm, O. Buchardt, L. Christensen, C. Behrens, S. M. Freier, D. A. Driver, R. H. Berg, S. K. Kim, B. Norden and P. E. Nielsen, *Nature*, 1993, **365**, 566–568.
31. S. Tomac, M. Sarkar, T. Ratilainen, P. Wittung, P. E. Nielsen, Bengt Nordén, and A. Gräslund, *J. Am. Chem. Soc.*, 1996, **118**, 5544–5552.
32. B. Hyrup and P. E. Nielsen, *Bioorg. Med. Chem.*, 1996, **4**, 5–23.
33. P. E. Nielsen, *Pure Appl. Chem.*, 1998, **70**, 105–110.
34. P. E. Nielsen, *et.al*, *Peptide nucleic acids: protocols and applications* (Second Edition). Horizon Bioscience, Wymondham, 2004.
35. E. Uhlmann, D. W. Will, G. Breipohl, D. Langner and A. Ryte, *Angew. Chem. Int. Ed.*, 1996, **35**, 2632–2635.
36. a) M. Leijon, A. Graeslund, P. E. Nielsen, O. Buchardt, B. Norden, S. M. Kristensen and M. Eriksson, *Biochemistry*, 1994, **22**, 9820–9825; b) M. Eriksson and P. E. Nielsen, *Nat. Struct. Biol.*, 1996, **3**, 410–413.
37. S. C. Brown, S. A. Thomson, J. M. Veal and D. G. Davis, *Science*, 1994, **265**, 777–780.
38. L. Bets, J. A. Josey, J. M. Veal and S. R. Jordan, *Science*, 1995, **270**, 1838–1841.
39. a) M. Egholm, O. Buchardt, L. Christensen, C. Behrens, S. M. Freier, D. A. Driver, R. H. Berg, S. K. Kim, B. Nordén and P. E. Nielsen, *Nature*, 1993, **365**, 566–568; b) K. K. Jensen, H. Ørum, P. E. Nielsen, and B. Nordén, *Biochemistry*, 1997, **36**, 5072–5077.
40. a) D. Praseuth, M. Grigoriev, A. L. Guieysse, L. L. Pritchard, A. Harel-Bellan, P. E. Nielsen and C. Hélène, *Biochim. Biophys. Acta.*, 1996, **1309**, 226–238; b) P. Wittung, P. E. Nielsen and B. Nordén, *Biochemistry*, 1997, **36**, 7973–7979; c) P. E. Nielsen and L. Christensen, *J. Am. Chem. Soc*., 1996, **118**, 2287–2288; d) L. Betts, J. A. Josey, J. M. Veal and S. Jordan, *Science*, 1995, **270**, 1838–1841; e) J. Lohse, O. Dahl and P. E. Nielsen, *Proc. Natl. Acad. Sci. U. S. A.*, 1999, **96**, 11804–11808.
41. B. Hyrup, M. Egholm, M. Rolland, P. E. Nielsen, R. H. Berg and O. Buchardt, *J. Chem. Soc. Chem. Commun.*, 1993, 518–519.

42. B. Hyrup, M. Egholm, P. E. Nielsen, P. Wittung, B. Nordén and O. Buchardt, *J. Am. Chem. Soc*., 1994, **116**, 7964–7970.
43. B. Hyrup, M. Egholm, O. Buchardt and P. E. Nielsen, *Bioorg. Med. Chem. Lett*., 1996, **6**, 1083–1088.
44. R. Schültz, M. Cantin, C. Roberts, B. Greiner, E. Uhlmann and C. Leumann, *Angew. Chem. Int. Ed.*, 2000, **39**, 1250–1253.
45. A. Gourishankar and K. N. Ganesh, *Artif. DNA: PNA XNA*, 2012, **3**, 5–13.
46. T. Govindaraju, V. Madhuri, V. A. Kumar and K. N. Ganesh, *J. Org. Chem.*, 2006, **71**, 14–21.
47. a) V. A. Kumar and K. N. Ganesh, *Acc. Chem. Res*., 2005, **38**, 404–412; b) T. Vilaivan, *Acc. Chem. Res.*, 2015, **48**, 1645–1656.
48. B. P. Gangamani, V. A. Kumar and K. N. Ganesh, *Tetrahedron*, 1996, **52**, 15017–15030.
49. T. Vilaivan and C. Srisuwannaket, *Org. Lett.*, 2006, **8**, 1897–1900.
50. a) G. Haaima, A. Lohse, O. Buchardt and P. E. Nielsen, *Angew. Chem. Int. Ed*., 1996, **35**, 1939–1942; b) S. Sforza, G. Haaima, R. Marchelli and P. E. Nielsen, *Eur. J. Org. Chem.*, 1999, 197–204.
51. a) N. T. S. De Costa and J. M. Heemstra, *PLoS One*, 2013, **8**, e58670; b) N. T. S. De Costa and J. M. Heemstra, *Bioorg. Med. Chem. Lett*., 2014, **24**, 2360–2363.
52. a) P. Zhou, M. Wang, L. Du, G. W. Fisher, A. Waggoner and D. H. Ly, *J. Am. Chem. Soc*. 2003, **125**, 6878–6879; b) A. Dragulescu-Andrasi, P. Zhou, G. He and D. H. Ly, *Chem. Commun.*, 2005, **41**, 244–246.
53. P. Zhou, A. Dragulescu-Andrasi, B. Bhattacharya, H. Okeefe, P. Vatta, J. J. Hyldig-Nielsen and D. H. Ly, *Bioorg. Med. Chem. Lett*., 2006, **16**, 4931–4935.
54. B. Sahu, V. Chenna, K. L. Lathrop, S. M. Thomas, G. Zon, K. J. Livak and D. H. Ly, *J. Org. Chem*., 2009, **74**, 1509–1516.
55. D. R. Jain, L. Anandi V, M. Lahiri and K. N. Ganesh, *J. Org. Chem.*, 2014, **79**, 9567–9577.
56. R. Mitra and K. N. Ganesh, *J. Org. Chem.*, 2012, **77**, 5696–5704.
57. G. Haaima, H. F. Hansen, L. Christensen, O. Dahl and P. E. Nielsen, *Nucleic Acids Res*., 1997, **25**, 4639–4643.
58. J. Lohse, O. Dahl and P. E. Nielsen, *Proc. Natl. Acad. Sci. U. S. A.*, 1999, **96**, 11804–11808.
59. M. Egholm, L. Christensen, K. L. Deuholm, O. Buchardt, J. Coull and P. E. Nielsen, *Nucleic Acids Res.*, 1995, **23**, 217–222.
60. B. P. Gangamani, V. A. Kumar and K. N. Ganesh, *Chem. Commun.*, 1997, 1913–1914.
61. H. F. Hansen, L. Christensen, O. Dahl and P. E. Nielsen, *Nucleosides Nucleotides*, 1999, **18**, 5–9.
62. V. Chenna, S. Rapireddy, B. Sahu, C. Ausin, E. Pedroso and D. H. Ly, *ChemBioChem*, 2008, **9**, 2388–2391.
63. H. Ikeda, Y. Nakamuraa and I. Saito, *Tetrahedron Lett.*, 2002, **43**, 5525–5528.
64. S. Müllar, J. Strohmeier and U. Diederichsen, *Org. Lett.*, 2011, **14**, 1382–1385.
65. F. Wojciechowski and R. H. E. Hudson, *J. Am. Chem. Soc.*, 2008, **130**, 12574–12575.
66. J. Hua, D. W. Dodd, R. H. E. Hudson, D. R. Corey, *Bioorg. Med. Chem. Lett*., 2009, **19**, 6181–6184.
67. C. Boonlua, C. Vilaivan, H.-A. Wagenknecht and T. Vilaivan, *Chem.-Asian J.*, 2011, **6**, 3251–3259.
68. a) O. Köhler, D. V. Jarikote, and O. Seitz, *ChemBioChem*, 2005, **6**, 69–77; b) S. Kummer, A. Knoll, E. Socher, L. Bethge, A. Herrmann and O. Seitz, *Angew. Chem. Int. Ed.*, 2011, **50**, 1931–1934; c) S. Kummer, A. Knoll, E. Socher, L. Bethge, A. Herrmann and O. Seitz, *Bioconjugate Chem.*, 2012, **34**, 2051–2060.

69. A. G. Torres, M. M. Fabani, E. Vigorito, D. Williams, N. Al-Obaidi, F. Wojciechowski, R. H. E. Hudson, O. Seitz, and M. J. Gait, *Nucleic Acids Res.*, 2012, **40**, 2152–2167.
70. Kam, Y., Rubinstein, A., Nissan, A., Halle, D., and Yavin, E. *Mol. Pharmacol.*, 2012, **9**, 685–693.
71. S. Ficht , A. Mattes and O. Seitz, *J. Am. Chem. Soc.*, 2004, **126**, 9970–9981.
72. T. Sato, Y. Sato, and S. Nishizawa, *J. Am. Chem. Soc.*, 2016, **138**, 9397–9400.
73. M. A. Bonham, S. Brown, A. L. Boyd, P. H. Brown, D. A. Bruckenstein, J. C. Hanvey, S. A. Thomson, A. Pipe, F. Hassman, J. E. Bisi, B. C. Froehler, M. D. Matteucci, R. W. Wagner, S. A. Noble and L. E. Babiss, *Nucleic Acids Res*., 1995, **23**, 1197–1203.
74. U. Koppelhus and P. E. Nielsen, *Adv. Drug Delivery Rev.*, 2003, **55**, 267–280.
75. M. M. Fabani and M. J. Gait, *RNA*, 2008, **14**, 336–346.
76. H. Yin, C. Betts, A. F. Saleh, G. D. Ivanova, H. Lee, Y. Seow, D. Kim, M. J. Gait and M. Wood, *Molecular Therapy*, 2010, **18**, 819–827.
77. J. C. Norton, M. A. Piatyszek, W. E. Wright, J. W. Shay and D. R. Corey, *Nat. Biotech.*, 1996, **14**, 615–620.
78. E. Fabbri, A. Manicardi, T. Tedeschi, S. Sforza, N. Bianchi, E. Brognara, A. Finotti, G. Breveglieri, M. Borgatti, R. Corradini, R. Marchelli and R. Gambari, *ChemMedChem*, 2011, **6**, 2192– 2202.
79. T. Shiraishi and P. E. Nielsen, *Artificial DNA: PNA XNA*, 2011, **2**, 90–99.
80. T. Shiraishi and P. E. Nielsen, *Bioconjugate Chem.*, 2012, **23**, 196–202.
81. G. Upert, A. Di Giorgio, A. Upadhyay, D. Manvar, N. Pandey, V. N. Pandey and N. Patino, *Journal of Nucleic Acids*, 2012, **12**, 1–9.
82. H. Ørum, P. E. Nielsen, M. Egholm, R. H. Berg, O. Buchardt and C. Stanley, *Nucleic Acids Res.*, 1993, **21**, 5332–5336.
83. a) Y. Nagai, H. Miyazawa, Huqun , T. Tanaka, K. Udagawa, M. Kato, S. Fukuyama, A. Yokote, K. Kobayashi, M. Kanazawa and K. Hagiwara, *Cancer Research*, 2005, **65**, 7276–7282; b) J. Soh, S. Toyooka, K. Aoe, H. Asano, S. Ichihara, H. Katayama, A. Hiraki, K. Kiura, M. Aoe, Y. Sano, K. Sugi, N. Shimizu and H. Date, *International Journal of Cancer*, 2006, **119**, 2353–2358; c) H. Miyazawa, T. Tanaka, Y. Nagai, M. Matsuoka, Huqun, A. Sutani, K. Udagawa, J. Zhang, T. Hirama, Y. Murayama, N. Koyama, K. Ikebuchi, M. Nagata, M. Kanazawa, T. Nukiwa, S. Takenoshita, K. Kobayashi and K. Hagiwara, *Cancer Science*, 2008, **99**, 595–600.
84. Affymetrix GeneChip Globin-Reduction Kit Handbook https://www.affymetrix.com/support/downloads/manuals/globin_reduction_protocol_manual.pdf.
85. D. S. Lundberg, S. Yourstone, P. Mieczkowski, C. D. Jones and J. L. Dangl, *Nat. Methods*, 2013, **10**, 999–1002.
86. O. Brandt and J. D. Hoheisel, *Trends Biotechnol*., 2004, **22**, 617–622.
87. N. Zhang and D. H. Appella, *J. Am. Chem. Soc.*, 2007, **129**, 8424–8425.
88. X. Su and R. Kanjanawarut, *ACS Nano*, 2009, **3**, 2751–2759.
89. S. Shin, B. Y. Won, C. Jung, S. C. Shin, D. Y. Cho, S. S. Lee and H. G. Park, *Chem. Commun.*, 2011, **47**, 6611–6613.
90. J. Das, I. Ivanov, E. H. Sargent and S. O. Kelley, *J. Am. Chem. Soc.*, 2016, **138**, 11009–11016.
91. D. Phelan, K. Hondorp, M. Choob, V. Efimov and J. Fernandez, *Nucleosides Nucleotides Nucleic Acids*, 2001, **20**, 1107–1111.
92. N. Winssinger, S. Ficarro, P. G. Schultz and J. L. Harris, *Proc. Natl. Acad. Sci. U. S. A.*, 2002, **99**, 11139–11144.
93. B. Liu, and G. C. Bazan, *Proc. Natl. Acad. Sci. U. S. A.*, 2005, **102**, 589–593.

94. V. Kotikam, M. Fernandes and V. A. Kumar, *Phys. Chem. Chem. Phys.*, 2012, **14**, 15003–15006.
95. H. Perry-O'Keefe, X-W. Yao, J. M. Coull, M. Fuchs and M. Egholm, *Proc. Natl. Acad. Sci. U. S. A.*, 1996, **93**, 14670–14675.
96. B. Williams, H. Stender and J. M. Coull, *Peptide nucleic acids; methods and protocols*, Totowa, New York: Humana Press Inc., 2002, 181–193.
97. F. Bonvicini, C. Filippone, E. Manaresi, G. A. Gentilomi, M. Zerbini, M. Musiani and G. Gallinel, *Clinical Chemistry*, 2006, **52**, 973–978.
98. J. P. Burton, J. K. McCormick, P. A. Cadieux and G. Reid, *Letters in Applied Microbiology*, 2003, **36**, 145–149.
99. P. M. Lansdorp, N. P. Verwoerd, F. M. van de Rijke, V. Dragowska, M.-T. Little, R. W. Dirks, A. K. Raap and H. J. Tanke, *Hum. Mol. Genet.*, 1996, **5**, 685–691.
100. K. L. Taneja, E. A. Chavez, J. Coull and P. M. Lansdorp, *Genes Chromosomes Cancer*, 2001, **30**, 57– 63.
101. C. Molenaar, K. Wiesmeijer, N. P. Verwoerd, S. Khazen, R. Eils, H. J. Tanke and R. W. Dirks, *EMBO J.*, 2003, **22**, 6631–6641.
102. H. Perry-O'Keefe, S. Rigby, K. Oliveira, D. Sørensen, H. Stender, J. Coull, J. J. Hyldig-Nielsen, *J. Microbiol. Methods*, 2001, **47**, 281–292.
103. S.-R. Ryoo, J. Lee, J. Yeo, H.-K. Na, Y.-K. Kim, H. Jang, H. H. Lee, S. W. Han, Y. Lee, V. N. Kim and D.-H Min, *ACS Nano*, 2013, **7**, 5882–5891.
104. a) S. Jin, C. V. Miduturu, D. C. McKinney and S. K. Silverman, *J. Org. Chem.*, 2005, **70**, 4284–4299; b) H. Sahoo, *RSC Adv.*, 2012, **2**, 7017–7029.
105. a) S. S. Ghosh, P. M. Kao, A. W. McCue and H. L. Chappelle, *Bioconjugate Chem*., 1990, **1**, 71–76; b) G. M. Blackburn, M. J. Gait, D. Loakes and D. M. Williams, RSC, UK, 3rd ed., 2006.
106. C. D. Spicer and B. G. Davis, *Nat. Commun.*, 2014, **5**, 4740.
107. a) J. A. Prescher, and C. R. Bertozzi, *Nat. Chem. Biol.*, 2005, **1**, 13–21; b) A. G. Neef and C. Schultz, *Angew. Chem. Int. Ed.*, 2009, **48**, 1498–1500; c) P. M. E. Gramlich, C. T. Wirges, A. Manetto and T. Carell, *Angew. Chem. Int. Ed.*, 2008, **47**, 8350–8358; d) A. H. El-Sagheer and T. Brown, *Chem. Soc. Rev.*, 2010, **39**, 1388–1405; e) S. S. van Berkel, M. B. van Eldijk and J. C. M. van Hest, *Angew. Chem. Int. Ed.*, 2011, **50**, 8806–8827.
108. K. Gogoi, M. V. Mane, S. S. Kunte and V. A. Kumar, *Nucleic acid Res.*, 2007, **35**, e139
109. A. H. St. Amant, C. Engbers and R. H. E. Hudson, *Artif. DNA: PNA XNA*, 2013, **4**, 4–10.
110. A. Manicardi, E. Gyssels, R. Corradinia and A. Madder, *Chem. Commun.*, 2016, **52**, 6930–6933.
111. J. D. Flory, T. Johnson, C. R. Simmons, S. Lin, G. Ghirlanda and P. Fromme, *Artif. DNA: PNA XNA*, 2014, **5**, 1–8.

Chapter 2

Synthesis, incorporation and responsiveness of heterobicycle-modified PNA base analogues

2.1 Introduction

Oligonucleotides (ONs) probes labeled with base modified fluorescent nucleoside analogues capable of binding to target nucleic acids have been elegantly utilized in studying nucleic-acid structure, folding, and recognition process.[1,2] Typically, such emissive nucleobase analogues are obtained by attaching known fluorophores as base surrogates or heterocycles to the nucleobase.[1c] Albeit, with few exception,[3] labeled ONs exhibit low fluorescence, compromised hybridization efficiency and less stability in nuclease environment, which eventually hampers their practical applications, in particular, as hybridization probes.[1c] In this regard, a synthetic nucleic acid mimic such as peptide nucleic acid (PNA) could be an ideal candidate. PNA oligomers consist of repeating units of *N*-(2-aminoethyl)glycine (*aeg*) linked via amide bonds in which the nucleobases are attached through methylene carbonyl linkage.[5] This pseudo-peptide backbone in PNA provides stability in cellular environment and better hybridization affinity towards the complementary ONs.[4] PNA oligomers were primarily developed as antisense and antigene therapeutic agents to control the expression of disease causing genes.[6] Notably, in recent years, PNAs has been widely used as hybridization probes for applications in clinical diagnosis.[7] Normally, the hybridization assays use PNA probes attached to large fluorophores, which could potentially reduce the hybridization efficiency of the probe to the target ON sequence. Alternatively, a few nucleobase analogues (e.g., 2-aminopurine, 8-vinylguanine, etc.) have been incorporated into PNA and used in studying nucleic acid topologies and hybridization process.[8] However, these analogues have excitation and emission maximum in the UV region and or exhibit decrease in fluorescence intensity upon hybridization to complementary ONs. Therefore, there is significant demand for the development of fluorescent PNA probes that could effectively report the binding event with an enhancement in fluorescence intensity, which greatly facilitate the development of robust diagnostic and therapeutic tools.

As a part of our efforts in developing nonperturbing fluorescent ribonucleoside analogues, we have introduced a small series of extended ribonucleosides by conjugating heterobicycles (indole, *N*-methylindole, benzothiophene and benzofuran) at the 5-position of uridine.[9,10] 5-benzofuran and 5-benzothiophene modified uridine analogues were moderately emissive and their fluorescence properties were highly sensitive to changes in their local environment.[9,10] More importantly, when incorporated into ONs and hybridized to complementary ONs, the nucleosides were structurally noninvasive and retained appreciable fluorescence efficiency, a property rarely exhibited by the majority of fluorophores. 5-

benzofuran uridine analogue (BFU) was utilized to distinguish different nucleic acid topologies and report the binding of small molecule ligands to telomeric DNA and RNA G-quadruplex structures in buffer solution.[11] Further, 5-benzothiophene uridine analogue (BTU) was implemented in a biophysical assay to study the ON dynamics in a cell-like confined environment.[12]

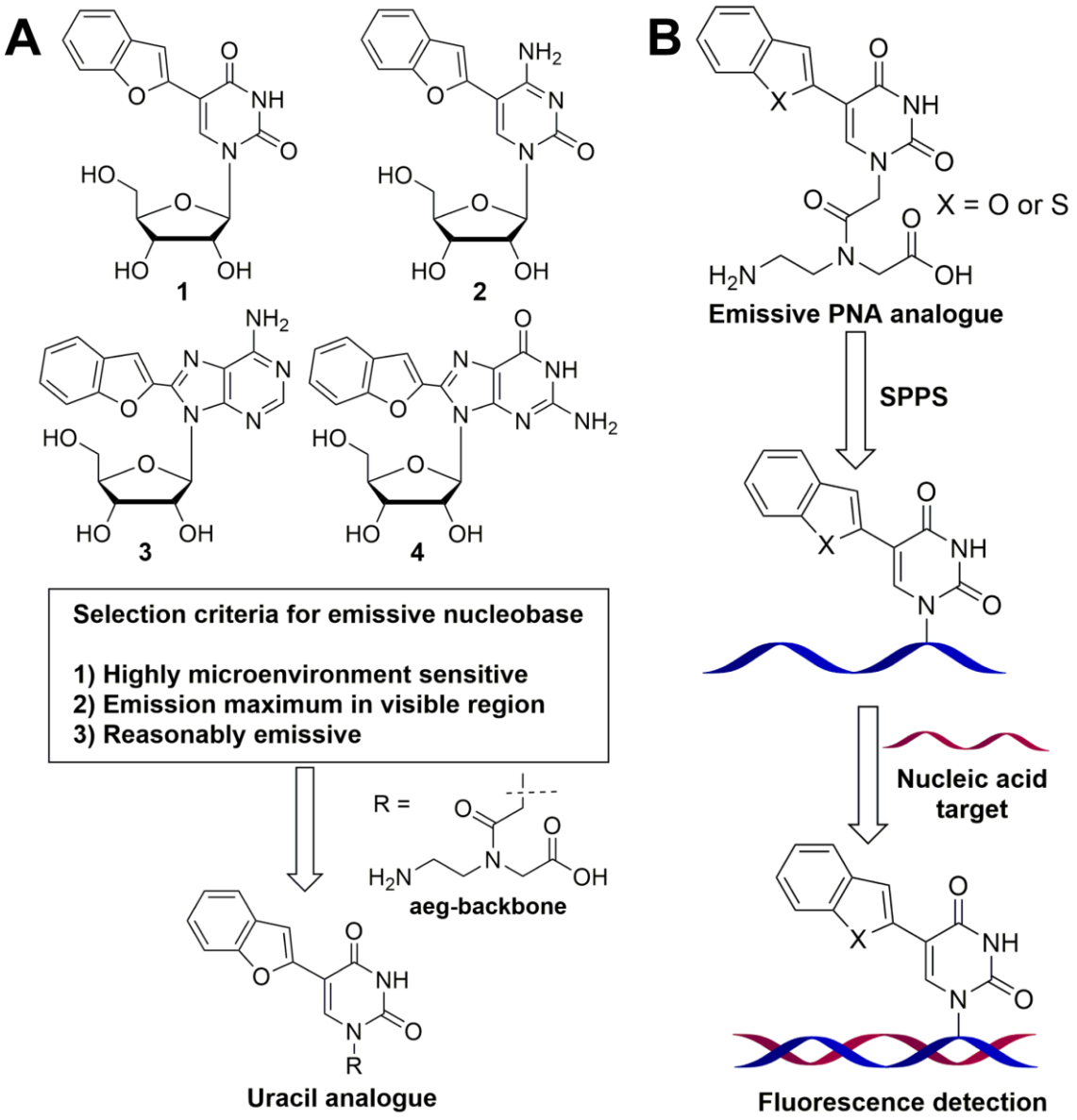

Figure 1. (**A**) Chemical structure of benzofuran-conjugated pyrimidine and purine ribonucleosides. Selection criteria for the development of fluorescent base-modified PNA analogues. (**B**) Design of benzofuran- and benzothiophene- modified uracil PNA oligomers as hybridization probes for nucleic acid detection.

In order to design a suitable emissive nucleobase (A/U/G/C) for incorporation into PNA oligomers, we have initially compared the photophysical properties of benzofuran modified pyrimidine and purine analogues (Figure 1A). To have a direct comparison with

BFU (**1**), we have synthesized remaining benzofuran-conjugated ribonucleoside analogues (**2**, **3** and **4**) and evaluated their photophysical properties in different solvents (Figure 1A).[13] The fluorescence properties of pyrimidine ribonucleosides (**1** and **2**) as compared to purine ribonucleosides (**3** and **4**) were highly sensitive to solvent polarity and or viscosity changes. Further, BFU (**1**) displayed better fluorescence efficiency and environment-sensitivity as compared to BFC (**2**). Therefore, we envisioned that base modified uracil analogue containing a heterocycle at the 5 position would be a better candidate to devise nucleobase probes. Hence, we decided to attach heterocycles at the 5 position of uracil PNA base and incorporate into PNA oligomers to devise robust hybridization probes (Figure 1B).

In this chapter, we report the synthesis and photophysical analysis of benzofuran-conjugated pyrimidine and purine ribonucleoside analogues. Further, synthesis, photophysical analysis and incorporation of 5-benzofuran and 5-benzothiophene conjugated uracil PNA analogues into PNA oligomers by solid-phase peptide synthesis (SPPS) are discussed. Next, the impact of neighboring base environment on the fluorescence properties of emissive PNA analogues incorporated into PNA oligomers and hybridized to complementary ONs has been discussed. The results obtained from these studies point out that both benzofuran- and benzothiophene-modified PNA uracil analogues are minimally perturbing and are highly responsive to changes in their neighboring based environment. In subsequent chapters we have used these highly useful features to develop PNA probes to detect G-quadruplex forming human telomeric DNA repeats and proto-oncogenes (e.g., c-kit and c-myc), and study the kinetics of depurination activity of ribosome inactivating protein toxins (e.g. saporin).

2.2 Results and Discussion

2.2.1 Synthesis and photophysical analysis of benzofuran-conjugated ribonucleoside analogues

2.2.1.1 Synthesis of full-set of benzofuran-conjugated ribonucleoside analogues

Benzofuran-conjugated adenosine (**3**) and guanosine (**4**) analogues were synthesized by performing palladium catalyzed Stille cross-coupling reaction between 2-(tri-*n*-butylstannyl)benzofuran and respective 8-bromopurines[14] under microwave conditions (Scheme 1). 5-benzofuran uridine (**1**) and 5-benzofuran cytidine (**2**) ribonucleosides were synthesized and studied by a colleagues from our group.[10,13]

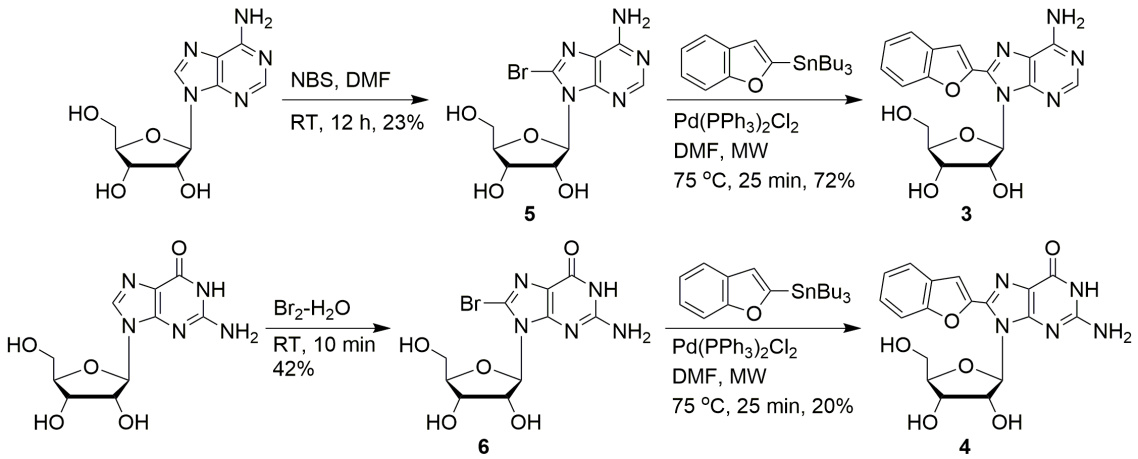

Scheme 1. Synthesis of fluorescent 8-benzofuran purine ribonucleoside analogues **3** and **4**.[15]

2.2.1.2 Photophysical characterization of fluorescent ribonucleoside analogues

Fluorescence properties of emissive nucleoside analogues, when incorporated into ONs, can be affected by changes in microenvironment and by various interactions with neighbouring bases. Generally, collisional and stacking interactions with adjacent bases and electron transfer between the fluorescent base and neighbouring bases result in fluorescence quenching.[16-19] If the nucleoside analogue is solvatochromic or conformation-sensitive, then its fluorescence properties are likely to be altered by solvation-desolvation effects or by structural rigidification-derigidification process, respectively.[17,20]

The solvatochromic property of an emissive nucleoside can be evaluated by performing UV-vis absorption and fluorescence measurements in solvents of different polarity. In nucleoside analogues the relative conformation of the benzofuran moiety with respect to the nucleobase separated by a rotatable aryl-aryl bond could influence the effective conjugation and hence, the fluorescence properties. It has been shown that the relative conformation of nucleoside analogues containing molecular rotor element, when incorporated into ONs, is influenced by molecular crowding effects due to interaction with neighbouring bases.[20] The conformation-sensitivity of a fluorophore, in this case, benzofuran-conjugated nucleosides, can be evaluated by performing photophysical characterization in solvents of different viscosity. Typically, rotation about the aryl-aryl bond is restricted in a viscous medium as compared to in a less viscous medium, which usually results in higher quantum yield. Nucleic acid-based assays to study the structure and function of nucleic acids often utilize fluorescent nucleoside analogues that photophysical respond to subtle changes in microenvironment (e.g., polarity and viscosity) and or conformation.[1] Therefore, in order to

assess the suitability of our emissive nucleosides as biophysical tools we have studied the photophysical behaviour of free nucleosides in different environments.

Fluorescence properties of ribonucleosides in solvents of different polarity: The absorption spectrum of **1** and **2** were marginally affected by solvent polarity change (Table 1). However, the excited-state properties of pyrimidine analogues were significantly affected by solvent polarity. When excited, nucleoside **1** and **2** displayed an emission band in the visible region corresponding to a quantum yield of 0.212[10] and 0.03[13] respectively (Table 1). As the solvent polarity was reduced from water to dioxane, a significant quenching in fluorescence intensity corresponding to a nearly 2-fold reduction in quantum yield with a blue-shifted emission maximum was observed for both the nucleoside analogues. Time-resolved fluorescence measurements revealed a longer excited-state lifetime for the nucleosides in water as compared to in dioxane (Table 1).

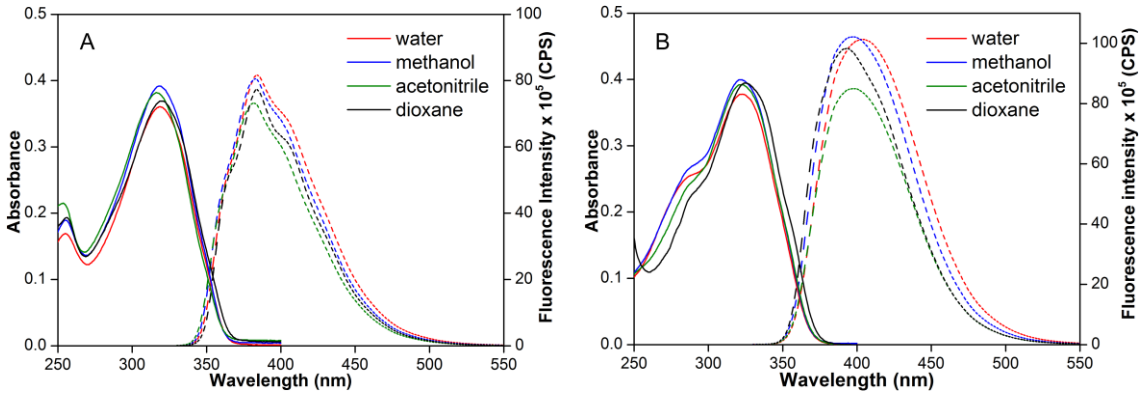

Figure 2. Absorption (25 µM, solid lines) and emission (5 µM, dashed lines) spectra of ribonucleoside **3** (**A**) and **4** (**B**) in different solvents. Samples were excited at respective lowest energy maximum, and excitation and emission slit widths were maintained at 2 and 3 nm, respectively. All solutions for absorption and emission studies contained 2.5% and 0.5% DMSO, respectively.

The absorption spectrum of benzofuran-modified adenosine analogue **3** showed a major absorption maximum at nearly 320 nm, which more or less remained unaltered as the solvent polarity was decreased from water to dioxane (Figure 2A, Table 1). Upon excitation at 320 nm, the nucleoside **3** in water displayed a strong emission band (λ_{em}=384 nm) corresponding to a quantum yield 0.62. Akin to ground-state properties, the excited-state properties such as emission maximum, quantum yield and lifetime were not significantly affected by solvent polarity changes (Figure 2A, Table 1, Figure 3). Benzofuran-modified guanosine analogue **4** exhibited a slightly red-shifted absorption maximum, which again was not significantly affected by solvent polarity changes (Figure 2B, Table 1). When a solution

of **4** in water was excited at 323 nm, it displayed an emission maximum in the visible region corresponding to a high quantum yield of 0.82 (Figure 2B, Table 1). Analogous to benzofuran-conjugated adenosine analogue, the solvent polarity changes had minor impact on the quantum yield and excited-state lifetime of nucleoside **4** (Table 1, Figure 4).

The ratio of radiative (K_r) to nonradiative (K_{nr}) decay rate constant calculated for ribonucleosides using quantum yield and lifetime in different solvents clearly indicates that the fluorescence emission of pyrimidine analogues was more favoured in polar solvents as opposed to in nonpolar solvents (Table 1). However, fluorescence properties of purine analogues were not substantially affected by solvent polarity changes (Table 1). Together, these results indicated that the photophysical behaviour of purine analogues, when incorporated into ONs, might not be affected by solvation-desolvation effects.

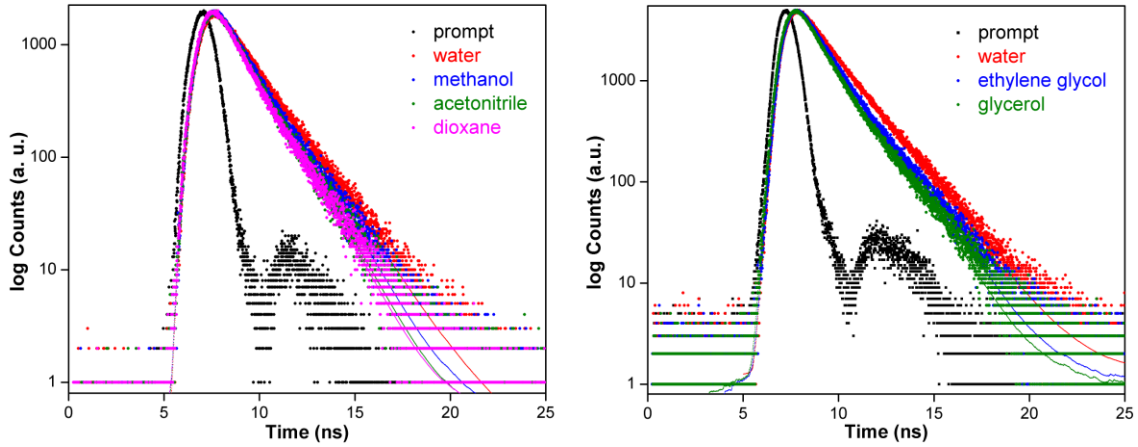

Figure 3. Excited state decay profile of ribonucleoside **3** (5 μM) in various solvents. Samples were excited using 339 nm LED source. Laser profile is shown in black (prompt). Curve fits are shown in solid lines.

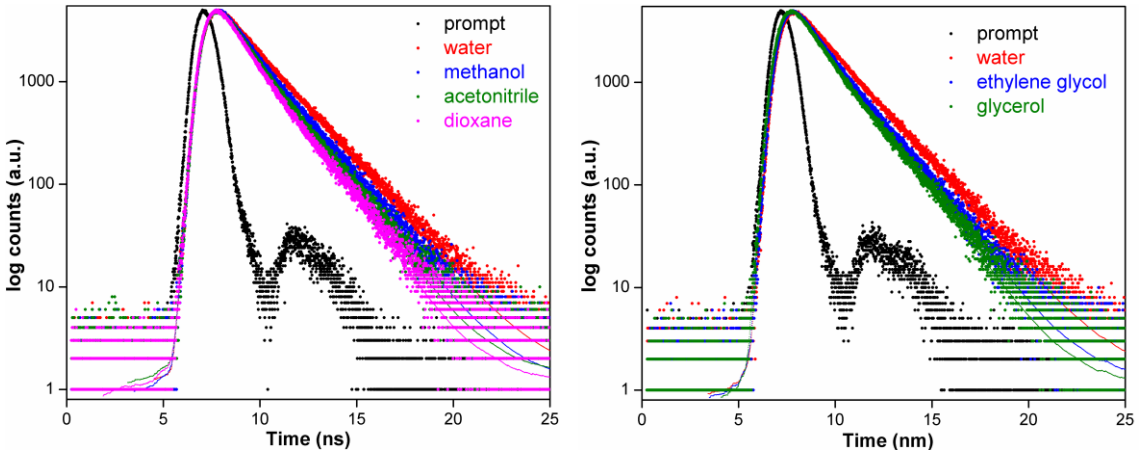

Figure 4. Excited state decay profile of ribonucleoside **4** (5 μM) in various solvents. Samples were excited using 339 nm LED source. Laser profile is shown in black (prompt). Curve fits are shown in solid lines.

Table 1. Photophysical properties of ribonucleosides **1**, **2**, **3** and **4** in various solvents

Ribonucleoside	Solvent	λ_{max} [a] (nm)	λ_{em} (nm)	I_{rel} [b]	Φ [c]	τ [c] (ns)	k_r/k_{nr}
	water	322	447	1.0	0.21	2.55	0.27
1	methanol	322	423	0.8	0.15	0.94	0.16
	acetonitrile	322	410	0.4	0.06	0.33	0.06
	dioxane	322	404	0.6	0.10	0.43	0.11
	ethylene glycol	322	428	1.9	0.38	3.13	0.61
	glycerol	322	427	2.4	0.53	3.40	1.12
	water	290	452	1.0	0.03	0.57	0.03
2	methanol	290	446	0.7	0.01	0.38	0.01
	acetonitrile	291	440	0.5	0.01	0.34	0.01
	dioxane	297	437	0.6	0.01	0.34	0.01
	ethylene glycol	292	444	2.3	0.06	1.25	0.06
	glycerol	292	447	5.0	0.13	3.07	0.15
	water	320	384	1.0	0.62	1.68	1.63
3	methanol	318	383	1.0	0.56	1.48	1.27
	acetonitrile	317	382	0.9	0.53	1.39	1.13
	dioxane	320	384	1.0	0.60	1.35	1.50
	ethylene glycol	322	385	0.9	0.61	1.45	1.56
	glycerol	323	384	1.0	0.66	1.34	1.94
	water	323	403	1.0	0.82	1.94	4.56
4	methanol	323	397	1.0	0.75	1.72	3.00
	acetonitrile	323	397	0.8	0.62	1.59	1.63
	dioxane	324	394	1.0	0.80	1.48	4.00
	ethylene glycol	327	403	0.9	0.74	1.70	2.85
	glycerol	327	399	0.9	0.84	1.60	5.25

[a] The lowest energy maximum is given. [b] Relative emission intensity with respect to intensity in water. [c] Standard deviations for quantum yield (Φ) and lifetime (τ) are ≤ 0.02 and ≤ 0.04 ns, respectively. Photophysical properties of ribonucleosides **1** and **2** have been adapted from reference 10 and 13 respectively.

Fluorescence properties of nucleosides in solvents of different viscosity: The conformational flexibility of pyrimidine and purine analogues has been studied by performing steady-state fluorescence and lifetime measurements in solvents of different viscosity. Fluorescence properties for ribonucleoside analogues **1** and **2** such as quantum yield and excited state lifetime increases as the solvent viscosity was increased from water to ethylene glycol to glycerol (Table 1). These results indicate the presence of a molecular rotor element in pyrimidine nucleosides, which is rigidified in a more viscous medium resulting in enhanced fluorescence efficiencies. Purine analogues **3** and **4** exhibited only minor alterations in fluorescence properties as the solvent viscosity was increased from water to ethylene glycol to glycerol (Table 1, Figure 5). These observations indicated that the benzofuran and purine rings in purine analogues were fairly coplanar and conformationally rigid, which explains their high quantum yields even in less viscous medium, water. These results confirmed that the purine analogues **3** and **4** are not conformation-sensitive.

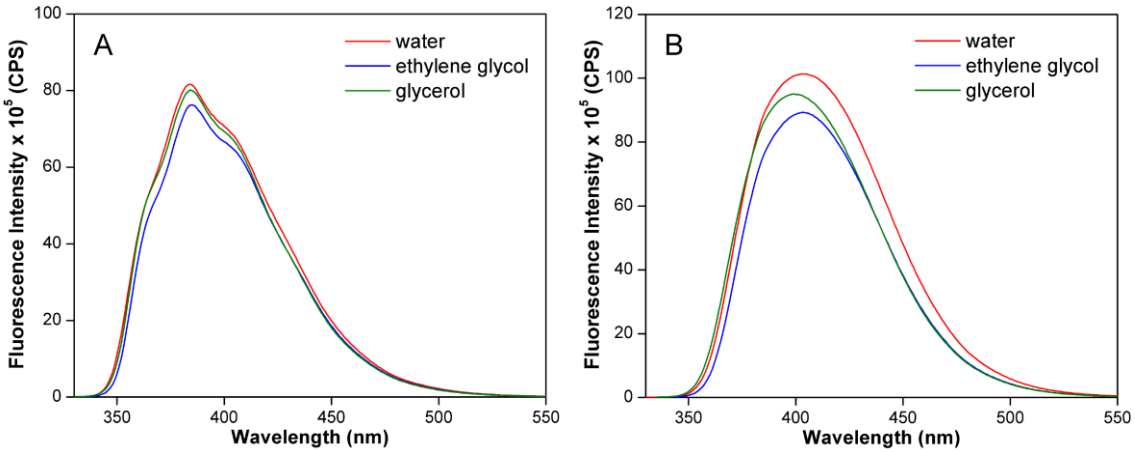

Figure 5. Emission spectra (5.0 μM) of nucleoside **3** (**A**) and **4** (**B**) in solvents of varying viscosity. Samples were excited at respective lowest energy maximum. Excitation and emission slit widths were 2 and 3 nm, respectively.

Effect of collisional interaction on fluorescence properties of ribonucleosides: Collisional interaction between a fluorescent nucleobase and neighbouring bases in an ON sequence can quench the fluorescence by nonradiative pathway.[17] Since these interactions can also take place when the nucleobases are free in solution, it is possible to study the effect of collisional interactions on the fluorescence by titrating the fluorophore with increasing concentrations of the natural bases. Typically, such fluorescence titrations are performed by adding increasing amounts of nucleotide phosphates (e.g., nucleoside monophosphates, NMPs), which are readily soluble in water compared to nucleobases. Increasing concentrations of AMP, CMP and UMP resulted in minor reduction in fluorescence intensity of purine ribonucleosides. Among the four NMPs used in this study, GMP exhibits the highest quenching effect on ribonucleosides **3** and **4** with a Stern-Volmer quenching constant (K_{sv}) of 26.6 and 24.8 μM^{-1}, respectively (Figure 6, Table 2). It is worth mentioning here that the quenching effect produced by NMPs on 2-AP fluorescence is very high compared to the benzofuran-modified nucleosides.[17] Hence, collisional interactions with neighbouring bases may not have an impact on the fluorescence outcome of the benzofuran-modified nucleosides within ONs.[21] Similar results were obtained for BFU (**1**) and BFC (**2**) in Stern-Volmer quenching experiment (Table 2). [10,13]

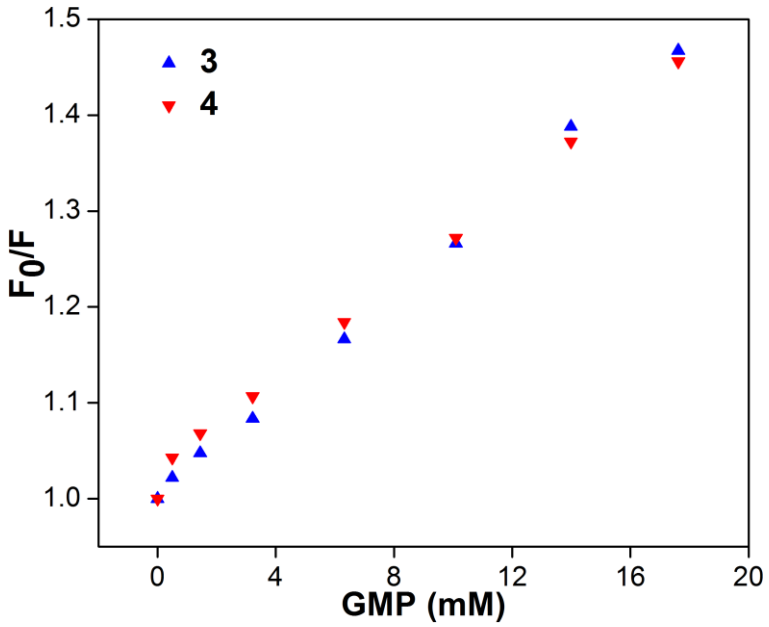

Figure 6. A representative Stern-Volmer plot for the titration of ribonucleosides **3** and **4** with GMP.

Table 2. Stern-Volmer quenching constant for the titration of emissive ribonucleosides with NMPs.[15]

Ribonucleoside	K_{sv} (μM^{-1})			
	AMP	GMP	CMP	UMP
1[a]	nd	26.2 ± 0.2	nd	8.3 ± 1.0
2[b]	nd	8.2 ± 0.7	nd	nd
3	15.0 ± 1.0	26.6 ± 0.4	5.8 ± 0.5	10.0 ± 0.5
4	6.7 ± 0.4	24.8 ± 0.6	11.9 ± 0.2	13.3 ± 0.4

[a]Ref. 10 and [b]Ref. 13. nd= not determined

The photophysical analysis of a complete set of benzofuran-modified fluorescent ribonucleoside analogues exhibited moderate to very high fluorescence efficiency with an emission maxima of 382–452 nm.[13] In particular, photophysical properties such as quantum yield, Stokes shift and lifetime of pyrimidine ribonucleosides as compared to purine ribonucleosides were highly sensitive to change in solvent polarity and or viscosity. From our results, it was observed that BFU exhibited useful probe like characteristics necessary for devising tools to investigate nucleic acids, when compared to other benzofuran-conjugated ribonucleoside analogues. Inspired by the interesting properties BFU and BTU analogues,[9-12] we have decided to further explore benzofuran- and benzothiophene-conjugated uracil base in the context to PNA oligomers for developing robust hybridization probes for important nucleic acid targets.

2.2.2 Synthesis, incorporation and photophysical analysis of 5-benzofuran and 5-benzothiophene-conjugated uracil PNA analogues

2.2.2.1 Synthesis of 5-benzofuran and 5-benzothiophene-conjugated uracil PNA monomers

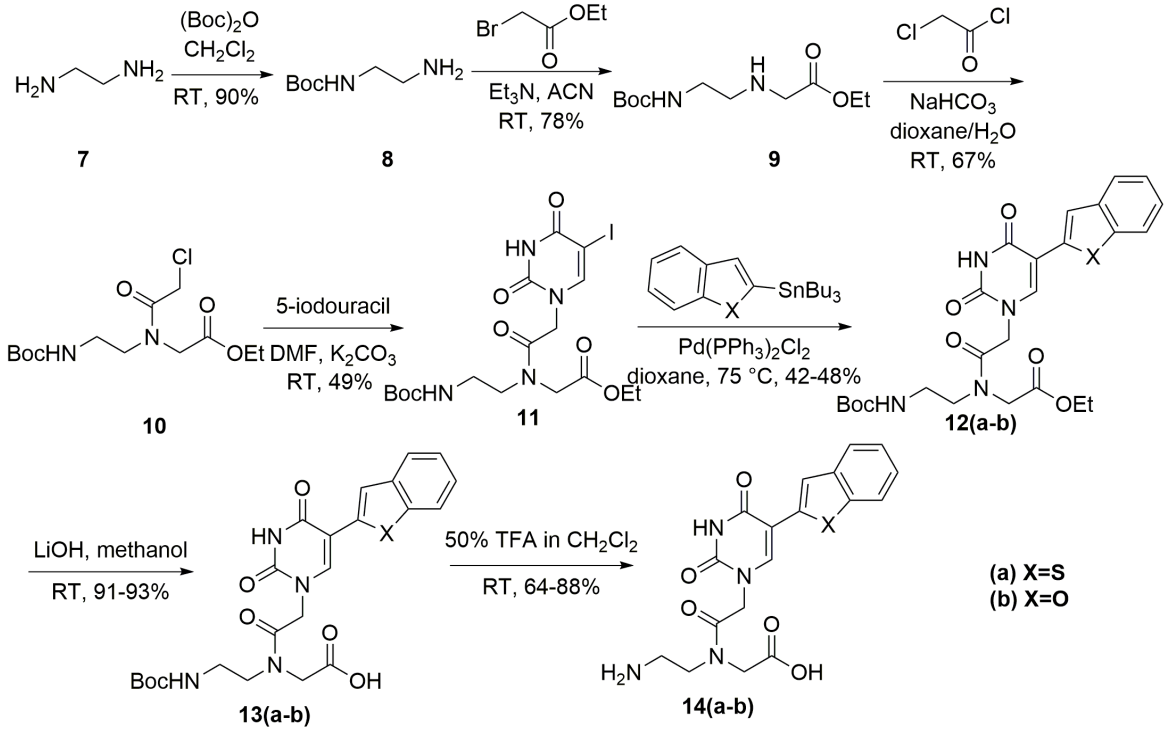

Scheme 2. Synthesis of 5-benzothiophene and benzofuran -modified uracil PNA monomers **13**(**a**-**b**) and **14**(**a**-**b**) used in the solid phase PNA synthesis and fluorescence studies respectively.[15]

The benzothiophene and benzofuran-modified uracil *aeg*PNA monomers **13a** and **13b** required for the SPPS were prepared by following the steps illustrated in Scheme 2. 5-Iodouracil-modified intermediate **11** containing *aeg* backbone was synthesized in four steps following known literature procedures.[22] First, ethylene diamine **7** was converted into mono-protected ethylene diamine **8** by treating with Boc-anhydride. Compound **8** was mono alkylated using ethyl bromoacetate to afford ethyl *N*-(Boc-amino ethyl) glycinate **9**. The compound **9** was acylated using acetyl chloride to give *N*-Boc-aminoethyl-*N*-chloroacetyl glycinate **10**. Further, compound **10** was converted into PNA ester **11** by reacting with 5-iodouracil in the presence of K_2CO_3. The respective fluorescent PNA esters **12**(**a**-**b**) were obtained by a Stille cross-coupling reaction with 2-(tri-*n*-butylstannyl)benzothiophene and 2-(tri-*n*-butylstannyl)benzofuran respectively, in the presence of a palladium catalyst. Subsequent ester hydrolysis of **12**(**a**-**b**) in the presence of lithium hydroxide afforded the fluorescent monomers **13**(**a**-**b**) necessary for solid phase PNA synthesis. The fully

deprotected PNA monomers **14**(**a**-**b**) required for photophysical analysis were obtained by treating **13**(**a**-**b**) with TFA.

2.2.2.2 Photophysical properties of 5-benzofuran and 5-benzothiophene-conjugated uracil PNA monomers

Prior to incorporation into PNA oligomers, the responsiveness of the monomers to microenvironment changes was evaluated by performing preliminary photophysical characterization in solvents of different polarity using completely deprotected PNA monomers **14**(**a**-**b**) (Scheme 2). The bands corresponding to the longest absorption maximum showed a minor hyperchromic effect and bathochromic shift as the solvent polarity was decreased from water to dioxane (Figure 7, Table 3). Upon exciting a solution of **14a** at 318 nm and **14b** at 322 nm in water, an emission band in the visible region (λ_{em} (**14a**) = 467 nm, λ_{em} (**14b**) = 447 nm) corresponding to a quantum yield of 0.06 and 0.28 was observed (Figure 7, Table 3). As the polarity of the medium was decreased by varying the water-dioxane ratio, PNA base analogues **14a** and **14b** displayed a significant hypsochromic shift in its emission maximum from 467 to 439 nm and 447 to 413 nm respectively.

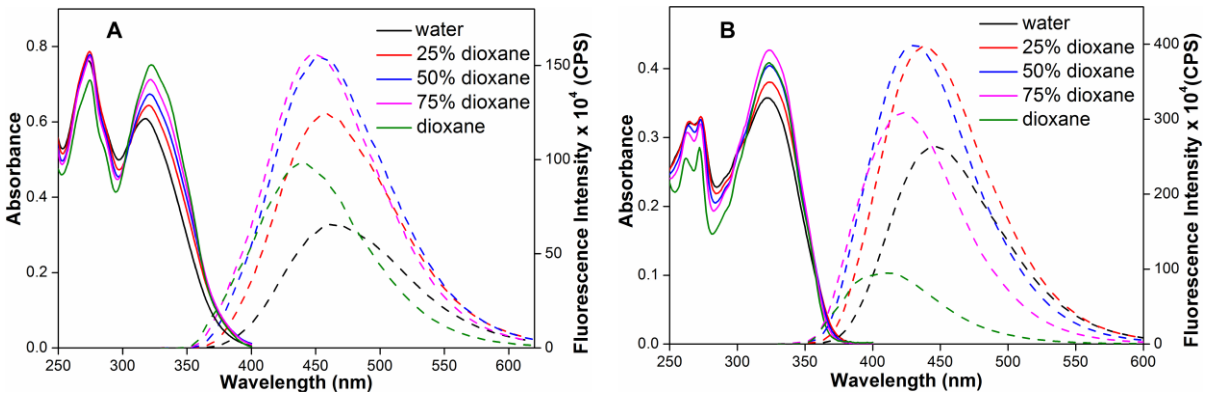

Figure 7. Absorption (solid line) and emission (dashed line) spectra of monomer in water, dioxane and their mixtures. (**A**) Absorption 50 µM and emission 5 µM for **14a** (**B**) absorption 25 µM and emission 5 µM for **14b**. Samples were excited at their respective lowest energy maximum. Excitation and emission slit widths were kept at 3 and 4 nm for **14a** and 2 and 3 nm for **14b** respectively. All solutions for absorption and emission studies contained 5% and 0.5% DMSO, respectively for **14a** and 2.5% and 0.5% DMSO, respectively for **14b**.

A nearly linear plot was obtained when Reichardt's microscopic solvent polarity parameter $E_T(30)$ was plotted against Stokes shift, which further confirmed the sensitivity of the analogues to microscopic polarity changes (Figure 8).[23] Although responsiveness of the benzofuran-modified PNA analogue (**14b**) and BFU nucleoside (**1**)[10] are similar (compared with the results reported in reference 10), the responsiveness of respective analogues (**1** or **14b**) could be different when incorporated into oligomer and hybridized to target

oligonucleotides. Interestingly, the fluorescence intensity, quantum yield and excited-state lifetime were found to change nonlinearly as solvent polarity was reduced by using water-dioxane system (Figure 7, Table 3 and Figure 9). The fluorophore system in **14a** and **14b** has an aryl-aryl rotatable bond between benzothiophene/benzofuran and uracil rings, and hence, its fluorescence could be also sensitive to solvent viscosity changes.[24,25] Although water and dioxane mixtures are commonly used to study the effect of polarity,[20,26] they exhibit small nonlinearity in viscosity.[27] The fluorophore system in PNA base analogues could undergo structural rigidification in viscous medium, and hence, the observed trend in fluorescence properties of **14a** and **14b** is likely due to the combined effect of polarity and viscosity of the medium. Such photophysical behavior in response to polarity and viscosity effects have been observed in case of fluorescent probes possessing similar molecular rotor element.[20,26]

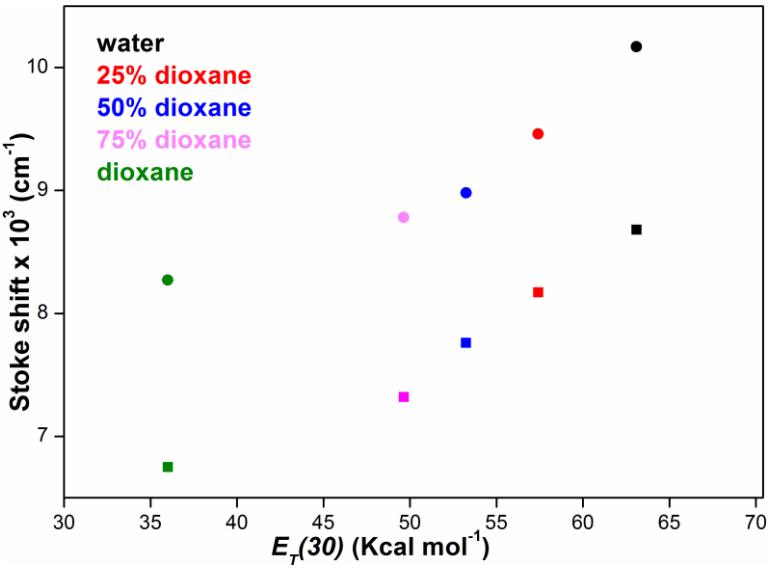

Figure 8. Plot of Stokes shift versus $E_T(30)$ (microscopic solvent polarity parameter)[23] for PNA monomer **14a** (circle) and **14b** (square) respectively.

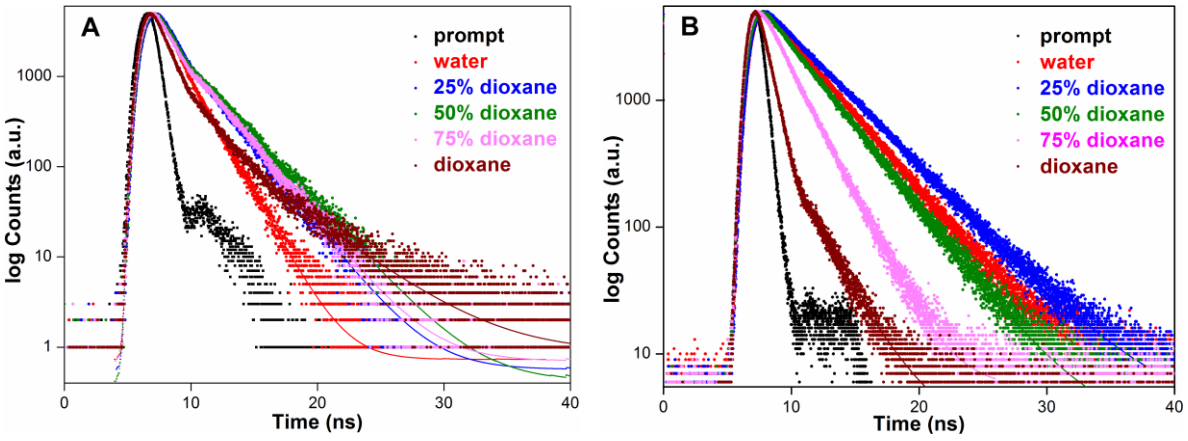

Figure 9. Excited-state decay profile (5.0 μM) of PNA monomer **14a** (**A**) and **14b** (**B**) in solvents of different polarity. Samples were excited using a 320 nm LED source. The laser profile is shown in black (prompt). Curve fits are depicted as solid lines.

Table 3. Photophysical properties of emissive PNA base analog **14a** and **14b**.

Monomer	solvent	λ_{max} [a] (nm)	λ_{em} (nm)	I_{rel} [b]	Φ [c]	τ_1 [d] (ns)	τ_2 [d] (ns)	τ_3 [d] (ns)	τ_{av} [c] (ns)
14a	water	318	467	1.00	0.06	0.82 (0.55)	1.70 (0.45)	-	1.22
	25% dioxane	320	459	1.90	0.10	0.92 (0.60)	2.49 (0.40)	-	1.54
	50% dioxane	321	457	2.35	0.11	0.67 (0.69)	2.88 (0.31)	-	1.35
	75% dioxane	322	449	2.39	0.11	0.45 (0.73)	2.58 (0.27)	-	1.03
	dioxane	322	439	1.50	0.06	0.04 (0.96)	1.29 (0.04)	4.477 (0.005)	0.11
14b	water	322	447	1.00	0.28	3.69	-	-	3.69
	25% dioxane	324	437	1.51	0.38	4.23	-	-	4.23
	50% dioxane	324	431	1.52	0.36	3.39	-	-	3.39
	75% dioxane	324	423	1.17	0.26	0.28 (0.18)	2.15 (1.18)	-	2.50
	dioxane	324	413	0.36	0.09	0.62 (0.96)	2.55 (0.04)	-	0.69

[a] Lowest energy maximum is given. [b] Intensity with respect to water. [c] Standard deviations for quantum yield (Φ) and average lifetime (τ_{av}) are ≤ 0.01 and ≤ 0.05 ns, respectively. [d]Relative amplitude is given in parenthesis.

2.2.2.3 Synthesis of model 15mer fluorescent PNA oligomers containing 14a and 14b

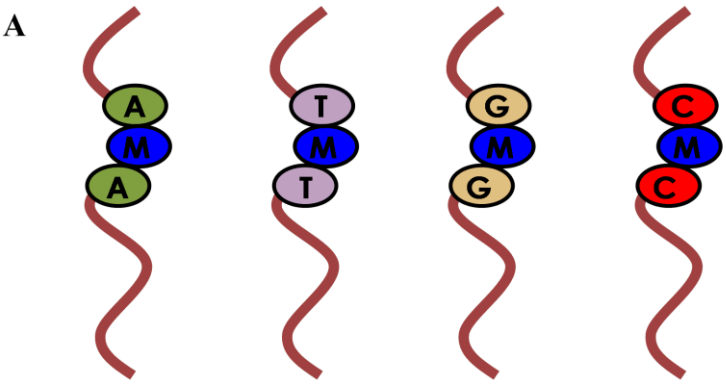

B

15	CGATCAA**T**AACTAGCKK	**16** CGATCAT**T**TACTAGCKK
15X	CGATCAA**14a**AACTAGCKK	**16X** CGATCAT**14a**TACTAGCKK
15Y	CGATCAA**14b**AACTAGCKK	**16Y** CGATCAT**14b**TACTAGCKK
15A	5' d(GCTAGTTATTGATCG) 3'	**16A** 5' d(GCTAGTAAATGATCG) 3'
15T	5' d(GCTAGTTTTTGATCG) 3'	**16T** 5' d(GCTAGTATATGATCG) 3'
15G	5' d(GCTAGTTGTTGATCG) 3'	**16G** 5' d(GCTAGTAGATGATCG) 3'
15C	5' d(GCTAGTTCTTGATCG) 3'	**16C** 5' d(GCTAGTACATGATCG) 3'
17	CGATCAG**T**GACTAGCKK	**18** CGATCAC**T**CACTAGCKK
17X	CGATCAG**14a**GACTAGCKK	**18X** CGATCAC**14a**CACTAGCKK
17Y	CGATCAG**14b**GACTAGCKK	**18Y** CGATCAC**14b**CACTAGCKK
17A	5' d(GCTAGTCACTGATCG) 3'	**18A** 5' d(GCTAGTGAGTGATCG) 3'
17T	5' d(GCTAGTCTCTGATCG) 3'	**18T** 5' d(GCTAGTGTGTGATCG) 3'
17G	5' d(GCTAGTCGCTGATCG) 3'	**18G** 5' d(GCTAGTGGGTGATCG) 3'
17C	5' d(GCTAGTCCCTGATCG) 3'	**18C** 5' d(GCTAGTGCGTGATCG) 3'

Figure 10. (**A**) Model 15mer PNA oligomers with modification **M** is 5-benzothiophene or 5-benzofuran conjugated uracil PNA monomer. (**B**) Sequence of control unmodified PNA oligomers **15**–**18** and fluorescent PNA oligomers **15X**–**18X** (contained **14a**) and **15Y**–**18Y** (contained **14b**) obtained by solid phase synthesis are shown in bold letters. PNA sequences are written from N- to C-terminus containing two lysine (K) residues at the C-terminus. Sequence of synthetic DNA ONs ("d" preceding the parentheses) used in this study are shown.

Numerous studies have shown that the photophysical behaviour of fluorescent base analogues incorporated into ONs greatly influenced by a variety of mechanisms involving neighbouring bases, which include stacking, collisional and H-bonding interactions, rigidification-derigidification of the fluorophore and electron transfer process between adjacent bases and the fluorophore.[16–19] To study the effect of neighboring bases on the fluorescence properties of PNA base analogues, we synthesized a series of model 15mer fluorescent PNA oligomers **15X**–**18X** and **15Y**–**18Y** containing modified base **14a** and **14b**, respectively (Figure 10).[15] The PNA oligomers were designed to contain the modification in-between different flanking bases (A, T, G and C residues). The control unmodified (**15**–**18**) and fluorescently modified PNA oligomers were synthesized by standard solid-phase PNA synthesis protocol using Boc-protected *aeg*-PNA monomers. Two lysine residues were attached at the C terminus of PNAs to enhance the solubility in aqueous buffer. The oligomers were purified by RP-HPLC and their integrity was confirmed by mass analysis (see 2.6 Appendix-I for HPLC profile and mass spectra, Table 4).[15]

Table 4. ε_{260} and MALDI-TOF mass analysis of PNA oligomers

PNA	Sequence[a]	ε_{260} ($M^{-1}cm^{-1}$)	Calculated mass	Observed mass
15	CGATCAATAACTAGCKK	15.78 x 10^4	4311.31 $[M]^+$	4311.41
15X	CGATCAA**14a**AACTAGCKK	15.94 x 10^4	4429.46 $[M]^+$	4429.47
15Y	CGATCAA**14b**AACTAGCKK	16.12 x 10^4	4414.41 $[M+H]^+$	4414.10
16	CGATCATTTACTAGCKK	14.76 x 10^4	4293.28 $[M]^+$	4293.43
16X	CGATCAT**14a**TACTAGCKK	14.92 x 10^4	4411.43 $[M]^+$	4411.97
16Y	CGATCAT**14b**TACTAGCKK	15.09 x 10^4	4395.37 $[M]^+$	4395.38
17	CGATCAGTGACTAGCKK	15.40 x 10^4	4344.32 $[M+H]^+$	4344.67
17X	CGATCAG**14a**GACTAGCKK	15.54 x 10^4	4461.46 $[M]^+$	4461.85
17Y	CGATCAG**14b**GACTAGCKK	15.74 x 10^4	4446.33 $[M+H]^+$	4446.39
18	CGATCACTCACTAGCKK	14.36 x 10^4	4263.26 $[M]^+$	4263.27
18X	CGATCAC**14a**CACTAGCKK	14.52 x 10^4	4382.42 $[M+H]^+$	4382.19
18Y	CGATCAC**14b**CACTAGCKK	14.72 x 10^4	4365.35 $[M]^+$	4365.89

[a]PNA sequences are written from N to C terminus.

2.2.2.4 Circular dichroism and thermal melting analysis of PNA-DNA duplexes

The introduction of benzothiophene and benzofuran modifications can potentially affect the native structure and the hybridization efficiency of PNA oligomer, and hence, the observed

fluorescence properties may not be a true reflection of the intact duplexes. A series of PNA-DNA heteroduplexes were assembled by annealing control unmodified and fluorescently modified PNA oligomers with complementary DNA ONs (Figure 10B). The duplexes were designed in such a fashion that the emissive base was placed opposite to its complementary base, mismatched bases and abasic site. UV-thermal denaturation and circular dichroism (CD) analyses of unmodified and modified PNA-DNA duplexes indicate that benzothiophene and benzofuran modifications marginally affect the structure and stability of duplexes (Figure 11 and Figure 12, Table 5). In addition, UV-thermal denaturation study showed that both the modification slightly, destabilizes the matched duplexes and stabilizes the mismatched duplexes (Table 5). Notably, the modified PNA oligomers formed a stable PNA-DNA hybrid at room temperature. Therefore, the observed fluorescence properties will be a true indication of intact duplex, which will be further useful for devising hybridization assays for the detection of clinically important nucleic acids at physiological conditions.

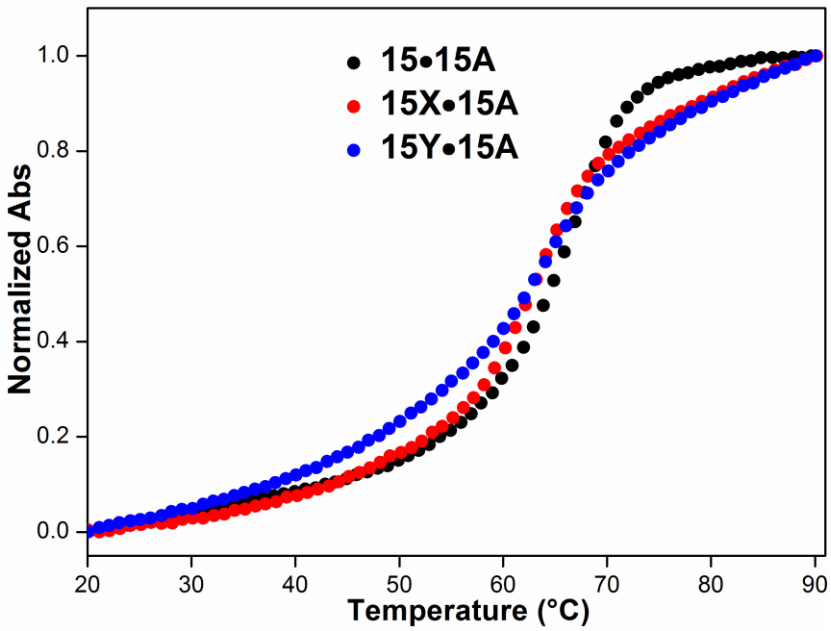

Figure 11. Representative UV-thermal melting profile (1.0 µM) of control unmodified (**15•15A**), benzothiophene-modified (**15X•8A**) and benzofuran-modified (**15Y•8A**) PNA-DNA duplexes in 10 mM phosphate buffer (pH 7.1, 100 mM NaCl, 0.1 mM EDTA). For T_m values see Table 5.[15]

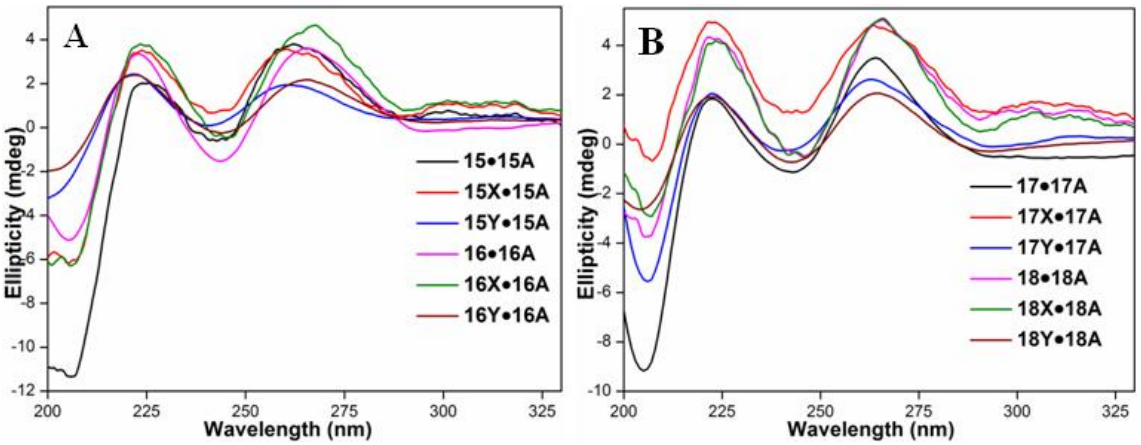

Figure 12. CD spectra (5.0 μM) of control unmodified and fluorescently modified duplexes in 10 mM phosphate buffer (pH 7.1, 100 mM NaCl, 0.1 mM EDTA). (**A**) **15•15A**, **15X•15A**, **15Y•15A, 16•16A**, **16X•16A**, **16Y•16A**. (**B**) **17•17A**, **17X•17A**, **17Y•17A, 18•18A**, **18X•18A**, **18Y•18A**.[15]

Table 5. T_m values of control and modified PNA-DNA duplexes

Control duplex	T_m (°C)	Duplex made of **14a**	T_m (°C)	Duplex made of **14b**	T_m (°C)
15•15A	66.8 ± 0.4	**15X•15A**	62.5 ± 0.8	**15Y•15A**	63.6 ± 0.5
15•15T	59.3 ± 0.9	**15X•15T**	59.1 ± 0.5	**15Y•15T**	58.6 ± 0.6
15•15G	57.4 ± 0.5	**15X•15G**	58.6 ± 0.6	**15Y•15G**	58.3 ± 1.0
15•15C	53.4 ± 0.7	**15X•15C**	59.6 ± 0.9	**15Y•15C**	58.3 ± 0.9
16•16A	62.3 ± 0.5	**16X•16A**	61.3 ± 0.5	**16Y•16A**	62.6 ± 0.5
16•16T	56.6 ± 1.0	**16X•16T**	57.3 ± 1.1	**16Y•16T**	58.0 ± 0.6
16•16G	52.7 ± 0.4	**16X•16G**	54.6 ± 0.6	**16Y•16G**	54.0 ± 0.7
16•16C	52.4 ± 0.7	**16X•16C**	54.1 ± 0.5	**16Y•16C**	55.1 ± 1.1
17•17A	74.6 ± 1.1	**17X•17A**	70.4 ± 0.5	**17Y•17A**	73.4 ± 0.5
17•17T	65.4 ± 1.0	**17X•17T**	66.3 ± 0.5	**17Y•17T**	66.2 ± 0.5
17•17G	65.6 ± 0.3	**17X•17G**	67.5 ± 0.6	**17Y•17G**	67.1 ± 0.5
17•17C	62.6 ± 0.8	**17X•17C**	67.8 ± 0.7	**17Y•17C**	66.1 ± 0.4
18•18A	70.1 ± 0.5	**18X•18A**	68.0 ± 0.9	**18Y•18A**	69.0 ± 0.5
18•18T	61.5 ± 0.5	**18X•18T**	62.6 ± 0.6	**18Y•18T**	63.3 ± 0.8
18•18G	62.6 ± 0.5	**18X•18G**	62.9 ± 0.7	**18Y•18G**	63.3 ± 0.8
18•18C	57.8 ± 0.7	**18X•18C**	62.3 ± 0.5	**18Y•18C**	62.1 ± 0.4

2.2.2.5 Photophysical properties of PNA oligomers containing fluorescent base analogues 14a and 14b

Numerous studies have shown that the photophysical behaviour of fluorescent base analogues incorporated into ONs is greatly influenced by a variety of mechanisms involving

neighbouring bases, which include stacking, collisional and H-bonding interactions, rigidification-derigidification of the fluorophore and electron transfer process between adjacent bases and the fluorophore.[17–20] Initially, we studied the impact of flanking bases on the fluorescence properties of emissive PNA analogues by performing steady state fluorescence of emissive PNA analogues (**14a** and **14b**) and fluorescent PNA oligomers **15X**–**18X** (contained **14a**) and **15Y**–**18Y** (contained **14b**). Benzothiophene-modified single stranded PNA oligomers **15X**, **16X** and **18X** in which **14a** is flanked between A, T and C residues, respectively, displayed significant enhancement in fluorescence intensity and slightly blue-shifted emission maximum as compared to free monomer **14a** (Figure 13A). PNA **17X** in which the modification is flanked by G residues exhibited a profile similar to the free PNA base **14a**. However, benzofuran-modified single stranded PNA oligomers **15Y**, **16Y** and **18Y** showed 3–6 fold quenching in fluorescence intensity with slight blue-shift in emission maximum as compared to free PNA base **14b** (Figure 13B). Modified base placed between G-residues in PNA **17Y** exhibited dramatic quenching in fluorescence intensity. It is well documented in literature that among nucleobases, guanine quenches the fluorescence of many fluorophores, especially when placed in the flanking position.[19]

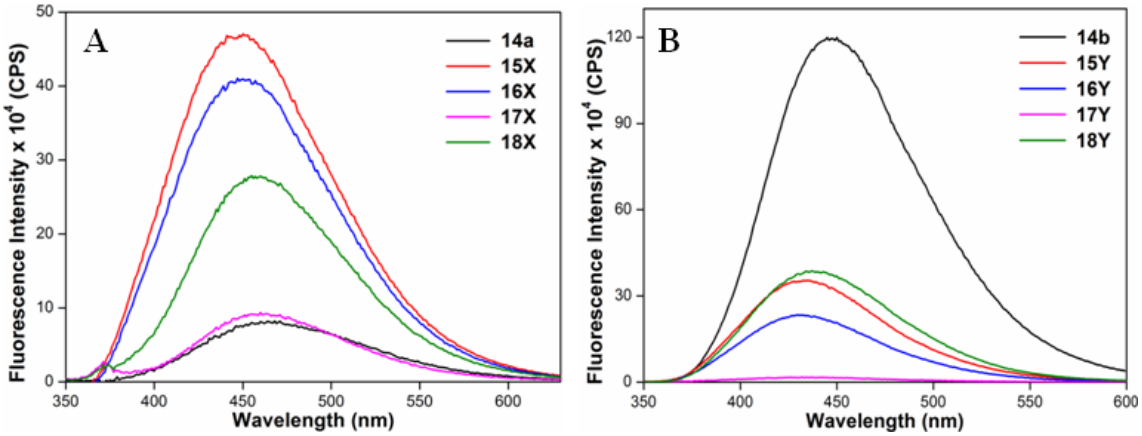

Figure 13. (**A**) Emission spectra (0.5 µM) of PNA monomer **14a** and PNA oligomers **15X**–**18X**. Excitation and emission slit widths were kept at 5 and 7 nm, respectively. (**B**) Emission spectra (0.5 µM) of PNA monomer **14b** and PNA oligomers **15Y**–**18Y**. Excitation and emission slit widths were kept at 3 and 5 nm, respectively. All Samples were excited at 330 nm.

Next, the effect of base pair substitution was studied by assembling a series of PNA-DNA duplexes constructed by hybridizing PNA **15X**–**18X** and **15Y**–**18Y** with complementary and mismatched DNA ONs (Figure 10B). For example, while hybridization of PNA **15X** or **15Y** with DNA ON **15A** would place the respective modified base analogue opposite to its complementary base dA, hybridization with ONs **15T**, **15G** and **15C** would place the analogues opposite to mismatched bases dT, dG and dC, respectively.

Benzothiophene-modified PNA base **14a** flanked by A residues (PNA **15X**) and paired with complementary and mismatched bases in PNA-DNA duplexes displayed substantial enhancement in fluorescence intensity (3–4 fold) as compared to single stranded PNA **15X** (Figure 14A). PNA oligomer **15Y** containing benzofuran-modified PNA base **14b**, when hybridized to complementary and mismatched DNA ONs, also showed enhancement in fluorescence intensity (2–5 fold) as compared to PNA **15Y** (Figure 14B). Similarly, PNA-DNA duplexes made of PNA **16X** and **16Y** (modification flanked by T residues) exhibited considerable enhancement in intensity as compared to respective PNA oligomers (Figure 15). Although **14a** and **14b** flanked by G residues and placed opposite to different bases in duplexes made of PNA **17X** and **17Y** exhibited different fluorescence intensity, the overall intensity was very low (Figure 16). In all the above duplexes along with enhancement in fluorescence intensity small differences in emission maximum were observed.

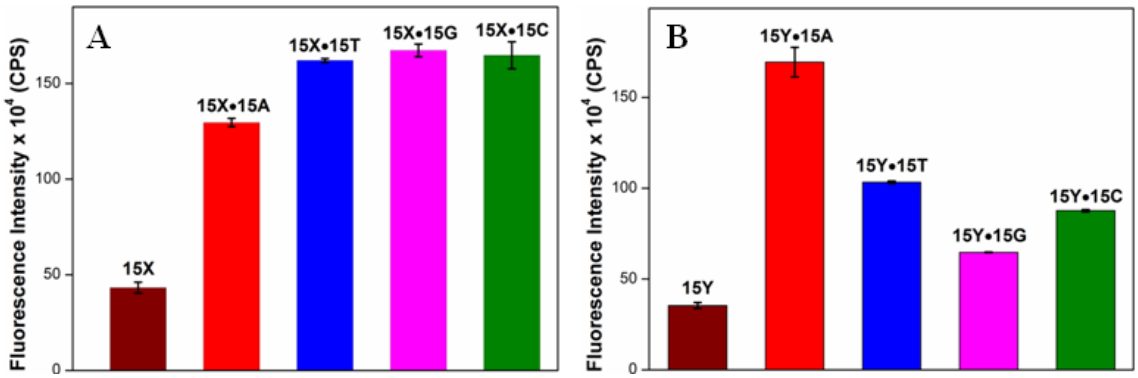

Figure 14. (**A**) Fluorescence intensity (0.5 µM) of PNA oligomer **15X** and its duplexes at respective emission maximum. Excitation and emission slit widths were kept at 5 nm and 7 nm, respectively. (**B**) Fluorescence intensity (0.5 µM) of PNA oligomer **15Y** and its duplexes at respective emission maximum. Excitation and emission slit widths were kept at 3 nm and 5 nm, respectively. All samples were excited at 330 nm.

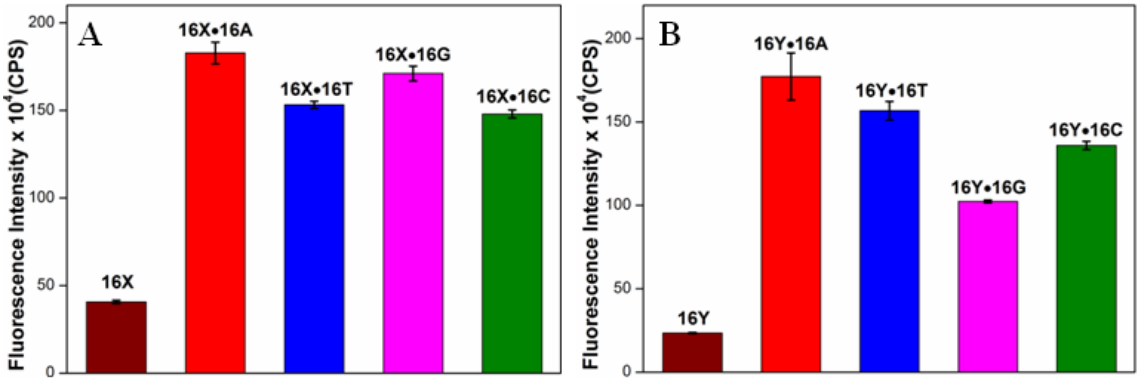

Figure 15. (**A**) Fluorescence intensity (0.5 µM) of PNA oligomer **16X** and its duplexes at respective emission maximum. Excitation and emission slit widths were kept at 5 nm and 7 nm, respectively. (**B**) Fluorescence intensity (0.5 µM) of PNA oligomer **16Y** and its duplexes at respective emission maximum. Excitation and emission slit widths were kept at 3 nm and 5 nm, respectively. All samples were excited at 330 nm.

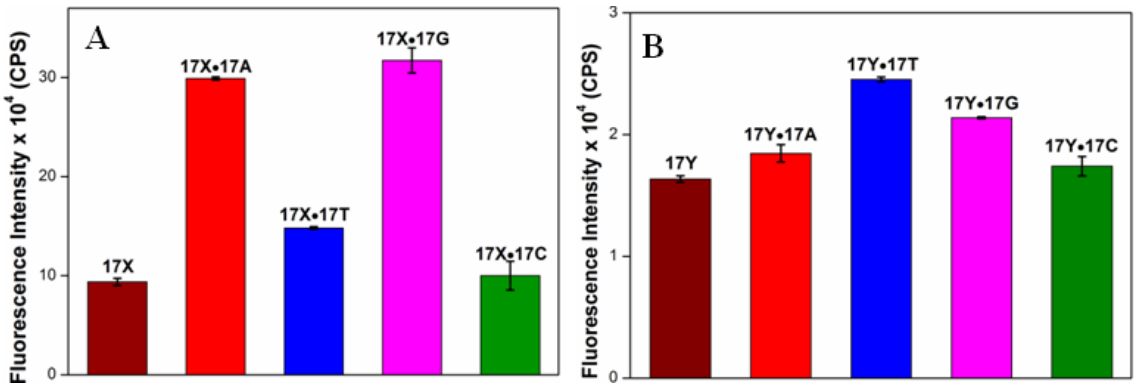

Figure 16. (**A**) Fluorescence intensity (0.5 µM) of PNA oligomer **17X** and its duplexes at respective emission maximum. Excitation and emission slit widths were kept at 5 nm and 7 nm, respectively. (**B**) Fluorescence intensity (0.5 µM) of PNA oligomer **17Y** and its duplexes at respective emission maximum. Excitation and emission slit widths were kept at 3 nm and 5 nm, respectively. All samples were excited at 330 nm.

Interestingly, duplex **18X•18A** in which **14a** is flanked by C residues and present opposite to its complementary base dA displayed significantly higher fluorescence intensity (~5-fold) with no apparent change in emission maximum as compared to single stranded PNA **18X** (Figure 17A). Furthermore, when **14a** was placed opposite to mismatched bases dT, dG and dC in duplexes **18X•18T**, **18X•18G**, **18X•18C**, respectively, a profile similar to that of PNA **18X** with no enhancement in fluorescence intensity was observed. Although benzofuran-modified uracil analogue **14b** base paired with dA in duplex **18Y•18A** showed enhancement in fluorescence intensity as compared to PNA **18Y**, the fold increase (~2-fold) was not substantial as compared to benzothiophene-modified uracil analogue **14a** in the same environment (compare Figure 17A and Figure 17B). Moreover, **14b** placed opposite to mismatched bases in duplexes **18Y•18T**, **18Y•18G**, **18Y•18C** exhibited lower intensity as compared to PNA **18Y**. This observation indicate that benzothiophene-modified PNA base **14a**, when flanked by C residues, selectively reports the presence of a complementary nucleobase (dA) in a GAG sequence with appreciable enhancement in fluorescence intensity. Although the exact morphology of the fluorescent nucleobase **14a** in the matched and mismatched PNA-DNA duplexes is unknown, we believe that the observed selectivity for the matched base dA can be possibly due to the following reasons. In the PNA-DNA (**18X•18A**) duplex benzothiophene-modification attached at 5-position of uracil is extrahelical and projected towards major groove because of effective H-bonding with dA. Therefore, it experiences less stacking interaction and also located away from guanosine residues of ON **18A**, which resulted into higher fluorescence intensity for **18X•18A** duplex. However, due to the absence of H-bonding in mismatched PNA-DNA duplexes (**18X•18T, 18X•18G** and

18X•18C), benzothiophene-modification could be intrahelical and closer to guanosine residues of ONs **18T**, **18G** and **18C**. Subsequently, the benzothiophene-modification experiences the stacking interaction from neighbouring guanosine residues and resulted into significantly lower fluorescence intensity. This observation was further supported by T_m values (Table 5), where the modified mismatched PNA-DNA duplexes displayed slightly higher T_m values as compared to corresponding control unmodified mismatched PNA-DNA duplexes. In general, the distinct fluorescence profile exhibited by emissive analogues in different nucleobase environment could be possibly due to the combined effect of π–π stacking and electron transfer process between the neighboring bases and emissive PNA base, and rigidification of emissive PNA base.[17-19,26]

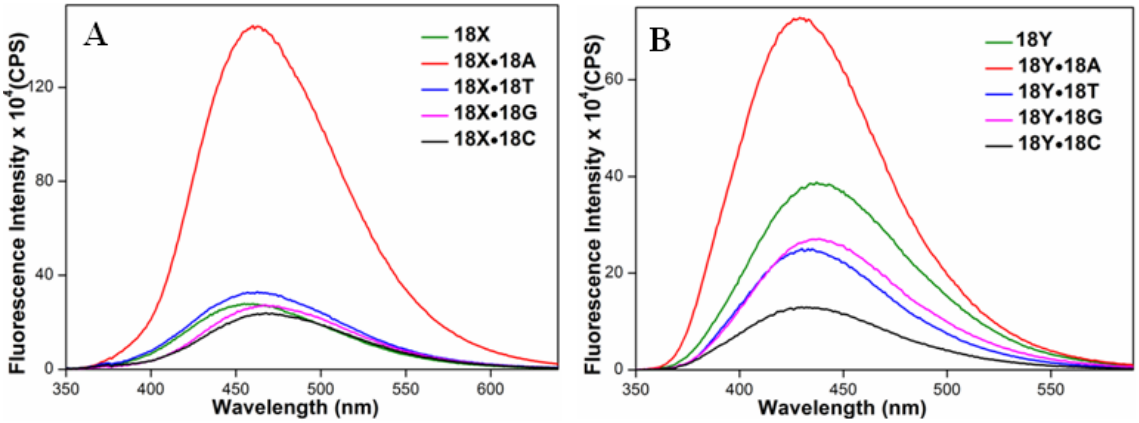

Figure 17. (**A**) Emission spectra (0.5 µM) of PNA **18X** and PNA-DNA duplexes formed by hybridizing **18X** with DNA ONs. Excitations and emission slit widths were kept at 5 and 7 nm, respectively. (**B**) Emission spectra (0.5 µM) of PNA **18Y** and PNA-DNA duplexes formed by hybridizing **18Y** with DNA ONs. Excitation and emission slit widths were kept at 3 and 5 nm, respectively. All PNA oligomers and duplexes were excited at 330 nm.

2.3 Conclusion

In conclusion, we have synthesized and systematically compared the photophysical properties of the full set of benzofuran-conjugated ribonucleoside analogues. In particular, BFU analogue showed probe-like fluorescence properties as compared to remaining benzofuran-conjugated ribonucleoside analogues, which essentially laid the foundation for the design of emissive benzofuran and benzothiophene-modified PNA probes. 5-benzothiophene and 5-benzofuran conjugated uracil PNA analogues (**14a** and **14b**) were synthesized and incorporated into PNA oligomers. These PNA analogues displayed emission maxima in the visible region, high conformational sensitivity and moderate quantum yields. Moreover, when incorporated into PNA oligomers and hybridized to complementary ONs, both the analogues displayed significant enhancement in fluorescence intensity. In particular, 5-

benzothiophene analogue **14a** showed significant enhancement in fluorescence intensity, when hybridized with the perfect complementary ON (**18A**) as compared to mismatched duplexes as well as single strand PNA **18X**. These interesting properties of emissive analogues **14a** and **14b** could be judicially utilized to develop hybridization assays to target and detect therapeutically relevant nucleic acid motifs.

2.4 Experimental Section

2.4.1 Materials

Chloroacetyl chloride, di-*t*-butyl dicarbonate, ethane-1,2-diamine, ethyl bromoacetate, TFA and silica gel (100-200 mesh) were purchased from Spectrochem India. Dry DMF and dry dichloromethane were purchased from Rankem India. Acetic anhydride was purchased from Thomas Baker India. Adenosine, guanosine, benzofuran, tributyltin chloride, *N*-bromosuccinimide (NBS), 5-Iodouracil, benzo[*b*]thiophene, *bis*(triphenylphosphine)-palladium (II) chloride, pyridine, *N*-hydroxybenzotriazole (HOBt), 3-[bis(dimethylamino)methyliumyl]-3*H*-benzotriazol-1-oxide hexafluorophosphate (HBTU), *N*,*N*-diisopropylethylamine (DIPEA), 1,2-ethanedithiol, thioanisole and trifluoromethanesulfonic acid (TFMSA) were purchased from Sigma-Aldrich. Chemicals for preparing buffer solutions were obtained from Sigma-Aldrich. 8-Bromo adenosine, 8-bromo gaunosine, 2-(tri-*n*-butylstannyl) benzo[*b*]thiophene and 2-(tri-*n*-butylstannyl)benzofuran were prepared by using a method described in the literature.[17,28] Ethyl-2-(*N*-(2-((*tert*-butoxycarbonyl)amino)ethyl)-2-chloroacetamido)acetate **10** was synthesized by using method reported in the literature.[22] Boc-protected *aeg*-PNA monomers were purchased from ASM Research Chemicals. The exocyclic amino group of adenine, guanine and cytosine PNA monomers was protected with cbz (Z) group. 4-Methylbenzhydrylamine•HCl (MBHA) resin LL (100-200 mesh) and Boc-Lys(2-Cl-Z)-OH were obtained from Novabiochem. DNA ONs were purchased from Integrated DNA Technologies. All ONs were purified by polyacrylamide gel electrophoresis (PAGE) under denaturing conditions and desalted on Sep-Pak Classic C18 cartridges (Waters Corporation). Autoclaved water was used in all biochemical reactions and fluorescence measurements.

2.4.2 Instrumentation

NMR spectra were recorded on a 400 MHz Jeol ECS-400 spectrometer (^{1}H 400 MHz and ^{13}C 100 MHz) and processed in Mnova NMR software from Mestrelab Research. All mass

measurements were recorded on an Applied Biosystems 4800 Plus MALDI-TOF/TOF analyzer instrument and Water Synapt G2 High Definition mass spectrometers. Reversed-phase (RP) flash chromatography (C18 RediSepRf column) purifications were carried out using Teledyne ISCO, Combi Flash Rf. Microwave reactions were performed using CEM discover microwave synthesizer. PNA oligomers were purified by using Agilent Technologies 1260 Infinity HPLC. Absorption spectra were recorded on a Shimadzu UV-2600 spectrophotometer. UV-thermal melting analysis of duplexes was performed on a Cary 300Bio UV-Vis spectrophotometer. Steady-state fluorescence experiments were carried out in a micro fluorescence cuvette (Hellma, path length 1.0 cm) on a Fluoromax-4 and Fluorolog-3 spectrophotometers (Horibha Scientific). Time-resolved fluorescence experiments were carried out on a TCSPC instrument (Horiba JobinYvon, Fluorolog 3). All CD spectra were recorded on JASCO J-815 CD spectrometer.

2.4.3 Synthesis of fluorescent ribonucleoside analogues 3 and 4

2.4.3.1 (2R,3R,4S,5R)-2-(6-Amino-8-(benzofuran-2-yl)-9H-purin-9-yl)-5 (hydroxymethyl)tetrahydrofuran-3,4-diol 3

To a mixture of 8-bromoadenosine **5**[17] (0.20 g, 0.58 mmol, 1.0 equiv) and *bis*(triphenylphosphine)-palladium(II) chloride (0.020 g, 0.04 mmol, 0.05 equiv) in degassed anhydrous DMF (6 ml) was added 2-(tri-n-butylstannyl)benzofuran (0.353 g, 0.87 mmol, 1.5 equiv). The reaction mixture was heated at 75 °C using microwave for 25 min, cooled to RT and filtered through celite pad. The celite pad was washed with DMF (2 × 15 ml) and solvent was evaporated using rota evaporator with high vacuum pump. Residue was purified by reversed phase column chromatography (C18 Redi*SepRf* column, CH_3CN:H_2O) to afford product **3** as white solid (0.160 g, 72%). R_f = 0.42 (CH_2Cl_2:MeOH = 8.5:1.5); ^{1}H-NMR (400 MHz, d_6-DMSO): δ = 8.19 (s, 1H), 7.84 (d, *J* = 7.6 Hz, 1H), 7.76 (bs, 2H), 7.75 (d, *J* = 8.4 Hz, 1H), 7.60 (s, 1H), 7.48-7.47 (m, 1H), 7.38 ($_{app}$t, *J* = 7.6 Hz, 1H), 6.21 (d, *J* = 6.8 Hz, 1H), 5.79 (dd, J_1 = 9.0 Hz, J_2 = 3.6 Hz, 1H), 5.52 (d, *J* = 6.4 Hz, 1H), 5.28 (d, *J* = 4.4 Hz, 1H), 5.18-5.13 (m, 1H), 4.26-4.23 (m, 1H), 4.06-4.04 (m, 1H), 3.76-3.71 (m, 1H), 3.61-3.55 (m, 1H) ppm; ^{13}C-NMR (100 MHz, d_6-DMSO): δ = 156.6, 154.6, 152.8, 149.9, 144.8, 141.2, 127.4, 126.4, 123.9, 122.3, 119.6, 111.6, 109.9, 89.5, 86.9, 71.8, 71.0, 62.2 ppm; HRMS: (*m/z*): Calculated for $C_{18}H_{18}N_5O_5$: 384.1308 $[M+H]^+$; found = 384.1308.

2.4.3.2 2-Amino-8-(benzofuran-2-yl)-9-((2R,3R,4S,5R)-3,4-dihydroxy-5-(hydroxymethyl)tetrahydrofuran-2-yl)-1,9-dihydro-6H-purin-6-one 4

To a mixture of 8-bromoguanosine **6**[17] (0.60 g, 1.65 mmol, 1.0 equiv) and *bis*(triphenylphosphine)-palladium(II) chloride (0.057 g, 0.081 mmol, 0.05 equiv) in degassed anhydrous DMF (6 ml) was added 2-(tri-n-butylstannyl)benzofuran (1.01 g, 2.48 mmol, 1.5 equiv). The reaction mixture was heated at 75 °C using microwave for 25 min, cooled to RT and filtered through celite pad. The celite pad was washed with DMF (2 × 15 ml) and solvent was evaporated using rota evaporator under reduced pressure. The resulting residue was purified by reversed phase column chromatography (C18 Redi*SepRf* column, CH_3CN:H_2O) to afford product **6** as white solid (0.130 g, 20%). R_f = 0.76 (CH_2Cl_2:MeOH = 8:2); ^{1}H-NMR (400 MHz, d_6-DMSO): δ = 10.87 (s, 1H), 7.77 (d, *J* = 7.2 Hz, 1H), 7.68 (d, *J* = 8.4 Hz, 1H), 7.45-7.40 (m, 2H), 7.36-7.32 (m, 1H), 6.54 (bs, 2H), 6.03 (d, *J* = 6.4 Hz, 1H), 5.40 (d, *J* = 6.4 Hz, 1H), 5.06-4.99 (m, 3H), 4.16 (dd, J_1 = 9.2 Hz, J_2 = 5.2 Hz, 1H), 3.90 (dd, J_1 = 9.2 Hz, J_2 = 4.8 Hz, 1H), 3.73-3.68 (m, 1H), 3.60-3.54 (m, 1H) ppm; ^{13}C-NMR (100 MHz, d_6-DMSO): δ = 157.0, 154.8, 154.0, 152.7, 146.2, 138.3, 128.1, 126.3, 124.2, 122.4, 118.3, 112.0, 108.6, 89.6, 86.4, 71.2, 70.9, 62.5 ppm; HRMS: (*m/z*): Calculated for $C_{18}H_{18}N_5O_6$: 400.1257 $[M+H]^+$; found = 400.1274.

2.4.4 Synthesis of fluorescent PNA monomers

The amide group in the *aeg* backbone of the PNA monomers is known to give two rotamers with different chemical shifts.[29] **11**–**14**(**a**-**b**) also gave two rotamers with different chemical shifts, and the rotamers have been indicated as major (ma.) and minor (mi.).

2.4.4.1 Ethyl-2-(*N*-(2-((*tert*-butoxycarbonyl)amino)ethyl)-2-(5-iodo-2,4-dioxo-3,4-dihydropyrimidin-1(*2H*)-yl)acetamido)acetate 11

To a solution of ethyl-2-(*N*-(2-((*tert*-butoxycarbonyl)amino)ethyl)-2-chloroacetamido)acetate **10**[22] (2.00 g, 6.20 mmol, 1.0 equiv.) in DMF (20 mL) was added potassium carbonate (1.88 g, 13.63 mmol, 2.2 equiv.) and 5-iodouracil (1.62 g, 6.82 mmol, 1.1 equiv.). The reaction mixture was stirred for 12 h at room temperature (RT). Water (100 mL) was added and the product was extracted using EtOAc (2 × 100 mL). The organic layer was evaporated and residue was purified by silica gel column chromatography to afford the product **11** as a white solid (1.60 g, 49%). R_f = 0.29 (petroleum ether:EtOAc = 30:70); ^{1}H-NMR (400 MHz, $CDCl_3$): δ = 9.66 (minor (mi.)) and 9.60 (major (ma.) (br, 1H), 7.65 (mi.) and 7.59 (ma.)

(s,1H), 5.65 (ma.) and 5.10 (mi.) (t, *J* = 6.0 Hz, 1H), 4.63 (ma.) and 4.48 (mi.) (s, 2H), 4.26–4.05 (m, 4H), 3.51 ($_{app}$t, *J* = 5.6 Hz, 2H), 3.34–3.24 (m, 2H), 1.44 (ma.) and 1.42 (mi.) (s, 9H), 1.31 (mi.) and 1.27 (ma.) (t, *J* = 7.1 Hz, 3H) ppm; ^{13}C-NMR (100 MHz, $CDCl_3$): δ = 169.7 (ma.) and 169.4 (mi.), 167.4 (mi.) and 167.1 (ma.), 160.8 (mi.) and 160.8 (ma.), 156.3, 150.9, 149.6, 80.2, 68.3 (ma.) and 68.2 (mi.), 62.5 (mi.) and 61.9 (ma.), 49.3, 48.9, 48.4, 38.8, 28.6 (ma.) and 28.5 (mi.), 14.2 (mi.) and 14.2 (ma.) ppm; HRMS: (*m/z*): Calc. for $C_{17}H_{25}IN_4O_7Na$: 547.0666 $[M+Na]^+$; found: 547.0666.

2.4.4.2 General procedure for synthesis of fluorescent PNA esters 12(a–b)

To a suspension of compound **11** (1.0 equiv.) and bis(triphenylphosphine)-palladium(II) chloride (0.05 equiv.) in degassed anhydrous dioxane (30 mL per g of **11**) was added 2-(tri-n-butylstannyl) benzo[*b*]thiophene or 2-(tri-n-butylstannyl)benzofuran [47] (1.5 equiv.). The reaction mixture was heated at 75 °C for 3 h, and filtered through celite pad. Celite pad was washed with hot dioxane. Dioxane was evaporated and the residue was purified by silica gel column chromatography to afford the desired products **12**(**a**–**b**).

Ethyl-2-(2-(5-(benzothiophene-2-yl)-2,4-dioxo-3,4-dihydropyrimidin-1(*2H*)-yl)-*N*-(2-((*tert*-butoxycarbonyl)amino)ethyl)acetamido)acetate 12a

Faint brown solid, 48% yield. R_f = 0.26 (petroleum ether:EtOAc = 3:7); ^{1}H-NMR (400 MHz, d_6-DMSO): δ = 11.83 (br, 1H), 8.29 (ma.) and 8.25 (mi.) (s, 1H), 7.92 (d, *J* = 7.6 Hz, 1H), 7.79 (d, *J* = 6.4 Hz, 2H), 7.37–7.29 (m, 2H), 6.98 (ma.) and 6.77 (mi.) (t, *J* = 5.2 Hz, 1H), 4.86 (ma.) and 4.68 (mi.) (s, 2H), 4.35–4.06 (m, 4H), 3.47–3.37 (m, 2H), 3.27–3.20 (ma.) and 3.08–3.03 (mi.) (m, 2H), 1.39 (ma.) and 1.36 (mi.) (s, 9H), 1.26 (mi.) and 1.18 (ma.) (t, *J* = 7.0 Hz, 3H) ppm; ^{13}C-NMR (100 MHz, d_6-DMSO): δ = 169.3 (mi.) and 169.0 (ma.), 167.5 (mi.) and 167.2 (ma.), 160.8, 155.9 (ma.) and 155.7 (mi.), 152.9, 149.9, 148.9, 142.6, 131.6 and 131.5, 128.9 (ma.) and 128.8 (mi.), 124.5, 123.2, 121.2, 110.4, 104.0, 78.2 (ma.) and 77.8 (mi.), 61.3 (mi.) and 60.6 (ma.), 48.3, 47.9, 47.0, 38.1, 28.2, 14.1 ppm; HRMS: Calcd. for $C_{25}H_{30}N_4O_7SNa$: 553.1733 $[M+Na]^+$; found: 553.1727.

Ethyl-2-(2-(5-(benzofuran-2-yl)-2,4-dioxo-3,4-dihydropyrimidin-1(*2H*)-yl)-*N*-(2-((*tert*-butoxycarbonyl)amino)ethyl)acetamido)acetate 12b

White solid, 42% yield. R_f = 0.63 (petroleum ether:EtOAc = 10:90); ^{1}H-NMR (400 MHz, d_6-DMSO): δ = 11.85 (br, 1H), 8.21 (ma.) and 8.15 (mi.) (s, 1H), 7.64 (d, *J* = 7.6 Hz, 1H), 7.49 (d, *J* = 7.6 Hz, 1H), 7.38 (s, 1H), 7.30–7.21 (m, 2H), 6.99 (ma.) and 6.77 (mi.) (t, *J* = 5.2 Hz,

1H), 4.93 (ma.) and 4.75 (mi.) (s, 2H), 4.33–4.07 (m, 4H), 3.46–3.37 (m, 2H), 3.23–3.04 (m, 2H), 1.40 (ma.) and 1.36 (mi.) (s, 9H), 1.27 (mi.) and 1.18 (ma.) (t, J = 7.0 Hz, 3H) ppm; ^{13}C-NMR (100 MHz, d_6-DMSO): δ = 169.0, 167.2, 160.7, 155.8, 152.9, 149.9, 148.9, 142.6, 131.5, 128.8, 124.5, 123.2, 121.2, 110.4, 103.9, 78.1, 60.6, 48.3, 47.9, 47.0, 38.1, 28.2, 14.0 ppm; HRMS: (*m/z*): Calc. for $C_{25}H_{30}N_4O_8Na$: 537.1961 $[M+Na]^+$; found: 537.1960.

2.4.4.3 General procedure for synthesis of fluorescent PNA acid 13(a–b)

To a solution of compound **12**(**a**–**b**) (1.0 equiv.) in methanol (40 mL per g **12**(**a**–**b**)) was added lithium hydroxide (3% solution in H_2O, 10.0 mL per g of **12**(**a**–**b**)) and the reaction mixture was stirred for 3 h at RT. Reaction mixture was evaporated to dryness, and residue was dissolved in water (minimum amount) and washed with diethyl ether. To the aqueous extract was added saturated $KHSO_4$ solution to adjust the pH to ~4. The product was then extracted in EtOAc and solvent was evaporated to afford the products **13**(**a**–**b**).

2-(2-(5-(Benzothiophene-2-yl)-2,4-dioxo-3,4-dihydropyrimidin-1(*2H*)-yl)-*N*-(2-((*tert* butoxycarbonyl)amino)ethyl)acetamido)acetic acid 13a

The residue was redissolved in DMF (1.5 mL) and purified by C18 RP column chromatography (C18 Redi *SepRf*, 0–100% methanol in 50 min) to afford the product **13a** as a faint brown solid, 91% yield. R_f = 0.26 (CH_2Cl_2:MeOH = 8:2); ^{1}H-NMR (400 MHz, d_6-DMSO): δ = 11.83 (ma.) and 11.80 (mi.) (br, 1H), 8.30 (ma.) and 8.25 (mi.) (s, 1 H), 7.93–7.90 (m, 1H), 7.80–7.77 (m, 2H), 7.36–7.28 (m, 2H), 6.99 (ma.) and 6.84 (mi.) ($_{app}$t, J = 5.0 Hz, 1H), 4.85 (ma.) and 4.66 (mi.) (s, 2H), 4.09 (mi.) and 3.99 (ma.) (s, 2H), 3.44–3.41 (ma.) and 3.35–3.32 (mi) (m, 2H), 3.22–3.17 (ma.) and 3.05–3.03 (mi.) (m, 2H), 1.39 (ma.) and 1.35 (mi.) (s, 9H) ppm; ^{13}C-NMR (100 MHz, d_6-DMSO): δ = 170.5, 167.4 (mi.) and 166.9 (ma.), 161.8, 155.8 (ma.) and 155.6 (mi.), 149.9, 143.7, 139.1, 138.7 (mi.) and 138.6 (ma.), 135.0, 124.5 (ma.) and 124.4 (m.), 124.1 (ma.) and 124.0 (mi.), 123.1, 122.0, 119.2 (ma.) and 119.1 (mi.), 107.1 and 107.0, 78.1 (ma.) and 77.7 (mi.), 48.4 (mi.) and 48.3 (ma.), 47.9, 47.2, 46.9, 38.1 (ma.) and 37.6 (mi.), 28.2 ppm (Note: trace amount of DMF impurity was present); HRMS: Calcd. for $C_{23}H_{26}N_4O_7SNa$: 525.1420 $[M+Na]^+$; found: 525.1422.

2-(2-(5-(Benzofuran-2-yl)-2,4-dioxo-3,4-dihydropyrimidin-1(*2H*)-yl)-*N*-(2-((*tert* butoxycarbonyl)amino)ethyl)acetamido)acetic acid 13b

White solid, 93% yield. R_f = 0.26 (CH_2Cl_2:MeOH = 70:30); ^{1}H-NMR (400 MHz, d_6-DMSO): δ = 11.83 (ma.) and 11.81 (mi.) (br, 1H), 8.22 (ma.) and 8.14 (mi.) (s, 1 H), 7.64 (d, J = 6.0

Hz, 1H), 7.51–7.49 (m, 1H), 7.37 (s, 1H), 7.30–7.22 (m, 2H), 6.97 (ma.) and 6.76 (mi.), 4.91 (ma.) and 4.73 (mi.) (s, 2H), 4.20 (mi.) and 4.00 (ma.) (s, 2H), 3.42 ($_{app}$t, J = 5.0 Hz, 2H), 3.22–3.17 (ma.) and 3.06–3.03 (mi.) (m, 2H), 1.40 (ma.) and 1.36 (mi.) (s, 9H) ppm; ^{13}C-NMR (100 MHz, d_6-DMSO): δ = 170.8 (ma.) and 170.5 (mi.), 167.4 (mi.) and 167.0 (ma.), 160.7, 155.8 (ma.) and 155.6 (mi.), 152.9, 149.9, 148.9, 142.7, 128.9, 124.5, 123.2, 121.2, 110.4, 103.9, 78.1, 48.3, 47.7, 46.9, 38.0, 28.2 ppm; HRMS: (*m/z*): Calc. for $C_{23}H_{26}N_4O_8Na$: 509.1648 $[M+Na]^+$; found: 509.1648.

2.4.4.4 General procedure for synthesis of fluorescent PNA acid 14(a–b)

A solution of compound **13(a–b)** (1.0 equiv.) in 50% TFA in CH_2Cl_2 (40 mL per g of **13**(**a–b**)) was stirred for 2 h at RT. Reaction mixture was evaporated and the residue was purified by reverse-phase (RP) column chromatography (C18 Redi *SepRf*, 0–50% acetonitrile in 50 min) to afford products **14**(**a–b**).

2-(*N*-(2-Aminoethyl)-2-(5-(benzothiophene-2-yl)-2,4-dioxo-3,4-dihydropyrimidin-1(*2H*)-yl)acetamido)acetic acid 14a

Off-white solid, 88% yield. R_f = 0.52 (CH_2Cl_2: MeOH = 3:7); ^{1}H-NMR (400 MHz, d_6-DMSO): δ = 8.40 (mi.) and 8.35 (mi.) and 8.31 (ma.) (s, 1H), 7.91 (d, J = 7.6 Hz, 1H), 7.80 (ma.) and 7.77 (mi.) (s, 2H), 7.36–7.27 (m, 2H), 4.89 (mi.) and 4.63 (ma.) (s, 2H), 3.85–3.61 (m, 4H), 3.06–2.88 (m, 2H) ppm; ^{13}C-NMR (100 MHz, d_6-DMSO): δ = 168.2, 167.2, 161.9, 150.0, 143.9, 139.1, 138.7, 135.0, 124.5, 124.0 123.1, 122.0, 119.2 (ma.) and 119.1 (mi.), 107.1 (ma.) and 106.9 (mi.), 50.0 (ma.) and 49.9 (mi.), 46.5 (mi.) and 46.2 (ma.), 36.7, 35.9 ppm; HRMS: Calcd. for $C_{18}H_{19}N_4O_5S$: 403.1076 $[M+H]^+$; found: 403.1078. λ_{max} (H_2O) = 273 nm and 318 nm; ε_{260} = 11970 $M^{-1}cm^{-1}$, ε_{322} = 12170 $M^{-1}cm^{-1}$.

2-(*N*-(2-Aminoethyl)-2-(5-(benzofuran-2-yl)-2,4-dioxo-3,4-dihydropyrimidin-1(*2H*)-yl)acetamido)acetic acid 14b

White solid, 64% yield. R_f = 0.44 (CH_2Cl_2:MeOH = 30:70); ^{1}H-NMR (400 MHz, d_6-DMSO): δ = 8.30 (mi.) and 8.18 (ma.) (s, 1H), 8.18 (br, 1H), 7.64 (d, J = 7.6 Hz, 1H), 7.51 (d, J = 8.0 Hz, 1H), 7.38–7.22 (m, 3H), 4.94 (mi.) and 4.73 (ma.) (s, 2H), 4.06 (ma.) and 3.98 (mi.) (br, 2H), 3.66 (mi.) and 3.58 (ma.) (br, 2H), 3.13 (mi.) and 2.98 (ma.) (br, 2H) ppm; ^{13}C-NMR (100 MHz, d_6-DMSO): δ =168.4, 167.2, 160.7(mi.) and 160.7 (ma.), 152.9, 150.0 (mi.) and 149.9 (ma.), 148.9, 142.7, 128.8, 124.5, 123.2, 121.2, 110.4, 104.0 (ma.) and 103.8 (mi.),

48.4, 45.2, 42.5 36.8 ppm; HRMS: (*m/z*): Calc. for $C_{18}H_{19}N_4O_6$: 387.1305 $[M+H]^+$; found: 387.1308. $\lambda_{max}(H_2O)$ = 263, 274 nm and 322 nm; ε_{260}= 12210 $M^{-1}cm^{-1}$, ε_{322}= 14340 $M^{-1}cm^{-1}$.

2.4.5 Photophysical characterization of emissive ribonucleoside analogues 3 and 4

UV-Vis absorption: Samples of **3** and **4** (25 μM) were prepared in solvents of different polarity such as water, methanol, acetonitrile and dioxane. Solutions of **3** and **6** contained 2.5% DMSO.

Steady-state fluorescence: Emission spectra of **3** and **4** (5 μM) in water, methanol, acetonitrile and dioxane were obtained by exciting the samples at respective longest absorption maximum (see Table 1) by maintaining the excitation and emission slit widths at 2 and 3 nm, respectively. All solutions contained 0.5% DMSO.

Time-resolved fluorescence measurements: Excited-state lifetimes of emissive ribonucleosides **3** and **4** in different solvents were determined using TCSPC fluorescence spectrophotometer (Horiba Jobin Yvon). Ribonucleoside analogues were excited using 339 nm LED source (IBH, UK, NanoLED) and fluorescence signal at respective emission maximum was collected. Lifetime measurements were performed in duplicate, and decay profiles were analyzed using IBH DAS6 analysis software. Fluorescence intensity decay kinetics of ribonucleosides in various solvents was found to be monoexponential with χ^2 (goodness of fit) values very close to unity.

Radiative and nonradiative decay rate constants: Radiative (k_r) and nonradiative decay (k_{nr}) rate constants of emissive ribonucleosides in different solvents were determined from their respective quantum yield (Φ) and average lifetime (τ) using following equations.

$$k_r = \Phi/\tau$$

$$1/\tau = k_r + k_{nr}$$

2.4.6 Quenching Studies and Stern-Volmer plot

Fluorescence quenching of ribonucleoside analogues **3** and **4** by other nucleobases were performed by adding aliquots of concentrated nucleotide monophosphate solution (AMP, GMP, CMP, TMP, 40 mM) into ribonucleoside solution, where both solutions contained equal concentration of the ribonucleoside (5 μM). All solutions were prepared in 20 mM cacodylate buffer containing 0.5% DMSO (100 mM NaCl, 0.5 mM EDTA, pH 7.1). Stern-Volmer plot was obtained by plotting F_0/F vs. concentration of the quencher (NMPs) and was fit using the following equation.

$$F_0/F = 1 + K_{sv}[NMP] \quad (1)$$

Where F_0 and F are the fluorescence intensities in the absence and presence of quencher (NMPs) respectively, and K_{sv} is the Stern-Volmer quenching constant.

2.4.7 Photophysical characterization of PNA base analogues 14a and 14b

UV-Vis absorption: Samples of **14a** (50 µM) and **14b** (25 µM) were prepared in solvents of different polarity such as water, dioxane and their mixtures (25% dioxane, 50% dioxane, 75% dioxane in water). Solutions of **14a** and **14b** contained 5% and 2.5% DMSO, respectively.

Steady-state fluorescence: Emission spectra of **14a** and **14b** (5 µM) in water, dioxane and water-dioxane mixture were obtained by exciting the samples at respective longest absorption maximum (see Table 1) by maintaining the excitation and emission slit widths at 3 and 4 nm, respectively, for **14a** and 2 and 3 nm, respectively, for **14b**. All solutions contained 0.5% DMSO.

Time-resolved fluorescence: Excited-state lifetime of PNA base analogues **14a** and **14b** (5 µM) in various solvents were determined using TCSPC instrument (Horiba Jobin Yvon, Fluorolog-3). Analogues **14a** and **14b** were excited using a 320 nm LED source (IBH, UK, NanoLED-320L) and fluorescence signal at respective emission maximum was collected. Lifetime measurements were performed in duplicate and decay profiles were analyzed using IBH DAS6 analysis software. Fluorescence intensity decay profiles were found to be monoexponential, biexponential or triexponential with χ^2 (goodness of fit) values very close to unity.

2.4.8 Quantum yield determination for emissive ribonucleosides and PNA base analogues

The quantum yield of emissive ribonucleoside **3** and **4** and PNA base analogues **14a** and **14b** in different solvents were determined with respect to 2-aminopurine standard using the following equation.[30]

$$\Phi_{F(x)} = (A_s/A_x)\,(F_x/F_s)\,(n_x/n_s)^2\Phi_{F(s)}$$

Where s is the standard, x is ribonucleoside (**3** or **4**)/ PNA analogue (**14a** or **14b)**, A is the absorbance at excitation wavelength, F is the area under the emission curve, n is the refractive index of the solvent, and Φ_F is the quantum yield.

2.4.9 Solid phase synthesis of control and fluorescently modified PNA oligomers

All control and modified PNA oligomers were synthesized by applying standard solid phase PNA synthesis protocol[31] on MBHA resin using Boc-protected *aeg*-PNA monomers and fluorescently modified PNA base analogues **13(a–b)**. In order to enhance aqueous solubility of PNA oligomers, two lysine residue were attached at the C-terminus. The fluorescent PNA oligomers **15X**–**18X** and **15Y**–**18Y** containing modified base **14a** and **14b**, respectively were synthesized by solid phase synthesis. Respective control unmodified PNA oligomers (**15**–**18**) were also synthesized by using the same protocol to compare the impact of the modification on the stability of PNA-DNA duplex.

General procedure: In a glass sintered flask, 4-methylbenzhydrylamine•HCl (MBHA) resin (250 mg, 0.65 mmol/g) was swelled in CH_2Cl_2 (10 mL) for 12 h. Then solvent was removed and resin was treated with 50% DIPEA in CH_2Cl_2 (10 mL) for 10 min. This step was repeated two more times. The resin was then washed sequentially with CH_2Cl_2 (3 x 3 mL), DMF (3 x 3 mL) and CH_2Cl_2 (3 x 3 mL). The resin was dried under nitrogen flow for few minutes. The coupling reaction was performed in dry DMF (1.8 mL) with Boc-Lys (2-Cl-Z)-OH (36 mg, 1.0 equiv. to obtain a loading of 0.35 mmol/g) in the presence of HOBt (1.0 equiv.), HBTU (1.0 equiv.) and DIPEA (1.0 equiv.) for 7–9 h at RT. The resin was further washed with CH_2Cl_2 (3 x 3 mL), DMF (3 x 3 mL) and CH_2Cl_2 (3 x 3 mL). Next, remaining amino groups on the resin was capped with acetic anhydride (1.0 mL) in pyridine (1.0 mL) for 1 h at RT. This step was repeated two more times, and the resin was then washed with CH_2Cl_2 (3 x 3 mL), DMF (3 x 3 mL) and CH_2Cl_2 (3 x 3 mL) and dried under nitrogen flow for few minutes. The resin was treated with 50% TFA in CH_2Cl_2 (6 mL) for 15 min to remove Boc-group. This step was repeated two more times, and the resin was then washed with CH_2Cl_2 (3 x 3 mL), DMF (3 x 3 mL) and CH_2Cl_2 (3 x 3 mL). Resin was further treated with 10% DIPEA in CH_2Cl_2 (6 mL) for 10 min three times. Resin was then washed with CH_2Cl_2 (3 x 3 mL), DMF (3 x 3 mL) and CH_2Cl_2 (3 x 3 mL). The coupling reactions were performed in dry DMF (1.8 mL) with Boc-Lys(2-Cl-Z)-OH (3.0 equiv.) in the presence of HOBt (3.0 equiv.), HBTU (3.0 equiv.) and DIPEA (3.0 equiv.) for 7–9 h at RT. The resin was then washed with CH_2Cl_2 (3 x 3 mL), DMF (3 x 3 mL) and CH_2Cl_2 (3 x 3 mL). The resin was dried under nitrogen flow for few minutes.

Above lysine loaded MBHA resin (25 mg, 0.35 mmol/g) was swelled in CH_2Cl_2 (2 mL) for 2 h in glass sintered flask. The solvent was removed and resin was treated with 50% TFA in CH_2Cl_2 (3 mL) for 15 min to remove Boc-group as mentioned above. The resin was then washed with CH_2Cl_2 (3 x 3 mL), DMF (3 x 3 mL) and CH_2Cl_2 (3 x 3 mL). Resin was

further treated with 10% DIPEA in CH_2Cl_2 (6 mL) for 10 min three times. The resin was then washed with CH_2Cl_2 (3 x 3 mL), DMF (3 x 3 mL) and CH_2Cl_2 (3 x 3 mL). The coupling reaction was performed in dry DMF (0.6 mL) with appropriate Boc-protected PNA monomers (3.0 equiv.) in the presence of HOBt (3.0 equiv.), HBTU (3.0 equiv.) and DIPEA (3.0 equiv.) for 7–9 h at RT. The resin was washed again and the coupling, Boc deprotection, neutralization and washing steps were repeated in cycle as mentioned above to synthesize the desired PNA sequence.

Cleavage procedure: The dried resin (20 mg) was transferred to a glass vial and treated with thioanisole (30 μL) and ethanedithiol (12 μL) in an ice bath for 10 min. TFA (300 μL) was then added and stirred for another 10 min. Next, TFMSA (24 μL) was added to the above mixture and was stirred for 2 h at room temperature. The resin was filtered, and the filtrate was concentrated and precipitated as a white solid by adding cold diethyl ether (1 mL). The solvent was decanted and the crude product was dissolved in autoclaved water and purified by RP-HPLC.

2.4.4.10 HPLC analysis of PNA oligomers

All control and fluorescently modified PNA oligomers were purified using a Luna C18 semi-preparative RP column (5 micron, 250 × 10 mm, Phenomenex) on an Agilent Technologies 1260 Infinity HPLC system. Conditions: 0–50% B in 25 min and 50–100% B in 15 min (Mobile phase A: 5% acetonitrile in H_2O containing 0.1% TFA. Mobile phase B: 50% acetonitrile in H_2O containing 0.1% TFA). Flow rate was 2 mL/min. The chromatogram of control PNA oligomers was recorded at 260 nm and fluorescently modified PNA oligomers was recorded at 260 nm and 330 nm. Concentration of the PNA oligomers were determined by using the molar extinction coefficients of nucleobases at 260 nm (ε_A = 13700, ε_T = 8600, ε_G = 11700, ε_C = 6600, $\varepsilon_{\mathbf{14a}}$ = 11970, $\varepsilon_{\mathbf{14b}}$ = 12210 $M^{-1}cm^{-1}$).[31]

2.4.4.11 MALDI-TOF mass measurement of PNA oligomers

1 μL of a ~150 μM stock solution of PNA oligomer was combined with 2,5-dihydroxybenzoic acid (DHB) or α-cyano-4-hydroxycinnamic acid (CHCA) matrix. The samples were spotted on a plate and air dried before mass analysis.

2.4.4.12 Thermal melting and CD analysis of PNA duplexes

The PNA-DNA and PNA-RNA duplexes were assembled by heating a 1:1 mixture of PNA and DNA oligomers (10.0 µM) in 10 mM phosphate buffer (pH 7.1, 100 mM NaCl, 0.1 mM EDTA) at 90 ºC for 3 min. Samples were slowly cooled to RT and kept in an ice bath for ~1 h. Samples were further diluted using phosphate buffer to give a final duplex concentration of 1.0 µM for T_m and 5.0 µM for CD analysis, respectively. UV-thermal melting analysis of PNA duplexes were performed in duplicate using quartz cuvette on a Cary 300Bio UV-Vis spectrophotometer. The temperature was increased from 20 ºC to 90 ºC at 1 ºC/min and the absorbance was measured every 1 ºC interval at 260 nm. CD spectra of PNA duplexes were recorded with an average of three scans from 350 to 200 nm using quartz cuvette (Starna Scientific, path length 2 mm) on a JASCO J-815 CD spectrometer at 20 ºC and scan speed of 100 nm/min.

2.4.4.13 Fluorescence of benzothiophene- and benzofuran-modified PNA oligomers and their duplexes

PNA-DNA duplexes were obtained by heating a 1:1 mixture of PNA and DNA (5.0 µM) in 10 mM phosphate buffer (pH 7.1, 100 mM NaCl, 0.1 mM EDTA) at 90 ºC for 3 min. Samples were slowly cooled to RT and kept in an ice bath for ~1 h. Samples were further diluted using phosphate buffer to give a final duplex concentration of 0.5 µM. Samples were excited at 330 nm. Excitation and emission slit widths were maintained at 5 nm and 7 nm, respectively, for duplexes made of **14a**, and 3 nm and 5 nm, respectively, for duplexes made of **14b**.

2.5 Notes and References

1. a) M. J. Rist and J. P. Marino, *Curr. Org. Chem.*, 2002, **6**, 775–793; b) L. M. Wilhelmsson, *Quart. Rev. Biophy.*, 2010, **43**, 159–183; c) R. W. Sinkeldam, N. J. Greco and Y. Tor, *Chem. Rev.*, 2010, **110**, 2579–2619; d) S. G. Srivatsan and A. A. Sawant, *Pure Appl. Chem.*, 2011, **83**, 213–232; e) K. Phelps, A. Morris and P. A. Beal, *ACS Chem. Biol.*, 2012, **7**, 100–109; f) M. Winnacker and E. T. Kool, *Angew. Chem. Int. Ed.*, 2013, **52**, 12498–12508.
2. Recent examples: a) A. Dierckx, P. Dinér, A. H. El-Sagheer, D. K. Joshi, T. Brown, M. Grøtli and L. M. Wilhelmsson, *Nucleic Acids Res.*, 2011, **39**, 4513–4524; b) T. Ehrenschwender and H.-A. Wagenknecht, *J. Org. Chem.*, 2011, **76**, 2301–2304; c) J. Guo, S. Wang, N. Dai, Y. N. Teo and E. T. Kool, *Proc. Natl. Acad. Sci. U.S.A.*, 2011, **108**, 3493–3498; d) A. S. Wahba, F. Azizi, G. F. Deleavey, C. Brown, F. Robert, M. Carrier, A. Kalota, A. M. Gewirtz, J. Pelletier, R. H. E. Hudson and M. J. Damha, *ACS Chem. Biol*., 2011, **6**, 912–919; e) J. Krim, C. Grünewald, M. Taourirte and J. C. Engels, *Bioorg. Med. Chem.*, 2012, **20**, 480–486; f) F. Wojciechowski, J. Lietard and C. J. Leumann, *Org. Lett*.,

2012, **14**, 5176–5179; g) S. S. Bag, S. Talukdar, K. Matsumoto and R. Kundu, *J. Org. Chem.*, 2013, **78**, 278–291. h) K. M. Rankin, M. Sproviero, K. Rankin, P. Sharma, S. D. Wetmore and R. A. Manderville, *J. Org. Chem.*, 2012, **77**, 10498–10508. i) J. Riedl, R. Pohl, N. P. Ernsting, P. Orság, M. Fojta and M. Hocek, *Chem. Sci*., 2012, **3**, 2797–2806; j) D. Dziuba, V. Y. Postupalenko, M. Spadafora, A. S. Klymchenko, V. Guérineau, Y. Mély, R. Benhida and A. Burger, *J. Am. Chem. Soc.*, 2012, **134**, 10209–10213; k) M. G. Pawar, A. Nuthanakanti and S. G. Srivatsan, *Bioconjugate Chem.*, 2013, **24**, 1367–1377; l) J. W. Park, Y. J. Seo and B. H. Kim, *Chem. Commun.*, 2014, **50**, 52–54; m) R. A. Mizrahi, D. Shin, R. W. Sinkeldam, K. J. Phelps, A. Fin, D. J. Tantillo, Y. Tor and P. A. Beal, *Angew. Chem. Int. Ed.*, 2015, **54**, 8713–8716; n) G. Mata and N. W. Luedtke, *J. Am. Chem. Soc.*, 2015, **137**, 699–707; o) Y. Saito, A. Suzuki, T. Yamauchi and I. Saito, *Tetrahedron Lett.*, 2015, **56**, 3034–3038; p) G. Hayashi, M. Yanase, K. Takeda, D. Sakakibara, R. Sakamoto, D. O. Wang and A. Okamoto, *Bioconjugate Chem.*, 2015, **26**, 412–417.

3. a) P. Cekan and S. T. Sigurdsson, *Chem. Commun.*, 2008, 3393–3395; b) K. Börjesson, S. Preus, A. H. El-Sagheer, T. Brown, B. Albinsson and L. M. Wilhelmsson, *J. Am. Chem. Soc.*, 2009, **131**, 4288–4293; c) A. A. Tanpure and S. G. Srivatsan, *ChemBioChem*, 2012, **13**, 2392–2399; d) T. Kanamori, H. Ohzeki, Y. Masaki, A. Ohkubo, M. Takahashi, K. Tsuda, T. Ito, M. Shirouzu, K. Kuwasako, Y. Muto, M. Sekine and K. Seio, *ChemBioChem*, 2015, **16**, 167–176.
4. K. N. Ganesh and P. E. Nielsen, *Curr. Org. Chem.*, 2000, **4**, 931–943; b) P. E. Nielsen, *Chem. Biodiv.*, 2010, **7**, 786–804; c) H. Knudsen and P. E. Nielsen, *Nucleic Acids Res.*, 1996, **24**, 494–500; d) N. J. Peffeer, J. C. Hanvey, J. E. Bisi, S. A. Thomson, C. F. Hassman, S. A. Noble and L. E. Babiss, *Proc. Natl. Acad. Sci. U. S. A.*, 1993, **90**, 10648–10652.
5. P. E. Nielsen, M. Egholm, R. H. Berg and O. Buchardt, *Science*, 1991, **254**, 1497–1500.
6. a) J. Hu and D. R. Corey, *Biochemistry*, 2007, **46**, 7581–7589; b) M. M. Fabani, M. J. Gait, *RNA*, 2008, **14**, 336–346; c) A. G. Torres, M. M. Fabani, E. Vigorito, D. Williams, N. Al-Obaidi, F. Wojciechowski, R. H. E. Hudson, O. Seitz and M. J. Gait, *Nucleic Acids Res.*, 2012, **40**, 2152–2167; d) C. Zhao, T. Hoppe, M. K. H. G. Setty, D. Murray, T.-W. Chun, I. Hewlett and D. H. Appella, *Nat. Commun.*, 2014, **5**, 5079; e) T. D. Canady, C. A. Telmer, S. N. Oyaghire, B. A. Armitage and M. P. Bruchez, *J. Am. Chem. Soc.*, 2015, **137**, 10268–10275.
7. a) K. L. Robertson, L. Yu, B. A. Armitage, A. J. Lopez and L. A. Peteanu, *Biochemistry*, 2006, **45**, 6066–6074; b) S. Kummer, A. Knoll, E. Socher, L. Bethge, A. Herrmann and O. Seitz, *Angew. Chem. Int. Ed.*, 2011, **50**, 1931–1934; c) T. Zengeya, P. Gupta and E. Rozners, *Angew. Chem. Int. Ed.*, 2012, **51**, 12593–12596; d) Y. Kam, A. Rubinstein, A. Nissan, D. Halle and E. Yavin, *Mol. Pharmaceutics*, 2012, **9**, 685–693; e) D. Sethi, C.-P. Chen, R.-Y. Jing, M. L. Thakur and E. Wickstrom, *Bioconjugate Chem.*, 2012, **23**, 158–163; f) I. Sacui, W.-C. Hsieh, A. Manna, B. Sahu and D. H. Ly, *J. Am. Chem. Soc.*, 2015, **137**, 8603–8610; g) S. Dickgiesser, N. Rasche, D. Nasu, S. Middel, S. Hörner, O. Avrutina, U. Diederichsen and H. Kolmar, *ACS Chem. Biol.*, 2015, **10**, 2158–2165; h) Y. Shemesh and E. Yavin, *Bioconjugate Chem.*, 2015, **26**, 1916–1922; i) P. R. Bohländer, T. Vilaivan and H.-A. Wagenknecht, *Org. Biomol. Chem.*, 2015, **13**, 9223–9230.
8. a) B. P. Gangamani, V. A. Kumar and K. N. Ganesh, *Chem. Commun.*, 1997, 1913–1914; b) F. Wojciechowski and R. H. E. Hudson, *J. Am. Chem. Soc.*, 2008, **130**, 12574–12575; c) C. Boonlua, C. Vilaivan, H.-A. Wagenknecht and T. Vilaivan, *Chem.-Asian J.*, 2011, **6**, 3251–3259; d) S. Müllar, J. Strohmeier and U. Diederichsen, *Org. Lett.*, 2011, **14**, 1382–1385; e) A. H. St. Amant and R. H. E. Hudson, *Org. Biomol. Chem.*, 2012, **10**, 876–881.
9. M. G. Pawar and S. G. Srivatsan, *Org. Lett.*, 2011, **13**, 1114–1117.

10. A. A. Tanpure and S. G. Srivatsan, *Chem. Eur. J.*, 2011, **17**, 12820–12827.
11. A. A. Tanpure and S. G. Srivatsan, *Nucleic Acids Res.*, 2015, **43**, e149.
12. M. G. Pawar and S. G. Srivatsan, *J. Phys. Chem. B*, 2013, **117**, 14273–14282.
13. P. M. Sabale, A. Nuthanakanti and S. G. Srivatsan, *Ind. J. Chem. A*, 2013, **52**, 1004–1013.
14. a) B. Zhang, V. C. Bailey and B. V. L. Potter, *J. Org. Chem.*, 2008, **73**, 1693–1703; b) R. A. Long, R. K. Robins and L. B. Townsend, *J. Org. Chem.*, 1967, **32,** 2751–2756.
15. See Experimental Section for details.
16. a) D. C. Ward, E. Reich and L. Stryer, *J. Biol. Chem*., 1969, **244**, 1228–1237; b) M. Kawai, M. J. Lee, K. O. Evans and T. M. Nordlund, *J. Fluorescence*, 2001, **11**, 23–32.
17. E. L. Rachofsky, R. Osman and J. B. A. Ross, *Biochemistry*, 2001, **40**, 946–956.
18. a) S. O. Kelley and J. K. Barton, *Science*, 1999, **283**, 375–381; c) M. Torimura, S. Kurata, K. Yamada, T. Yokomaku, Y. Kamagata, T. Kanagawa and R. Kurane, *Anal. Sci.*, 2001, **17**, 155–160; c) I. Nazarenko, R. Pires, B. Lowe, M. Obaidy and A. Rashtchian, *Nucleic Acids Res.*, 2002, **30**, 2089–2195.
19. a) C. A. M. Seidel, A. Schulz and M. H. M. Sauer, *J. Phys. Chem.*, 1996, **100**, 5541–5553; b) S. Doose, H. Neuweiler and M. Sauer, *ChemPhysChem*, 2009, **10**, 1389–1398.
20. R. W. Sinkeldam, A. J. Wheat, H. Boyaci and Y. Tor, *ChemPhysChem*, 2011, **12,** 567–570.
21. 2-AP exhibits up to 100-fold quenching in fluorescence intensity, when placed in between different bases in ON sequences. See ref. 16.
22. a) P. C. Meltzer, A. Y. Liang and P. Matsudaira, *J. Org. Chem.*, 1995, **60**, 4305–4308; b) G. Breipohl, D. W. Will, A. Peyman and E. Uhlmann, Tetrahedron, 1997, **53**, 14671–14686.
23. C. Reichardt, *Chem. Rev.*, 1994, **94,** 2319–2358.
24. A. A. Tanpure, M. G. Pawar and S. G. Srivatsan, *Isr. J. Chem.*, 2013, **53**, 366–378
25. R. W. Sinkeldam and Y. Tor, *Org. Biomol. Chem.*, 2007, **5**, 2523–2528.
26. a) M. S. Noé, R. W. Sinkeldam and Y. Tor, *J. Org. Chem.*, 2013, **78**, 8123–8128; b) R. W. Sinkeldam, A. J. Wheat, H. Boyaci and Y. Tor, *ChemPhysChem*, 2011, **12**, 567–570.
27. N. Ouerfelli, O. Iulian and M. Bouaziz, *Phys. Chem. Liq.*, 2010, **48**, 488–513.
28. L. S. Liebeskind and J. Wang, *J. Org. Chem.*, 1993, **58**, 3550–3556.
29. a) K. L. Dueholm, M. Egholm, C. Behrens, L. Christensen, H. F. Hansen, T. Vulpius, K. H. Petersen, R. H. Berg, P. E. Nielsen and O. Buchardt, *J. Org. Chem.*, 1994, **59**, 5767–5773; b) B. Sahu, V. Chenna, K. L. Lathrop, S. M. Thomas, G. Zon, K. J. Livak and D. H. Ly, *J. Org. Chem.*, 2009, **74**, 1509–1516.
30. D. Lavabre and S. Fery-Forgues, *J. Chem. Educ.*, 1999, **76**, 1260–1260.
31. P. E. Nielsen and M. Egholm, *Peptide nucleic acids-protocols and applications.* Horizon Scientific Press, Wymondham, 1999.

2.6 Appendix-I: Characterization data of synthesized compounds

^{1}H-NMR of benzofuran-conjugated adenosine **3** in d_6-DMSO

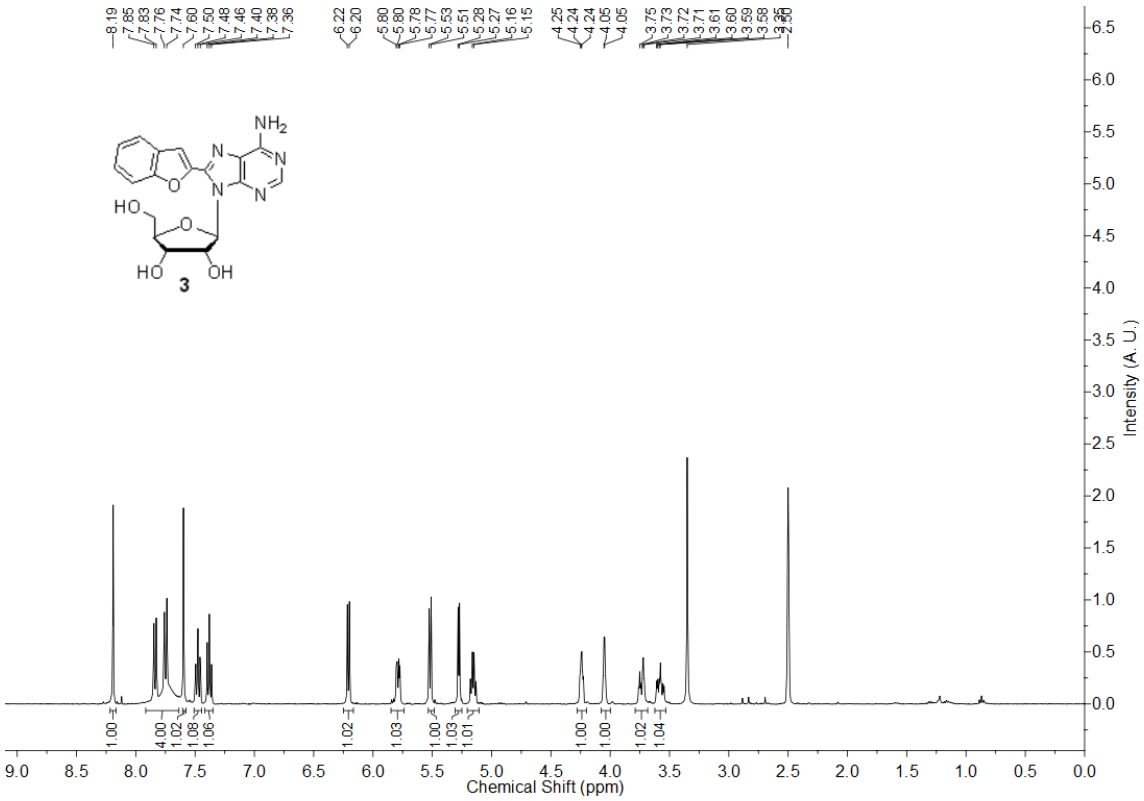

^{13}C-NMR of benzofuran-conjugated adenosine **3** in d_6-DMSO

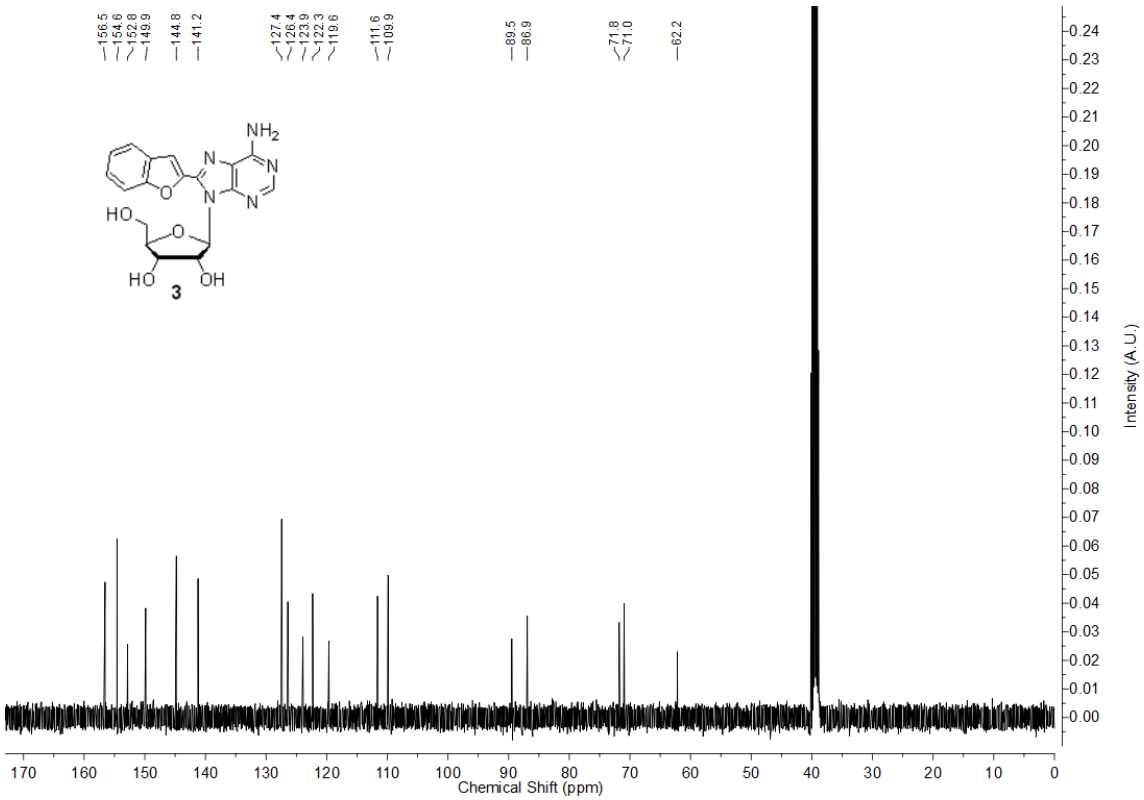

[1]H-NMR of benzofuran-conjugated guanosine **4** in d_6-DMSO

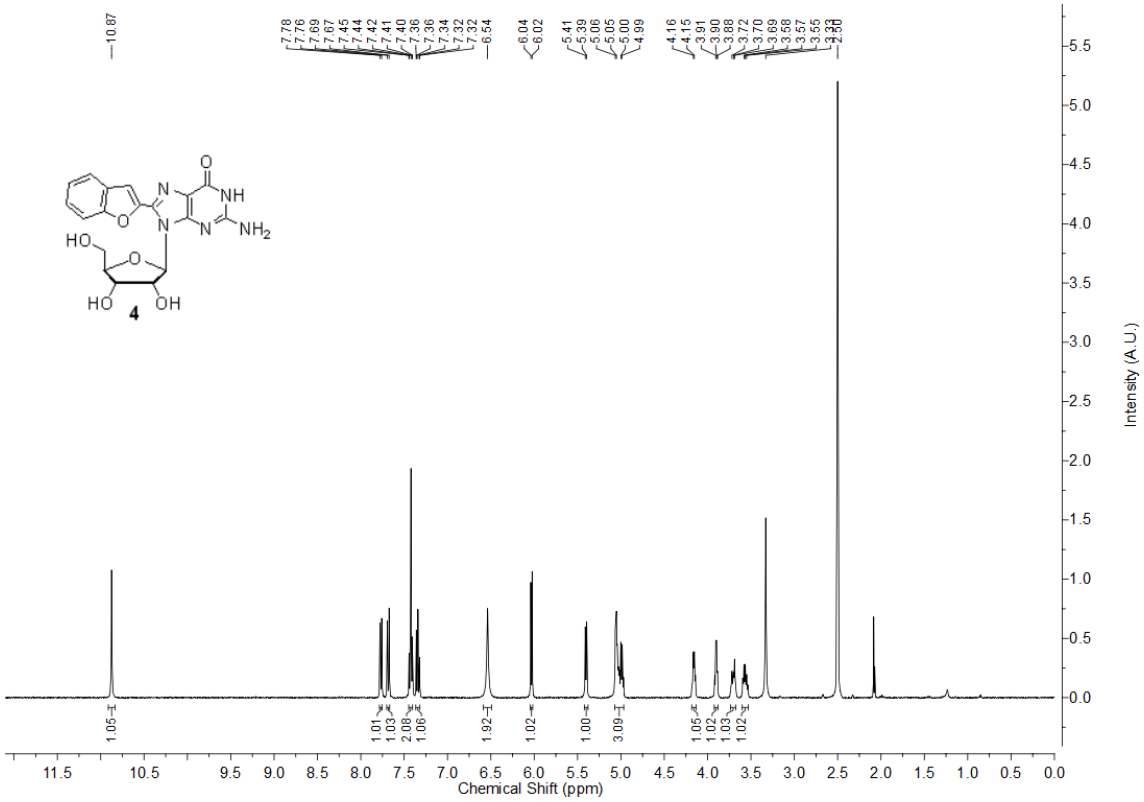

[13]C-NMR of benzofuran-conjugated guanosine **4** in d_6-DMSO.

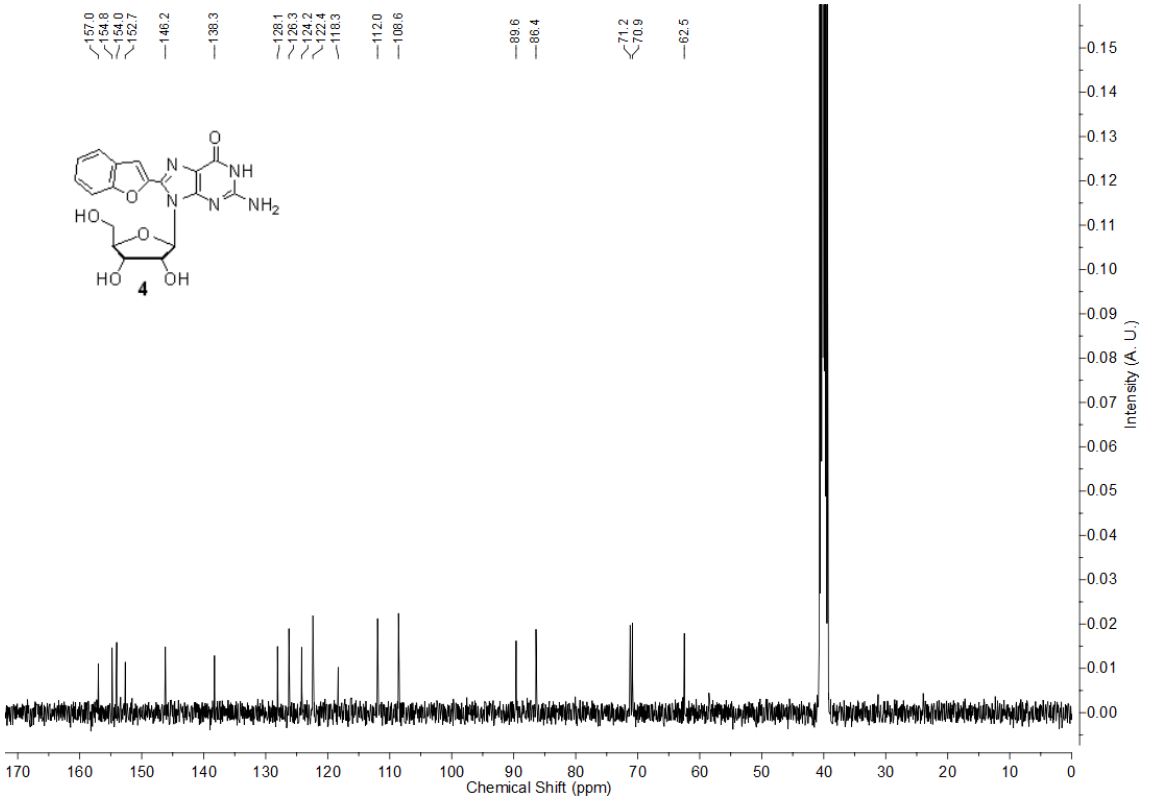

^{1}H-NMR of 5-iodouracil PNA ester **11** in $CDCl_3$

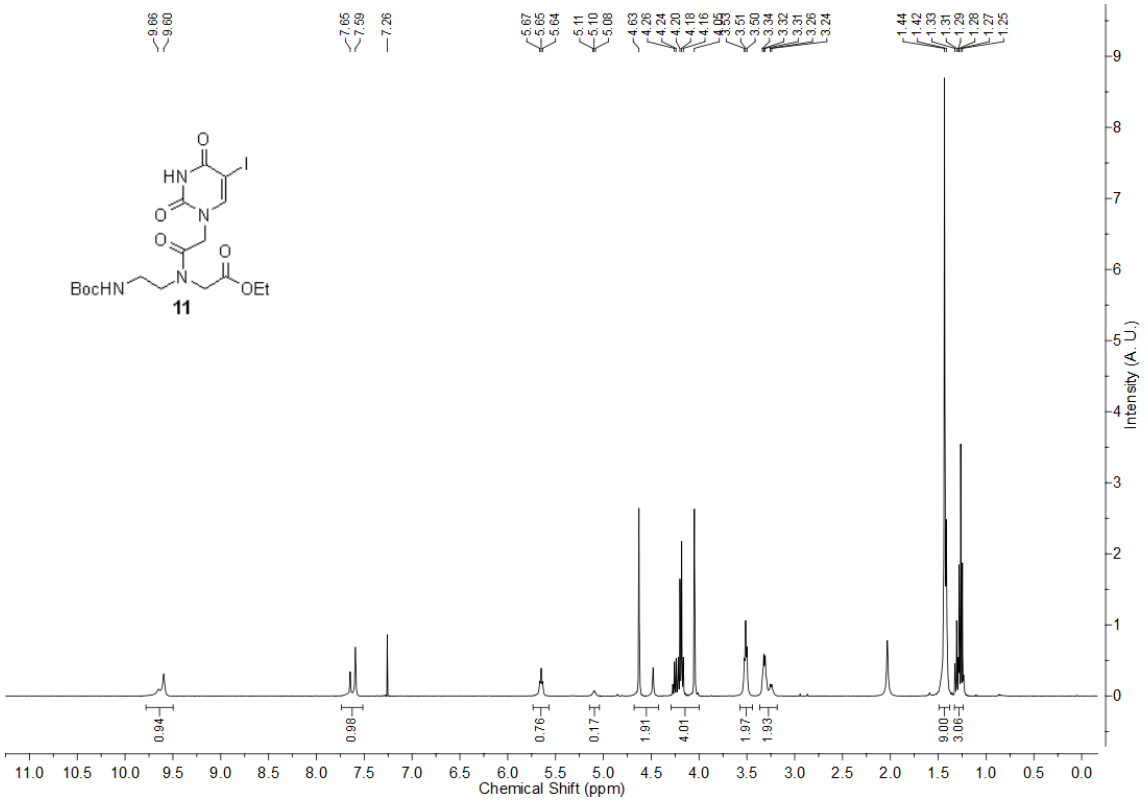

^{13}C-NMR of 5-iodouracil PNA ester **11** in $CDCl_3$

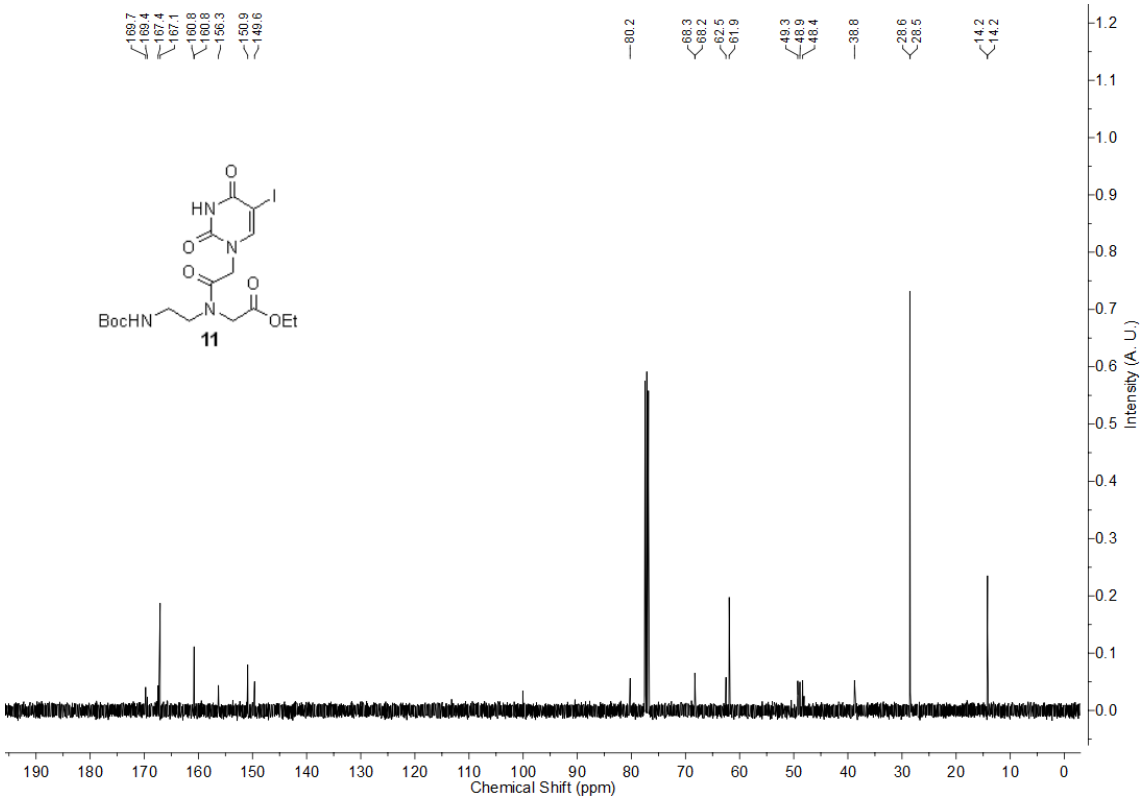

^{1}H-NMR of fluorescent benzothiophene PNA ester **12a** in d_6-DMSO

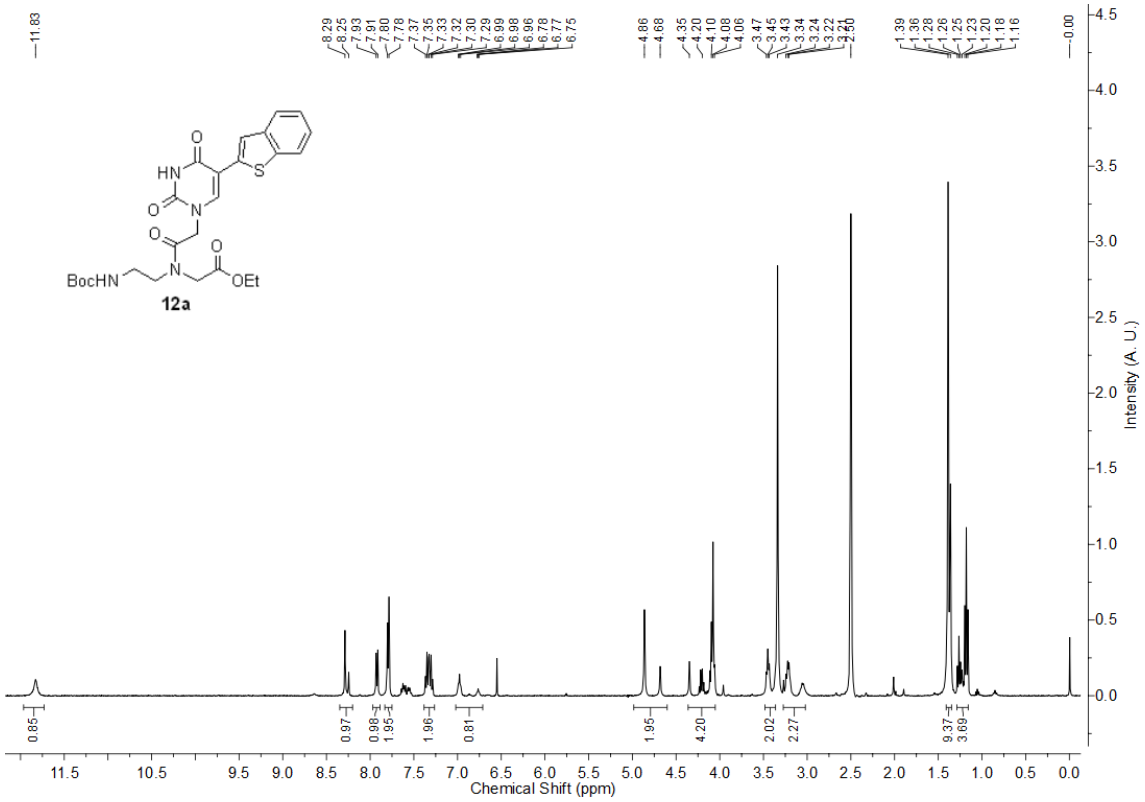

^{13}C-NMR of fluorescent benzothiophene PNA ester **12a** in d_6-DMSO

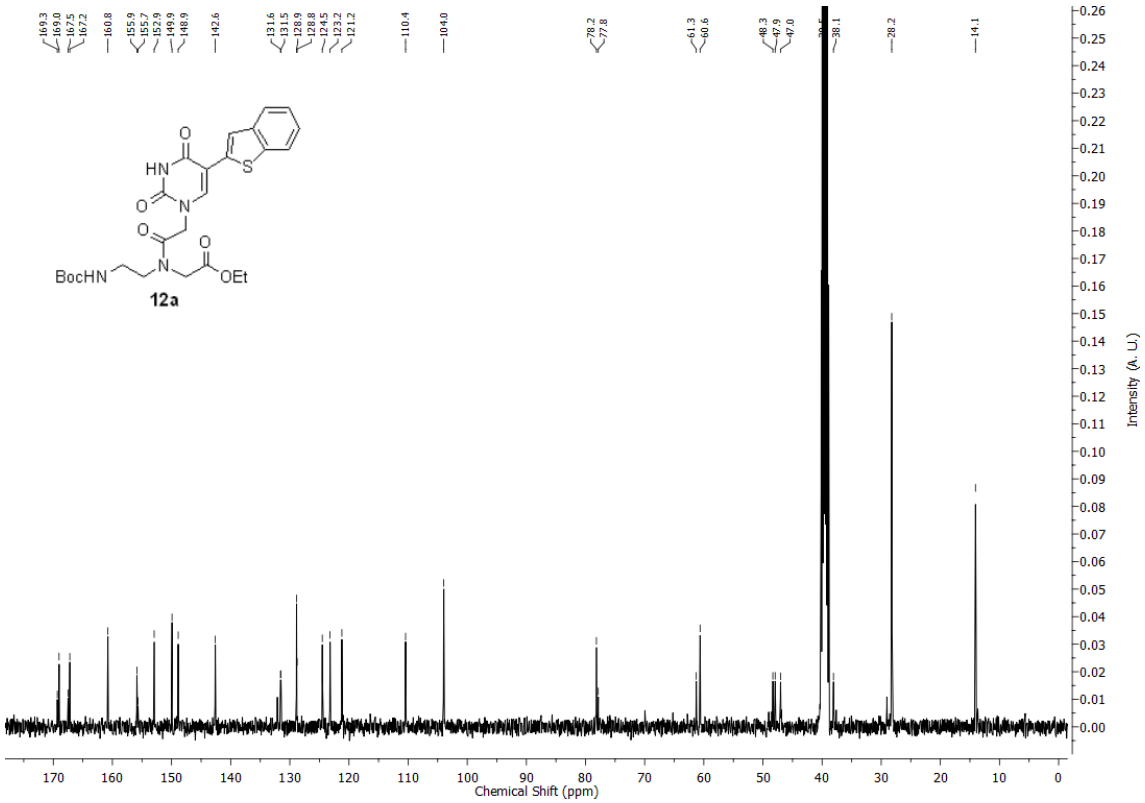

^{1}H-NMR of fluorescent benzofuran PNA ester **12b** in d_6-DMSO

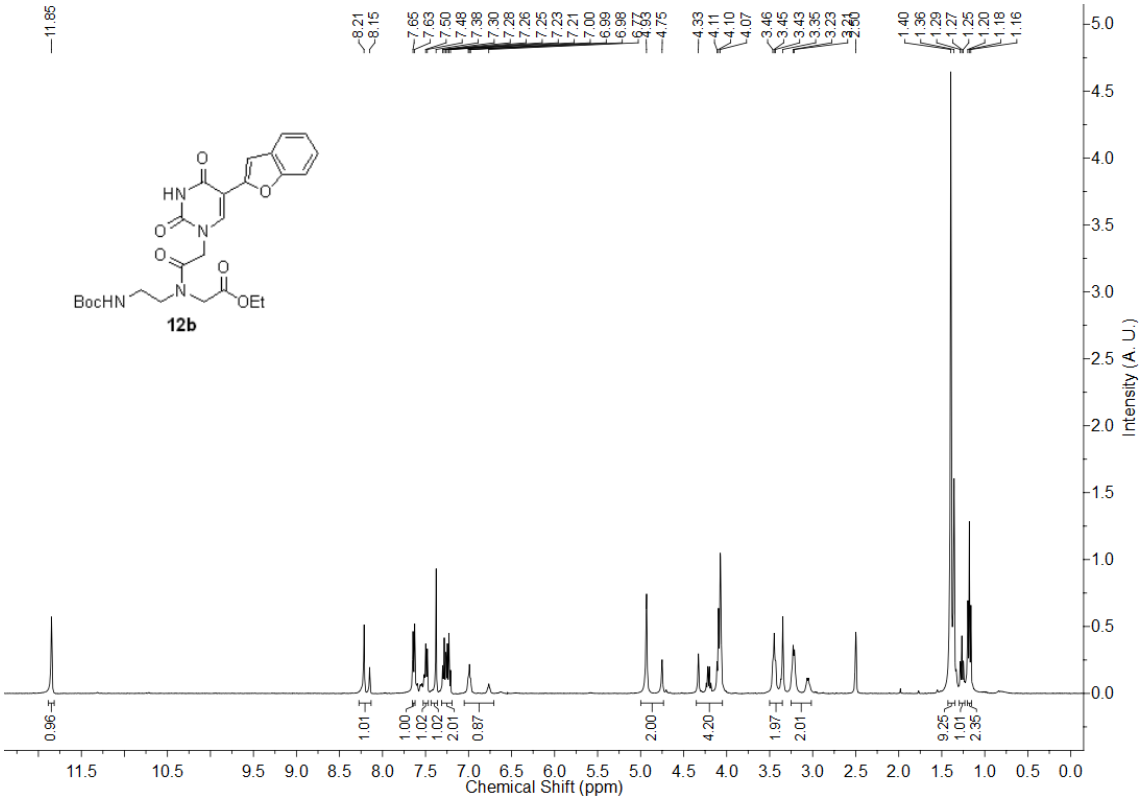

^{13}C-NMR of fluorescent benzofuran PNA ester **12b** in d_6-DMSO

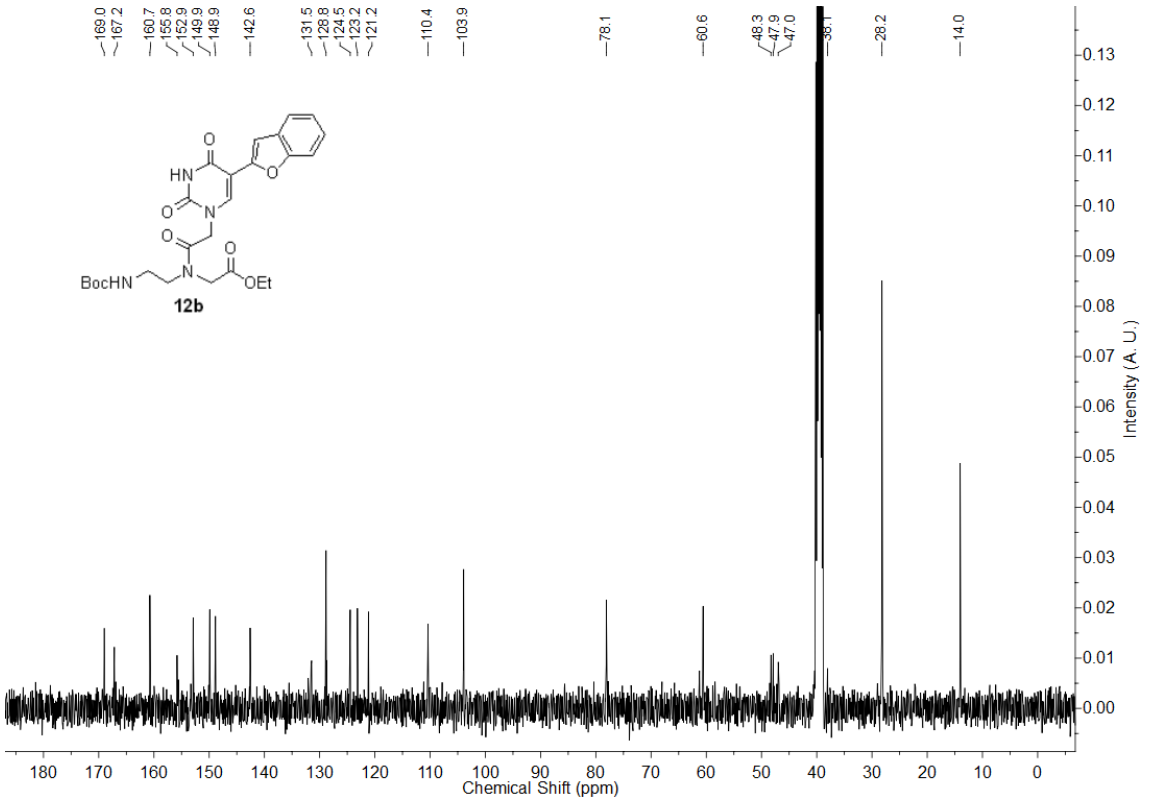

^{1}H-NMR of fluorescent benzothiophene PNA acid **13a** in d_6-DMSO

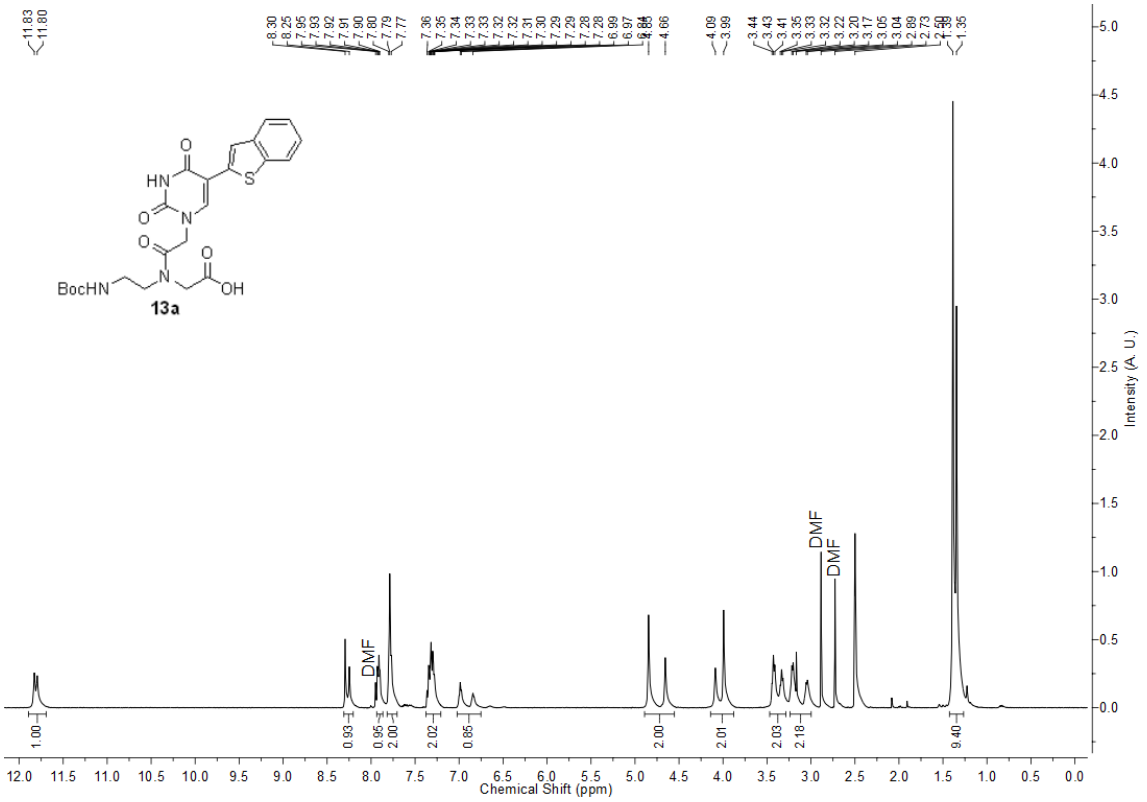

^{13}C-NMR of fluorescent benzothiophene PNA acid **13a** in d_6-DMSO

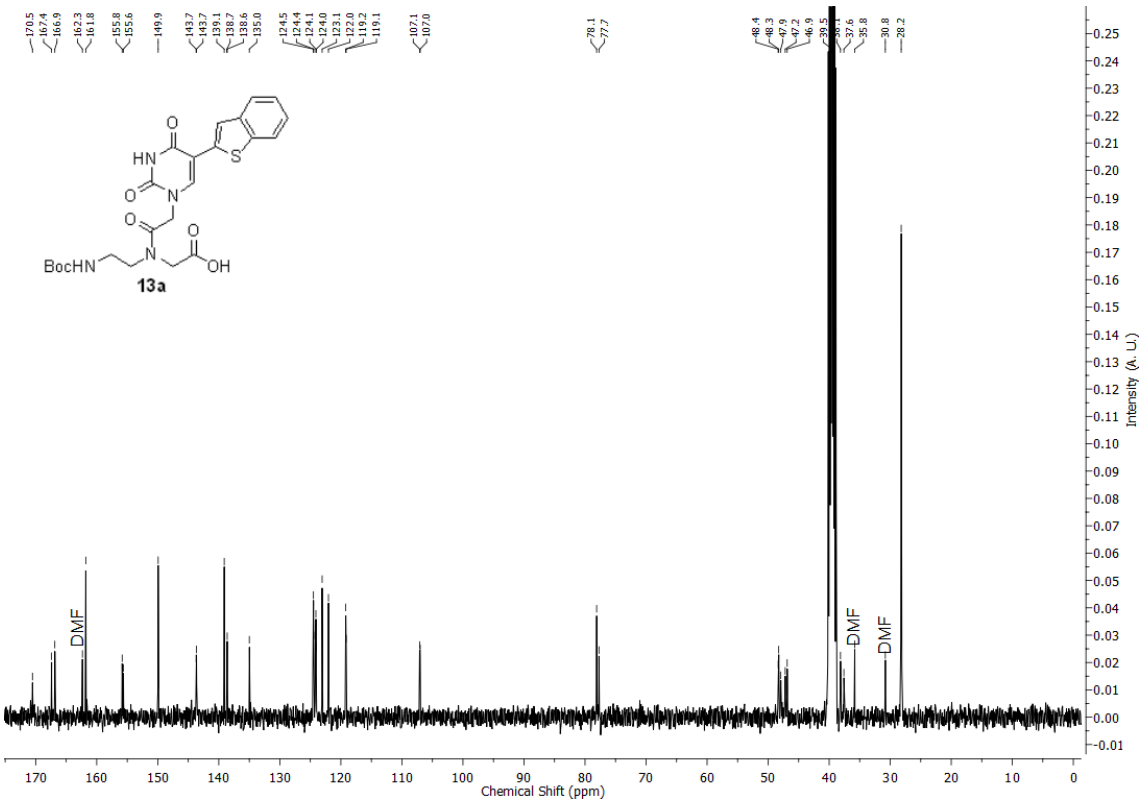

^{1}H-NMR of fluorescent benzofuran PNA acid **13b** in d_6-DMSO

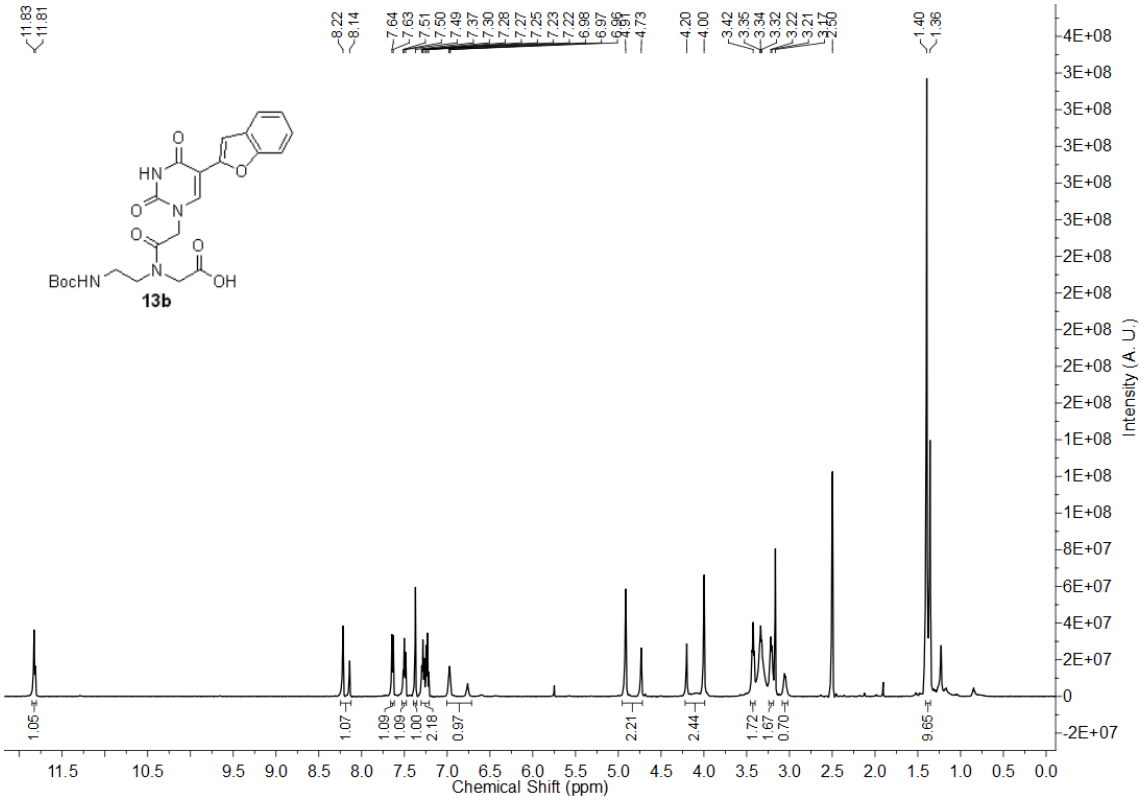

^{13}C-NMR of fluorescent benzofuran PNA acid **13b** in d_6-DMSO

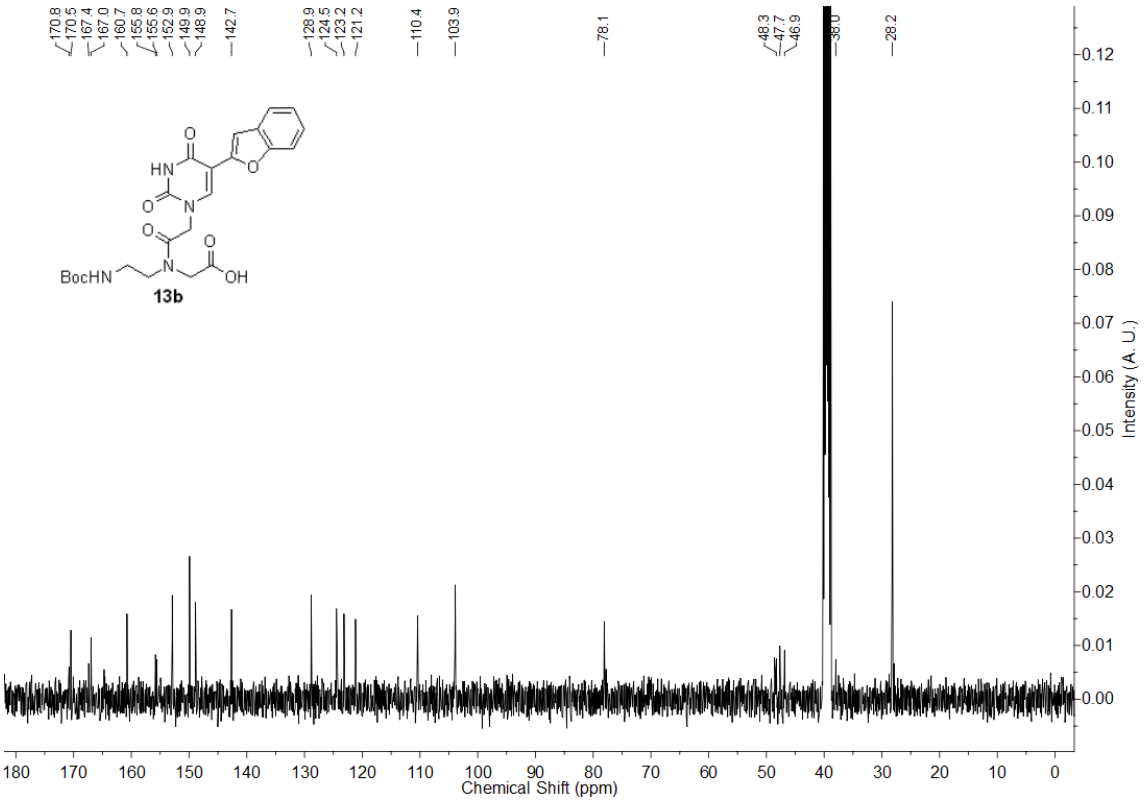

^{1}H-NMR of fluorescent benzothiophene PNA monomer **14a** in d_6-DMSO

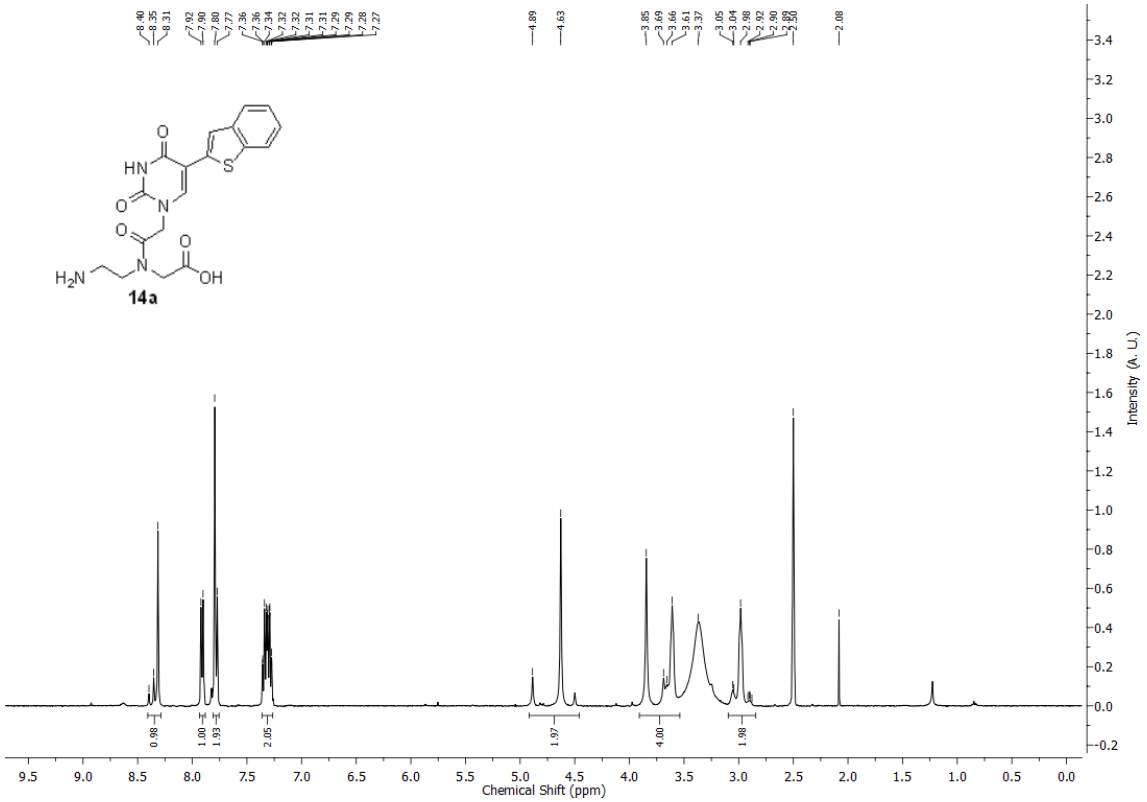

^{13}C-NMR of fluorescent benzothiophene PNA monomer **14a** in d_6-DMSO

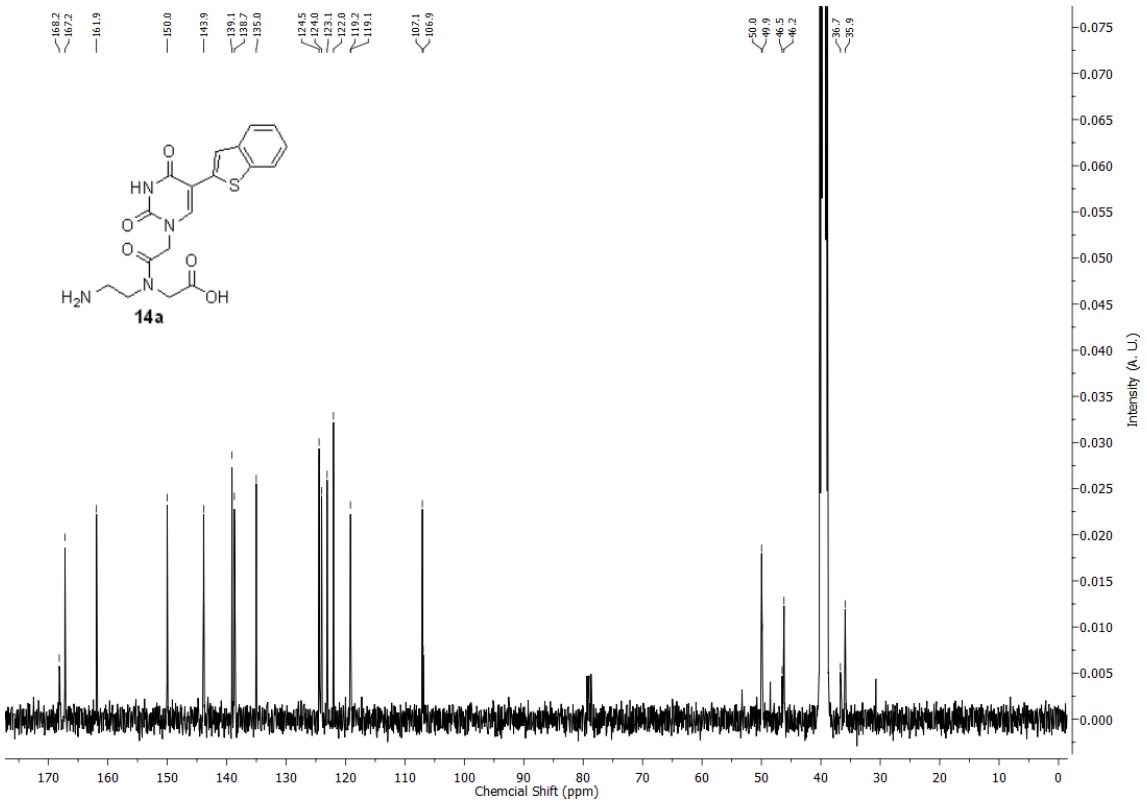

^{1}H-NMR of fluorescent benzofuran PNA monomer **14b** in d_6-DMSO

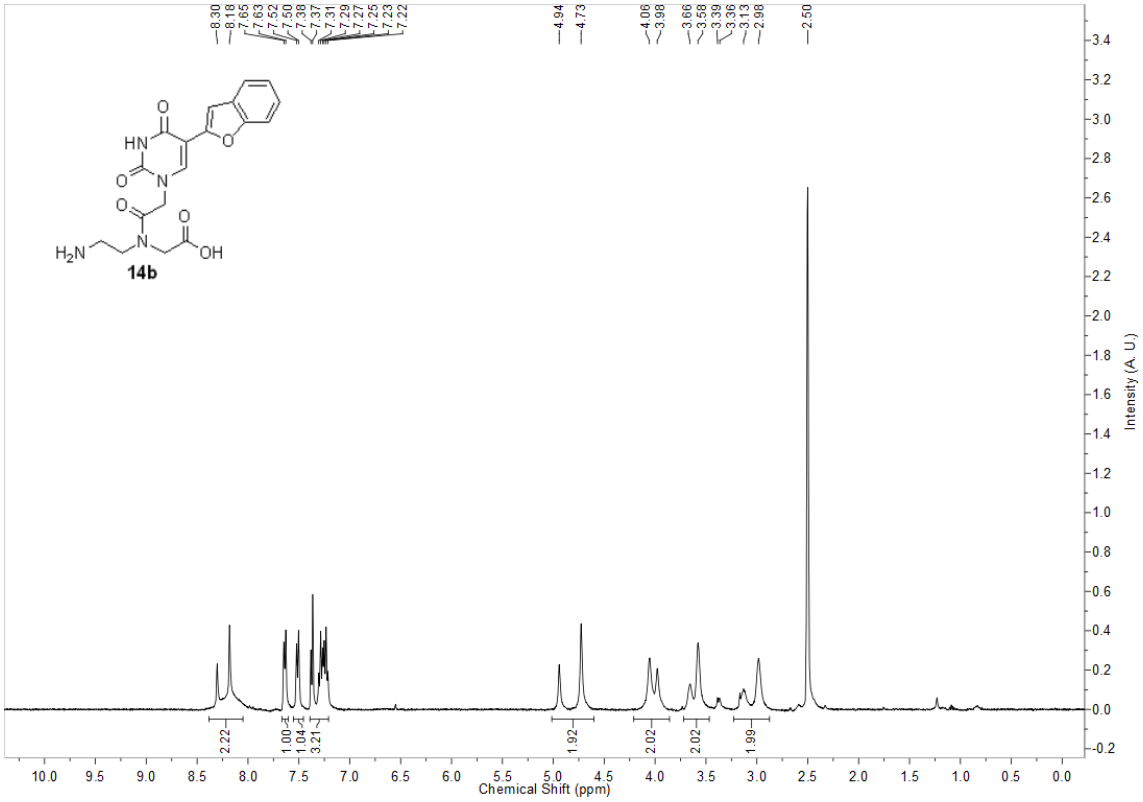

^{13}C-NMR of fluorescent benzofuran PNA monomer **14b** in d_6-DMSO

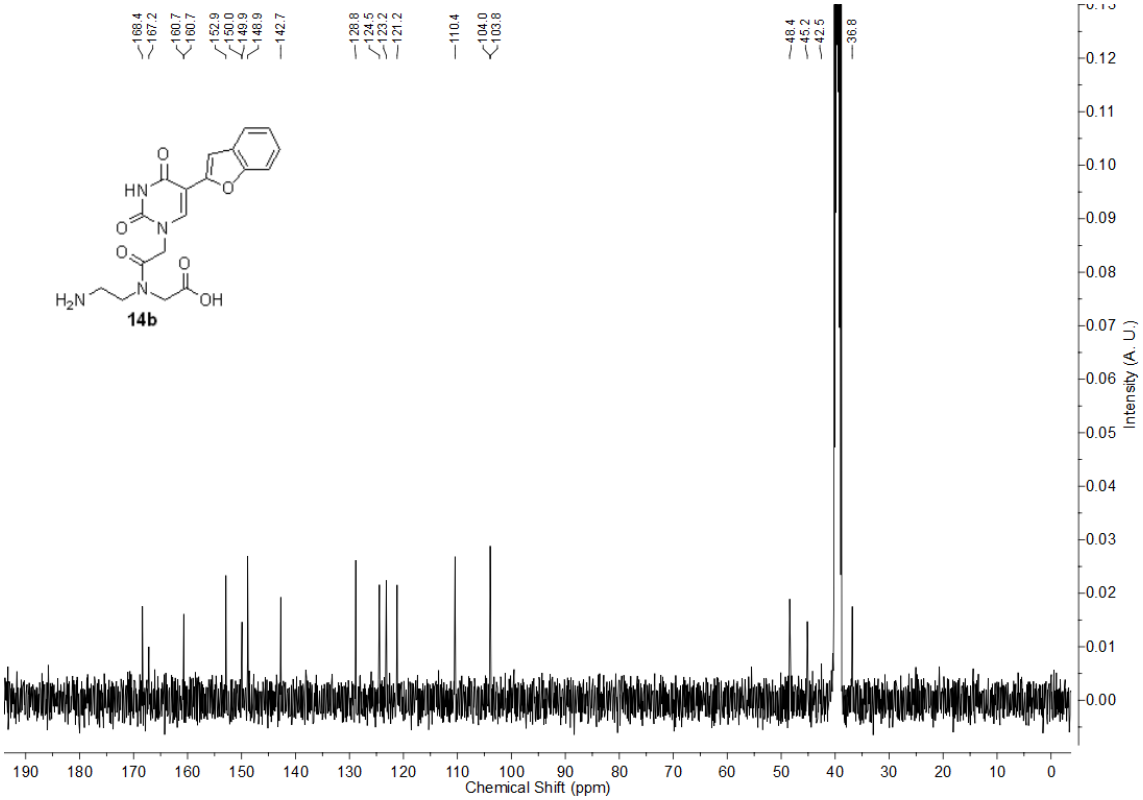

RP-HPLC chromatogram of fluorescent PNA oligomers **15X**–**18X** (contained **14a**) and **15Y**–**18Y** (contained **14b**) at 260 nm. Conditions: 0–50% B in 25 min and 50–100% B in 15 min (Mobile phase A: 5% acetonitrile in H_2O containing 0.1% TFA. Mobile phase B: 50% acetonitrile in H_2O containing 0.1% TFA). Flow rate was 2 mL/min.

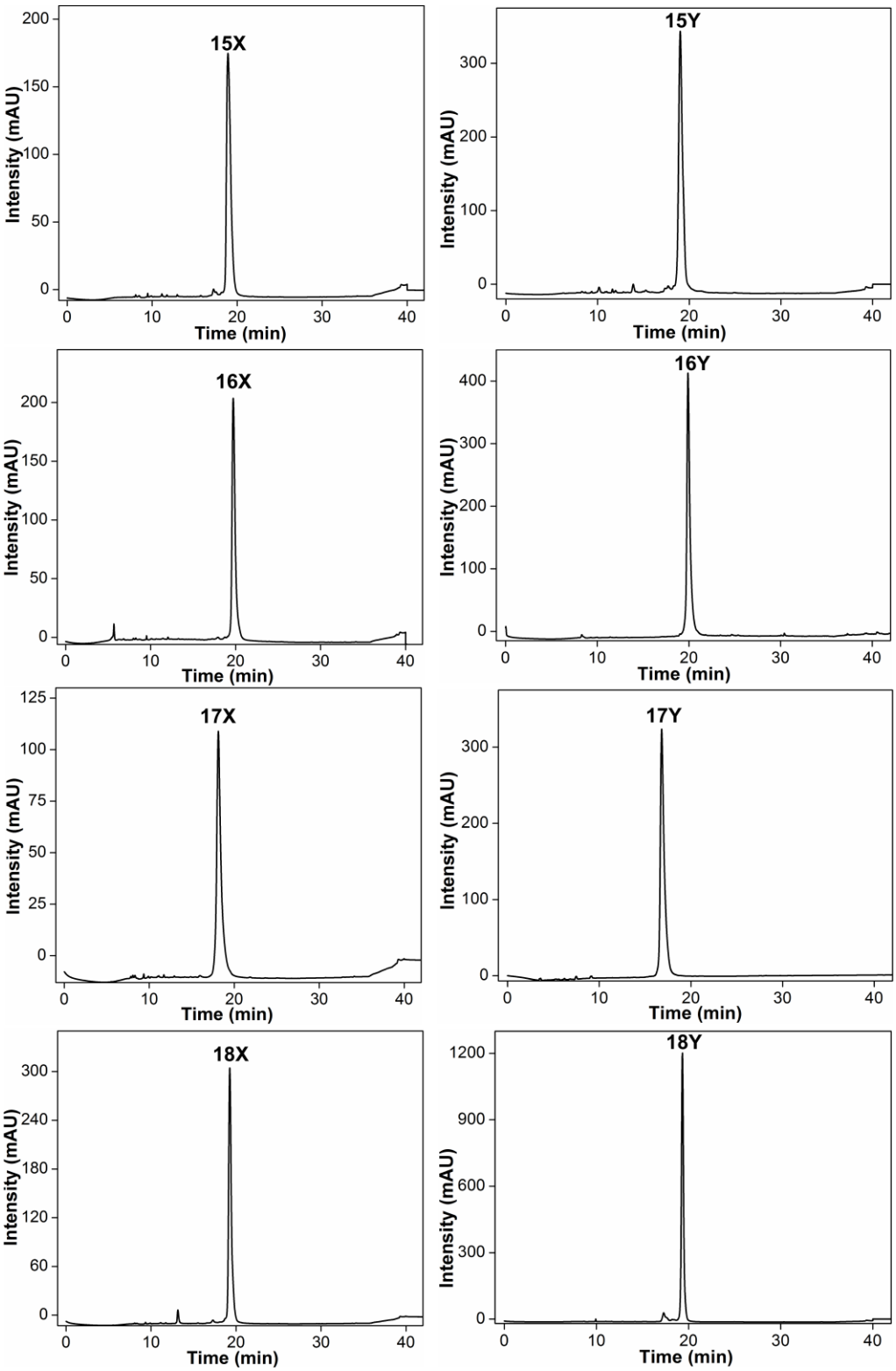

MALDI-TOF mass spectra of fluorescently modified PNA oligomers **15X**–**18X** and **15Y**–**18Y**. See Table 4 for mass data of all PNA oligomers.

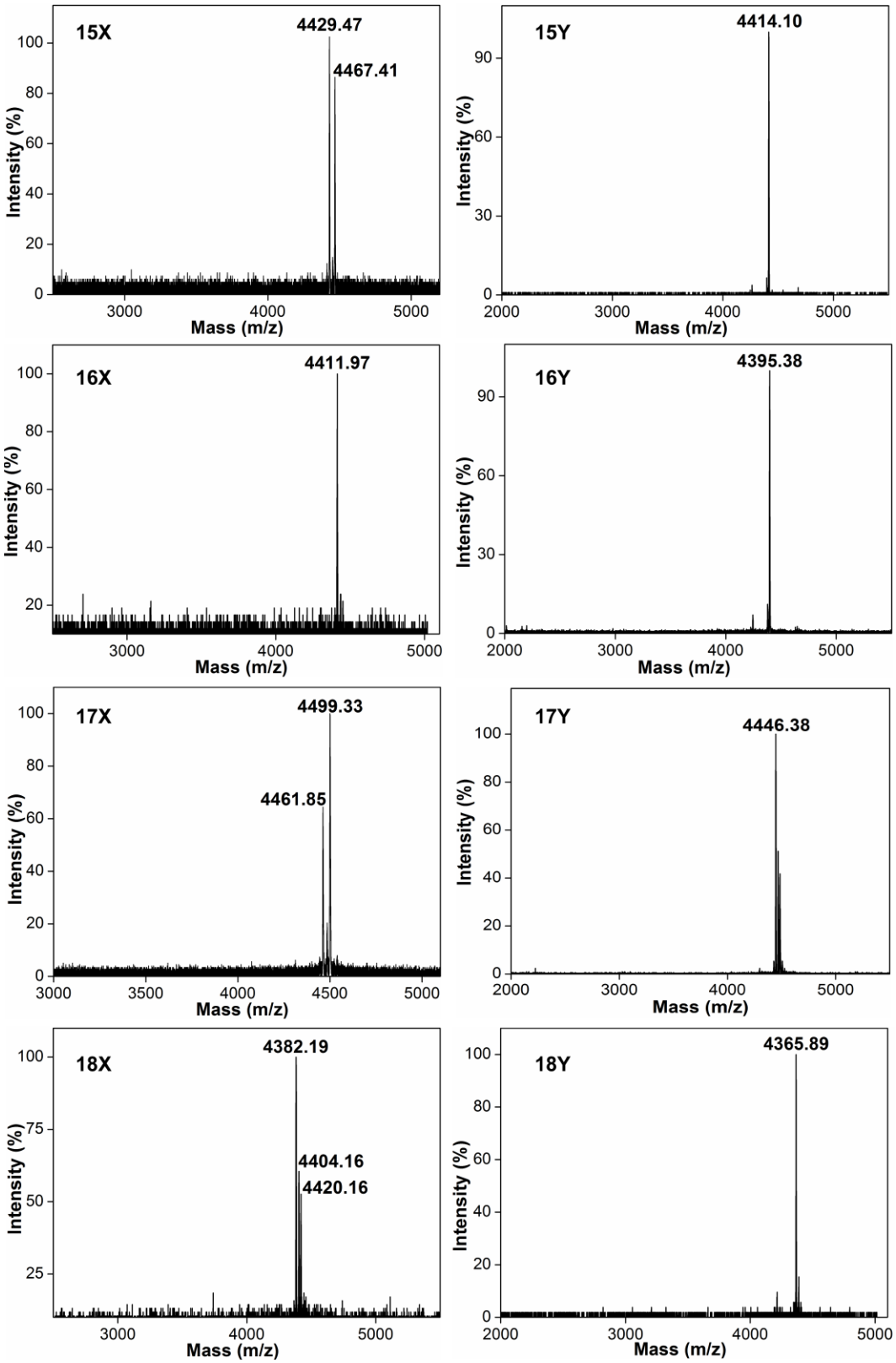

Chapter 3

Fluorescence detection of noncanonical nucleic acid motifs and depurination activity of plant toxins using fluorescent PNA probes

Chapter 3A

Fluorescent PNA-graphene oxide platform as a turn-on sensor for the detection of human telomeric DNA repeats

3A.1 Introduction

Telomeres, which endcap and protect eukaryotic chromosomes from end-to-end fusion and degradation, are typically composed of a few hundred bases to over 20 kilobases of tandem hexameric repeats $(TTAGGG)_n$.[1,2] The G-rich strand, orientated in the 5'–3' direction, terminates in a 100–200 bases 3' single stranded overhang.[3,4] During cell division the telomeric repeats shorten progressively with each cycle inducing replicative senescence or apoptosis in human somatic cells.[5] While aberrant loss of telomeric repeats has been implicated in genomic instability and aging-associated diseases,[6] the maintenance of telomere length in tumor cells by telomerase activity has been implicated in carcinogenesis.[7] In terms of structure, the G-rich telomeric sequences from various organisms are known to form G-quadruplexes (GQs) *in vitro*.[8] In one of the seminal contributions in the study of telomeres, it has been recently shown that telomeric repeats do fold into GQ structures *in vivo* (e.g., ciliate macronuclei and genomic DNA of human cells).[9,10] These studies also indicate that the telomerase activity is tightly regulated by the unfolding of GQ structures, which further underscores the importance of telomeric repeats as a very important target for therapeutic intervention.[11,12]

Telomere structure and function studies greatly relies on the detection and estimation of telomeric repeats in genomic DNA.[13] Conventionally, telomeres have been measured by forming terminal restriction fragments from genomic DNA using frequently cutting restriction enzymes, which produce short genomic fragments and longer uncut telomeres. The telomere fragments are then detected by southern blotting or in-gel hybridization using telomere-specific probes.[3,5,14] Quantitative PCR and more recently, monochrome multiplex quantitative PCR techniques have also been used in the analysis of telomeres.[15] Alternate to enzyme-based techniques, fluorescence *in situ* hybridization (FISH) technique using fluorescently labeled oligonucleotides (ONs) and peptide nucleic acids (PNA) that are complementary to telomeric repeats have been used to detect and measure telomeres in chromosomes.[16,17] Although widely used, these methods have certain disadvantage, which preclude accurate, easy and rapid detection and measurements of telomeres. For example, terminal restriction fragment analysis reports subtelomeric and variant repeats along with pure telomeric repeats and in situ hybridization technique suffers from variation in the hybridization efficiency of the probes to telomeric target.[13] Moreover, these techniques are either time consuming and or use elaborate assay and sophisticated instrumental setups, and hence, are not suitable for high throughput screening (HTS) for the discovery of telomere-

specific ligands. Therefore, given the biological and therapeutic significance of telomeres and other GQ forming sequences, it will be highly useful to develop GQ structure-specific detection methods that are simple and amenable to HTS.[18,19]

In the previous chapter, we have introduced the environment-sensitive fluorescent 5-benzofuran uracil PNA analogue (**1**), which displays enhanced fluorescence intensity when hybridized to complementary ONs. The probe like property of benzofuran PNA analogue motivated us to develop a simple hybridization assay for the detection of human telomeric DNA repeats (TTAGGG)n. Moreover, developing a turn-on fluorescence sensor for such G-rich ON sequences remain a challenge, because guanine is known to quench fluorescence of majority of fluorophores by electron transfer process.[20,21,22] In this chapter, we describe a simple homogeneous fluorescence turn-on assay to detect the human telomeric DNA repeats $(TTAGGG)_n$ by using a benzofuran-modified fluorescent PNA oligomer on the graphene oxide (GO) platform. This turn-on telomere sensor assembly combines the properties of (i) a structurally nonperturbing and environment-sensitive fluorescent PNA base analogue (**1**), based on the 5-(benzofuran-2-yl)uracil core, which when incorporated into PNA oligomers and hybridized to complementary oligonucleotides retains its fluorescence efficiency, (ii) a PNA oligomer labeled with the fluorescent analogue **1**, which strongly binds to human telomeric DNA repeats, and (iii) GO, an excellent fluorescence quencher, which shows significantly higher binding affinity for single stranded (ss) ONs over the double stranded (ds) and folded ONs (Figure 1).[23,24] The choice of PNA over ON and GO over other carbon-based nanomaterials in devising this detection assay is based on the following reasons. PNA oligomer containing uncharged pseudo-peptide backbone, *N*-(2-aminoethyl)glycine (*aeg*), which is homomorphous with the nucleic acid backbone, has certain notable features: (i) the stability of PNA-DNA or PNA-RNA duplex is discernibly higher compared to the corresponding DNA-DNA or RNA-RNA duplex and (ii) the backbone is highly resistant to hydrolysis by nucleases and proteases.[25] GO, which can be conveniently obtained by extensive oxidation followed by mechanochemical exfoliation of graphite, is highly dispersible in water as compared to carbon nanotubes, carbon nanofibers, graphene and fullerenes.[26] Furthermore, GO sheets have high planar surface area, which enhances its optical quenching property as well as its binding affinity for biomolecules by noncovalent interactions.[27] Utilizing these properties several GO-based homogeneous optical biosensing platforms have been conceived to detect biomolecules.[28] In this design strategy, we expect that the binding of ssPNA probe to GO will first result in drastic quenching in fluorescence intensity by energy transfer process.[23a] Subsequent addition of the human telomeric DNA

target would then displace the PNA from GO surface and form a PNA-DNA heteroduplex resulting in an enhancement in fluorescence intensity (Figure 1). Utilizing this strategy, we have also explored the suitability of setting up an assay to detect the displacement of a small molecule GQ binder with our PNA probe.

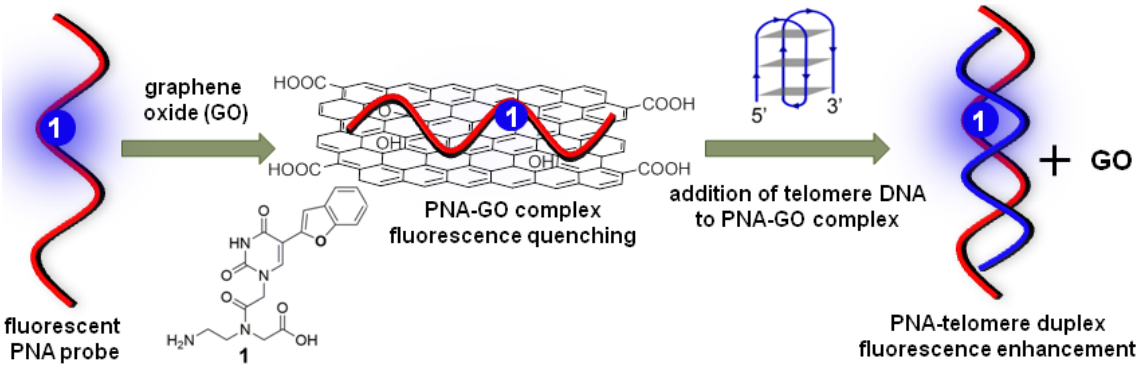

Figure 1. A schematic illustration of the fluorescence turn-on assay to detect the human telomeric DNA repeats by using benzofuran-modified fluorescent PNA-GO platform.

3A.2 Results and discussion

3A.2.1 Synthesis of fluorescent PNA oligomer probe 3

In order to develop a fluorescence hybridization assay for the detection of human telomeric DNA repeat, $(TTAGGG)_3$, we synthesized fluorescently modified 18-mer PNA oligomers **3** and a control unmodified PNA **2** by using SPPS (Figure 2). PNA oligomers were purified by RP-HPLC and integrity was confirmed by MALDI-TOF mass analysis (Figure 3, Table 1). Further, introduction of benzofuran modification can potentially affect the native structure and the hybridization efficiency of PNA oligomer, and hence, the observed fluorescence properties may not be a true reflection of the intact duplexes. To study this, we first examined the stability of PNA-DNA duplexes by performing UV-thermal melting and circular dichroism (CD) experiments in phosphate buffer (10 mM, 100 mM NaCl, pH 7.1). The difference between T_m values of unmodified (**2•5a**) and modified (**3•5a**) PNA-DNA duplex was negligible (Table 2). Also, CD spectra of modified duplex (**3•5a**) was comparable to that of unmodified duplex (**2•5a**), which indicated that benzofuran modification had only marginally affect the structure and stability of duplexes (Figure 4 and Table 2). In addition, significantly higher T_m values (ΔT_m = ~12 °C) exhibited by PNA-DNA duplexes over corresponding DNA-DNA duplex (**4•5a**) support our choice of using fluorescent PNA oligomer over corresponding DNA in devising this telomere detection assay.

2 **CCCTAACCCTAACCCTAAKK**
3 **CCC<u>1</u>AACCCTAACCCTAAKK**
4 5' $_d$(CCCTAACCCTAACCCTAA) 3'

5a 5' $_d$(TTAGGGTTAGGGTTAGGG) 3'
5b 5' $_d$(TTAGGGTTAGGGTTAGGG)$_2$ 3'
5c 5' $_d$(TTAGGGTTAGGGTTAGGG)$_3$ 3'
6 5' $_d$(CGCTAGTCACTGATCGC) 3'

Figure 2. Sequence of control unmodified PNA (**2**), fluorescently modified PNA probe (**3**) and control unmodified DNA ONs (**4**) complementary to telomeric DNA are shown. Telomere DNA sequences **5a**–**5c** containing hexameric repeats of 3, 6 and 9, respectively. Control random DNA ON **6** used in the hybridization assay. PNA sequences (highlighted in bold) are written from N to C terminus and contain two lysine (K) residues at the C terminus.

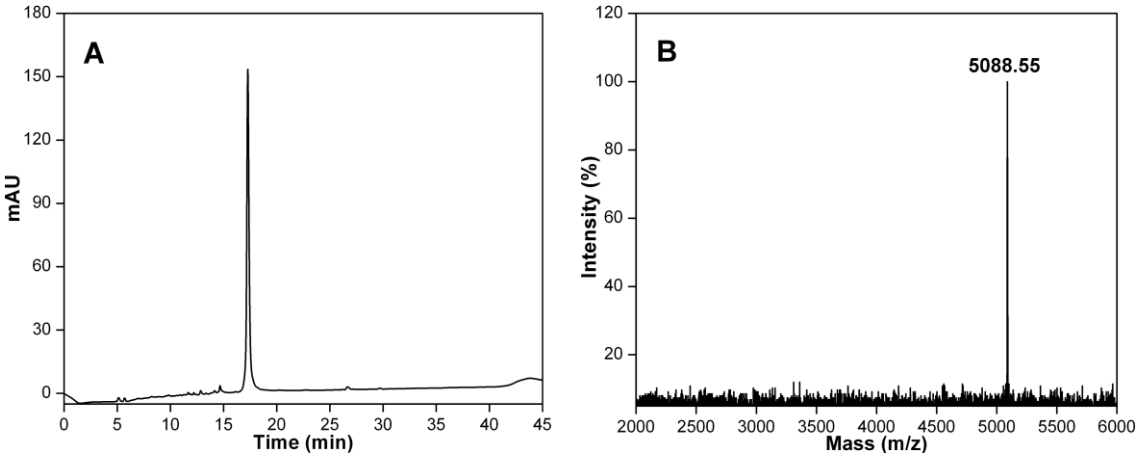

Figure 3. (**A**) RP-HPLC chromatogram of PNA telomere probe **3.** Mobile phase A: 5% acetonitrile in H_2O containing 0.1% TFA, mobile phase B: 50% acetonitrile in H_2O containing 0.1% TFA. Flow rate: 3 mL/min. Gradient: 0–50% B in 25 min and 50–100% B in 20 min. (**B**) MALDI-TOF mass spectrum of PNA telomere probe **3**. Calculated for $[M+H]^+$ = 5088.01 and observed = 5088.55.

Table 1. ε_{260} and MALDI-TOF mass analysis of PNA oligomers

PNA	Sequence[a]	ε_{260} ($M^{-1}cm^{-1}$)	Calculated mass	Observed mass
2	CCCTAACCCTAACCCTAAKK	16.7 x 10^4	5007.90 $[M+Na]^+$	5007.15
3	CCC**<u>1</u>**AACCCTAACCCTAAKK	17.1 x 10^4	5088.01 $[M+H]^+$	5088.55

[a]PNA sequences are written from N to C terminus.

Table 2. T_m values of control and modified PNA-DNA and DNA-DNA duplexes

Control unmodified duplex	T_m (°C)	Fluorescently modified duplex	T_m (°C)
2•5a	71.2 ± 0.8	**3•5a**	71.0 ± 1.0
4•5a	59.3 ± 0.9		

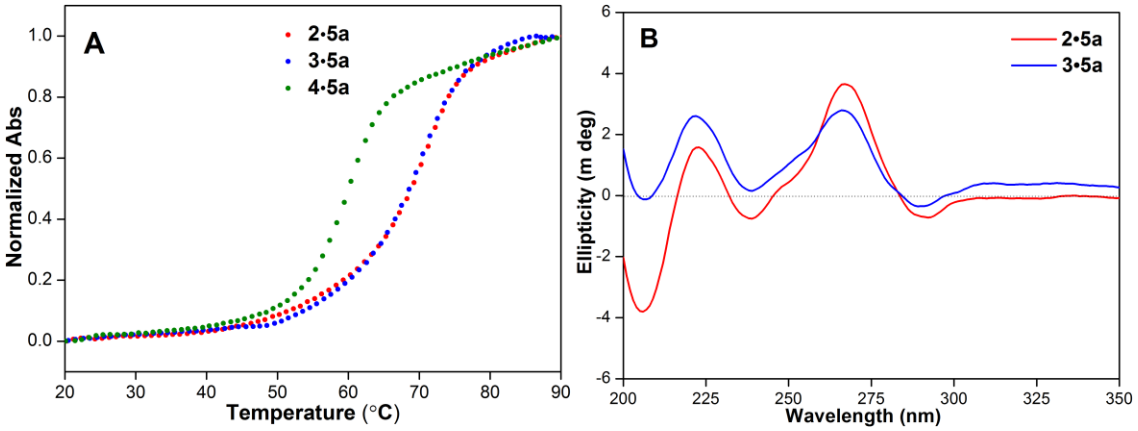

Figure 4. (**A**) UV-thermal melting analysis (2.0 µM) of control unmodified (**2•5a**) and fluorescently modified (**3•5a**) PNA-DNA duplexes and corresponding DNA-DNA duplex (**4•5a**) in 10 mM phosphate buffer (pH 7.1, 100 mM NaCl, 0.1 mM EDTA). For T_m values see Table 2. (**B**) CD spectra (5.0 µM) of control unmodified **2•5a** and fluorescently modified **3•5a** duplexes in 10 mM phosphate buffer (pH 7.1, 100 mM NaCl, 0.1 mM EDTA). A 1:1 mixture of PNA and DNA in the above mentioned buffer was heated at 90 ºC for 3 min and cooled slowly to room temperature. The samples were placed on crushed ice bath for at least 1 h before thermal melting and CD analyses.

3A.2.2 Fluorescence hybridization assay to detect telomeric DNA repeats

To setup a telomere detection assay, we took advantage of the nucleic acid-binding and excellent fluorescence quenching properties of GO.[23,24] GO is a water-dispersible graphene derivative, which preferentially adsorbs ss ONs over ds ONs via π–π, hydrogen bonding and van der Waals interactions between the nucleobase rings and GO surface.[24,30] Utilizing these properties of GO, several bioanalytical tools have been developed recently to detect nucleic acids, proteins and enzyme activities.[24,31,32] However, most of these methods use ON probes attached to large fluorophores (e.g., fluorescein derivatives) via a linker, which by themselves could bind to GO even after desorption and hybridization to ON sequence (binding of fluorescein to reduced GO (rGO) has been reported in literature).[32o] In this context, constructing a PNA probe containing a nonperturbing fluorescent base analogue as an integral part of the oligomer sequence would be appropriate as it would have adsorption, desorption and hybridization properties similar to that of the native oligomer. GO required for these studies were synthesized with known literature procedure[29] and characterized by a colleague from our group.[33]

We performed preliminary fluorescence experiments to optimize the concentration of the PNA probe, GO and telomere DNA target required to setup an efficient telomere detection assay. Based on initial observations (data not shown), concentration of PNA **3**, GO and telomere DNA target was set to 100 nM, 1.0 µg/mL and 1.0 µM, respectively. This combination produced significant fluorescence quenching upon adsorption of **3** onto GO surface and fluorescence enhancement upon desorption and subsequent hybridization with

telomere DNA target. When excited, a solution of PNA **3** in phosphate buffer (10 mM, 100 mM NaCl, pH 7.1) displayed a strong emission band with an emission maximum at 409 nm (Figure 5). Upon addition of GO, a three-fold quenching in fluorescence intensity with no apparent change in emission maximum was observed due to the adsorption of fluorescent PNA oligomer on the GO surface (Figure 5). The formation of PNA-GO complex (**3**-GO) was further confirmed by steady-state fluorescence anisotropy measurements. The fluorescence anisotropy of free PNA **3** was 0.029 ± 0.005, while that of PNA-GO complex was 0.062 ± 0.004, which indicated that the ssPNA was adsorbed on GO surface.[24a] Subsequent addition of a short telomere DNA **5a** to **3**-GO resulted in a red-shifted emission band (λ_{em} = 422 nm) and a significant increase in fluorescence intensity (~4-fold) and anisotropy (0.168 ± 0.008, ~3-fold, Figure 5 and Table 3). To estimate the recovery of fluorescence intensity upon addition of telomere DNA **5a** to PNA-GO complex, the emission profile of prehybridized PNA-telomere DNA duplex **3•5a** in the presence of GO under similar conditions was recorded. The prehybridized duplex in GO gave a similar emission profile (λ_{em} = 422 nm), albeit with enhanced intensity, indicating a nearly 75% fluorescence recovery due to the addition of target DNA **5a** to **3**-GO (Figure 5). Importantly, addition of a noncomplementary control ON **6** to PNA-GO complex resulted in a very small increase in intensity. On the basis of these observations, it is likely that the added telomere DNA target displaces the PNA probe from the GO surface resulting in an intense fluorescence band corresponding to the PNA-telomere DNA duplex **3•5a**.[34]

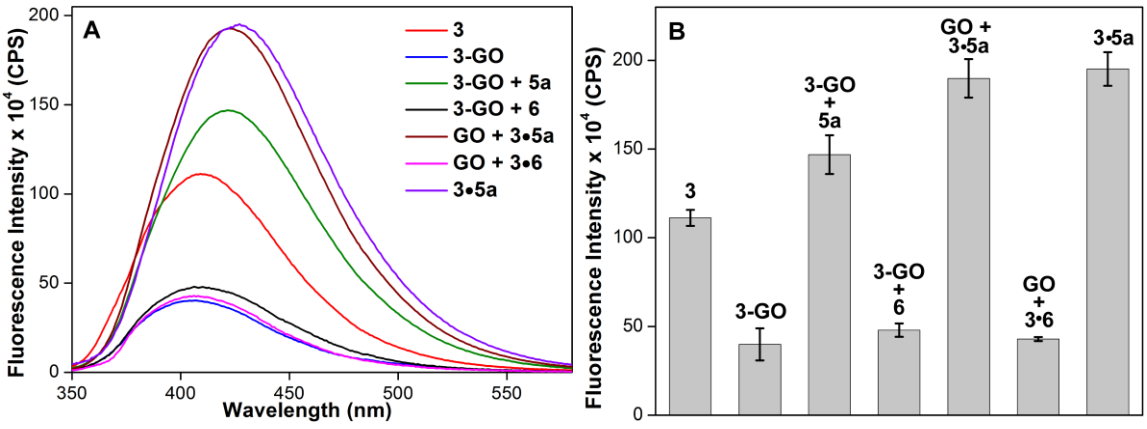

Figure 5. (**A**) Fluorescence spectra of PNA probe **3**, **3**-GO complex and **3**-GO complex in the presence of telomere DNA target **5a** and control DNA **6** in phosphate buffer (10 mM, 100 mM NaCl, pH 7.1). (**B**) Comparison of fluorescence intensity at respective emission maximum (see Table 3). Conc. of PNA **3** (100 nM), DNA **5a** and **6** (1.0 μM) and GO (1.0 μg/mL). Samples were excited at 330 nm and excitation and emission slit widths were kept at 6 and 8 nm, respectively. [35]

Table 3. Emission maximum of PNA probe **3**, PNA-GO complex (**3**-GO) and PNA-GO complex in the presence of telomere target **5a** and control DNA **6**.

Sample[a]	λ_{em} (nm)	I_{rel}[b]
3	409	2.8
3-GO	409	1.0
3-GO + **5a**	422	3.7
3-GO + **6**	406	1.2
GO + **3•5a**	422	4.8
GO + **3•6**	406	1.1
3•5a	427	4.9

[b]Relative emission intensity with respect to PNA-GO complex.[35]

To study the utility of our PNA probe in detecting the number of telomere repeats present in same sequence (for increase in telomere length), DNAs of increasing hexameric repeats (**5a**–**5c**) were added to PNA-GO complex. Rewardingly, as the hexameric repeats increased from 3 to 6 to 9, a progressive increase in fluorescence intensity corresponding to the emission profile of PNA-telomere hybrid was observed (Figure 6). The increase in fluorescence intensity as a function of telomere repeats could be possibly due to effective desorption and multiple hybridization of the PNA probe onto the longer telomere targets.

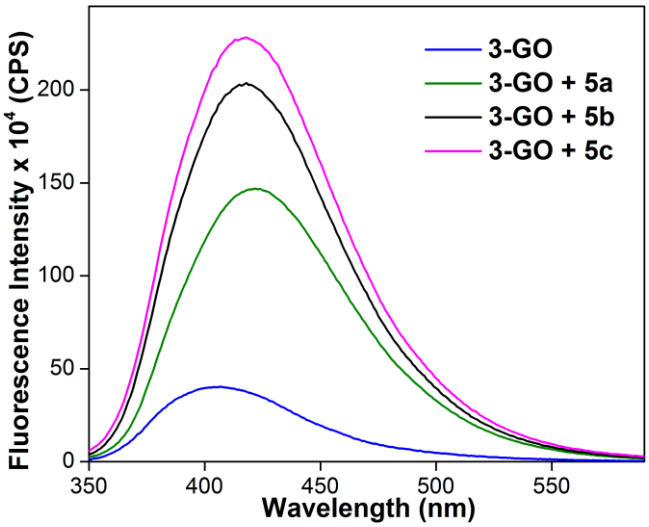

Figure 6. Fluorescence spectra of PNA-GO complex in the presence of telomere DNAs (**5a**–**5c**) of increasing hexameric repeats in phosphate buffer (10 mM, 100 mM NaCl, pH 7.1). Samples were excited at 330 nm and excitation and emission slit widths were kept at 6 and 8 nm, respectively. [35]

In order to further explore the utility of this method, the detection limit of the PNA-GO platform was determined by monitoring the fluorescence response as a function of

increasing concentration of the telomere DNA target. A significant increase in fluorescence intensity was observed upon addition of telomere DNA 5c (25–1000 nM) to the PNA-GO complex, with a good linear correlation until 100 nM of DNA (Figure 7).[34] The detection limit of the PNA-GO platform for the telomeric DNA, based on three times the signal-to-noise level, was estimated to be ~30 nM, which is comparable to other GO-based biosensing systems.[23a,32d,32l]

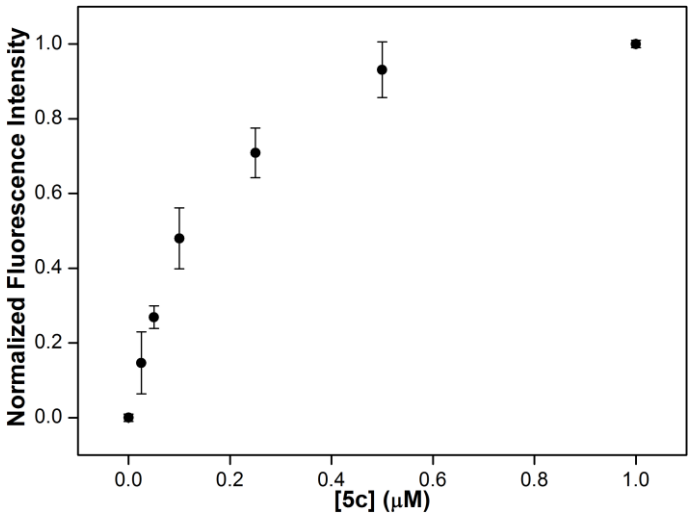

Figure 7. A plot of normalized fluorescence intensity at λ_{em} = 422 nm versus increasing concentration of telomere DNA **5c**. Conc. of PNA **3** (50 nM), GO (0.5 μg/mL) and DNA **5c** (25–1000 nM). Samples were excited at 330 nm and excitation and emission slit widths were kept at 10 nm and 12 nm, respectively. A linear correlation was obtained until 100 nM of DNA **5c** ($y = 4.74x + 0.02$, R^2 = 0.99).[35]

3A.2.3 Displacement of small molecule GQ binder using telomere PNA probe 3

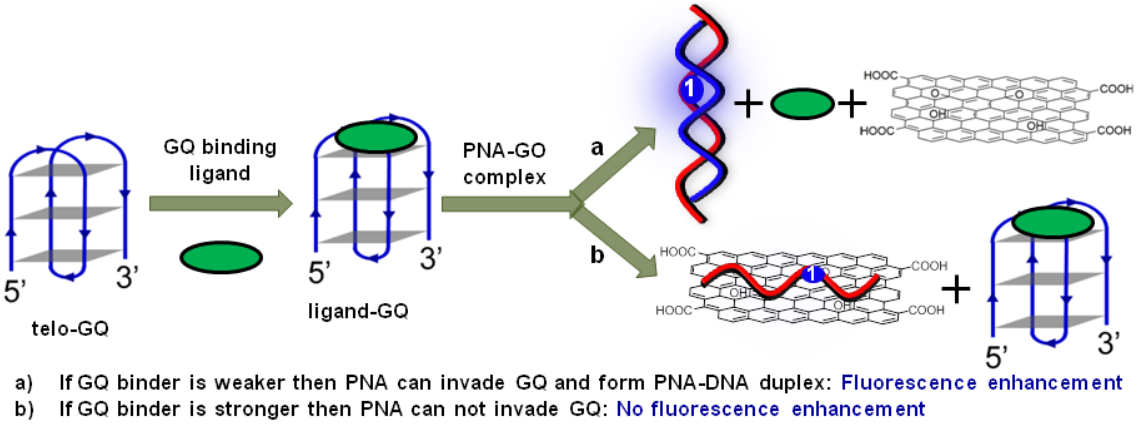

Figure 8. Schematic representation of hybridization assay to detect the displacement of small molecule GQ binder with fluorescent PNA probe.

Next, we evaluated the suitability of this telomere detection assay in identifying small molecules that strongly bind and stabilize GQ structures (Figure 8). For this purpose, we

used two known GQ stabilizing ligands, pyridostatin (**Py**) and BRACO19 (**Bc**), which have been very well studied in the biophysical assays of GQ structures.[36,37]

Telomere targets **5a**–**5c**[37] were first annealed in phosphate buffer containing Na^+ and K^+ to form anti-parallel and parallel GQ structures, respectively.[8] Then 1:1 telomere DNA-**Py**/**Bc** (**5a-Py/Bc**, **5b-Py/Bc** and **5c-Py/Bc**) complexes were prepared by mixing annealed telomere DNAs and **Py**/**Bc** in phosphate buffer.[35] Upon addition of telomere DNA-**Py**/**Bc** complexes to **3**-GO, a significant enhancement in fluorescence intensity corresponding to the emission profile of PNA-telomere DNA duplex was observed in buffer solution containing Na^+ and K^+ ions (Figure 9 and Figure 10). Importantly, in a control experiment, addition of **Py**/**Bc** to PNA-GO complex produced only a small increase in fluorescence intensity. Together, these observations reveal that the desorbed PNA probe displaces **Py**/**Bc** from the telomere DNA-**Py**/**Bc** complex (irrespective of the parallel or anti-parallel nature of the telomere DNA) and forms a stable hybrid with telomeric DNA, resulting in an enhancement in fluorescence intensity. Therefore, in a screening assay using this method, only a very strong GQ binder would resist displacement by the PNA probe, and such a state would be signaled by a low intensity and blue-shifted emission band associated with the PNA-GO complex. Although, this method may not be suitable for estimating the binding constant, low intensity due to PNA-GO complex or high intensity due to PNA-telomere hybrid could indicate if a small molecule ligand, in a screening assay, is a strong or weak GQ binder, respectively. Such displacement methods have been useful in identifying high affinity nucleic acid and protein binders.[39]

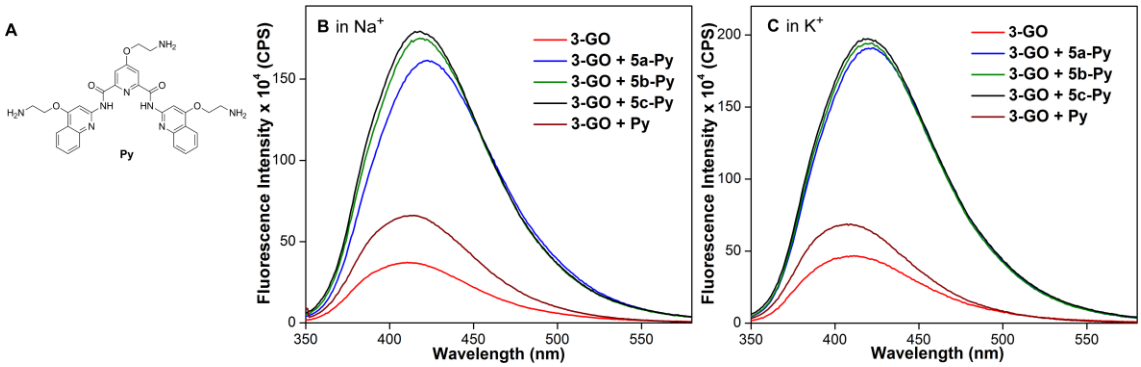

Figure 9. (**A**) Chemical structure of pyridostatin (**Py**). Fluorescence spectra of PNA-GO complex in the presence of telomere DNA-**Py** complexes (**5a-Py**, **5b-Py** and **5c-Py**) in 10 mM phosphate buffer (pH 7.1, 0.1 mM EDTA) containing 100 mM NaCl (**B**) and 100 mM KCl (**C**). Conc. of PNA (100 nM), DNA (1.0 μM), **Py** (1.0 μM) and GO (1.0 μg/mL). Samples were excited at 330 nm and excitation and emission slit widths were kept at 6 and 8 nm, respectively .[35]

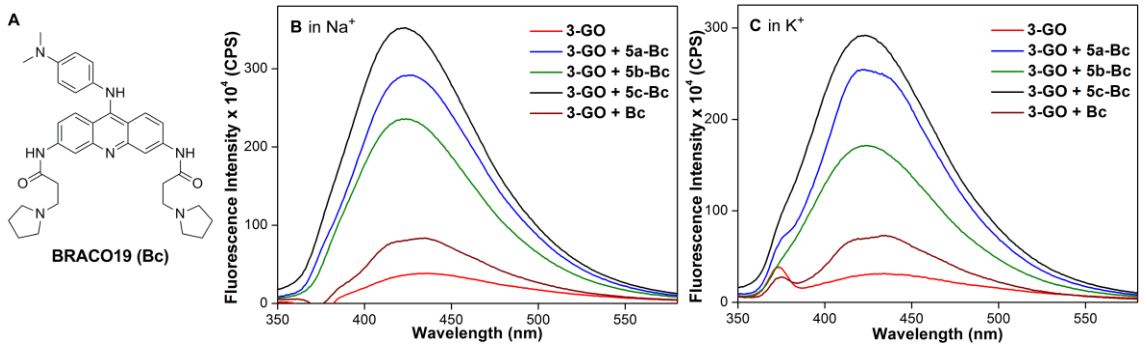

Figure 10. (**A**) Chemical structure of BRACO19 (**Bc**). Fluorescence spectra of PNA-GO complex in the presence of telomere DNA-**Bc** complexes (**5a**-**Bc**, **5b**-**Bc** and **5c**-**Bc**) in 10 mM phosphate buffer (pH 7.1, 0.1 mM EDTA) containing 100 mM NaCl (**B**) and 100 mM KCl (**C**). Conc. of PNA (100 nM), DNA (1.0 μM), **Bc** (1.0 μM) and GO (1.0 μg/mL). Samples were excited at 330 nm and excitation and emission slit widths were kept at 6 and 8 nm, respectively .[35]

3A.3 Conclusion

We have developed a robust and simple homogeneous turn-on fluorescence assay to detect the human telomeric DNA repeats using a unique combination of an environment-sensitive fluorescent nucleobase analogue **1**, the superior base pairing property of PNA, and surface and electronic properties of GO. Notably, long human telomeric sequences can form higher order GQ structures in cells, and hence, methods to detect and identify ligands that bind higher-order GQ could be more useful for studying telomeric GQ structures.[39] In this context, the ability of our PNA-GO platform to detect smaller as well as longer telomeric DNA repeats could be an alternative to existing methods (use of small molecule e.g., thioflavin T)[12e] as most of the investigations use GQ formed by short telomere DNA repeat to study the structure or to indentify GQ-binding ligands. Further, as a proof of principle we have shown the displacement of **Py**/**Bc** ligand from DNA-**Py**/**Bc** (**5a**-**Py**/**Bc**, **5b**-**Py**/**Bc** and **5c**-**Py**/**Bc**) complex using our fluorescent PNA probe **3** with significant enhancement in fluorescence, which suggest that ligands (**Py**/**Bc**) are weak GQ binder. Therefore, given the importance of GQ structures in biology and paucity in discovery assays to identify higher-order GQ binders, we believe that this method, which does not involve rigorous assay and sophisticated instrument setups, would provide new avenues in the study of GQ structures.

3A.4 Experimental Section

3A.4.1 Materials

Pyridostatin (Py) and BRACO19 (Bc) were purchased from Sigma-Aldrich. DNA ONs were purchased from Integrated DNA Technologies. All oligonucleotides were purified by polyacrylamide gel electrophoresis (PAGE) under denaturing conditions and desalted on Sep-

Pak Classic C18 cartridges (Waters Corporation). Autoclaved water was used in all biochemical reactions and fluorescence measurements.

3A.4.2 Instrumentation

All mass measurements were recorded on an Applied Biosystems 4800 Plus MALDI-TOF/TOF analyzer instrument and Water Synapt G2 High Definition mass spectrometers. PNA oligomers were purified by using Agilent Technologies 1260 Infinity HPLC. UV-thermal melting analysis of duplexes was performed on a Cary 300Bio UV-Vis spectrophotometer. Steady-state fluorescence experiments were carried out in a micro fluorescence cuvette (Hellma, path length 1.0 cm) on Fluorolog-3 spectrophotometers (Horibha Scientific). Time-resolved fluorescence experiments were carried out on a TCSPC instrument (Horiba JobinYvon, Fluorolog 3). All CD spectra were recorded on JASCO J-815 CD spectrometer.

3A.4.3 Fluorescence of PNA oligomer 3 and duplexes made of 3

PNA-DNA duplexes **3•5a** and **3•6** were prepared by heating a mixture of PNA **3** (1.0 µM) and DNA **5a** or **6** (10.0 µM) in 10 mM phosphate buffer (pH 7.1, 100 mM NaCl, 0.1 mM EDTA) at 90 °C for 3 min. Samples were cooled to RT slowly and kept on an ice bath for ~1 h. Samples were further diluted using phosphate buffer to give a final duplex concentration of PNA **3** and DNA **5a** or **6** as 100 nM and 1.0 µM respectively. Samples were excited at 330 nm, and excitation and emission slit widths were maintained at 10 nm and 12 nm, respectively. Fluorescence experiments were performed in triplicate in a micro fluorescence cell (Hellma, pathlength 1.0 cm) on a Horiba Scientific Fluoromax-4 spectrofluorometer.

3A.4.4 Fluorescence hybridization assay to detect telomeric DNA repeats using PNA probe 3

Fluorescence of a solution of PNA **3** (100 nM) in 10 mM phosphate buffer (pH 7.1, 100 mM NaCl, 0.1 mM EDTA) was recorded (40 ºC) by exciting the sample at 330 nm with an excitation and emission slit widths of 6 nm and 8 nm, respectively. A spectral blank in the absence of the fluorescence PNA probe was corrected from the above spectrum.

A stock dispersion of GO (100 µg/mL) in water was sonicated for 1 h. The PNA-GO complex (**3**-GO) was prepared by mixing an aqueous solution of PNA **3** with GO in 10 mM phosphate buffer (pH 7.1, 100 mM NaCl, 0.1 mM EDTA) such that the final concentration of **3** and GO was 100 nM and 1.0 µg/mL, respectively. The sample was incubated at room

temperature for 3 h. To another set of solution containing PNA-GO complex was added telomere DNA target **5a** such that the final concentration of PNA **3**, GO and DNA **5a** was 100 nM, 1.0 μg/mL and 1.0 μM, respectively. Similarly, samples were also prepared in the presence of control DNA **6** (1.0 μM) and longer telomeric DNA repeats **5b** and **5c** (1.0 μM). The final volume of each sample was maintained at 400 μL. The samples were incubated for another 75 min at 40 °C, and their fluorescence were recorded at 40 °C under the same conditions mentioned above. A spectrum of GO (1.0 μg/mL) alone in 10 mM phosphate buffer was used for blank correction. All fluorescence measurements were performed at least in triplicate.

3A.4.5 Fluorescence of PNA-GO complex in the presence of telomere DNA-ligand (pyridostatin or BRACO19) complexes

Telomere DNA targets **5a**–**5c** in phosphate buffer, containing either NaCl or KCl, were heated at 90 ºC for 3 min and cooled slowly to RT. After an hour at RT, pyridostatin (**Py**) or BRACO19 (**Bc**) was added to prepare 1:1 telomere-Py/Bc complexes (**5a**-**Py/Bc**, **5b**-**Py/Bc** and **5c**-**Py/Bc**, 50.0 μM). The telomere-**Py**/**Bc** complexes were incubated at RT for an hour and were added to the PNA-GO complex (**3**-GO) as mentioned above. Control experiment was carried out by mixing **3**-GO and **Py**/**Bc**. The total volume of each sample was maintained at 400 μL. The final concentration of PNA **3**, GO and telomere-**Py**/**Bc** complex was 100 nM, 1.0 μg/mL and 1.0 μM, respectively. The samples were incubated for another 75 min at 40 °C, and their fluorescence was recorded under the same conditions as mentioned above. A spectrum of GO (1.0 μg/mL) alone in 10 mM phosphate buffer was used for blank correction. All fluorescence measurements were performed in triplicate.

3A.4.6 Detection limit for PNA-GO platform

The detection limit was calculated based on three times the signal-to-noise level using the following equation.[24a, 32d,32l]

Detection limit = $3\sigma/S$

Where, σ is the variation in fluorescence intensity of PNA-GO complex in the absence of telomere DNA target and S is the slope of the linear fit.

3A.5 Notes and References

1. E. H. Blackburn, *Nat. Struct. Biol.*, 2000, **7**, 847–850.
2. a) R. E. Verdun and J. Karlseder, *Nature*, 2007, **447**, 924–931; b) R. J. O'Sullivan and J. Karlseder, *Nat. Rev. Mol. Cell Biol.*, 2010, **11**, 171–181.
3. V. L. Makarov, Y. Hirose and J. P. Langmore, *Cell*, 1997, **88**, 657–666.
4. W. E. Wright, V. M. Tesmer, K. E. Huffman, S. D. Levene and J. W. Shay, *Genes Dev.*, 1997, **11**, 2801–2809.
5. C. B. Harley, A. B. Futcher and C. W. Greider, *Nature*, 1990, **345**, 458–460.
6. a) R. A. DePinho, *Nature*, 2000, **408**, 248–254; b) Y.-L. Zheng, N. Hu, Q. Sun, C. Wang and P. R. Taylor, *Cancer Res.*, 2009, **69**, 1604–1614.
7. J. W. Shay and I. B. Roninson, *Oncogene*, 2004, **23**, 2919–2933.
8. P. L. T. Tran, J.-L. Mergny and P. Alberti, *Nucleic Acids Res.*, 2011, **39**, 3282–3294.
9. a) K. Paeschke, T. Simonsson, J. Postberg, D. Rhodes and H. J. Lipps, *Nat. Struct. Mol. Biol.*, 2005, **12**, 847–854; b) K. Paeschke, S. Juranek, T. Simonsson, A. Hempel, D. Rhodes and H. J. Lipps, *Nat. Struct. Mol. Biol.*, 2008, **15**, 598–604.
10. a) G. Biffi, D. Tannahill, J. McCafferty and S. Balasubramanian, *Nat. Chem.*, 2013, **5**, 182–186; b) E. Y. N. Lam, D. Beraldi, D. Tannahill and S. Balasubramanian, *Nat. Commun.*, 2013, **4**, 1796–1804; c) Y. Xu, M. Komiyama, *Chembiochem*, 2013, **14**, 927–928; d) A. Henderson, Y. Wu, Y. C. Huang, E. A. Chavez, J. Platt, F. B. Johnson, R. M. Brosh Jr., D. Sen and P. M. Lansdrop, *Nucleic Acids Res.*, 2013, **42**, 860–869.
11. Compounds that bind and stabilize G-quadruplex structures can be potential anticancer agents. a) S. Balasubramanian and S. Neidle, *Curr. Opin. Chem. Biol.*, 2009, **13**, 345–353; b) Y. Xu, *Chem. Soc. Rev.*, 2011, **40**, 2719–2740. See ref. 12 for recent examples.
12. a) D. Monchaud and M.-P. Teulade-Fichou, *Org. Biomol. Chem.*, 2008, **6**, 627–636; b) T.-M. Ou, Y.-J. Lu, J.-H. Tan, Z.-S. Huang, K.-Y. Wong and L.-Q. Gu, *ChemMedChem*, 2008, **3**, 690–713; c) S. N. Georgiades, N. H. Abd Karim, K. Suntharalingam and R. Vilar, *Angew. Chem., Int. Ed.*, 2010, **49**, 4020–4034; d) C. Zhao, L. Wu, J. Ren, Y. Xu and X. Qu, *J. Am. Chem. Soc.*, 2013, **135**, 18786–18789; e) J. Mohanty, N. Barooah, V. Dhamodharan, S. Harikrishna, P. I. Pradeepkumar and A. C. Bhasikuttan, *J. Am. Chem. Soc.*, 2013, **135**, 367–376; f) K. Iida, T. Nakamura, W. Yoshida, M. Tera, K. Nakabayashi, K. Hata, K. Ikebukuro and K. Nagasawa, *Angew. Chem., Int. Ed.*, 2013, **52**, 12052–12055; g) W. J. Chung, B. Heddi, F. Hamon, M.-P. Teulade-Fichou and A. T. Phan, *Angew. Chem., Int. Ed.*, 2013, **53**, 999–1002; h) T. Agarwal, M. K. Lalwani, S. Kumar, S. Roy, T. K. Chakraborty, S. Sivasubbu and S. Maiti, *Biochemistry*, 2014, **53**, 1117−1124.
13. G. Aubert, M. Hills and P. M. Lansdorp, *Mutation Res.*, 2012, **730**, 59–67.
14. a) Y. Gan, K. J. Engelke, C. A. Brown and J. L.-S. Au, *Pharm. Res.*, 2001, **18**, 1655–1659; b) M. Kimura, R. C. Stone, S. C. Hunt, J. Skurnick, X. Lu, X. Cao, C. B. Harley and A. Aviv, *Nat. Protoc.*, 2010, **5**, 1596–1607.
15. a) R. J. Callicott and J. E. Womack, *Comp. Med.* 2006, **56**, 17–22; b) R. M. Cawthon, *Nucleic Acids Res.*, 2009, **37**, e21; c) M. Yamasuji, T. Shibata, T. Kabashima and M. Kai, *Anal. Biochem.*, 2011, **413**, 50–54.
16. J. G. Hacia, E. A. Novotny, R. A. Mayer, S. A. Woski, M. A. Ashlock and F. S. Collins, *Nucleic Acids Res.*, 1999, **27**, 4034–4039.
17. P. M. Lansdorp, N. P. Verwoerd, F. M. van de Rijke, V. Dragowska, M.-T. Little, R. W. Dirks, A. K. Raap and H. J. Tanke, *Hum. Mol. Genet.*, 1996, **5**, 685–691.
18. G-quadruplex forming sequences, which are prevalent in human genome, play important role in replication, transcriptional regulation and telomere maintenance. S.

Balasubramanian, L. H. Hurley and S. Neidle, *Nat. Rev. Drug Discovery*, 2011, **10**, 261–275.
19. Quarfloxin is the only G-quadruplex-binding ligand that reached the Phase II clinical trials for the treatment of neuroendocrine and carcinoid tumors. D. Drygin, A. Siddiqui-Jain, S. O'Brien, M. Schwaebe, A. Lin, J. Bliesath, C. B. Ho, C. Proffitt, K. Trent, J. P. Whitten, J. K. C. Lim, D. Von Hoff, K. Anderes and W. G. Rice, *Cancer Res.*, 2009, **69**, 7653–7661.
20. S. Doose, H. Neuweiler and M. Sauer, *ChemPhysChem*, 2009, **10**, 1389–1398.
21. B. R. Vummidi, J. Alzeer and N. W. Luedtke, *ChemBioChem*, 2013, **14**, 540–558.
22 a) A. Dumas and N. W. Luedtke, *J. Am. Chem. Soc.*, 2010, **132**, 18004–18007; b) A. Nadler, J. Strohmeier and U. Diederichsen, *Angew. Chem., Int. Ed.*, 2011, **50**, 5392–5396; c) Y. Xu, Y. Suzuki, K. Ito and M. Komiyama, *Proc. Natl. Acad. Sci. U. S. A.*, 2010, **107**, 14579–14584; d) S. Müllar, J. Strohmeier and U. Diederichsen, *Org. Lett.*, 2012, **14**, 1382–1385.
23. a) R. S. Swathi and K. L. Sebastiana, *J. Chem. Phys.*, 2009, **130**, 086101; b) J. Liu, *Phys. Chem. Chem. Phys.*, 2012, **14**, 10485–10496.
24. a) C.-H. Lu, H.-H. Yang, C.-L. Zhu, X. Chen and G.-N. Chen, *Angew. Chem. Int. Ed.*, 2009, **48**, 4785–4787; b) S. He, B. Song, D. Li, C. Zhu, W. Qi, Y. Wen, L. Wang, S. Song, H. Fang and C. Fan, *Adv. Funct. Mater.*, 2010, **20**, 453–459; c) L. Tang, H. Chang, Y. Liu and J. Li, *Adv. Funct. Mater.*, 2012, **22**, 3083–3088.
25. P. E. Nielsen, *Acc. Chem. Res*., 1999, **32**, 624–630.
26. W. Yang, K. R. Ratinac, S. P. Ringer, P. Thordarson, J. J. Gooding and F. Braet, *Angew. Chem. Int. Ed*., 2010, **49**, 2114–2138.
27. (*a*) S. Stankovich, D. A. Dikin, G. H. B. Dommett, K. M. Kohlhaas, E. J. Zimney, E. A. Stach, R. D. Piner, S. T. Nguyen and R. S. Ruoff, *Nature*, 2006 , **442** , 282–286; (*b*) E. Morales-Narváez, B. Pérez-López, L. B. Pires and A. Merkoçi, *Carbon*, 2012, **50**, 2987–2993.
28. E. Morales-Narváez and A. Merkoçi, *Adv. Mater.*, 2012, **24**, 3298–3308.
29. a) W. S. Hummers and Jr. R. E. Offeman, *J. Am. Chem. Soc.*, 1958, **80**, 1339–1339; b) Y. Pan, H. Bao, N. G. Sahoo, T. Wu and L. Li, *Adv. Funct. Mater.*, 2011, **21**, 2754–2763.
30. N. Varghese, U. Mogera, A. Govindaraj, A. Das, P. K. Maiti, A. K. Sood and C. N. R. Rao, *ChemPhysChem*, 2009, **10**, 206–210.
31. Reviews: a) Y. Wang, Z. Li, J. Wang, J. Li and Y. Lin, *Trends Biotechnol.*, 2011, **29**, 205–212; b) J. Liu, *Phys. Chem. Chem. Phys.*, 2012, **14**, 10485–10496; c) L. Cui, Y. Song, G. Ke, Z. Guan, H. Zhang, Y. Lin, Y. Huang, Z. Zhu and C. J. Yang, *Chem. –Eur. J.*, 2013, **19**, 10442–10451.
32. Examples: a) H. Chang, L. Tang, Y. Wang, J. Jiang and J. Li, *Anal. Chem.*, 2010, **82**, 2341–2346; b) H. Wang, Q. Zhang, X. Chu, T. Chen, J. Ge and R. Yu, *Angew. Chem., Int. Ed.*, 2011, **50**, 7065–7069; c) V. Kotikam, M. Fernandes, V. A. Kumar, *Phys. Chem. Chem. Phys.*, 2012, **14**, 15003–15006. d) P.-J. J. Huang and J. Liu, *Anal. Chem.*, 2012, **84**, 4192−4198; e) Z. Wang, Z. Ge, X. Zheng, N. Chen, C. Peng, C. Fan and Q. Huang, *Nanoscale*, 2012, **4**, 394–399; f) J. S. Park, A. Baek, I.-S. Park, B.-H. Junb and D.-E. Kim, *Chem. Commun.*, 2013, **49**, 9203–9205; g) M. Zhang, H.-N. Le and B.-C. Ye, *ACS Appl. Mater. Interfaces*, 2013, **5**, 8278–8282; h) E. J. Lee, H. K. Lim, Y. S. Cho and S. S. Hah, *RSC Adv.*, 2013, **3**, 5828–5831; i) S. J. Moon, S. H. Park, J. Jaworski and J. H. Jung, *Chem. Commun.*, 2013, **49**, 11698–11700; j) S.-R. Ryoo, J. Lee, J. Yeo, H.-K. Na, Y.-K. Kim, H. Jang, H. H. Lee, S. W. Han, Y. Lee, V. N. Kim and D.-H Min, *ACS Nano*, 2013, **7**, 5882–5891; k) A. H. Loo, A. Bonanni and M. Pumer, *Nanoscale*, 2013, **5**, 4758–4762; l) S. Guo, D. Du, L. Tang, Y. Ning, Q. Yao and G.-J. Zhang, *Analyst*, 2013, **138**, 3216–3220; m) R. K. Koninti, A. Sengupta, K. Gavvala, N. Ballav and P. Hazra,

Nanoscale, 2014, **6**, 2937–2944; n) J. Lee, G. Park and D.-H. Min, *Chem. Commun.*, 2015, **51**, 14597–14600; o) S. T. Huang, Y. Shi, N. B. Li and H. Q. Luo, *Analyst*, 2012, **137**, 2593–2599.
33. P. M. Sabale, J. T. George and S. G. Srivatsan, *Nanoscale*, 2014, **6**, 10460–10469.
34. B. Liu, Z. Sun, X. Zhang and J. Liu, *Anal. Chem.*, 2013, **85**, 7987–7993.
35. See Experimental Section for details.
36. R. Rodriguez, S. Müller, J. A. Yeoman, C. Trentesaux, J.-F. Riou and S. Balasubramanian, *J. Am. Chem. Soc.*, 2008, **130**, 15758–15759.
37. M. J. B. Moore, C. M. Schultes, J. Cuesta, F. Cuenca, M. Gunaratnam, F. A. Tanious, W. D. Wilson and S. Neidle, *J. Med. Chem.*, 2006, **49**, 582–599.
38. M. Hafner, A. Schmitz, I. Grune, S. G. Srivatsan, B. Paul, W. Kolanus, T. Quast, E. Kremmer, I. Bauer and M. Famulok, *Nature*, 2006, **444**, 941–944.
39. Higher-order G-quadruplex structures could be an important factor in recognition and function of telomeric DNA in vivo. L. Petraccone, *Top. Curr. Chem.*, 2013, **330**, 23–46.

Chapter 3B

Benzothiophene-conjugated uracil PNA analogue as a fluorescence tool for detecting oncogenic G-quadruplex motifs and activity of toxic ribosome inactivating proteins

3B.1 Introduction

Environment-sensitive fluorescent PNA nucleobase analogues that show enhancement in fluorescence intensity upon hybridization with complementary DNA/RNA oligonucleotides (ONs) can be used to develop turn-on fluorescence assays for the detection of therapeutically relevant nucleic acid targets. As a part of our efforts in this direction, we have discussed the synthesis and photophysical properties of 5-benzofuran- (BF) and 5-benzothiophene-modified uracil (BT) PNA oligomer probes in Chapter 2.[1] In general, both the analogues exhibit enhancement in fluorescence intensity, when hybridized to complementary ONs. In the first section of this chapter, we have introduced a turn-on fluorescence hybridization assay for the detection of telomeric DNA repeats by BF PNA probe. However, this assay requires a graphene oxide (GO) platform to quench the fluorescence of single stranded (ss) BF PNA probe.[2] In order to develop a simple and robust hybridization assay, an ideal ss PNA probe should be weakly fluorescent while its duplex with complementary ONs should be highly fluorescent.

GAG triplet base sets are constituents of many functionally important nucleic acid motifs such as G-quadruplex (GQ) forming sequences in the promoter (c-myc, c-myb, c-kit etc.) and untranslated regions (UTRs) of mRNA (NRAS, BCL-2 etc.) of a number of oncogenes.[3] In addition, GAG base set is also present in the highly conserved sarcin-ricin loop of eukaryotic 28S rRNA, which is a critical site for the binding of elongation factors to ribosome during protein synthesis.[4] Interestingly, PNA oligomers containing BT modification flanked in between C-residue (C**7**C), displayed significant enhancement in fluorescence intensity when hybridized to perfect complementary DNA ON (with GAG base set) as compared to ss PNA and mismatched duplexes.[1] The responsiveness of BT-modified PNA oligomers in different neighbouring bases has been discussed in the previous chapter. In this chapter, the development of a turn-on fluorescence hybridization assay for the detection of biologically important GQ forming promoter oncogenes such as c-myc and c-kit using the sensitivity of the BT-modified PNA base analogue has been described (Figure 1A). Further, the ability of the PNA probe to photophysically distinguish between a complementary base in a GAG base set and an abasic site in an RNA-PNA duplex has been utilized in setting up a method to monitor and estimate the depurination activity of ribosome inactivating protein toxins (RIPs, e.g. saporin, Figure 1B).

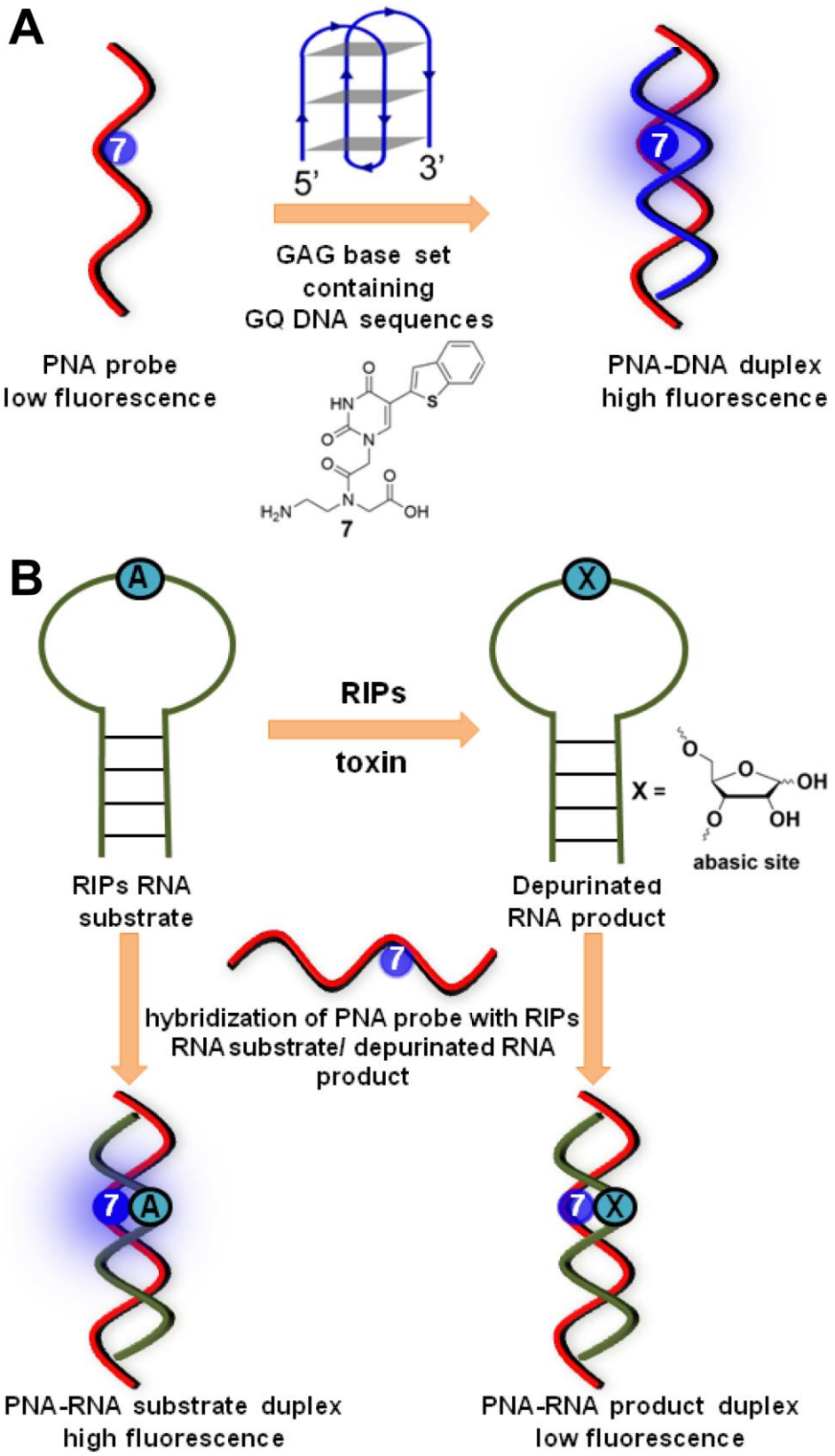

Figure 1. (**A**) A schematic illustration of the fluorescence turn-on assay to detect the GAG base set containing GQ forming DNA sequences using emissive PNA probes. (**B**) Study of depurination activity of ribosome inactivating protein (RIP) toxin using fluorescent PNA oligomer probe.

3B.2 Results and discussion

3B.2.1 Fluorescence detection of GQ forming oncogenic promoter DNA sequences

GQ sequences are majorly found in telomeric DNA repeats, telomeric repeat-containing RNA (TERRA), and in promoter regions and untranslated regions (UTR) of mRNA of a number of oncogenes.[3,5] These GQ structures play a crucial roles in the cellular processes such as maintaining the chromosomal stability, replication, transcription and recombination.[6] The detection of putative GQ forming sequences in human genome greatly relies on techniques such as fluorescence *in situ* hybridization, FRET and immunofluorescence microscopy.[7] Several fluorescent non-covalent GQ binders have been implemented in stabilization and detection of these GQ structures.[8,9] Additionally, fluorescent analogues incorporated into oligomers have been developed to study the formation of GQ structures.[10] While these fluorescence-based detection tools are very useful, however certain disadvantages hamper their practical applications. Many of the small molecule ligands and ON probes poorly distinguish different GQ topologies and or display unfavorable fluorescence properties such as low fluorescence when bound to G-rich sequences.[8a,11] In this context, PNA hybridization probes containing a minimally perturbing fluorescent nucleobase analogue that could report its binding to target G-rich ONs with significant enhancement in fluorescence would serve as robust tool to detect G-rich sequences in human genome. Coincidentally, GAG triplet base sets are present in human oncogenic GQ forming promoter DNA sequences (e.g., c-myc, c-kit).[3,12] Importantly, such GAG base sets are not found in the GQ forming regions of telomeric DNA repeats and TERRA. Therefore, it could be possible to detect such promoter GQ sequences in cellular conditions selectively over telomeric DNA/RNA repeats using these emissive PNA probes.

To setup a turn-on fluorescence hybridization assay for the detection GQ forming c-myc and c-kit2 ONs using benzothiophene-modified PNA analogue **7**, we synthesized fluorescent PNA oligomers **8** and **9** by using SPPS (Figure 2A). PNA oligomers **8** and **9** are complementary to c-myc and c-kit2 ONs respectively. PNA oligomers were purified by RP-HPLC and their integrity was confirmed by MALDI-TOF mass analysis (Figure 2 and Table 1). PNA probes **8** and **9** contain C**7**C base set, which upon hybridization to c-myc and c-kit2 ONs would place the emissive analogue **7** opposite to complementary base dA in GAG base set of the target ONs. Initially, CD and UV-thermal melting studies were performed to confirm the formation of parallel GQ structure by c-myc and c-kit2 ONs in a buffer solution containing 100 mM KCl (Figure 3 and Table 2). The GQ structure formed by c-kit2 (T_m =

67.5 ± 0.8) has much lower T_m value as compared to c-myc ON (T_m = 79.0 ± 0.5, Table 2). This difference in the T_m value of GQ structures are due to different number of tetrads present in respective GQ structures; c-myc GQ structure consists of four tetrads whereas c-kit2 consists of three tetrads.[12a,12d] The T_m of GQ structures also depend on the number nucleotides presents in the loop; with increase in number of nucleotide in loop increases the flexibility and decreases the stability. In the c-myc GQ structure, only one nucleotide is present in all four loops and one of the A-residues in the loop participate in the tetrad formation. Alternatively, c-kit2 GQ structure consists of three loops (two with single nucleotide and one with five nucleotides), which provides extra flexibility but lower stability.

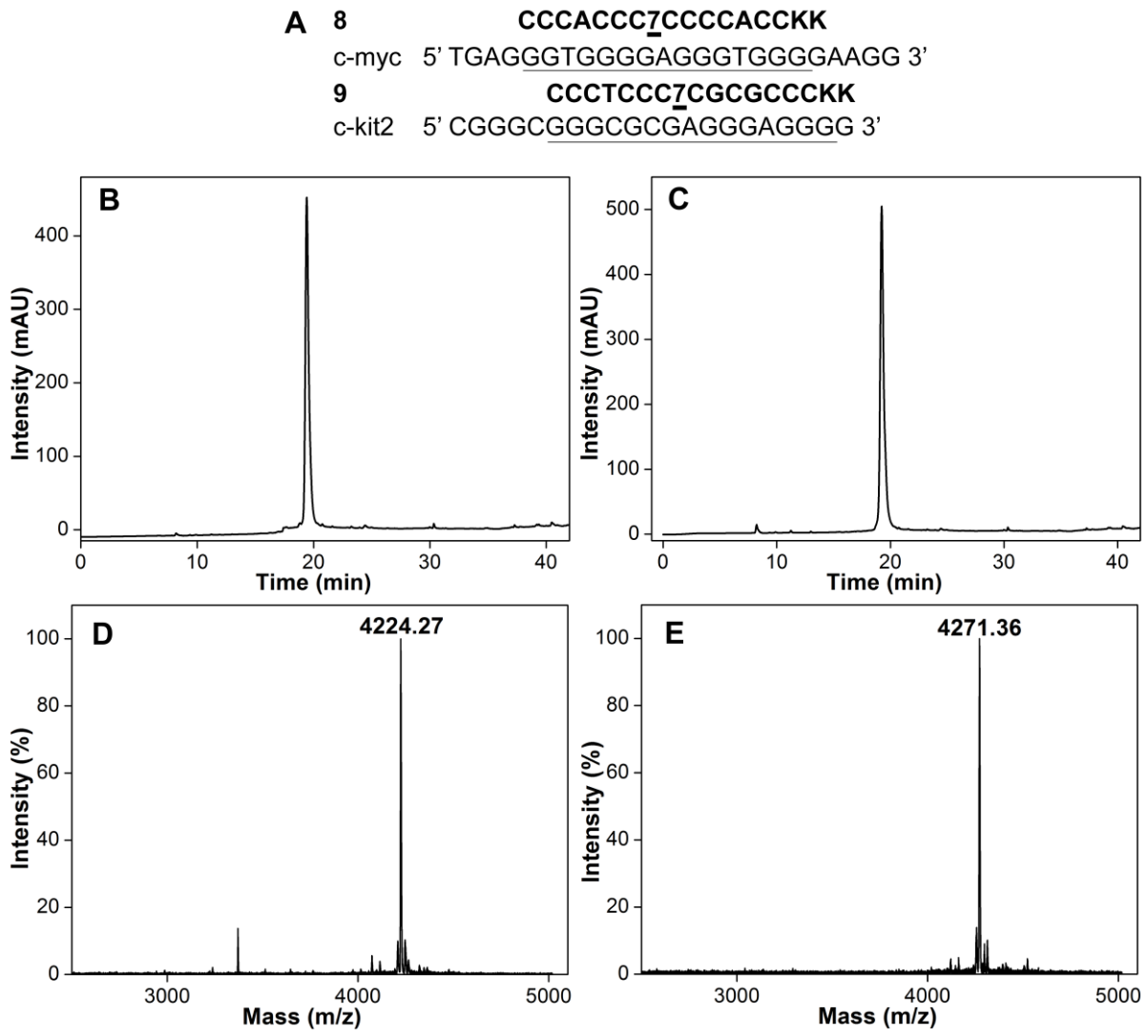

Figure 2. (**A**) Sequence of GQ forming c-myc and c-kit2 DNA ONs used in this study. Fluorescent PNA oligomers **8** and **9** complementary to c-myc and c-kit2, respectively were synthesized by solid-phase synthesis. PNA oligomers (highlighted in bold) are written from N to C terminus and contain two lysine (K) residues at the C terminus. RP-HPLC chromatogram of benzothiophene-modified PNA oligomers **8** (**A**) and **9** (**B**) at 260 nm. MALDI-TOF mass spectrum of benzothiophene-modified PNA oligomers **8** (**C**) and **9** (**D**). For mass data see Table 1.

Table 1. ε_{260} and MALDI-TOF mass analysis of PNA oligomers

PNA	Sequence[a]	ε_{260} ($M^{-1}cm^{-1}$)	Calculated mass	Observed mass
8	CCCACCC**7**CCCCACCKK	11.68 x 10^4	4223.29	4224.27
9	CCCTCCC**7**CGCGCCCKK	11.48 x 10^4	4270.30	4271.36

[a]PNA sequences are written from N to C terminus.

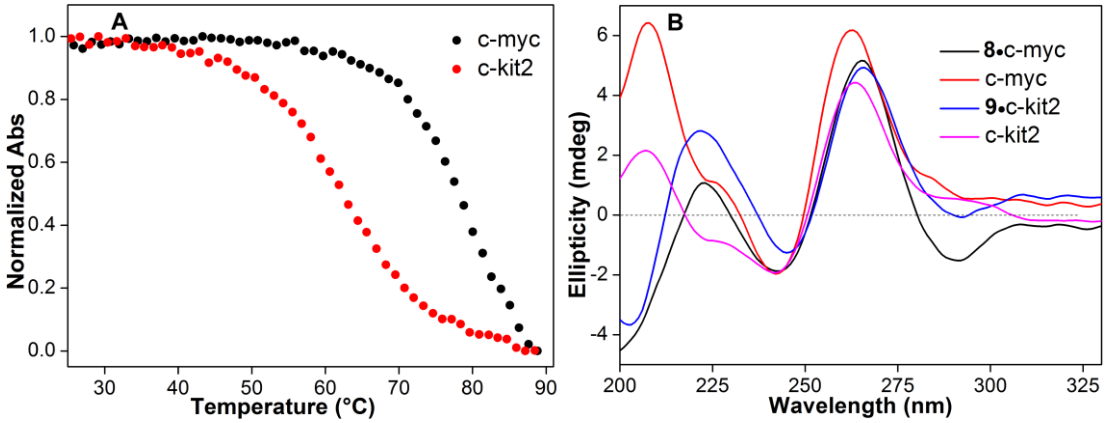

Figure 3. (**A**) UV-thermal melting profile of GQ forming DNA ONs c-myc and c-kit2 (1.0 µM) in 10 mM phosphate buffer (pH 7.1, 100 mM KCl, 0.1 mM EDTA) at 295 nm. (**B**) CD spectra (5.0 µM) of benzothiophene-modified PNA-DNA duplexes (**8**•c-myc and **9**•c-kit2) and GQ forming DNA ONs (c-myc and c-kit2) in 10 mM phosphate buffer (pH 7.1, 100 mM KCl, 0.1 mM EDTA). For T_m values see Table 2.[13]

Table 2. T_m values of GQ of c-myc and c-kit2 and their respective duplexes with fluorescent PNA probes **8** and **9**.

GQ	T_m (°C)	Duplex made of **7**	T_m (°C)
c-myc	79.0 ± 0.5	**8**•c-myc	77.2 ± 0.8
c-kit2	67.5 ± 0.8	**9**•c-kit2	79.8 ± 0.6

PNA probes **8** and **9** were hybridized with c-myc and c-kit2 ONs and subjected to fluorescence studies. A hybrid of **8** and c-myc displayed discernible enhancement in fluorescence intensity (~2-fold) as compared to single stranded PNA **8** (Figure 4). Remarkably, a hybrid of **9** and c-kit2 displayed nearly 7-fold enhancement in fluorescence intensity as compared to free PNA **9**. In the absence of structural information, it is likely that the enhancement in fluorescence intensity exhibited by duplexes could be due to rigidification of the PNA base analogue in the base paired state as compared to in single stranded PNAs. Reduced stacking interaction between the base paired fluorophore (projected in the major groove) and adjacent bases, and solvation-desolvation effects could have also influenced the overall outcome of fluorescence.

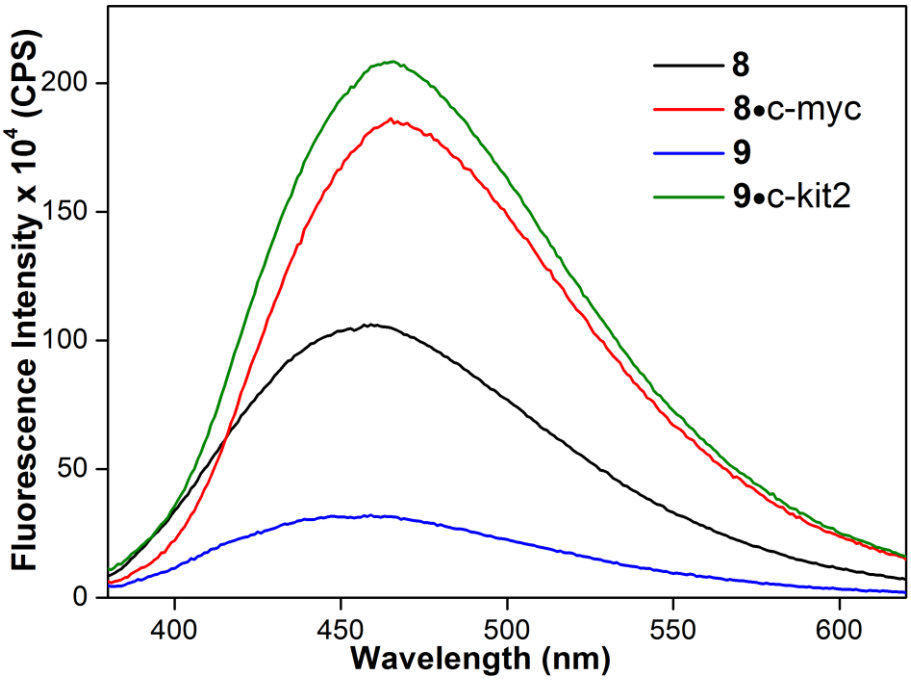

Figure 4. Emission spectra (0.5 µM) of single stranded PNA (**8** and **9**) and their duplex with c-myc and c-kit2 (**8**•c-myc and **9**•c-kit2) in phosphate buffer containing 100 mm KCl. Samples were excited at 330 nm and excitation and emission slit widths were kept at 4 and 5 nm, respectively.[13]

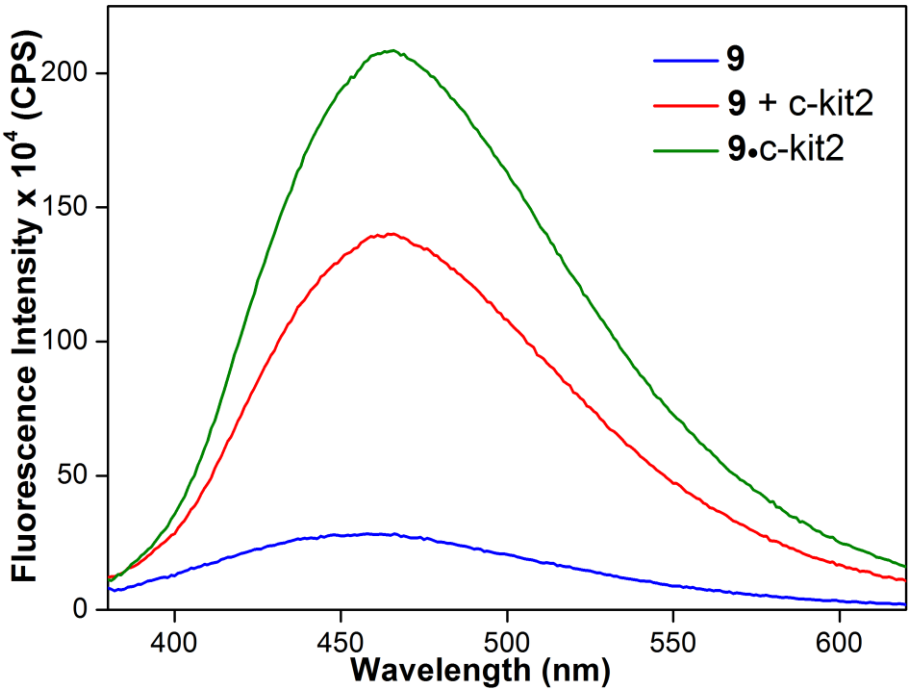

Figure 5. Fluorescence analysis of c-kit2 GQ strand invasion using complementary PNA probe **9**. PNA **9** (1 µM) was added to a preformed GQ structure of c-kit2 (1 µM) in 10 mM phosphate buffer (pH 7.1, 100 mM KCl, 0.1 mM EDTA) and incubated for 4 h. The final concentration of **9** + c-kit2 mix was 0.5 µM. Samples were excited at 330 nm and fluorescence was recorded with excitation and emission slit widths of 4 and 5 nm, respectively. For comparison, the fluorescence profile of annealed **9**•c-kit2 duplex (0.5 µM, green) was also recorded under similar conditions. A nearly 5-fold enhancement in fluorescence intensity was observed when PNA probe **9** was incubated with preformed GQ structure of c-kit2 (red), which indicates that benzothiophene-modified PNA **9** disrupts the GQ structure of c-kit2 and forms a more emissive **9**•c-kit2 heteroduplex.

Notably, T_m of PNA-DNA hybrid **9**•c-kit2 was found to be significantly higher than GQ of c-kit2, which indicates that **9** could potentially invade the GQ structure of c-kit2 and form PNA-DNA heteroduplex (Table 2). We performed strand invasion experiment by adding PNA **9** to a preformed GQ structure of c-kit2 in a buffer containing 100 mM KCl. The sample was incubated for 4 hr at 37 °C and fluorescence was measured. Rewardingly, we observed a nearly 5-fold enhancement in fluorescence intensity as compared to free PNA probe **9**, which indicates that benzothiophene-modified PNA **9** disrupts the GQ structure of c-kit2 and forms a more emissive **9**•c-kit2 heteroduplex (Figure 5). On the other hand, PNA **8** did not show appreciable enhancement in fluorescence intensity upon incubation with preformed GQ structure of c-myc (Figure 6). This could be due to similar T_m values exhibited by both GQ of c-myc and **8**•c-myc duplex, which would have prevented PNA from invading the c-myc GQ structure effectively. It has been shown earlier that homologus PNA oligomers can invade and form stable heteroquadruplex with c-myc, while complementary PNA oligomers fail to strand invade GQ of c-myc to form a duplex.[14]

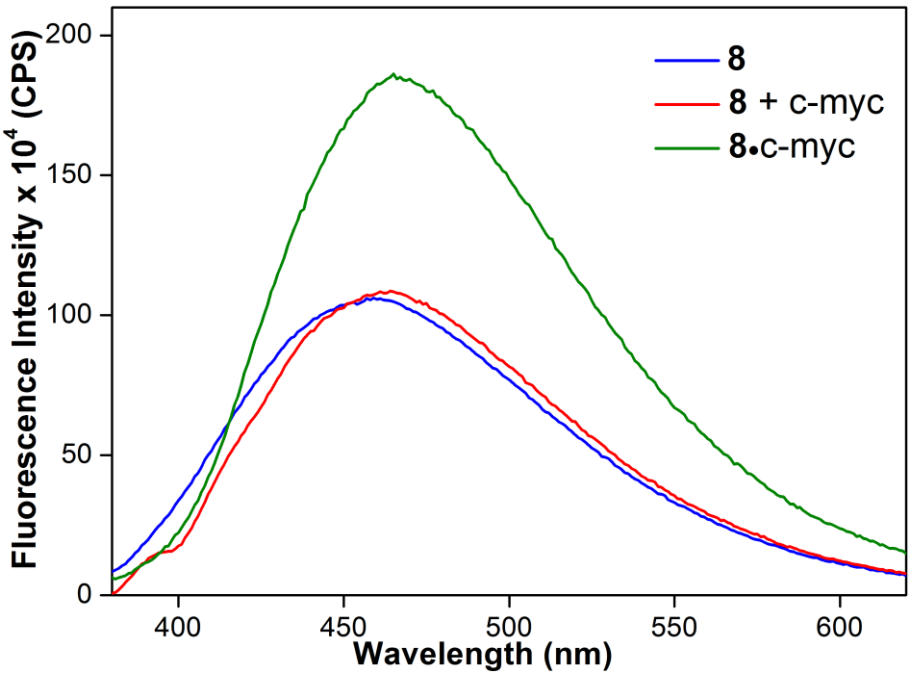

Figure 6. Fluorescence analysis of c-myc GQ strand invasion using complementary PNA probe **8**. PNA **8** (1 µM) was added to a preformed GQ structure of c-myc (1 µM) in 10 mM phosphate buffer (pH 7.1, 100 mM KCl, 0.1 mM EDTA) and incubated for 4 h. The final concentration of **8** + c-myc mix was 0.5 µM. Samples were excited at 330 nm and fluorescence was recorded with excitation and emission slit widths of 4 and 5 nm, respectively. For comparison, the fluorescence profile of annealed **8**•c-myc duplex (0.5 µM, green) was also recorded under similar conditions. There was no enhancement in fluorescence intensity, when PNA probe **8** was incubated with preformed GQ structure of c-myc (red), which indicates that benzothiophene-modified PNA **8** did not disrupts the GQ structure of c-myc and forms a slightly more emissive **8**•c-myc heteroduplex.

Taken together, these results substantiate that benzothiophene-modified PNA oligomers could be potentially utilized as fluorescence turn-on probes to detect certain GQ forming motifs. Transcription and translation regulation of protein expression by targeting such GQ structures is being actively pursued. Ligands and oligomer probes that specifically bind to GQs have been shown to regulate the activity of oncogenic promoter DNA and RNA sequences.[5] Hence, these PNA probes might also enable the study of the functional roles of GQ-forming sequences. Currently, we are evaluating the role of PNA probes in invading the GQ structures of c-myc and c-kit2 gene *in vitro,* using luciferase assay. Results will be further extended to study the down regulation of genes *in vivo* by dual luciferase assay.

3B.2.2 Fluorescence detection of the depurination activity of RIP toxin

DNA abasic sites are common lesions and several methods are available to study their formation and repair.[15] However, the formation of RNA abasic sites are rare. RNA abasic sites are formed by the depurination activity of a certain class of protein toxins called ribosome inactivating proteins (RIPs).[4] RIPs toxin is known to bind to sarcin-ricin loop of 28S rRNA and specifically depurinate adenosine residue from the GAG base set, which results in the formation of abasic site.[4] This reduces the affinity of ribosome to elongation factors that are critical for protein synthesis, and further lead to cell death. While immunoassays have been usually used in the detection of RIPs toxin.[16] Radiolabeling, electrochemiluminescence, fluorescence and mass spectrometry techniques have also been utilized to detect their activity.[17,18] In particular, fluorescent probes placed opposite or adjacent to an abasic site have enabled the detection of abasic sites in nucleic acids.[18,19a-19d] However, some of these methods are laborious involving rigorous chemical manipulations, assay set-ups and also there are no effective antidotes for the treatment of RIPs (e.g., ricin) exposure. Alternatively, the PNA as well as LNA FIT probes developed by Seitz *et al.* could also be useful for developing a hybridization assay for the detection of abasic sites in target nucleic acids.[19e] Hence, the development of methods that can quantitatively report the depurination activity of these protein toxins and are amenable to screening formats could facilitate the discovery of RIP inhibitors.

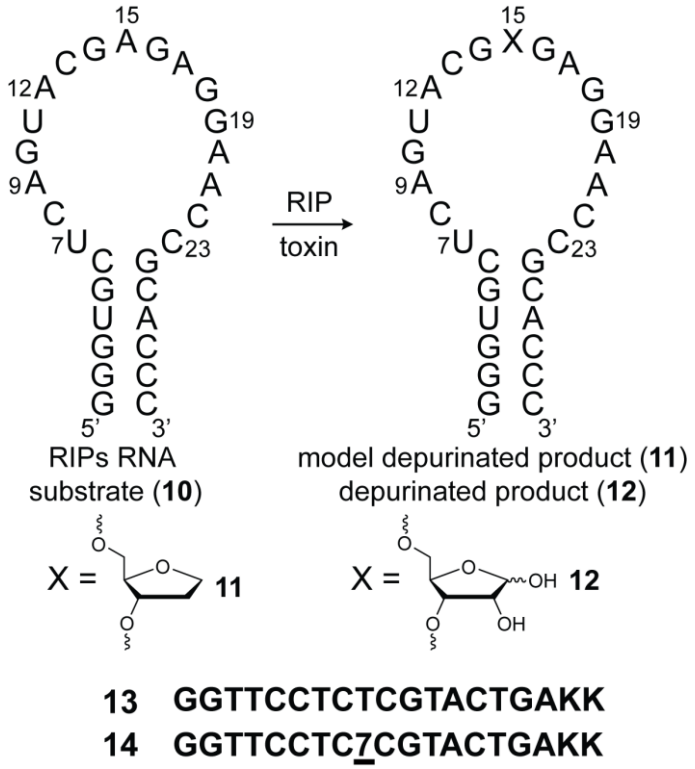

Figure 7. Sequence of synthetic RIPs RNA substrate **10** and depurinated product mimic **11** containing a chemically stable abasic site substitute X. Adenosine residue A_{15} corresponding to A_{4324} of 28S rRNA is specifically depurinated by RIP toxins to produce RNA **12**. Control unmodified **13** and fluorescently modified **14** PNA oligomers complementary to loop of RIPs RNA.

RIP toxins such as ricin and saporin specifically depurinate an adenosine residue (A_{4324}) present in the highly conserved sarcin-ricin loop of eukaryotic 28S rRNA (Figure 7).[20] The C**7**C triplet PNA base set is complementary to the triplet residue $GA_{4324}G$ of the rRNA motif, which is the target of RIP toxins (Figure 7). The ability of emissive PNA base **7** to selectively signal the presence of a complementary base (dA) in duplex with appreciable enhancement in fluorescence intensity motivated us to evaluate its behavior opposite an abasic site (site devoid of a nucleobase). Hence, if the fluorescence of the PNA base analogue placed opposite to a complementary base and abasic site in a RIP RNA substrate and its depurinated product respectively, is distinguishable, then it would be possible to develop a fluorescence hybridization assay to detect the activity of RIP toxins, irrespective of the protein's identity.

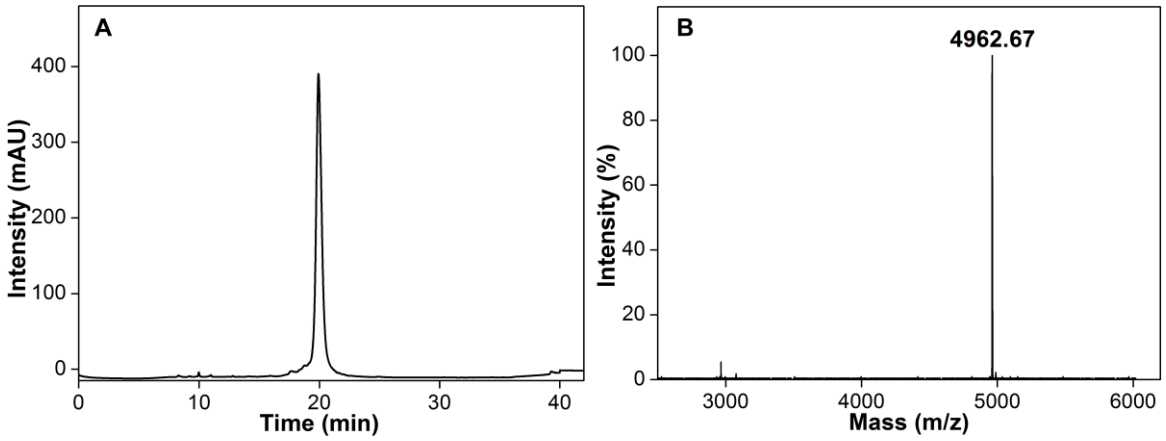

Figure 8. (**A**) RP-HPLC chromatogram of PNA probe **14** at 260 nm. Mobile phase A: 5% acetonitrile in H_2O containing 0.1% TFA, mobile phase B: 50% acetonitrile in H_2O containing 0.1% TFA. Flow rate: 2 mL/min. Gradient: 0–50% B in 25 min and 50–100% B in 20 min. (**B**) MALDI-TOF mass spectrum of PNA probe **14**. Calculated for $[M]^+$ = 4960.93 and observed = 4962.67.

Table 3. Molar absorption coefficient and MALDI-TOF mass data of PNA oligomers

PNA	Sequence[a]	ε_{260} ($M^{-1}cm^{-1}$)	Calculated mass $[M]^+$	Observed mass
13	GGTTCCTCTCGTACTGAKK	15.88 x 10^4	4842.78	4842.60
14	GGTTCCTC**7**CGTACTGAKK	16.04 x 10^4	4960.93	4962.67

[a]PNA sequences are written from N to C terminus.

Initially, control unmodified **13** and fluorescently modified PNA oligomers **14** complementary to RNA ONs **10** and **11** containing the conserved region of the sarcin-ricin stem-loop domain of rRNA were synthesized using SPPS (Figure 8, Table 3). While **10** is a commonly used RIPs RNA substrate for *in vitro* applications, **11** represents a depurinated RNA product mimic with a chemically stable abasic site surrogate, tetrahydrofuran.[18] First, the effectiveness of PNA base analogue **7** to report the presence of an abasic site in RNA was evaluated by performing fluorescence studies of single strand PNA **14** and its duplex with RNA ONs **10** and **11**. Hybridization of PNA **14** with RNA ONs **10** and **11** will place **7** opposite to its complementary base (A_{15} = A_{4324}) and an abasic site, respectively. Rewardingly, the PNA analogue signaled the presence of an abasic site in the model product duplex **14•11** with a significant reduction (~3.5-fold) in fluorescence intensity as compared to the substrate duplex **14•10** (Figure 9). Interestingly, the melting temperature of duplex **14•11** containing fluorescent analogue opposite to an abasic site was discernibly higher than that of control unmodified duplex **13•11** containing the native uracil base opposite to an abasic site (Figure 10, Table 4). This observation points out that the benzothiophene ring is possibly intrahelical and stacked between the guanine residues of the RNA strand as the conformation of **7** placed opposite to an abasic site is not restricted by base pair interaction. PNA base

analogue in such a conformation would provide additional stabilization to duplex (**14•11**) and show significant quenching in fluorescence intensity.[21]

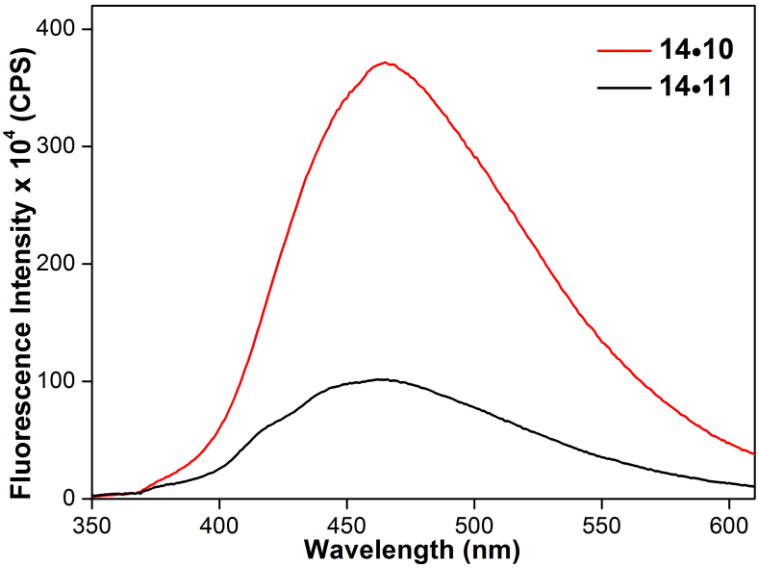

Figure 9. Emission spectra (1.0 µM) of PNA-RNA substrate (**14•10**) and model depurinated product duplexes (**14•11**). Samples were excited at 330 nm and excitation and emission slit widths were kept at 5 nm and 7 nm, respectively.[13]

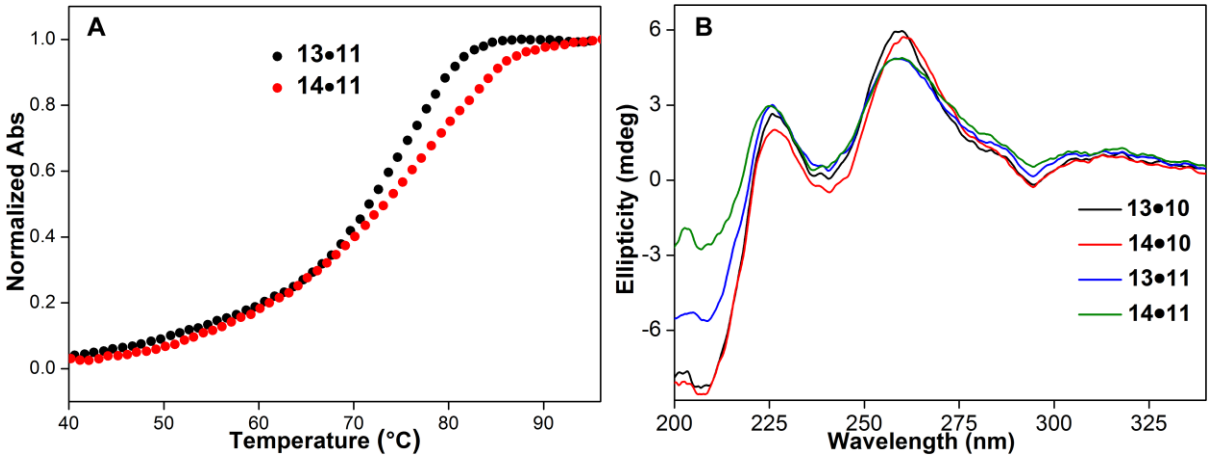

Figure 10. (**A**) UV-thermal melting profile (1.0 µM) of control unmodified (**13•11**) and fluorescently modified (**14•11**) model depurinated product duplex in 10 mM phosphate buffer (pH 7.1, 100 mM NaCl, 0.1 mM EDTA). For T_m values see Table 4. (**B**) CD spectra (5.0 µM) of control unmodified (**13•10** and **13•11**) and fluorescently modified (**14•10** and **14•11**) PNA-RNA duplexes in 10 mM phosphate buffer (pH 7.1, 100 mM NaCl, 0.1 mM EDTA).

Table 4. T_m values of duplexes assembled by hybridizing control PNA **13**/ fluorescent PNA probe **14** with RIPs RNA substrate **10** and abasic site-containing RNA product mimic **11**.

Control duplex	T_m (°C)	Duplex made of **7**	T_m (°C)
13•10	89.7 ± 1.0	**14•10**	87.2 ± 1.4
13•11	75.2 ± 1.0	**14•11**	80.3 ± 0.4

Further, to study the suitability of **7** in detecting and estimating the depurination activity of RIP toxins, we selected saporin as a representative toxin. Saporin is commercially available and has been shown to specifically depurinate the adenosine residue corresponding to A_{4324} of synthetic RNA substrates containing the conserved region of the sarcin-ricin stem-loop domain of rRNA.[17,18] Thermally folded RNA substrate **10** was incubated in the presence of different concentrations of saporin in Tris-HCl buffer (30 mM, 25 mM NaCl, 2 mM $MgCl_2$, pH 6.0) at 37 °C. Aliquots of reaction solution at different time intervals were immediately quenched by adding fluorescent PNA **14** followed by rapid thermal denaturation by heating the samples at 90 °C and rehybridization by flash cooling on an ice bath. Fluorescence spectra of aliquots revealed a time-dependent quenching in emission intensity as a result of generation of an abasic site by saporin and subsequent formation of product duplex **14•12** (Figure 11). Further, the fluorescence data was fitted using an exponential rate equation to determine the apparent rate constant (k_{ap}) of the depurination reaction (Figure 12). A positive correlation between rate and toxin concentration was obtained, and the rates were comparable with literature reports, which used similar synthetic RIP substrate (Table 5).[17a,18] These results clearly demonstrate that the emissive PNA base analogue **7**, when placed opposite to a developing abasic site in RNA, can be used to detect and estimate the depurination activity of RIP toxins. It should be mentioned that a benzofuran-modified DNA ON that reported an abasic site in a custom synthesized model RNA[22] failed to report the depurination activity of the RIP toxin (data not shown).

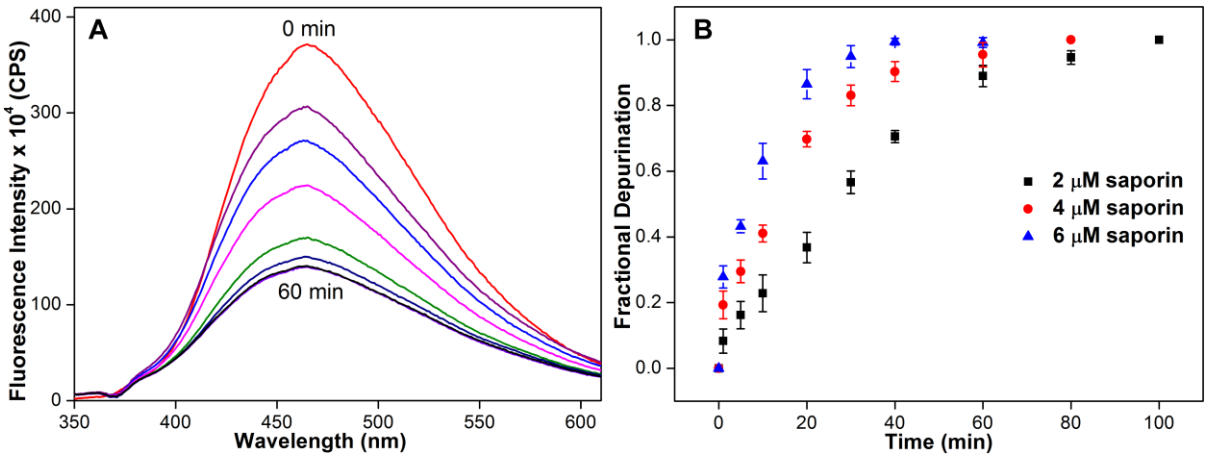

Figure 11. (**A**) Representative plot showing the saporin-mediated (6 μM) depurination of RIP RNA substrate **10**. Reaction aliquots at regular time intervals were hybridized with PNA oligomer **14** and change in fluorescence intensity was measured. Samples were excited at 330 nm with an excitation and emission slit width of 5 nm and 7 nm, respectively. (**B**) A plot of fractional depurination versus reaction time at different concentrations of saporin.[13]

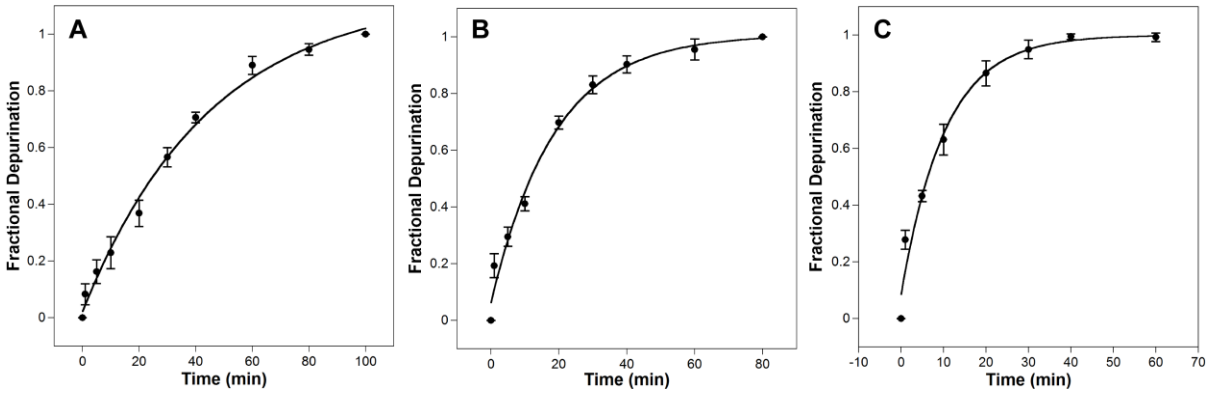

Figure 12. Curve fit for the depurination of RIPs RNA substrate **10** in the presence of saporin (**A**) 2 μM, (**B**) 4 μM and (**C**) 6 μM. Apparent rate constants were determined from the plot of fractional depurination *vs* time. R^2 values were very close to unity.[13]

Table 5. Apparent rate constant (k_{ap}) of depurination of RIPs RNA substrate **10** in the presence of different concentration of saporin.[13]

[saporin] (μM)	k_{ap} (min^{-1})
2.0	0.022 (±0.003)
4.0	0.054 (±0.007)
6.0	0.097 (±0.018)

3B.3 Conclusion

We have demonstrated the practical utility of benzothiophene-conjugated PNA analogue **7** in developing a fluorescence turn-on hybridization assay for the detection of GQ-forming sequences in proto-oncogenes (e.g. c-myc and c-kit2). The ability of the PNA probe, containing emissive PNA base **7**, to invade GQ structure formed by c-kit2 ON under near physiological conditions suggests that such turn-on fluorescence probes could potentially enable the detection and targeting of GQ sequences in cellular environment. Furthermore, the sensitivity of emissive PNA base **7** to the RNA abasic site allowed the monitoring and estimation of the depurination activity of a RIP toxin. The straight forward synthesis and useful fluorescence properties highlight the potential of the BT-modified PNA base as efficient fluorescent probes for nucleic acid analysis. Currently, we are evaluating the structure-function relationship of c-myc and c-kit2 genes using our PNA probes in cells by luciferase assay.

3B.4 Experimental Section

3B.4.1 Materials

Saporin was purchased from Sigma-Aldrich. DNA ONs were purchased from Integrated DNA Technologies. Custom synthesized RNA ONs were purchased from Dharmacon RNAi Technologies were deprotected according to the supplier's procedure. All oligonucleotides were purified by polyacrylamide gel electrophoresis (PAGE) under denaturing conditions and desalted on Sep-Pak Classic C18 cartridges (Waters Corporation). Autoclaved water was used in all biochemical reactions and fluorescence measurements.

3B.4.2 Instrumentation

All mass measurements were recorded on an Applied Biosystems 4800 Plus MALDI-TOF/TOF analyzer instrument and Water Synapt G2 High Definition mass spectrometers. PNA oligomers were purified by using Agilent Technologies 1260 Infinity HPLC. Absorption spectra were recorded on a Shimadzu UV-2600 spectrophotometer. UV-thermal melting analysis of duplexes was performed on a Cary 300Bio UV-Vis spectrophotometer. Steady-state fluorescence experiments were carried out in a micro fluorescence cuvette (Hellma, path length 1.0 cm) on Fluorolog-3 spectrophotometers (Horibha Scientific). Time-resolved fluorescence experiments were carried out on a TCSPC instrument (Horiba JobinYvon, Fluorolog 3). All CD spectra were recorded on JASCO J-815 CD spectrometer.

3B.4.3 Thermal melting and CD analysis of GQ of c-myc and c-kit2 ONs

GQ structures (10.0 μM) of c-myc and c-kit2 ONs were obtained by heating in 10 mM phosphate buffer (pH 7.1, 100 mM KCl, 0.1 mM EDTA) at 90 ºC for 3 min. Samples were slowly cooled to RT and kept in an ice bath for ~1 h. Samples were further diluted using phosphate buffer to give a final quadruplex concentration of 1.0 μM for T_m and 5.0 μM for CD analysis, respectively. UV-thermal melting analysis of G-quadruplex structures were performed in duplicate at 295 nm using quartz cuvette on a Cary 300Bio UV-Vis spectrophotometer. CD spectra of ONs were recorded with an average of three scans from 350 to 200 nm using quartz cuvette (Starna Scientific, path length 2 mm) on a JASCO J-815 CD spectrometer at 20 ºC and scan speed of 100 nm/min.

3B.4.4 Thermal melting and CD analysis of PNA duplexes

The PNA-DNA and PNA-RNA duplexes were assembled by heating a 1:1 mixture of PNA and DNA oligomers (10.0 µM) in 10 mM phosphate buffer (pH 7.1, 100 mM NaCl, 0.1 mM EDTA) at 90 ºC for 3 min. Samples were slowly cooled to RT and kept in an ice bath for ~1 h. Samples were further diluted using phosphate buffer to give a final duplex concentration of 1.0 µM for T_m and 5.0 µM for CD analysis, respectively. UV-thermal melting analysis of PNA duplexes were performed in duplicate using quartz cuvette on a Cary 300Bio UV-Vis spectrophotometer. The temperature was increased from 20 ºC to 90 ºC at 1 ºC/min and the absorbance was measured every 1 ºC interval at 260 nm. CD spectra of PNA duplexes were recorded with an average of three scans from 350 to 200 nm using quartz cuvette (Starna Scientific, path length 2 mm) on a JASCO J-815 CD spectrometer at 20 ºC and scan speed of 100 nm/min.

3B.4.5 Fluorescence study of benzothiophene-modified PNA oligomers and their DNA duplexes

PNA-DNA duplexes were obtained by heating a 1:1 mixture of PNA and DNA (5.0 µM) in 10 mM phosphate buffer (pH 7.1, 100 mM NaCl, 0.1 mM EDTA) at 90 ºC for 3 min. Samples were slowly cooled to RT and kept in an ice bath for ~1 h. Samples were further diluted using phosphate buffer to give a final duplex concentration of 0.5 µM. Samples were excited at 330 nm, and excitation and emission slit widths were maintained at 5 nm and 7 nm, respectively. Fluorescence experiments were performed in duplicate in a micro fluorescence cell (Hellma, path length 1.0 cm).

3B.4.6 Fluorescence study of benzothiophene-modified PNA-RNA duplexes

PNA-RNA duplexes were formed by heating a 1:1 mixture of PNA **14** and RNA ON (**10**/**11**) (5.0 µM) in the combination of 10 mM phosphate (pH 7.1, 100 mM NaCl, 0.1 mM EDTA) and 15 mM Tris-HCl (pH 6.0, 10 mM $MgCl_2$) buffer at 90 ºC for 3 min. Samples were slowly cooled to RT and kept in an ice bath for ~1 h. Samples were further diluted using phosphate and Tris-HCl 1x buffer to give a final duplex concentration of 1.0 µM. Samples were excited at 330 nm, and excitation and emission slit widths were maintained at 5 nm and 7 nm, respectively. Fluorescence experiments were performed in duplicate in a micro fluorescence cell (Hellma, path length 1.0 cm) using Horiba JobinYvon, Fluorolog-3 instrument.

3B.4.7 Fluorescence detection of depurination of RNA

A solution of RIPs RNA substrate **10** (2.2 μM) in 30 mM Tris buffer (25 mM NaCl, 2 mM $MgCl_2$, pH 6.0) was hybridized to form a stem-loop structure by heating the sample to 75 °C for 3 min and slowly cooling the solution to RT. The sample was placed in crushed ice for 1 h and later incubated at 37 °C for 10 min. The depurination reaction was initiated by adding different concentrations of saporin (2.0, 4.0, and 6.0 μM). At regular time intervals aliquots of reaction mixture (80 μL) were mixed with the complementary fluorescent PNA oligomer **14** (2.0 μM, 80 μL in 20 mM phosphate buffer, 175 mM NaCl, 0.2 mM EDTA, pH 7.1) and was immediately hybridized by heating at 90 °C for 3 min and flash cooled on crushed ice over 15 min. The final concentration of **14** was 1.0 μM. Hybridized samples were brought to RT over 10 min, centrifuged and the fluorescence spectrum was recorded. Samples were excited at 330 nm with an excitation and emission slit width of 5 nm and 7 nm, respectively. The depurination activity was monitored by measuring the changes in fluorescence intensity at λ_{em} = 465 nm. All reactions were performed in triplicate.

Rate of depurination reaction. Fluorescence intensity at each time point of the depurination reaction of RIPs RNA substrate **10** by saporin corresponds to the sum of fluorescence intensity of the substrate duplex (**10•14**) and product duplex (**12•14**) (equation 1). The rate of depurination reaction is directly proportional to the formation of product duplex (**12•14**).The fluorescence intensity contribution of the product duplex (**12•14**) at a given time, which is associated to the fraction of substrate depurinated, can be determined by using equation 1 and 2. The apparent rate constant (k_{ap}) was obtained by fitting the fluorescence data (fractional depurination I_P *vs* time) using an exponential rise equation 3 in Kaleidagraph software (Figure 12 and Table 5).[18b,18d]

$$I_t = I_S + I_P \qquad (1)$$

$$I_S = I_{S0} - \{(I_{S0}-I_t)/(I_{S0}-I_{Sat})\}I_{S0} \qquad (2)$$

I_t = fluorescence intensity at time = t
I_S = fluorescence intensity of substrate duplex (**10•14**) at time t
I_P = fluorescence intensity of product duplex (**12•14**) at time t
I_{S0} = fluorescence intensity of substrate duplex (**10•14**) at time t = 0 min
I_{Sat} = fluorescence intensity at saturation point

$$y = a + b(1-e^{-k_{ap}t}) \qquad (3)$$

y is fractional depurination (I_P), k_{ap} is apparent rate constant, t is time, a and b are coefficients, respectively.

3B.5 Notes and references

1. P. M. Sabale and S. G. Srivatsan, *ChemBioChem*, 2016, **17**, 1665–1673.
2. P. M. Sabale, J. T. George and S. G. Srivatsan, *Nanoscale*, 2014, **6**, 10460–10469.
3. G. W. Collie and G. N. Parkinson, *Chem. Soc. Rev.*, 2011, **40**, 5867–5892.
4. a) Y. Endo, A. Glück and I. G. Wool, *J. Mol. Biol.*, 1991, **221**, 193–207; b) L. Barbieri, M. G. Battelli and F. Stirpe, *Biochim. Biophys. Acta.*, 1993, **1154**, 237–282.
5. a) D. J. Patel, A. T. Phan and V. Kuryavyi, *Nucleic Acids Res.*, 2007, **35**, 7429–7455; b) S. Balasubramanian, L. H. Hurley and S. Neidle, *Nat. Rev. Drug Discov.*, 2011, **10**, 261–275; c) P. Murat and S. Balasubramanian, *Curr. Opin. in Genet. & Develop.*, 2014, **25**, 22–29.
6. T. Simonsson, *Biol. Chem.*, 2001, **382**, 621–628.
7. a) J. G. Hacia, E. A. Novotny, R. A. Mayer, S. A. Woski, M. A. Ashlock and F. S. Collins, *Nucleic Acids Res.*, 1999, **27**, 4034–4039; b) Y. Xu, Y. Suzuki, K. Ito and M. Komiyama, *Proc. Natl. Acad. Sci. U. S. A.*, 2010, **107**, 14579–14584; c) D. Renčiuk, J. Zhou, L. Beaurepaire, A. Guédin, A. Bourdoncle and J.-L. Mergny, *Methods*, 2012, **57**, 122–128; d) A. Henderson, Y. Wu, Y. C. Huang, E. A. Chavez, J. Platt, F. B. Johnson, Jr. R. M. Brosh, D. Sen and P. M. Lansdrop, *Nucleic Acids Res.*, 2013, **42**, 860–869; e) G. Biffi, M. Di Antonio, D. Tannahill and S. Balasubramanian, *Nat. Chem.*, 2014, **6**, 75–80.
8. a) B. R. Vummidi, J. Alzeer and N. W. Luedtke, *ChemBioChem*, 2013, **14**, 540–558; b) E. Largy, A. Granzhan, F. Hamon, D. Verga and M.-P. Teulade-Fichou, *Top. Curr. Chem.*, 2013, **330**, 111–177; c) A. C. Bhasikuttan and J. Mohanty, *Chem. Commun.* 2015, **51**, 7581–7597.
9. a) M. Nikan, M. Di Antonio, K. Abecassis, K. McLuckie and S. Balasubramanian, *Angew. Chem. Int. Ed.*, 2013, **52**, 1428–1431; b) K. Iida, T. Nakamura, W. Yoshida, M. Tera, K. Nakabayashi, K. Hata, K. Ikebukuro and K. Nagasawa, *Angew. Chem. Int. Ed.*, 2013, **52**, 12052–12055; c) J. Mohanty, N. Barooah, V. Dhamodharan, S. Harikrishna, P. I. Pradeepkumar and A. C. Bhasikuttan, *J. Am. Chem. Soc.*, 2013, **135**, 367–376; d) T.-Y. Tseng, Z.-F. Wang, C.-H. Chien and T.-C. Chang, *Nucleic Acids Res.*, 2013, **41**, 10605–10618; e) Y. P. Kumar, S. Bhowmik, R. N. Das, I. Bessi, S. Paladhi, R. Ghosh, H. Schwalbe and J. Dash, *Chem.-Eur. J.*, 2013, **19**, 11502–11506; f) A. R. de la Faverie, A. Guédin, A. Bedrat, L. A. Yatsunyk and J.-L. Mergny, *Nucleic Acids Res.*, 2014, **42**, e65; g) A. Laguerre, K. Hukezalie, P. Winckler, F. Katranji, G. Chanteloup, M. Pirrotta, J.-M. Perrier-Cornet, J. M. Y. Wong and D. Monchaud, *J. Am. Chem. Soc.*, 2015, **137**, 8521–8525; h) S. Xu, Q. Li, J. Xiang, Q. Yang, H. Sun, A. Guan, L. Wang, Y. Liu, L. Yu, Y. Shi, H. Chen and Y. Tang, *Nucleic Acids Res.*, 2015, **43**, 9575–9586; i) L. Hahn, N. J. Buurma and L. H. Gade, *Chem.-Eur. J.*, 2016, **22**, 6314–6322; j) S. Wu, L. Wang, N. Zhang, Y. Liu, W. Zheng, A. Chang, F. Wang, S. Li and D. Shangguan, *Chem.-Eur. J.*, 2016, **22**, 6037–6047.
10. a) T. Kimura, K. Kawai, M. Fujitsuka and T. Majima, *Chem. Commun.*, 2006, 401–402; b) V. L. Marin and B. A. Armitage, *Biochemistry*, 2006, **45**, 1745–1754; c) R. D. Gray, L. Petraccone, J. O. Trent and J. B. Chaires, *Biochemistry*, 2010, **49**, 179–194; d) A. Nadler, J. Strohmeier and U. Diederichsen, *Angew. Chem. Int. Ed.*, 2011, **50**, 5392–5396; e) A. Dumas and N. W. Luedtke, *Nucleic Acids Res.*, 2011, **39**, 6825–6834; f) M. Sproviero, K. L. Fadock, A. A. Witham and R. A. Manderville, *ACS Chem. Biol.*, 2015, **10**, 1311–1318; g) C. Y. Lee, K. S. Park and H. G. Park, *Chem. Commun.*, 2015, **51**, 13744–13747.
11. S. Müllar, J. Strohmeier and U. Diederichsen, *Org. Lett.*, 2011, **14**, 1382–1385.

12. a) A. T. Phan, V. Kuryavyi, H. Y. Gaw and D. J. Patel, *Nat. Chem. Biol.*, 2005, **1**, 167–173; b) N. Kumar, A. Patowary, S. Sivasubbu, M. Petersen and S. Maiti, *Biochemistry*, 2008, **47**, 13179–13188; c) H. Fernando, A. P. Reszka, J. Huppert, S. Ladame, S. Rankin, A. R. Venkitaraman, S. Neidle and S. Balasubramanian, *Biochemistry*, 2006, **45**, 7854–7860; d) S.-T. Danny Hsu, P. Varnai, A. Bugaut, A. P. Reszka, S. Neidle and S. Balasubramanian, *J. Am. Chem. Soc.*, 2009, **131**, 13399–13409.
13. See Experimental section for more detail.
14. a) S. Roy, F. A. Tanious, W. D. Wilson, D. H. Ly and B. A. Armitage, *Biochemistry*, 2007, **46**, 10433–10443; b) A. Gupta, L.-L. Lee, S. Roy, F. A. Tanious, W. D. Wilson, D. H. Ly and B. A. Armitage, *ChemBioChem*, 2013, **14**, 1476–1484.
15. a) T. Lindahl, *Nature (London)* 1993, **362**, 709–715; b) H. Atamna, I. Cheung and B. N. Ames, *Proc. Natl. Acad. Sci. U. S. A.*, 2000, **97**, 686–691; c) S. Nishizawa, Y. Sato and N. Teramae, *Anal Sci.*, 2014, **30**, 137–142.
16. C. Lubelli, A. Chatgilialoglu, A. Bolognesi, P. Strocchi, M. Colombatti and F. Stirpe, *Anal. Biochem.*, 2006, **355**, 102–109.
17. a) S. Tang, R.-G. Hu, W.-Y. Liu and K.-C. Ruan, *Biol. Chem.*, 2000, **381**, 769–772; b) W. K. Keener, V. R. Rivera, C. C. Young and M. A. Poli, *Anal. Biochem.*, 2006, **357**, 200–207.
18. a) S. Roday, M. B. Sturm, D. Blakaj and V. L. Schramm, *J. Biochem. Biophys. Methods*, 2008, **70**, 945–953; b) S. G. Srivatsan, N. J. Greco and Y. Tor, *Angew. Chem. Int. Ed.*, 2008, **47**, 6661–6665; c) Q.-Q. Tan, D.-X. Dong, X.-W. Yin, J. Sun, H.-J. Ren and R.-X. Li, *J. Biotechnol.*, 2009, **139**, 156–162; d) A. A. Tanpure, P. Patheja and S. G. Srivatsan, *Chem. Commun.*, 2012, **48**, 501–503.
19. a) L. Valis, N. Amann and H. A. Wagenknecht, *Org. Biomol. Chem.*, 2005, **3**, 36–38; b) E. Shipova and K. S. Gates, *Bioorg. Med. Chem. Lett.*, 2005, **15**, 2111– 2113; c) Z. Xu, Y. Sato, S. Nishizawa and N. Teramae, *Chem. Eur. J.*, 2009, **15**, 10375– 10378; d) Y. Sato, Y. Toriyabe, S. Nishizawa and N. Teramae, *Chem. Commun.*, 2013, **49**, 9983–9985; e) F. Hövelmann and O. Seitz, *Acc. Chem. Res.*, 2016, **49**, 714–723.
20. P. Ghosh and J. K. Batra, *Biochem. J.*, 2006, **400**, 99–104.
21. R. W. Sinkeldam, A. J. Wheat, H. Boyaci and Y. Tor, *ChemPhysChem*, 2011, **12**, 567–570.
22. A. A. Tanpure and S. G. Srivatsan, *ChemBioChem*, 2012, **13**, 2392–2399.

Chapter 4

Lucifer chromophore-based fluorescent PNA probe for imaging poly(A) tail of mRNA

4.1 Introduction

Fluorescent PNA oligomers that can report a binding event with a change in fluorescence properties have been highly useful in setting up assays to detect specific nucleic acids sequences in cell-free and cellular environments. Over the years, few base-modified emissive PNA oligomer probes have been developed and effectively used for the detection of nucleic acids by a hybridization process.[1] In a similar approach, we have also introduced two emissive PNA analogues, based on 5-benzofuran and 5-benzothiophene modified uracil cores.[2] The 5-benzofuran uracil PNA analogue was effectively utilized for the detection of human telomeric DNA repeats, and 5-benzothiophene uracil PNA analogue was employed in devising a turn-on sensor for the detection of G-quadruplex (GQ) forming human promoter oncogenes (c-myc and c-kit).[2] Additionally, 5-benzothiophene uracil PNA analogue was utilized to study the depurination activity of ribosome inactivating protein (RIP) toxins.[2] Although these analogues were highly environment-sensitive and retained reasonable quantum yields upon hybridization to nucleic acid targets, they exhibit excitation maximum in UV region, which limit their practical application such as hybridization probes for detection or imaging therapeutically relevant nucleic acid targets in cellular conditions. Recently, Seitz and co-workers have reported PNA FIT (forced intercalation) probes, where one of the nucleobase is completely replaced by thiazole orange fluorophore.[3] FIT PNA probe exhibited low fluorescence at the single-stranded level whereas fluorescence intensity was significantly increased upon hybridization to target nucleic acids. Further, these FIT-probes have been utilized to simultaneously image two different viral mRNA molecules expressed during the replication cycle of the H1N1 influenza A virus in cellular milieu.[3] Alternatively, the fluorescent nucleobase analogues, which preserve the base recognition property through hydrogen bonding as that of native nucleobase and have the ability to detect target nucleic acid with significant enhancement in fluorescence intensity, would be highly useful as a turn-on sensor for nucleic acid diagnostics. Therefore, developing such environment-sensitive fluorescent PNA analogues would be advantageous for imaging specific nucleic acid sequences in cellular conditions.

As a part of the development of emissive nucleosides, recently our group has introduced highly emissive 5-naphthalimide uridine analogue based on Lucifer chromophore.[4] This nucleoside analogue was found to be highly sensitive to its microenvironment with excitation and emission maximum (λ_{ex} = 400 nm and λ_{em} = 540 nm) in the visible region and exhibited reasonable quantum yield (Φ_{water} = 0.15). When

incorporated into ONs, fluorescence outcome of nucleoside analogue was highly sensitive to neighbouring bases. Comparatively, pyrene attached to a nucleobase or sugar has been widely explored for the detection of nucleic acids.[5] It exhibits useful fluorescence properties via exciplex and excimer formation in different conformations caused by stacking interactions.[5] Further, the properties of pyrene have been adequately evaluated for developing DNA-multichromophoric systems called oligodeoxyfluorosides (ODFs) as alternative fluorescent probes for biological assays by Kool and co-workers.[6]

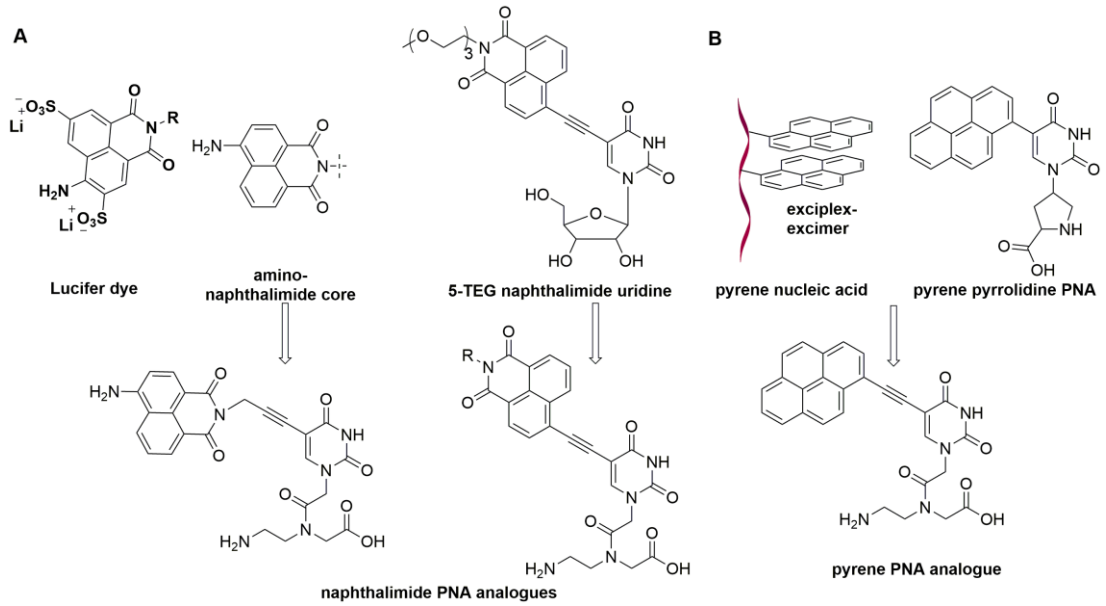

Figure 1. (**A**) Chemical structures of Lucifer dye, amino naphthalimide core, and 5-TEG naphthalimide uridine analogue are shown. Design of fluorescent naphthalimide *aeg*-PNA analogues from Lucifer dye is given. (**B**) Excimer formation of pyrene nucleic acid and structure of pyrene pyrrolidine PNA analogue are shown. Design of fluorescent pyrene *aeg*-PNA analogue through ethyne spacer is given.

Inspired by these attractive properties of naphthalimide and pyrene fluorophores, we have explored both the fluorophores in context to PNA oligomers. In the present study, we report the synthesis and photophysical analysis of 5-naphthalimide-TEG-, 5-aminonaphthalimide-, and 5-pyrene-modified uracil PNA analogues (Figure 1). Further, incorporation and detailed photophysical analysis of 5-naphthalimide-TEG uracil PNA analogue into PNA oligomers were carried out to evaluate the probe-like behaviour of the PNA base analogue. The fluorescence of 5-naphthalimide-TEG modified PNA oligomers was highly sensitive to its neighbouring bases. Results obtained from model PNA oligomers helped us to develop a PNA oligomer probe containing 5-naphthalimide-TEG uracil analogue for the imaging of poly(A) tail of mRNA in a human colon cancer cells (DLD1). Our results

demonstrate that this highly emissive naphthalimide-modified PNA probe could potentially serve as a robust hybridization probe for visualizing specific nucleic acid targets in cells.

4.2 Results and Discussion

4.2.1 Synthesis and photophysical properties of emissive naphthalimide and pyrene PNA analogues 8a–8c

Fluorescent naphthalimide PNA analogues **8a** and **8b** were designed based on Lucifer dye, which is made of the naphthalimide core.[7] The dye displayed excitation and emission maximum at 430 and 540 nm, respectively with the quantum yield of 0.25 in water (Figure 1A). The photophysical properties of the naphthalimide core are mainly influenced by substituent present at the 4-position of the ring.[7b] In general, electron donating groups at the 4-position impart very high fluorescence efficiency due to charge transfer excited state. Several derivatives of Lucifer dye have been introduced and successfully evaluated as biological markers, sensors, and electroluminescent materials.[7b] 5-TEG naphthalimide uridine introduced by our group also exhibited an excellent solvatochromism (Figure 1A).[4] Encouraged by these results, we designed two naphthalimide alkynes, one with the intact amino group as that of Lucifer dye (alkyne **4b**) and 5-TEG naphthalimide (alkyne **4a**). Further, both alkynes were attached at the 5-position of uracil base of *aeg*-PNA monomer (Figure 1A).

Tirayut and co-workers utilized excimer properties of pyrene attached to pyrrolidine PNA oligomer, as hybridization probes, for the detection of complementary nucleic acids.[8a] Additionally, pyrene was also incorporated into pyrrolidine PNA oligomers by attaching it at 5-position of uracil base and employed for nucleic acid analysis (Figure 1B).[8b] However, attachment of pyrene directly to uracil base could potentially destabilize the PNA-DNA/RNA heteroduplexes due to its bulky nature, and might not serve as good conformational sensitive analogue. Therefore, we envisioned to attach pyrene at 5-position of uracil base in *aeg*-PNA oligomer through an ethyne spacer, which could enhance the stability of PNA-DNA/RNA duplexes by increasing the distance between pyrene and uracil base (Figure 1B). This can impart conformational flexibility in pyrene analogue for better fluorescence properties.

Naphthalimide alkynes **4a** and **4b** were synthesized from 8-bromo naphthalic anhydride **1** by employing steps illustrated in Scheme 1. 8-bromo naphthalic anhydride **1** was refluxed with monomethyl TEG amine **2** in ethanol to afford bromo napthalimide **3**. Further, compound **3** was reacted with TMS acetylene under Sonogashira cross-coupling

reaction condition followed by TMS deprotection using TBAF afforded naphthalimide TEG alkyne **4a** in good yield.[4] Similarly, alkyne **4b** was obtained in three steps, first by refluxing 8-bromo naphthalic anhydride **1** with propargylamine in ethanol to afford 8-bromopropargyl naphthalimide **5**. Then bromine from compound **5** was replaced by nucleophilic substitution reaction with sodium azide, which was further reduced to amine using sodium ascorbate to afford alkyne **4b**. Fluorescent *aeg*-PNA esters **7a**–**7c** were synthesized by palladium catalyzed Sonogashira reaction between 5-iodouracil PNA ester **6** and respective alkynes **4a**–**4c** at RT. Further, fluorescent PNA esters **7a**–**7c** were hydrolysed to give Boc-protected PNA monomers **8a**–**8c** in quantitative yields, which were used in the solid-phase synthesis of PNA oligomers.

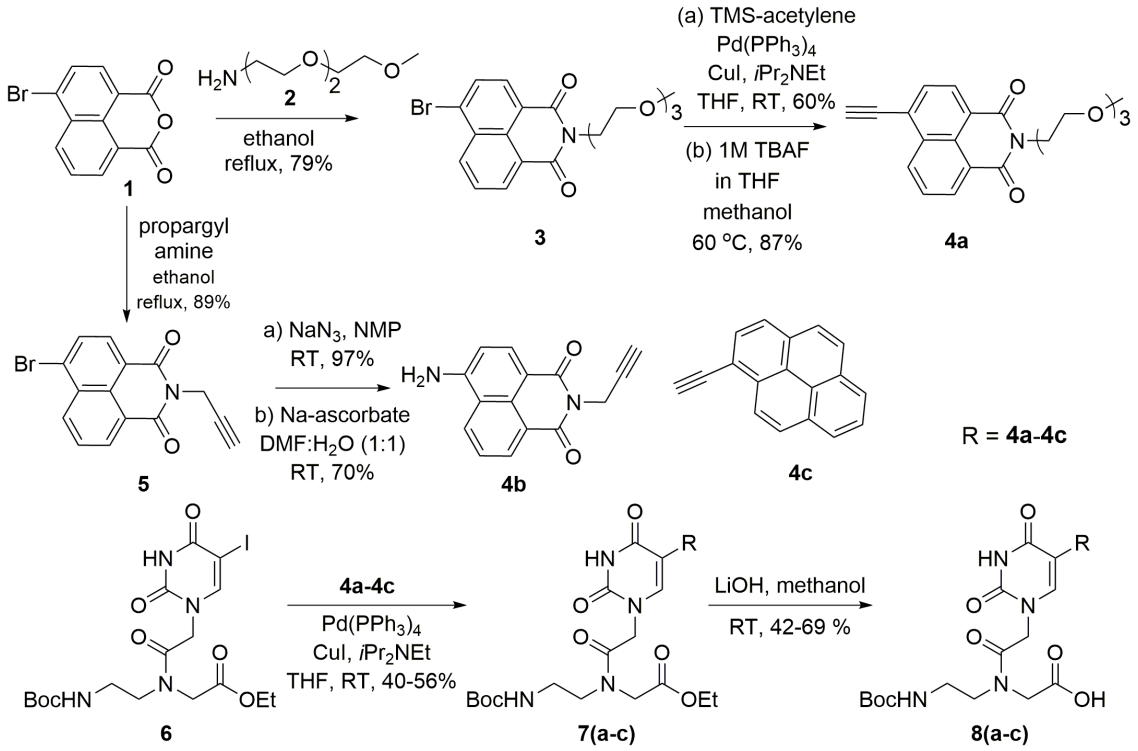

Scheme 1. Synthesis of napthalimide alkynes **4a** and **4b** for Sonogashira coupling reaction. The structure of commercially available pyrene alkyne **4c** is shown. Synthesis of 5-naphthalimide-conjugated uracil PNA monomers **8a** and **8b** and 5-pyrene-conjugated uracil PNA monomer **8c** required for the solid phase synthesis by Boc-strategy.[9]

Prior to solid phase PNA synthesis, preliminary photophysical analysis of Boc-protected emissive PNA monomers **8a**–**8c** were carried out in solvents of different polarity such as water, methanol, and dioxane. The ground-state electronic spectrum of **8a**–**8c** was marginally affected by changes in solvent polarity (Figure 2, Table 1). However, the excited-state spectrum of **8a**–**8c** was reasonably affected as solvent polarity was changed from water

to dioxane. An aqueous solution of the PNA monomer **8a** and **8b**, when excited at its lowest energy maximum, gave an emission band centered at 518 and 541 nm with a quantum yield of 0.09 and 0.08, respectively (Figure 2A and 2B, Table 1). As the solvent polarity was changed from water to dioxane, a significant increase in fluorescence intensity and quantum yield along with a blue-shifted emission band was observed. However, the fluorescence of pyrene monomer **8c** in water was completely quenched. When **8c** was excited at 391 nm in methanol, it showed an emission band centered at 423 nm with a quantum yield of 0.22. Interestingly, the quantum yield increased in dioxane by 2-fold (46%) with no apparent change in emission maximum (Figure 2C, Table 1). From these results, it is clear that fluorescence properties of PNA monomers **8a**–**8c** are sensitive to solvent polarity changes. However, naphtahlimide PNA monomers **8a** and **8b** were slightly better than **8c**, because of naphthalimide fluorophores, when conjugated to uracil nucleobase, exhibited better quantum yield in water and very good solvatochromism. Therefore, fluorescence behaviour of naphthalimide PNA analogues **8a** and **8b** in the different neighbouring base environment was further evaluated by incorporating them into model 15mer PNA oligomers, where the modification was placed in-between T residues.

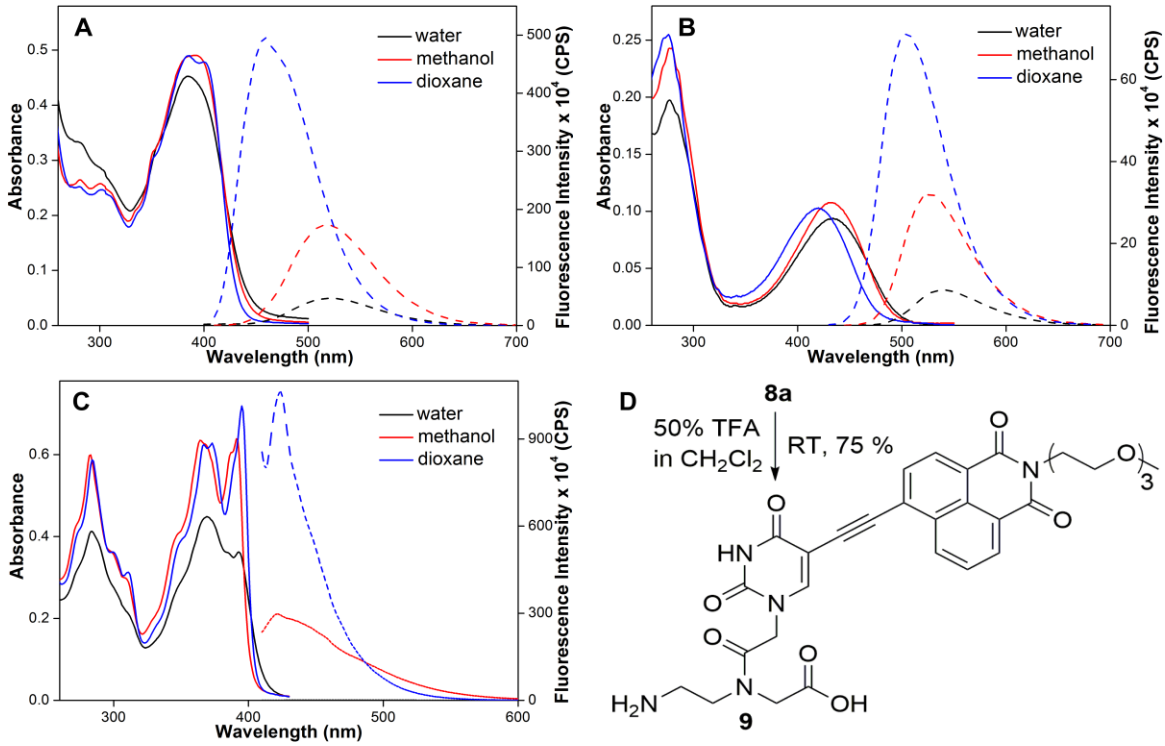

Figure 2. Absorption (25.0 µM) and emission (5.0 µM) spectra of PNA monomers **8a** (**A**), **8b** (**B**) and **8c** (**C**) in solvents of different polarity. Samples were excited at their respective lowest energy maximum. Excitation and emission slit widths were kept at 1 and 2 nm, respectively. All solutions for absorption and emission studies contained 2.5% and 0.5% DMSO, respectively. (**D**) Synthesis of free emissive TEG naphthalimide PNA analogue **9** by deprotection of **8a** is shown.[9]

Table 1. Photophysical properties of PNA monomer **8a**–**8c** in various solvents.

Monomer	Solvent	λ_{max} [a] (nm)	λ_{em} (nm)	I_{rel} [b]	Φ [d]
8a	water	385	518	1.0	0.09
	methanol	392	518	3.7	0.27
	dioxane	400	457	10.5	0.79
8b	water	434	541	1.0	0.08
	methanol	430	527	3.7	0.24
	dioxane	420	504	8.2	0.55
8c	water	394	nd	nd	nd
	methanol	391	423	1.0	0.22
	dioxane	395	424	3.6[c]	0.46

[a]Lowest energy maximum is given. [b]Intensity with respect to water. [c]Intensity with respective methanol. nd means fluorescence of **8c** was completely quenched in water. [d]Standard deviations for quantum yield (Φ) ≤ 0.02.

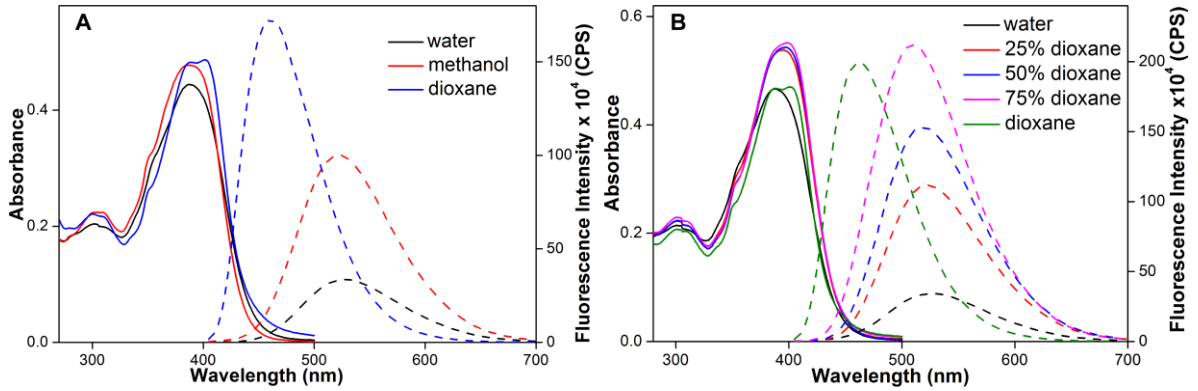

Figure 3. Absorption (25.0 µM) and emission (5.0 µM) spectra of PNA monomer **9** in various solvents such as water, methanol, and dioxane (**A**) and water, dioxane and its mixtures (**B**). Samples were excited at their respective lowest energy maximum. Excitation and emission slit widths were kept at 1 and 3 nm, respectively. All solutions for absorption and emission studies contained 2.5% and 0.5% DMSO, respectively.[9]

We decided to evaluate the photophysical properties of completely deprotected PNA monomers to investigate the role of Boc-protecting group. Hence, as a representative example, Boc-group of emissive PNA monomer **8a** was deprotected using TFA to afford the free emissive 5-TEG naphthalimide PNA analogue **9** (Figure 2D). Photophysical analysis of monomer **9** in solvents of different polarity such as water, methanol, and dioxane indicated that the ground-state electronic spectrum was slightly affected as solvent polarity changed from water to dioxane (Figure 3A Table 2). When excited at 388 nm, monomer **9** displayed an emission band centered at 528 nm with the quantum yield of 0.13 in water. As solvent polarity was reduced from water to methanol to dioxane, there was a significant increase in

fluorescence intensity (~6-fold) with a blue shift in emission maximum from 535 nm to 463 nm. Similarly, quantum yield and lifetime of analogue **9** also increased linearly with decrease in solvent polarity from water to methanol to dioxane (Table 2)

Table 2. Photophysical properties of PNA monomer **9** in various solvents.

solvent	λ_{max} [a] (nm)	λ_{em} (nm)	I_{rel} [b]	Φ [c]	τ_{av} [c] (ns)
water	388	528	1.0	0.13	1.16
25% dioxane	395	522	3.2	0.34	2.51
50% dioxane	398	520	4.4	0.47	3.07
75% dioxane	399	509	6.2	0.65	3.46
methanol	388	521	3.0	0.37	2.34
dioxane	401	463	5.8	0.62	2.46

[a]Lowest energy maximum is given. [b]Intensity with respect to water. [c]Standard deviations for quantum yield (Φ) and average lifetime (τ_{av}) are ≤ 0.01 and ≤ 0.05 ns, respectively.[9]

Additionally, photophysical properties of **9** were also evaluated in water, dioxane and water-dioxane mixtures; as such solvent systems have been used to study the impact of polarity on fluorescence properties of several fluorophores. The UV-visible spectrum showed slight hyperchromicity for the mixture of water-dioxane as compared to pure water or dioxane (Figure 3B, Table 2). On the other hand, excited-state properties such as emission maximum, quantum yield and lifetime were significantly affected by solvent polarity changes (Figure 3B, Table 2). When PNA monomer **9** was excited in water at its lowest energy maximum (388 nm), the emission profile depicted an emission maximum at 528 nm with a quantum yield of 0.13 and lifetime of 1.16 ns (Figure 3B, Figure 4A, Table 2). Since, there was a reduction in solvent polarity upon changing water-dioxane ratio, PNA analogue **9** showed a blue shift in emission maximum from 528 to 463 nm in combination with an enhancement in fluorescence intensity (~6-fold). Also, there was a significant increase in quantum yield and lifetime upon changing the polarity of medium (Table 2, Figure 4A). The microenvironment sensitivity of fluorescent analogue **9** was further confirmed by a positive correlation obtained by plotting the Stokes shift in solvents of different polarity against Reichardt's microscopic solvent polarity parameter, $E_T(30)$ (Figure 4B). The photophysical properties of PNA analogue **8a** containing Boc-group and completely deprotected emissive PNA monomer **9** in water, methanol, and dioxane were slightly different (for comparison see Table 1 and Table 2), which could be due to the better solubility of the free monomer **9** compared to Boc-protected **8a**, in respective solvents. Overall, the trend in the fluorescence

properties was similar for **8a** and **9** in various solvents. Analogue **9** showed absorption and emission in the visible region, and their fluorescence properties were highly sensitive to its microenvironment change. Therefore, this probe like property of analogue **9** would be further explored for designing PNA probes for the detection of important nucleic acid targets.

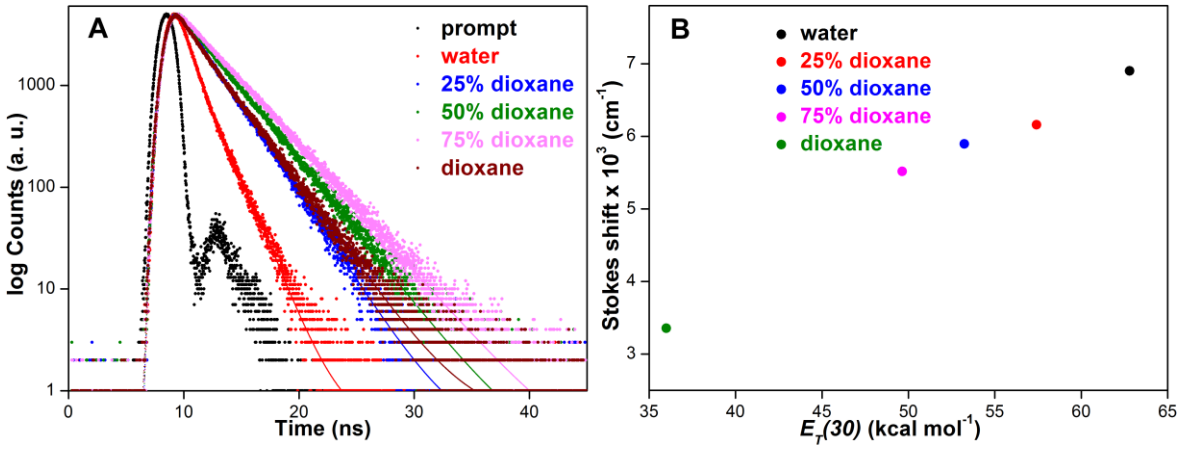

Figure 4. (**A**) Excited-state decay profile (5.0 μM) of free PNA analogue **9** in solvents of different polarity. Samples were excited using a 371 nm LED sources. The laser profile is shown in black (prompt). Curve fits are depicted as solid lines. (**B**) The plot of Stokes shift versus $E_T(30)$ (microscopic solvent polarity parameter)[10] for PNA monomer **9**.

4.2.2 Synthesis of model fluorescent PNA oligomers containing TEG naphthalimide and amino naphthalimide PNA analogues

In order to understand the photophysical behaviour of Lucifer chromophore-containing PNA base analogues in the different neighboring base environment, model 15mer PNA oligomers **10** (containing TEG naphthalimide PNA analogue **9**) and **10X** (containing amino naphthalimide PNA analogue **X**) were synthesized by using solid-phase PNA synthesis protocol (For detailed procedure see Chapter 2, section 2.4.9). L-lysine preloaded MBHA resin and Boc-protected *aeg*-PNA monomers were used for the synthesis of PNA oligomers (Figure 5). Additionally, emissive PNA oligomers **11**–**13** containing modification **9** flanked in between A, G, and C respectively, were also synthesized by above procedure. In order to enhance the solubility in aqueous medium, all PNA oligomers were synthesized with two C-terminal lysine residues.[9] The PNA oligomers were purified by RP-HPLC and well characterized by MALDI-TOF mass analysis (see 4.6 Appendix-II for HPLC profile and mass spectra and Table 3).

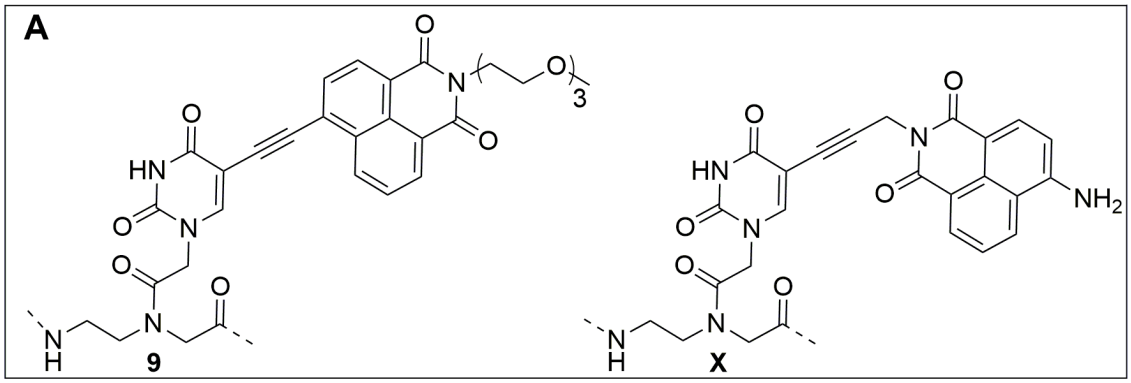

B

10 CGATCAT**9**TACTAGCKK	
10X CGATCAT**X**TACTAGCKK	**11** CGATCAA**9**AACTAGCKK
10A 5' d(GCTAGTAAATGATCG) 3'	**11A** 5' d(GCTAGTTATTGATCG) 3'
10T 5' d(GCTAGTATATGATCG) 3'	**11T** 5' d(GCTAGTTTTTGATCG) 3'
10G 5' d(GCTAGTAGATGATCG) 3'	**11G** 5' d(GCTAGTTGTTGATCG) 3'
10C 5' d(GCTAGTACATGATCG) 3'	**11C** 5' d(GCTAGTTCTTGATCG) 3'
12 CGATCAG**9**GACTAGCKK	**13** CGATCAC**9**CACTAGCKK
12A 5' d(GCTAGTCACTGATCG) 3'	**13A** 5' d(GCTAGTGAGTGATCG) 3'
12T 5' d(GCTAGTCTCTGATCG) 3'	**13T** 5' d(GCTAGTGTGTGATCG) 3'
12G 5' d(GCTAGTCGCTGATCG) 3'	**13G** 5' d(GCTAGTGGGTGATCG) 3'
12C 5' d(GCTAGTCCCTGATCG) 3'	**13C** 5' d(GCTAGTGCGTGATCG) 3'

Figure 5. (**A**) Structures of TEG naphthalimide (**9**) and amino naphthalimide (**X**) PNA analogues in with internal modification in PNA oligomer are shown. (**B**) Sequence of fluorescently modified PNA **10**–**13** (containing **9**) and **10X** (containing **X**) oligomers obtained by solid-phase synthesis. Sequence of synthetic DNA ONs ("d" preceding the parentheses) used in this study is shown. PNA sequences (highlighted in bold) are written from N-to C-terminus containing two lysine (**K**) residues at the C-terminus.[9]

Table 3. ε_{260} and MALDI-TOF mass analysis of PNA oligomers

PNA	Sequence[a]	ε_{260} ($M^{-1}cm^{-1}$)	Calculated mass	Observed mass
10	CGATCAT**9**TACTAGCKK	14.87 x 10^4	4644.56 $[M]^+$	4645.09
10X	CGATCAT**X**TACTAGCKK	14.57 x 10^4	4527.41 $[M]^+$	4532.78
11	CGATCAA**9**AACTAGCKK	15.89 x 10^4	4662.67 $[M]^+$	4663.84
12	CGATCAG**9**GACTAGCKK	15.49 x 10^4	4694.67 $[M]^+$	4697.30
13	CGATCAC**9**CACTAGCKK	14.47 x 10^4	4614.54 $[M]^+$	4616.70

[a]PNA sequences are written from N to C terminus.

4.2.3 Fluorescence behaviour of naphthalimide-modified PNA oligomers in different neighboring base environment

Several biophysical investigations have suggested that the fluorescence properties of emissive analogues incorporated into oligomers are affected by interactions with neighboring bases. Collisional, stacking and H-bonding interactions with adjacent bases and electron transfer process between an emissive base and neighbouring bases are known to significantly influence the fluorescence efficiency, emission maximum and excited state lifetime. Also, environment-sensitive fluorescent nucleobase analogues are known to change its fluorescence properties by structural rigidification-derigidification and by solvation-desolvation depending on its neighbouring bases.[11–14]

In order to investigate the effect of neighbouring bases on fluorescence properties of 5-TEG naphthalimide **9** and amino naphthalimide **X** PNA analogues, single-stranded (ss) PNA oligomers **10** and **10X**, and their duplexes with DNA ONs **10A, 10T, 10G, 10C** were subjected to steady-state fluorescence analysis. The PNA-DNA heteroduplexes were formed by annealing fluorescent PNA oligomers (**10** and **10X**) with DNA ONs in such a way that emissive PNA analogue **9/X** was placed opposite to the perfect complementary and mismatched bases. For example, when PNA**10/10X** was hybridized to **10A**, modification **9/X** is placed opposite to complementary base dA. Hybridization with ONs **10T**, **10G**, and **10C** would place the modification **9**/**X** opposite to mismatched base dT, dG, and dC respectively.

5-TEG naphthalimide PNA base analogue **9**, flanked in-between T-residues in PNA oligomer **10**, displayed a weak fluorescence band at 535 nm. Upon hybridization, there was ~5-fold enhancement in fluorescence intensity when the modification was opposite to pyrimidine bases (dT and dC) and ~2-fold enhancement when opposite to dG (Figure 6A). More interestingly, when PNA**10** was hybridized to ON **10A**, where **9** was located opposite to a perfect complementary base dA, a significant enhancement in fluorescence intensity (~14-fold) as compared to PNA **10** was observed (Figure 6A). This is possibly because, TEG naphthalimide-modification in **10•10A** duplex is extrahelical and oriented into major groove due to the H-bonding with complementary base dA. While in mismatched PNA-DNA duplexes, TEG naphthalimide-modification could be intrahelical and experiences the π–π stacking with neighboring bases (opposite strand) due to the absence of H-bonding, which results into quenching in fluorescence intensity as compared to matched **10•10A** duplex. Alternatively, upon excitation of amino naphthalimide PNA analogue **X** flanked in-between

T-residues in PNA oligomer **10X** at 455 nm, it showed an emission band at 530 nm, and a slight increment was observed upon hybridization with ONs **10A**, **10T**, **10G** and **10C** (Figure 6B). These results clearly depict the importance of emissive analogue **9** over **X** when incorporated into PNA **10** and **10X** for the detection of complementary ON (**10A**) with significant enhancement in fluorescence intensity. This observation could be because of the naphthalimide core in **9**, which is in conjugation with uracil ring via triple bond, while in **X**, aminonaphthalimide core is attached to the uracil ring via a propargyl linker, which results in effective conformational sensitivity for **9** over **X** upon incorporation into PNA oligomers and subsequent hybridization with complementary DNA ONs. Therefore, we explored the emissive 5-TEG naphthalimide PNA analogue **9** to study the impact of the flanking bases. For this, PNA oligomers **11** (**9** flanked in-between A), **12** (**9** flanked in-between G) and **13** (**9** flanked in-between C) were synthesized and performed steady-state fluorescence analysis (Figure 5 and Figure 7).

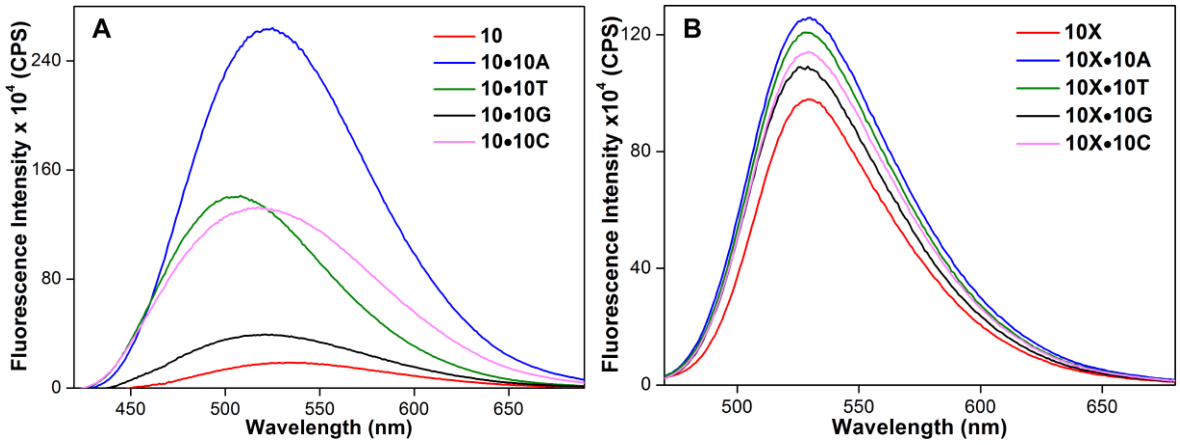

Figure 6. (**A**) Emission spectra (0.5 µM) of PNA oligomer **10** and duplexes made up of **10**. Excitation and emission slit widths were kept at 6 and 8 nm, respectively. All Samples were excited at 400 nm. (**B**) Emission spectra (0.5 µM) of PNA oligomer **10X** and duplexes made up of **10X**. Excitation and emission slit widths were kept at 3 and 5 nm, respectively. All Samples were excited at 455 nm.

Upon excitation at 400 nm, PNA**11** showed emission band around 548 nm (Figure 7A). Interestingly, PNA-DNA duplexes with modification **9** placed opposite to pyrimidine bases dT and dC displayed ~10-fold (**11•11T** and **11•11C**), and to purine bases dA and dG exhibited ~3–7-fold (**11•11G** and **11•11A**) increment in fluorescence intensity as compared to ssPNA**11** with small shift in emission maximum (Figure 7A). However, the 30% enhancement in fluorescence intensity for mismatched PNA-DNA (**11•11T** and **11•11C**) duplexes as compared to matched **11•11A** duplex is possibly due to the following reason. The TEG naphthalimide-modification in mismatched duplexes might have experienced the

rigidification and hydrophobic environment effect due to the complementary pyrimidine residues (dT or dC) as well as neighboring dT residues from opposite strand. Therefore, combination of above two effects could be responsible for the 30% enhancement in fluorescence intensity for emissive analogue **9** in mismatched duplexes as compared to matched duplex. Alternatively, PNA**12** (**9** flanked in-between G) and its duplexes (**12•12A**, **12•12T**, **12•12G** and **12•12C**) gave similar fluorescence intensity, and overall fluorescence was very low (data not shown). Moreover, PNA**13** (**9** flanked in-between **C**) exhibited an emission band at 540 nm, and fluorescence intensity was decreased to ~1.8-fold and ~4.5-fold for modification **9** placed opposite to complementary base dA (**13A**) and mismatched bases (**13T**, **13G**, **13C**) respectively, in PNA-DNA duplexes (Figure 7B). These observations point out that the 5-TEG naphthalimide-modified PNA analogue **9**, when flanked in-between T-residues, selectively reports the presence of AAA triplet base set in ON with significant enhancement (~14-fold) in fluorescence intensity. Analogue **9**, when incorporated into PNA oligomers and hybridized to DNA ONs experience change in solvent polarity as well as rigidification-derigidification. Therefore, discrete fluorescence profile exhibited by emissive analogue **9** in the different base environment is perhaps due to combined effect of rigidification-derigidification of the emissive PNA base, electron transfer process between the neighboring bases and emissive PNA base as well as solvation-desolvation effect.[11–15]

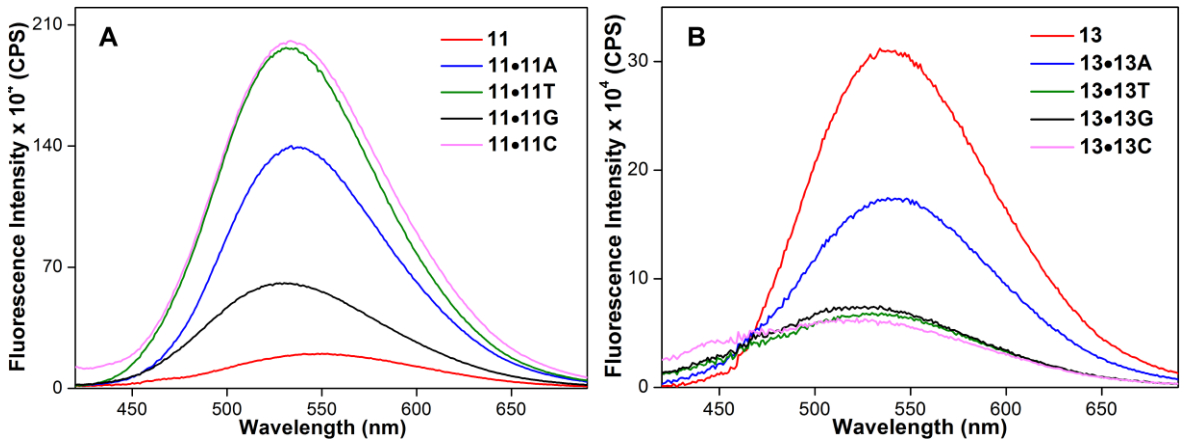

Figure 7. (**A**) Emission spectra (0.5 µM) of PNA oligomer **11** and duplexes made up of **11**. (**B**) Emission spectra (0.5 µM) of PNA oligomer **13** and duplexes made up of **13**. Excitation and emission slit widths were kept at 6 and 8 nm, respectively. All Samples were excited at 400 nm.

Most of the fluorescent nucleoside analogues reported in the literature structurally deviate from the natural nucleobases and destabilize the native duplex structures. Therefore, the impact of naphthalimide modification on the structure and stability of PNA-DNA heteroduplexes was evaluated by performing thermal melting and CD analysis. The thermal

melting analysis showed significantly lower T_m values ($\Delta T_m \leq 12$ °C) for modified PNA-DNA duplexes as compared to control unmodified PNA-DNA duplexes discussed in Table 5 of Chapter 2 (Figure 8A, Table 4). Furthermore, CD spectra of modified duplex were in good agreement with control duplex shown in Figure 12 of Chapter 2 (Figure 8B). Above results confirmed that the PNA oligomers containing 5-TEG naphthalimide-modified PNA analogue **9** formed stable duplexes at RT and the observed fluorescence properties are a reflection of the intact PNA-DNA duplexes.

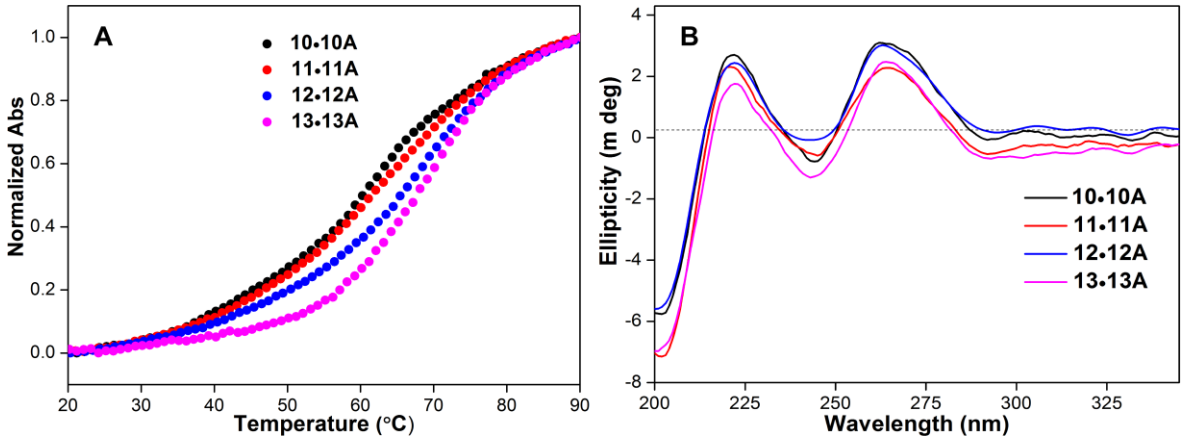

Figure 8. (**A**) UV-thermal melting profile (1.0 µM) of fluorescently modified (**10•10A, 11•11A, 12•12A** and **13•13A**) model PNA-DNA duplex in 10 mM phosphate buffer (pH 7.1, 100 mM NaCl, 0.1 mM EDTA). For T_m values see Table 4. (**B**) CD spectra (5.0 µM) of fluorescently modified PNA-DNA (**10•10A, 10X•10A, 11•11A, 12•12A** and **13•13A**) duplexes in 10 mM phosphate buffer (pH 7.1, 100 mM NaCl, 0.1 mM EDTA).

Table 4. T_m values of fluorescent PNA-DNA duplexes made up with **9**.

Duplex made of **9**	T_m (°C)
10•10A	61.5 ± 0.8
11•11A	61.8 ± 1.2
12•12A	63.2 ± 0.9
13•13A	64.2 ± 1.3

4.2.4 Fluorescence detection and imaging of poly(A) tail of mRNA

Poly(A) tail is present in most of the mRNAs of eukaryotic organisms, which provides stability to particular mRNA in the cytoplasm and also promotes the translations process.[16] Poly(A) tail length shortening is related to mRNA splicing and degradation process.[16] Techniques such as microarray, sequencing, and fluorescence *in situ* hybridization are widely explored for the detection and quantification of poly(A) tail in mRNA.[17] Among them,

fluorescence *in situ* hybridization (FISH) is one of the most powerful techniques to study the dynamics of poly(A) tail of mRNA in the real time.[18] Fluorescent oligo-dT nucleic acid probes are being routinely used to visualize poly(A) tail of mRNA in fixed as well as in live cell.[18] However, natural sugar phosphate backbone of the oligo-dT probe makes it less stable in nuclease environment, and they also exhibit no change in fluorescence property upon binding to target poly(A) mRNA, which additionally shows background fluorescence problem. Therefore, development of a synthetic nucleic acid hybridization probe, which is nuclease stable, base pairs strongly and sequence specifically, and reports poly(A) repeats with significant enhancement in fluorescence intensity would be advantageous for cell-based analysis.

Our initial study suggested that the emissive PNA oligomer **10** (**9** flanked in-between T-residues) were able to detect the AAA triplet base sets upon hybridization to a DNA ON with significant enhancement (~14-fold) in fluorescence intensity (Figure 6A). Therefore, we envisioned that this valuable turn-on fluorescence property of the emissive PNA analogue **9** could be utilized in setting up a hybridization assay to image poly(A) tail of mRNA. In this regards, fluorescently modified **14** (TTTTT**9**TTTTTTKK) and control unmodified **15** (TTTTTTTTTTTTKK) PNA oligomers complementary to poly(A) DNA and RNA ONs were synthesized by SPPS on Rink amide resin (Figure 9A). Fmoc-chemistry was preferred over Boc-chemistry, because of its mild cleavage condition for the synthesis of PNA oligomers (for detailed protocol see experimental section).[9]

Fmoc-protected fluorescent PNA acid **20** required for SPPS was synthesized as illustrated in Scheme 2. First, 5-iodouracil **16** was reacted with ethyl bromoacetate in K_2CO_3 to obtain compound **17**. Iodo compound **17** was converted into emissive ester **18** by palladium-catalysed Sonogashira cross-coupling reaction. The ester **18** was then hydrolyzed using aqueous LiOH in THF to fluorescent acid **19**. Further, acid **19** was coupled with Fmoc PNA backbone **20** using coupling reagent EDC and DIPEA as a base in dry DMF to afford emissive PNA ester **21**. Finally, *t*Bu-ester of compound **21** was hydrolysed using 50% TFA in dichloromethane to obtain the emissive Fmoc-protected PNA acid **22**, which was subsequently used for the SPPS using Fmoc-strategy. PNA oligomer probe **14** was then synthesized by Fmoc-chemistry with L-lysine preloaded rink amide resin and Fmoc *aeg*-thymine PNA monomer (Figure 9A). PNA probe **14** was purified with RP-HPLC and characterized by mass analysis (Figure 9B and Figure 9C).

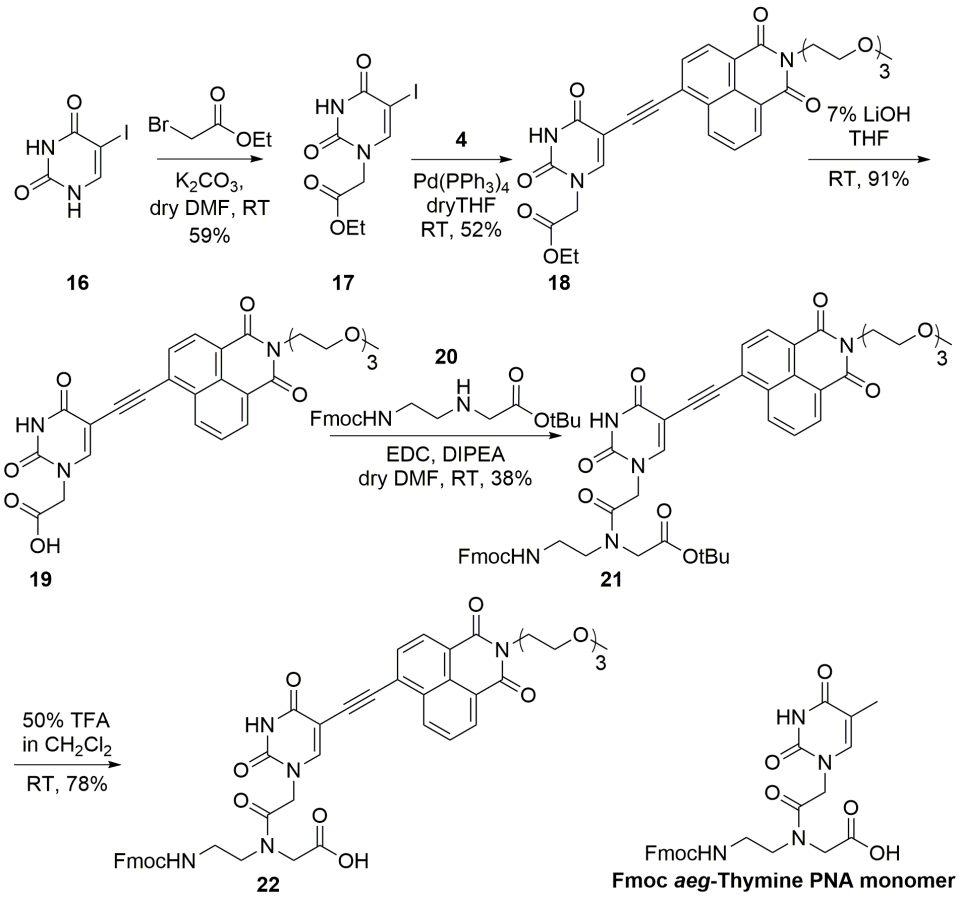

Scheme 2. Synthesis of Fmoc-protected 5-TEG naphthalimide-conjugated uracil PNA monomer **22** for SPPS by Fmoc-chemistry. The structure of Fmoc *aeg*-thymine PNA monomer is also given.[9]

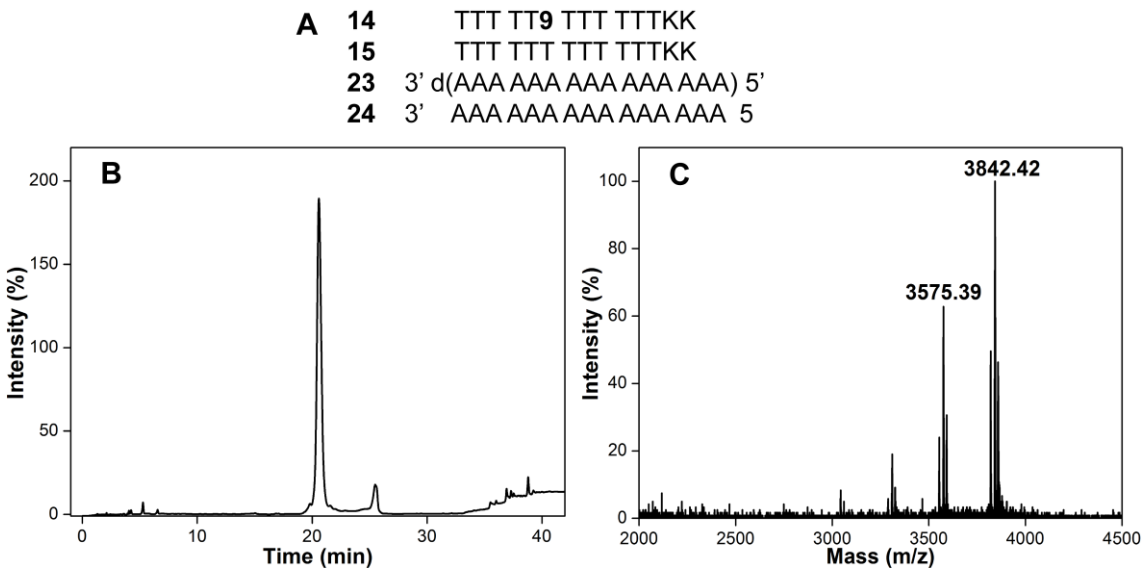

Figure 9. (**A**) Sequence of fluorescently modified **14** and control unmodified **15** PNA oligomers. Sequences of poly(A) DNA **23** ("d" preceding the parentheses) and RNA **24** ONs are also given. (**B**) RP-HPLC chromatogram of fluorescent PNA probe **14** at 260 nm. Conditions: 0-50% B in 25 min and 50-100% B in 15 min (Mobile phase A: 5% acetonitrile in H_2O containing 0.1% TFA. Mobile phase B: 50% acetonitrile in H_2O containing 0.1% TFA). Flow rate was 2 mL/min. (**C**) MALDI-TOF mass spectrum of fluorescently modified PNA probe **14**. Calculated for $[M+Na]^+$ = 3842.81 and observed = 3842.42.[9]

Next, PNA probe **14** and its duplexes with poly(A) DNA **23** and RNA **24** were subjected to steady-state fluorescence analysis (Figure 10). Upon excitation, PNA probe **14** gave an emission profile centered around 527 nm with a quantum yield of 0.22 (Figure 10, Table 5). PNA-DNA duplex **14•23** exhibited quenching in fluorescence intensity and reduces quantum yield to 0.17 as compared to PNA**14** (Figure 10, Table 5). Interestingly, PNA-RNA duplex **14•24** displayed noticeable enhancement in fluorescence intensity with a quantum yield of 0.29 (Figure 10, Table 5).

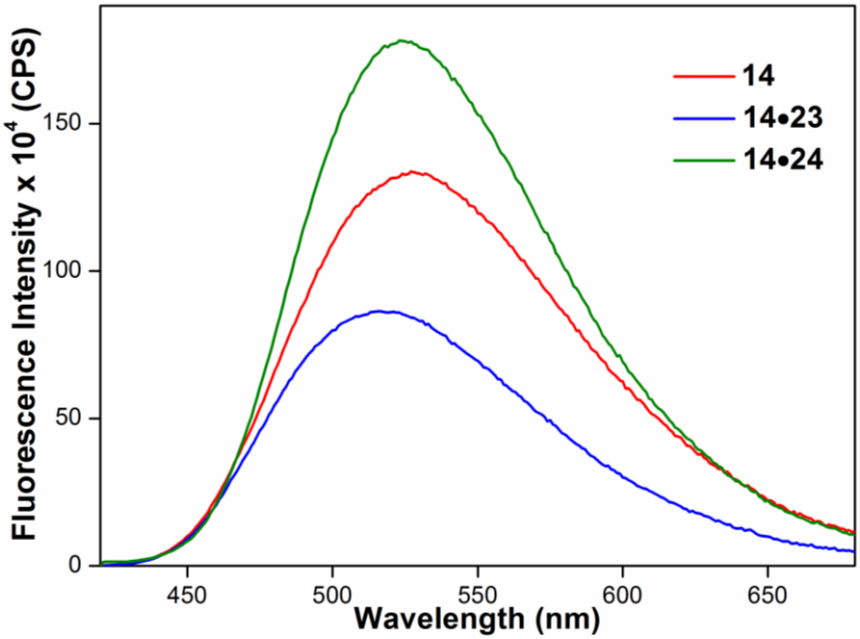

Figure 10. Emission spectra (0.5 µM) PNA probe **14**, PNA-DNA (**14•23**) and PNA-RNA duplex (**14•24**) made up of **15**. Excitation and emission slit widths were kept at 2 and 3 nm, respectively. All Samples were excited at 400 nm.

Table 5. Fluorescence properties of PNA oligomer **14** and its duplexes with poly(A) DNA and RNA.

sample	λ_{em} (nm)	I_{rel}[a]	Φ[b]
14	527	1.00	0.22
14•23	516	0.65	0.17
14•24	524	1.33	0.29

[a]Intensity with respect to water. [b]Standard deviations for quantum yield (Φ) is ≤ 0.01. [b]Quantum yields were calculated with respect to TEG-naphthalimide PNA monomer **9** as standard.[9]

Although the extent of enhancement for the poly(A) RNA was not that great as we excepted from model 15mer PNA **10** (~14-fold for **10•10A**), still PNA **14** was able to preferentially detect poly(A) RNA **24** with enhancement in fluorescence as compared to

poly(A) DNA ON **23**. This observation is possibly due to less polar environment experienced by modification **9** in PNA-RNA duplex (**14•24**) as compared to PNA-DNA duplex (**14•24**), which is in correlation with the fluorescence intensity of **9**, higher in dioxane than water (Figure 3 and Table 2). Moreover, the overall fluorescence of PNA **14** (**9** flanked in-between T) was significantly higher than model 15mer PNA **10** (**9** flanked in-between T) under the same conditions (data not shown). This observation is possibly due to more hydrophobic environment experienced by modification **9** in poly(T) PNA probe **14**. This observation clearly explained that the fluorescence outcome of emissive analogue not only depends on neighboring bases, but also depends on other nucleobases in the sequence. Further, the ability to retain fluorescence upon binding to poly(A) RNA (**24**) prompted us to study the usefulness of emissive PNA analogue **9** in imaging poly(A) tails of mRNA in cellular conditions.

Typically, mRNA is polyadenalyted in the nucleus and transported into the cytoplasm for protein synthesis.[19] To track the poly(A) mRNA in the nucleus as well as cytoplasm, FISH technique would be highly useful. Therefore, we evaluated the suitability of fluorescent PNA **14** for the imaging of poly(A) mRNA in DLD1 (human colon cancer) cells. The cells cultured in 12-well plates were sequentially fixed, permeabilized, hybridized with poly(A) probe (DNA/PNA), and imaged by fluorescence microscopy. Initially, we performed a control experiment with 30-mer Cy5-d$(T)_{30}$, which has previously been very well explored for the imaging of poly(A) mRNA in cells.[18] Conventional poly(A) FISH protocol with Cy-5d$(T)_{30}$ (0.5 μM) displayed a characteristic poly(A) mRNA distribution pattern (red colour in Cy-5 channel) with punctated nuclear staining, which was consistent with literature reports (Figure 11). Next, the appropriate concentration 1.0 μM of PNA **14** for poly(A) imaging was determined by performing a preliminary experiment (data not shown). When PNA **14** (1.0 μM) was used for poly(A) FISH experiment, we observed staining pattern (green colour in naphthalimide channel) with punctated nuclear staining, similar to that of Cy-5d$(T)_{30}$ (Figure 11). In a parallel experiment, staining of poly(A) mRNA by Cy-5d$(T)_{30}$ and PNA **14**, after RNase A (single-stranded RNA cleaving enzyme) treatment resulted in complete abolishment in the signal from both Cy-5 and naphthalimide channels (Figure 11). Emissive TEG naphthalimide PNA probe **14** was excited with 405 nm laser and emission were collected in a range of 510–580 nm (green-naphthalimide channel). Collectively, these results demonstrate that PNA probe **14** can be used to image poly(A) mRNA in cells similar to Cy-5d$(T)_{30}$. Cell culture was done by a colleague from lab.

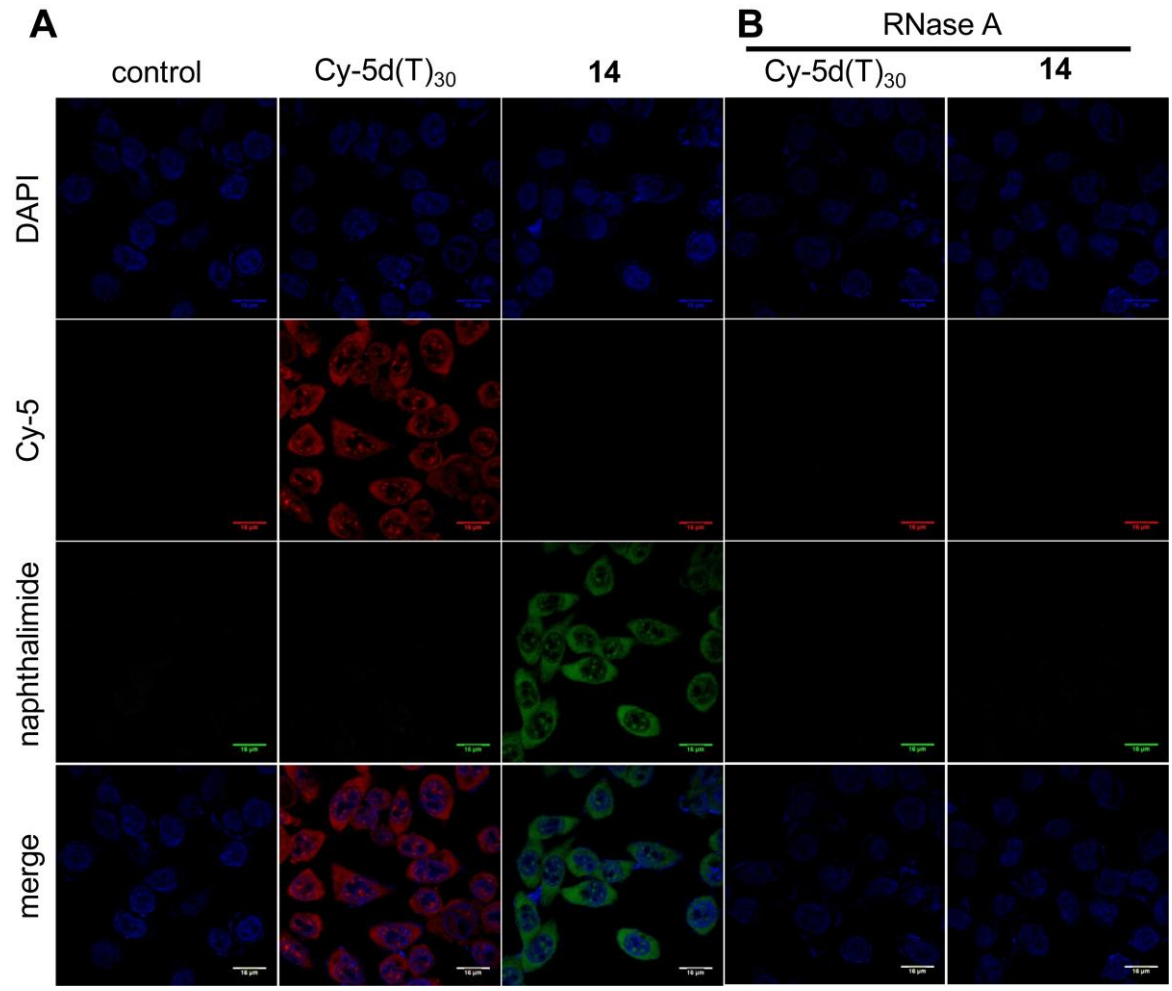

Figure 11. (**A**) Imaging cellular poly(A) mRNA using Cy-5d(T)$_{30}$ and PNA probe **14**. Cultured DLD1 cells were fixed, permeabilized and hybridized with Cy-5d(T)$_{30}$ (0.5 μM) and PNA probe **14** (1.0 μM) for 2.5 h at 37 °C. (**B**) Cells were treated with RNase A (single-stranded RNA cleaving enzyme) and hybridized with Cy-5d(T)$_{30}$ (1.0 μM) and PNA probe **14** (1.0 μM) under similar conditions. For detailed protocol, please see the experimental section.[9]

Next, we examined the selective binding of PNA over conventional DNA probe (Cy-5d(T)$_{30}$) by designing a competition assay. Upon mixing Cy-5d(T)$_{30}$ probe (0.5 μM) with various concentrations of PNA **14**, 1.0 μM, 0.5 μM and 0.25 μM in hybridization buffer, we observed punctate green coloured staining pattern for poly(A) mRNA with nuclear staining suggesting preferential binding of **14** to poly(A) mRNA over Cy-5d(T)$_{30}$ (Figure 12). We observed highly specific staining pattern by **14** over Cy-5d(T)$_{30}$ probe, but the overall fluorescence intensity was slightly reduced as the concentration of **14** was gradually decreased from 1.0 to 0.25 μM. This observation points out the selective and preferential binding affinity of PNA probe over the DNA probe.

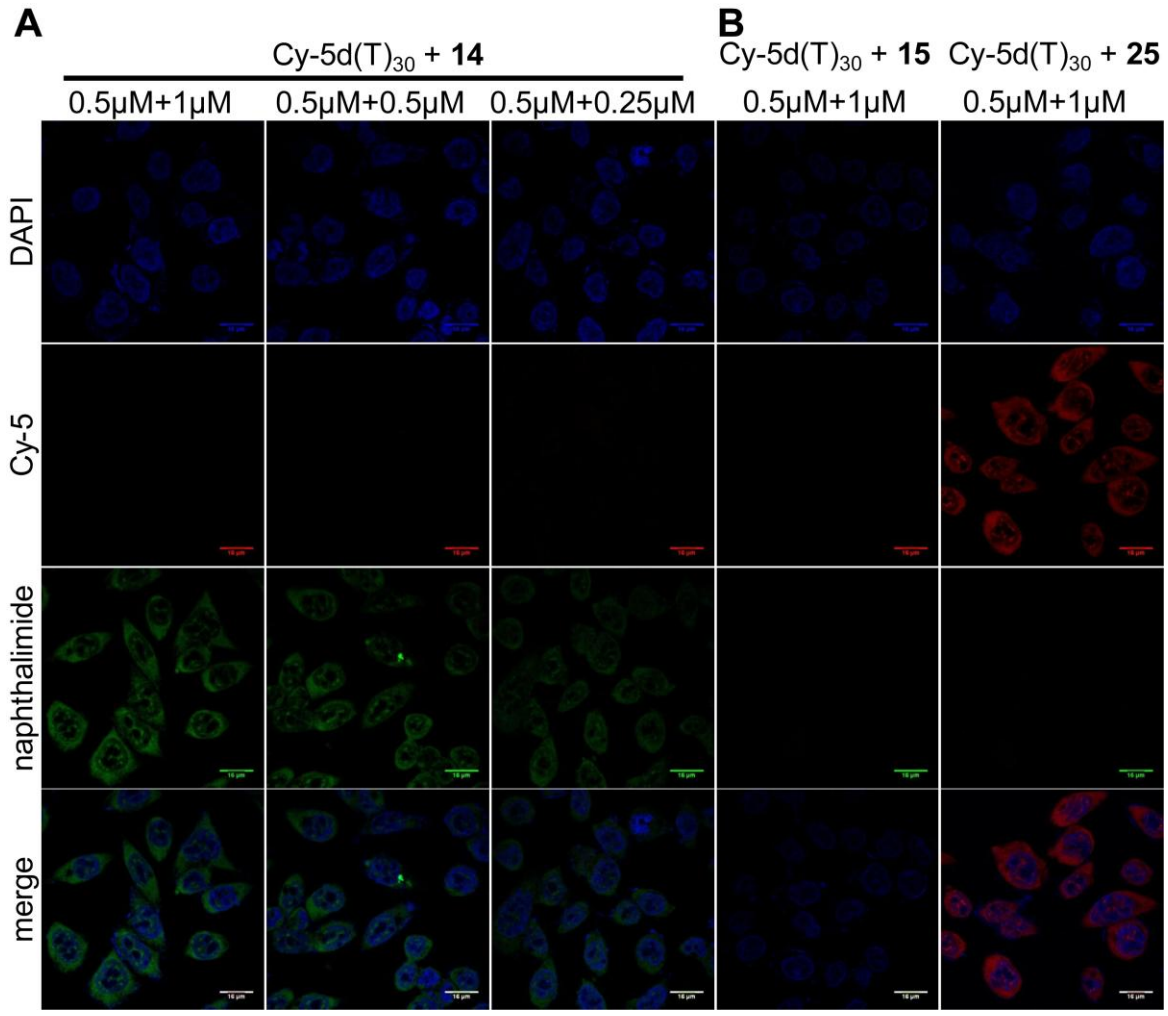

Figure 12. Competition assay, (**A**) Imaging cellular poly(A) mRNA using mixture of Cy-5d(T)$_{30}$ (0.5 μM) and PNA probe **14** (1.0, 0.5 and 0.25 μM). (**B**) Imaging cellular poly(A) mRNA using mixtures of Cy-5d(T)$_{30}$ (0.5 μM) and PNA oligomer **15**/**25** (1.0 μM). For detailed protocol please see the experimental section.[9]

In parallel, when we carried out competition assay with unmodified control PNA **15** (1.0 μM) and Cy-5d(T)$_{30}$ (0.5 μM), there was no staining from both Cy-5 (red) and naphthalimide (green) channels. This is because of the preferential binding of unmodified PNA **15** to poly(A) mRNA in the presence of Cy-5d(T)$_{30}$. Moreover, the specificity of poly(A) PNA oligomers **14** and **15** was confirmed by control experiment with 1.0 μM of random unmodified PNA oligomer **25** (CGATCAGTGACTAGCKK) and 0.5 μM of Cy-5d(T)$_{30}$ probe (Figure 12). The similar staining pattern was observed as that of Cy-5d(T)$_{30}$ probe (compare Figure 11 and 12). Thus, above competition assays confirmed the strong and selective binding affinity of PNA probe over the oligo-dT probe for imaging of poly(A) mRNA in cellular conditions. This observation was further supported by thermal melting analysis, where the modified PNA-RNA duplex **14•24** exhibited a significantly higher T_m =

78 ± 1.6 °C as compared to control unmodified DNA-RNA duplex **26•24** (T_m = 29 ± 0.5 °C, **26** = 5' d(TTTTTTTTTTTT) 3'). In addition, CD analysis was also carried for the above modified PNA-RNA (**14•24**) and control DNA-RNA (**26•24**) duplexes at 5.0 µM concentration (data not shown). Although, the CD spectra of PNA-RNA (**14•24**) duplex was similar to that of DNA-RNA (**26•24**) duplex, the possibility of triplex formation cannot be ruled out (for poly-pyrimidine PNA).[20] However, in PNA-RNA duplex naphthalimide-modification is pointed towards major groove, which could destabilize the $(PNA)_2$-RNA triplex and subsequently eliminate the possibility of triplex formation. Even if the polyT PNA probe forms triplex with poly(A) RNA, application of imaging poly(A) mRNA in cellular conditions should not be affected. Currently, we are utilizing PNA probe **14** for imaging of poly(A) mRNA in different cell lines.

4.3 Conclusion

A small set of emissive PNA base analogues based on Lucifer and pyrene fluorophores was developed, which has excitation and emission maximum in the visible region. In particular, the fluorescence of naphthalimide PNA analogue **9** was found to be highly sensitive to changes in surrounding microenvironment (e.g., polarity). Upon incorporation into PNA oligomers and hybridization with complementary and mismatched ONs, the emission properties of **9** were found to be responsive to neighbouring base environment. Interestingly, a PNA-DNA duplex in which the emissive PNA base was flanked by T residues and base paired with dA preferentially reported the presence of an A-repeat with significant enhancement in fluorescence intensity. These observations prompted the design of a poly(T) PNA oligomer probe against poly(dA) and poly(A) sequences. The poly(T) PNA probe containing the emissive naphthalimide analogue, when hybridized to poly(dA) and poly(A) DNA and RNA ONs, respectively, detected the poly(A) RNA ON with enhancement in fluorescence intensity, which was more than the single stranded PNA probe and PNA-poly(dA) duplex. The fluorescence properties (excitation and emission profile), which are compatible to confocal microscopy, and ability of the PNA probe to detect poly(A) RNA repeat enabled the development of a robust assay to image endogenous poly(A) mRNA sequences in fixed cells. Importantly, competition experiment and RNase treatment revealed that our fluorescent PNA probe is highly selective and binds to poly(A) mRNA with significantly higher affinity over a commercially available poly(A) mRNA probe, Cy5-oligo-dT_{30}. Collectively, the ability of PNA to displace/invade nucleic acid structures and the

results presented in this chapter underscore the potential of Lucifer-based PNA oligomers as efficient probes for detecting and imaging specific nucleic acid sequences in cells.

4.4 Experimental Section

4.4.1 Materials

Chloroacetyl chloride, di-*t*-butyl dicarbonate, ethane-1,2-diamine, ethyl bromoacetate, TFA, piperidine, EDC and silica gel (100-200 mesh) were purchased from Spectrochem India. Dry DMF and dry dichloromethane were purchased from Rankem India. Acetic anhydride was purchased from Thomas Baker India. 5-Iodouracil, sodium ascorbate, propargylamine tetrakis(triphenylphosphine) palladium (0), pyridine, *N*-hydroxybenzotriazole (HOBt), 3-[bis(dimethylamino)methyliumyl]-3*H*-benzotriazol-1-oxide hexafluorophosphate (HBTU), *N*,*N*-diisopropylethylamine (DIPEA), 1,2-ethanedithiol, thioanisole, anisole, Fmoc-Lys(Boc)-OH and trifluoromethanesulfonic acid (TFMSA), Vanadyl ribonucleoside complex (VRC) solution, paraformaldehyde, dextran sulphate, formamide, salmon sperm DNA, RNase A and DAPI were purchased from Sigma-Aldrich. Chemicals for preparing buffer solutions were obtained from Sigma-Aldrich. Monomethyl TEG amine **2** was prepared by using a method described in the literature. 5-iodo uracil PNA ester **6** was synthesized by using our reported procedure. Boc-and Fmoc-protected *aeg*-PNA monomers were purchased from ASM Research Chemicals. The exocyclic amino group of adenine, guanine, and cytosine of Boc-PNA monomers the with cbz (Z) group. While, Fmoc-PNA monomers was protected with Bhoc-group. 4-Methylbenzhydrylamine•HCl (MBHA) resin LL (100-200 mesh) and Boc-Lys(2-Cl-Z)-OH were obtained from Novabiochem. Rink amide AM resin (100-200 mesh) was purchased from GL Biochem (Shanghai) Ltd. DNA ONs were purchased from Integrated DNA Technologies. Custom synthesized RNA ON purchased from Dharmacon RNAi Technologies was deprotected according to the supplier's procedure. Reagents for cell culture experiments such as RPMI1640 medium (gibco®), fetal bovine serum (gibco®) and penicillin streptomycin (gibco®) and anti-fade mounting media were obtained from Life Technology, India. Fluorescent Cy-5 oligo-dT probe (5'Cy5-$(T)_{30}$ 3') was purchased from Sigma-Aldrich. All ONs were purified by polyacrylamide gel electrophoresis (PAGE) under denaturing conditions and desalted on Sep-Pak Classic C18 cartridges (Waters Corporation). Autoclaved water was used in all biochemical reactions and fluorescence measurements. All PNA oligomers were prewarmed at 60 °C for 2 min to avoid self-aggregation before the experiments.

4.4.2 Instrumentation

NMR spectra were recorded on a 400 MHz Jeol ECS-400 spectrometer (^{1}H 400 MHz and ^{13}C 100 MHz) and processed in Mnova NMR software from Mestrelab Research. All mass measurements were recorded on an Applied Biosystems 4800 Plus MALDI-TOF/TOF analyzer instrument and Water Synapt G2 High Definition mass spectrometers. Reverse-phase (RP) flash chromatography (C18 RediSepRf column) purifications were carried out using Teledyne ISCO, Combi Flash Rf. Microwave reactions were performed using CEM discover microwave synthesizer. PNA oligomers were purified by using Agilent Technologies 1260 Infinity HPLC. Absorption spectra were recorded on a Shimadzu UV-2600 spectrophotometer. UV-thermal melting analysis of duplexes was performed on a Cary 300Bio UV-Vis spectrophotometer. Steady-state fluorescence experiments were carried out in a microfluorescence cuvette (Hellma, path length 1.0 cm) on a Fluoromax-4 and Fluorolog-3 spectrophotometer (Horibha Scientific). Time-resolved fluorescence experiments were carried out on a TCSPC instrument (Horiba JobinYvon, Fluorolog 3). All CD spectra were recorded on JASCO J-815 CD spectrometer. Confocal imaging was carried out on a Zeiss LSM710 Confocal Laser Scanning Microscope with oil immersion using 40X lens. The channel used for acquiring an image is DAPI filter (λ_{ex} = 405 nm and λ_{em} = 420–476 nm). Emissive TEG naphthalimide PNA probe **14** was also excited with 405 nm laser and emission were collected in a range of 510–580 nm (green-naphthalimide channel). Images for oligo-dT probe were acquired in the red Cy-5 filter (λ_{ex} = 633 nm and λ_{em} = 640–760 nm). The Zen 2012 software has been used for image acquisition. Java Image J software was used to process the images acquired from the instrument.

4.4.3 Synthesis of fluorescent PNA monomers

6-Bromo-2-(2-(2-(2-methoxyethoxy)ethoxy)ethyl)-1*H*-benzo[*de*]isoquinoline-1,3(2H)-dione 3

A mixture of 4-bromo-1,8-napthalic anhydride **1** (2.50 g, 9.02 mmol, 1.0 equiv.) and 2-(2-(2-methoxyethoxy)ethoxy)ethanamine **2** (1.62 g, 9.92 mmol, 1.1 equiv.) in ethanol (25 mL) was refluxed for 12 h under nitrogen atmosphere. The solvent was evaporated completely; residue was then dissolved in dichloromethane (120 mL) and washed with water (2 x 50 mL). Organic layer was then evaporated and residue was purified by silica gel column chromatography to afford the product **3** as pale yellow solid (3.03 g, 79%). TLC R_f = 0.39 ($CHCl_3$); ^{1}H-NMR (400 MHz, $CDCl_3$): δ = 8.64 (dd, *J* = 7.4 & 1.0 Hz, 1H), 8.55 (dd, *J* = 8.6

& 1.0 Hz, 1H), 8.39 (d, *J* = 7.6 Hz, 1H), 8.03 (d, *J* = 7.6 Hz, 1H), 7.83 (dd, *J* = 8.6 & 7.4 Hz, 1H), 4.42 (t, *J* = 6.0 Hz, 2H), 3.82 (t, *J* = 6.2 Hz, 2H), 3.71–3.67 (m, 2H), 3.62–3.60 (m, 2H), 3.58–3.56 (m, 2H), 3.45–3.42 (m, 2H), 3.31 (s, 3H) ppm; ^{13}C-NMR (100 MHz, $CDCl_3$): δ = 163.8, 163.7, 133.4, 132.2, 131.4, 131.2, 130.7, 130.4, 129.2, 128.2, 123.2, 122.3, 72.0, 70.7, 70.6, 70.3, 68.0, 59.1, 39.4 ppm; HRMS: Calcd. for $C_{19}H_{20}BrNO_5Na$: 444.0423 $[M+Na]^+$; found: 444.0421.

6-Ethynyl-2-(2-(2-(2-methoxyethoxy)ethoxy)ethyl)-1*H*-benzo[*de*]isoquinoline-1,3(2H)-dione 4a

A mixture of 4-bromo napthalimide derivative **3** (3.03 g, 7.2 mmol, 1.0 equiv.), tetrakis(triphenylphosphine) palladium(0) (0.414 g, 0.36 mmol, 0.05 equiv.) and CuI (0.14 g, 0.72 mmol, 0.1 equiv.) were dissolved in degassed anhydrous THF (60 mL). Trimethylsilylacetylene (4.1 mL, 28.7 mmol, 4 equiv.) and *N*,*N*-diisopropylethylamine (4.4 mL, 25.1 mmol, 3.5 equiv.) were added slowly to the above solution and reaction mixture was stirred at RT for 12 h in nitrogen atmosphere. Solvent was evaporated completely and the residue was purified by silica gel column chromatography to afford the brown viscous oil (1.90 g, 60%), TLC R_f = 0.77 (CH_2Cl_2).

Above coupled product (1.9 g, 4.3 mmol, 1.0 equiv.) and 1 M tetrabutylammonium fluoride solution in THF (17.3 mL, 17.3 mmol, 4.0 equiv.) was heated at 60 °C for 1 h in anhydrous methanol (38 mL). Solvent was evaporated and residue was re-dissolved in ethyl acetate (100 mL). Ethyl acetate layer was washed with water (50 mL) and brine (50 mL). Organic layer was separated and dried over sodium sulphate. Organic layer was then completely evaporated using rotary evaporator and residue was purified by silica gel column chromatography to afford as lemon yellow solid **4a** (1.31 g, 87%). TLC R_f = 0.56 (EtOAc); ^{1}H-NMR (400 MHz, $CDCl_3$): δ = 8.66–8.61 (m, 2H), 8.51 (d, *J* = 7.6 Hz, 1H), 7.92 (d, *J* = 7.6 Hz, 1H), 7.61 (t, *J* = 8.0 Hz, 1H), 4.43 (t, *J* = 6.0 Hz, 2H), 3.82 (t, *J* = 6.0 Hz, 2H), 3.74 (s, 1H), 3.71–3.69 (m, 2H), 3.63–3.60 (m, 2H), 3.58–3.56 (m, 2H), 3.45–3.42 (m, 2H), 3.31 (s, 3H) ppm; ^{13}C-NMR (100 MHz, $CDCl_3$): δ = 164.1, 163.8, 132.4, 132.0, 131.8, 131.7, 130.3, 128.1, 127.8, 126.4, 123.0, 122.8, 86.7, 80.4, 72.0, 70.7, 70.6, 70.3, 68.0, 59.1, 39.3 ppm; HRMS: Calcd. for $C_{21}H_{21}NO_5Na$: 390.1317 $[M+Na]^+$; found: 390.1317.

6-Bromo-2-(prop-2-yn-1-yl)-1*H*-benzo[*de*]isoquinoline-1,3(2*H*)-dione 5

A mixture of 4-bromo-1,8-napthalic anhydride **1** (2.12 g, 7.65 mmol, 1.0 equiv.) and propargyl amine (0.98 mL, 15.3 mmol, 2.0 equiv.) in ethanol (21.2 mL) was refluxed for 12 h under nitrogen atmosphere. The solvent was evaporated completely; residue was then dissolved in dichloromethane (100 mL) and washed with water (2 x 50 mL). Organic layer was then evaporated and residue was purified by silica gel column chromatography to afford the product as faint white solid **5** (2.10 g, 89%). TLC R_f = 0.54 (CH_2Cl_2); ^{1}H-NMR (400 MHz, $CDCl_3$): δ = 8.71 (dd, *J* = 7.6 & 1.2 Hz, 1H), 8.61 (dd, *J* = 8.6 & 1.0 Hz, 1H), 8.46 (d, *J* = 8.0 Hz, 1H), 8.06 (d, *J* = 7.6 Hz, 1H), 7.87 (dd, *J* = 8.6 & 7.4 Hz, 1H), 4.96 (d, *J* = 2.8 Hz, 2H), 2.20 (t, *J* = 2.4 Hz, 1H) ppm; ^{13}C-NMR (100 MHz, $CDCl_3$): δ = 163.0, 133.9, 132.6, 131.8, 131.4, 131.0, 130.9, 129.2, 128.3, 122.9, 122.0, 78.5, 70.9, 29.7 ppm; HRMS: Calcd. For $C_{15}H_9BrNO_2$: 313.9817 $[M+H]^+$; found: 313.9810.

6-Amino-2-(prop-2-yn-1-yl)-1*H*-benzo[*de*]isoquinoline-1,3(2*H*)-dione 4b

A mixture of 4-bromo napthalimide derivative **5** (1.10 g, 3.51 mmol, 1.0 equiv.) and NaN_3 (1.14 g, 17.55 mmol, 5.0 equiv.) in *N*-methyl pyrrolidone (15 mL) was stirred at RT for 16 h. Then 50 mL de-ionized water was added to above reaction mixture and the crude product was extracted using dichloromethane (2 x 100 mL). The Organic layer was evaporated using a rotary evaporator to afford the crude product as faint brown solid (0.87 g, 97%) TLC R_f = 0.53 (CH_2Cl_2).

Above product (0.544 g, 1.97 mmol, 1.0 equiv.) and sodium ascorbate (3.92 g, 19.78 mmol, 10.0 equiv.) in 10 mL of DMF-H_2O mixture (4:1) was stirred for 14 h at RT. Solvent was evaporated using high vacuum pump and residue was dissolved into CH_2Cl_2 (100 mL). Dichloromethane layer was further washed with water (2 x 30 mL) and dried over sodium sulphate. Organic layer was then completely evaporated using rotary evaporator and residue was purified by silica gel column chromatography to afford as yellow solid **4b** (0.35 g, 70%). TLC R_f = 0.24 (Ethyl acetate: Hexane = 5:5); ^{1}H-NMR (400 MHz, d_6-DMSO): δ = 8.63 (d, *J* = 8.4, 1H), 8.45–8.43 (m, 1H), 8.20 (d, *J* = 8.4 Hz, 1H), 7.66 ($_{app}$t, *J* = 7.6 & 6.8 Hz, 1H), 7.53 (br, 2H), 4.73 (s, 2H), 3.06 ($_{app}$t, *J* = 2.4 & 2.0 Hz, 1H) ppm; ^{13}C-NMR (100 MHz, d_6-DMSO): δ = 163.1, 162.0, 153.1, 134.3, 131.3, 129.8, 129.7, 124.1, 121.4, 119.4, 106.3, 107.0, 80.0, 72.4, 26.6 ppm; HRMS: Calcd. for $C_{15}H_{11}N_2O_2$: 251.0821 $[M+H]^+$; found: 251.0819.

General procedure for the synthesis of fluorescent PNA esters 7(a-c)

A mixture of 5-iodouracil PNA ester **6**[2] (1.0 equiv.), CuI (0.2 equiv.), tetrakis(triphenylphosphine) palladium(0) (0.1 equiv.) and alkyne (**4a**–**4c**) (1.1 equiv.) were dissolved in degassed anhydrous THF (25 mL per g of **6**) under nitrogen atmosphere. DIPEA (3.5 equiv.) was then slowly added, and the reaction mixture was stirred in the dark at RT for 12h. Solvent was evaporated using rotary evaporator. The residue was dissolved in ethyl acetate and further washed with water. The organic layer was separated and dried over sodium sulphate. The residue obtained after evaporation was purified using silica gel Combi-flash column chromatography (methanol-dichloromethane solvent systems) to afford desired products **7**(**a-c**).

Ethyl *N*-(2-((*tert*-butoxycarbonyl)amino)ethyl)-*N*-(2-(5-((2-(2-(2-(2-methoxyethoxy)ethoxy)ethyl)-1,3-dioxo-2,3-dihydro-1*H*-benzo[*de*]isoquinolin-6-yl)ethynyl)-2,4-dioxo-3,4-dihydropyrimidin-1(2*H*)-yl)acetyl)glycinate 7a: Yellow solid, (0.63 g of product **7a** from 1.1 g of **6**) 40% yield. TLC R_f = 0.48 ($CHCl_3$:MeOH = 9:1); ^{1}H-NMR (400 MHz, $CDCl_3$): δ = 8.73 (d, *J* = 8.4 Hz, 1H), 8.54 ($_{app}$t, *J* = 6.8 & 5.6 Hz, 1H), 8.42 ($_{app}$t, *J* = 7.6 & 5.2 Hz, 1H), 7.80–7.76 (m, 2H), 7.70 (br, 1H), 5.64 (ma.) and 5.07 (mi.) ($_{app}$t, *J* = 5.2 Hz, 1H), 4.76 (ma.) and 4.60 (mi.) (s, 2H), 4.40 (t, *J* = 6 Hz, 2H), 4.24 (m, 4H), 3.81 (t, *J* = 6 Hz, 2H), 3.71–3.69 (m, 2H), 3.62–3.60 (m, 2H), 3.58–3.56 (m, 4H), 3.45–3.42 (m, 2H), 3.37–3.34 (m, 2H), 3.30 (s, 3H), 1.46 (ma.) and 1.42 (mi.) (s, 9H), 1.34 (mi.) and 1.27 (ma.) (t, *J* = 7.2 Hz, 3H) ppm; ^{13}C-NMR (100 MHz, $CDCl_3$): δ = 169.7 (ma.) and 169.4 (mi.), 167.3 (mi.) and 166.9 (ma.), 164.1 (mi.) and 163.8 (ma.), 161.6, 156.2, 149.9, 148.5 (mi.) and 148.4 (ma.), 133.0, 132.3, 132.2, 131.8, 131.5, 130.3 (ma.) and 130.2 (mi.), 128.7, 128.6, 128.0 (mi.) and 127.8 (ma.), 127.1, 122.7 (ma.) and 122.2 (mi.), 99.7, 91.4, 90.2, 80.3, 72.0, 70.7, 70.6, 70.3, 68.0, 62.6, 62.0, 59.1, 49.4, 49.0, 48.6, 46.2, 39.3 (ma.) and 38.9 (mi.), 28.6 (ma.) and 28.5 (mi.), 14.2 ppm; HRMS: Calcd. for $C_{38}H_{45}N_5O_{12}Na$: 786.2962 $[M+Na]^+$; found: 786.2956. (Note: trace amount of impurity was present).

Ethyl *N*-(2-(5-(3-(6-amino-1,3-dioxo-1*H*-benzo[*de*]isoquinolin-2(3*H*)-yl)prop-1-yn-1-yl)-2,4-dioxo-3,4-dihydropyrimidin-1(2*H*)-yl)acetyl)-*N*-(2-((*tert*-butoxycarbonyl)amino)ethyl)glycinate 7b: Yellow solid, (0.19 g of product **7b** from 0.39 g of **6**) 40% yield. TLC R_f = 0.38 ($CHCl_3$:MeOH = 9:1); ^{1}H-NMR (400 MHz, d_6-DMSO): δ = 11.63 (ma.) and 11.62 (mi.) (br, 1H), 8.64 (d, *J* = 8.4 Hz, 1H), 8.46 (d, *J* = 7.2 Hz, 1H), 8.22

(d, *J* = 8.4 Hz, 1H), 7.79 (s, 1H), 7.67 ($_{app}$t, *J* = 8.0 & 7.6 Hz, 1H), 7.54 (br, 2H), 4.94 (s, 2H), 4.67 (ma.) and 4.51 (mi.) (s, 2H), 4.23–4.00 (m, 4H), 3.35–3.27 (m, 2H), 3.14–3.11 (ma.) and 3.01–2.97 (mi.) (m, 2H), 1.32 (mi.) and 1.31 (ma.) (s, 9H), 1.21 (mi.) and 1.15 (ma.) ($_{app}$t, *J* = 7.2 & 6.8 Hz, 3H) ppm; ^{13}C-NMR (100 MHz, d_6-DMSO): δ = 169.2, 168.9, 167.3, 166.9, 163.1, 162.1 (ma.) and 162.0 (mi.), 155.7, 153.1, 149.9, 134.3, 131.4, 129.6, 124.1, 121.5, 119.4, 108.3, 107.1, 96.9, 88.5 (ma.) and 88.4 (mi.), 78.0 (ma.) and 77.7 (mi.), 73.3, 61.2, 60.3, 47.9, 47.6, 46.9, 37.9, 29.4, 28.2 (mi.) and 28.1 (ma.), 14.0 ppm; HRMS: Calcd. for $C_{32}H_{34}N_6O_9Na$: 669.2284 $[M+Na]^+$; found: 669.2291.

Ethyl *N*-(2-((*tert*-butoxycarbonyl)amino)ethyl)-*N*-(2-(2,4-dioxo-5-(pyren-4-ylethynyl)-3,4-dihydropyrimidin-1(2*H*)-yl)acetyl)glycinate 7c: Faint yellow solid, (0.22 g of product **7c** from 0.21 g of **6**) 56% yield; TLC R_f = 0.43 (EtOAc); ^{1}H-NMR (400 MHz, d_6-DMSO): δ = 11.89 (ma.) and 11.73 (mi.) (br, 1H), 8.65–8.61 (m, 1H), 8.39–8.11 (m, 7H), 7.64–7.52 (m, 2H), 7.01–6.73 (m, 1H), 4.85–4.54 (m, 2H), 4.35–4.04 (m, 4H), 3.47–3.37 (m, 2H), 3.24–3.03 (m, 2H), 1.40 (ma.) and 1.37 (mi.) (s, 9H), 1.27 (mi.) and 1.20 (ma.) (t, *J* = 7.2 Hz, 3H) ppm; ^{13}C-NMR (100 MHz, d_6-DMSO): δ = 169.7 (mi.) and 169.4 (ma.), 167.8 (mi.) and 167.5 (ma.), 162.6 (ma.) and 161.6 (mi.), 156.3, 151.1 (mi.) and 150.5 (ma.), 132.5, 132.0, 131.9, 131.4, 131.3, 131.0, 129.4, 129.3, 129.2, 128.8, 127.7, 127.3, 126.5 (mi.) and 126.4 (ma.), 125.4 (ma.) and 125.3 (mi.), 124.1, 123.9, 117.3, 98.1, 91.7, 88.4, 78.6 (ma.) and 78.3 (mi.), 61.7 (mi.) and 61.1 (ma.), 48.7, 48.4, 47.5, 38.5, 28.6, 14.5 ppm; HRMS: Calcd. for $C_{35}H_{35}N_4O_7$: 623.2506 $[M+H]^+$; found: 623.2497.

General procedure for the synthesis of fluorescent PNA acids 8(a-c)

To a solution of fluorescent PNA esters (**7a**/**7b**/**7c**, 1.0 equiv.) in methanol (20 mL per g of **7**(**a**-**c**)) was added lithium hydroxide (3% solution in H_2O, 10 mL per g of **7**(**a**-**c**) and the reaction mixture was stirred for 3 h at RT. The solvent was evaporated to dryness, and the residue was dissolved in water and washed with diethyl ether. To the aqueous extract was added saturated $KHSO_4$ solution to adjust the pH to ~4. The product was then extracted with EtOAc and solvent was evaporated. The residue was purified by reversed phase column chromatography (C18 Redi*SepRf* column, MeOH: H_2O) to afford the desired products **7** (**a**-**c**).

***N*-(2-((*tert*-Butoxycarbonyl)amino)ethyl)-*N*-(2-(5-((2-(2-(2-(2-ethoxyethoxy)ethoxy)ethyl)-1,3-dioxo-2,3-dihydro-1*H*-benzo[*de*]isoquinolin-6-yl)ethynyl)-2,4-dioxo-3,4-dihydropyrimidin-1(2*H*)-yl)acetyl)glycine 8a**: Yellow solid, (0.3 g of product **8a** from 0.45 g of **7a**) 69% yield. TLC R_f = 0.12 (CH_2Cl_2:MeOH = 9:1); ^{1}H-NMR (400 MHz, d_6-DMSO): δ = 11.93 (br, 1H), 8.75 (d, *J* = 8.4 Hz, 1H), 8.54–8.26 (m, 3H), 8.00–7.88 (m, 2H), 7.64–7.55 (m, 2H), 7.00 (ma.) and 6.85 (mi.) (br, 1H), 4.82 (ma.) and 4.65 (mi.) (s, 2H), 4.24–3.99 (m, 4H), 3.67–3.41 (m, 13H), 3.14 (s, 3H), 1.39 (ma.) and 1.36 (mi.) (s, 9H) ppm; ^{13}C-NMR (100 MHz, d_6-DMSO): δ = 167.2 (mi.) and 166.6 (ma.), 163.2, 162.9, 161.9, 155.8 (ma.) and 155.6 (mi.), 151.2 (mi.) and 150.9 (ma.), 149.9, 132.1 (ma.) and 131.9 (mi.), 131.5, 131.3, 130.7 (ma.) and 130.6 (mi.), 130.2 (ma.) and 130.0 (mi.), 128.8 (ma.) and 128.7 (mi.), 128.1 (ma.) and 128.0 (mi.), 127.4 (ma.) and 127.3 (mi.), 126.5 (mi.) and 126.4 (ma.), 122.6 (ma.) and 122.5 (mi.), 121.5 (ma.) and 121.4 (mi.), 96.6, 92.3, 89.5, 78.1, 77.7, 71.2, 69.7, 69.6, 66.9, 58.0, 48.4, 47.9, 46.9, 38.0, 28.2 ppm; HRMS: Calcd. for $C_{36}H_{41}N_5O_{12}Na$: 758.2649 $[M+Na]^+$; found: 758.2657.

***N*-(2-(5-(3-(6-Amino-1,3-dioxo-1*H*-benzo[*de*]isoquinolin-2(3*H*)-yl)prop-1-yn-1-yl)-2,4-dioxo-3,4-dihydropyrimidin-1(2*H*)-yl)acetyl)-*N*-(2-((*tert*-butoxycarbonyl)amino)ethyl)glycine 8b:** Yellow solid, (20 mg of product **8b** from 50 mg of **7b**) 42% yield; TLC R_f = 0.09 (CH_2Cl_2:MeOH = 9:1); ^{1}H-NMR (400 MHz, d_6-DMSO): δ = 11.65 (br, 1H), 8.65 (d, *J* = 8.4 Hz, 1H), 8.46 (d, *J* = 7.2 Hz, 1H), 8.22 (d, *J* = 8.4 Hz, 1H), 7.80 (ma.) and 7.78 (mi.) (s, 1H), 7.67 ($_{app}$t, *J* = 8.0 and 7.6 Hz, 1H), 7.55 (br, 2H), 6.94–6.73 (m, 2H), 4.94 (s, 2H), 4.66 (ma.) and 4.49 (mi.) (s, 2H), 4.07 (mi.) and 3.93 (ma.) (s, 2H), 3.33–3.26 (m, 2H), 3.13–2.98 (m, 2H), 1.31 (s, 9H) ppm; ^{13}C-NMR (100 MHz, d_6-DMSO): δ = 170.4, 166.7, 163.1, 162.1, 155.7, 153.2, 150.0, 134.3, 131.4, 129.8, 124.1, 121.5, 119.4, 108.3, 107.1, 96.9, 88.4, 78.0, 73.3, 47.9, 47.6, 46.7, 37.8, 29.4, 28.1 ppm; HRMS: Calcd. for $C_{30}H_{30}N_6O_9Na$: 641.1972 $[M+Na]^+$; found: 641.1964. (Note: trace amount of DMSO impurity was present).

***N*-(2-((*tert*-Butoxycarbonyl)amino)ethyl)-*N*-(2-(2,4-dioxo-5-(pyren-1-ylethynyl)-3,4-dihydropyrimidin-1(2*H*)-yl)acetyl)glycine 8c:** Faint yellow solid, (0.1 g of product **8c** from 0.21 g of **7c**) 50% yield; TLC R_f = 0.13 (CH_2Cl_2:MeOH = 9:1); ^{1}H-NMR (400 MHz, d_6-DMSO): δ = 12.81 (br, 1H), 11.88 (ma.) and 11.72 (mi.) (br, 1H), 8.64 (mi.) and 8.63 (ma.) (d, *J* = 9.2 Hz, 1H), 8.39–8.11 (m, 9H), 6.99 (ma.) and 6.77 (mi.) ($_{app}$t, *J* = 6.0 and 5.6 Hz, 1H), 4.83 (ma.) and 4.66 (mi.) (s, 2H), 4.24 (mi.) and 4.02 (ma.) (s, 2H), 3.45–3.35 (m, 2H), 3.24–3.19 (ma.) and 3.09–3.05 (mi.) (m, 2H), 1.40 (ma.) and 1.37 (mi.) (s, 9H) ppm; ^{13}C-

NMR (100 MHz, d_6-DMSO): δ = 170.9, 167.7 (ma.) and 167.3 (mi.), 162.6, 156.3, 150.5, 132.0, 131.9, 131.3, 131.0, 129.4, 129.3, 129.2, 128.8, 127.7, 127.3, 126.5 (mi.) and 126.4 (ma.), 125.4 (ma.) and 125.3 (mi.), 124.1, 123.9, 117.4 (mi.) and 117.3 (ma.), 98.1 (ma.) and 98.0 (mi), 91.7 (ma.) and 91.6 (mi.), 88.4, 78.6 (ma.) and 78.3 (mi.), 48.7, 48.1, 47.3, 38.5, 28.6 ppm; HRMS: Calcd. for $C_{33}H_{31}N_4O_7$: 595.2193 $[M+H]^+$; found: 595.2184.

_N_-(2-Aminoethyl)-_N_-(2-(5-((2-(2-(2-(2-methoxyethoxy)ethoxy)ethyl)-1,3-dioxo-2,3-dihydro-1_H_-benzo[_de_]isoquinolin-6-yl)ethynyl)-2,4-dioxo-3,4-dihydropyrimidin-1(2_H_)-yl)acetyl)glycine 9

Solution of compound **8a** (0.300 g, 0.41 mmol, 1.0 equiv.) in 50% TFA in dichloromethane (15 mL) was stirred for 3 h at RT. Reaction mixture was evaporated to dryness using NaOH trap, and residue was co-evaporated with dichloromethane (3 x 20 mL). Residue was further purified using RP-HPLC with semipreparative column [conditions: 0–50% B in 10 min and 50–100% B in 10 min (Mobile phase A: 5% acetonitrile in H_2O containing 0.1% TFA. Mobile phase B: 100% acetonitrile in H_2O containing 0.1% TFA) and flow rate: 1 mL/min] to afford yellow solid **9** (0.133 g, 51%). ^{1}H-NMR (400 MHz, d_6-DMSO): δ = 11.99 (mi.) and 11.95 (ma.) (s, 1H), 8.81–8.69 (m, 1H), 8.59–8.54 (m, 1H), 8.46–8.30 (m, 2H), 7.99–7.77 (m, 5H), 5.12–4.69 (m, 2H), 4.36–4.06 (m, 4H), 3.69–3.64 (m, 3H), 3.57–3.53 (m, 3H), 3.48–3.45 (m, 2H), 3.43–3.40 (m, 2H), 3.29–3.27 (m, 2H), 3.14 (s, 3H), 3.11–2.96 (m, 2H) ppm; ^{13}C-NMR (100 MHz, d_6-DMSO): δ = 170.9 (mi.) and 170.8 (ma.), 168.2, 167.0, 163.2 (mi.) and 162.9 (ma.), 161.9, 151.1, 150.0, 131.9, 131.3, 130.7, 130.2, 130.0, 128.2, 127.4, 126.4, 122.6, 121.6, 96.7 (mi.) and 96.6 (ma.), 92.4 (ma.) and 92.3 (mi.), 89.6 (mi.) and 89.5 (ma.), 71.2, 69.7, 69.6, 66.9, 58.0, 48.8 (mi.) and 48.5 (ma.), 47.8, 45.0, 36.9 ppm; HRMS: Calcd. for $C_{31}H_{34}N_5O_{10}$: 636.2306 $[M+H]^+$; found: 636.2318. λ_{max} (H_2O) = 388 nm; ε_{260} = 9680 $M^{-1}cm^{-1}$, ε_{388} = 17700 $M^{-1}cm^{-1}$.

Ethyl 2-(5-iodo-2,4-dioxo-3,4-dihydropyrimidin-1(2_H_)-yl)acetate 17

To a suspension of iodouracil **16** (3.97 g, 16.69 mmol, 1.0 equiv.) and K_2CO_3 (2.31 g, 16.69 mmol, 1.0 equiv.) in DMF (99 mL) was added ethyl bromoacetate (1.86 mL, 16.69 mmol, 1.0 equiv.) drop wise. The reaction mixture was vigorously stirred for 12 h at RT. The DMF was evaporated using rotary evaporator with high vacuum pump and then water (100 mL) was added and the product was extracted using EtOAc (2 × 100 mL). The organic layer was evaporated and residue was purified by silica gel column chromatography to afford the

product **17** as a white solid (3.23 g, 59%). TLC R_f = 0.43 (Hexane:EtOAc = 5:5); ^{1}H-NMR (400 MHz, d_6-DMSO): δ = 11.81 (br, 1H), 8.21 (s,1H), 4.50 (s, 2H), 4.15 (q, *J* = 7.2 Hz , 2H), 1.21 (t, *J* = 7.2 Hz, 3H) ppm; ^{13}C-NMR (100 MHz, d_6-DMSO): δ = 167.9, 161.0, 150.6, 150.0, 68.2, 61.2, 48.5, 14.0 ppm; HRMS: (*m/z*): Calc. for $C_8H_{10}IN_2O_4$: 324.9685 $[M+H]^+$; found: 324.9685. (Note: trace amount of acetone impurity was present)

Ethyl 2-(5-((2-(2-(2-(2-methoxyethoxy)ethoxy)ethyl)-1,3-dioxo-2,3-dihydro-1*H*-benzo[*de*]isoquinolin-6-yl)ethynyl)-2,4-dioxo-3,4-dihydropyrimidin-1(2*H*)-yl)acetate 18

To a suspension of compound **17** (0.610 g, 1.88 mmol, 1.0 equiv.), **4** (0.680 g, 1.88 mmol, 1.0 equiv.), $Pd(Ph_3)_4$ (0.214 g, 0.19 mmol, 0.1 equiv.) and CuI (0.071 g, 0.38 mmol, 0.2 equiv.) in degassed dry THF (6 mL) was added *N*,*N*-diisopropylethylamine (1.13 mL, 6.58 mmol, 3.5 equiv.). The reaction mixture was stirred for 12 h at RT and filtered through celite pad, washed with THF (2 x 10 mL). The filterate was then evaporated and the residue was washed with petroleum ether (2 x 20 mL). The crude product was further re-crystalized using EtOAc (30 mL) to afford the product **18** as a yellow solid (0.545 g, 52%). TLC R_f = 0.41 (EtOAc); ^{1}H-NMR (400 MHz, d_6-DMSO): δ = 12.03 (br, 1H), 8.74 (d, *J* = 8.4 Hz, 1H), 8.53 (d, *J* = 7.2 Hz, 1H), 8.49 (s, 1H), 8.43 (d, *J* = 7.6 Hz, 1H), 7.98–7.92 (m, 2H), 4.65 (mi.) and 4.63 (ma.) (s, 2H), 4.25–4.17 (m, 4H), 3.66 (t, *J* = 6.4 Hz, 2H), 3.56–3.53 (m, 2H), 3.47–3.41 (m, 4H), 3.30–3.27 (m, 2H), 3.15 (s, 3H), 1.24 ($_{app}$t, *J* = 7.2 and 6.8 Hz, 3H) ppm; ^{13}C-NMR (100 MHz, d_6-DMSO): δ = 167.6, 163.1, 162.8, 161.7, 150.3, 149.8, 131.8, 131.2, 130.6, 130.1, 130.0, 128.0, 127.3, 126.2, 122.5, 121.6, 96.9, 92.0, 89.5, 71.1, 69.6, 69.5, 66.8, 61.4, 57.9, 49.0, 14.0 ppm; HRMS: (*m/z*): Calc. for $C_{29}H_{29}N_3O_9Na$: 586.1801 $[M+Na]^+$; found: 586.1797.

2-(5-((2-(2-(2-(2-Methoxyethoxy)ethoxy)ethyl)-1,3-dioxo-2,3-dihydro-1*H*-benzo[*de*]isoquinolin-6-yl)ethynyl)-2,4-dioxo-3,4-dihydropyrimidin-1(2*H*)-yl)acetic acid 19

To a solution of compound **18** (0.545 g, 0.97 mmol, 1.0 equiv.) in THF (11 mL), lithium hydroxide (7% solution in H_2O, 5.0 mL) was added dropwise and the reaction mixture was stirred for 2 h at RT. Reaction mixture was evaporated to dryness, and residue was dissolved in water (20 mL) and washed with diethyl ether (15 ml). To the aqueous extract was added saturated $KHSO_4$ solution (~5 mL) to adjust the pH to ~5 and product was precipitated out as yellow solid. Which was further collected upon filteration as a yellow solid **19** (0.47 g, 91%).

TLC R_f = 0.18 (CH_2Cl_2:MeOH = 8:2); ^{1}H-NMR (400 MHz, d_6-DMSO): δ = 11.98 (br, 1H), 8.72 (d, *J* = 8.4 Hz, 1H), 8.53–8.49 (m, 1H), 8.48 (s, 1H), 8.41 (d, *J* = 7.6 Hz, 1H), 7.97–7.87 (m, 2H), 4.53 (s, 2H), 4.22 (t, *J* = 6.4 Hz, 2H), 3.65 (t, *J* = 6.4 Hz, 2H), 3.55–3.53 (m, 2H), 3.47–3.41 (m, 4H), 3.30–3.27 (m, 2H), 3.14 (s, 3H) ppm; ^{13}C-NMR (100 MHz, d_6-DMSO): δ = 169.1, 165.7, 163.1, 162.8, 161.7, 150.6, 149.9, 131.8, 131.2, 130.6, 130.1, 129.9, 128.0, 127.3, 126.3, 122.5, 121.5, 96.7, 92.2, 89.4, 71.1, 69.6, 69.5, 66.9, 57.9, 49.1 ppm; HRMS: Calcd. for $C_{27}H_{25}N_3O_9Na$: 558.1488 $[M+Na]^+$; found: 558.1492.

tert-Butyl _N_-(2-((((9_H_-fluoren-9-yl)methoxy)carbonyl)amino)ethyl)-_N_-(2-(5-((2-(2-(2-(2-methoxyethoxy)ethoxy)ethyl)-1,3-dioxo-2,3-dihydro-1_H_-benzo[_de_]isoquinolin-6-yl)ethynyl)-2,4-dioxo-3,4-dihydropyrimidin-1(2_H_)-yl)acetyl)glycinate 21

Solution of compound **19** (0.430 g, 0.80 mmol, 1.2 equiv.), Fmoc PNA backbone **20** (0.290 g, 0.67 mmol, 1.0 equiv.), EDC (0.153 g, 0.80 mmol, 1.2 equiv.), HOBt (0.108 g, 0.80 mmol, 1.2 equiv.) and DIPEA (0.23 mL, 1.34 mmol, 2.0 equiv.) in dry DMF (8.6 mL) were stirred for 4 h at RT under nitrogen atmosphere. Solvent was evaporated and residue was purified using silica gel chromatography with dichloromethane and methanol solvent system to afford yellow solid **21** (0.28 g, 38%). TLC R_f = 0.53 (EtOAc); ^{1}H-NMR (400 MHz, d_6-DMSO): δ = 11.94 (br, 1H), 8.73 (d, *J* = 8.4 Hz, 1 H), 8.55–8.48 (m, 1H), 8.40 (t, *J* = 7.0 Hz, 1H), 8.33 (ma.) and 8.30 (mi.) (s, 1H), 7.95–7.82 (m, 4H), 7.69–7.64 (m, 2H), 7.46–7.26 (m, 5H), 4.83 (ma.) and 4.65 (mi.) (s, 2H), 4.35–4.22 (m, 6H), 3.97 (s, 1H), 3.66 (t, *J* = 6.4 Hz, 2H), 3.56–3.53 (m, 2H), 3.47–3.40 (m, 6H), 3.29–3.27 (m, 4H), 3.14 (s, 3H), 1.48 (mi.) and 1.40 (ma.) (s, 9H) ppm; ^{13}C-NMR (100 MHz, d_6-DMSO): δ = 167.9, 166.7, 163.1, 162.8, 161.8, 157.4, 150.9, 149.9, 142.5, 139.4, 137.4, 131.9, 131.2, 130.6, 130.1, 129.9, 128.9, 128.0, 127.4, 127.2, 126.4, 122.5, 121.5, 121.3, 120.0, 109.7, 96.6, 92.4, 92.3, 89.4, 82.0, 81.0, 71.1, 69.6, 69.5, 66.9, 57.9, 54.9, 48.7, 48.4, 47.2, 38.8, 27.7 (ma.) and 27.6 (mi.) ppm; HRMS: (*m/z*): Calc. for $C_{50}H_{51}N_5O_{12}Na$: 936.3432 $[M+Na]^+$; found: 936.3406. (Note: trace amount of dichloromethane impurity was present).

_N_-(2-((((9_H_-Fluoren-9-yl)methoxy)carbonyl)amino)ethyl)-_N_-(2-(5-((2-(2-(2-(2-methoxyethoxy)ethoxy)ethyl)-1,3-dioxo-2,3-dihydro-1_H_-benzo[_de_]isoquinolin-6-yl)ethynyl)-2,4-dioxo-3,4-dihydropyrimidin-1(2_H_)-yl)acetyl)glycine 22

Solution of compound **21** (0.13 g, 0.14 mmol, 1.0 equiv.) in 50% TFA in dichloromethane (15 mL) was stirred for 2 h at RT. Solvent was evaporated to dryness using NaOH trap, and

residue was co-evaporated using dichloromethane (3 x 20 mL). Crude product was purified using silica gel column chromatography with dichloromethane and methanol solvent system to afford yellow product **22** (95 mg, 78%). TLC R_f = 0.33 (CH_2Cl_2:MeOH = 8.5:1.5); ^{1}H-NMR (400 MHz, d_6-DMSO): δ = 11.95 (mi.) and 11.90 (ma.) (br, 1H), 8.69–8.61 (m, 1 H), 8.48–8.24 (m, 3H), 7.84–7.47 (m, 7H), 7.39–7.26 (m, 4H), 4.83 (mi.) and 4.68 (ma.) (s, 2H), 4.33–4.13 (m, 5H), 3.99 (br, 2H), 3.66–3.63 (m, 2H), 3.55–3.53 (m, 2H), 3.47–3.45 (m, 3H), 3.43–3.41 (m, 4H), 3.31–3.27 (m, 3H), 3.15 (ma.) and 3.14 (mi.) (s, 3H) ppm; ^{13}C-NMR (100 MHz, d_6-DMSO): δ = 167.4, 166.5, 163.1, 162.8, 161.9, 156.4, 156.1, 151.1 (mi.) and 151.0 (ma.), 150.0, 143.8, 140.7, 140.6, 131.9, 131.2, 131.7, 130.6 (mi.) and 130.5 (ma.), 130.1, 130.0, 129.9, 129.8, 129.7, 128.0, 127.9, 127.8, 127.6 (mi.) and 127.5 (ma.), 127.3, 127.1, 126.4, 125.2, 120.1 (mi.) and 120.0 (ma.), 96.6, 92.5 and 92.4, 89.5, 71.2, 69.7, 69.6, 66.9, 65.6, 58.0, 51.2, 48.6, 46.8 (mi.) and 46.7 (ma.), 37.9 ppm; HRMS: Calcd. for $C_{46}H_{43}N_5O_{12}Na$: 880.2806 $[M+Na]^+$; found: 880.2799.

4.4.4 Photophysical characterization of PNA base analogues 8a–8c and 9

UV-Vis absorption: Samples of **8a–8c** and **9** (25.0 μM) were prepared in solvents of different polarity such as water, methanol and dioxane. Sample of analogue **9** (25.0 μM) were also prepared in water, dioxane and their mixtures (25% dioxane, 50% dioxane, 75% dioxane in water). All solutions contained 2.5% DMSO.

Steady-state fluorescence: Emission spectra of **8a–8c** and **9** (5.0 μM) in water, methanol, and dioxane were obtained by exciting the samples at respective longest absorption maximum (see Table 1 and 2) by maintaining the excitation and emission slit widths at 1 and 2 nm, respectively, for **8a–8c** and 1 and 3 nm, respectively, for **9**. Emission spectra of analogue **9** (5.0 μM) in water, dioxane and their mixtures (25% dioxane, 50% dioxane, 75% dioxane in water) were also recorded by exciting the samples at respective longest absorption maximum (Table 2). All solutions contained 0.5% DMSO.

Time-resolved fluorescence: Excited-state lifetime of Lucifer PNA analogue **9** (5.0 μM) in various solvents were determined using TCSPC instrument (Horiba Jobin Yvon, Fluorolog-3). Analogue **9** were excited using a 371 nm LED source (IBH, UK, NanoLED-371L) and fluorescence signal at respective emission maximum was collected. Lifetime measurements were performed in duplicate and decay profiles were analyzed using IBH DAS6 analysis software. Fluorescence intensity decay profiles were found to be biexponential with χ^2 (goodness of fit) values very close to unity.

4.4.5 Quantum yield determination for emissive PNA base analogues 8a–8c and 9

The quantum yield of emissive PNA analogues **8a–8c** and **9** in different solvents relative to cumarin 153 standard were determined using the following equation.[21]

$\Phi_{F(x)} = (A_s/A_x)\ (F_x/F_s)\ (n_x/n_s)^2\Phi_{F(s)}$

Where s is the standard, x is PNA analogue (**8a–8c** and **9**), A is the absorbance at excitation wavelength, F is the area under the emission curve, n is the refractive index of the solvent, and Φ_F is the quantum yield. Quantum yield of cumarin 153 in acetonitrile is 0.56.[22]

4.4.6 Solid phase synthesis of TEG naphthalimide-modified PNA probe 14 by Fmoc-chemistry

Model 15mer fluorescent PNA oligomers were synthesized on MBHA resin by SPPS using Boc-chemistry according to protocol mentioned in Chapter 2. PNA probe **14** was synthesized by applying SPPS protocol on rink amide resin using Fmoc-protected *aeg*-thymine and fluorescent 5-TEG naphthalimide PNA acid **22**.[23] To enhance aqueous solubility of PNA oligomer, two lysine residues were attached at the C-terminus.

General procedure: In a glass sintered flask, Rink-amide resin (250 mg, 0.65 mmol/g) was swelled in CH_2Cl_2 (8 mL) for 12 h. The solvent was then removed, and the resin was treated with 20% piperidine in DMF (6 mL) for 10 min to remove Fmoc-group from resin. This step was repeated two more times. The resin was then washed sequentially with DMF (3 x 3 mL), CH_2Cl_2 (3 x 3 mL), and DMF (3 x 3 mL). The resin was dried under nitrogen flow for few minutes. The coupling reaction was performed in dry DMF (1.8 mL) with Fmoc-Lys(Boc)-OH (36 mg, 1.0 equiv. to obtain a loading of 0.35 mmol/g) in the presence of HOBt (1.0 equiv.), HBTU (1.0 equiv.) and DIPEA (1.0 equiv.) for 7–9 h at RT. The resin was further washed with DMF (3 x 3 mL), CH_2Cl_2 (3 x 3 mL), and DMF (3 x 3 mL). Next, remaining amino groups on the resin was capped with acetic anhydride (1.0 mL) in pyridine (1.0 mL) for 1 h at RT. This step was repeated two more times, and the resin was then washed with DMF (3 x 3 mL), CH_2Cl_2 (3 x 3 mL), and DMF (3 x 3 mL) and dried under nitrogen flow for few minutes. The resin was treated with 20% piperidine in DMF (5 mL) for 10 min to remove Fmoc-group. This step was repeated two more times, and the resin was washed with DMF (3 x 3 mL), CH_2Cl_2 (3 x 3 mL), and DMF (3 x 3 mL). Then coupling reaction was performed in dry DMF (1.8 mL) with Fmoc-Lys(Boc)-OH (3.0 equiv.) in the presence of HOBt (3.0 equiv.), HBTU (3.0 equiv.) and DIPEA (3.0 equiv.) for 7–9 h at RT. The resin was then

washed with DMF (3 x 3 mL), CH_2Cl_2 (3 x 3 mL), and DMF (3 x 3 mL). The resin was dried under nitrogen flow for few minutes.

Above lysine loaded Rink-amide resin (25 mg, 0.35 mmol/g) was swelled in CH_2Cl_2 (2 mL) for 2 h in glass sintered flask. The solvent was removed and the resin was treated with 20% piperidine in DMF (1.0 mL) for 10 min to remove Fmoc-group as mentioned above. The resin was then washed with DMF (3 x 3 mL), CH_2Cl_2 (3 x 3 mL), and DMF (3 x 3 mL). The coupling reaction was performed in dry DMF (0.6 mL) with appropriate Fmoc-protected PNA monomers (3.0 equiv.) in the presence of HOBt (3.0 equiv.), HBTU (3.0 equiv.) and DIPEA (3.0 equiv.) for 6 min at 65 °C using microwave peptide synthesizer (Note: Coupling reaction for fluorescent PNA monomer **22** was carried out at RT for 7–9 h). The resin was washed again, and the coupling, Fmoc deprotection, and washing steps were repeated in the cycle as mentioned above to synthesize the desired PNA sequence. Also, the re-coupling reaction was performed for only fluorescently modified PNA monomer **22** in the presence of HOBt (3.0 equiv.), HBTU (3.0 equiv.) and DIPEA (3.0 equiv.) for 7–9 h at RT.

Cleavage procedure: The dried resin (20 mg) was transferred to a glass vial and treated with H_2O (10 μL) and anisole (10 μL) in an ice bath for 10 min. TFA (380 μL) was then added to the above mixture and was stirred for 1.5 h at room temperature. The resin was filtered, and the filtrate was concentrated and precipitated as a white solid by adding cold diethyl ether (1 mL). The solvent was decanted, and the crude product was dissolved in autoclaved water and purified by RP-HPLC.

4.4.7 HPLC analysis of PNA oligomers

All control and fluorescently modified PNA oligomers were purified using a Luna C18 semi-preparative RP column (5 micron, 250 × 10 mm, Phenomenex) on an Agilent Technologies 1260 Infinity HPLC system. Conditions: 0–50% B in 25 min and 50–100% B in 15 min (Mobile phase A: 5% acetonitrile in H_2O containing 0.1% TFA. Mobile phase B: 50% acetonitrile in H_2O containing 0.1% TFA). Flow rate was 2 mL/min. The chromatogram of control PNA oligomers was recorded at 260 nm, and fluorescently modified PNA oligomers were recorded at 260 nm, and 330 nm. Concentration of the PNA oligomers were determined by using the molar extinction coefficients of nucleobases at 260 nm (ε_A = 13700, ε_T = 8600, ε_G = 11700, ε_C = 6600, $\varepsilon_{\mathbf{9}}$ = 9680 $M^{-1}cm^{-1}$).[23]

4.4.8 MALDI-TOF mass measurement of PNA oligomers

1 μL of a ~150 μM stock solution of PNA oligomer was combined with 2,5-dihydroxybenzoic acid (DHB) or α-cyano-4-hydroxycinnamic acid (CHCA) matrix. The samples were spotted on a plate and air dried before mass analysis.

4.4.9 Thermal melting and CD analysis of PNA duplexes

The PNA-DNA and PNA-RNA duplexes were assembled by heating a 1:1 mixture of PNA and DNA/RNA oligomers (10.0 μM) in 10 mM phosphate buffer (pH 7.1, 100 mM NaCl, 0.1 mM EDTA) at 90 ºC for 3 min. Samples were slowly cooled to RT and kept in an ice bath for ~1 h. Samples were further diluted using phosphate buffer to give a final duplex concentration of 1.0 μM for T_m and 5.0 μM for CD analysis, respectively. UV-thermal melting analysis of PNA duplexes were performed in duplicate using quartz cuvette on a Cary 300Bio UV-Vis spectrophotometer. The temperature was increased from 20 ºC to 90 ºC at 1 ºC/min, and the absorbance was measured every 1 ºC interval at 260 nm. CD spectra of PNA duplexes were recorded with an average of three scans from 350 to 200 nm using quartz cuvette (Starna Scientific, path length 2 mm) on a JASCO J-815 CD spectrometer at 20 ºC and scan speed of 100 nm/min.

4.4.10 Fluorescence of naphthalimide-modified PNA oligomers and their duplexes

PNA-DNA and PNA-RNA duplexes were obtained by heating a 1:1 mixture of PNA and DNA/RNA (5.0 μM) in 10 mM phosphate buffer (pH 7.1, 100 mM NaCl, 0.1 mM EDTA) at 90 ºC for 3 min. Samples were slowly cooled to RT and kept in an ice bath for ~1 h. Samples were further diluted using phosphate buffer to give a final duplex concentration of 0.5 μM. All Samples were excited at 400 nm, and excitation and emission slit widths were maintained at 6 nm and 8 nm, respectively for **9**. However, all Samples were excited at 455 nm, and excitation and emission slit widths were kept at 3 and 5 nm, respectively for **X**. Samples made for PNA probe **14** and its duplexes with poly(A) DNA **23** and RNA **24** were excited at 400 nm, and excitation and emission slit widths were kept at 2 and 3 nm, respectively.

4.4.11 Quantum yield determination for PNA 14 and its duplex with DNA 23 and RNA 24: Quantum yield of fluorescently-modified PNA **14** and its duplexes (**14•23** and **14•23**) were determined relative to the quantum yield of the PNA analogue **9** in 10 mM phosphate buffer (pH 7.1, 100 mM NaCl, 0.1 mM EDTA) using the equation given in section 4.4.5.

4.4.12 Cell culture experiments

Cell culture

DLD-1 (Human colon cancer cells ATCC® CCL-221™) cells were cultured in RPMI1640 medium (gibco® by life technologies™, 61870-036) supplemented with 10% fetal bovine serum (gibco® by life technologies™, 10437028) and penicillin-streptomycin (gibco® by life technologies™, 15070-063) under humidified atmosphere at 37 ºC with 5% CO_2. Cells were seeded with 0.1–0.3 million in 12 well plates on glass coverslips and allowed to grow for nearly 48 hours before the experiment.

Fluorescence *in situ* hybridization

Cells grown on coverslips were washed with 500 µL of 1X PBS (10 mM Na_2HPO_4, 1.8 mM KH_2PO_4, 2.7 mM KCl, 137 mM NaCl, 500 µM VRC, pH 7.4) and fixed in 500 µL of 4% paraformaldehyde (500 µM VRC) for 15 min. Subsequently, cells were permeabilized with 95% chilled methanol for 5 min. Cells were then washed with 500 µL of 2X SSC buffer (0.3 M sodium citrate, 0.03 M sodium chloride, 500 µM VRC, pH 7.4) and prehybridized in 50 µL of hybridization buffer (10% (w/v) dextran sulphate, 40% (v/v) formamide, 5 ng/µL salmon sperm DNA and 500 µM VRC prepared in 2X SSC) for 30 min at 37 ºC in an incubator. After prehybridization, cells were washed with 500 µL of 2X SSC buffer and incubated in 0.5 µM of Cy-5d$(T)_{30}$ or 1.0 µM of PNA **14** in hybridization buffer for 2.5 h at 37 ºC in an incubator. Next, cells were washed with 500 µL of 2X SSC followed by 500 µL of 0.1X SSC. Cells were counterstained with 500 µL of DAPI (50 nM in 2X SSC) for 5 min and washed with 500 µL of 0.1X SSC. Coverslips were then placed on a microscope slide with 7 µL anti-fade mounting media and sealed with nail polish. Finally, cells were imaged using Confocal Laser Scanning Microscope with an oil immersion using 40X lens.

RNase A treatment

Cells were incubated in 500 µL of RNase A (0.5µg/mL in 1X PBS) solution for 1 h at 37 ºC in an incubator. Cells were then washed with 500 µL of 2X SSC and subjected for prehybridization in hybridization buffer. Finally, cells were incubated with 0.5 µM of Cy-5d$(T)_{30}$ or 1.0 µM of PNA **14** in hybridization buffer for 2.5 h at 37 ºC in an incubator and imaged using a confocal microscope as mentioned above.

Competition assay

Cells were hybridized with mixture of Cy-5d$(T)_{30}$ (0.5 µM) and PNA **14** (1.0, 0.5, 0.25 µM) in hybridization buffer for 2.5 h at 37 ºC in an incubator. Cells were also incubated with the mixture of Cy-5d$(T)_{30}$ (0.5 µM) and PNA **15/25** (1.0 µM) in hybridization buffer for 2.5 h at 37 ºC in an incubator. Finally, cells were counterstain with 500 µL DAPI (50 nM) and imaged using a confocal microscope as mentioned above.

4.5 Notes and References

1. a) B. P. Gangamani, V. A. Kumar and K. N. Ganesh, *Chem. Commun.*, 1997, 1913–1914; b) F. Wojciechowski and R. H. E. Hudson, *J. Am. Chem. Soc.*, 2008, **130**, 12574–12575; c) C. Boonlua, C. Vilaivan, H.-A. Wagenknecht and T. Vilaivan, *Chem.-Asian J.*, 2011, **6**, 3251–3259; d) S. Müllar, J. Strohmeier and U. Diederichsen, *Org. Lett.*, 2011, **14**, 1382–1385; e) A. H. St. Amant and R. H. E. Hudson, *Org. Biomol. Chem.*, 2012, **10**, 876–881.
2. P. M. Sabale and S. G. Srivatsan, *ChemBioChem*, 2016, **17**, 1665–1673.
3. a) S. Kummer, A. Knoll, E. Socher, L. Bethge, A. Herrmann and O. Seitz, *Angew. Chem. Int. Ed.*, 2011, **50**, 1931–1934; b) S. Kummer, A. Knoll, E. Socher, L. Bethge, A. Herrmann and O. Seitz, *Bioconjugate Chem.*, 2012, **34**, 2051–2060.
4. A. A. Tanpure and S. G. Srivatsan, *ChemBioChem*, 2014, **15**, 1309–1316.
5. a) C. Wu, C. Wang, L. Yan and C. J. Yang, *J. Biomed. Nanotechnol.*, 2009, **5**, 495–504; b) M. E. Østergaard and P. J. Hrdlicka, *Chem. Soc., Rev.*, 2011, **40**, 5771–5788.
6. J. N. Wilson, J. Gao and E. T. Kool, *Tetrahedron***,** 2007**, 63,** 3427–3433.
7. a) W. W. Stewart, *Nature*, 1981, **292**, 17–21; b) R. M. Duke, E. B. Veale, F. M. Pfeffer, P. E. Kruger and T. Gunnlaugsson, *Chem. Soc. Rev.*, 2010, **39**, 3936–3953.
8. C. Boonlua, C. Vilaivan, H.-A. Wagenknecht and T. Vilaivan, *Chem. Asian J.*, 2011, **6**, 3251–3259.
9. See Experimental Section for details.
10. C. Reichardt, Chem. Rev., 1994, **94**, 2319–2358.
11. E. L. Rachofsky, R. Osman and J. B. A. Ross, *Biochemistry*, 2001, **40**, 946–956.
12. a) S. O. Kelley and J. K. Barton, *Science*, 1999, **283**, 375–381; c) M. Torimura, S. Kurata, K. Yamada, T. Yokomaku, Y. Kamagata, T. Kanagawa and R. Kurane, *Anal. Sci.*, 2001, **17**, 155–160; c) I. Nazarenko, R. Pires, B. Lowe, M. Obaidy and A. Rashtchian, *Nucleic Acids Res.*, 2002, **30**, 2089–2195.
13. a) C. A. M. Seidel, A. Schulz and M. H. M. Sauer, *J. Phys. Chem.*, 1996, **100**, 5541–5553; b) S. Doose, H. Neuweiler and M. Sauer, *ChemPhysChem*, 2009, **10**, 1389–1398.
14. R. W. Sinkeldam, A. J. Wheat, H. Boyaci and Y. Tor, *ChemPhysChem*, 2011, **12,** 567–570.
15. a) M. S. Noé, R. W. Sinkeldam and Y. Tor, *J. Org. Chem.*, 2013, **78**, 8123–8128; b) R. W. Sinkeldam, A. J. Wheat, H. Boyaci and Y. Tor, *ChemPhysChem*, 2011, **12**, 567–570.
16. a) D. F. Colgan and J. L. Manley, *Genes & Dev.*, 1997, **11**, 2755–2766; b) A. O. Subtelny, S. W. Eichhorn, G. R. Chen, H. Sive and D. P. Bartel, *Nature*, 2014, **508**, 66–71; c) T. H. Beilharz, T. Preiss, *Methods*, 2009, **48**, 294–300.

17. a) R. P. Perry, J. La Torre, D. E. Kelley and J. R. Greenberg, *Biochim. Biophys. Acta.*, 1972, **262**, 220–226; b) J. A. Bantle, I. H. Maxwell and W. E. Hahn, *Anal Biochem.*, 1976, **72**, 413–427; c) J. H. Pringle, L. Primrose, C. N. Kind, I. C. Talbot and I. Lauder, *J. Pathol.*, 1989, **158**, 279–286; d) T. Koji and P. K. Nakane, *Acta Pathol Jpn.*, 1990, **40**, 793–807.
18. a) D. O. Wang, H. Matsuno, S. Ikeda, A. Nakamura, H. Yanagisawa, Y. Hayashi and A. Okamoto, *RNA*, 2012, **18**, 166–175; b) R. S. McIsaac, S. J. Silverman, L. Parsons, P. Xu, R. Briehof, M. N. McClean, D. Botstein, *J. Vis. Exp.*, 2013, **76**, e50382; c) A. Gebhardt, M. Habjan, C. Benda, A. Meiler, D. A. Haas, M. Y. Hein, A. Mann, M. Mann, B. Habermann and A. Pichlmair, *Nat. Commun.*, 2015, **6**, 8192; d) A. S. Labade, K. Karmodiya and K. Sengupta, *Epigenetics & Chromatin*, 2016, **9**, 54.
19. a) D. Munroe and A. Jacobson, *Mol. Cell Biol.*, 1990, **10**, 3441–3455; b) S. S. Bradrick, E. Y. Dobrikova, C. Kaiser, M. Shveygert, and M. Gromeier, *RNA*, 2007, **13**, 1582–1593; c) F. Besse and A. Ephrussi, *Nat. Rev. Mol. Cell Biol.*, 2008, **9**, 971–980.
20. S. K. Kim, P. E. Nielsen, M. Egholm, O. Buchardt, R. H. Berg and B. Norden, *J. Am. Chem. Soc.*, 1993, **115**, 6477–6481
21. D. Lavabre and S. J. Fery-Forgues, *Chem. Educ.*, 1999, **76**, 1260–1264.
22. G. Jones II, W. R. Jackson and C-Y. Choi, *J. Phys. Chem.*, 1985, **89**, 294–300.
23. P. E. Nielsen and M. Egholm, *Peptide nucleic acids-protocols and applications.* Horizon Scientific Press, Wymondham, 1999.

4.6 Appendix-II: Characterization data of synthesized compounds

^{1}H-NMR of compound **3** in $CDCl_3$

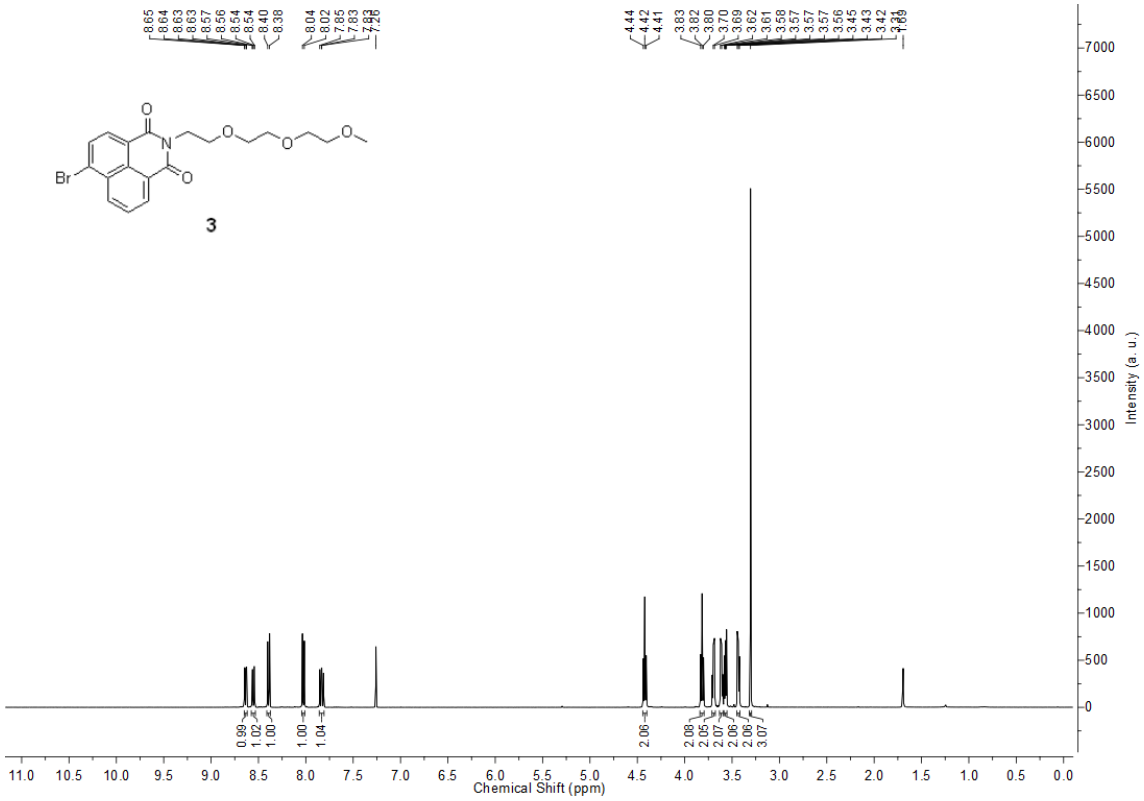

^{13}C-NMR of compound **3** in $CDCl_3$

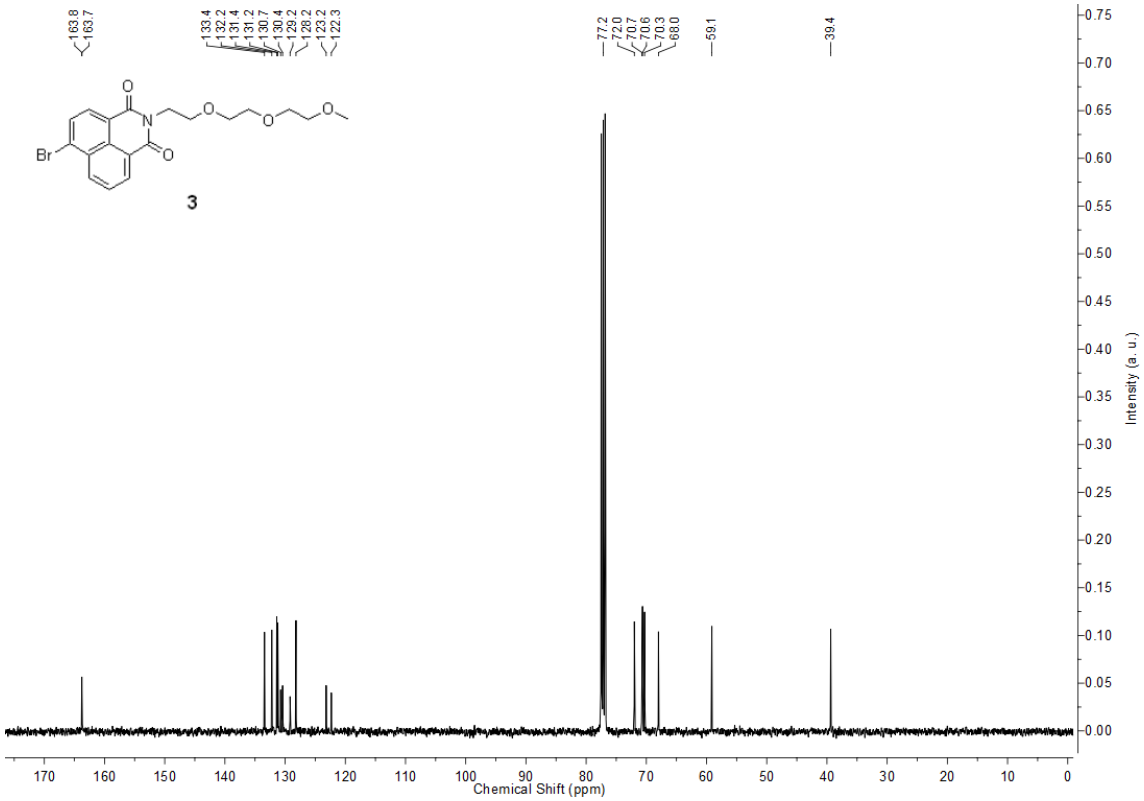

^{1}H-NMR of compound **4a** in $CDCl_3$

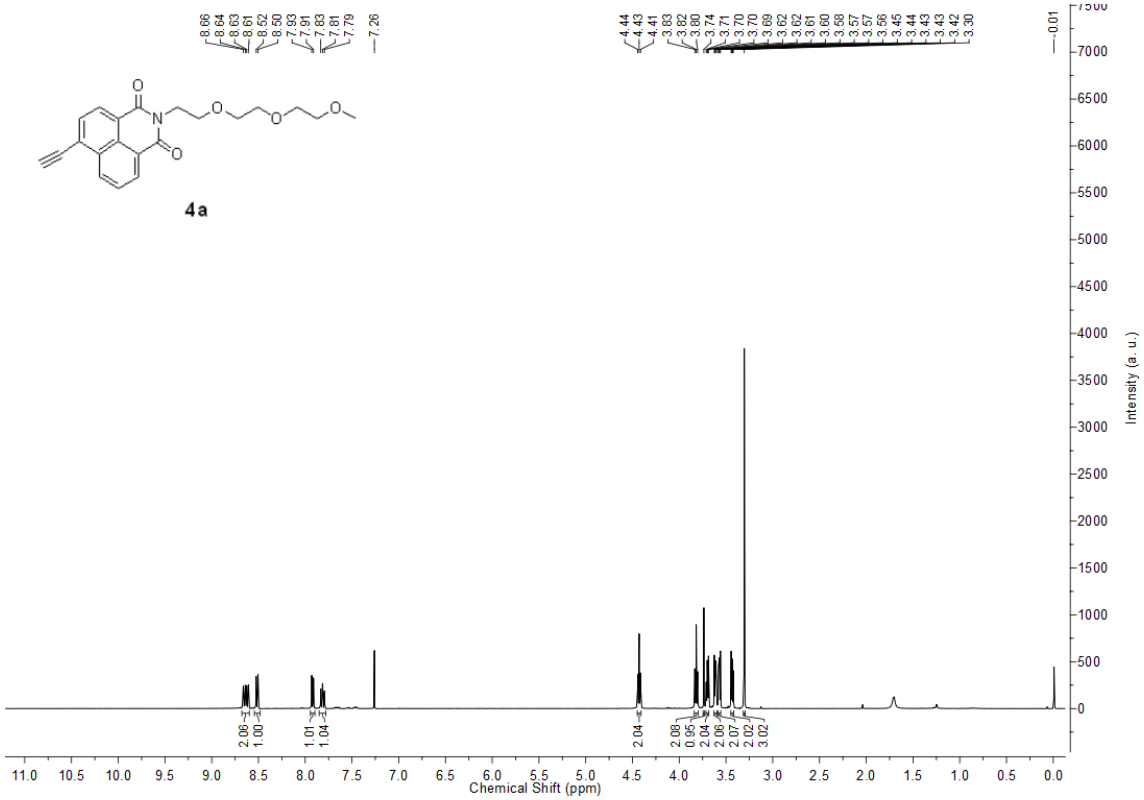

^{13}C-NMR of compound **4a** in $CDCl_3$

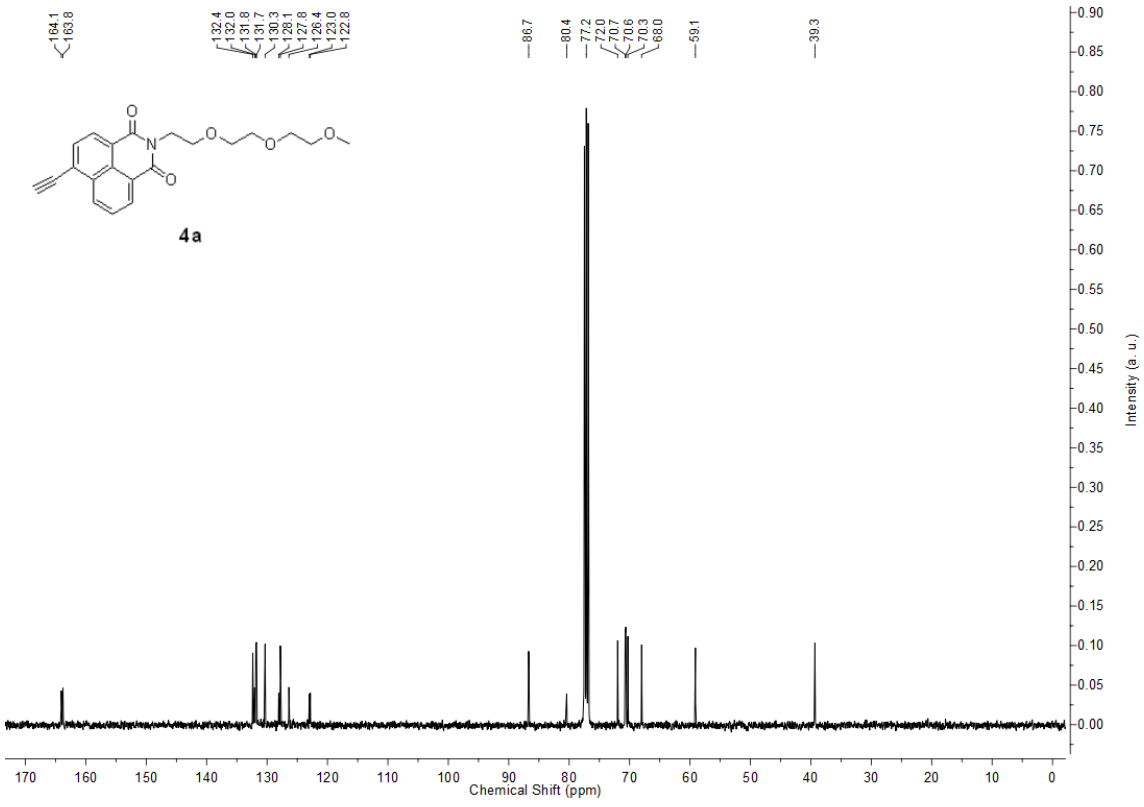

^{1}H-NMR of compound **5** in $CDCl_3$

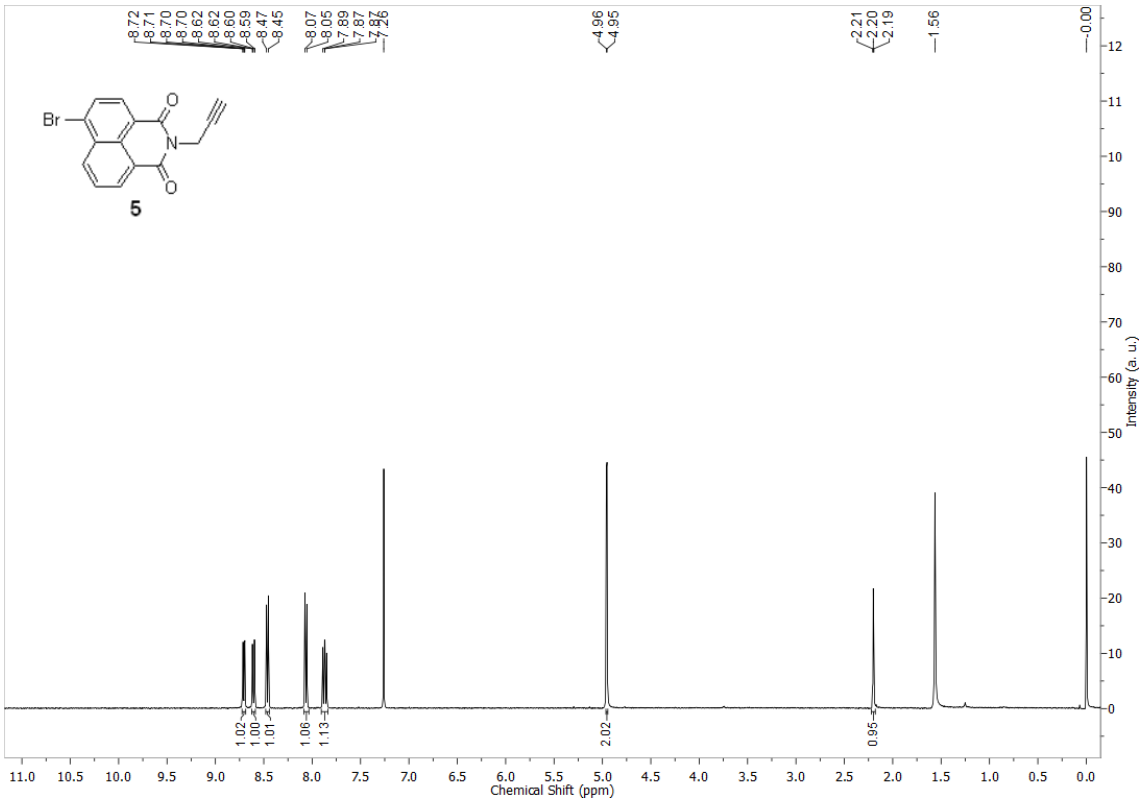

^{13}C-NMR of compound **5** in $CDCl_3$

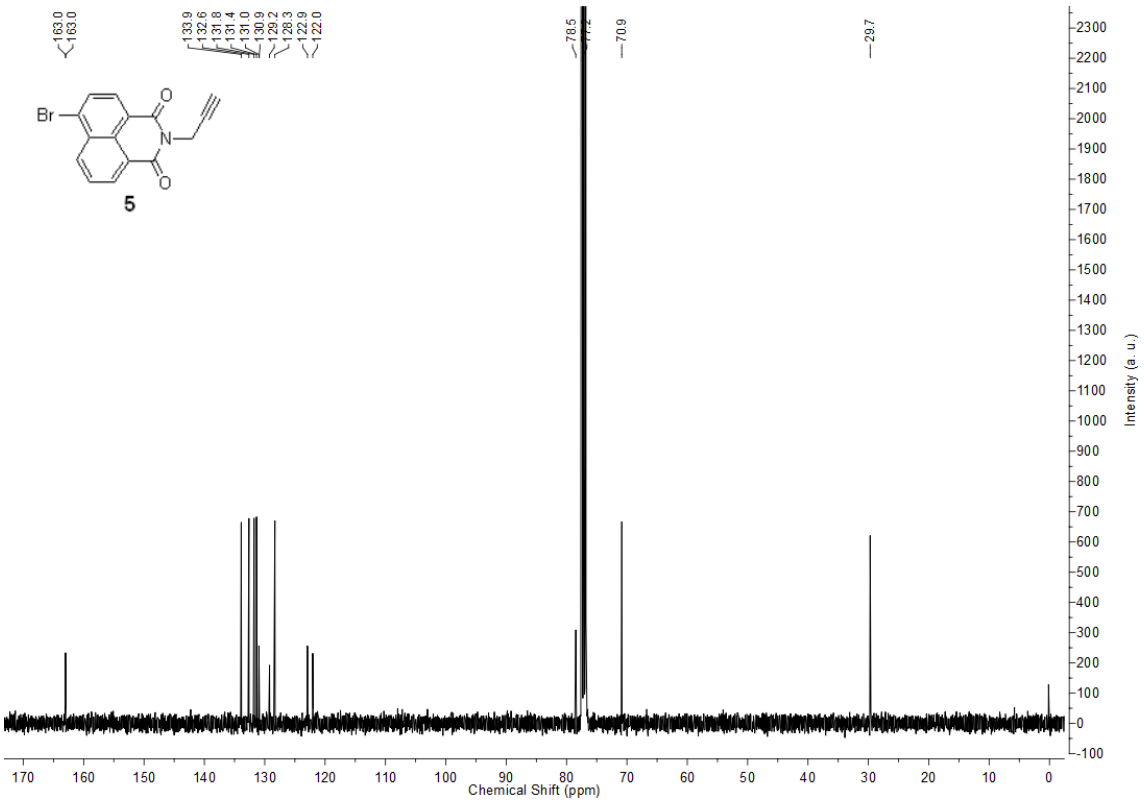

[1]H-NMR of compound **4b** in d_6-DMSO

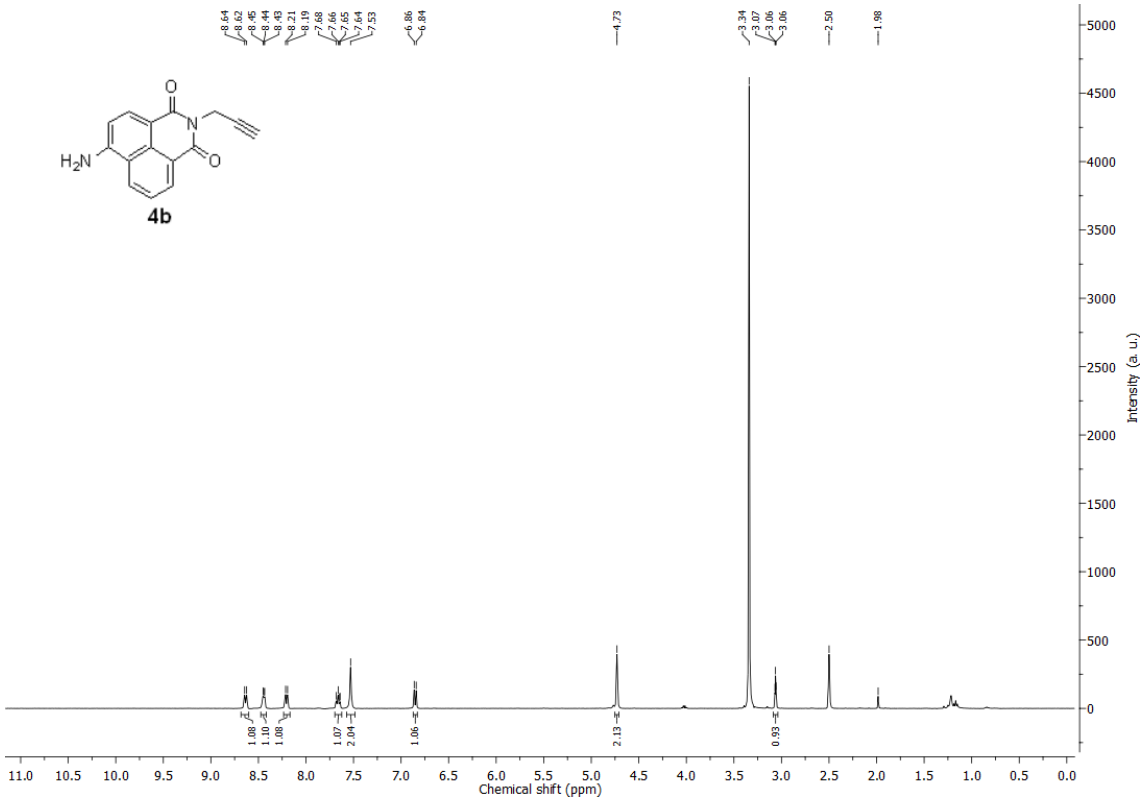

[13]C-NMR of compound **4b** in d_6-DMSO

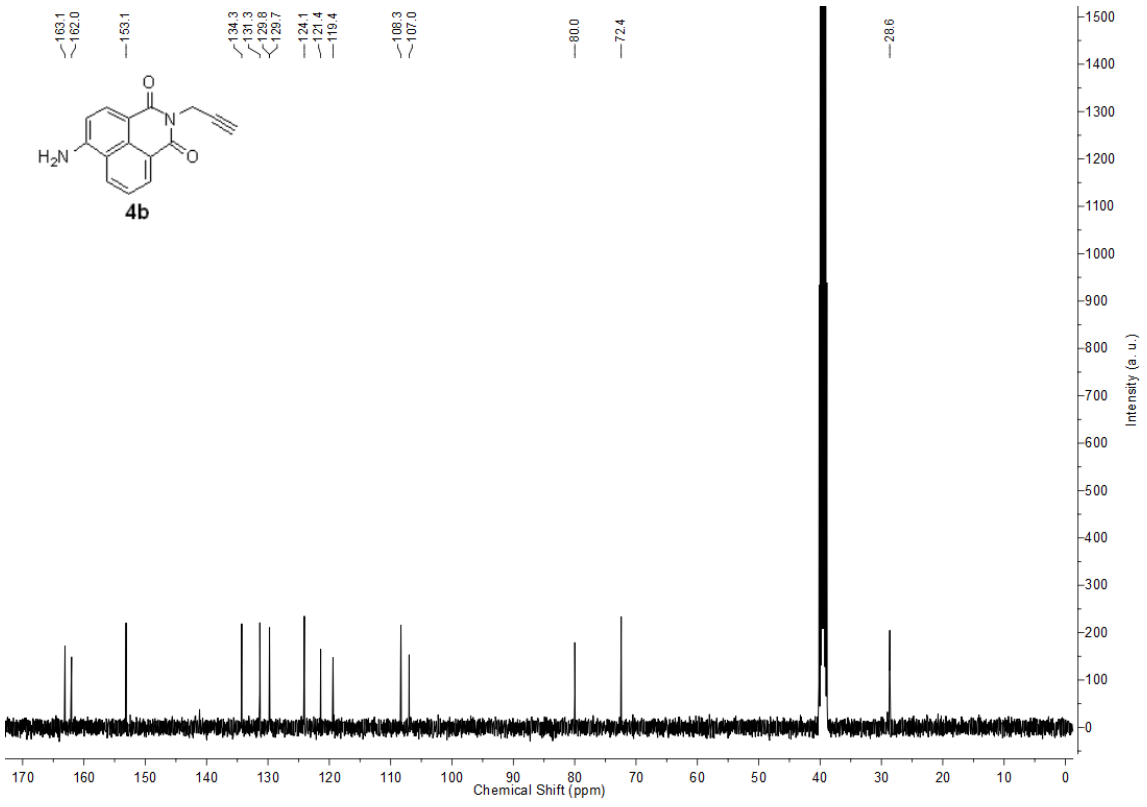

^{1}H-NMR of compound **7a** in $CDCl_3$

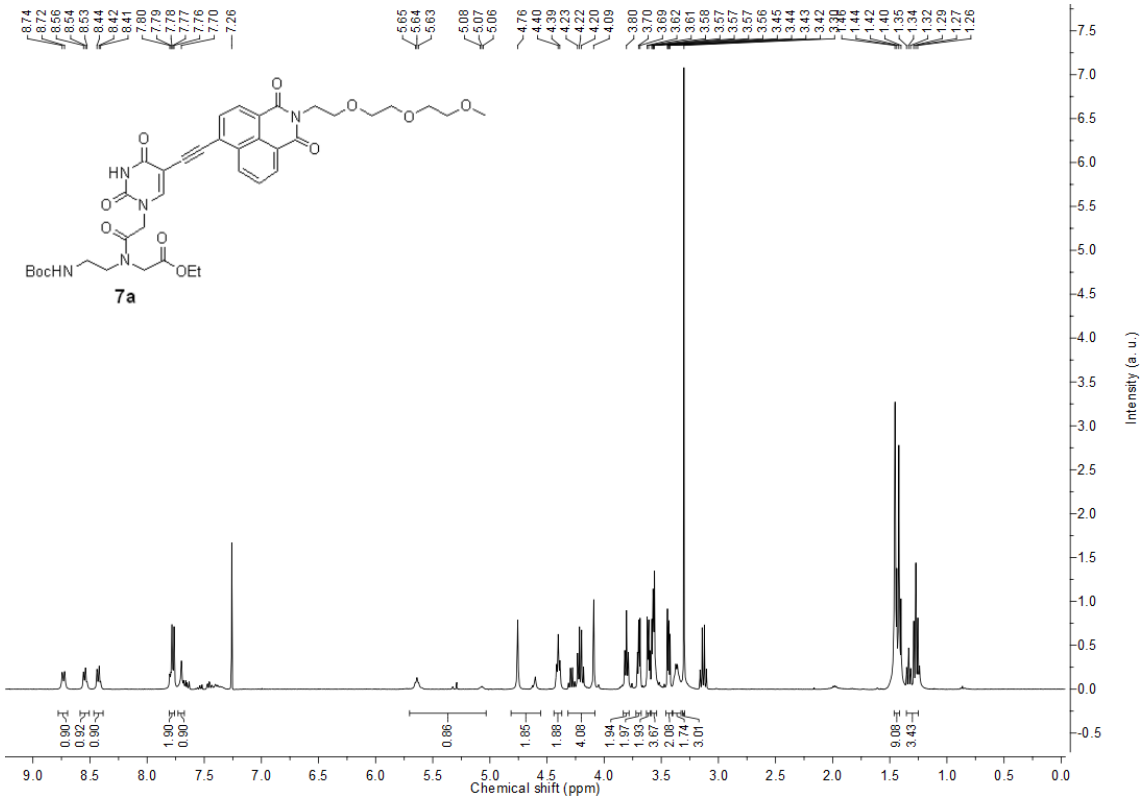

^{13}C-NMR of compound **7a** in $CDCl_3$

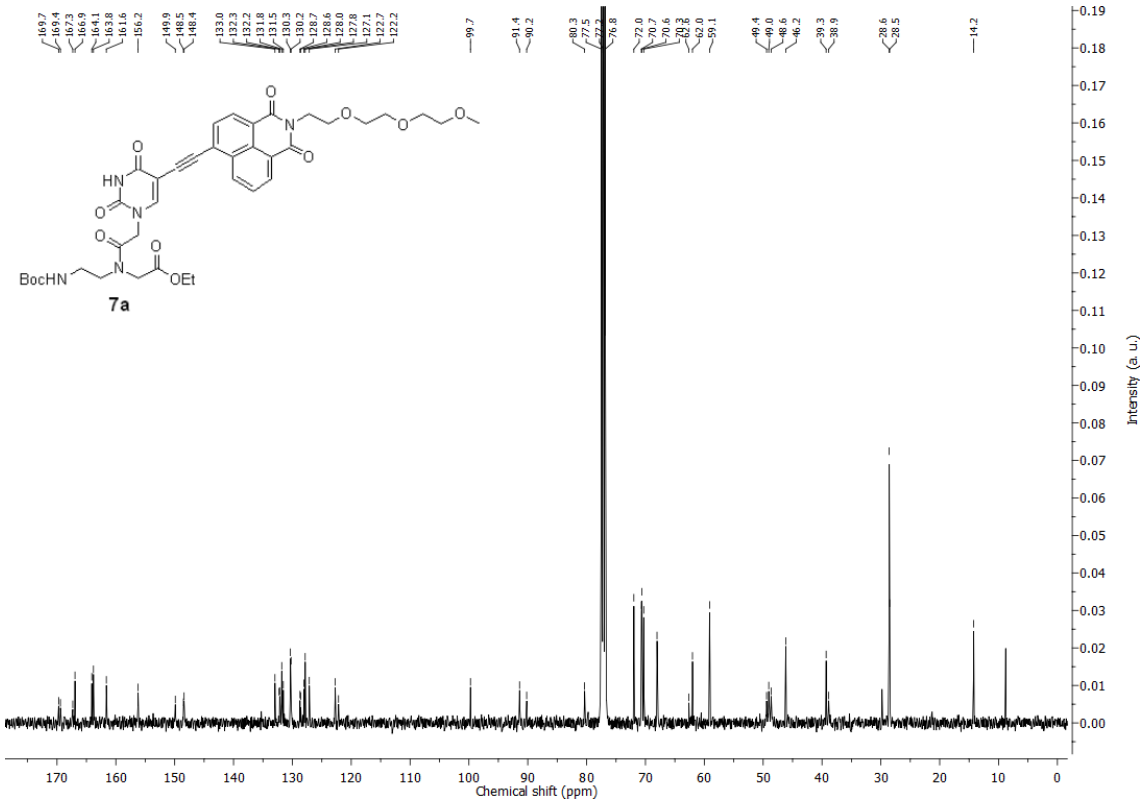

^{1}H-NMR of compound **7b** in d_6-DMSO

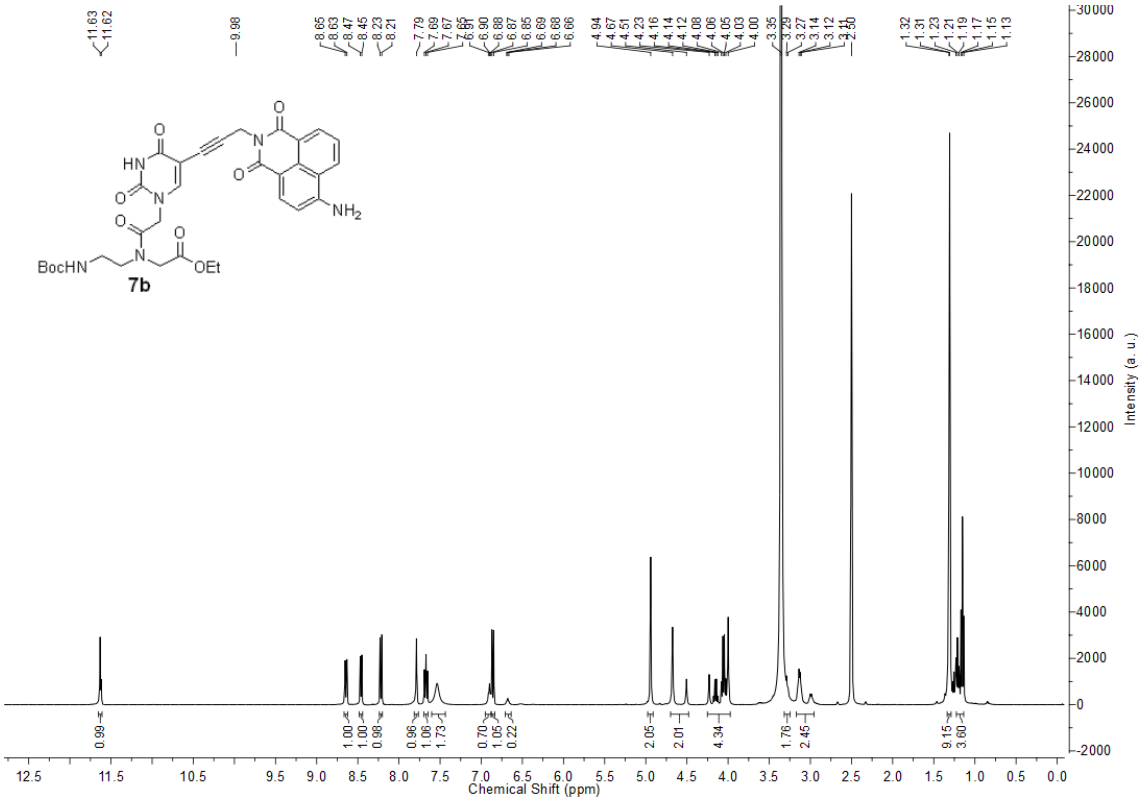

^{13}C-NMR of compound **7b** in d_6-DMSO

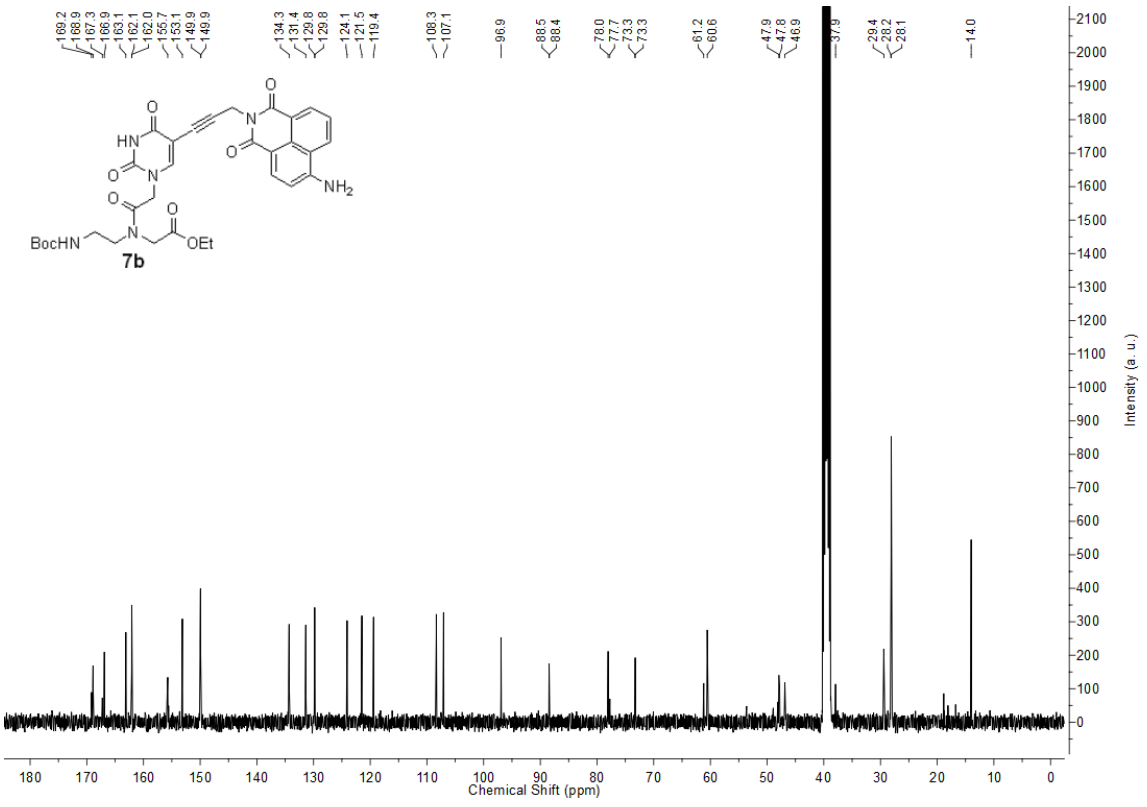

^{1}H-NMR of compound **7c** in d_6-DMSO

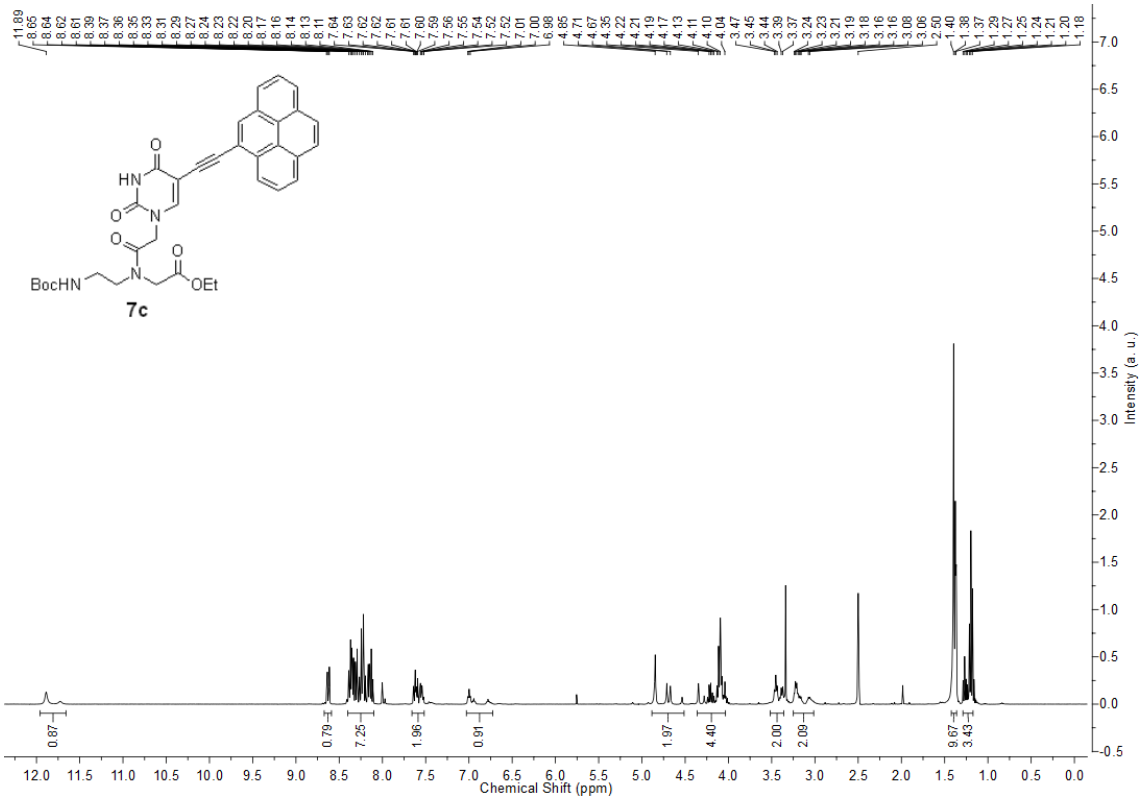

^{13}C-NMR of compound **7c** in d_6-DMSO

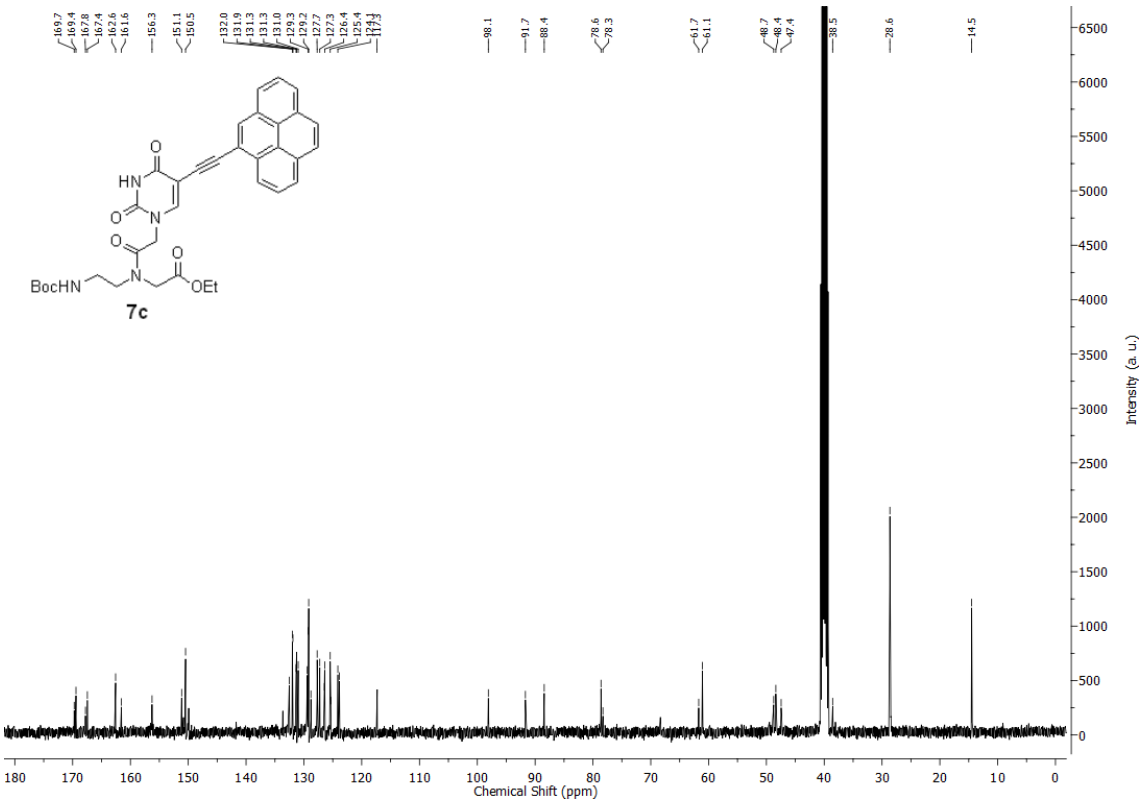

^{1}H-NMR of compound **8a** in d_6-DMSO

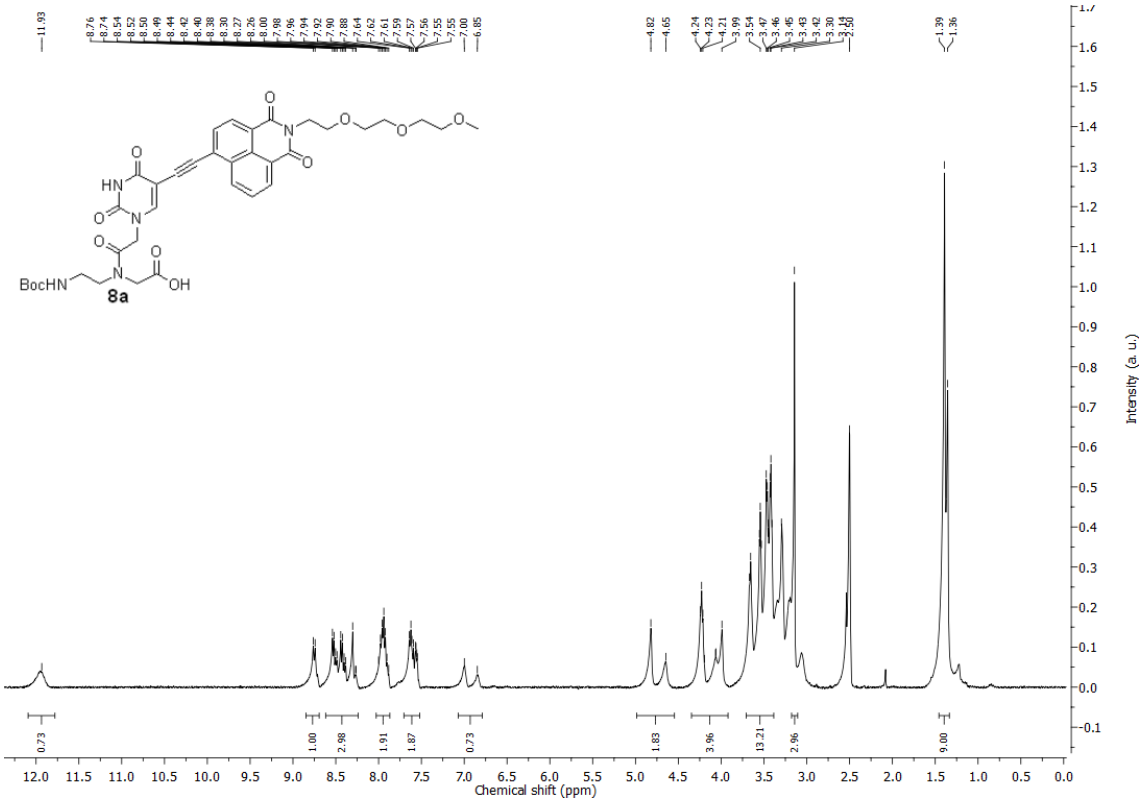

^{13}C-NMR of compound **8a** in d_6-DMSO

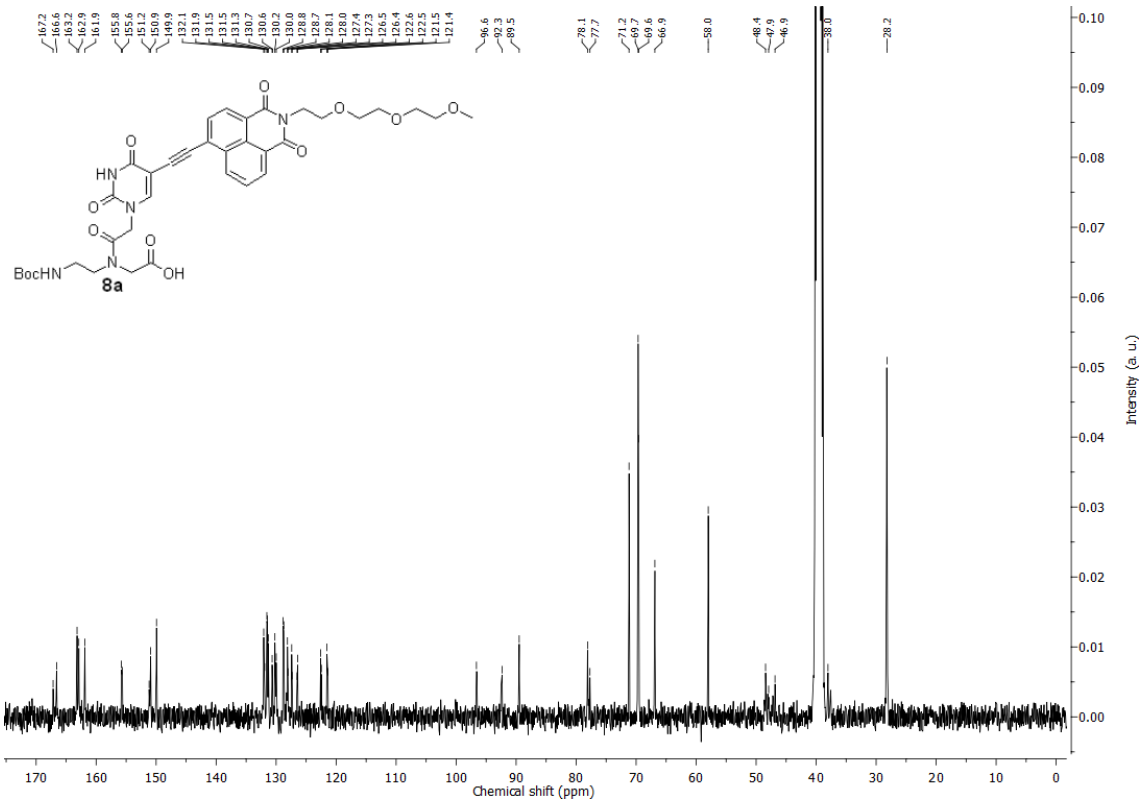

^{1}H-NMR of compound **8b** in d_6-DMSO

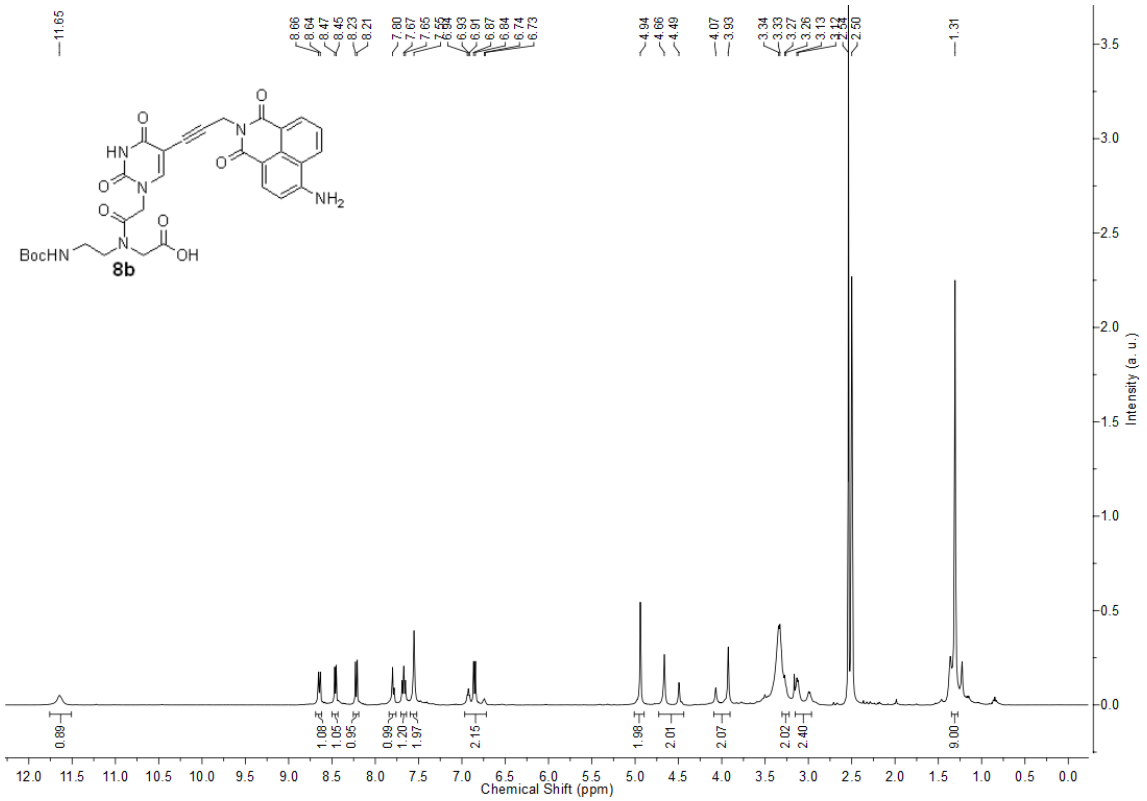

^{13}C-NMR of compound **8b** in d_6-DMSO

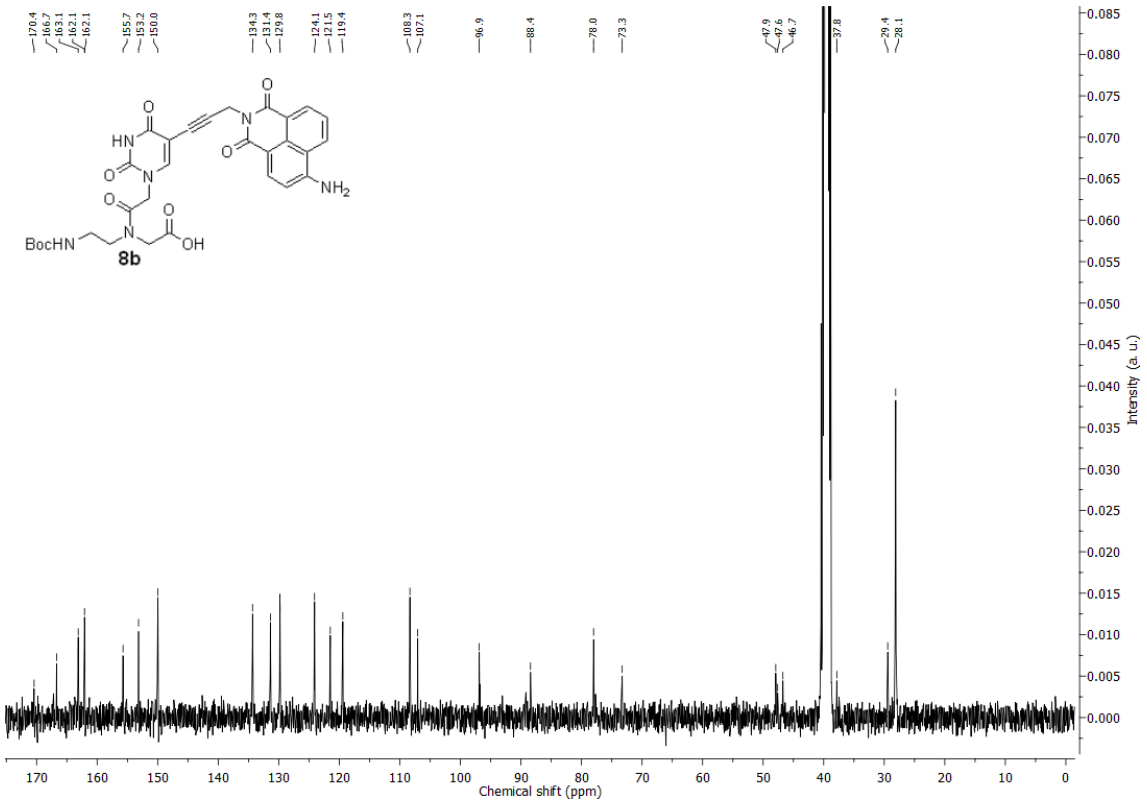

^{1}H-NMR of compound **8c** in d_6-DMSO

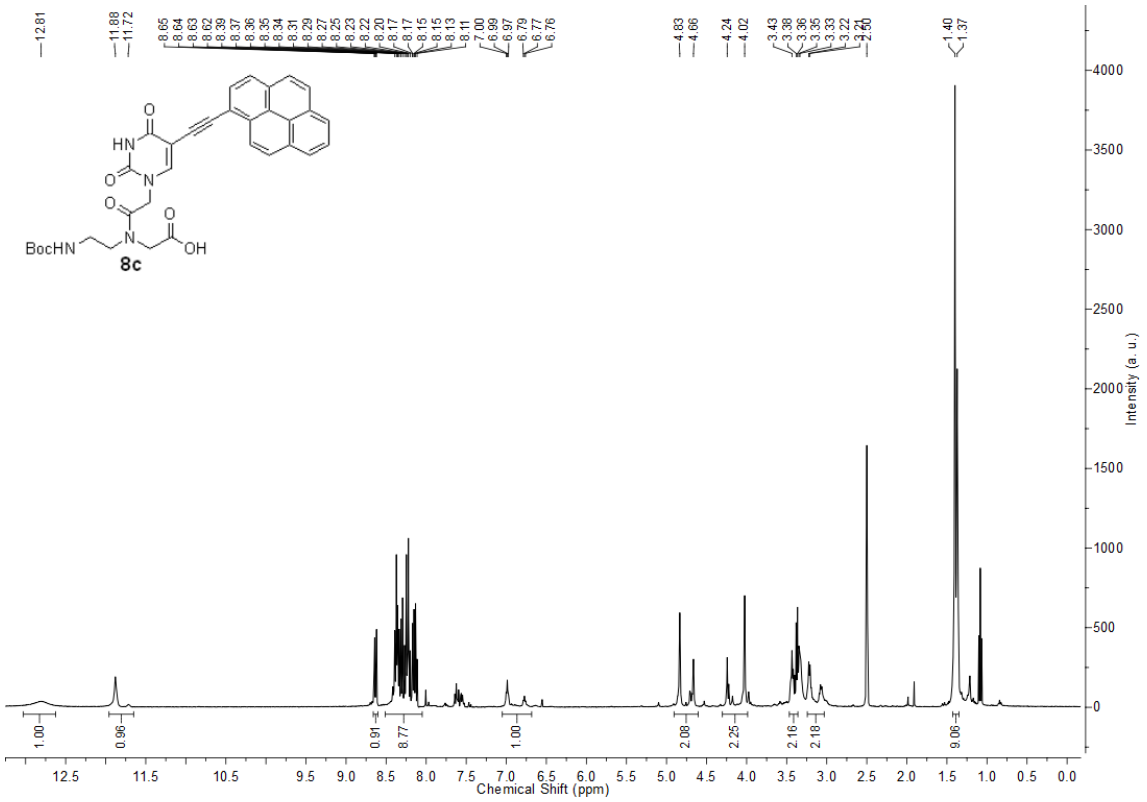

^{13}C-NMR of compound **8c** in d_6-DMSO

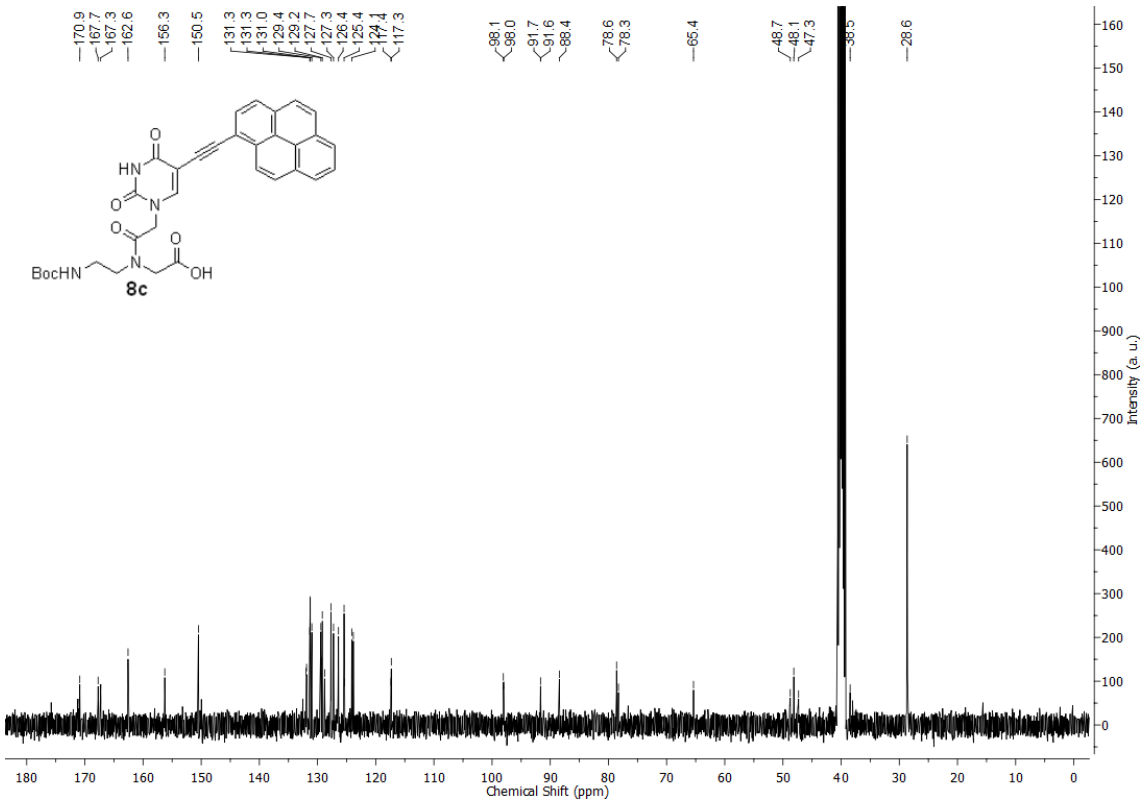

^{1}H-NMR of compound **9** in d_6-DMSO

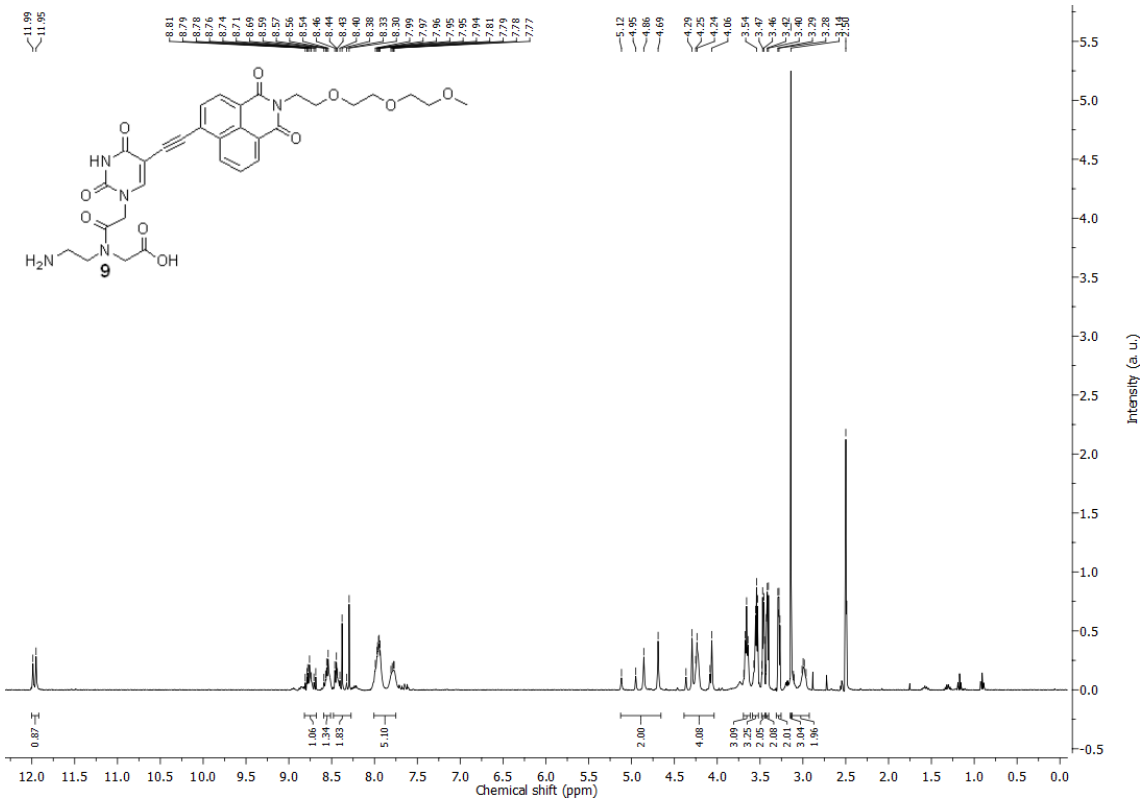

^{13}C-NMR of compound **9** in d_6-DMSO

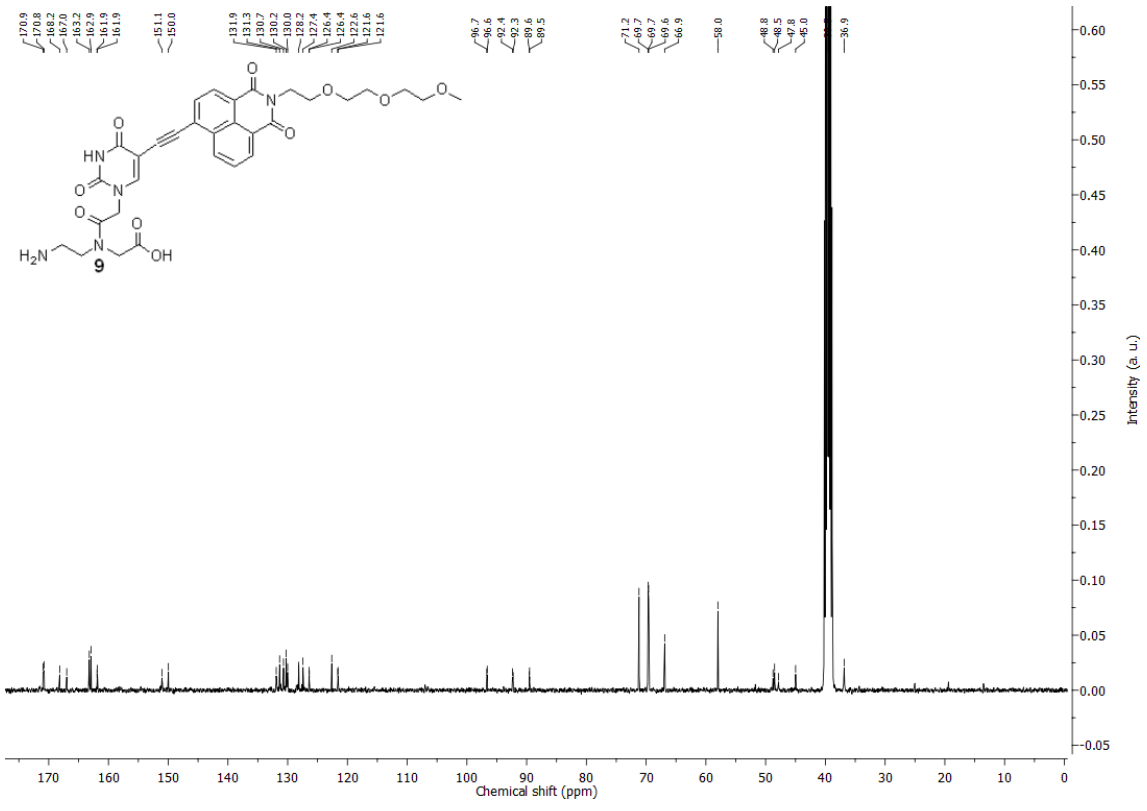

[1]H-NMR of compound **17** in d_6-DMSO

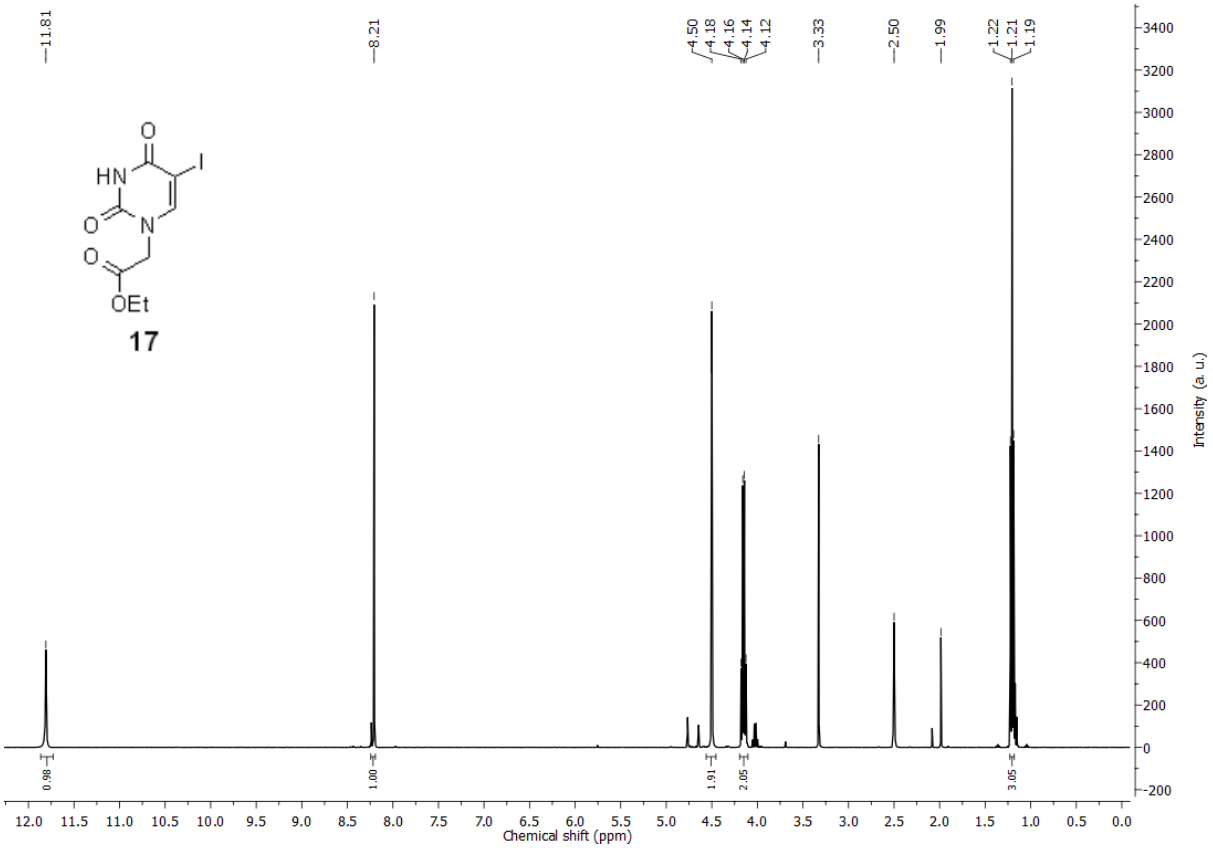

[13]C-NMR of compound **17** in d_6-DMSO

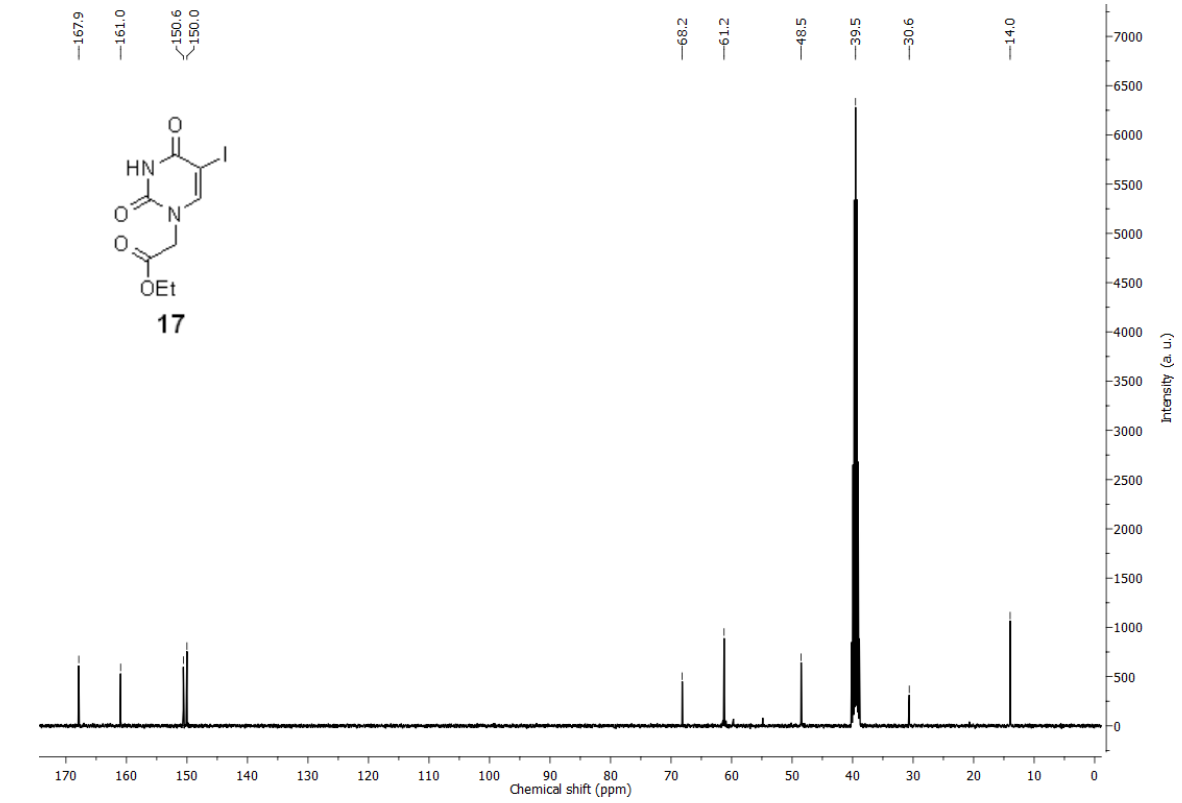

^{1}H-NMR of compound **18** in d_6-DMSO

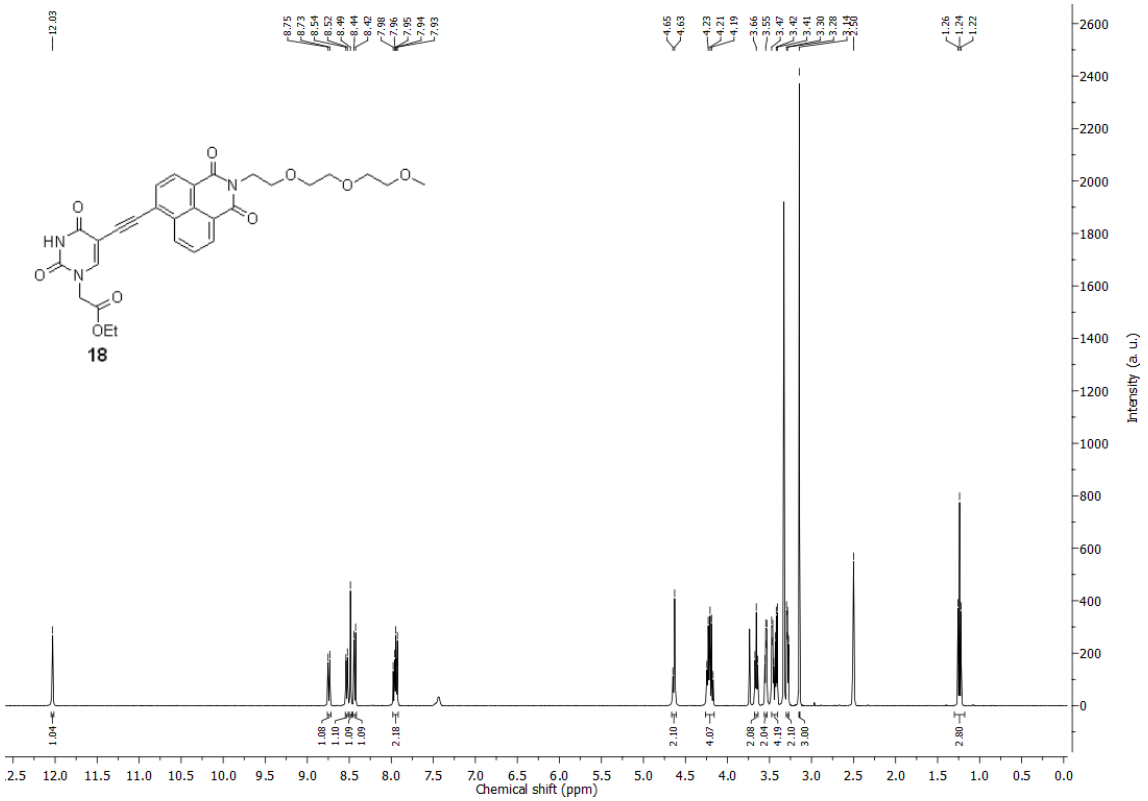

^{13}C-NMR of compound **18** in d_6-DMSO

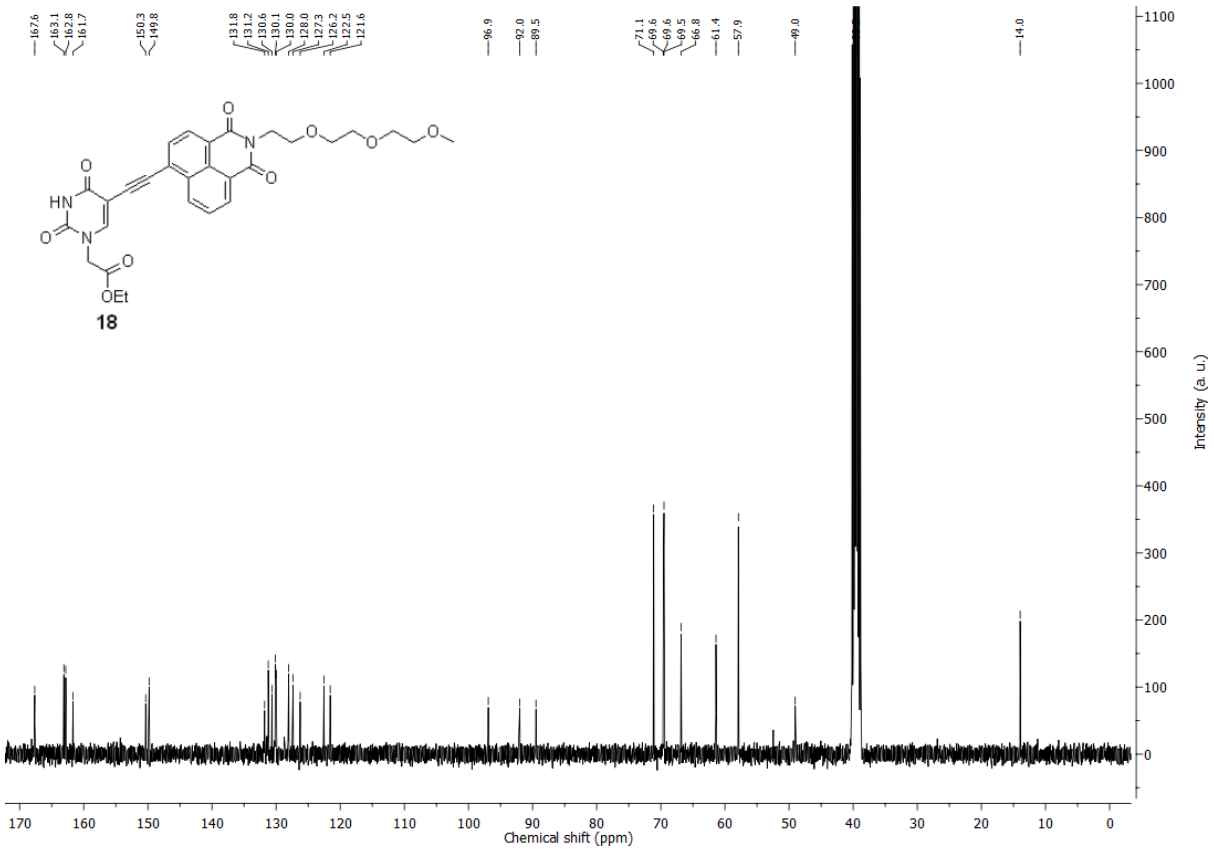

^{1}H-NMR of compound **19** in d_6-DMSO

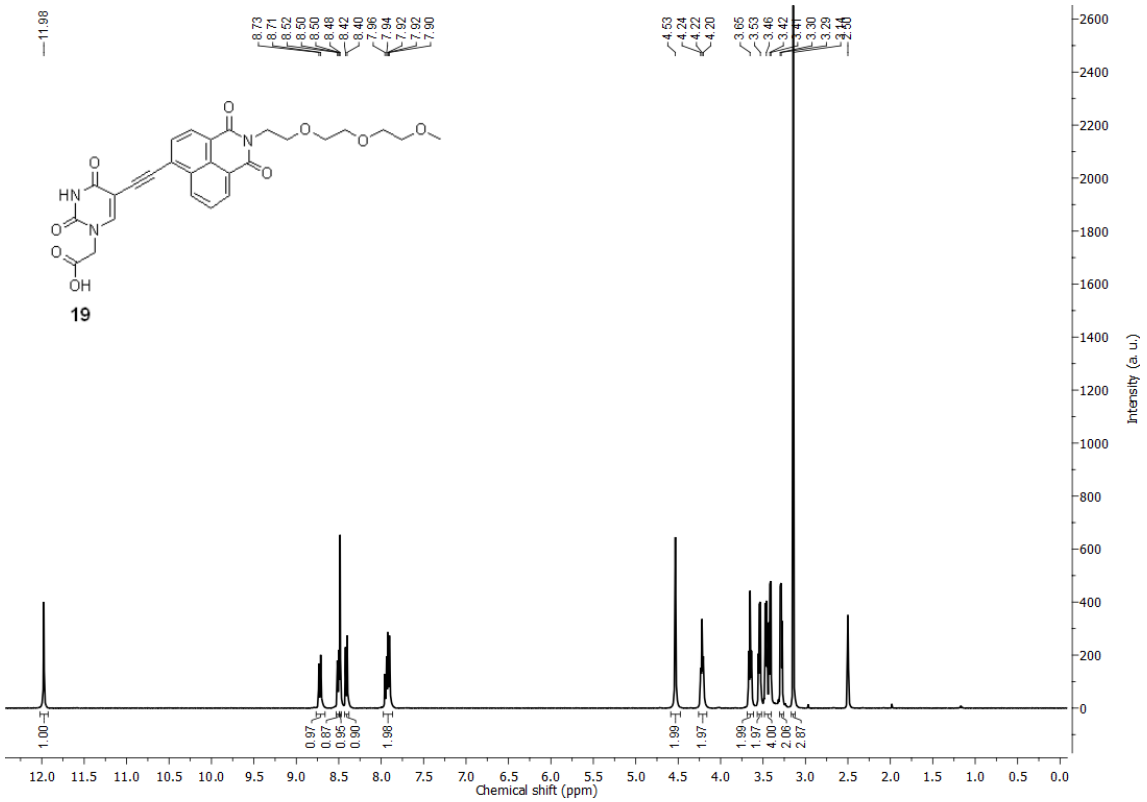

^{13}C-NMR of compound **19** in d_6-DMSO

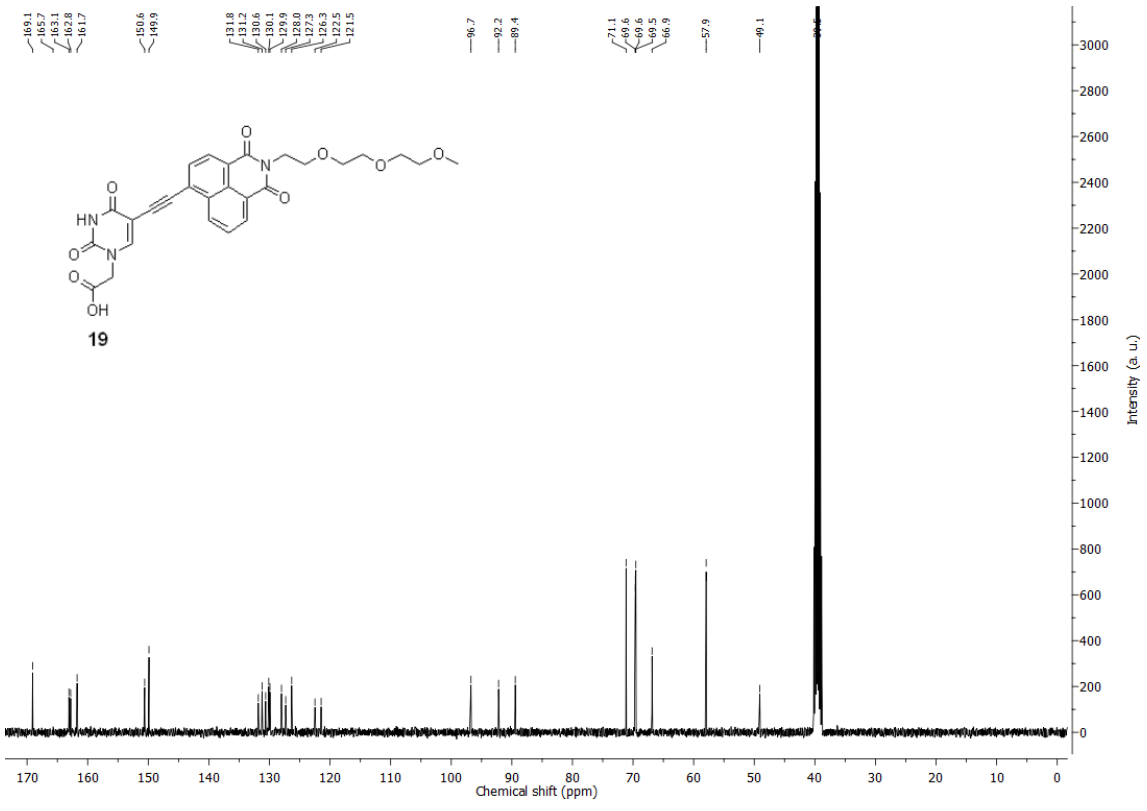

^{1}H-NMR of compound **21** in d_6-DMSO

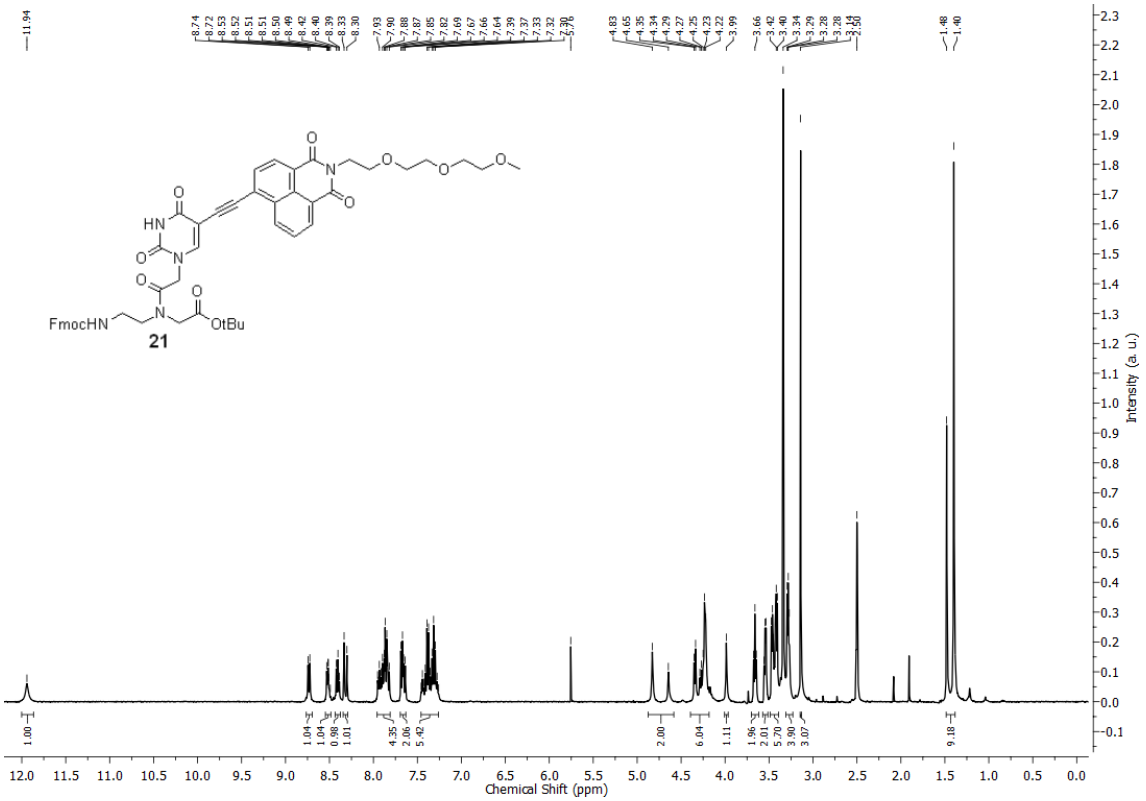

^{13}C-NMR of compound **21** in d_6-DMSO

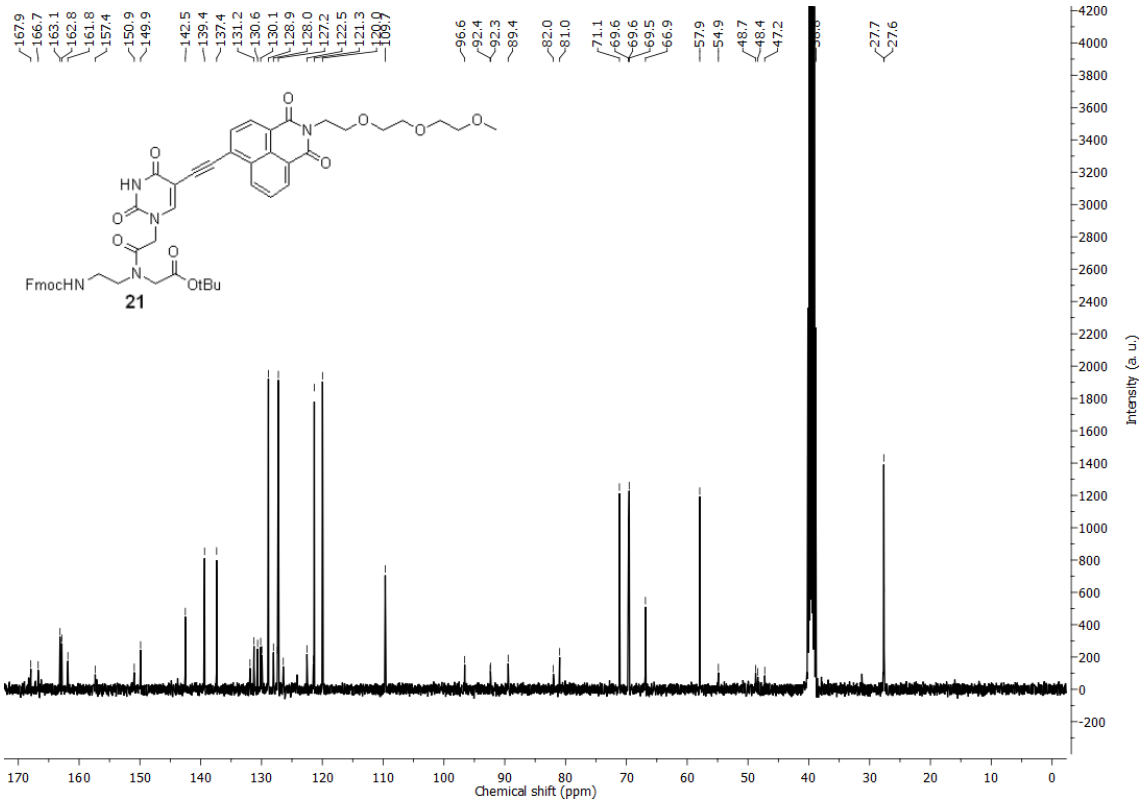

^{1}H-NMR of compound **22** in d_6-DMSO

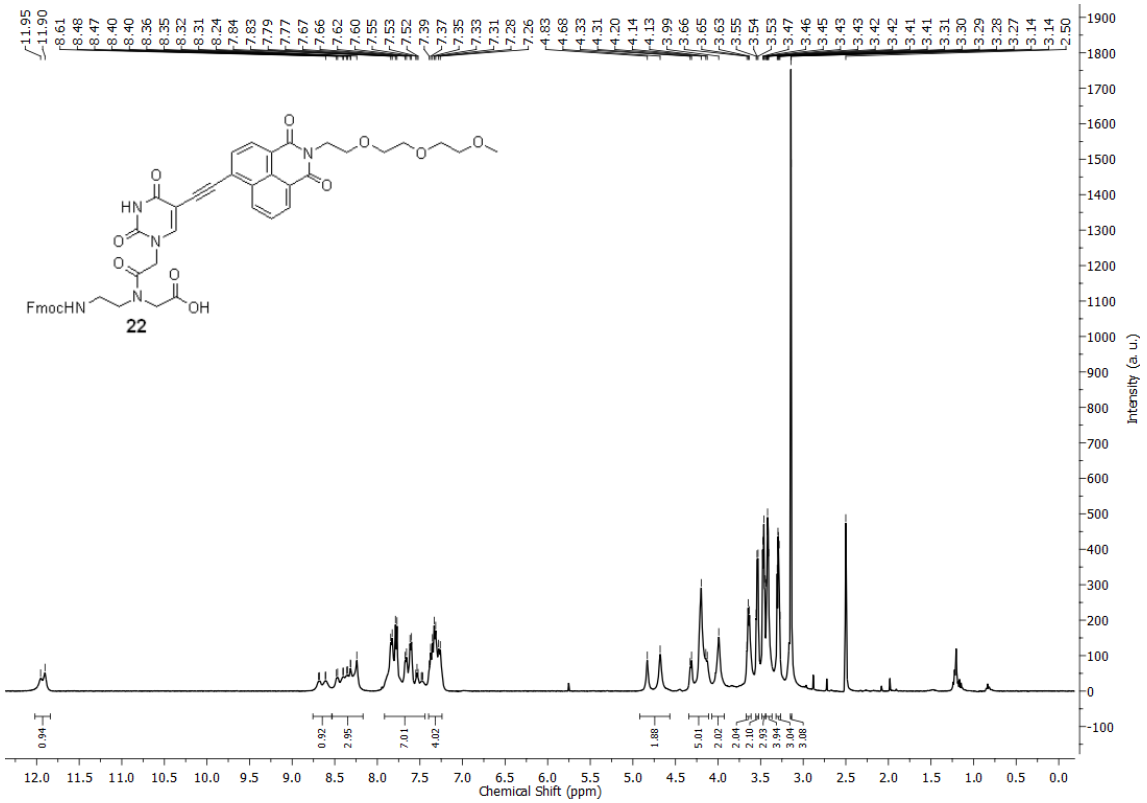

^{13}C-NMR of compound **22** in d_6-DMSO

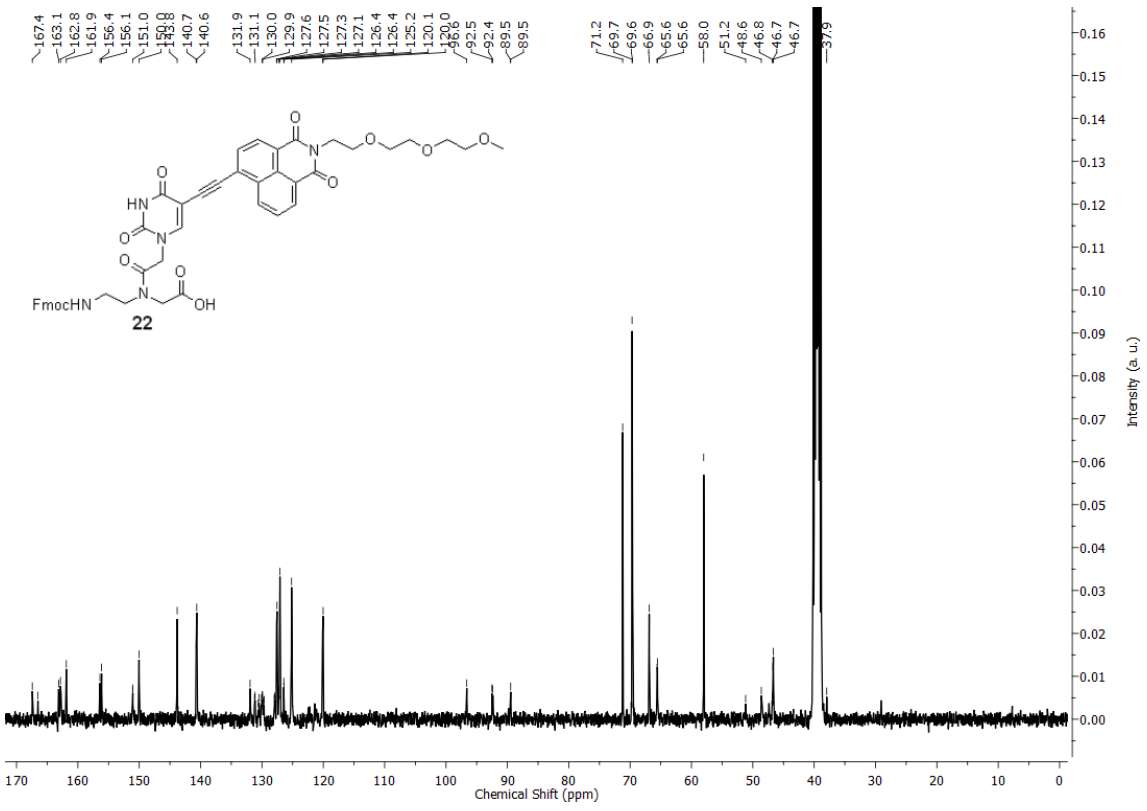

RP-HPLC chromatogram of fluorescent PNA oligomers **10**–**13** (contained **9**) and **10X** (contained **8b**) at 260 nm. Conditions: 0–50% B in 25 min and 50–100% B in 15 min (Mobile phase A: 5% acetonitrile in H_2O containing 0.1% TFA. Mobile phase B: 50% acetonitrile in H_2O containing 0.1% TFA). Flow rate was 2 mL/min.

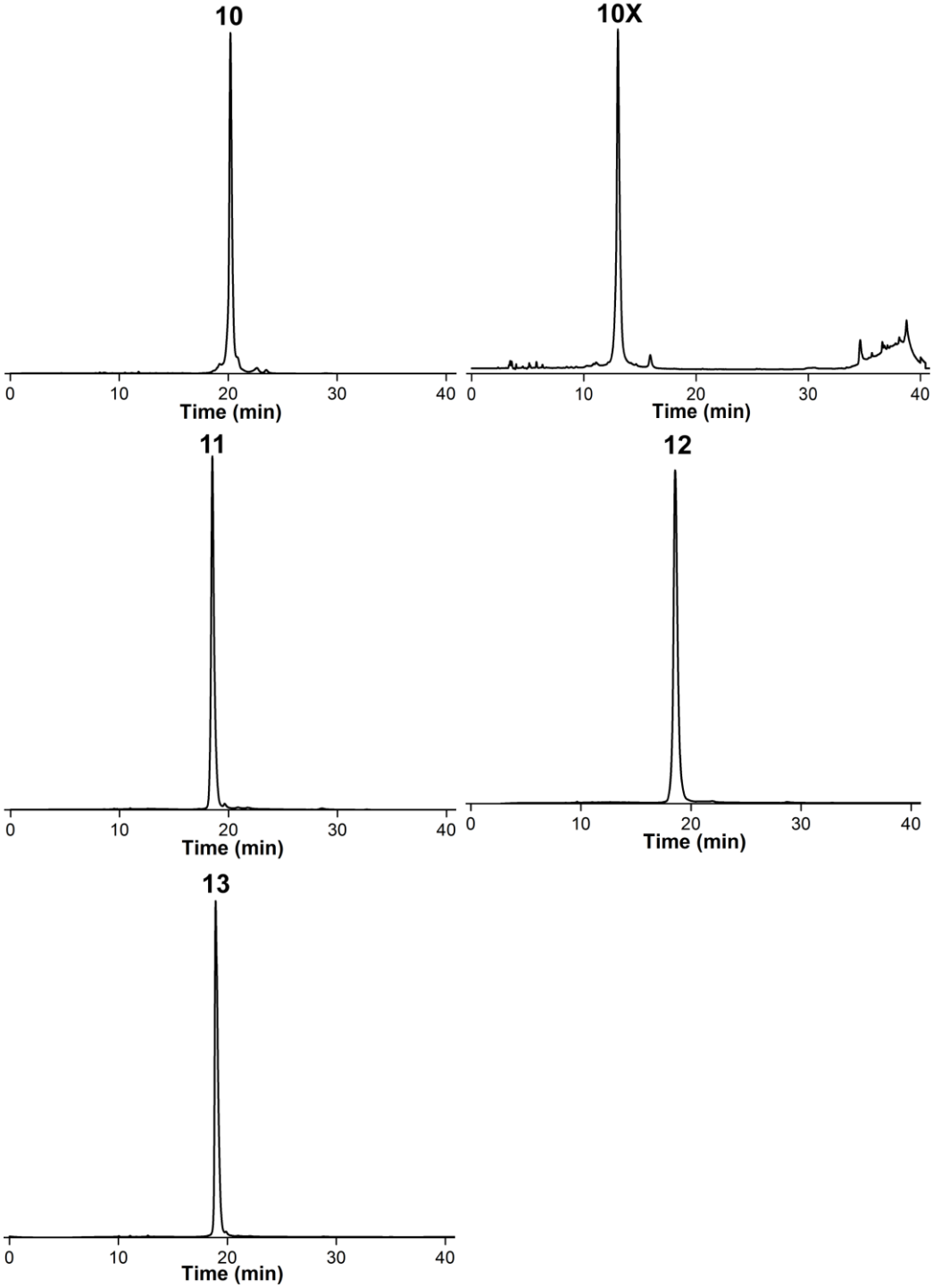

MALDI-TOF mass spectra of fluorescently modified PNA oligomers **10**–**13** and **10X**. See Table 3 for mass data of all PNA oligomers.

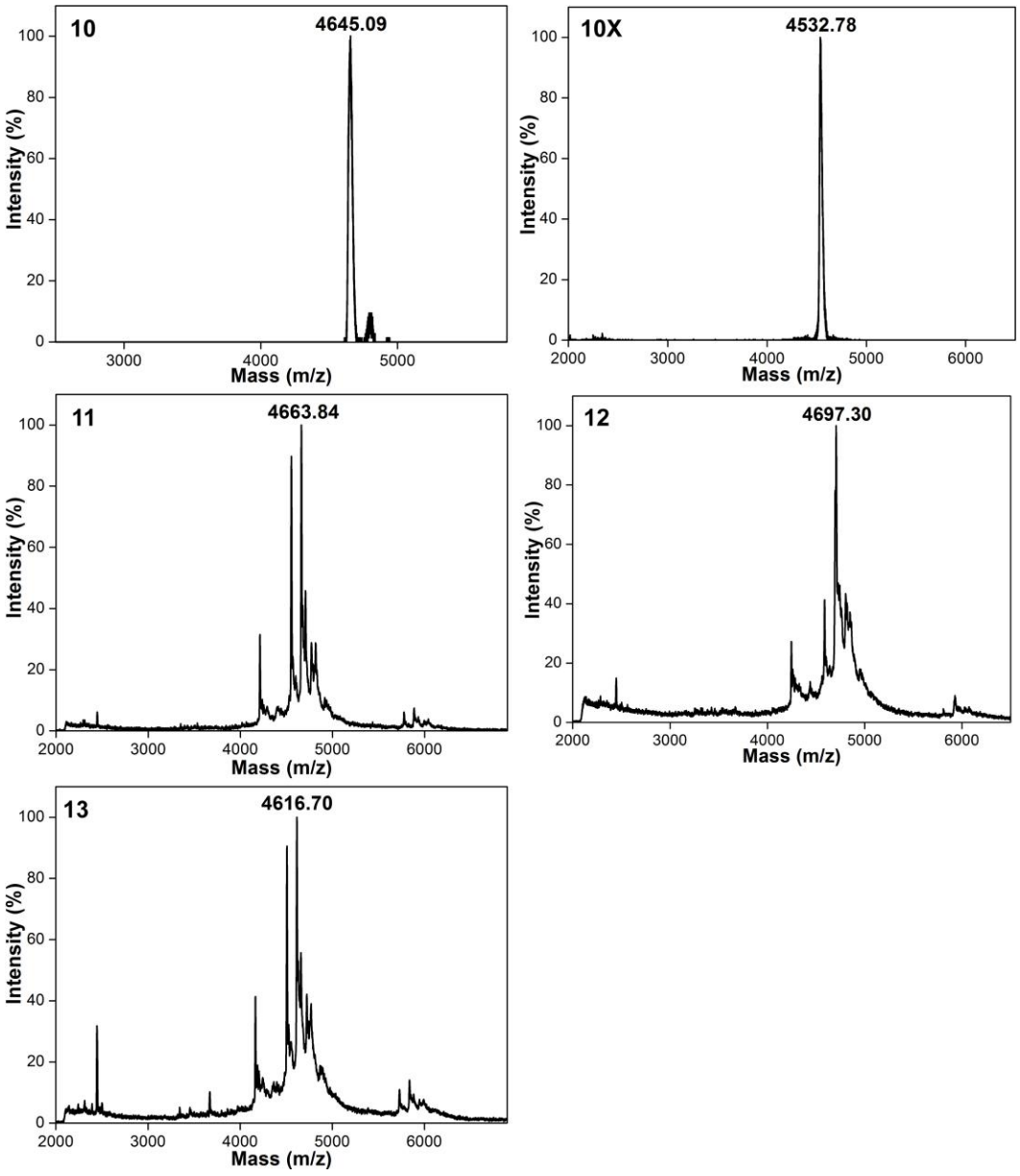

Chapter 5

Postsynthetic chemical labeling of PNA oligomers by using bioorthogonal chemical reactions

5.1 Introduction

Peptide nucleic acids (PNAs) have frequently been utilized in various applications including detection, quantification, and visualization of biologically important nucleic acid targets *in vitro* as well as *in vivo*.[1] Recently, various biophysical techniques have been developed to study the application of PNA oligomers in cell-free and cellular conditions. Therefore, there is a continuous demand to develop chemical functionalization methods for the labeling of PNA oligomers with a variety of biophysical reporters. Postsynthetic chemical functionalization has been widely explored as a valuable tool for the labeling of biomolecules such as proteins, lipids, glycans and nucleic acids to elucidate their structure and functions.[2] Typically, postsynthetic labeling is achieved in two sequential step wherein, a small reactive functional group is incorporated into an oligomer by using solid-phase synthesis or enzymatic method and in the subsequent step chemoselective reaction is carried out with an appropriate reactive counterpart containing a variety of biophysical reporters to afford the desired labeled oligomer (Figure 1A). Traditionally, chemoselective reactions such as acid-amine coupling and thiol-maleimide reaction have been developed for the labeling of biomolecules.[3] Unfortunately, these chemoselective reactions exhibit certain shortcomings such as acid-amine coupling are pH sensitive, and thiols tend to undergo oxidation.[4] Moreover, poor stability of the activated esters and less chemoselectivity due to intrinsic amine and alcohol groups in biomolecules have restricted their utility. To use postsynthetic strategy for labeling biomolecules, the following criteria have to be considered a) reaction should be highly chemoselective and b) reaction should proceed significantly faster at physiological conditions. Recently, several bioorthogonal chemical reactions including copper(I)-catalyzed azide-alkyne cycloaddition (CuAAC), strain-promoted azide-alkyne cycloaddition (SPAAC), azide-phosphine Staudinger ligation and, inverse electron demand Diels-Alder reactions (IEDDA), and palladium-catalyzed reactions have been described for labeling proteins, glycans and nucleic acids in cell-free as well as in cellular conditions (Figure 1B).[5] Among these reactions, azide-alkyne cycloaddition reaction has been extensively performed for bioorthogonal labeling, because of its fast reaction kinetics.[6]

Azide-alkyne cycloaddition reactions have been utilized for the synthesis of labeled PNA oligomers with different cargo molecules (fluorophores, peptide) on a solid support and in solution.[7] Bulky reporters such as fluorophore and affinity tags attached to PNAs are majorly used for cellular applications.[8] Due to these bulky groups, PNA oligomer could exhibit poor hybridization efficiency for complementary nucleic acids in cellular conditions.

The labeling of single-stranded PNA oligomers has been performed in solution,[6] however labeling of PNA-ON duplex (post-hybridization) using CuAAC and SPAAC reactions is less explored. Therefore, we envisioned to develop a postsynthetic chemical strategy for labeling of PNA-DNA duplex using CuAAC or SPAAC reactions in cell-free as well as in cellular conditions. Among azide and alkyne modification in PNA oligomer, azide is the most versatile modification because it can be further functionalized using CuAAC, SPAAC and Staudinger ligation reactions. Moreover, to avoid the toxicity of copper in the cell, SPAAC reaction could be highly useful for labeling and imaging of hybridized PNA oligomers in a live cell.

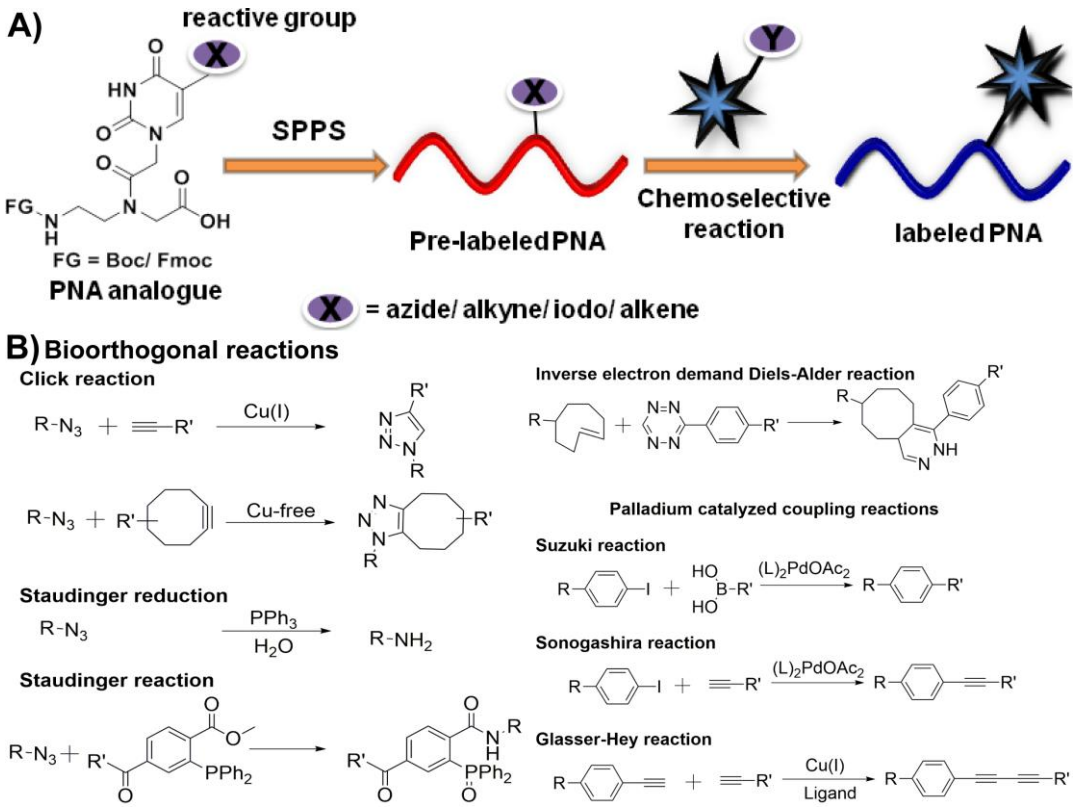

Figure 1. (**A**) Design for postsynthetic chemical functionalization of PNA oligomers with different biophysical probes. (**B**) Various bioorthogonal chemical reactions explored for labeling of biomolecules in cell-free as well as cellular conditions.[2,5]

In this chapter, we report synthesis, incorporation and postsynthetic chemical functionalization of alkyne- and azide-modified PNA analogues (**7** and **16**). In addition, we have also demonstrated the end labeling of PNA oligomer using azido acetic acid as azide surrogate at the *N*-terminus. Subsequently, azide and alkyne PNA oligomers were functionalized with different reporters by CuAAC reaction. Further, azide PNA oligomers were functionalized by SPAAC and Staudinger ligation reactions with different biophysical probes.

In parallel, we have also worked on developing palladium-catalyzed bioorthogonal chemical reactions to synthesize labeled PNA oligomers. Palladium-catalyzed bioorthogonal reactions have been employed for labeling of proteins and to a certain extent nucleic acids.[9] Labeling single-stranded PNA oligomers in cell free-conditions has not been carried out using palladium-catalyzed reactions. However, reactions such as Suzuki-Miyaura, Sonogashira, Heck and Stille couplings have been very well explored for the synthesis of base-modified PNA analogues by various research groups including us (as mentioned in Chapter 2 and Chapter 4). Furthermore, labeling of 7mer-iodo PNA on solid support (on resin) was demonstrated with propargyl alcohol using Sonogashira cross-coupling reactions by Hudson and co-workers.[10] The main advantage of palladium-catalyzed reactions are; i) their cognate reactive partners are either commercially available or easy to synthesize, ii) it is possible to synthesize conformation-sensitive emissive PNA probes (as discussed in Chapter 2 and Chapter 4). To perform palladium catalyzed reactions, we incorporated 5-iodouracil PNA analogue (**22**) into PNA oligomers by SPPS and subsequently functionalized by Suzuki-Miyaura and Cu-free Sonogashira reactions to generate labeled PNA oligomers.

We have also incorporated alkyne-, azide- and iodo-modified PNA analogues into PNA oligomers complementary to telomeric DNA repeats and subjected for post-hybridization labeling of a PNA-telomere DNA duplex with different biophysical probes (e.g. fluorophores and affinity tag). This post-hybridization labeling methodology is being currently evaluated for imaging telomeric DNA repeats in cellular conditions.

5.2 Results and Discussion

5.2.1 Postsynthetic chemical labeling of alkyne and azide-modified PNA oligomers

5.2.1.1 Synthesis of 5-ODU-and 5-tetraethylene glycol azide-conjugated uracil PNA base analogues 7 and 16

Base-modified alkyne- (**7**) and azide- (**16**) PNA monomers were synthesized according to steps illustrated in Scheme 1 and 2. 5-Iodouracil **1** was converted into 5-iodouracil ethyl ester **2** using K_2CO_3 in DMF at RT. Iodo compound **2** was further converted into 5-ODU uracil ethyl ester **3** by palladium catalyzed Sonogashira coupling reaction with octa-1,7-diyne in dry THF at RT. ODU uracil ester **3** was hydrolysed into ODU uracil acid **4** in quantitative yield using an aqueous solution of LiOH. Further, acid **4** was coupled with commercially available Fmoc PNA backbone **5** to afford 5-ODU uracil PNA ester **6** using EDC and DIPEA in dry DMF at RT. Finally, base-modified alkyne PNA acid analogue **7** required for SPPS by

Fmoc-chemistry was obtained by hydrolysis of *t*Bu-ester using TFA in DCM at RT in a quantitative amount.

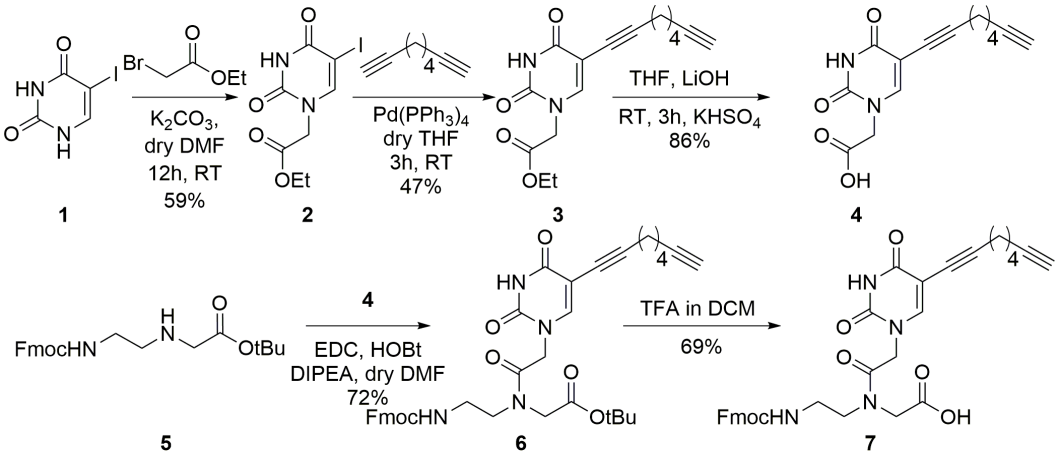

Scheme 1. Synthesis of 5-ODU conjugated uracil PNA monomer **7** for SPPS.[11]

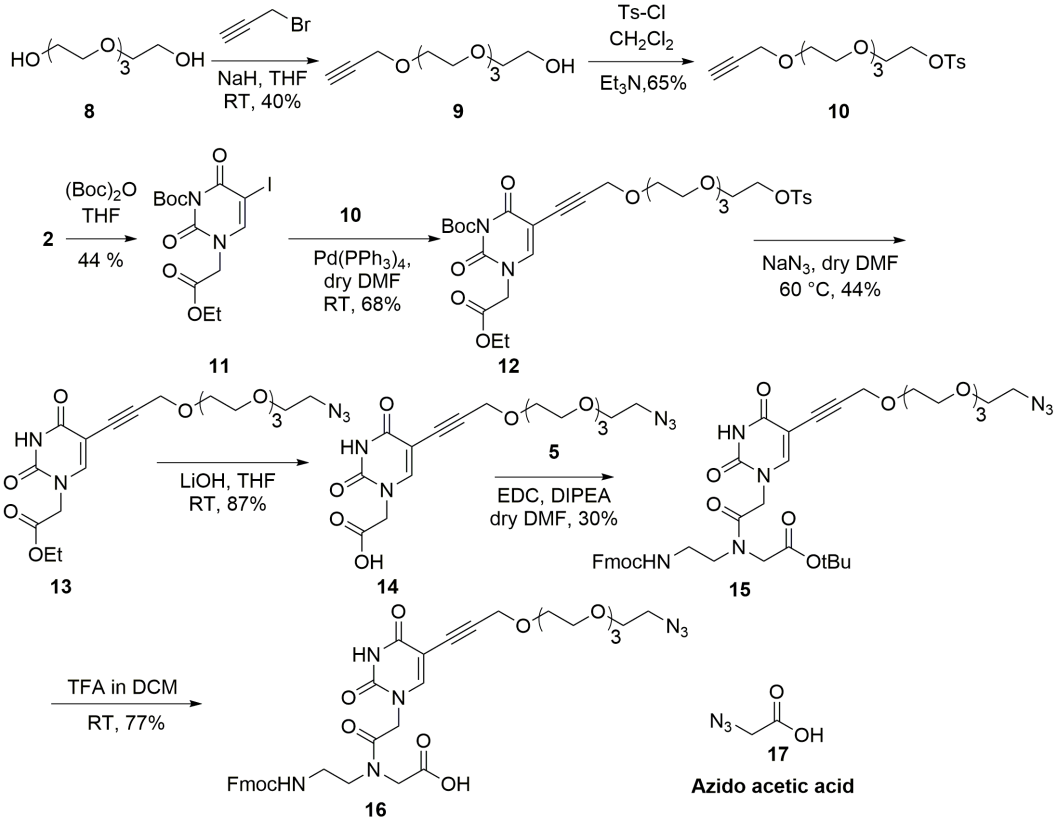

Scheme 2. Synthesis of 5-tetraethylene glycol azide-conjugated uracil PNA monomer **16** for SPPS. The structure of azidoacetic acid **17** is also shown.[11]

Initially, alkyne-tetraethylene glycol-OTs **10** was synthesized in two steps first by reacting triethylene glycol **8** with propargyl bromide in the presence of NaH, followed by tosylation of compound **9** using tosyl chloride in dichloromethane (Scheme 2). Further, synthesis of 5- tetraethylene glycol azide uracil PNA acid **16** was started from compound **2**

with Boc-protection to afford compound **11** (Scheme 2). Palladium-catalyzed Sonogashira reaction was performed between Boc-protected iodo compound **11** and compound **10** in dry THF at RT to afford compound **12**. Tosyl group of **12** was replaced by azide using NaN_3 in dry DMF at 60 °C to get **13**. Next, **13** was hydrolyzed using aqueous LiOH to acid **14** in quantitative yield at RT. Acid **14** was then coupled with Fmoc-PNA backbone **5** in the presence of EDC and DIPEA to obtained ester **15**. Finally, base-modified tetraethylene glycol azide uracil PNA acid **16** was prepared by hydrolysis of ester **15** using TFA in DCM.

In order to establish postsynthetic chemical functionalization of PNA using click reactions, base-modified alkyne- (**18**) and azide-(**19**) PNA oligomers were prepared by using PNA monomers **7** and **16**, respectively. We also used azidoacetic acid **17** to synthesize an end-labeled azide PNA oligomer **20**. All the PNA oligomers were prepared by using an L-lysine preloaded rink amide resin and Fmoc-protected *aeg*-PNA monomers (Table 1). PNA oligomers were synthesized with two C-terminal lysine residues to enhance the aqueous solubility. The PNA oligomers were further purified by RP-HPLC and characterized by mass analysis (see 5.6 Appendix-III for HPLC profile and mass spectra, Table 1).

Table 1. ε_{260} and MALDI-TOF mass analysis of PNA oligomers

PNA	Sequence[a]	ε_{260} ($M^{-1}cm^{-1}$)	Calcd mass	Obsvd mass
18	**7**TACTAGCKK	7.33×10^4	2506.58 $[M]^+$	2506.48
19	**16**TACTAGCKK	7.29×10^4	2657.71 $[M]^+$	2658.25
20	**17**TACTAGCKK	6.95×10^4	2233.25 $[M]^+$	2233.70

[a]Sequence of alkyne-and azide-modified PNA oligomers (**18**–**20**) obtained by the SPPS. PNA sequences are written from N-to C-terminus containing two lysine (**K**) residues at the C-terminus.

5.2.1.2 Postsynthetic chemical functionalization of alkyne- and azide-modified PNA oligomers

To evaluate the utility of alkyne- (**18**) and azide- (**19** and **20**) modified PNA oligomers towards postsynthetic chemical modifications, CuAAC, SPAAC and Staudinger ligation reactions were performed with respective alkyne, azide and phosphine substrates attached with fluorescent, affinity, sugar and amino acid tags (**a**–**j**, Figure 2).[5f,5g] In this regards, TEG-naphthalimide alkyne (**e**) was synthesized by a procedure mentioned in Chapter 4, while azide (**a**–**d**), alkyne (**f**–**h**) and biotinylated triaryl phosphine (**j**) substrates were prepared using reported literature procedure by colleagues from my lab.[5f,5g] Click reaction was performed by incubating alkyne PNA **18**, and azide PNA oligomers **19** and **20** with azide

substrates **a**–**d** and alkyne substrates **e**–**h**, respectively, under CuAAC reaction conditions (Figure 3, Scheme 3 and 4). Reactions were carried out in the presence of water-soluble Cu(I) stabilizing ligand, tris-(3-hydroxypropyltriazolylmethyl)amine (THPTA), $CuSO_4$ and a reducing agent, sodium ascorbate, at 37 °C for 2 h. CuAAC reaction was performed using the following condition; final concentration of alkyne/azide PNA, cognate biophysical probe, CuSO4, THPTA and sodium ascorbate was 0.3 mM, 1.5 mM, 3.75 mM, 7.5 mM and 7.5 mM, respectively.

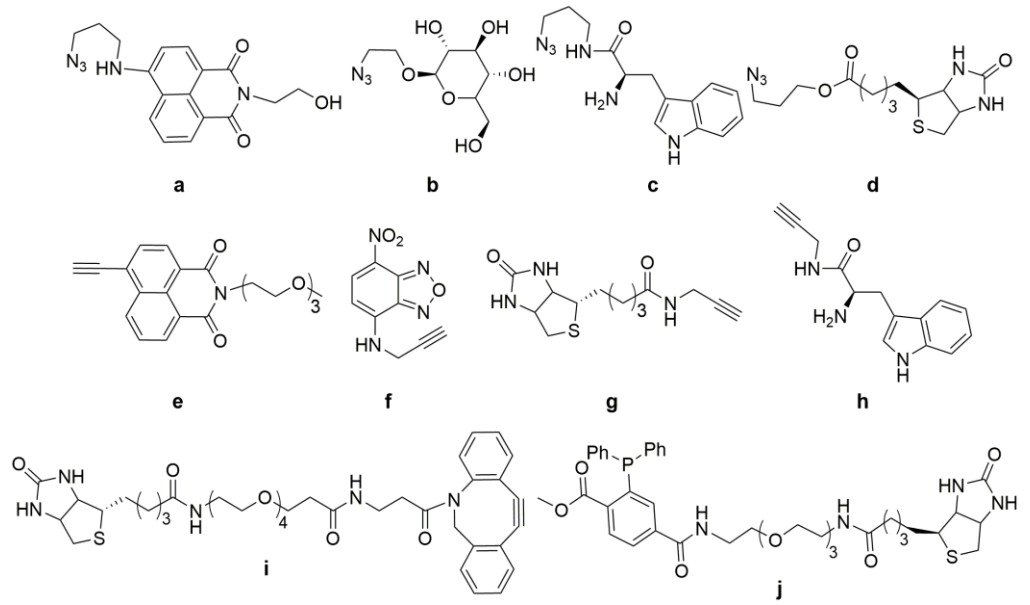

Figure 2. Building blocks for postsynthetic chemical modification by CuAAC, SPAAC and Staudinger ligation reactions.[5f,5g]

As a first attempt, naphthalimide-azide (**a**) and naphthalimide-alkyne (**e**) were allowed to react with alkyne PNA (**18**) and azide PNAs (**19** and **20**), respectively, under CuAAC reaction conditions (Figure 2, Scheme 3 and 4). This resulted in the formation of respective fluorescent clicked products (**18a**, **19e** and **20e**) within 2 h at 37 °C, which was further confirmed by mass analysis of HPLC purified fractions (Table 2, entry 1, 5 and 9, Figure 3). The scope of CuAAC reaction for conjugating diverse biophysical probes was explored by reacting azide-(**b**–**d**) and alkyne-(**f**–**h**) substrates with respective alkyne-(**18**) and azide-(**19** and **20**) PNA oligomers (Figure 2 and 3, Scheme 3 and 4, Table 2). In addition, mass analyses revealed the formation of an undesired adduct of alkyne PNA **18** with ascorbic acid, when CuAAC reactions were performed between alkyne PNA **18** and different azide substrates (**a**–**d**) (See Figure 3A for a representative example, the peak corresponding to ~20 min). Moreover, CuAAC reaction of biotin-azide (**d**) and biotin-alkyne (**g**) with respective alkyne/azide PNA oligomers gave an additional peak corresponding to the biotin-oxidized

product, which was characterized by mass analysis. Unexpectedly, clicked products isolated after CuAAC reaction of azide- (**19** and **20**) PNA oligomers with nitrobenzoxadiazole (NBD) alkyne (**f**) displayed a mass, which is less than the expected (Cal. 2875.88 and Obs. 2846.36 for **19f**; Cal. 2451.42 and Obs. 2423.07 for **20f**, Table 2). This observation is possibly due to removal of NO-functional group (molecular weight = 30) during mass analysis.

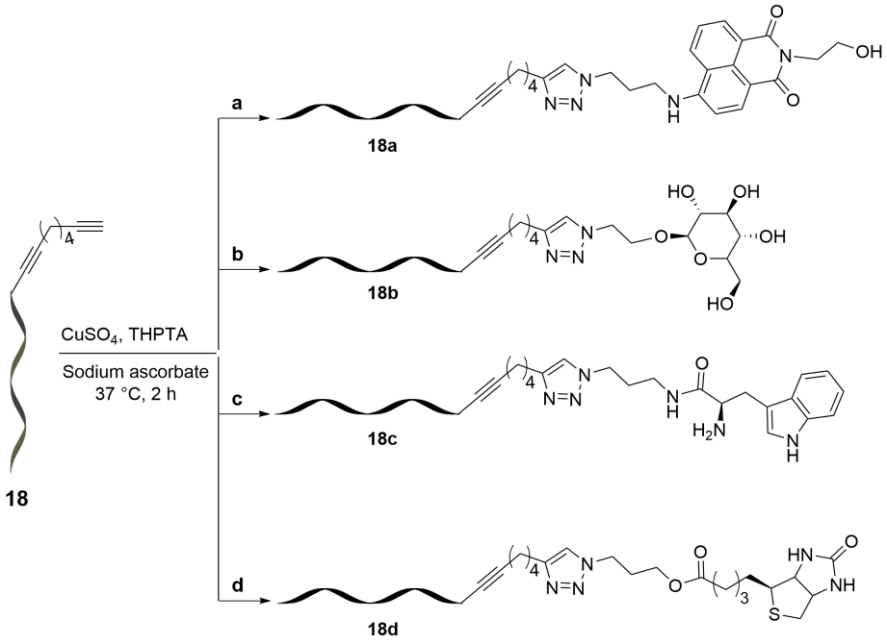

Scheme 3. Postsynthetic chemical functionalization of alkyne-modified PNA oligomer **18** by CuAAC reaction using azide substrates **a**–**d**.[11]

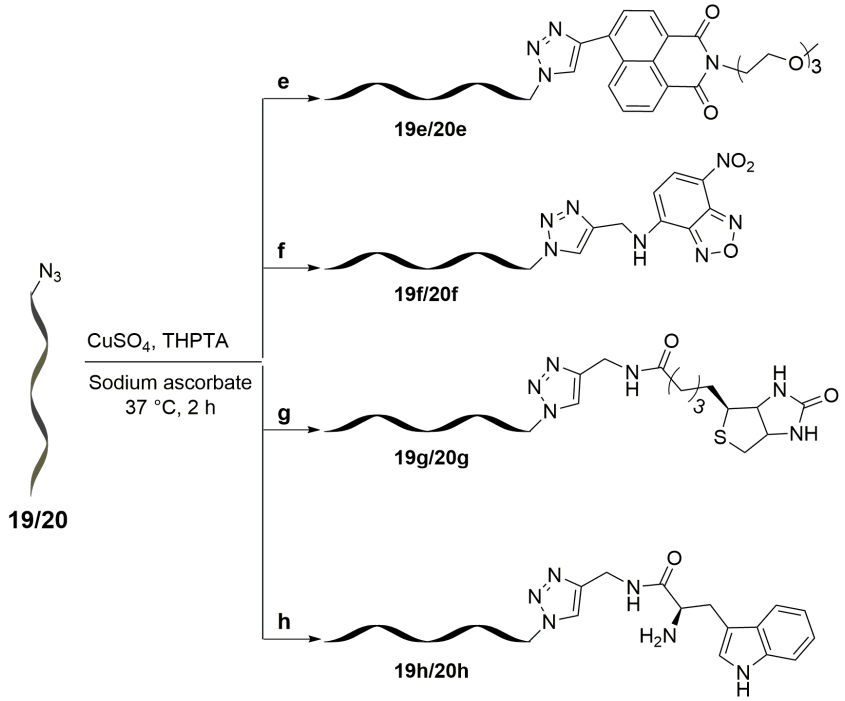

Scheme 4. Postsynthetic chemical functionalization of azide-modified PNA oligomers **19** and **20** by CuAAC reaction using alkyne substrate **e**–**h**.[11]

Table 2. Yield and mass data of CuAAC reaction on PNA oligomers **18**–**20**

Entry	PNA	Substrate	Product	Yield (nmol)	Isolated Yield (%)[a]	MALDI-TOF mass analysis of products (*m/z*)	
						Calcd mass	Obsvd mass
1	**18**	**a**	**18a**	7.8	52	2845.94	2845.74
2	**18**	**b**	**18b**	6.8	45	2755.81	2755.13
3	**18**	**c**	**18c**	6.1	41	2792.92	2792.20
4	**18**	**d**	**18d**	5.8	39	2833.99	2833.27
5	**19**	**e**	**19e**	1.5	50	3025.11	3026.61
6	**19**	**f**	**19f**	1.1	37	2875.88	2846.36
7	**19**	**g**	**19g**	0.5	17	2939.08	2938.56
8	**19**	**h**	**19h**	1.4	46	2899.00	2898.65
9	**20**	**e**	**20e**	7.7	51	2600.65	2600.32
10	**20**	**f**	**20f**	8.8	59	2451.42	2423.07
11	**20**	**g**	**20g**	7.9	53	2514.63	2514.09
12	**20**	**h**	**20h**	5.3	35	2474.55	2474.38

[a]All reactions were performed on 15 nmol scale (except for PNA **19**, it was 3 nmol) of alkyne-and azide-modified PNA oligomers. Yields reported are with respect to the PNA products isolated after HPLC purification. The yields were calculated by using ε_{260} values of reactant PNA oligomers given in Table 1.[11]

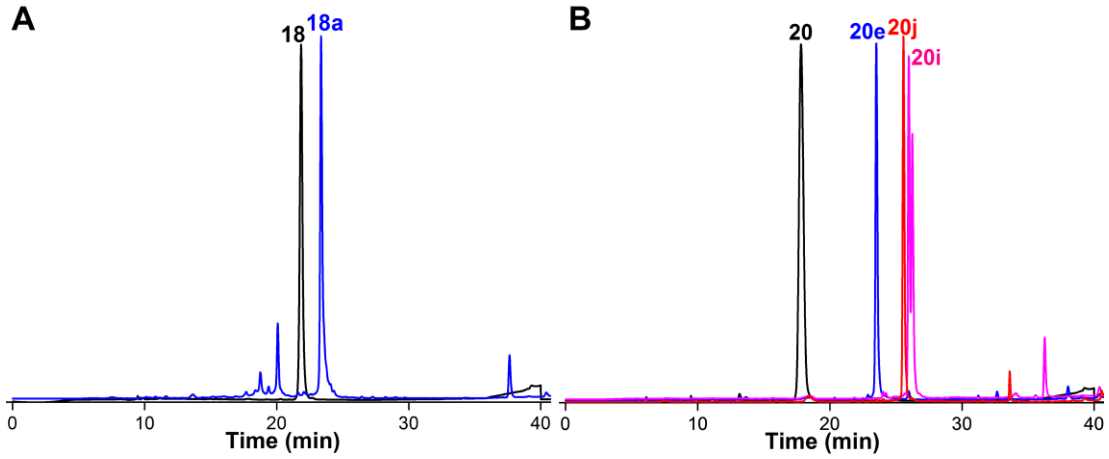

Figure 3. (**A**) Representative RP-HPLC chromatogram of starting alkyne PNA **18** and its CuAAC reaction product (**18a**) with naphthalimide azide (**a**) at 260 nm. (**B**) Representative RP-HPLC chromatogram of starting azide PNA **20** and its CuAAC (**20e**), SPAAC (**20i**) and Staudinger ligation (**20j**) reaction products with naphthalimide alkyne (**e**), biotin-DBCO (i) and biotinylated triaryl phosphine (**j**), respectively at 260 nm. Conditions: 0–50% B in 25 min and 50–100% B in 15 min (Mobile phase A: 5% acetonitrile in H_2O containing 0.1% TFA. Mobile phase B: 50% acetonitrile in H_2O containing 0.1% TFA). Flow rate was 2 mL/min.[11]

Furthermore, the integrity of fluorescent clicked products (**18a**, **19e**, **20e**, **19f** and **20f**) was confirmed by steady-state fluorescence analysis (Figure 4). PNA product **18a** displayed a significant enhancement in fluorescence as compared to naphthalimide-alkyne (**a**) substrate (Figure 4A). Surprisingly, there was significant reduction in fluorescence intensity for clicked PNA products **19e** and **20e** as compared to naphthalimide-alkyne (**e**) with red shifted emission maximum (419 nm to 462 nm, Figure 4B). NBD-alkyne (**f**) and their clicked PNA products **19f** and **20f** gave a similar fluorescence profile (Figure 4C). In summary, we isolated a good to moderate yields for clicked products after HPLC purifications.

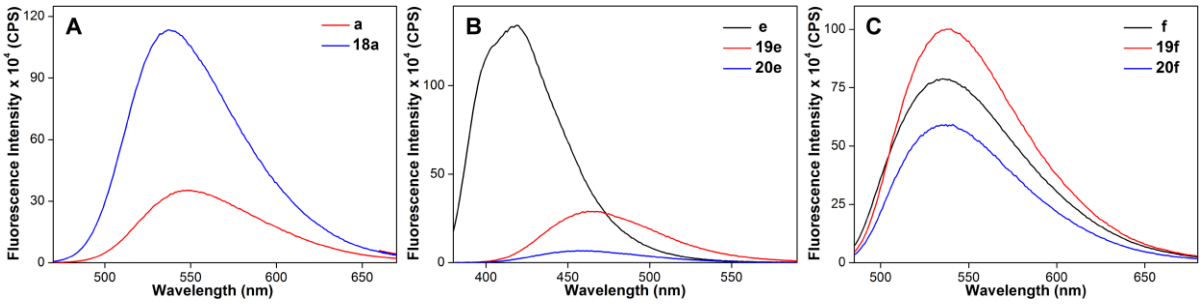

Figure 4. (**A**) Emission spectra (0.5 µM) of naphathlimide-azide (**a**) and clicked PNA product **18a**. Excitation and emission slit widths were kept at 2 and 5 nm, respectively. Samples were excited at 455 nm. (**B**) Emission spectra (0.5 µM) of naphathlimide-alkyne (**e**) and clicked PNA products **19e** and **20e**. Excitation and emission slit widths were kept at 2 and 4 nm, respectively. Samples were excited at 362 nm. (**C**) Emission spectra (0.5 µM) of NBD-alkyne (**f**) and clicked PNA products **19f** and **20f**. Excitation and emission slit widths were kept at 4 and 5 nm, respectively. Samples were excited at 473 nm.[11]

Since, azide is an common functionality in many chemoselective reactions, azide PNA **19** and **20** were further subjected to copper-free SPAAC and Staudinger ligation reactions with commercially available cyclooctyne building blocks of biotin (**i**) and biotinylated triaryl phosphine substrate (**j**) synthesized by a colleague from my group (Figure 2 and 3B, Scheme 5 and 6). SPAAC and Staudinger ligation reactions were performed for 1 h and 12 h, respectively at 37 °C, we observed moderate to good yields in all these reactions (Figure 2 and 3B, and Table 3). In particular, we observed good yields for PNA oligomer **20**, where azide functionality was placed at the end of backbone as compared to PNA oligomer **19**, where azide functionality was incorporated on the 5-position of uracil base. This is possibly due to the better accessibility of azide functionality in **20** as compared to **19**. These postsynthetic chemical labeling strategies are simple, robust and efficient to generate labeled PNA oligomers with a variety of biophysical probes in sufficient amounts. These labeled PNA probes could be further utilized for the detection of nucleic acid targets by different biophysical techniques.

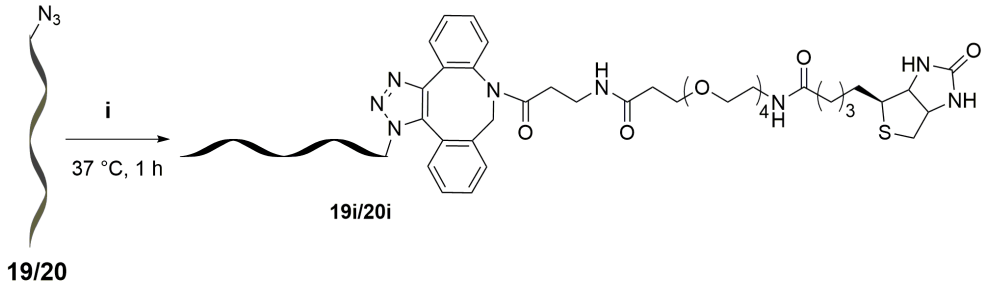

Scheme 5. Postsynthetic chemical functionalization of azide-modified PNA oligomers **19** and **20** by SPAAC reaction using alkyne substrate **i**.[11]

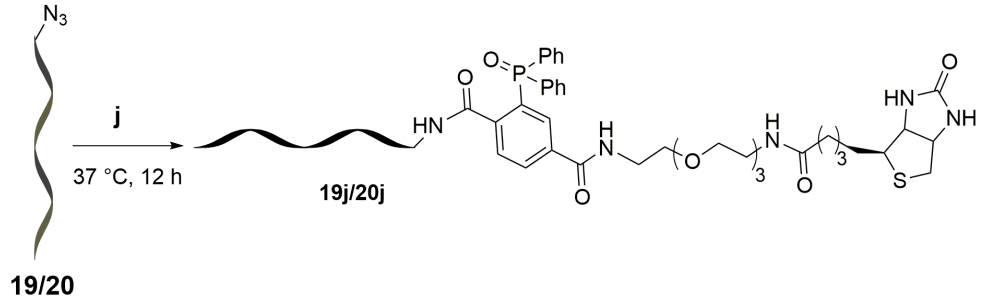

Scheme 6. Postsynthetic chemical modification of azide-modified PNA oligomers **19** and **20** by Staudinger ligation reaction with biotinylated triaryl phosphine substrate **j**.[11]

Table 3. Yield and mass data of postsynthetically functionalized PNA oligomers **19** and **20**

Entry	PNA	Substrate	Product	Yield (nmol)	Isolated Yield (%)[a]	MALDI-TOF mass analysis of products (*m/z*)	
						Calcd mass	Obsvd mass
1	**19**	**i**	**19i**	2.2	73	3407.63	3407.50
2	**19**	**j**	**19j**	0.04	1.3	3380.54	3380.45
3	**20**	**i**	**20i**	2.4	40	2983.18	2983.47
4	**20**	**j**	**20j**	4.3	72	2956.08	2956.12

[a]Reactions were performed on 3 nmol and 6 nmol scales for azide-modified PNA **19** and **20**, respectively. Yields reported are on the PNA products isolated after HPLC purification. The yields were calculated by using ε_{260} values of reactant PNA oligomers given in Table 1.[11]

5.2.2 Palladium-catalyzed reactions on an iodo-modified PNA oligomer

5.2.2.1 Synthesis of 5-iodouracil PNA monomer 22

The synthesis was initiated (Figure 5A) with 5-iodouracil PNA ester **21**, which was prepared according to the procedure discussed in Chapter 2 (Section 2.2.2.1). The ethyl ester of 5-compound **21** was hydrolyzed in quantitative yield using 10% LiOH to afford 5-iodouracil PNA acid **22** (Figure 5A). Further, Iodo PNA oligomer **23** (containing two lysine residues at

C-terminus for the aqueous solubility) was prepared using, Boc-protected 5-iodouracil (**22**) and *aeg*-thymine PNA monomers on MBHA resin (Figure 5B, Table 4).

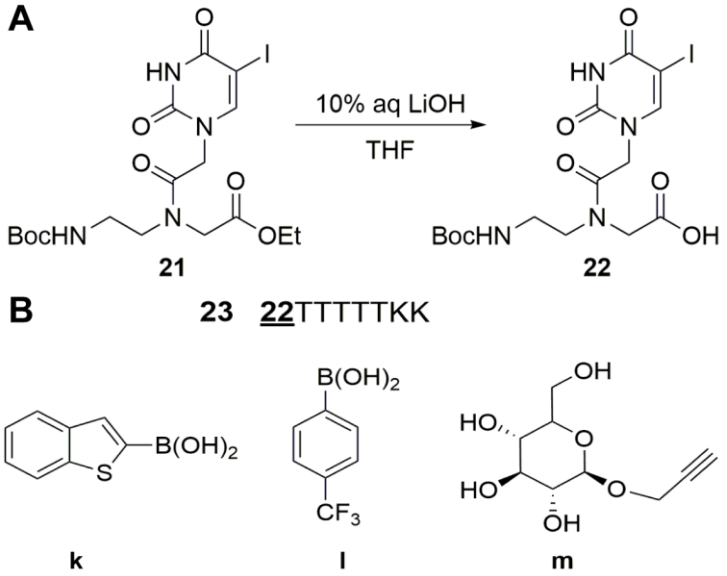

Figure 5. (**A**) Synthesis of 5-iodouracil PNA acid **22** for SPPS using Boc-chemistry. (**B**) The sequence of 5-iodouracil-modified PNA oligomer **23** obtained by the solid-phase synthesis (Boc-chemistry). PNA sequence is written from N-to C-terminus containing two lysine (**K**) residues at the C-terminus. Boronic acid and alkyne building blocks for palladium-catalyzed Suzuki-Miyaura and Cu-free Sonogashira reactions. [11]

Table 4. ε_{260} and MALDI-TOF mass analysis of iodo PNA oligomer **23**

PNA	Sequence[a]	ε_{260} ($M^{-1}cm^{-1}$)	Calcd mass	Obsvd mass
23	**22**TTTTTKK	4.61 x 10^4	1982.80 $[M]^+$	1982.59

[a]Sequence of alkyne-and azide-modified PNA oligomers **23** obtained by the SPPS. PNA sequence is written from N-to C-terminus containing two lysine (**K**) residues at the C-terminus.

5.2.2.2 Palladium-catalyzed Suzuki-Miyaura and Cu-free Sonogashira reactions on an iodo-modified PNA oligomer

Davis and co-workers have introduced a series of pyrimidine and guanidine based ligands for aqueous phase palladium-catalyzed Suzuki-Miyaura reaction on iodo-modified peptides as well as proteins.[12] The ligands form a complex with $Pd(OAc)_2$, that is easily soluble in water. Among them, complex of dimethylguanidine (DMG) with $Pd(OAc)_2$ [$Pd(OAc)_2$•$(DMG)_2$ catalyst] exhibited high yields for Suzuki-Miyaura reaction on peptides. In parallel, Cu-free Sonogashira reaction for labeling of iodo-modified proteins with variety of probes was explored using a complex of 2-dimethylamino-4,6-dihydroxypyrimidine with $Pd(OAc)_2$ [$Pd(OAc)_2$•$(DMADHP)_2$ catalyst] by Lin's group.[9b] Therefore, by considering the importance of palladium-catalyzed reactions in bioconjugation, we sought to utilize these

reactions for labeling PNA oligomers with biophysical tags, espacially for the preparation of microenvironment-sensitive emissive PNA probes.

In this regards, iodo-modified PNA **23** was subjected to palladium-catalyzed Suzuki-Miyaura and Cu-free Sonogashira coupling reactions using $Pd(OAc)_2$•$(DMG)_2$ and $Pd(OAc)_2$•$(DMADHP)_2$ catalyst, respectively (Figure 5 and Scheme 7). We performed preliminary experiments to optimize the concentration of iodo-PNA **23** and the equivalence of boronic acid substrates (**k** and **l**) and palladium catalyst required for coupling reactions. Based on the initial observations (data not shown), following conditions were finalized for Suzuki-Miyaura; concentration of iodo PNA, boronic acid, and palladium catalyst was set to 100 µM, 1 mM and 1 mM, respectively, whereas for Cu-free Sonogashira; concentration of iodo PNA, alkyne, a palladium catalyst, and sodium ascorbate was set to 100 µM, 5 mM, 0.5 mM, and 1 mM, respectively.

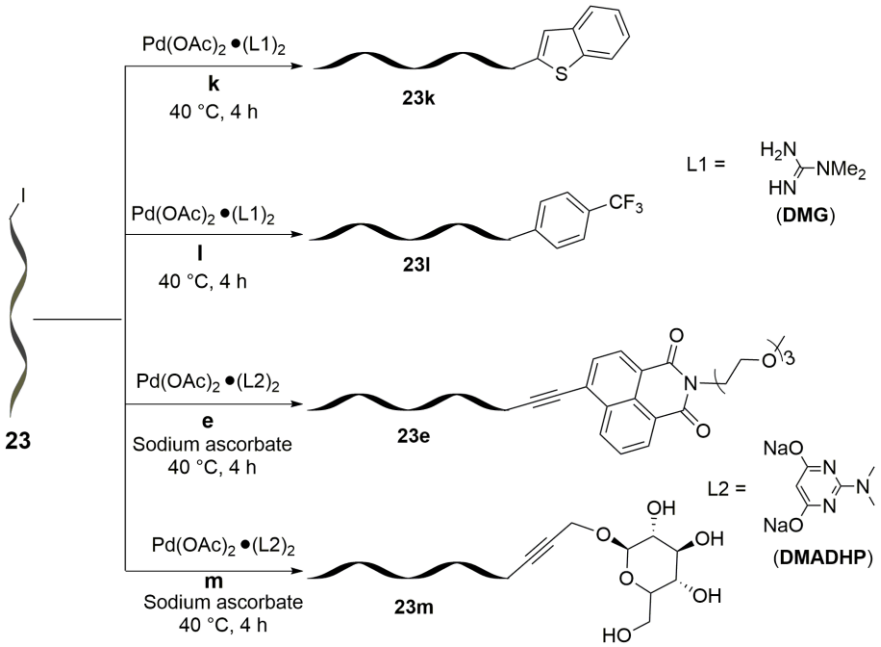

Scheme 7. Palladium-catalyzed Suzuki-Miyaura and Cu-free Sonogashira reactions on iodo-PNA **23** with boronic acids (**k** and **l)** and alkyne (**e** and **m**) substrates. Structure of ligands L1 and L2 used for palladium-catalyzed reactions are also given.

Having identified the appropriate conditions, iodo-PNA **23** was incubated with commercially available benzothiophene (**k**) and 4-trifluoromethyl benzene (**l**) boronic acids in the presence of $Pd(OAc)_2$•$(DMG)_2$ in 50 mM phosphate buffer (pH 8.0) under Suzuki-Miyaura coupling conditions (Figure 5 and Scheme 7). In parallel, iodo-PNA **23** was also subjected to Cu-free Sonogashira reaction with naphthalimide (**e**) and glucose (**m**, prepared by a colleague from my group) alkyne substrates in the presence of $Pd(OAc)_2$•$(DMADHP)_2$

in 50 mM Tris-HCl buffer (pH 8.5, Figure 5 and Scheme 7). Each of the reactions were incubated at 40 °C for 4 h, and subsequently monitored by RP-HPLC. Respective coupled products (**23k**, **23l**, **23e** and **23m**) were characterized by mass spectrometry (see 5.6 Appendix-I for HPLC profile, Table 5). Additionally, fluorescent benzothiophene-(**23k**) and naphthalimide-(**23e**) modified PNA products exhibited enhancement in fluorescence intensity as compared to their respective benzothiophene-(^{BT}**U**) and naphthalimide-(^{Nap}**U**) modified PNA monomers as discussed in Chapter 2 and Chapter 4 (Figure 6). HPLC chromatogram showed significant amount of impurities, along with desired products (see 5.6 Appendix-I for HPLC profile, Table 5). Typically, a reaction scale of 5 nmole, after HPLC purification, yielded ~0.6–1.3 nmoles of the labeled PNA products (**23k**, **23l**, **23e** and **23m**, Table 5). Further, optimizations to improve yields for palladium-catalyzed reactions are under progress.

Table 5. Yield and mass data of palladium-catalyzed reactions on PNA oligomer **23**

Entry	PNA	Substrate	Product	Yield (nmol)	Isolated Yield (%)[a]	MALDI-TOF mass analysis of products (*m/z*)	
						Calcd mass	Obsvd mass
1	**23**	**k**	**23k**	1.3	26	1989.08	1989.34
2	**23**	**l**	**23l**	1.1	22	2000.99	2001.58
3	**23**	**e**	**23e**	1.1	22	2222.28	2222.37
4	**23**	**m**	**23m**	0.6	12	2073.09	2073.48

[a]Reactions were performed on 5 nmol scale for iodo-modified PNA oligomers. Yields reported are with respect to the PNA products isolated after HPLC purification. The yields were calculated by using ε_{260} values of reactant PNA oligomer **23** given in Table 4.

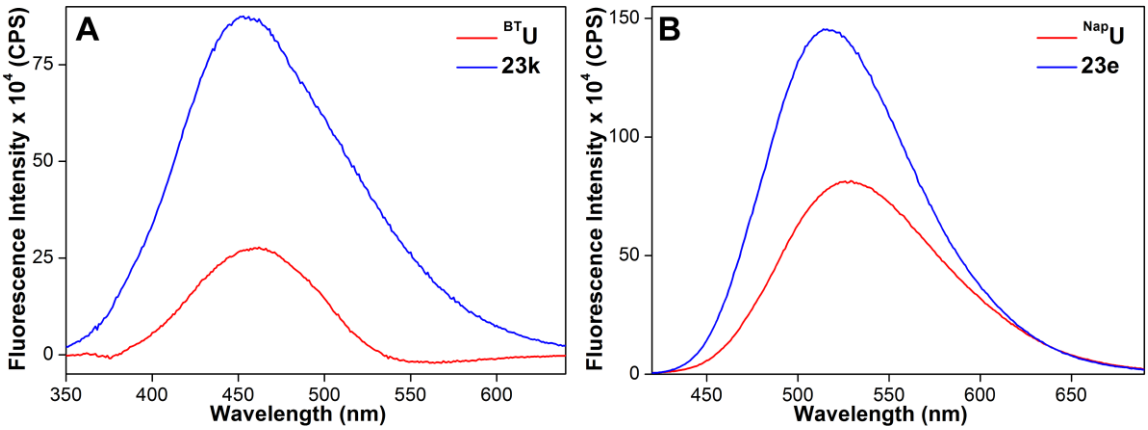

Figure 6. (**A**) Emission spectra (0.5 µM) of benzothiophene-conjugated uracil PNA analogue (^{BT}**U**) and coupled PNA product **23k**. Excitation and emission slit widths were kept at 7 and 9 nm, respectively. Samples were excited at 330 nm. (**B**) Emission spectra (0.5 µM) of naphthalimide-conjugated uracil PNA analogue (^{Nap}**U**) and coupled PNA product **23e**. Excitation and emission slit widths were kept at 3 and 4 nm, respectively. Samples were excited at 400 nm.[11]

5.2.3 Synthesis of telomere-targeting PNA probes

Telomeric DNA repeats present at the end of chromosomes protect the chromosomes from degradation and also play a crucial role in the maintenance of chromosomes.[13,14] A typical telomeric DNA sequence contains thousands of hexameric nucleotide repeats $(TTAGGG)_n$. These telomeric DNA repeats have the ability to form G-quadruplex (GQ) structures *in vitro* and *in vivo*, and have been implicated in cancer and ageing-related diseases (Figure 7).[15–17] Hence, the detection and estimation of telomeric DNA repeats is paramount to understand its structure and functions. Methods such as terminal restriction fragments (TRF) analysis, quantitative PCR, fluorescence *in situ* hybridization (FISH) etc. have been widely used for detection and quantification of telomeres.[18–20] Unlike the TRF and PCR-based assays, the FISH provides the spatio-temporal distribution of telomeres in cells.[21] For this purposes, PNA oligomers conjugated to bulky fluorophores (e.g., fluorescein, Cy-5, Rhodamine, etc.) are commercially available for imaging human telomeric DNA repeats in-side cells by FISH assay. Although, these commercial fluorescent PNA probes are highly useful for visualizing telomere dynamics in fixed as well as live cells, they exhibit background fluorescence problem. In addition to this, customized PNA probes with different fluorophores and affinity tags have to be prepared every time separately depending upon the applications such as imaging or pulldown, which makes this approach cumbersome and expensive

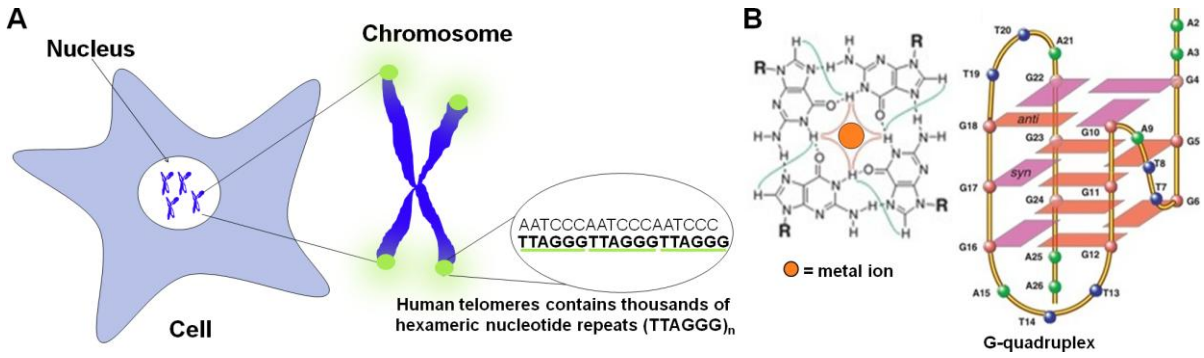

Figure 7. (**A**) Chromosomes (shown in blue) and human telomeric repeats present at its ends (shown in green). (**B**) A guanine-rich sequence of human telomeric DNA known to form G-quadruplex structure is also given.[22] Figure adapted from reference 22.

Therefore, we envisioned to develop a modular postsynthetic approach for attaching such reporters (fluorescent or affinity tags) to PNA oligomer after hybridization with telomeres under physiological conditions. In this regard, base-modified internal-labeled alkyne-(**24**), azide-(**25**), and iodo-(**27**) and end-labeled azide-(**26**) PNA oligomers complementary to human telomeric DNA repeats were synthesized using the protocol described in the earlier Chapters (PNA oligomers **24**–**26** by Fmoc-chemistry, and **27** and **28**

by Boc-chemistry, Figure 8, Table 6). Initially, postsynthetic chemical modifications by CuAAC, SPAAC, Staudinger ligation, and palladium-catalyzed Suzuki-Miyaura and Cu-free Sonogashira reactions were carried on the respective single-stranded PNA oligomers (Scheme 8 and 9, Table 7).

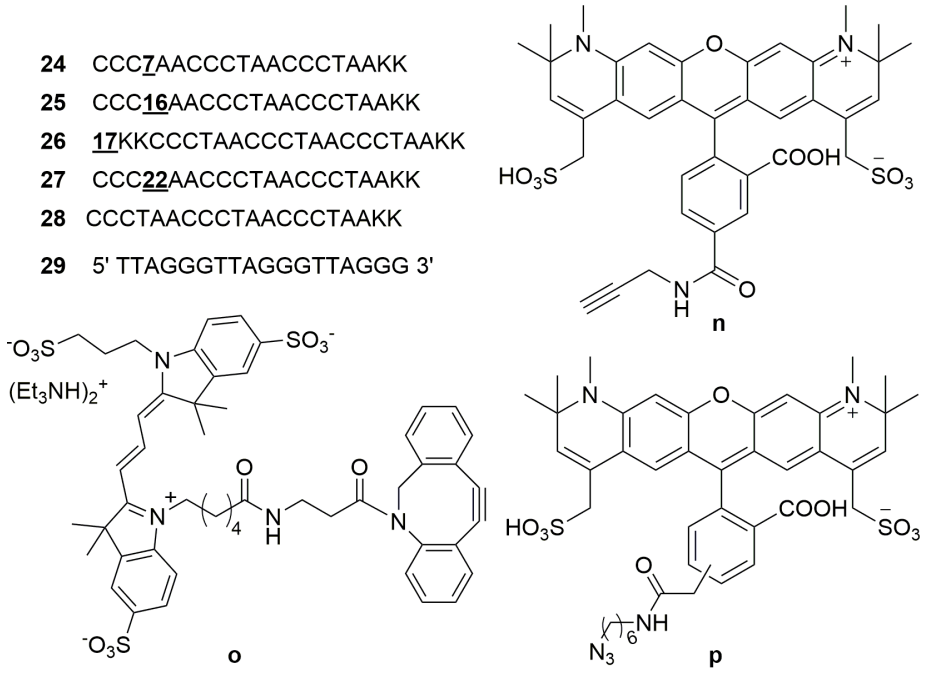

Figure 8. Sequences of PNA oligomer probes complementary to human telomeric DNA repeats synthesized by SPPS using Fmoc (**24**–**26**) and Boc (**27** and **28**) strategy. The sequence of custom telomeric DNA ON **29** is also given. Fluorescent alkyne, activated cyclooctyne and azide substrates (**n**–**p**) for CuAAC and SPAAC reactions on PNA-DNA duplex are also shown.[11]

Table 6. ε_{260} and MALDI-TOF mass analysis of PNA oligomers

PNA	Sequence[a]	ε_{260} ($M^{-1}cm^{-1}$)	Cal. Mass	Obs. mass
24	CCC**7**AACCCTAACCCTAAKK	16.26 x 10^4	5075.12 $[M]^+$	5075.09
25	CCC**16**AACCCTAACCCTAAKK	16.22 x 10^4	5249.24 $[M+Na]^+$	5253.01
26	**17**KKCCCTAACCCTAACCCTAAKK	16.70 x 10^4	5324.40 $[M]^+$	5323.63
27	CCC**22**AACCCTAACCCTAAKK	16.19 x 10^4	5096.87 $[M]^+$	5097.74
28	CCCTAACCCTAACCCTAAKK	16.70 x 10^4	5007.90 $[M+Na]^+$	5007.15

[a]Sequence of alkyne-, azide- and iodo-modified PNA oligomers (**24**–**27**) and control unmodified PNA oligomer **28** obtained by SPPS. PNA sequences are written from N-to C-terminus containing two lysine (**K**) residues at the C-terminus.[11]

Labeling of single-stranded telomere targeting PNA using click and Staudinger ligation reactions: Single-stranded internal-labeled alkyne-(**24**) and azide-(**25**), and end-labeled azide-(**26**) PNA oligomers were functionalized with respective naphthalimide-azide (**a**) and naphthalimide-alkyne (**e**) substrates, using CuAAC reaction described in section 5.2.1.2

(Scheme 8 and Table 7). Corresponding fluorescent clicked products (**24a**, **25e** and **26e**) were isolated and characterized by RP-HPLC and mass analysis (Table 7). A typical 7.5 nmole scale reactions of **24** and **26** resulted in ~1.5 nmoles of the clicked products **24a** and **26e** (Table 7). However, CuAAC reaction on **25** with naphthalimide alkyne (**e**) gave a fluorescent clicked product **25e** in poor yield (3%), indicating that the base-modified 5-tetraethylene glycol azide (**16**) at internal position in azide PNA **25** might not be easily accessible for click reaction. Hence, terminal labeled azide PNA **26** (azido acetic acid **17** at N-terminus) was further labeled with biotin cyclooctyne (**i**) and biotin phosphine (**j**), using SPAAC and Staudinger ligation reactions, respectively (Scheme 8 and Table 7). The desired ligated products (**26i** and **26j**) were isolated using RP-HPLC and their integrity was confirmed by mass analysis (Table 7). In addition, we compared the fluorescence of emissive clicked PNA products **24a** and **26e** along with respective naphthalimide azide-(**a**) and naphthalimide alkyne-(**e**) substrates (Figure 9). The clicked PNA product **24a** gave intense fluorescence band to that of naphthalimide-azide (**a**) substrate (Figure 9A). Despite the considerable red shift in emission maximum form 419 nm to 461 nm, clicked product **26e** showed significant quenching in fluorescence efficiency (Figure 9B).

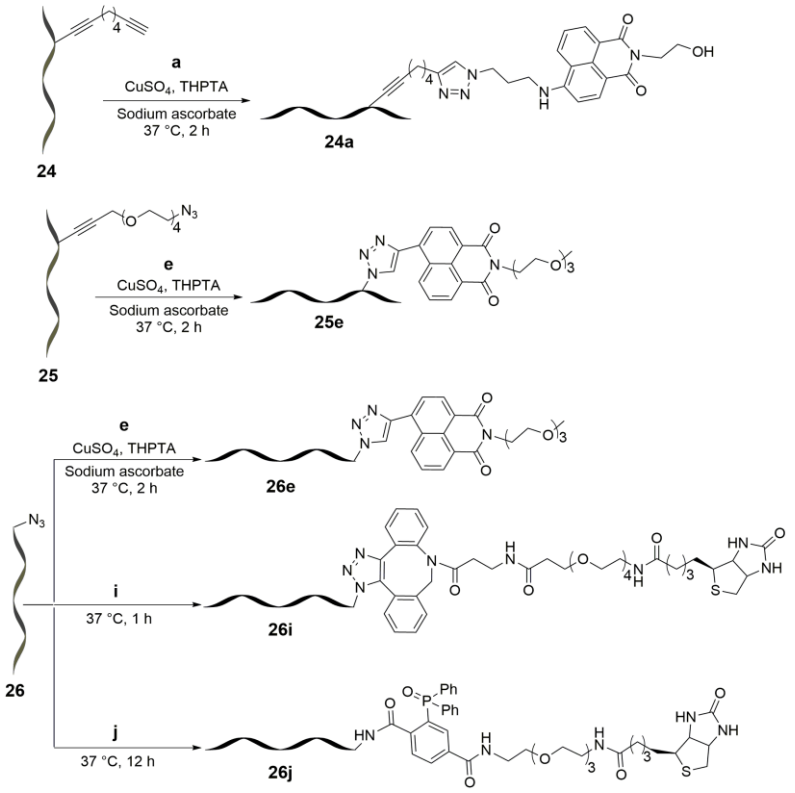

Scheme 8. Postsynthetic chemical functionalization on telomere targeting internal-labeled alkyne-(**24**) and azide-(**25**), and end-labeled azide-(**26**) PNA oligomers by CuAAC, SPAAC and Staudinger ligation reactions using respective substrates (**a**, **e**, **i**, and **j**).[11]

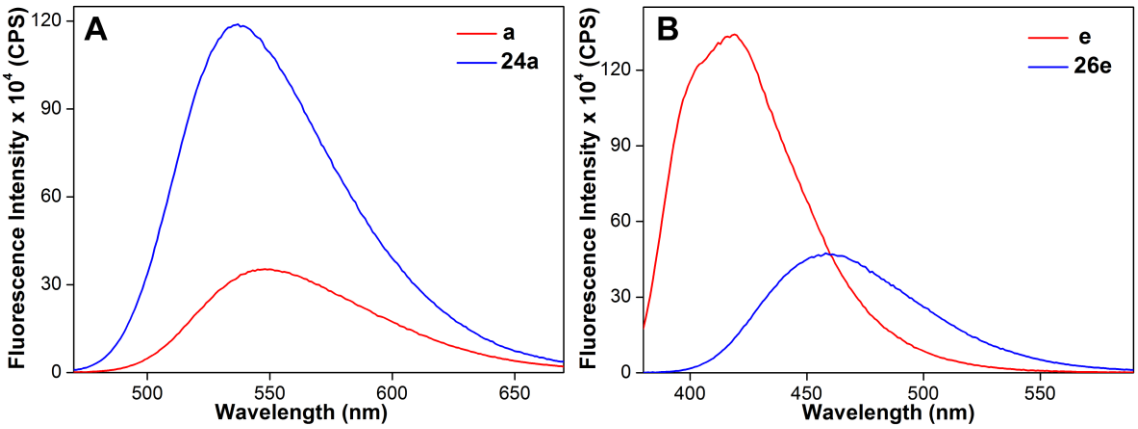

Figure 9. (**A**) Emission spectra (0.5 µM) of naphathlimide-azide (**a**) and clicked PNA product **24a**. Excitation and emission slit widths were kept at 2 and 5 nm, respectively. Samples were excited at 455 nm. (**B**) Emission spectra (0.5 µM) of naphathlimide-alkyne (**e**) and clicked PNA product **26e**. Excitation and emission slit widths were kept at 2 and 4 nm, respectively. Samples were excited at 362 nm.[11]

Palladium-mediated cross-coupling reactions to label single-stranded telomere targeting PNA: Palladium-catalyzed Suzuki-Miyaura and Cu-free Sonogashira reactions on iodo-PNA **27** were performed in presence of benzothiophene boronic acid (**k**) and naphthalimide alkyne (**e**), respectively, using conditions mentioned in section 5.2.2.2 (Scheme 9). After HPLC purification, a peak corresponding to coupled products (**27k** and **27e**) was isolated, which was further confirmed by MALDI-TOF mass analysis (Scheme 9 and Table 7). We observed that yields of palladium-catalyzed reactions were very poor (from HPLC profile), hence quantification was difficult. Therefore, further optimizations to get desired coupled product in good yields for biophysical studies are currently under progress.

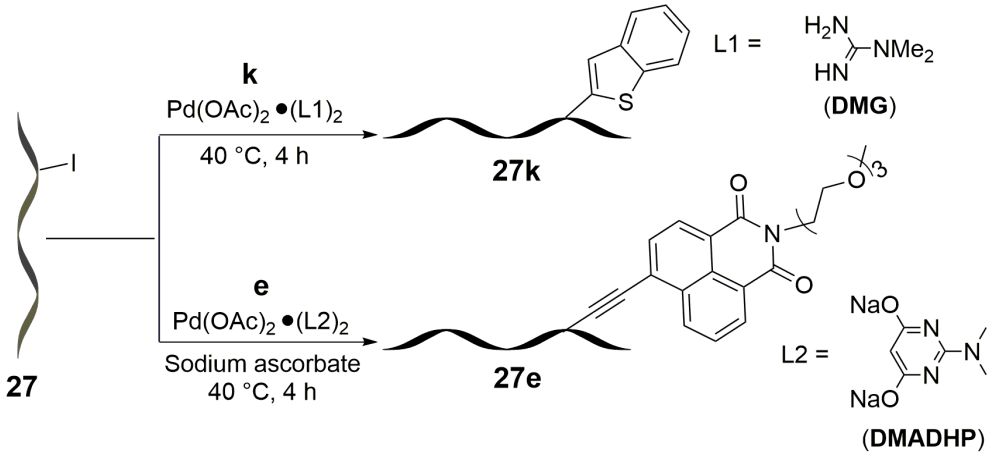

Scheme 9. Palladium-catalyzed Suzuki-Miyaura and Cu-free Sonogashira reactions on telomere targeting internal-labeled iodo PNA **27** with benzothiophene boronic acid (**k**) and naphthalimide alkyne (**e**). Structure of ligands L1 and L2 used for palladium-catalyzed reactions are also given.[11]

Table 7. Yield and mass data of postsynthetically functionalized telomere PNAs

Entry	PNA	Substrate	Product	Yield (nmol)	Isolated Yield (%)[a]	MALDI-TOF mass analysis of products (*m/z*)	
						Calcd mass	Obsvd mass
1	**24**	**a**	**24a**	1.4	19	5414.5	5416.1
2	**25**	**e**	**25e**	0.17	3[b]	5593.6	5613.66
3	**26**	**e**	**26e**	1.5	20	5691.8	5691.8
4	**26**	**i**	**26i**	1.5	20	6074.3	6074.5
5	**26**	**j**	**26j**	1.0	17	6047.2	6048.0
6[c]	**27**	**k**	**27k**	nd	nd	5103.2	5104.0
7[c]	**27**	**e**	**27e**	nd	nd	5336.4	5337.3

[a]Reactions were performed on 7.5 nmol scale (except, for entry 2 and 4, it was 6 nmol and for entry 6 and 7, it was 5 nmol) for PNA oligomers. Yields reported are with respect to the PNA products isolated after HPLC purification. The yields were calculated by using ε_{260} values of reactant PNA oligomer given in Table 6. [b]Major amount of starting azide PNA **25** was isolated after HPLC purification. [c]Yields of palladium-catalyzed reactions were poor and therefore desired products were not quantified.

Altogether, these experiments clearly demonstrate that the efficiency of CuAAC, SPAAC and Staudinger ligation reactions in labeling single-stranded PNA oligomers are superior as compared to palladium-catalyzed reactions. This prompted us to examine the utility of click labeling strategy in functionalizing PNA oligomer hybridized to complementary ON targets (post-hybridization labeling) with a variety of reporters. Further, this approach could be extended for multiplex imaging, and pulldown of specific nucleic acid sequences.

Labeling of telomere-PNA heteroduplex using click and Staudinger ligation reactions: Traditionally, PNA containing bulky reporter molecules such as fluorophore and affinity tags are used for the detection of nucleic acid targets (e.g., telomere) by *in situ* hybridization techniques.[21] Although, this strategy is highly advantageous, its hybridization efficiency is compromised due to bulky reporter molecules. Moreover, every time one has to prepare customized PNA probes labeled with appropriate reporter molecules for applications such as imaging and pulldown of nucleic acids in cell-free and cellular conditions. To overcome this problem, we decided to perform post-hybridization chemical labeling of a PNA-telomere duplex with a variety of biophysical probes including fluorescent and affinity tags (Figure 2, 8 and 10A). Initially, PNA oligomers **24** and **26** containing azide and alkyne functionalities were hybridized with telomeric DNA ON **29** and subsequent post hybridization labeling was

achieved by reacting with respective alkyne and azide-containing fluorophores (**n**–**p**) and a biotin tag (**j**) to obtain labeled PNA-telomere duplexes (Figure 2 and 8). All reactions were performed at 0.15 mM (2.1 nmole) concentration of PNA-telomere duplex in 10 mM phosphate buffer (pH 7.1) and labeled PNA-telomere product duplexes were resolved by 15% native PAGE under non-denaturing conditions, followed by UV-shadowing (Figure 10B).

Azide PNA-telomere duplex (**26•29**) displayed nearly complete conversion of starting **26•29** duplex into labeled duplexes when subjected to CuAAC, SPAAC and Staudinger ligation reactions with substrates **n**, **o**, and **p**, respectively (Figure 2 and 8, Figure 10B, lane 2, 3 and 4). CuAAC reaction on **26•29** duplex with Alexa-594 alkyne **n** gave labeled duplex, which was moving faster compared to control **26•29** duplex in the gel electrophoresis (compare lane 1and 2, Figure 10B). Further, SPAAC and Staudinger ligation reaction on **26•29** duplex with Cy-5 DBCO (**o**) and biotinylated triaryl phosphine (**j**) gave a labeled product duplexes with either similar or retarded mobility (compare lane 1 and 3, 4, Figure 10B). The observed mobility of labeled product duplexes on PAGE could be possibly due to a combined effect of additional charge on substrates and increased molecular weight of the labeled product duplexes as compared to control **26•29** duplex. Interestingly, no degradation of the substrate or product was observed under the reaction conditions employed for labeling PNA-DNA duplex.

Next, CuAAC reaction on alkyne PNA-telomere duplex (**24•29**) with Alexa-594 azide (**p**) was performed and it gave a band corresponding to labeled duplex with higher mobility probably due to a charge on fluorophore (**p**) as compared to control **24•29** duplex (compare lane 5 and 6, Figure 10B). However, some amount of unreacted alkyne-modified PNA-telomere duplex **24•29** was also noticed as the reaction did not proceed to completion (lane 6, Figure 10B). The specificity of postsynthetic click reaction was confirmed by performing a CuAAC reaction on control unmodified PNA-telomere duplex **28•29** with Alexa-594 azide **p**. The reaction mixture gave a band, which did not contain the Alexa probe, and was found to be similar to the control duplex **28•29** band (compare lane 7 and 8, Figure 10B). These observations ascertained the chemoselectivelty of the reactions. Notably, we observed good yields for azide PNA oligomer **26**, in which azide functionality was at the N-terminus through lysine residues, as compared to alkyne PNA oligomer **24**, where alkyne functionality at 5-position of uracil base was incorporated in the internal position of the PNA oligomer. The differences in labeling efficiency could be due to better accessibility of end-labeled (N-terminus) azide over internally labeled alkyne group in PNA oligomers. These experiments clearly demonstrated that azide or alkyne modified PNA oligomers hybridized to the target

telomeric DNA ON can be effectively labeled with biophysical probes using chemoselective reactions. Therefore, these postsynthetic chemical strategies could be further explored for the imaging of therapeutically relevant nucleic acid targets (telomere) by post-hybridization based labeling of PNA oligomers, hybridized to the telomere in cellular conditions.

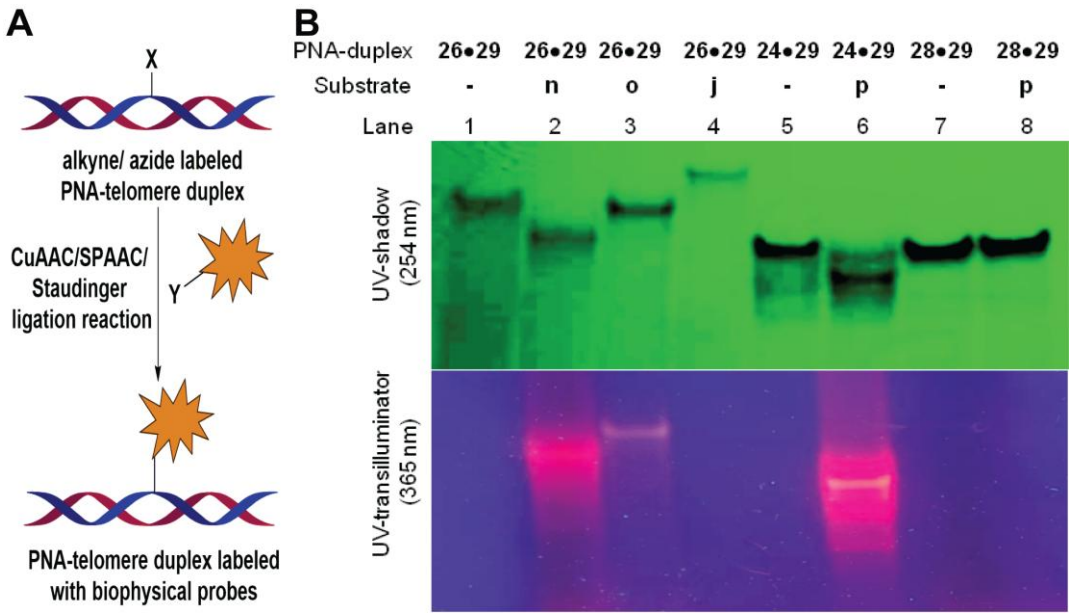

Figure 10. (**A**) Schematic illustration of postsynthetic chemical modification on PNA-telomere heteroduplex using postsynthetic chemical reactions. (**B**) UV-shadow (260 nm) of PAGE-resolved control unmodified (lane 1, 5 and 7) and modified (lane 2, 3, 4, 6 and 8) PNA-telomere duplexes with CuAAC, SPAAC and Staudinger ligation reactions. The fluorescent clicked products (lane 2, 3, and 6) were clearly visualized by UV-transilluminator (365 nm). Some amount of unreacted alkyne-modified PNA-telomere duplex (**24•29**) was noticed (lane 6) as the reaction did not proceed to completion.[11]

5.3 Conclusion

In summary, we have developed clickable alkyne- and azide-modified uracil PNA analogues and incorporated them into PNA oligomers by using Fmoc-chemistry. The alkyne- and azide-modified PNA oligomers were conveniently labeled by using postsynthetic chemical reactions with variety of biophysical reporters that include fluorescent probes, affinity tag, amino acid and sugar residues. Further, this postsynthetic approach was effectively explored for labeling PNA-telomeric DNA heteroduplexes with different reporters. Taken together, this post-hybridization labeling of PNA-DNA heteroduplex could be potentially useful to overcome certain limitations such as background fluorescence problem and facilitate labeling of PNA oligomer in a modular fashion. Therefore, currently we are evaluating the utility of this post-hybridization labeling methodology for imaging and pulldown of specific nucleic acid sequences from human genome (e.g., telomeric DNA repeats) and transcriptome

[poly(A) mRNA]. This post-hybridization labeling could be further extended for multicolor fluorescence imaging of therapeutically relevant nucleic acid sequences in the cells by using a combination of chemoselective reactions.

5.4 Experimental Section

5.4.1 Materials

Chloroacetyl chloride, di-*t*-butyl dicarbonate, ethane-1,2-diamine, ethyl bromoacetate, TFA, EDC and silica gel (100-200 mesh) were purchased from Spectrochem India. Dry DMF and dry dichloromethane were purchased from Rankem India. Acetic anhydride was purchased from Thomas Baker India. 5-Iodouracil, tetrakis(triphenylphosphine) palladium (0), pyridine, *N*-hydroxybenzotriazole (HOBt), 3-[bis(dimethylamino)methyliumyl]-3*H*-benzotriazol-1-oxide hexafluorophosphate (HBTU), *N*,*N*-diisopropylethylamine (DIPEA), 1,2-ethanedithiol, thioanisole and trifluoromethanesulfonic acid (TFMSA) were purchased from Sigma-Aldrich. Chemicals for preparing buffer solutions were obtained from Sigma-Aldrich. 5-iodouracil PNA ester **21** was synthesized by using method reported in chapter 2. Boc-and Fmoc-protected *aeg*-PNA monomers were purchased from ASM Research Chemicals. The exocyclic amino group of adenine, guanine, and cytosine of Boc-PNA monomers the with cbz (Z) group. While, Fmoc-PNA monomers was protected with Bhoc group. 4-Methylbenzhydrylamine•HCl (MBHA) resin LL (100-200 mesh) and Boc-Lys(2-Cl-Z)-OH were obtained from Novabiochem. Rink amide AM resin (100-200 mesh) was purchased from GL Biochem (Shanghai) Ltd. Autoclaved water was used in all biochemical reactions.

5.4.2 Instrumentation

NMR spectra were recorded on a 400 MHz Jeol ECS-400 spectrometer (^{1}H 400 MHz and ^{13}C 100 MHz) and processed in Mnova NMR software from Mestrelab Research. All mass measurements were recorded on an Applied Biosystems 4800 Plus MALDI-TOF/TOF analyzer instrument and Water Synapt G2 High Definition mass spectrometers. Reversed-phase (RP) flash chromatography (C18 RediSepRf column) purifications were carried out using Teledyne ISCO, Combi Flash *Rf*. Microwave reactions were performed using CEM discover microwave synthesizer. PNA oligomers were purified by using Agilent Technologies 1260 Infinity HPLC. Absorption spectra were recorded on a Shimadzu UV-2600 spectrophotometer.

5.4.3 Synthesis of azide and alkyne modified PNA monomers.

Ethyl 2-(5-iodo-2,4-dioxo-3,4-dihydropyrimidin-1(2*H*)-yl)acetate 2

To a suspension of iodouracil **1** (3.97 g, 16.69 mmol, 1.0 equiv.) and K_2CO_3 (2.31 g, 16.69 mmol, 1.0 equiv.) in DMF (99 mL) was added ethyl bromo acetate (1.86 mL, 16.69 mmol, 1.0 equiv.) drop wise. The reaction mixture was vigorously stirred for 12 h at room temperature (RT). The DMF was evaporated using rotary evaporator with high vacuum pump and then water (100 mL) was added and the product was extracted using EtOAc (2 × 100 mL). The organic layer was evaporated and residue was purified by silica gel column chromatography to afford the product **2** as a white solid (3.23 g, 59%). R_f = 0.43 (Hexane:EtOAc = 5:5); ^{1}H-NMR (400 MHz, d_6-DMSO): δ = 11.81 (br, 1H), 8.21 (s,1H), 4.50 (s, 2H), 4.15 (q, *J* = 7.2 Hz , 2H), 1.21 (t, *J* = 7.2 Hz, 3H) ppm; ^{13}C-NMR (100 MHz, d_6-DMSO): δ = 167.9, 161.0, 150.6, 150.0, 68.2, 61.2, 48.5, 14.0 ppm; HRMS: (*m/z*): Calcd. for $C_8H_{10}IN_2O_4$: 324.9685 $[M+H]^+$; found: 324.9685. (Note: trace amount of acetone impurity was present).

Ethyl 2-(5-(octa-1,7-diyn-1-yl)-2,4-dioxo-3,4-dihydropyrimidin-1(2*H*)-yl)acetate 3

A mixture of 5-iodouracil ester **2** (0.71 g, 2.19 mmol, 1.0 equiv.), CuI (0.083 g, 0.438 mmol, 0.2 equiv.), tetrakis(triphenylphosphine) palladium(0) (0.25 g, 0.22 mmol, 0.1 equiv.) were kept in the vacuum for 30 min. Degassed anhydrous THF (10.6 mL) was then added to above mixture under nitrogen atmosphere. Finally, octa-1,7-diyne (1.45 mL, 11.0 mmol, 5.0 equiv.) and DIPEA (1.10 mL, 7.67 mmol, 3.5 equiv.) were added drop wise to above solution. The reaction mixture was then stirred for 12 h at RT and filtered through Celite pad. Celite pad was washed with THF (2 x 10 mL). THF was evaporated and the residue was purified by silica gel column chromatography to afford the product **3** as a faint brown solid (0.31 g, 47%). R_f = 0.43 (Hexane:EtOAc = 5:5); ^{1}H-NMR (400 MHz, $CDCl_3$): δ = 8.82 (br, 1H), 7.31 (s, 1H), 4.45 (s, 2H), 4.26 (q, *J* = 7.2 Hz, 2H), 2.43 (t, *J* = 6.6 Hz, 2H), 2.23 (td, *J* = 6.8 Hz and 2.8 Hz, 2H), 1.95 (t, *J* = 2.8 Hz, 1H), 1.70–1.63 (m, 4H), 1.30 (t, *J* = 7.2 Hz, 3H) ppm; ^{13}C-NMR (100 MHz, $CDCl_3$): δ = 167.1, 161.9, 149.8, 146.1, 101.4, 95.3, 84.2, 71.1, 68.7, 62.5, 49.1, 27.7, 27.5, 19.3, 18.1, 14.2 ppm; HRMS: Calcd. for $C_{16}H_{18}N_2O_4Na$: 325.1164 $[M+Na]^+$; found: 325.1157.

2-(5-(Octa-1,7-diyn-1-yl)-2,4-dioxo-3,4-dihydropyrimidin-1(2*H*)-yl)acetic acid 4

To a solution of compound **3** (0.14 g, 0.46 mmol, 1.0 equiv.) in THF (5.6 mL) at 0 °C, lithium hydroxide (10% solution in H_2O, 2.8 mL) was added dropwise and the reaction

mixture was further stirred for 3 h at RT. Solvent was evaporated to dryness, and residue was dissolved in water (20 mL) and washed with diethyl ether (15 ml). To the aqueous extract was added saturated $KHSO_4$ solution (~5 mL) to adjust the pH ~5 and product was precipitated out as faint yellow solid **4** (0.11 g, 86%). R_f = 0.27 (MeOH: EtOAc = 3:7); ^{1}H-NMR (400 MHz, d_6-DMSO): δ = 11.63 (s, 1H), 7.97 (s, 1H), 4.40 (s, 2H), 2.76 (br, 1H), 2.41–2.38 (m, 2H), 2.21–2.16 (m, 2H), 1.57 (br, 4H) ppm; ^{13}C-NMR (100 MHz, d_6-DMSO): δ = 169.3, 162.3, 150.0, 148.4, 98.0, 92.9, 84.3, 72.6, 71.4, 48.7, 27.2, 27.1, 18.2, 17.3 ppm; HRMS: (*m/z*): Calcd. for $C_{14}H_{14}N_2O_4K$: 313.0591 $[M+K]^+$; found: 313.0506.

***tert*-Butyl *N*-(2-((((9*H*-fluoren-9-yl)methoxy)carbonyl)amino)ethyl)-*N*-(2-(5-(octa-1,7-diyn-1-yl)-2,4-dioxo-3,4-dihydropyrimidin-1(2*H*)-yl)acetyl)glycinate 6**

A mixture of compound **4** (0.167 g, 0.61 mmol, 1.2 equiv.), Fmoc PNA backbone **5** (0.220 g, 0.51 mmol, 1.0 equiv.), EDC (0.117 g, 0.61 mmol, 1.2 equiv.) and HOBt (0.082 g, 0.61 mmol, 1.2 equiv.) were kept in the vacuum for 30 min. Degassed dry DMF (3.34 mL) was then added to above mixture under nitrogen atmosphere. Finally, DIPEA (0.21 mL, 1.22 mmol, 2.0 equiv.) was then added to above reaction mixture drop wise. Then reaction was stirred for 12 h at RT under nitrogen atmosphere. Solvent was then evaporated and residue was purified using silica gel chromatography with hexane and ethyl acetate solvent system to afford off white solid **6** (0.181 g, 72%). R_f = 0.56 (EtOAc); ^{1}H-NMR (400 MHz, $CDCl_3$): δ = 7.75 (d, *J* = 7.6 Hz, 2H), 7.60 (t, *J* = 6.8 Hz, 2H), 7.41–7.36 (m, 2H), 7.30 ($_{app}$t, *J* = 8.0 and 6.8 Hz, 2H), 7.26 (s, 1H), 5.95 (ma.) and 5.41 (mi.) (br, 1H), 4.49–4.36 (m, 4H), 4.23–4.19 (m, 1H), 4.06 (mi.) and 3.94 (ma.) (s, 2H), 3.57–3.49 (m, 2H), 3.39–3.35 (m, 2H), 2.38–2.37 (m, 2H), 2.21–2.19 (m, 2H), 1.94 (m, 1H), 1.65–1.64 (br, 4H), 1.50 (ma.) and 1.46 (mi.) (s, 9H) ppm; ^{13}C-NMR (100 MHz, $CDCl_3$): δ = 168.8, 168.5, 162.0, 147.3, 147.0, 144.1, 143.9, 141.5, 127.9, 127.8, 127.2, 125.3, 125.1, 120.1, 100.9, 100.7, 94.9, 84.2, 84.0, 82.9, 77.4, 71.4, 68.7, 66.9, 50.0, 49.1, 48.1, 47.4, 28.2, 27.7, 27.6, 19.3, 18.1 ppm; HRMS: (*m/z*): Calcd. for $C_{37}H_{40}N_4O_7Na$: 675.2794 $[M+Na]^+$; found: 675.2796.

***N*-(2-((((9*H*-Fluoren-9-yl)methoxy)carbonyl)amino)ethyl)-*N*-(2-(5-(octa-1,7-diyn-1-yl)-2,4-dioxo-3,4-dihydropyrimidin-1(2*H*)-yl)acetyl)glycine 7**

A solution of compound **6** (0.285 g, 0.44 mmol, 1.0 equiv.) in dry CH_2Cl_2 (5.7 mL) was added TFA (4.2 mL) under stirring at 0 °C. Reaction mixture was stirred at RT for 2 h. Solvent was evaporated to dryness using NaOH trap, and residue was co-evaporated using CH_2Cl_2 (3 x 20 mL) to afford product **7** as white solid (178 mg, 69%). R_f = 0.22 (CH_2Cl_2:

MeOH = 9:1); ^{1}H-NMR (400 MHz, d_6-DMSO): δ = 11.56 (br, 1H), 7.88 (d, *J* = 7.6 Hz, 2H), 7.74–7.60 (m, 4H), 7.41 (d, *J* = 7.2 Hz, 2H), 7.33 (d, *J* = 7.2 Hz, 2H), 6.28 (mi.) and 5.75 (ma.) (s,1H), 4.66 (mi.) and 4.53 (ma.) (s, 2H), 4.30 (mi.) and 4.22 (ma.) (s, 2H), 3.77–3.75 (br, 2H), 3.26–3.13 (m, 4H), 2.75 (s, 1H), 2.30 (br, 2H), 2.15 (br, 2H), 1.51 (br, 4H) ppm; ^{13}C-NMR (100 MHz, d_6-DMSO): δ = 168.0, 162.3, 150.0, 148.8, 142.5, 139.4, 137.4, 128.9, 127.2, 121.3, 120.0, 109.6, 97.8, 92.7, 84.2, 79.3, 78.9, 78.6, 72.8, 71.3, 54.8, 53.2, 48.2, 46.7, 36.8, 27.2, 27.1, 18.2, 17.2 ppm; HRMS: (*m/z*): Calcd. for $C_{33}H_{32}N_4O_7Na$: 619.2168 $[M+Na]^+$; found: 619.2170.

3,6,9,12-Tetraoxapentadec-14-yn-1-ol 9

To a solution of tetraethylene glycol **8** (12.0 g, 61.78 mmol, 1.0 equiv.) in degassed dry THF (100 mL) at 0 °C under nitrogen atmosphere was added 60% sodium hydride (1.61 g, 40.16 mmol, 0.65 equiv.). The mixture was stirred at 0 °C for 30 min under nitrogen. Finally, 80% propargyl bromide solution in toluene (3.44 mL, 30.89 mmol, 0.5 equiv.) was added slowly to the reaction flask. The mixture was stirred at 0 °C for 2 h and at RT for 12 h. Reaction mixture was poured into water (100 mL), extracted with CH_2Cl_2 (2 x 100 mL) and dried over sodium sulphate. The crude product was purified by silica gel chromatography eluting with CH_2Cl_2 and MeOH solvent system to afford **9** as a yellow oil (5.80 g, 40%). R_f = 0.53 (CH_2Cl_2: MeOH = 8:2); ^{1}H-NMR (400 MHz, $CDCl_3$): δ = 4.19 (d, *J* = 2 Hz, 2H), 3.12–3.67 (m, 6H), 3.65 (s,8H), 3.59 ($_{app}$t, *J* = 4.8 and 4.0 Hz, 2H), 2.42 (br, 1H) ppm; ^{13}C-NMR (100 MHz, $CDCl_3$): δ = 79.7, 74.7, 72.7, 70.7, 70.5, 70.4, 69.2, 61.9, 58.7 ppm; HRMS: (*m/z*): Calcd. for $C_{11}H_{20}O_5Na$: 255.1208 $[M+Na]^+$; found: 255.1207.

3,6,9,12-Tetraoxapentadec-14-yn-1-yl 4-methylbenzenesulfonate 10

A mixture of compound **9** (3.15 g, 13.56 mmol, 1.0 equiv.) in CH_2Cl_2 was cooled to 0 °C, and tosyl chloride (5.17 g, 27.12 mmol, 2.0 equiv.) was then added to it slowly under a nitrogen atmosphere. Finally, triethyl amine (4.72 mL, 33.90 mmol, 2.5 equiv.) was added drop wise under stirring in a nitrogen atmosphere. The reaction mixture was stirred at RT for 12 h. Organic layer was washed with water (2 x 20 mL). The organic layer was separated, dried over anhydrous sodium sulphate and evaporated using rotary evaporator. The crude product was purified using silica gel chromatography with hexane and ethyl acetate solvent system to afford the product **10** as a pale yellow oil (3.43 g, 65%). R_f = 0.36 (Hexane: EtOAc = 5:5); ^{1}H-NMR (400 MHz, $CDCl_3$): δ = 7.79 (d, *J* = 8.4 Hz, 2H), 7.33 (d, *J* = 8.8 Hz, 2H), 4.20–4.18 (m, 2H), 4.16–4.14 (m, 2H), 3.69–3.62 (m, 11H), 3.58 (s,3H), 2.44 (s, 3H), 2.43–

2.41 (m, 1H) ppm; ^{13}C-NMR (100 MHz, $CDCl_3$): δ = 144.9, 133.2, 129.9, 128.1, 79.8, 74.6, 70.9, 70.7, 70.5, 69.4, 69.3, 68.8, 58.5, 21.7 ppm; HRMS: (*m/z*): Calcd. for $C_{18}H_{26}O_7SNa$: 409.1296 $[M+Na]^+$; found: 409.1299.

***tert*-Butyl 3-(2-ethoxy-2-oxoethyl)-5-iodo-2,6-dioxo-3,6-dihydropyrimidine-1(2*H*)-carboxylate 11**

To a mixture of compound **2** (0.339 g, 1.04 mmol, 1.0 equiv.) and DMAP (0.254 g, 2.08 mmol, 2.0 equiv.) was added dry THF (3.39 mL) at 0 °C under nitrogen atmosphere. The $(Boc)_2O$ (0.45 mL, 2.08 mmol, 2.0 equiv.) was further added to above mixture slowly and allowed to react at RT for 18 h. Reaction mixture was concentarted and residue was dissolved in CH_2Cl_2 (100 mL) and washed with water (2 x 50 mL). The organic layer was separated, dried over anhydrous sodium sulphate and evaporated using rotary evaporator. The crude product was further purified using silica gel chromatography with hexane and ethyl acetate solvent system to afford product **11** as a light-yellow foam (0.194 g, 44%). R_f = 0.69 (Hexane: EtOAc = 5:5), ^{1}H-NMR (400 MHz, $CDCl_3$): δ = 7.56 (s, 1H), 4.47 (s, 2H), 4.27 (q, *J* = 7.2 Hz, 2H), 1.60 (s, 9H), 1.31 (t, *J* = 7.2 Hz, 3H) ppm; ^{13}C-NMR (100 MHz, $CDCl_3$): δ = 166.9, 157.9, 148.7, 148.0, 146.8, 87.7, 67.9, 62.7, 49.1, 27.5, 14.2 ppm; HRMS: (*m/z*): Calcd. for $C_{13}H_{18}IN_2O_6$: 425.0210 $[M+H]^+$; found: 425.0208.

***tert*-Butyl 3-(2-ethoxy-2-oxoethyl)-2,6-dioxo-5-(14-(tosyloxy)-3,6,9,12-tetraoxatetradec-1-yn-1-yl)-3,6-dihydropyrimidine-1(2*H*)-carboxylate 12**

A mixture of compound **11** (0.594 g, 1.40 mmol, 1.0 equiv.), tosyl- tetraethylene glycol alkyne **10** (0.814 g, 2.10 mmol, 1.5 equiv.), CuI (0.053 g, 0.28 mmol, 0.2 equiv.), tetrakis(triphenylphosphine) palladium(0) (0.162 g, 0.14 mmol, 0.1 equiv.) were kept in the vacuum for 30 min. The degassed anhydrous THF (8.9 mL) was then added to above mixture under nitrogen atmosphere. Finally, DIPEA (0.68 mL, 4.9 mmol, 3.5 equiv.) were added drop wise to above solution and stirred at RT for 18 h. The reaction mixture was then filtered through Celite pad and Cellite pad was washed with THF (2 x 10 mL). THF was evaporated and the residue was dissolved into EtOAc and extracted with water (2 x 50 mL). The organic layer was separated, dried over anhydrous sodium sulphate and evaporated using rotary evaporator. The crude product was further purified by silica gel column chromatography in hexane and ethyl acetate system to afford the product **12** as off white solid (0.65 g, 68%). R_f = 0.33 (Hexane: EtOAc = 2:8), ^{1}H-NMR (400 MHz, $CDCl_3$): δ = 7.78 (d, *J* = 8.4 Hz, 2H), 7.44 (s, 1H), 7.34 (d, *J* = 8.0 Hz, 2H), 4.47 (s, 2H), 4.36 (s, 2H), 4.24 (q, *J* = 7.2 Hz, 2H), 4.16–

4.13 (m, 2H), 3.71–3.61 (m, 10H), 3.57 (s,4H), 2.43 (s, 3H), 1.58 (s, 9H), 1.28 (t, *J* = 7.2 Hz, 3H) ppm; ^{13}C-NMR (100 MHz, $CDCl_3$): δ = 166.8, 159.3, 148.1, 146.9, 146.7, 145.0, 133.1, 130.0, 128.1, 99.8, 90.7, 87.5, 76.5, 70.8, 70.7, 70.5, 69.4, 69.3, 68.8, 62.6, 59.1, 49.3, 27.5, 21.7, 14.2 ppm; HRMS: Calcd. for $C_{31}H_{42}N_2O_{13}SNa$: 705.2305 $[M+Na]^+$; found: 705.2295.

Ethyl 2-(5-(1-azido-3,6,9,12-tetraoxapentadec-14-yn-15-yl)-2,4-dioxo-3,4-dihydropyrimidin-1(2*H*)-yl)acetate 13

A mixture of compound **12** (0.44 g, 0.64 mmol, 1.0 equiv.) and NaN_3 (0.125 g, 1.92 mmol, 3.0 equiv.) in dry DMF (4.4 mL) was heated at 60 °C for 12 h under nitrogen atmosphere. The DMF was evaporated to dryness using high vacuum pump and residue was dissolved in EtOAc. EtOAc layer was further washed with water to remove unreacted NaN_3. Finally, organic layer was separated, dried over anhydrous sodium sulphate and evaporated using rotary evaporator. Crude product was then purified using silica gel chromatography with a gradient from 50% to 95% EtOAc in hexane to afford the product **13** as pale yellow thick oil (0.127 g, 44%). R_f = 0.23 (Hexane: EtOAc = 2:8); ^{1}H-NMR (400 MHz, $CDCl_3$): δ = 8.70 (br, 1H), 7.43 (s, 1 H), 4.46 (s, 2H), 4.39 (s, 2H), 4.26 (q, *J* = 7.2 Hz, 2H), 3.73–3.71 (m, 2H), 3.69–3.66 (m, 12H), 3.39 (t_{app}, *J* = 5.2 and 4.8 Hz, 2H), 1.31 (t, *J* = 7.2 Hz, 3H) ppm; ^{13}C-NMR (100 MHz, $CDCl_3$): δ = 167.0, 161.4, 149.6, 147.5, 100.1, 90.5, 70.8, 70.7, 70.5, 70.1, 69.4, 62.6, 59.2, 50.8, 49.2, 14.2 ppm; HRMS: (*m/z*): Calc. for $C_{19}H_{27}N_5O_8Na$: 476.1757 $[M+Na]^+$; found: 476.1760. (**Note:** during the course of reaction we observed deprotection of Boc-group, this was possibly due to the generation of p-toulene sulphonic acid as by product).

2-(5-(1-Azido-3,6,9,12-tetraoxapentadec-14-yn-15-yl)-2,4-dioxo-3,4-dihydropyrimidin-1(2*H*)-yl)acetic acid 14

Lithium hydroxide (10% solution in H_2O, 1.2 mL) was added to a solution of compound **13** (0.12 g, 0.26 mmol, 1.0 equiv.) in THF (4.8 mL) and the reaction mixture was stirred for 3 h at RT. The reaction mixture was evaporated to dryness, the residue was redissolved in water (15 mL) and washed with diethyl ether (10 ml). To the aqueous phase saturated $KHSO_4$ solution (~3 mL) was added to adjust the pH to ~4. The product was then extracted in EtOAc (2 × 40 mL) and solvent was evaporated to afford the product **14** as off white solid (0.098 g, 87%). R_f = 0.06 (CH_2Cl_2:MeOH = 9:1); ^{1}H-NMR (400 MHz, d_6-DMSO): δ = 11.74 (br, 1H), 8.11 (s, 1H), 4.42 (s, 2H), 4.34 (s, 2H), 3.61–3.58 (m, 4H), 3.56–3.52 (m, 10H), 3.39 (t, *J* = 4.8 Hz, 2H) ppm; ^{13}C-NMR (100 MHz, d_6-DMSO): δ = 169.1, 162.0, 149.9, 149.6, 96.9,

88.8, 78.1, 69.8, 69.7, 69.5, 69.2, 68.5, 58.1, 50.0, 48.8 ppm; HRMS: Calcd. for $C_{17}H_{23}N_5O_8Na$: 448.1444 $[M+Na]^+$; found: 448.1455.

***tert*-Butyl *N*-(2-((((9H-fluoren-9-yl)methoxy)carbonyl)amino)ethyl)-*N*-(2-(5-(1-azido-3,6,9,12-tetraoxapentadec-14-yn-15-yl)-2,4-dioxo-3,4-dihydropyrimidin-1(2*H*)-yl)acetyl)glycinate 15**

A mixture of compound **14** (0.170 g, 0.40 mmol, 1.2 equiv.), Fmoc PNA backbone **5** (0.143 g, 0.33 mmol, 1.0 equiv.) and EDC (0.077 g, 0.40 mmol, 1.2 equiv.) were kept in the vacuum for 30 min. The degassed anhydrous DMF (3.4 mL) was then added to above mixture under nitrogen atmosphere. Finally, DIPEA (0.12 mL, 0.66 mmol, 2.0 equiv.) was added drop wise to above reaction mixture. Then reaction mixture was stirred for 12 h at RT under nitrogen atmosphere. Solvent was then evaporated and residue was redissolved in EtOAc. EtOAc layer was further washed with water. The organic layer was separated, dried over anhydrous sodium sulphate and evaporated using rotary evaporator. The crude product was then purified by silica gel column chromatography with a gradient from 40% to 95% EtOAc in hexane to afford the product **15** as a white solid (0.095 g, 30%). R_f = 0.34 (EtOAc); ^{1}H-NMR (400 MHz, $CDCl_3$): δ = 8.63 (br, 1H), 7.75 (d, *J* = 7.6 Hz, 2H), 7.59 (t_{app}, *J* = 7.2 and 6.8 Hz, 2H), 7.46–7.28 (m, 5H), 5.91 (ma.) and 5.38 (mi.) (t_{app}, *J* = 5.6 and 4.8 Hz, 1H), 4.49–4.35 (m, 5H), 4.23–4.20 (m, 1H), 4.05 (mi.) and 3.94 (ma.) (s, 1H), 3.72–3.65 (m, 14H), 3.56–3.47 (m, 2H), 3.38 (t, *J* = 4.8 Hz, 4H), 1.74 (br, 2H), 1.50 (ma.) and 1.47 (mi.) (s, 9H) ppm; ^{13}C-NMR (100 MHz, $CDCl_3$): δ = 168.7, 168.4, 161.6, 156.8, 149.8, 148.7, 144.1, 143.9, 141.4, 127.9, 125.3, 125.1, 120.2, 120.1, 99.5, 90.2, 84.0, 83.0, 77.4, 70.8, 70.7, 70.5, 70.1, 69.3, 59.2, 50.8, 50.0, 49.1, 48.2, 47.4, 31.1, 28.2 ppm; HRMS: Calcd. for $C_{40}H_{49}N_7O_{11}Na$: 826.3387 $[M+Na]^+$; found: 826.3386.

***N*-(2-((((9*H*-Fluoren-9-yl)methoxy)carbonyl)amino)ethyl)-*N*-(2-(5-(1-azido-3,6,9,12-tetraoxapentadec-14-yn-15-yl)-2,4-dioxo-3,4-dihydropyrimidin-1(2*H*)-yl)acetyl)glycine 16**

A solution of compound **15** (0.09 g, 0.11 mmol, 1.0 equiv.) in dry CH_2Cl_2 (4.0 mL) was added TFA (2 mL) under stirring at 0 °C. Reaction mixture was stirred at RT for 3h and solvent was evaporated to dryness using NaOH trap. The residue was co-evaporated using CH_2Cl_2 (3 x 20 mL) and redissolved in water. Aqueous layer was washed with diethyl ether and acidified using saturated $KHSO_4$ solution (~3 mL) to adjust the pH to ~4. The product was extracted in EtOAc and solvent was evaporated to afford **16** as white solid (65 mg, 77%).

R_f = 0.11 (CH_2Cl_2: MeOH = 9:1); ^{1}H-NMR (400 MHz, d_6-DMSO): δ = 11.68 (br, 1H), 7.94–7.88 (m, 3 H), 7.68 (d, J = 7.2 Hz, 2H), 7.43–7.26 (m, 6H), 4.72 (ma.) and 4.55 (mi.) (s, 2H), 4.34–4.28 (m, 4H), 4.23 (t, J = 6.4 Hz, 1H), 4.18 (mi.) and 3.99 (ma.) (s, 2H), 3.60–3.51 (m, 12H), 3.39–3.38 (m, 4H), 3.14–3.11 (m, 2H), 1.23 (br, 2H) ppm; ^{13}C-NMR (125 MHz, d_6-DMSO): δ = 170.3, 167.3, 166.9, 162.1, 156.3, 156.1, 150.1, 150.0, 143.9, 140.7, 127.6, 127.1, 125.1, 120.1, 96.7, 88.8, 78.2, 69.8, 69.7, 69.5, 69.2, 68.5, 65.5, 58.1, 54.9, 50.0, 48.1, 47.7, 46.7, 30.7 ppm; HRMS: Calcd. for $C_{36}H_{41}N_7O_{11}Na$: 770.2761 $[M+Na]^+$; found: 770.2754.

_N_-(2-((_tert_-Butoxycarbonyl)amino)ethyl)-_N_-(2-(5-iodo-2,4-dioxo-3,4-dihydropyrimidin-1(2_H_)-yl)acetyl)glycine 22

Lithium hydroxide (10% solution in H_2O, 6.2 mL) was added to a solution of compound **21** (0.62 g, 1.18 mmol, 1.0 equiv.) in THF (12.4 mL) under stirring at 0 °C and further reaction mixture was stirred for 3 h at RT. The reaction mixture was evaporated to dryness, the residue was redissolved in water (15 mL) and washed with diethyl ether (10 ml). To the aqueous phase saturated $KHSO_4$ solution (~3 mL) was added to adjust the pH to ~5. The product was then extracted in EtOAc (2 × 40 mL) and solvent was evaporated to afford the product **22** as off white solid (0.532 g, 91%). R_f = 0.23 (CH_2Cl_2: MeOH = 8:2); ^{1}H-NMR (400 MHz, d_6-DMSO): δ = 12.70 (br, 1H), 11.71 (ma.) and 11.69 (mi.) (s, 1H), 8.01 (ma.) and 7.97 (mi.) (s, 1H), 6.93 (ma.) and 6.73 (mi.) ($_{app}$t, J = 5.6 and 5.2 Hz, 1H), 4.71 (ma.) and 4.53 (mi.) (s, 2H), 4.18 (mi.) and 3.98 (ma.) (s, 2H), 3.40–3.30 (m, 2H), 3.19–3.01 (m, 2H), 1.39 (ma.) and 1.38 (mi.) (s, 9H) ppm; ^{13}C-NMR (100 MHz, d_6-DMSO): δ = 170.7 (mi.) and 170.4 (ma.), 167.3 (mi.) and 166.9 (ma.), 161.1, 155.7, 150.7 (ma.) and 150.4 (mi.), 78.1, 67.8, 54.9, 47.8, 47.6, 46.8, 37.9, 28.2 ppm; HRMS: Calcd. for $C_{15}H_{22}IN_4O_7$: 497.0533 $[M+H]^+$; found: 497.0535.

5.4.4 Solid phase synthesis of alkyne- and azide- modified PNA oligomers by Fmoc chemistry

All alkyne- and azide-modified PNA oligomers were synthesized by applying standard solid phase PNA synthesis protocol on rink amide resin using Fmoc-protected *aeg*-PNA monomers, alkyne, and azide PNA base analogues and azido acetic acid. In order to enhance aqueous solubility of PNA oligomers, two lysine residue were attached at the C-terminus.

General procedure: In a glass sintered flask, Rink-amide resin (250 mg, 0.65 mmol/g) was swelled in CH_2Cl_2 (8 mL) for 12 h. Then the solvent was removed, and the resin was treated

with 20% piperidine in DMF (6 mL) for 10 min to remove Fmoc-group from resin. This step was repeated two more times. The resin was then washed sequentially with DMF (3 x 3 mL), CH_2Cl_2 (3 x 3 mL), and DMF (3 x 3 mL). The resin was dried under nitrogen flow for few minutes. The coupling reaction was performed in dry DMF (1.8 mL) with Fmoc-Lys(Boc)-OH (36 mg, 1.0 equiv. to obtain a loading of 0.35 mmol/g) in the presence of HOBt (1.0 equiv.), HBTU (1.0 equiv.) and DIPEA (1.0 equiv.) for 7–9 h at RT. The resin was further washed with DMF (3 x 3 mL), CH_2Cl_2 (3 x 3 mL) and DMF (3 x 3 mL). Next, remaining amino groups on the resin was capped with acetic anhydride (1.0 mL) in pyridine (1.0 mL) for 1 h at RT. This step was repeated two more times, and the resin was then washed with DMF (3 x 3 mL), CH_2Cl_2 (3 x 3 mL) and DMF (3 x 3 mL) and dried under nitrogen flow for few minutes. The resin was treated with 20% piperidine in DMF (5 mL) for 10 min to remove Fmoc-group. This step was repeated two more times, and the resin was then washed with DMF (3 x 3 mL), CH_2Cl_2 (3 x 3 mL), and DMF (3 x 3 mL). Then coupling reaction was performed in dry DMF (1.8 mL) with Fmoc-Lys(Boc)-OH (3.0 equiv.) in the presence of HOBt (3.0 equiv.), HBTU (3.0 equiv.) and DIPEA (3.0 equiv.) for 7–9 h at RT. The resin was then washed with DMF (3 x 3 mL), CH_2Cl_2 (3 x 3 mL) and DMF (3 x 3 mL). The resin was dried under nitrogen flow for few minutes.

Above lysine loaded Rink-amide resin (25 mg, 0.35 mmol/g) was swelled in CH_2Cl_2 (2 mL) for 2 h in glass sintered flask. The solvent was removed and the resin was treated with 20% piperidine in DMF (1.0 mL) for 10 min to remove Fmoc-group as mentioned above. The resin was then washed with DMF (3 x 3 mL), CH_2Cl_2 (3 x 3 mL) and DMF (3 x 3 mL). The coupling reaction was performed in dry NMP (0.6 mL) with appropriate Fmco-protected PNA monomers (3.0 equiv.) in the presence of HOBt (3.0 equiv.), HBTU (3.0 equiv.) and DIPEA (3.0 equiv.) for 7–9 h RT. The resin was washed again, and the coupling, Fmoc deprotection, and washing steps were repeated in the cycle as mentioned above to synthesize the desired PNA sequence.

Cleavage procedure: The dried resin (20 mg) was transferred to a glass vial and treated with H_2O (10 μL) and anisole (10 μL) in an ice bath for 10 min. TFA (380 μL) was then added to the above mixture and was stirred for 1.5 h at room temperature. The resin was filtered, and the filtrate was concentrated and precipitated as a white solid by adding cold diethyl ether (1 mL). The solvent was decanted, and the crude product was dissolved in autoclaved water and purified by RP-HPLC.

5.4.5 HPLC analysis of PNA oligomers

All azide and alkyne modified PNA oligomers were purified using a Luna C18 semi-preparative RP column (5 micron, 250 × 10 mm, Phenomenex) on an Agilent Technologies 1260 Infinity HPLC system. Conditions: 0–50% B in 25 min and 50–100% B in 15 min (Mobile phase A: 5% acetonitrile in H_2O containing 0.1% TFA. Mobile phase B: 50% acetonitrile in H_2O containing 0.1% TFA). The flow rate was 2 mL/min. The chromatogram of control PNA oligomers was recorded at 260 nm, and fluorescently modified PNA oligomers was recorded at 260 nm and 330 nm. Concentration of the PNA oligomers were determined by using the molar extinction coefficients of nucleobases at 260 nm (ε_A = 13700, ε_T = 8600, ε_G = 11700, ε_C = 6600 $M^{-1}cm^{-1}$).

5.4.6 MALDI-TOF mass measurement of PNA oligomers

1 μL of a ~150 μM stock solution of PNA oligomer was combined with 2,5-dihydroxybenzoic acid (DHB) or α-cyano-4-hydroxycinnamic acid (CHCA) matrix. The samples were spotted on a plate and air dried before mass analysis.

5.4.7 Bioorthogonal chemical reactions

5.4.7.1 Postsynthetic modification of azide-and alkyne-modified PNA oligomers by CuAAC reaction

The Cu-mix was prepared by mixing a solution of THPTA (4.2 μL, 90 mM), CuSO4 (4.2 μL, 45 mM) and sodium ascorbate (4.2 μL, 90 mM) in water. Above mixture was added to an aqueous solution of alkyne- or azide-modified PNA oligomers **18**/**19**/**20** in water (25 μL, 0.6 mM). Stock solutions (7.5 mM) of azide (**a**–**d**) or alkyne (**e**–**h**) substrates were prepared in DMSO. Azide or alkyne substrates (10 μL, 7.5 mM) were added to respective alkyne or azide-containing individual reaction mix, and the reaction volume was adjusted to 50 μL by adding water. The final concentration of reaction components was the following: THPTA (7.50 mM), $CuSO_4$ (3.75 mM), sodium ascorbate (7.50 mM), PNA oligomer (0.30 mM, 15 nmol), azide or alkyne substrate (1.5 mM) and DMSO (20%). The reaction mixtures were allowed to react at 37 °C for 2 h on thermomixer (500 rpm). The clicked product was purified by RP-HPLC using conditions mentioned above. The corresponding peak for clicked product was isolated and characterized by MALDI-TOF mass analysis. For the structure of clicked products see Scheme 3 and Scheme 4 and for yields and mass data see Table 2.

5.4.7.2 Postsynthetic modification of azide-modified PNA oligomers by copper-free SPAAC reaction with cyclooctyne building blocks of biotin i

A solution of azide-modified PNA oligomers **19/20** in water (12.5 µL, 0.6 mM) was mixed with cyclooctyne substrate **i** (2.25 µL, 10 mM) dissolved in DMSO. The 2.27 µL of DMSO was added to above reaction mixture, and total volume was adjusted to 25 µL by adding water. Final, concentration of PNA oligomers was 0.3 mM (7.5 nmol), cyclooctyne substrate **i** was 0.9 mM, and DMSO was 20 %. The individual reaction mixture was incubated at 37 °C for 1 h, and the clicked product was purified by RP-HPLC using conditions mentioned above. The corresponding peak for clicked product was isolated and characterized by MALDI-TOF mass. For the structure of clicked products see Scheme 5 and for yields and mass data see Table 3.

5.4.7.3 Postsynthetic modification of azide-modified PNA oligomers by Staudinger ligation reaction with biotinylated triaryl phosphine substrate j

A solution of azide-modified PNA oligomers **19/20** (6.0 µL, 1.0 mM) in water was mixed with 50 mM PBS buffer (10 µL, pH 8.0). The biotinylated phosphine substrate **j** (1.2 µL, 50 mM) in DMSO was then added to the above solution and mixed well. Then 8.8 µL of DMSO was added to above reaction mixture. Finally, reaction volume was adjusted to 50 µL by adding water. The final concentration of reaction components was the following: PNA (0.12 mM, 6 nmol), **j** (1.2 mM) and DMSO (20%). The reaction mixture was incubated at 37 °C for 12 h, and the ligated product was purified by RP-HPLC using conditions mentioned above. The corresponding peak for ligated product was isolated and characterized by MALDI-TOF mass. For the structure of ligated products see Scheme 6 and for yields and mass data see Table 3.

5.4.7.4 Postsynthetic chemical functionalization of iodo-modified PNA oligomer 23 by palladium catalyzed Suzuki-Miyaura and Cu-free Sonogashira reactions

Suzuki-Miyaura: A solution of iodo-modified PNA oligomers **23** in water (8.33 µL, 0.6 mM) and boronic acids **k/l** (0.5 µL, 100 mM) in DMSO was mixed with 50 mM PBS buffer (10 µL, pH 8.0). The 9.5 µL of DMSO was added to above reaction mixture and total volume was adjusted to 45 µL by adding water. Finally, palladium catalyst $Pd(OAc)_2$•$(DMG)_2$ (5.0 µL, 10 mM) was added to above reaction mixture. The final concentration of PNA oligomers was 0.1 mM (5.0 nmol), boronic acids **k/l** was 1.0 mM, DMSO was 20 % and reaction volume was 50 µL. The reaction was allowed to react at 40 °C for 4 h on thermomixer (500

rpm) and finally, allowed to react with 3-mercaptopropionic acid (5 mM, 5-equiv. to Pd) for 30 min at 40 °C.

Cu-free Sonogashira: A solution of iodo-modified PNA oligomers **23** in water (8.33 μL, 0.6 mM) and alkyne substrates **e/m** (2.5 μL, 100 mM) in DMSO was mixed with 50 mM Tris-HCl buffer (10 μL, pH 8.5). The 7.5 μL of DMSO was added to above reaction mixture, and total volume was adjusted to 42.5 μL by adding water. Finally, palladium catalyst $Pd(OAc)_2$•$(DMADHP)_2$ (2.5 μL, 10 mM) and sodium ascorbate (5.0 μL, 10 mM) was added to above reaction mixture. The final concentration of PNA oligomers was 0.1 mM (5.0 nmol), alkyne substrates **e/m** was 1.0 mM, DMSO was 20 % and reaction volume was 50 μL. The reaction was allowed to react at 40 °C for 4 h on thermomixer (500 rpm).

Coupled products were purified by RP-HPLC (analytical column) using conditions mentioned above. The corresponding product peaks were isolated and characterized by MALDI-TOF mass. For the structure of coupled products see Scheme 7 and for yields and mass data see Table 5.

5.4.7.5 Postsynthetic labeling of azide- and alkyne-modified PNA-telomere duplexes by CuAAC, SPAAC and Staudinger ligation reactions with cognate biophysical probes

The PNA-telomere duplexes were assembled by heating a 1:1 mixture of PNA oligomers (**24** and **26**) and telomere DNA **29** (0.30 mM) in 10 mM phosphate buffer (pH 7.1, 100 mM NaCl, 0.1 mM EDTA) at 90 ºC for 3 min. Samples were slowly cooled to RT and kept in an ice bath for ~1 h.

CuAAC: Cu-mix was prepared by mixing a solution of THPTA (0.58 μL, 90 mM), $CuSO_4$ (0.58 μL, 45 mM) and sodium ascorbate (0.58 μL, 90 mM) in water. Above mixture was added to alkyne- or azide-modified PNA-telomere duplexes **24•29** and **26•29** (7.0 μL, 0.30 mM), in 10 mM phosphate buffer (pH 7.1, 100 mM NaCl, 0.1 mM EDTA). Finally, azide (**p**) or alkyne (**n**) substrates (1.4 μL, 7.5 mM) were added to above respective alkyne or azide-modified PNA-telomere duplexes (**24•29** and **26•29**) containing individual reaction mix, and the reaction volume was adjusted to 14 μL. The final concentration of reaction components was the following: THPTA (3.75 mM), $CuSO_4$ (1.87 mM), sodium ascorbate (3.75 mM), PNA-telomere duplex (0.15 mM, 2.1 nmol), azide or alkyne substrate (0.75 mM), DMSO (20%) and 10 mM phosphate buffer (pH 7.1, 100 mM NaCl, 0.1 mM EDTA). The reaction mixtures were allowed to react at 37 °C for 2 h on thermomixer (500 rpm). The labeled PNA-telomere duplexes were analyzed by 15% native PAGE. Respective labeled products were visualized by UV-shadowing and UV-transilluminator. For gel picture, please see Figure 7B.

SPAAC: Azide-modified PNA-telomere duplex **26•29** (7.0 μL, 0.30 mM) in 10 mM phosphate buffer (pH 7.1, 100 mM NaCl, 0.1 mM EDTA) was mixed with cyclooctyne substrate (0.63 μL, 10 mM) dissolved in DMSO. The 2.17 μL of DMSO was added to above reaction mixture, and total volume was adjusted to 14 μL by adding water. Final, concentration of PNA-telomere duplex was 0.15 mM (2.1 nmol), cyclooctyne substrate **o** was 0.45 mM, DMSO was 20 % and 10 mM phosphate buffer (pH 7.1, 100 mM NaCl, 0.1 mM EDTA). The individual reaction mixture was incubated at 37 °C for 1 h. The labeled PNA-telomere duplex was analyzed by 15% native PAGE. Respective labeled product was visualized by UV-shadowing and UV-transilluminator. For gel picture please see Figure 7B.

Staudinger ligation: Azide-modified PNA-telomere duplex **26•29** (7.0 μL, 0.30 mM) in 10 mM phosphate buffer (pH 7.1, 100 mM NaCl, 0.1 mM EDTA) was mixed with biotinylated phosphine substrate **j** (0.42 μL, 50 mM) dissolved in DMSO. The 2.38 μL of DMSO was added to above reaction mixture and total volume was adjusted to 14 μL by adding water.

The final concentration of reaction components was the following: azide-modified PNA-telomere duplex (0.15 mM, 2.1 nmol), **j** (1.5 mM), DMSO (20%) and 10 mM phosphate buffer (pH 7.1, 100 mM NaCl, 0.1 mM EDTA). The reaction mixture was incubated at 37 °C for 12 h and the ligated product was analyzed by 15% native PAGE. Respective labeled product was visualized by UV-shadowing. For gel picture, please see Figure 7B.

5.4.8 Fluorescence spectra of labeled PNA oligomer products

Fluorescence experiments were performed in a micro fluorescence cuvette (Hellma, path length 1.0 cm) on Fluoromax-4 spectrophotometer (Horibha Scientific). Emission profile (0.5 μM) of the clicked PNA products (**18a** and **24a)** and naphthalimide-azide substrate (**a**) were obtained by exciting the samples at 455 nm with an excitation and emission slit width of 2 nm and 5 nm, respectively (see Figure 4 and 9). Emission profile (0.5 μM) of the clicked PNA products (**19e**, **20e** and **26e**) and naphthalimide-alkyne substrate (**e**) were obtained by exciting the samples at 362 nm with an excitation and emission slit width of 2 nm and 4 nm, respectively (see Figure 4 and 9). Emission profile (0.5 μM) of the clicked PNA products (**19f**, **20f** and **26f**) and NBD-alkyne substrate (**f**) were obtained by exciting the samples at 473 nm with an excitation and emission slit width of 4 nm and 5 nm, respectively (see Figure 4 and 9).

Emission profile (0.5 μM) of the coupled PNA product **23k**, and benzothiophene-conjugated uracil PNA analogue (^{BT}**U**) were obtained by exciting the samples at 330 nm with an excitation and emission slit width of 7 nm and 9 nm, respectively. While, emission profile

(0.5 μM) of the coupled PNA product **23k**, and naphthalimide-conjugated uracil PNA analogue (^{Nap}**U**) were obtained by exciting the samples at 400 nm with an excitation and emission slit width of 3 nm and 4 nm, respectively (see Figure 6).

5.5 Notes and References

1. a) M. Pooga, T. Land, T. Bartfai, Ü. Langel, *Biomolecular Engineering*, 2001, **17**, 183–192; b) F. Pellestor and P. Paulasova, *Eur. J. Hum. Genet.*, 2004, **12**, 694–700; c) Joseph Wang, *Current Issues Molec. Biol.*, 1999, **1**, 117–122.
2. C. D. Spicer and B. G. Davis, *Nat. Commun.*, 2014, **5**, 4740.
3. a) S. Jin, C. V. Miduturu, D. C. McKinney and S. K. Silverman, *J. Org. Chem.*, 2005, **70**, 4284–4299; b) H. Sahoo, *RSC Adv.*, 2012, **2**, 7017–7029.
4. a) S. S. Ghosh, P. M. Kao, A. W. McCue and H. L. Chappelle, *Bioconjugate Chem*., 1990, **1**, 71–76; b) G. M. Blackburn, M. J. Gait, D. Loakes and D. M. Williams, RSC, UK, 3rd ed., 2006.
5. a) J. A. Prescher, and C. R. Bertozzi, *Nat. Chem. Biol.*, 2005, **1**, 13–21; b) A. G. Neef and C. Schultz, *Angew. Chem. Int. Ed. Engl.*, 2009, **48**, 1498–1500; c) P. M. E. Gramlich, C. T. Wirges, A. Manetto and T. Carell, *Angew. Chem. Int. Ed. Engl.*, 2008, **47**, 8350–8358; d) A. H. El-Sagheer and T. Brown, *Chem. Soc. Rev.*, 2010, **39**, 1388–1405; e) S. S. van Berkel, M. B. van Eldijk and J. C. M. van Hest, *Angew. Chem.Int. Ed.*, 2011, **50**, 8806–8827; f) A. A. Sawant, P. P. Mukherjee, R. K. Jangid, S. Galande and S. G. Srivatsan, *Org. Biomol. Chem.*, 2016, **14**, 5832–5842; g) A. A. Sawant, A. A. Tanpure, P. P. Mukherjee, S. Athavale, A. Kelkar, S. Galande and S. G. Srivatsan, *Nucleic Acids Res.*, 2016, **44**, e16.
6. F. Himo, T. Lovell, R. Hilgraf, V. V. Rostovtsev, L. Noodleman, K. B. Sharpless and V. V. Fokin, *J. Am. Chem. Soc*., 2005, **127**, 210–216.
7. a) K. Gogoi, M. V. Mane, S. S. Kunte and V. A. Kumar, *Nucleic acid Res.*, 2007, **35**, e139; b) A. Manicardi, A. Accetta, T. Tedeschi, S. Sforza, R. Marchelli and R. Corradini, *Artif. DNA: PNA XNA*, 2012, **3**, 1–10; c) A. H. St. Amant, C. Engbers and R. H. E. Hudson, *Artif. DNA: PNA XNA*, 2013, **4**, 4–10; d) J. D. Flory, T. Johnson, C. R. Simmons, S. Lin, G. Ghirlanda and P. Fromme, *Artif. DNA: PNA XNA*, 2014, **5**, 1–8; e) A. Manicardi, E. Gyssels, R. Corradinia and A. Madder, *Chem. Commun.*, 2016, **52**, 6930–6933.
8. a) R. W. Dirks and H. J. Tanke, *Bio Techniques*, 2006, **40**, 489–496; b) J. Guo, J. Ju and N. J. Turro, *Anal. Bioanal. Chem*., 2012, **402**, 3115–3125.
9. (a) J. M. Chalker, C. S. C. Wood and B. G. Davis, *J. Am. Chem. Soc.*, 2009, **131**, 16346–16347; (b) N. Li, R. K. V. Lim, S. Edwardraja, Q. Lin, *J. Am. Chem. Soc.*, 2011, **133**, 15316–15319; c) L. Lercher, J. F. McGouran, B. M. Kessler, C. J. Schofield, and B. G. Davis, *Angew. Chem. Int. Ed.*, 2013, **52**, 10553–10558; d) J. T. George and S. G. Srivatsan, *Bioconjugate Chem.*, **DOI:** 10.1021/acs.bioconjchem.7b00169.
10. R. H. E. Hudson, G. Li and J. Tse, *Tetrahedron Lett.*, 2002, **43**, 1381–1386.
11. See Experimental Section for details.
12. Z. Gao, V. Gouverneur and B. G. Davis, *J. Am. Chem. Soc.*, 2013, **135**, 13612–13615.
13. E. H. Blackburn, *Nat. Struct. Biol.*, 2000, **7**, 847–850.
14. a) R. E. Verdun and J. Karlseder, *Nature*, 2007, **447**, 924–931; b) R. J. O'Sullivan and J. Karlseder, *Nat. Rev. Mol. Cell Biol.*, 2010, **11**, 171–181.
15. P. L. T. Tran, J.-L. Mergny and P. Alberti, *Nucleic Acids Res.*, 2011, **39**, 3282–3294.

16. a) K. Paeschke, T. Simonsson, J. Postberg, D. Rhodes and H. J. Lipps, *Nat. Struct. Mol. Biol.*, 2005, **12**, 847–854; b) K. Paeschke, S. Juranek, T. Simonsson, A. Hempel, D. Rhodes and H. J. Lipps, *Nat. Struct. Mol. Biol.*, 2008, **15**, 598–604.
17. a) G. Biffi, D. Tannahill, J. McCafferty and S. Balasubramanian, *Nat. Chem.*, 2013, **5**, 182–186; b) E. Y. N. Lam, D. Beraldi, D. Tannahill and S. Balasubramanian, *Nat. Commun.*, 2013, **4**, 1796–1804; c) Y. Xu, M. Komiyama, *ChemBioChem*, 2013, **14**, 927–928; d) A. Henderson, Y. Wu, Y. C. Huang, E. A. Chavez, J. Platt, F. B. Johnson, R. M. Brosh Jr., D. Sen and P. M. Lansdrop, *Nucleic Acids Res.*, 2013, **42**, 860–869.
18. a) Y. Gan, K. J. Engelke, C. A. Brown and J. L.-S. Au, *Pharm. Res.*, 2001, **18**, 1655–1659; b) M. Kimura, R. C. Stone, S. C. Hunt, J. Skurnick, X. Lu, X. Cao, C. B. Harley and A. Aviv, *Nat. Protoc.*, 2010, **5**, 1596–1607.
19. a) R. J. Callicott and J. E. Womack, *Comp. Med.*, 2006, **56**, 17–22; b) R. M. Cawthon, *Nucleic Acids Res.*, 2009, **37**, e21; c) M. Yamasuji, T. Shibata, T. Kabashima and M. Kai, *Anal. Biochem.*, 2011, **413**, 50–54.
20. J. G. Hacia, E. A. Novotny, R. A. Mayer, S. A. Woski, M. A. Ashlock and F. S. Collins, *Nucleic Acids Res.*, 1999, **27**, 4034–4039.
21. P. M. Lansdorp, N. P. Verwoerd, F. M. van de Rijke, V. Dragowska, M.-T. Little, R. W. Dirks, A. K. Raap and H. J. Tanke, *Hum. Mol. Genet.*, 1996, **5**, 685–691.
22. A. Ambrus, D. Chen, J. Dai, T. Bialis, R. A. Jones, and D. Yang, *Nucleic Acids Res.*, 2006, **34**, 2723–2735.

5.6 Appendix-III: Characterization data of synthesized compounds

^{1}H-NMR of compound **3** in $CDCl_3$

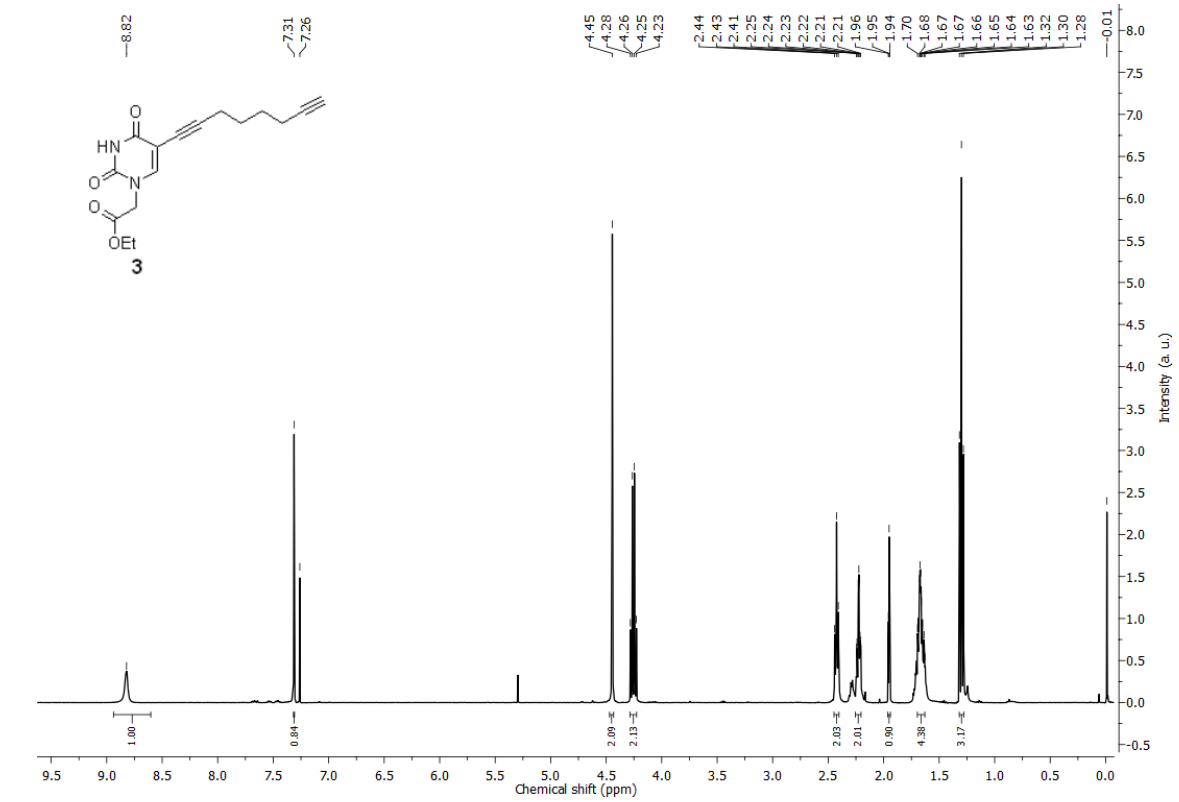

^{13}C-NMR of compound **3** in $CDCl_3$

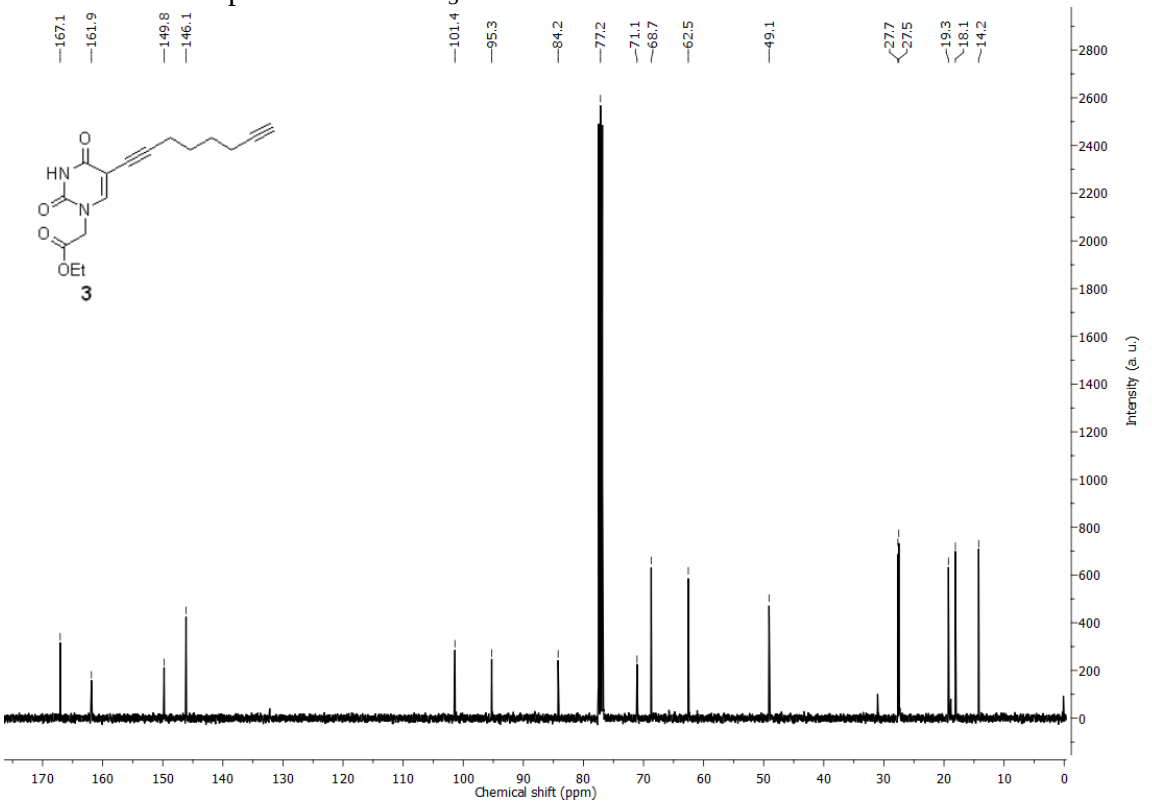

^{1}H-NMR of compound **4** in d_6-DMSO

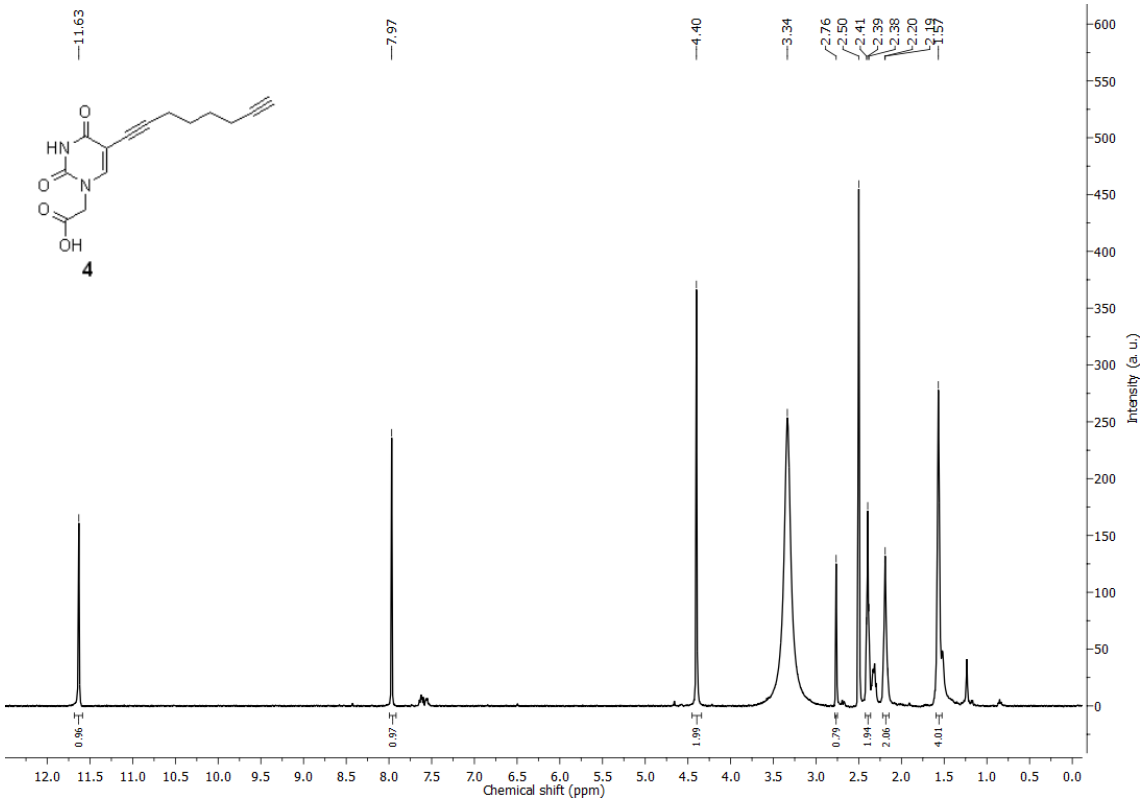

^{13}C-NMR of compound **4** in d_6-DMSO

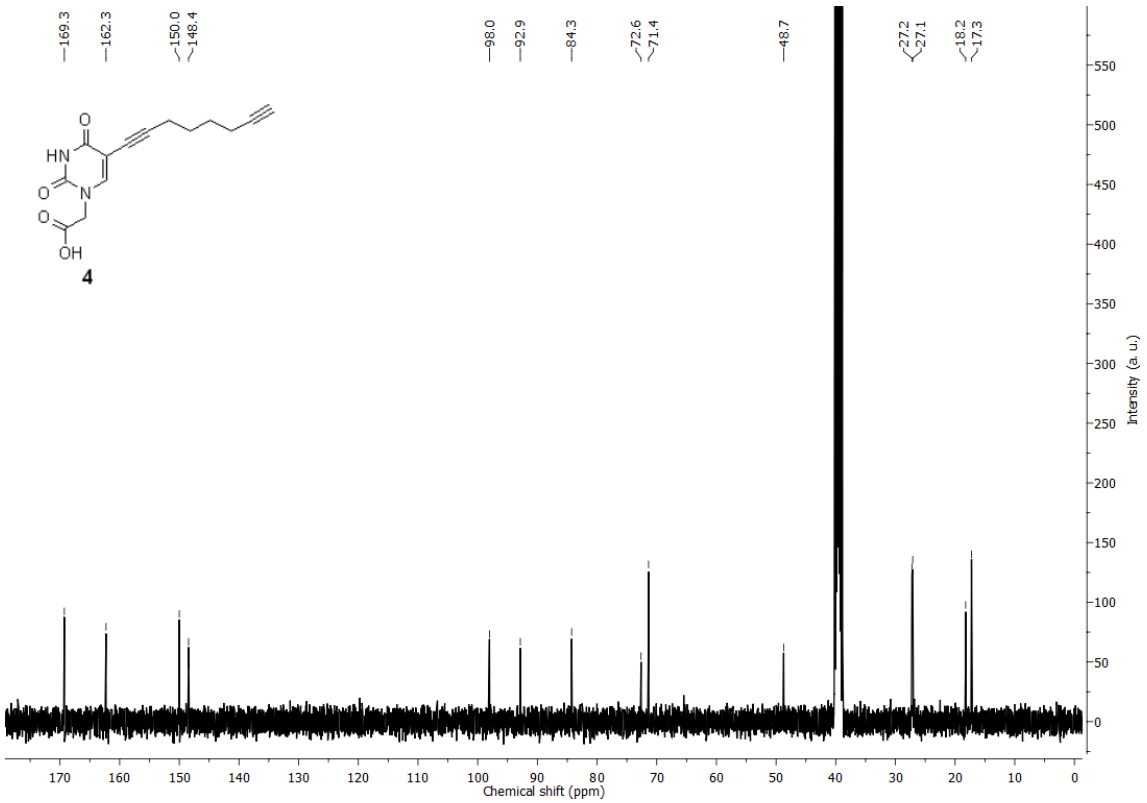

^{1}H-NMR of compound **6** in d_6-DMSO

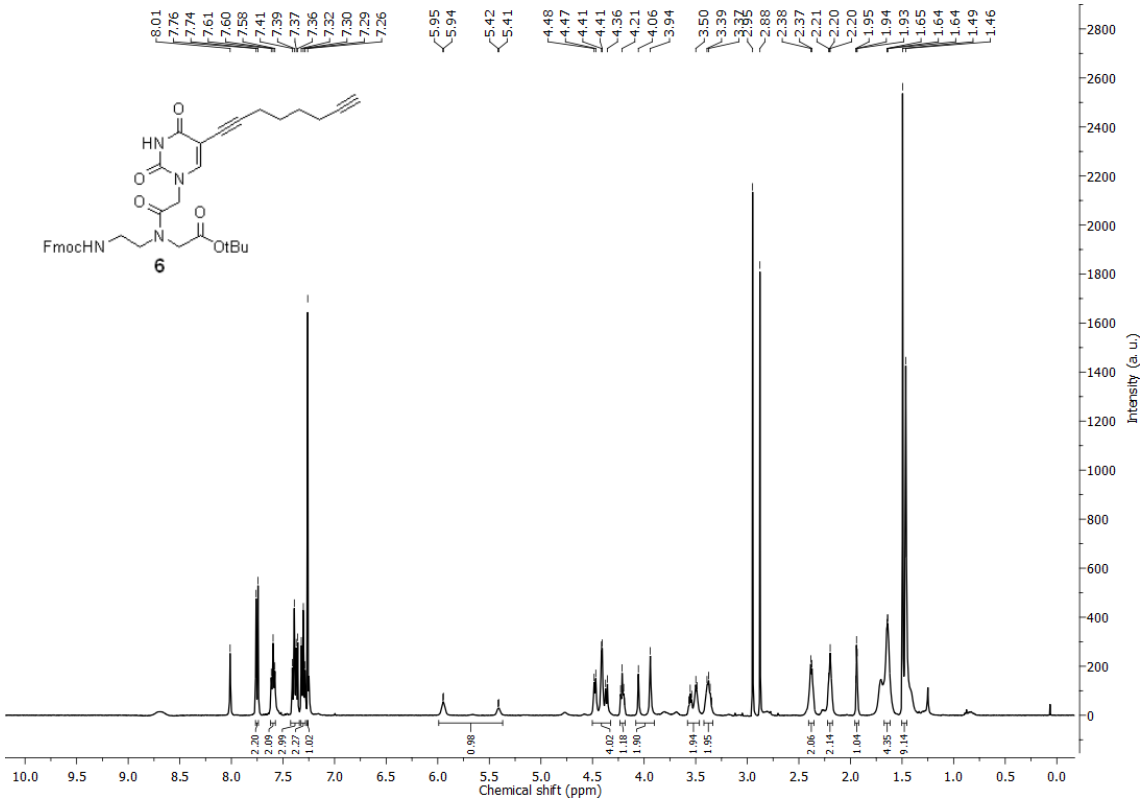

^{13}C-NMR of compound **6** in d_6-DMSO

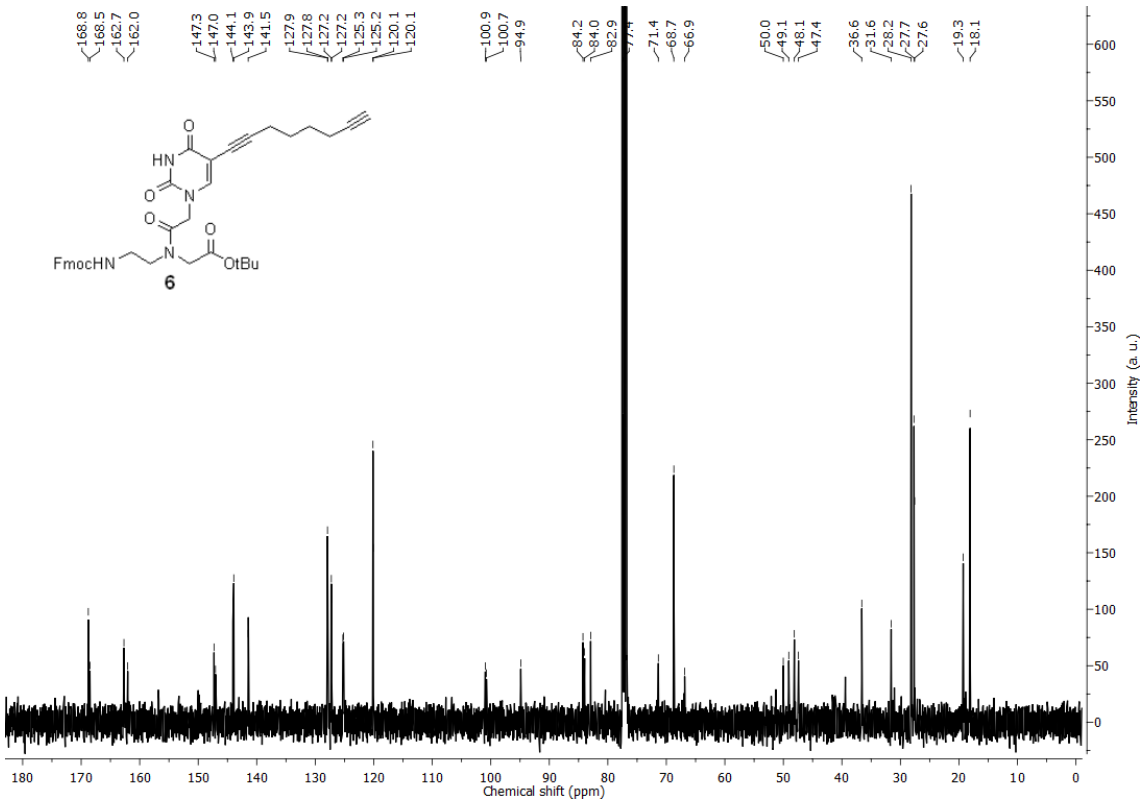

^{1}H-NMR of compound **7** in d_6-DMSO

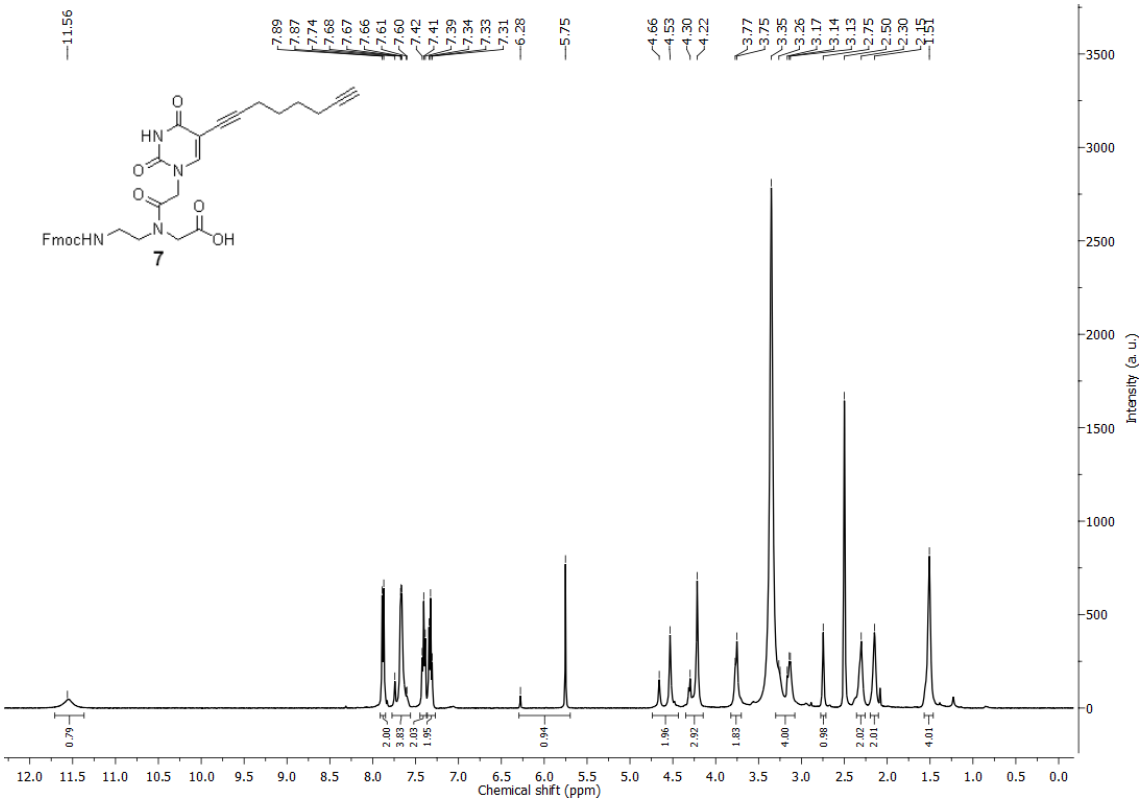

^{13}C-NMR of compound **7** in d_6-DMSO

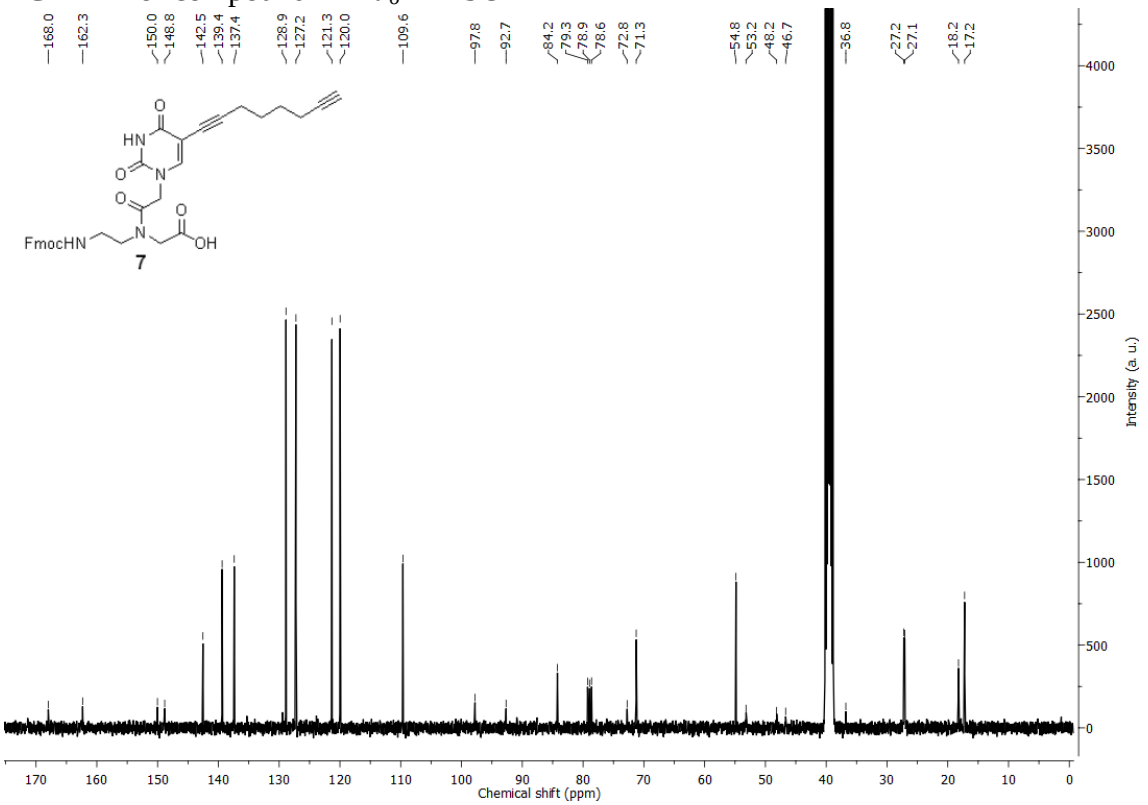

^{1}H-NMR of compound **9** in $CDCl_3$

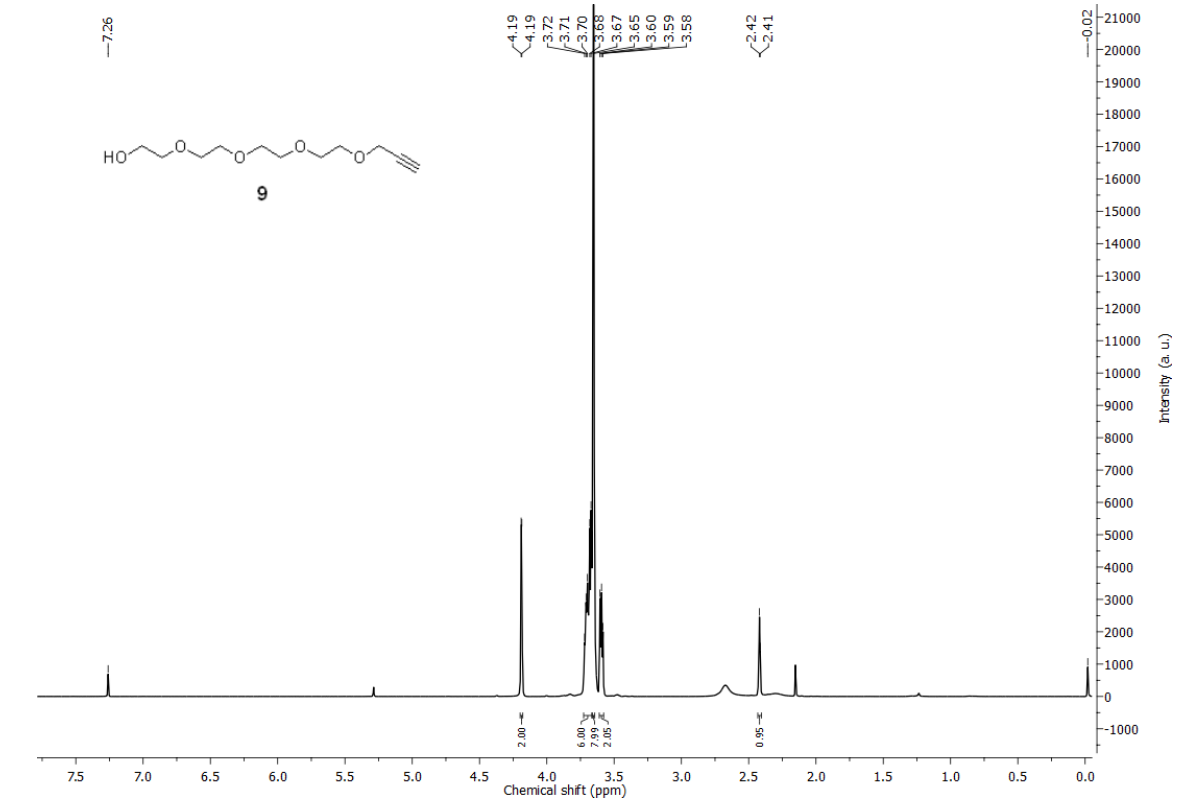

^{13}C-NMR of compound **9** in $CDCl_3$

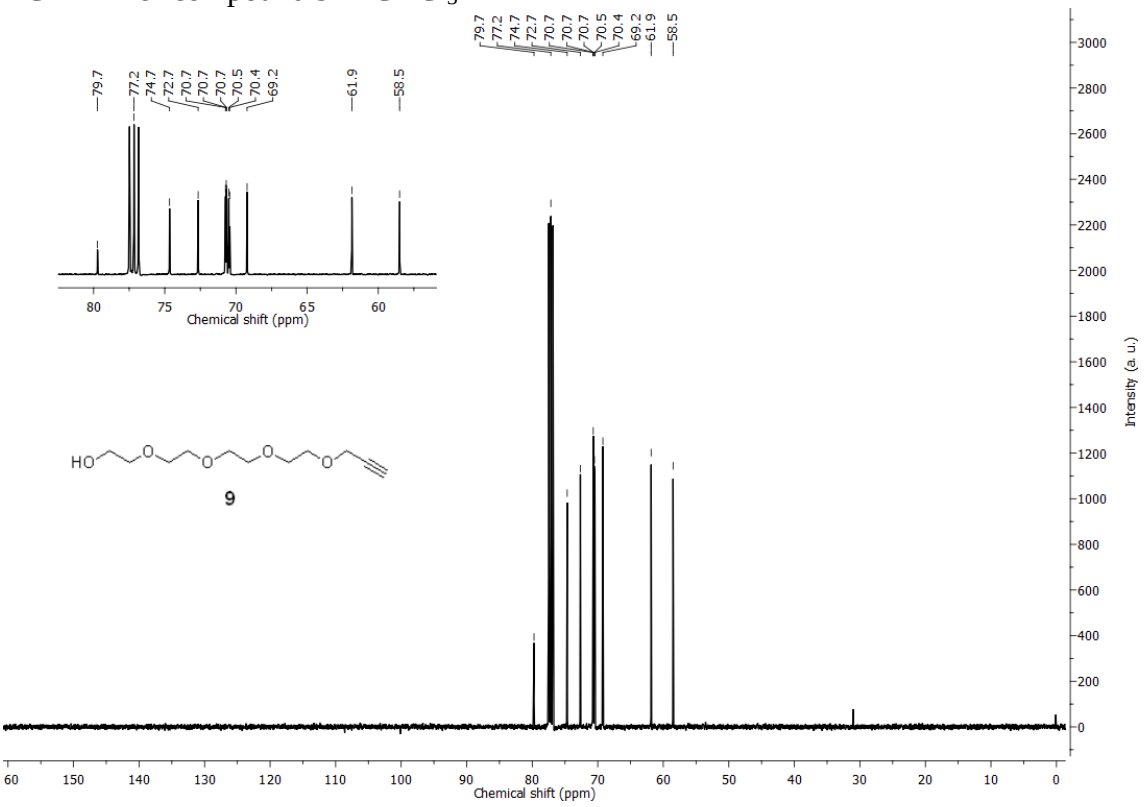

^{1}H-NMR of compound **10** in $CDCl_3$

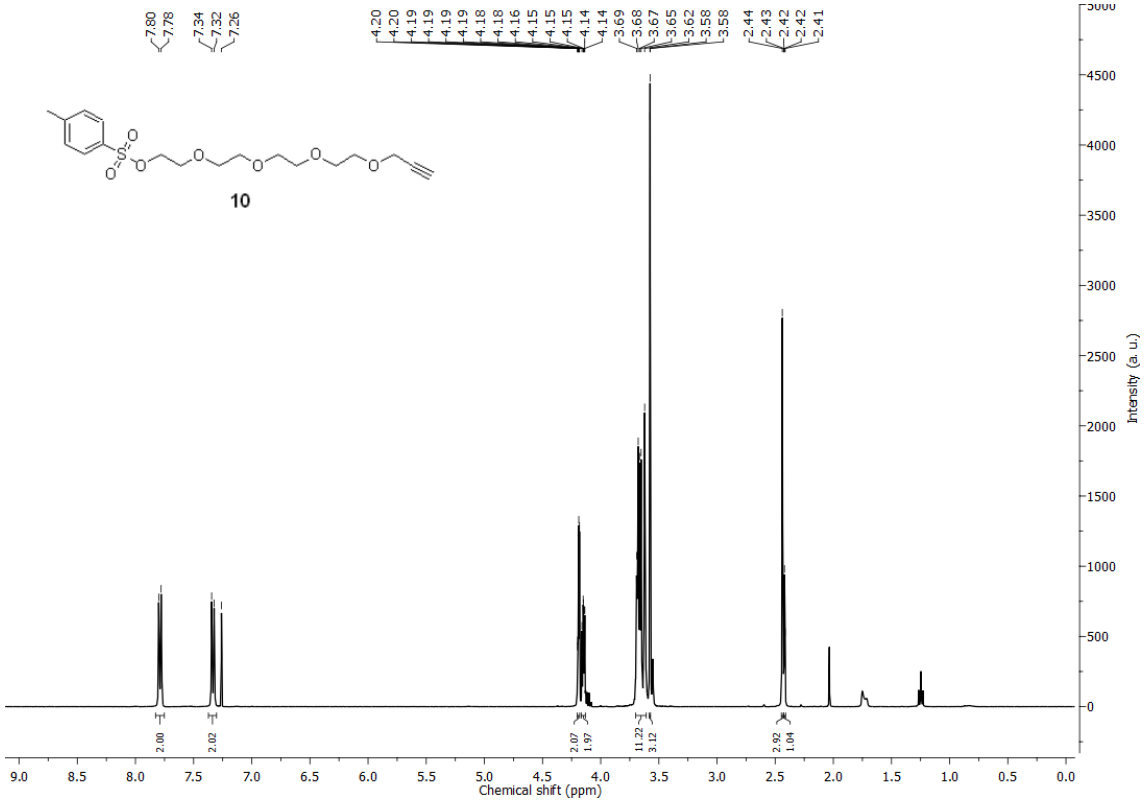

^{13}C-NMR of compound **10** in $CDCl_3$

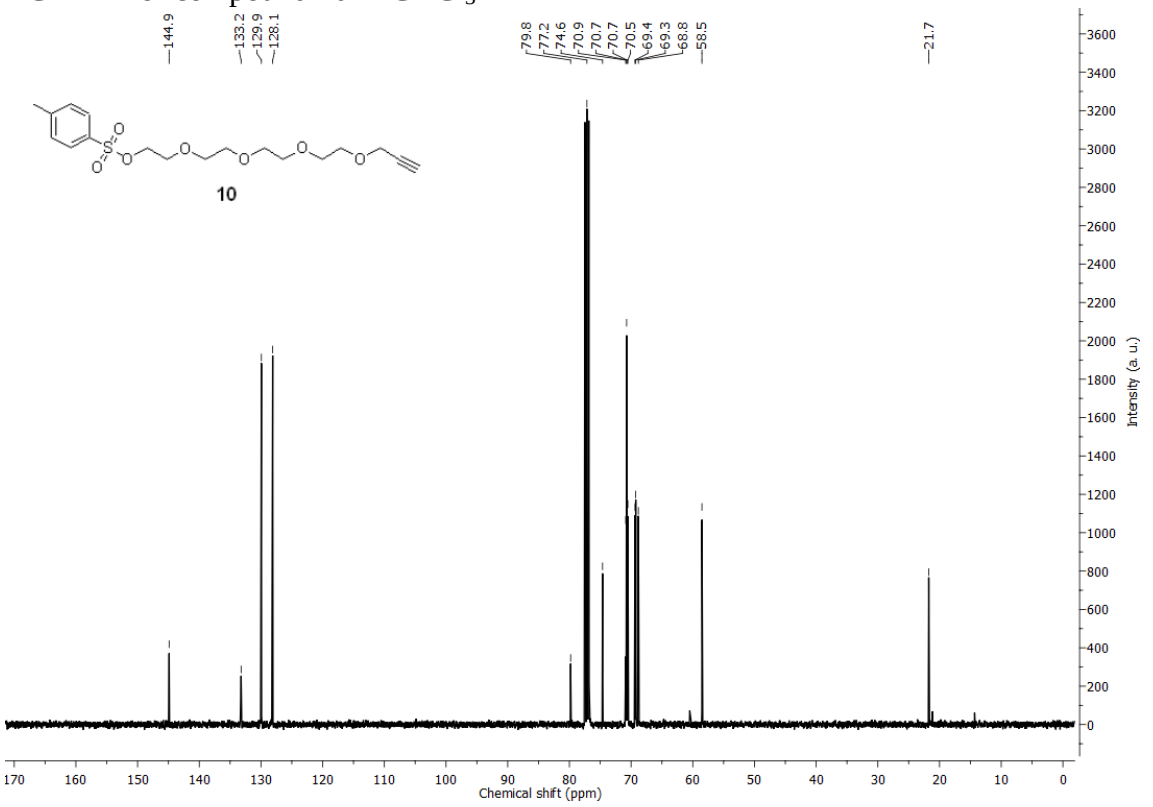

^{1}H-NMR of compound **11** in $CDCl_3$

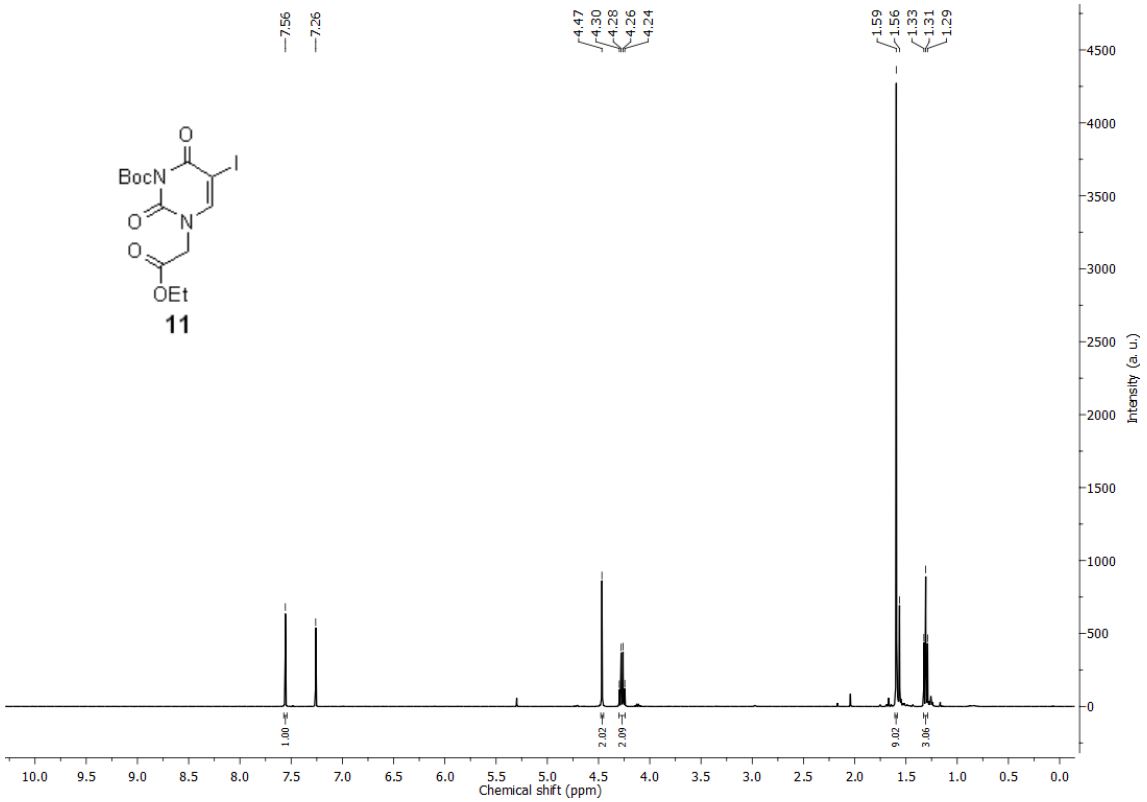

^{13}C-NMR of compound **11** in $CDCl_3$

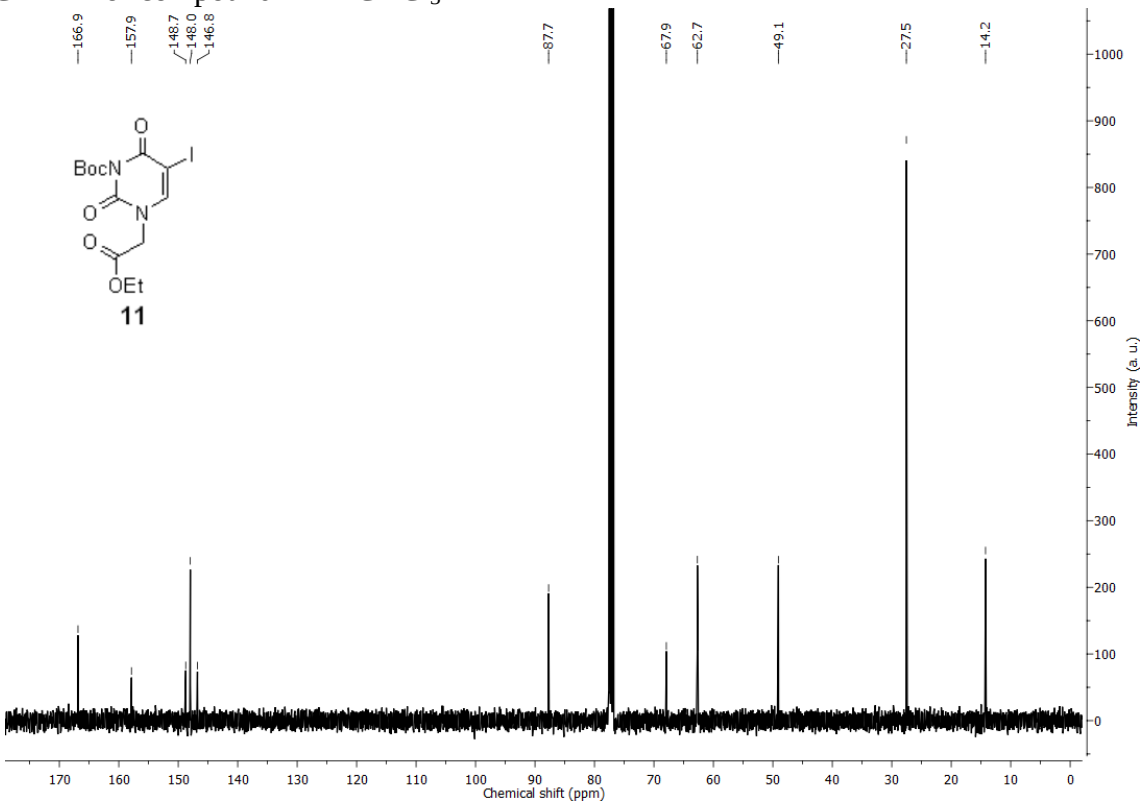

^{1}H-NMR of compound **12** in $CDCl_3$

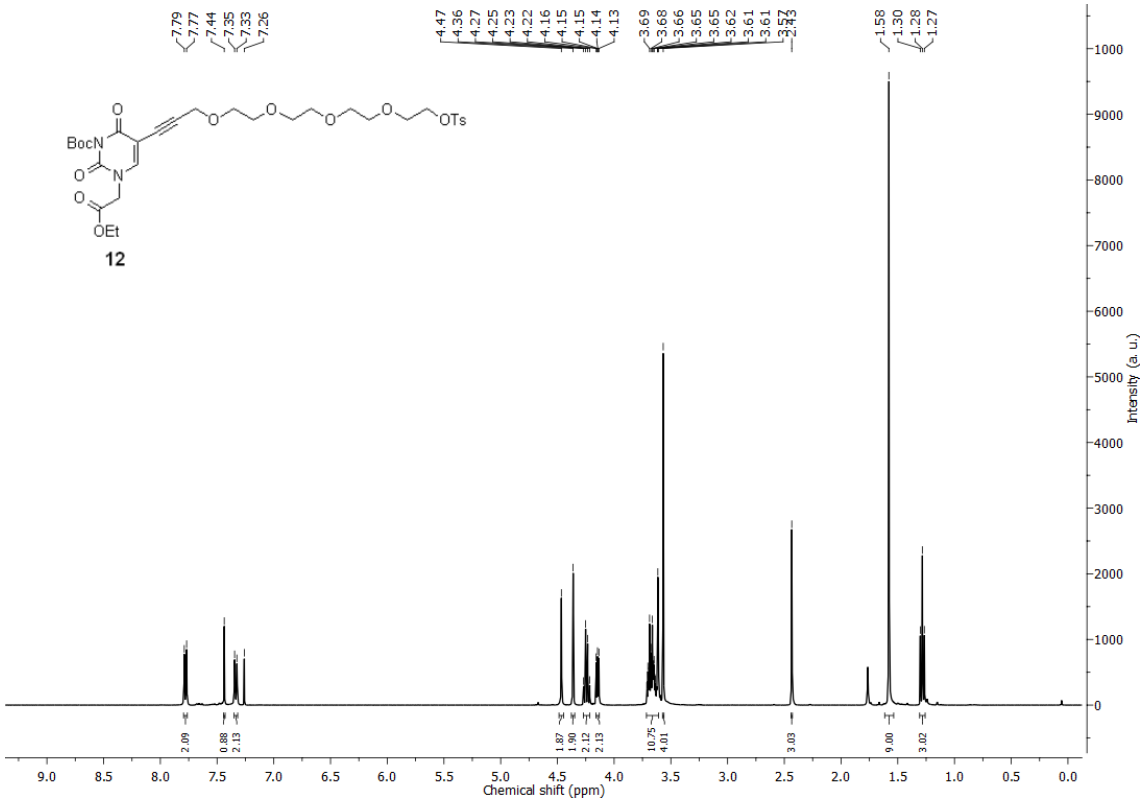

^{13}C-NMR of compound **12** in $CDCl_3$

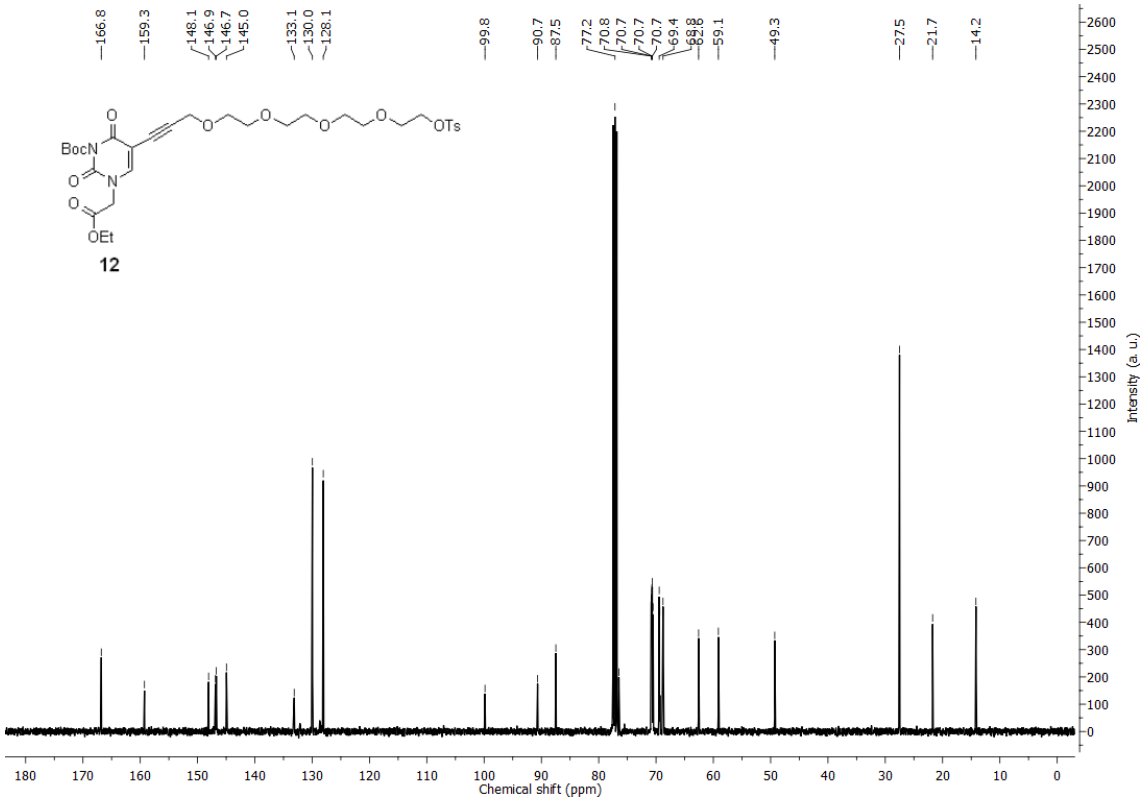

^{1}H-NMR of compound **13** in $CDCl_3$

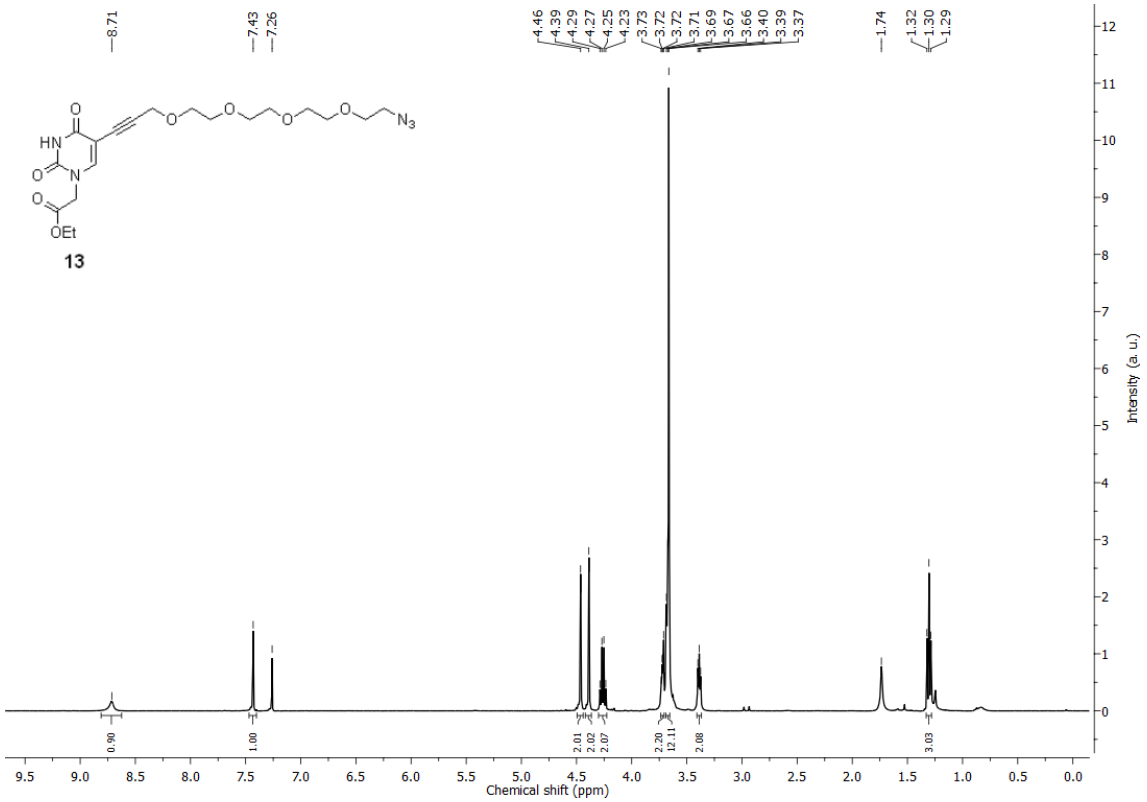

^{13}C-NMR of compound **13** in $CDCl_3$

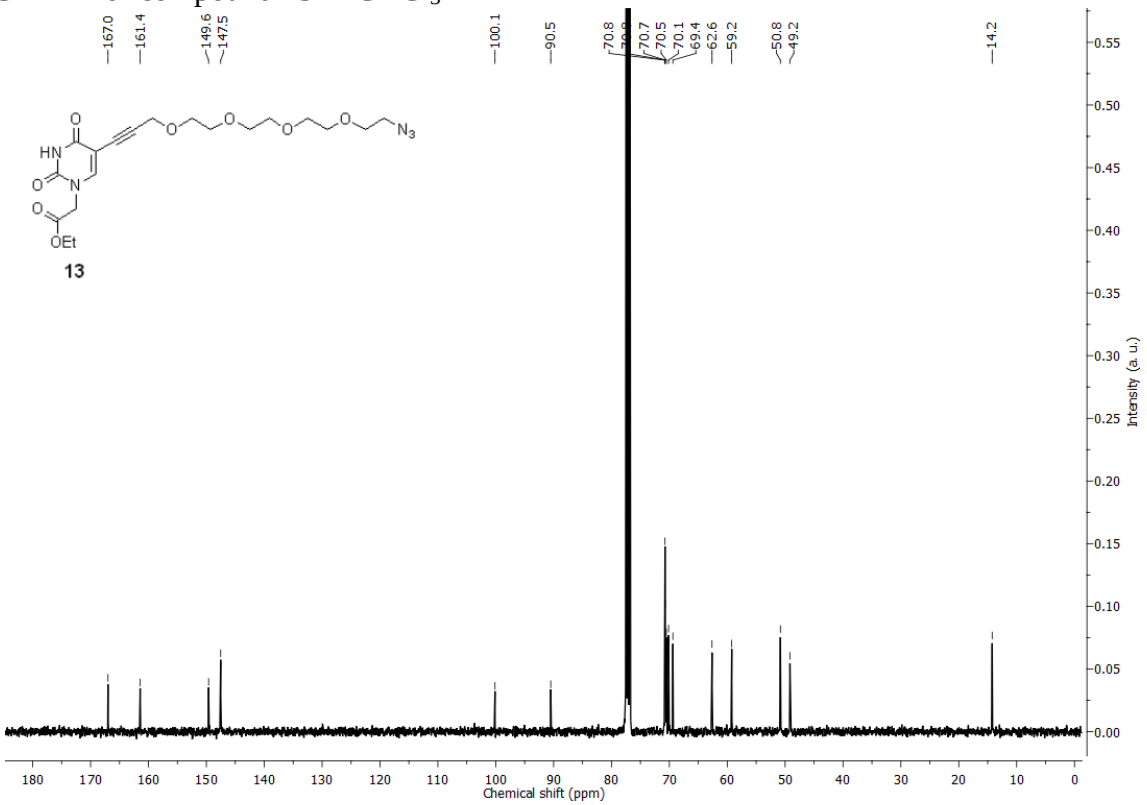

^{1}H-NMR of compound **14** in d_6-DMSO

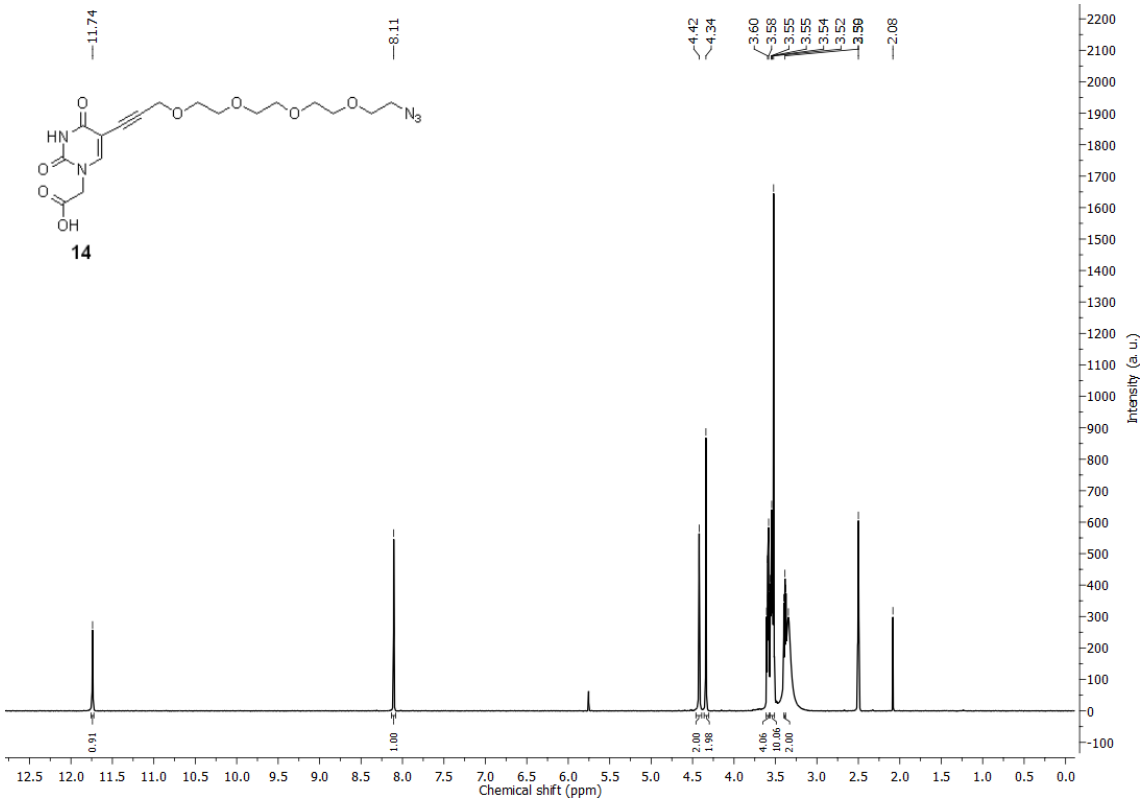

^{13}C-NMR of compound **14** in d_6-DMSO

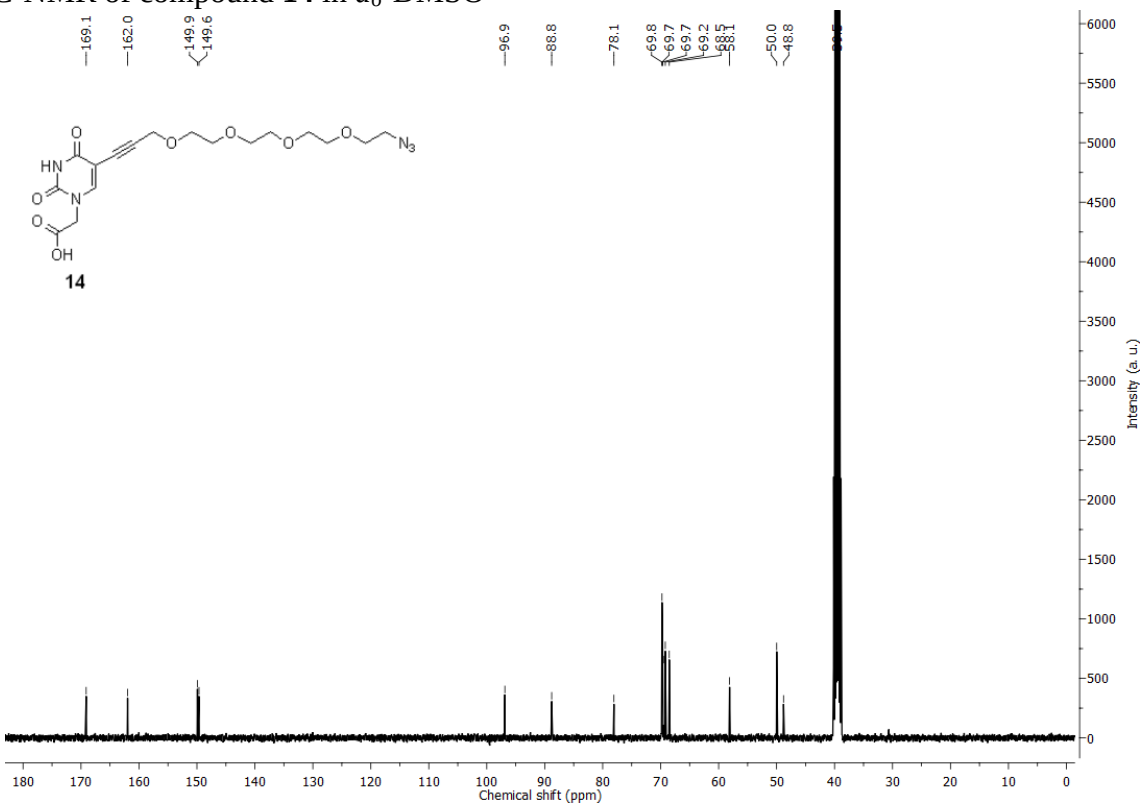

[1]H-NMR of compound **15** in d_6-DMSO

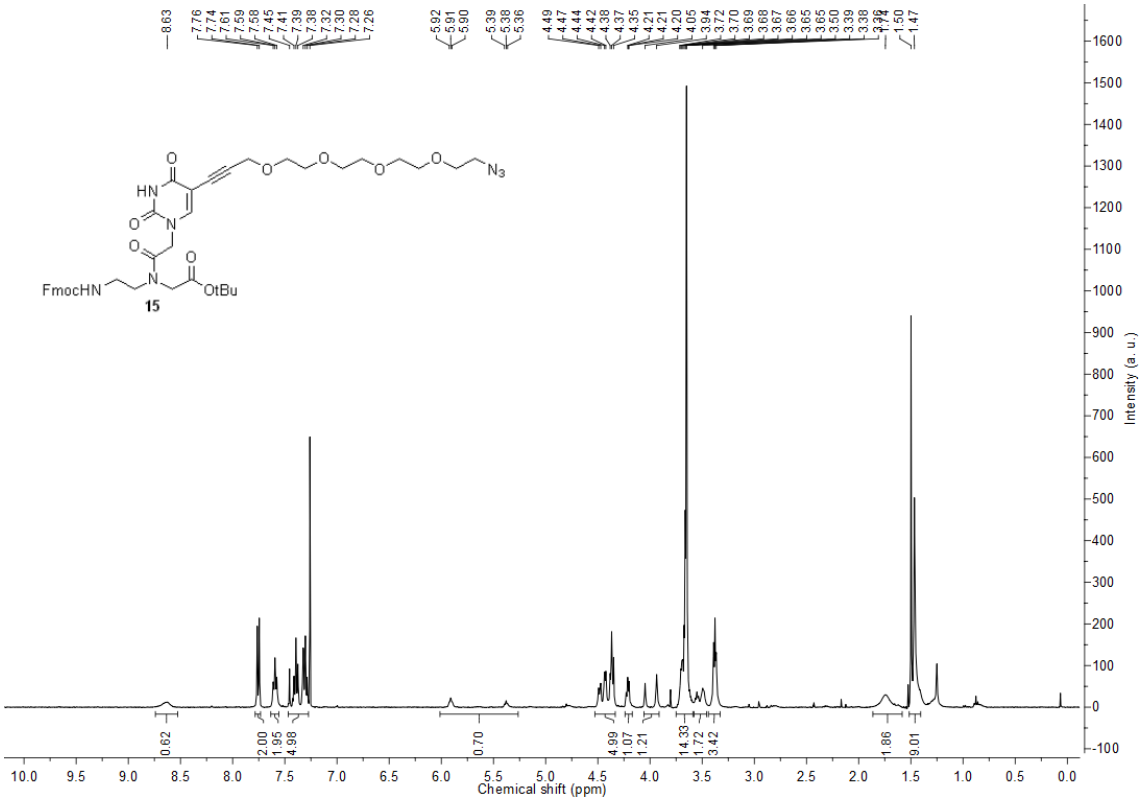

[13]C-NMR of compound **15** in d_6-DMSO

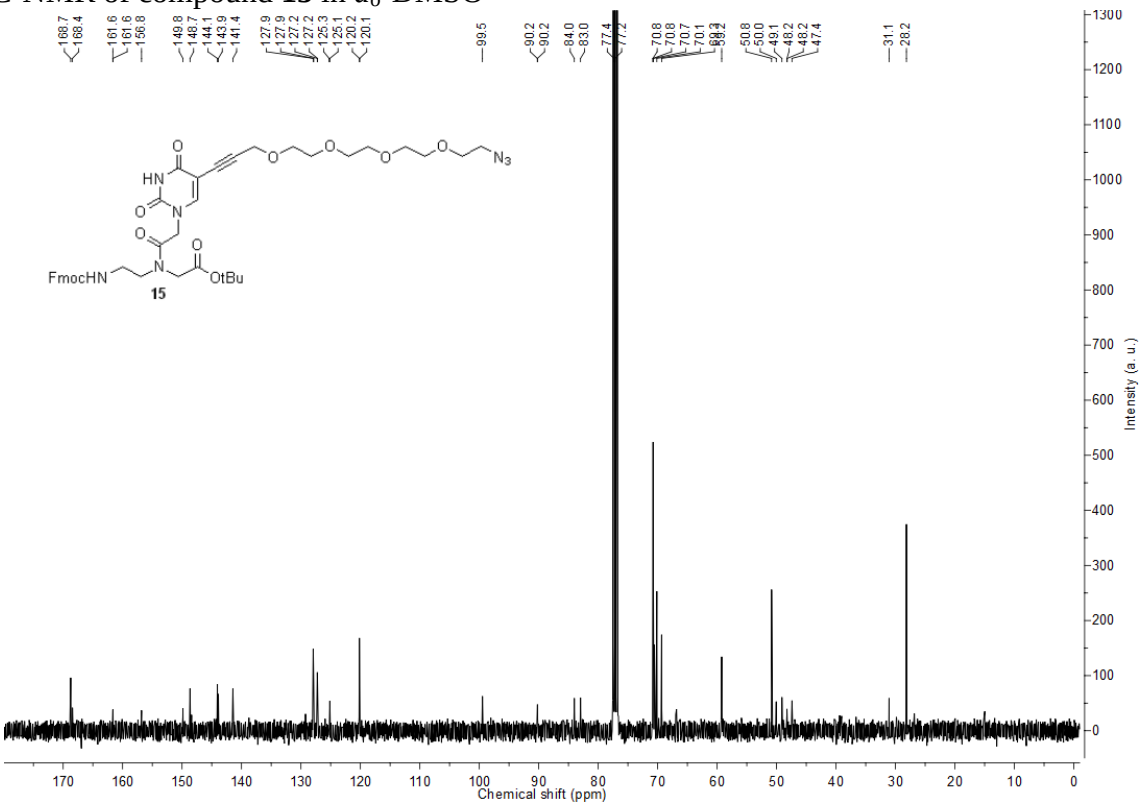

^{1}H-NMR of compound **16** in d_6-DMSO

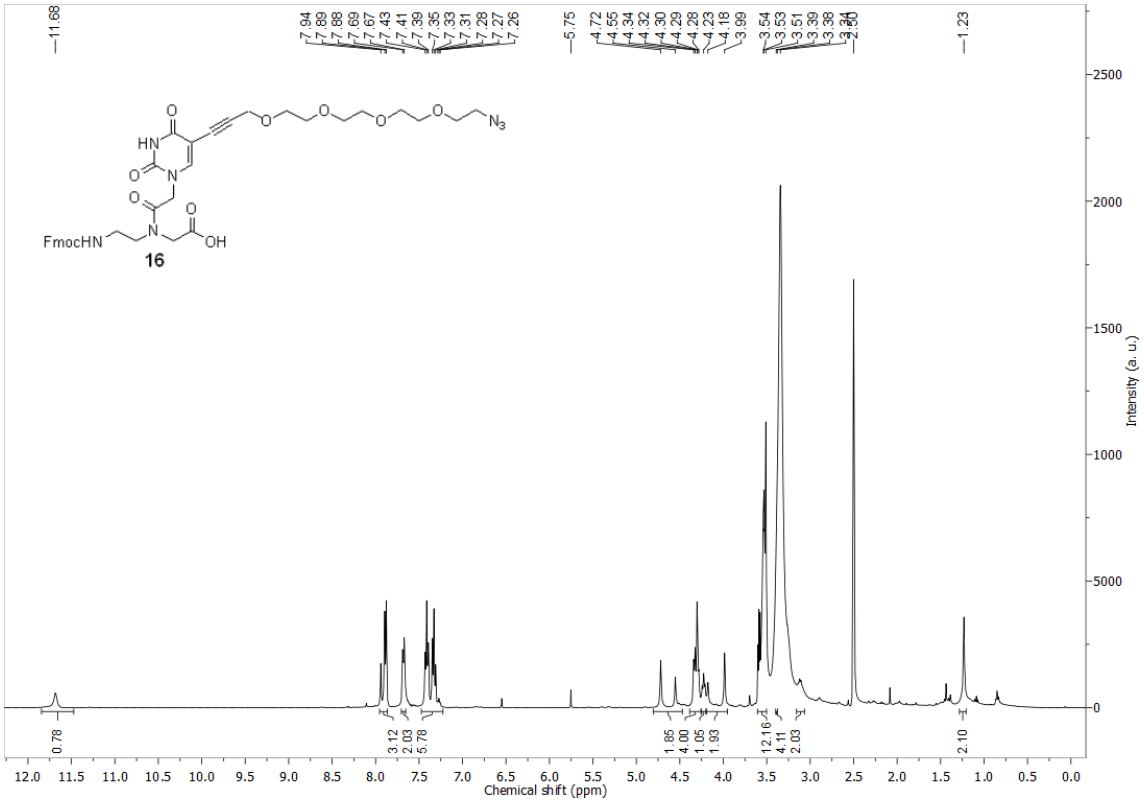

^{13}C-NMR of compound **16** in d_6-DMSO

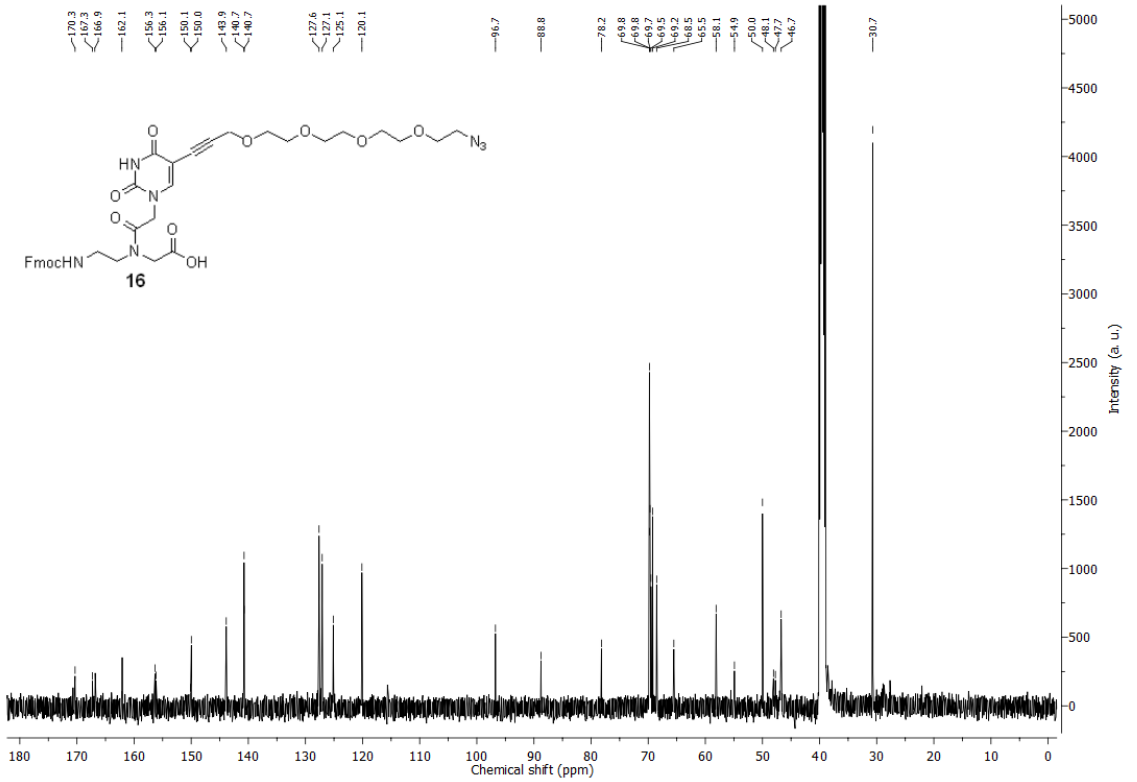

RP-HPLC chromatogram of azide-and alkyne-modified PNA oligomers **18** (**A**), **19** (**B**) and **20** (**C**) at 260 nm. Conditions: 0–50% B in 25 min and 50–100% B in 15 min (Mobile phase A: 5% acetonitrile in H_2O containing 0.1% TFA. Mobile phase B: 50% acetonitrile in H_2O containing 0.1% TFA). Flow rate was 2 mL/min. MALDI-TOF mass spectra of azide-and alkyne-modified PNA oligomers **18** (**D**), **19** (**E**) and **20** (**F**). See Table 1 for mass data of all PNA oligomers.

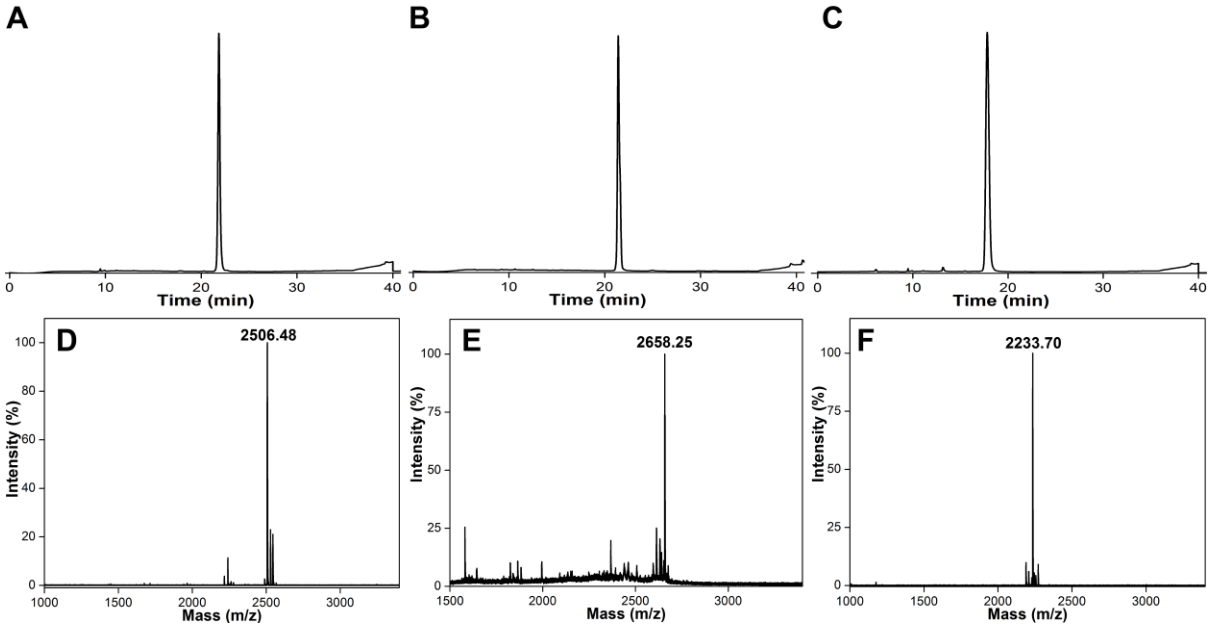

(**A**) Representative RP-HPLC chromatogram of iodo PNA **23** and its Suzuki-Miyaura reaction product (**23k**) with benzothiophene boronic acid (**k**) at 260 nm. (**B**) Representative RP-HPLC chromatogram of iodo PNA **23** and its Cu-free Sonogashira reaction product (**23k**) with naphthalimide alkyne (**e**) at 260 nm. Conditions: 0–50% B in 25 min and 50–100% B in 15 min (Mobile phase A: 5% acetonitrile in H_2O containing 0.1% TFA. Mobile phase B: 50% acetonitrile in H_2O containing 0.1% TFA). Flow rate was 1 mL/min.

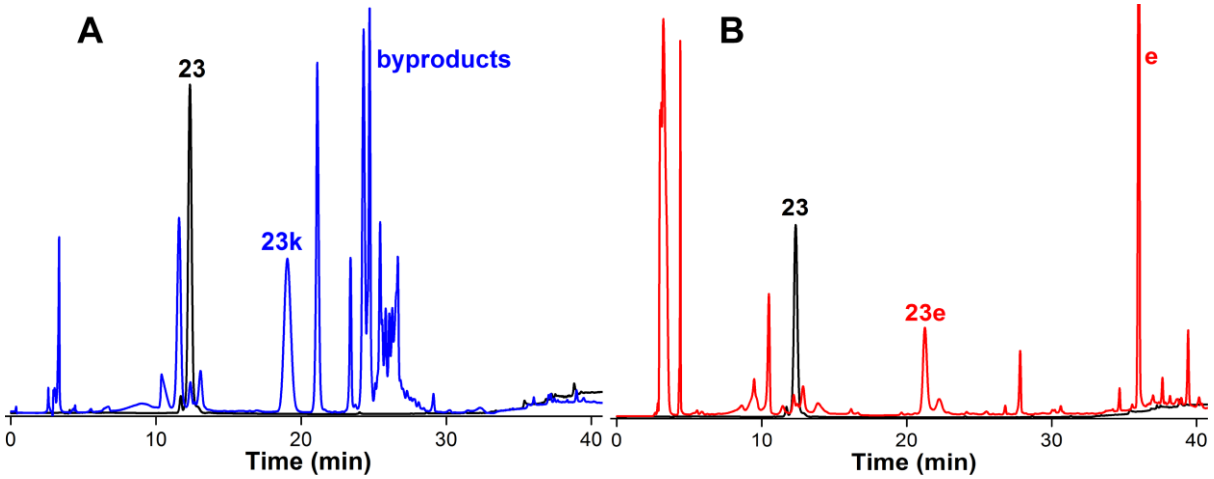

Representative absorption spectra of clicked PNA oligomers at 6.5 µM for **18a** and **20e**, and at 3.5 µM for **23k** and **23e**, respectively, in water.